

REPORT 1926

NACA INVESTIGATION OF FUEL PERFORMANCE IN PISTON-TYPE ENGINES

By HENRY C. BARNETT

PREFACE

It is generally recognized that the piston-type engine will continue to play an important role in air transportation for an indefinite period in spite of the intensive effort now being devoted to gas-turbine power plants. For this reason, past researches conducted in piston engines are still of interest in the solution of current problems relating to such engines. In order to simplify the task of using the data from previous investigations, an effort has been made to compile a portion of these data into a single reference source.

This particular report is a compilation of many of the pertinent research data acquired by the National Advisory Committee for Aeronautics on fuel performance in piston engines. The original data for this compilation are contained in many separate NACA reports which have in the present report been assembled in logical chapters that summarize the main conclusions of the various investigations. Complete details of each investigation are not included in this summary; however, such details may be found, in the original reports cited at the end of each chapter.

REPORT 1026

TABLE OF CONTENTS

Chapter		Page
I	HIGH-SPEED PHOTOGRAPHIC STUDIES OF KNOCKING COMBUSTION-----	455
II	CORRELATIONS OF KNOCK-LIMITED PERFORMANCE DATA-----	500
III	ANTIKNOCK PERFORMANCE SCALES-----	511
IV	PREIGNITION-----	520
V	HYDROCARBONS AND ETHERS AS ANTIKNOCK BLENDING AGENTS-----	532
VI	AROMATIC AMINES AS FUEL ADDITIVES-----	556
VII	TETRAETHYL LEAD AS A FUEL ADDITIVE-----	569
VIII	ANTIKNOCK BLENDING CHARACTERISTICS OF FUELS-----	581
IX	FUEL VOLATILITY-----	599
X	INTERNAL COOLING-----	612
	APPENDIX A—ADDITIONAL DATA ON PERFORMANCE OF VARIOUS FUELS-----	621
	APPENDIX B—ADDITIONAL BLENDING CHARTS FOR TERNARY AND QUATERNARY FUEL BLENDS-----	638

REPORT 1026

CHAPTER I

HIGH-SPEED PHOTOGRAPHIC STUDIES OF KNOCKING COMBUSTION

By C. DAVID MILLER*

At the Summer Meeting of the Society of Automotive Engineers in 1946, Mr. C. David Miller of the NACA presented a paper entitled "Roles of Detonation Waves and Autoignition in Spark-Ignition Engine Knock as Shown by Photographs Taken at 40,000 and 200,000 Frames per Second." This paper was a summary of the NACA high-speed photographic studies of combustion in engine cylinders and it is reproduced substantially in its original form as chapter I of this report. The same material, under the title given above, was previously published in the Transactions of the Society of Automotive Engineers in January, 1947.

The National Advisory Committee for Aeronautics has been using high-speed motion-picture photography in research over a period of more than 20 years and has applied this method to the study of combustion within engine cylinders since 1933. By the early part of 1936 it had become apparent that commercially available cameras were not fast enough for the study of engine combustion, particularly for the study of spark-ignition engine knock. For this reason work was begun at Langley Field early in 1936 on the development of a high-speed camera using a newly invented optical system (reference 1). This camera, which was fully described in reference 2, will be referred to throughout this paper as the high-speed camera. It was operated successfully at 40,000 photographs (or frames) per second on its first test late in 1938 and has been used since that time principally in the study of knock in the spark-ignition engine at Langley Field, Va., and at Cleveland, Ohio. It was soon found, however, that even 40,000 frames per second was inadequate for the study of spark-ignition engine knock, and work was begun in 1939 at Langley Field on the development of a still faster camera. This development was based on another optical system (invented early in 1939) entirely unlike that of the high-speed camera developed in the years 1936 to 1938. (See reference 3.) Construction of a camera incorporating the new optical system was completed in 1941. This camera will be referred to throughout this paper as the ultra-high-speed camera. The ultra-high-speed camera could not be operated satisfactorily according to the original design. The difficulties were not directly associated with the optical system of the camera but with incidental mechanical details. Development of the design, continued since 1941, has not yet been completed. One

photograph of the phenomenon of spark-ignition engine knock, however, was secured with the ultra-high-speed camera at Cleveland at the rate of 200,000 frames per second. It is believed that pictures can eventually be obtained with this camera at a speed several times greater than 200,000 frames per second.

Results of the research work done with the high-speed camera and the ultra-high-speed camera have been reported on a restricted basis during the war years except for one paper (reference 4) presenting a small amount of work on diesel combustion. A report on spark-ignition engine combustion printed in 1941 (reference 5) presented preliminary results and showed that the knock reaction occurred in less than 50 microseconds, and that this reaction may be preceded by much slower exothermic end-gas reactions. Reference 6 printed in 1942 included additional preliminary results and included indications that the knock reaction may sometimes originate at a point outside of the end gas and that the knock reaction may be preceded by mild vibrations which become manyfold intensified at the instant of knock. In references 5 and 6, the characteristic reaction occupying less than 50 microseconds as seen in the photographs was more or less assumed to be the knock reaction on the basis of the general appearance of the motion pictures. In reference 7, issued in 1943, this characteristic reaction was definitely shown to begin simultaneously, within 25 microseconds, with the onset of violent knocking gas vibrations as shown by a piezoelectric pressure pickup exposed to the end gas in the combustion chamber. Reference 7 included additional indications that the knock reaction does not necessarily originate in the end gas. Reports released in 1944 showed that the knock reaction instantly rendered a large part of the unreleased energy of combustion chemically unavailable (reference 8), revealed several definite facts about the previously noted preknock vibrations, and showed the development of several types of preknock end-gas autoignition as well as autoignition in a large end-gas volume practically without any resultant knock (reference 9). In 1946 a report was released presenting analyses of some of the high-speed pictures indicating knocking detonation-wave velocities ranging from one to two times the speed of sound in the burned gases (reference 10), and ultra-high-speed photographs taken at 200,000 frames per second have been released confirming the detonation-wave character of knock with a wave speed of 6800 feet per second (reference 11).

*Now with Battelle Memorial Institute.

It is the purpose of the present paper to offer a unified report of the facts concerning spark-ignition engine knock that have been previously reported on a restricted basis and to include as an introduction to the unified report the results of a literature study which the author believes support the new concept of knock that he and his coworkers have obtained from the high-speed pictures. A synopsis of the unified report has also been prepared in the form of a motion-picture film (reference 12). For a general history of the application of photographic methods to engine combustion, see references 4, 10, and 11.

Knock, one of the most serious limitations on the performance of the present-day reciprocating aircraft engine, has been plaguing the designers and users of spark-ignition engines in general at least since 1880, when Clerk suppressed extremely violent knock by the use of water (references 13 and 14). Knock has been the subject of intensive research by groups in various countries for about 25 years.

The past researches on knock have uncovered an immense amount of information, not only concerning the basic nature of knock but also concerning the question of what to do about it. The information available on the basic nature of knock has led most writers, at least in the United States, to accept the autoignition theory in preference to all others. (Though many writers refer to knock as "detonation," they do not mean to imply that they believe knock is caused by a detonation wave.) Only a few dissenters (references 14 to 19) have questioned the adequacy of the autoignition theory.* The photographs obtained with the high-speed camera and the ultra-high-speed camera have forced the author and his coworkers to join the ranks of the dissenters.

The available information on what should be done about knock is outside the scope of this paper and is so well known that it needs no review here. The available information is undoubtedly accurate as far as it goes and is so extensive that many practical workers with engines and fuels even discount the need for definite knowledge as to what knock is.

Aside from the fact that any kind of knowledge concerning any process of nature rarely proves in the end to be of no practical value, some urgent reasons exist for determining exactly what knock is. Probably the most important reason is associated with the fact that little is definitely known even about the harmfulness of knock. As will be shown in this paper, there are probably more than one and perhaps even more than two phenomena that are regarded as knock when they occur in the combustion chamber. In view of the possibility that these phenomena may not all be harmful, it seems urgently desirable to learn which are harmful and how to distinguish between one of the phenomena and another. As was pointed out by Boerlage in 1937 (reference 19), the noise of knock cannot be regarded too seriously until the harm done has been demonstrated to be proportional to the noise. In order to distinguish between the forms of knock and to know which are harmful and which are not, the logical first step appears to be that of learning what the phenomena are and under what conditions the various phenomena occur.

Other reasons for seeking the true explanation of knock are the possible saving of much labor involved in developing and testing ideas based on a possibly false conception of the nature of knock, acquisition of additional fundamental knowledge concerning chemical laws that might prove useful in other fields, and the possibility, however remote, that some new and simpler solution to the knock problem might be suggested.

Next to autoignition, the detonation-wave theory probably is generally regarded as the most plausible of the many theories that have been advanced to explain knock. Study of the photographs taken at 40,000 frames per second over a period of 6 years has convinced the author that a detonation wave, or some phenomenon very much like a detonation wave, actually is involved in the type of knock most frequently encountered in the modern aircraft engine. Autoignition also appears to be often involved in knock. A combined autoignition and detonation-wave theory has been proposed (reference 10) on the basis of a study of the high-speed photographs and the available literature concerning knock.

The autoignition and detonation-wave theories of knock are actually in agreement in many respects. According to either theory knock occurs only after the flame has traveled from the spark plug through most of the fuel-air mixture at speeds ranging from below 50 feet per second to several hundred feet per second, depending on engine speed, fuel-air ratio, and a number of other variables. This speed of 50 to several hundred feet per second is a low speed from the standpoint of tendency to produce shock; it is the normal rate of burning in nonknocking operation. Again according to either theory, the shock known as knock is produced by the sudden inflammation of the end gas, the gas that has not yet been ignited at the time knock occurs by the normal travel of the flame from the spark plug.

If the end gas is considered as being divided into a very large number of extremely small cells or increments, it is clear that no great shock will result from the burning of the individual increments at widely different times, however fast the burning of each increment may be, and it is also clear that shock will not result from the simultaneous burning of all the increments unless each increment goes through the burning process within an extremely small time interval. Shock will result, according to either theory, only if each increment burns within a very small time interval and all increments burn at the same time within a very small limit. If these two conditions are satisfied, then the end gas does not have time to expand during the burning of the increments and a very high pressure is produced in the end gas relative to the gas in the other parts of the chamber. The subsequent expansion of the end gas sets up a violent vibration or system of standing waves throughout the entire contents of the combustion chamber. Such a system of standing waves was shown to be the cause of audible knock, at least under certain conditions, by the researches reported by investigators at the Massachusetts Institute of Technology and at General

*Since the presentation of this paper in June 1946, prior opposition to the autoignition theory by several others has come to the author's attention.

Motors between 1933 and 1939 (references 20 to 23). Slow-motion pictures of these vibrations taken at 40,000 frames per second were first presented at an SAE meeting in March 1940 (reference 23).

The only point of difference between the autoignition and detonation-wave theories is in the means of synchronizing the ignition of the end-gas increments, that is, the mechanism that causes all end-gas increments to burn at the same time within a small enough limit to cause shock.

The argument presenting the synchronizing mechanism of the autoignition theory is as follows: Each end-gas increment will burn explosively when it attains some certain combination of temperature and density (or the equivalent of some particular temperature-density history, as suggested by Leary and Taylor of M. I. T. in reference 24). All end-gas increments are adiabatically compressed at the same time and at the same rate by the expansion of the burning gas behind the flame front. All increments of end gas should, therefore, reach the critical combination of temperature and density at which they will explode at the same time.

In an analysis of the synchronizing mechanism of the autoignition theory, it should be considered that the compression of the end gas by the burning gases is accomplished by an infinite series of sound waves. A given condition of temperature and density should, therefore, be expected to travel through the end gas from the burning zone at the speed of sound. The combination of temperature and density in any end-gas increment may be expressed as some function F , so defined that each end-gas increment will explode when $F=F_c \pm \delta$, the term δ representing an element of uncertainty due to random variation in the behavior of the end-gas increments or to random inhomogeneities. The value of F in each end-gas increment will increase by an amount equal to 2δ in some time interval τ . Now if τ is not greater than the order of the time interval τ' required for a sound wave to pass through the unignited end gas, then it should be expected that autoignition would take place as an explosive reaction traveling through the unignited end gas at least at the speed of sound. It would not take place as a simultaneous reaction throughout the end gas. The explosive reaction would constitute some kind of explosive wave, if not an actual detonation wave. This wave might travel too slowly to produce shock and to be regarded as a true detonation wave. Obviously, however, the less shock the wave produced the less the knocking sound heard outside the engine.

If τ is assumed to be much greater than the order of τ' , then autoignition should be expected to develop homogeneously throughout the end zone. The pressure built up by the combustion of the end gas, however, is relieved also by an infinite series of sound waves. Consequently, if τ is many times greater than the order of a time interval τ'' required for a sound wave to pass through the *autoigniting* end gas, the pressure in the end gas would be relieved many times during the process of autoignition and shock would not occur.

The magnitude of the time interval τ apparently must

lie within a range somewhat greater than τ' but not many times greater than τ'' if knock is to be caused by a homogeneous autoignition of the end gas. Above this range of values for τ no shock can occur; below this range of values the autoignition must occur as something similar to a detonation wave, and becoming more and more like a detonation wave as the knock intensity increases. (Knocks of different intensity can occur with the same end-zone volume according to unpublished NACA photographic records.) The time interval τ'' is a variable for different stages of the homogeneous autoignition process and reaches a value much less than τ' during the later stages of the process. The range of values of τ greater than τ' but not many times greater than τ'' must, therefore, be quite narrow.

Autoignition, either as a detonation wave or as a homogeneous reaction with τ slightly greater than τ' , seems a very plausible synchronizing mechanism. Before it is accepted conclusively, however, the available evidence should be carefully studied as to whether it actually is an adequate synchronizing mechanism. The evidence should also be investigated as to whether autoignition of the individual gas increments proceeds to completion within a short enough time interval to produce shock. A considerable amount of evidence exists against autoignition as the sole cause of the standing waves of knock on both counts, as will be shown in the later parts of this paper.

The synchronizing mechanism postulated by the detonation-wave theory is an intense compressive shock wave that travels through the end gas at supersonic velocity. Each gas increment is ignited probably by the combination of the sudden intense compression occurring in the shock front, the action of chain carriers in the shock front, and the radiation of heat from the shock front. The entire combustion, or some definite stage of the combustion, of each gas increment is presumed to occur in the shock front and to release a large amount of energy immediately behind the shock front. The energy released by the gas increments immediately behind the shock front maintains the high pressure required to propagate the shock front through the charge. Such a phenomenon, being an intense shock wave, would obviously set up vibration of the gases throughout the combustion chamber. If, as the author holds, simple homogeneous autoignition can no longer be accepted as the sole cause of the knocking gas vibrations, the detonation wave appears to be the only remaining plausible explanation that has been suggested. The detonation wave, however, may be only the end result of a comparatively slow homogeneous end-gas autoignition or the detonation wave may act as the initiator of a very rapid homogeneous combustion which in its turn sets up the violent gas vibrations.

A literature-based argument in favor of a combined detonation-wave and autoignition theory of knock will be found in the first part of the section called "Discussion and Analysis," and the unified report of the findings obtained from the high-speed and ultra-high-speed photographs will be found in the second part of the same section.

DEFINITION OF TERMS

Throughout the present paper the following terms are used with the meanings indicated:

1. Knock: Any type of reaction occurring within combustion-chamber contents and producing objectionable noise outside the engine, but not including the phenomenon of early combustion caused by too early spark timing or by early ignition from a hot spot.

2. Explosive knock reaction: A specific reaction observed in NACA photographs of knocking combustion taken at 40,000 frames per second, usually appearing instantaneous when the photographs are projected at the normal rate of 16 frames per second and coinciding chronologically with the onset of gas vibrations as seen in the photographs. (This reaction, being regarded as one form of knock, will sometimes be referred to simply as "knock" when the context makes the meaning clear.)

3. Flame front: The continuously changing surface that separates uninflamed parts of the cylinder charge from the burning parts of the charge that have been ignited by the advance of the flame from the spark plug.

4. Autoignition: Spontaneous burning in any part of the cylinder charge not caused by a spark, by contact with a flame front, or by contact with a hot spot, and including not only the initiation of burning but the entire process of burning resulting from the spontaneous ignition.

5. Shock wave: An intense compressive wave traveling through gas at supersonic velocity, the front of such wave constituting an abrupt increase or practical discontinuity in temperature, density, and velocity of the gas.

6. Detonation wave: A type of wave often observed in long tubes consisting of a shock wave traveling through a gas or a gas mixture and causing a reaction of the gas in the shock front, such reaction releasing energy immediately behind the shock front, the energy so released serving to maintain the pressure needed behind the shock front to propagate the wave.

DISCUSSION AND ANALYSIS: LITERATURE-BASED ARGUMENT FOR COMBINED DETONATION-WAVE AND AUTOIGNITION THEORY OF KNOCK

Autoignition theory.—The autoignition theory of knock was suggested by Ricardo in 1919 (reference 25). Midgley in 1920 declined to accept the autoignition theory and held to the detonation-wave theory (reference 14). A year later Woodbury, Lewis, and Canby of the du Pont laboratories (reference 26) presented streak photographs of combustion in a bomb, taken by the method of Mallard and Le Chatelier (reference 27), and drew conclusions favoring the autoignition theory. These du Pont investigators seem to have regarded the detonation-wave theory as the one having had general credence up to that time. From an analysis of their streak photographs and from consideration of various facts reported by previous investigators, they concluded that "the possibility of detonation under such conditions [conditions existing in the engine cylinder] appears exceedingly remote." After mentioning that detonation is set up in a closed cylinder of small dimensions only with great difficulty, they further

stated: "On the other hand, autoignition of the high-density gases ahead of the flame front occurs over a wide range of fuel mixtures and conditions [in their tests] and gives a sudden development of pressure similar, in our opinion, to that characteristic of a knocking explosion. It is possible that this autoignition may set up detonation [a detonation wave] in some cases, thereby acting as an intermediate stage in knocking. Our experiments have not been carried to a definite conclusion, and present data do not warrant presentation of autoignition as a positive explanation for knocking. It is our feeling, however, that information at hand favors more strongly the theory of autoignition of the high-density gases ahead of the flame front than that of detonation [the detonation wave]."

Actual motion pictures of knocking combustion were first published in 1936 by Withrow and Rassweiler of General Motors Corp. (reference 28). These excellent photographs, taken at the rate of 2250 frames per second, showed the development of autoignition in the end gas and greatly increased the already existing confidence in the autoignition theory. They were taken at too low a rate to show a detonation wave, however, even though such a wave might actually have occurred after the autoignition that was photographed.

The autoignition theory, with the additional assumption of preflame chain reactions, has the advantage of explaining and correlating many of the known facts concerning knock. During the period of 1939 to 1945, however, urgent need for a modification of the simple autoignition theory of knock was shown by photographs of knocking combustion taken at the rate of 40,000 frames per second with the NACA high-speed motion-picture camera. The first of these photographs, presented in references 23 and 5, showed a reaction completed in 50 microseconds or less. The authors believed that this reaction was the true knock reaction because they could see in the projected motion pictures that this reaction occurred at the same time as the beginning of the violent vibration of the gases, which by then had come to be regarded as an indication of knock. Later NACA tests (reference 7) showed that this extremely quick reaction did occur simultaneously with the beginning of the vibrations. Serruys had previously (in 1932) concluded that knock generally occupies a time interval less than 100 microseconds in reference 29 and, in 1933, on a basis more in harmony with the standing-wave concept of knock, in reference 30. Considerations presented in the present paper have caused the author to abandon the exclusiveness of the concept "true knock reaction." The reaction will hereinafter be referred to as the "explosive knock reaction."

The need for a modification of the autoignition theory of knock lies in the fact that the evidence available in the literature indicates autoignition requires for its completion a time interval of an entirely higher order than the 50 microseconds involved in the explosive knock reaction, even under conditions of severity approaching those of the modern aircraft engine. The previously mentioned photographs by Withrow and Rassweiler (reference 28) clearly show brightly luminous autoignition occupying a time interval of the order

of 1000 microseconds. NACA high-speed photographs have shown autoignition flames slowly propagating themselves from point to point throughout the end gas before the explosive knock reaction occurs (reference 9); and another NACA high-speed photograph has shown autoignition developing slowly and simultaneously in all parts of the end gas before the occurrence of the explosive knock reaction (reference 5). These two types of autoignition shown in the NACA high-speed photographs, preceding the explosive knock reaction, occupied time intervals ranging from 500 to 1250 microseconds. Streak photographs were published as early as 1911 by Dixon and coworkers (references 31 and 32) showing slow autoignition in glass tubes resulting from quick compression. This autoignition progressed at a rate comparable with the rates of the autoignitions shown by Withrow and Rassweiler and by the NACA investigators.

The evidence showing that autoignition occupies a time interval of a higher order than 50 microseconds is not the only reason for believing simple autoignition to be an inadequate explanation of knock. Many investigations have shown that autoignition can occur without causing marked gas vibrations, which are probably the best known characteristic of knock in the present-day spark-ignition engine. These gas vibrations, if they occur, are visible in streak photographs taken by the method of Mallard and Le Chatelier (reference 27) as a series of bright bands extending across the photograph in a direction perpendicular to the direction of film movement. The gas vibrations also cause oscillations in pressure-time records.

Some excellent streak photographs presented by Withrow and Boyd (reference 33) are examples of nonvibratory autoignition in the engine cylinder. These General Motors investigators stated that both the pressure-time records and the flame traces show that the autoignition required 2° to 5° of crankshaft rotation (400 to 1000 microsec) for its completion. Figures 11 to 16 of their work clearly show the flame front traversing the greater part of the chamber at the normal rate and show the end gas then being consumed at a much higher rate. All of these figures except figure 14, however, reveal not the slightest indication of gas vibrations. It is difficult to conclude from the printed picture of figure 14 whether there is any evidence of vibrations. Moreover, the pressure-time records of figures 11 to 16 of reference 33 show no evidence of gas vibrations. Though audible gas vibrations probably did not occur in those tests, some kind of disturbing noise surely must have occurred, as is discussed in the present paper under "Detonation-Wave and Autoignition Theories Combined."

Withrow and Boyd did not comment on the absence of gas vibrations in their tests. Up to about the time of the writing of their paper (1931), gas vibrations do not seem to have been regarded as a usual feature of knock. The only recognized criterion of knock as seen in pressure-time records appears to have been simply a sharp increase in the rate of pressure rise. In 1932 Rassweiler and Withrow (reference 34) presented streak photographs clearly showing the gas vibrations; and in 1934 (reference 21) they showed that the vibrations as

seen in the photographs coincided, cycle by cycle, with fluctuations shown in the pressure-time records.

Woodbury, Lewis, and Canby in 1921 did not regard the gas vibrations as being associated with knock, for in the previously quoted passage (reference 26) they concluded on the basis of their own experiments that autoignition of the high-density gases ahead of the flame front gives a sudden development of pressure similar, in their opinion, to that characteristic of a knocking explosion. The pressure-time traces presented for the cases of autoignition referred to showed, in general, no gas vibrations but only a sharp increase in rate of pressure rise near the end of combustion. Almost without exception the streak photographs also showed no trace of gas vibrations; the exception was with ether-air mixtures. With initial temperature of 150° C and initial pressure of 65 pounds per square inch, neither the flame trace nor the pressure-time trace for an ether-air mixture showed any sign of gas vibrations, whereas with the same initial temperature and with initial pressure of 75 pounds per square inch, both the flame trace and the pressure-time trace showed the gas vibrations with agreement in frequency. The change that occurred in the phenomena studied in a bomb by these investigators, when passing from 65 to 75 pounds per square inch with ether-air mixture at 150° C, appears to correspond to the change in the recognized criterion of spark-ignition engine knock that developed in the early 1930's.

No particular note appears to have been made in the literature of the change in the recognized criterion of knock that developed in the early 1930's. Sufficient data do not appear to be available to explain the change or to indicate whether it was a real change caused by altered engine design and altered fuels or an apparent change developing with the securing of more extensive data.

In 1939 Boyd (reference 35) compared a streak photograph of autoignition without gas vibrations (fig. 10 of reference 35, same as fig. 16 of reference 33) and a streak photograph of autoignition with gas vibrations (fig. 12 of reference 35, same as fig. 10 of reference 34). He very reasonably regarded the case of his figure 12 as involving a much more violent knock than the case of his figure 10. Examination of his figures 10 and 12, however, discloses that the end zone was of nearly the same size in the two cases at the time the autoignition, or knock, occurred. The comparison therefore indicates that the violence of knock or at least the violence of the gas vibrations is not dependent on the size of the autoigniting end zone. Moreover, NACA high-speed photographs have shown plainly visible gas vibrations in cases where the end zone, if any existed at the time of start of the gas vibrations, was too small even to be seen in the photographs (references 6 and 7).

Other streak photographs showing autoignition without trace of gas vibrations may be found in papers by General Motors investigators (references 36 to 38). The most striking examples of this phenomenon, however, are to be found in the work of Duchene (reference 39). In this work many streak photographs are presented of combustion, with spark ignition, in a bomb equipped with a piston providing compression by

a blow from a heavy pendulum. Many of these flame traces show a sudden darkening extending entirely across the trace, which Duchene considered as indicative of a detonation wave. Only three of the records, however, 21, 35, and 36, show any trace of gas vibrations. In most cases the darkening is quite diffuse instead of practically instantaneous, as it should be if caused by a detonation wave. The records all distinctly show slow autoignition preceding the sudden darkening. The fraction of the total charge involved in the nonvibratory autoignition in the different records covers the entire range from near zero to practically the entire charge. Gas vibrations should not, of course, be expected from simultaneous autoignition of the entire charge at constant volume. Records 23, 28, 29, and 31 of Duchene's work, however, clearly show autoignition of about half the contents of the chamber without any trace of vibrations.

The inadequacy of simple autoignition as an explanation of the phenomenon of knock has been clearly recognized by some investigators. In 1928 Maxwell and Wheeler in reference 15 reported frequently observing autoignition flame, with 50-50 mixtures of pentane and benzene in a bomb, starting from the far end of the cylinder and progressing back to meet the spark flame. They reported that explosions in which this phenomenon occurred were no louder than usual and that the pressure records showed no unusual features. They concluded, in consequence, that such an ignition of unburnt residual mixture is not likely to be the cause of a pinking explosion in an engine cylinder. In reference 16 the same investigators stated: "Our objection to the 'autoignition' theory is that, when such ignitions occur during an explosion in a closed cylinder (for example, figs. 2 and 5), the explosion is no more violent than in their absence. Moreover, what we have termed a 'pink' in our cylinder, because it so closely resembles the pink in an engine cylinder, is obtained most commonly without the occurrence of 'autoignition.'"

In 1935 Egerton, Smith, and Ubbelohde (reference 17), in discussing the work of other investigators, stated: "'Autoignition,' that is, ignition in a region of the gas prior to the arrival of the flame front, was observed both in the knocking zone and elsewhere, but does not necessarily give rise to the knocking type of combustion, though it was supposed that the high rate of combustion in the knocking zone was due to autoignition within it."

In 1936 Boerlage (reference 19), in discussing the results of his own streak photographs, stated: "What surprised us, however, in the results obtained with the test engine, was the relatively slow character of the combustion due to autoignition. The development of the second center of ignition was at all points similar to the progression of the primary flame due to the spark. The 'simultaneous' combustion of the 'end gas,' which we have believed responsible for the knock, thus seems to be reduced to the rather calm development of a secondary center of ignition." He further stated: "* * * the velocity of the secondary flame front is practically equal at each instant to that of the primary flame front. We have never been able to make out any speed equal to the speed of sound, but at most, speeds of 150 meters per second, and

these only in the case of excessive detonation (knock). In the case of slight detonation (knock) the speeds do not attain even half this figure. * * * The pressure diagrams show only moderate pressure rises, and this is still another indirect proof of the fact that the speeds of the flames are relatively low and remain much below the speed of sound. We have not succeeded in demonstrating the existence of extreme local pressures."

The investigations mentioned have shown beyond possible doubt that autoignition can, and in many cases actually does, occur too slowly to cause the gas vibrations characteristic of knock. This fact does not prove that autoignition cannot, under any conditions, occur quickly enough to cause the gas vibrations. It does, however, preclude the possibility of regarding the occurrence or nonoccurrence of autoignition as a criterion for the occurrence or nonoccurrence of the type of knock characterized by gas vibrations. A different criterion must be sought, either the occurrence of autoignition at a rate above some critical value or the occurrence of some other phenomenon.

Indeed the criterion of autoignition at a rate above some critical value seems to be precluded by some of the NACA photographs (references 5* and 9), for in those cases slow autoignition was seen to occur, followed by the much faster reaction that set up the gas vibrations. In this connection it should be noted that some investigators (references 24 and 40) have regarded the apparent autoignition shown in one of the NACA papers (reference 5) as a preflame reaction. The slow apparent autoignitions shown in reference 9, however, are more difficult to explain as preflame reactions because they propagate themselves from point to point in the same manner and at about the same speed as a normal flame.

The available literature, as reviewed in this section, points to the conclusion that some phenomenon other than simple autoignition must be sought as the cause of the gas vibrations associated with knock in the modern spark-ignition engine.

Detonation-wave theory.—Prior to the NACA investigations that will be summarized in the present paper the occurrence of a detonation wave in a bomb or a knocking engine had not been supported by any such abundance of direct experimental evidence as the occurrence of autoignition. This fact is, of course, readily explained by the consideration that the detonation wave, being a many times faster phenomenon than autoignition, requires very much more powerful methods for its detection. A very important consideration in favor of the detonation wave as the explanation of gas vibrations is the unquestionable fact that it would cause gas vibrations if it did occur, whereas it has been shown that simple autoignition does not necessarily cause the vibrations when it occurs.

Many writers have long been strongly opposed to the detonation-wave theory of knock, principally because it is very difficult to set up detonation waves in containers as small as an engine cylinder, or indeed in hydrocarbon-air mixtures at all, and because many variables have unlike effects on the tendency of a combustible charge to knock in an engine and to develop a detonation wave in a tube.

In 1936 the Russian investigators Sokolik and Voinov (reference 18) furnished direct experimental evidence of propagated combustion, as contrasted with the concept of simultaneous autoignition, traveling through the end zone in a knocking engine at the correct speed to be regarded as a detonation wave. This evidence is in the form of streak photographs for which a sufficiently high film speed was used to resolve the slope of the luminosity front developed by the detonation wave. It is unfortunate that this work has not, in the past few years, received more careful consideration. The photographs of Sokolik and Voinov were taken through a narrow window extending across the combustion chamber in the direction of the flame travel. The results show the flame traversing the greater part of the chamber at a mean velocity usually less than 20 meters per second, then traversing the remaining part of the chamber at a velocity of the order of 2000 meters per second.

The photographs of Sokolik and Voinov are, of course, open to the criticism that they show the performance of only a narrow zone in the combustion chamber. For this reason, the illusion of a detonation wave traveling at 2000 meters per second could have been caused by a much slower autoignition traveling through the end gas at a considerable angle to the visible zone. Such an illusion should not be expected to be consistent throughout many records. Sokolik and Voinov, however, do not state how many records they studied.

NACA high-speed motion pictures of knock in references 6, 7, and 11 have suggested that the explosive knock reaction does not necessarily originate in the flame front but that it originates at random anywhere within the normal flame or the autoigniting end gas. For this reason NACA investigators have been slow to accept the results of Sokolik and Voinov as having general validity, suspecting that some difference in test conditions may have caused a type of knocking phenomenon to occur in their work different from any knocking phenomenon that has been found in the NACA investigations.

The new evidence for the occurrence of a detonation wave in the knocking engine, based on the high-speed and ultra-high-speed photographs of references 10 and 11 will be discussed in the second part of the section called "Discussion and Analysis."

Intermediate flame velocity.—Intermediate between the slow autoignition found by various investigators and the detonation-wave velocity determined by the Russian investigators in reference 18 is the finding by Schnauffer (reference 41) of a speed of 265 to 300 meters per second for the travel of a flame through the end zone in knock. Schnauffer made this determination by means of ionization gaps mounted in different parts of the combustion chamber. The ionization current across the successive gaps was amplified and used to light neon bulbs. The time interval between the lighting of the successive bulbs was measured by the record of the bulbs on a photosensitive drum rotating at high speed.

Flame travel at 265 to 300 meters per second through an end zone 2 to 3 centimeters long would be almost fast enough to satisfy the 50-microsecond limitation imposed by the

NACA photographs (reference 5), and such a rate of flame travel might, therefore, very well be regarded as a satisfactory cause of the explosive knock reaction. Note should be made, however, that the speed of 265 to 300 meters per second has not been verified by other investigators. Schnauffer did not indicate how many ionization gaps were used in the actual knocking zone to determine the velocity of 265 to 300 meters per second. Examination of the pattern of the gap locations as shown in the figures of his paper indicates either that the velocity was determined from the time interval between ionization of only two gaps or that the distance over which the velocity was measured was much greater than 2 or 3 centimeters, in which case the 50-microsecond limitation was not satisfied. Measurement of rate of flame travel on the basis of the time interval between ionization of two gaps would not be valid in case of any type of greatly accelerated reaction in the end gas. In such a case the normal flame travel through an indeterminate fraction of the distance between the last two gaps would be erroneously treated as the flame travel across the entire distance; the result would be a meaningless velocity.

In Schnauffer's paper oscillograph records were shown for the ionization currents produced both by the normal flame and the knock reaction in the end zone. The oscillograph records for the two types of combustion look very much alike. Hastings has shown in reference 42, with the vibratory type of knock, that the total time interval throughout which ionization currents are measurable in the end gas is only a small fraction of the time interval throughout which the ionization currents are measurable in the earlier-burned parts of the cylinder charge. The similarity in the oscillograph traces of Schnauffer's work therefore indicates that he was dealing with simple autoignition, not vibratory knock.

Nature of gas vibrations.—Many investigators have shown the occurrence of gas vibrations in bombs and in engine cylinders, both by photography and by pressure-time records. When the vibrations were first observed on indicator records of engine combustion, the question was raised whether they were not natural vibrations of the indicator set up by the blow of knock. Undoubtedly in many cases of simple autoignition this explanation was correct. In this connection the observation by Schnauffer in 1931 (reference 43) is of interest. With the ionization-gap method he found apparently simultaneous ignition of end gas amounting to approximately 50 percent of the entire cylinder charge; the indicator record showed no vibrations but only a sharp increase in rate of pressure rise. Schnauffer commented: "Figures 4 and 5 show that with a pressure indicator sufficiently free of inertia it is very well possible to record the knocking blow without the appearance of pressure oscillations. It is thereby demonstrated that the oscillations are not pressure oscillations." When Withrow and Rassweiler in 1934 (reference 21) showed a precise agreement between the oscillations recorded by an indicator and the bright bands on a streak photograph of the combustion, it was no longer possible to doubt the validity of the vibrations recorded by the best indicators.

Examination of the published records of gas vibrations in bombs and in engine cylinders reveals that with comparatively slow-burning mixtures, such as are used in the spark-ignition engine, these vibrations are generally of two types: With the first type the first cycle of vibration recorded has a larger amplitude than any of the later vibrations and the decay of the vibrations is gradual; with the second type both the buildup and the decay of the vibrations are gradual. A detonation wave, by definition, would cause the first type of vibration but not the second. With auto-ignition ruled out as a cause of the first type of vibration, the detonation wave is probably the only known physical phenomenon that could cause it. This type of vibration will, therefore, be referred to hereinafter, for convenience, as the "detonation wave" type of vibration. The many investigations that have shown the detonation-wave type of gas vibration in bombs or engine cylinders, either photographically or by means of pressure indicators, include some of those previously mentioned (references 5 to 7, 18, 21, 26, 30, 34, 35, and 38), as well as investigations by Souders and Brown (fig. 6 of reference 44), Boerlage, Broeze, van Driel, and Peletier (reference 45), and Rothrock and Spencer (reference 46).

The type of vibration having a gradual buildup obviously requires a gradual feeding in of energy over a period of many cycles. This gradual feeding in of energy could occur only if the vibrations themselves affected the local rates of combustion, or energy release, in such manner as to speed up the combustion in the high-pressure regions relative to the low-pressure regions. Such an effect would cause any slight accidental vibration to become self-amplifying. The cause of an accidental vibration is not hard to find. Ignition at a point in a vessel will unavoidably send forth a pressure wave which, after reflection from the far wall, will return to the point of ignition and may speed up the combustion upon its arrival. Souders and Brown at the University of Michigan (reference 44) found that a very pronounced occurrence of this type of vibration could be eliminated by shortening their spark commutator contact so as to decrease the intensity of the pressure disturbance at ignition. The type of gas vibration having a gradual buildup will be referred to hereinafter as the "vibratory combustion" type of vibration.

The possibility, of course, exists that the inertia and damping characteristics of a pressure indicator might cause it to indicate a gradual buildup of vibrations even though the gas vibrations actually were of the detonation-wave type, particularly in cases where the vibration frequency is nearly the same as the natural frequency of the indicator. The failure of such spurious records to occur in practice, however, is indicated by the fact that all the records to be found in the literature fall very distinctly into the detonation-wave or the vibratory-combustion type; there is apparently no middle ground. A middle ground would be expected when the detonation-wave type of vibration is

modified by a pressure indicator with only slightly too much inertia to produce a faithful record.

The vibratory-combustion type of vibration, as should be expected, generally occurs in fairly long cylindrical bombs, in which the natural frequency is comparatively low and the total time of flame travel is comparatively long. Under such conditions this type of vibration may occur without any evidence of autoignition, hot-spot ignition, or any other type of combustion except the normal flame from the igniting spark, as in the previously mentioned work at the University of Michigan (figs. 5, 7, and 13 of reference 44).

Gas vibrations of the vibratory-combustion type in bombs have also been shown by Hunn and Brown, Kirkby and Wheeler, Lorentzen, Duchene, Wawrziniok, and Köchling in references 47, 48, 49, 39, 50, and 51, respectively. The photographs by Kirkby and Wheeler show how the vibratory combustion requires a bomb of considerable length. Lorentzen pointed out that the vibrations, which he apparently believed were caused by the same phenomenon as knock in the engine cylinder, could not have been caused by detonation because they set in before the attainment of maximum pressure. The vibrations shown by Duchene (records 21, 35, and 36) are of particular interest because they developed long after the charge had been completely inflamed, yet appear to have been built up gradually. The work by Wawrziniok showed gradual buildup not only of the vibrations in a bomb but also of the air vibrations outside a knocking engine. It is possible, however, that the forced vibrations of the engine walls built up gradually even with a detonation-wave type of gas vibration in the combustion chamber. The gradual buildup of the air vibrations in this case was very rapid as compared with the buildup of the gas vibrations in the bomb; in fact, this case seems to be the middle ground that is lacking in indicator records exposed directly to gas vibrations within the combustion chamber.

The work of Maxwell and Wheeler (references 15, 16, and 52) seems unique in the fact that they appear to have encountered both vibratory combustion and the detonation-wave type of vibration in the same explosion, and the one occurring just before the end of the flame travel and the other just after the flame front reached the far wall of the bomb. There seems to be no reason, however, why the two types of vibration should not occur, one after the other in the same combustion cycle. Moreover, two independent vibrations, each of the detonation-wave type, can be set up one after the other in the same combustion cycle, as has been shown in reference 9.

The excellent streak photographs by Payman and Titman (reference 53) are probably not pertinent to the present discussion because they involve only much faster-burning mixtures than are ordinarily used in spark-ignition engines. Inasmuch as pressure-time records are not included with the photographs by Payman and Titman, any discussion of the type of vibration set up by the phenomena shown in those pictures would be only speculation.

Detonation-wave and autoignition theories combined.—The foregoing discussion clearly indicates a need for some kind of combination of the detonation-wave and autoignition theories of knock, inasmuch as the occurrence of both autoignition and an apparent detonation wave has been demonstrated in the knocking engine. The combined theory proposed herein involves an affirmative decision on the controversial question as to whether afterburning takes place in a volume of gas for a considerable time after the flame front has passed through that volume of gas, or after the entire volume of gas has become inflamed through autoignition. For the purpose of this discussion "afterburning" will be understood to mean continued oxidation of combustible or any other reaction that causes continued spontaneous expansion of gases or pressure increase at constant volume.

If the concept is accepted of a body of end gas inflamed throughout its entire volume by autoignition, then it would seem reasonable that under severe conditions such an inflamed body of gas might be highly susceptible to the propagation of a detonation wave and that a detonation wave traveling through the inflamed body of gas might be the immediate result of autoignition. Such a high susceptibility to the detonation wave might be caused not only by the high temperature within the inflamed gases but by high concentrations of molecular fragments that might be of importance in the propagation of the detonation wave. If the possibility is accepted of a detonation wave traveling through a body of gas previously inflamed by autoignition, it seems almost necessary also to accept the possibility of such a wave traveling through a body of gas in which afterburning is taking place behind the normal flame front. In this manner a detonation wave could develop without autoignition after the entire contents of the combustion chamber had been ignited by the normal flame front. Larger volumes of inflamed gas at any one instant would be expected, however, with autoignition than without autoignition; therefore, a detonation wave should be expected to develop principally in the autoigniting end gas rather than in afterburning gas behind the flame front.

Concerning the possibility of burning after passage of the flame front through a body of gas, Withrow and Rassweiler in reference 36 concluded that the spectrum of the afterglow emitted by such supposedly afterburning gas is the same as that emitted during the CO-O₂ reaction and caused by active CO, O₂, CO₂, or O₃ molecules. They suggested that the H₂+CO₂↔CO+H₂O reaction is in equilibrium after the flame front has passed and that the afterglow is due to a readjustment of the equilibrium when the pressure and consequently the temperature are increased. They remarked: "The distribution of intensity of the afterglow throughout the combustion chamber accords well with the idea that the emission is by carbon dioxide heated by the increase in pressure brought about by combustion of the rest of the charge."

The suggestion that afterglow is entirely caused by readjustment of equilibrium due to compression does not seem

compatible with the results of Stevens' work at the National Bureau of Standards with a soap-bubble bomb in which no appreciable compression of the earlier-burned gas by the later-burned gas was possible. Some of Stevens' streak photographs show very considerable afterglow (references 54 to 56). On the other hand two of his photographs (references 57 and 58) show only the trace of the luminous flame front without afterglow.

Other sound explanations of the afterglow may exist independent of the concept of afterburning, but the possibility of other explanations only precludes use of the afterglow as support for the afterburning hypothesis; that is, the possibility of such explanations may not be regarded as evidence against afterburning.

Lewis and von Elbe in reference 59 have regarded Stevens' results (references 56 and 57) as evidence against the concept of afterburning, stating " * * * thousands of explosions * * * failed to reveal the slightest indication of further expansion of the burned sphere after the flame had traveled across the entire gas mixture." If close measurements are made on figure 2 of Stevens' 1923 report (reference 54) and figure 2 of his 1930 report (reference 56) it seems questionable whether a positive statement can be made that these figures show not even the slightest continued expansion of the luminous zone after the constant-velocity expansion of the spherical shell of flame had come to an end. (The end of the constant-velocity expansion of the flame shell seems to be the only means of determining from the photographs when the flame "had traveled across the entire gas mixture.") In one of the flame traces of figure 4 of reference 58 in which the afterglow is absent, continued expansion is plainly visible after completion of the constant-velocity expansion of the flame shell. The printed reproductions of photographs in reference 55 show the flame-front trace too indistinctly for judgment on continued expansion after completion of the constant-velocity expansion. Figure 2 of reference 54 shows luminosity fading progressively from the outer edge of the luminous sphere toward the center after some slight expansion has possibly taken place; the progressive fading is probably caused by rapid cooling of the outer shell of hot gases after the combustion is nearly complete. Figure 4 of a report by Randolph and Silsbee (reference 60), obtained with the same Bureau of Standards apparatus as used by Stevens, shows continued expansion most distinctly after completion of the constant-velocity expansion. A consideration that must always be given attention in Stevens' photographs, as well as in all photographs taken by flame radiations, is the fact that these photographs may not represent the true flame front because of low luminosity in the early stages of burning and because of the finite exposure time required to make a record on the photosensitive material.

The experimental work reported and the arguments advanced by Lewis and von Elbe in reference 59 were concerned mainly with the question of whether combustion in a constant-volume bomb is complete at the time peak pressure is reached and not with the question of whether peak pressure is reached at the instant the flame front has passed through

the last increment of gas. The afterburning required by the proposed combined detonation-wave and autoignition theory would cover a time interval of an entirely lower order than that considered in the question of whether combustion is complete at the instant of maximum pressure. The only consideration offered by Lewis and von Elbe, other than the photographs of Stevens, that would have a bearing on the question of afterburning on the smaller time scale is the suggestion that with afterburning the sharp breaks obtained with fast-burning mixtures between the rising pressure curve and the cooling curve would not occur. By the same token it might be suggested that the extremely flat pressure maxima of slower-burning mixtures, such as shown in figure 16 of reference 7, would not occur if there were no afterburning.

Probably the strongest experimental evidence against afterburning is the work presented in papers by General Motors investigators. Tests with a sampling valve (reference 61) showed that free oxygen disappeared from the charge immediately after passage of the flame front, but this evidence is open to the question of whether burning was not completed after the gases were removed from the combustion chamber by the sampling valve. The General Motors investigators also checked flame-front positions as shown by high-speed motion pictures against pressure rise obtained from indicator records. (See references 62 to 64.) The results indicated completion of burning at the flame front, with some exceptions in reference 64. This evidence is open to the previously mentioned objection that the photographs may not show the true flame front. The agreement between flame-front positions as shown by the photographs and as calculated from the pressure records on the assumption of complete combustion in the flame front may be a coincidence or the greater part of the combustion may actually be completed in a very small part of the deep combustion zone.

That the General Motors photographs may not actually have recorded the true flame fronts is indicated by some of the NACA schlieren photographs of reference 7. In this work it was shown that peak pressure was reached, at top center, very nearly at the same time that the schlieren flame pattern completely disappeared from the high-speed motion pictures, or about 10° of crank angle at 500 rpm after the flame front had completely filled the chamber. This finding that peak pressure at constant volume coincides with the final fadeout of the schlieren flame pattern is supported by the previous demonstration of the same fact in a bomb by Lindner (reference 65).

Other evidence in favor of the concept of afterburning has been furnished by various investigators. The ionization records obtained by Hastings (reference 42) showed ionization persisting over 20° to 30° of crank angle at 2000 rpm with normal combustion. With his records of ionization in the end zone during knock, the persistence had only a fraction of that magnitude. He attributed the difference to the much faster combustion in the end zone during knock. It is of interest, in Hastings' records of ionization with normal combustion, that the ionization did not decrease steadily after passage of the flame front but irregularly with even several sharp increases in ionization after the original passage of the flame front.

Souders and Brown (reference 44) with their streak photographs and simultaneous pressure records of combustion in a constant-volume bomb noted an appreciable increase in pressure after the flame front reached the end of the bomb. Marvin and Best (reference 66), observing flame stroboscopically through small windows mounted in a cylinder head, reported pressure rise after complete inflammation of the charge with very low compression ratios. Wawrziniok in reference 55 found maximum pressure developing in his bomb considerably after the flame front had ionized a gap at the end of the bomb. In this case the ionization gap was located at the most distant position in a hemispherical end of the bomb so that error due to curvature of flame front was minimized; yet the lag between ionization of this gap and peak pressure was about 20 percent of the total burning time. Marvin, Caldwell, and Steele (reference 67) observed that total radiation from burning gases increased after inflammation throughout a time interval equivalent to about 20° of crankshaft rotation at 600 rpm.

Bureau of Standards investigators (reference 68), taking streak photographs of combustion in a spherical bomb, suspended fine grains of gunpowder at various points on a diameter of the bomb by means of human hairs. With central ignition, the brilliantly burning grains of gunpowder continued to move toward the center of the bomb for some time after the flame reached the wall of the bomb. This experiment seems to be particularly strong evidence of afterburning in the outer parts of the bomb.

Lewis and von Elbe have done work determining the temperature zones in burner flames in reference 69. Much uncertainty would be involved, however, in applying the results to the much different conditions existing in engine combustion.

In a discussion of combustion in a turbulent stream (reference 70) Shelkin has drawn a model of flame structure that might well apply under the highly turbulent conditions existing during combustion in the engine cylinder. According to this model, the turbulence in the flame front causes the flame to advance in microscopic, or near-microscopic, tongues. The structure behind the flame front is cellular; the cell walls constitute burning gas and the interiors of the cells constitute unignited gas. According to this model, the unignited gas within each cell is gradually consumed as the flame front progresses beyond the cell. With this structure, in the microscopic sense the burning zones might all be very thin; in the microscopic sense a deep afterburning zone would exist beyond the flame front. In any event, the preponderance of experimental evidence available at this time appears to favor the existence of a rather deep zone of combustion behind the flame front in the engine cylinder, though the main part of the combustion may take place only within a small part of this zone. Whether the combustion zone is cellular on the microscopic scale or only on a submicroscopic molecular scale does not seem important in the presentation of the combined theory of knock. In either case there is a possibility that the gases in the combustion zone may be peculiarly susceptible to the propagation of a detonation wave, and the available evidence on this point should be carefully considered.

The concept of autoignition followed by the development of a detonation wave was given passing attention in the previously quoted remarks of Woodbury, Lewis, and Canby in reference 26. Among the streak photographs of autoignition resulting from quick compression of the charge in a glass tube presented by Dixon and his coworkers (references 31 and 32) were included some records of what they believed to be detonation waves. Dixon and his coworkers pointed out the fact that the development of the detonation wave was always preceded by autoignition at some point within the charge. The concept of the development of a detonation wave in autoigniting end gas has also been suggested by Boerlage and van Dyck in reference 71. They pointed out that "simultaneous combustion" at the beginning should be considered as a slow pressure rise in comparison with "true detonation" but that it ultimately may have the same character. The reverse concept, autoignition triggered by a shock wave, has been suggested by Dreyhaupt in reference 72.

The concept of autoignition followed by the development of a detonation wave is consistent with the high-speed motion pictures presented in various NACA reports (references 5 to 9) if the explosive knock reaction is considered to be a detonation wave. In these photographs, in most cases where end gas was visible at the time of the explosive knock reaction, this reaction has been preceded by some form of apparent autoignition. In one case the apparent autoignition developed at definite centers within the end gas and spread out in all directions from those centers to fill the end zone before the explosive knock reaction occurred. (See fig. 10 of reference 9 on preknock vibrations.) In another case the autoignition began at the chamber wall and propagated throughout the end zone before the explosive knock reaction occurred. (See fig. 12 of reference 9.) In this case the visible explosive knock reaction was light. In other cases the autoignition developed uniformly and simultaneously throughout the end zone before the explosive knock reaction occurred. (See fig. 5 of the preliminary report, reference 5.) In yet other cases autoignition was not clearly visible in the photographs but a visible vibration of the gases of the detonation-wave type was set up before the explosive knock reaction occurred (reference 9). The occurrence of a visible vibration before the explosive knock reaction is an effect apparently not frequently encountered. It appears likely that this phenomenon is comparable with the explosive knock reaction in speed and it may, therefore, be a mild detonation wave followed later by the development of a many-times more-powerful detonation wave.

The evidence of the NACA high-speed schlieren photographs of references 5 to 9 is open to the criticism that the end-zone reactions shown before knock may not represent true flame because the schlieren system may reveal reactions much less intense than flame combustion. The same phenomenon has been shown, however, in photographs exposed by direct flame radiation presented by Rothrock and Spencer (reference 46). With 18- and 30-octane fuels at a compression ratio of 7, photographs taken at about 2000 frames per second (fig. 7 of the report by Rothrock and Spencer) showed autoignition in the end gas one frame before the development of the brilliant illumination caused by

knock. In the same paper Rothrock and Spencer showed that this brilliant illumination coincided chronologically with the beginning of the gas vibrations.

The concept of a detonation wave set up in afterburning gases behind the normal flame front has been proposed previously by Maxwell and Wheeler in references 15, 16, and 52. In streak photographs of combustion in a bomb with knocking fuels they found only very faint afterglows behind the flame front during the travel of the flame through the bomb. After the flame had traveled completely through the charge they observed an extremely high-speed travel of a more brilliant glow through the chamber. With non-knocking fuels, however, the afterglow behind the normal flame front was brilliant. They reported invariably a correlation between the pinking tendencies of fuels and the lack of brilliancy in the afterburning, and they reported that the addition of ethyl ether or amyl nitrate to a fuel decreased the brilliancy of the afterglow, and that decomposed tetraethyl lead increased the brilliancy of the afterglow. These investigators concluded in part that the tendency to knock was dependent on slow afterburning, leaving sufficient energy behind the flame front to maintain a shock wave (detonation wave) set up by collision of the flame front with the chamber wall. Lorentzen in reference 49 found evidence from experiments with a combustion bomb that he believed supported the theory proposed by Maxwell and Wheeler. The finding that knocking fuels show less brilliant afterglows than nonknocking fuels has been verified by Duchene (reference 39) and by Rothrock and Spencer (reference 46). Rothrock and Spencer have also presented in figure 12 of the same paper 2000-frame-per-second motion pictures of combustion of 65-octane gasoline in which the combustion chamber was entirely inflamed before the occurrence of knock, as indicated by very brilliant reillumination of the entire chamber. In figure 4 of one of the NACA reports (reference 6) a knocking reaction is seen to have occurred not only after complete inflammation of the cylinder charge but even so late that the schlieren combustion pattern was almost gone.

The combined detonation-wave and autoignition theory, to be complete, must account for the fact that combustion cycles involving nothing more than simple autoignition have been found by General Motors investigators in references 33, 36, and 37 and have been regarded by those investigators as knocking cycles. It is clear that gas vibrations can cause forced vibrations of the combustion-chamber walls of the same frequency as the gas vibrations and thus cause a high-pitched ping. As gas vibrations apparently did not occur in the combustion cycles reported in those papers, however, the question naturally arises as to the cause of the knock that was heard. The only possible answer appears to be that the knocking sound was due to natural vibrations of engine parts.

The autoignition that occurred in the General Motors investigations has been seen to require a period of approximately one-thousandth part of a second for its completion. The sharp increase of pressure in the combustion chamber within the period of one-thousandth part of a second could set up natural vibrations in some of the stressed engine

parts. The energy imparted to the natural vibrations by the autoignition would, in general, be greater in the case of low-frequency vibration than in the case of high-frequency vibration. The influence of vibration frequency on the energy imparted to the vibration by the autoignition could be determined mathematically only if definite information were available as to the rate at which energy is released by autoignition at each instant throughout the autoignition process. Though no such information is available, the experimental evidence at least indicates that energy is released by the autoignition in such a manner that it does not excite appreciable vibration of the gases. It may, therefore, be reasonably assumed that the autoignition would excite natural vibrations of the stressed engine parts only in such modes as have a natural frequency considerably less than the natural frequency of the vibrating gases.

The suggestion that knock is due to vibration of engine parts caused by autoignition and that pink is caused by gas vibrations had previously been made by Boerlage and his coworkers (references 19, 45, and 71).

Summary of literature-based argument for combined knock theory.—The following facts appear to be supported by the weight of experimental evidence:

1. Autoignition of comparatively large bodies of end gas occurs too slowly under certain conditions to produce audible gas vibrations.

2. Under suitable conditions one or both of two types of gas vibration may occur, the detonation-wave type and the vibratory-combustion type.

3. Either type of gas vibration may occur independently of autoignition, but under some conditions the detonation-wave type of gas vibration tends to occur very soon after slow autoignition has taken place.

4. Under suitable conditions apparent detonation waves can develop in the engine cylinder.

5. Under a wide range of conditions, either combustion continues for a distance sometimes as great as several inches behind the flame front or some adjustment of equilibrium takes place through the same distance, resulting in increased pressure, continued ionization, and continued emission of light.

The foregoing facts, supported by the experimental evidence, suggest the following explanation of knock in the spark-ignition engine:

(a) Knock of a comparatively low pitch is caused by simple autoignition of end gas at a rate too slow to produce audible gas vibrations.

(b) Knock involving both low- and high-pitched tones may be caused by autoignition followed by the development of a detonation wave in the autoignited gases.

(c) Knock of high pitch may be caused by a detonation wave in afterburning gases behind the flame front. This detonation wave, having originated in the afterburning gases behind the flame front, may also pass through unignited end gas.

This explanation of knock harmonizes with the findings of the NACA photographic knock investigations that will be summarized in the second part of this section.

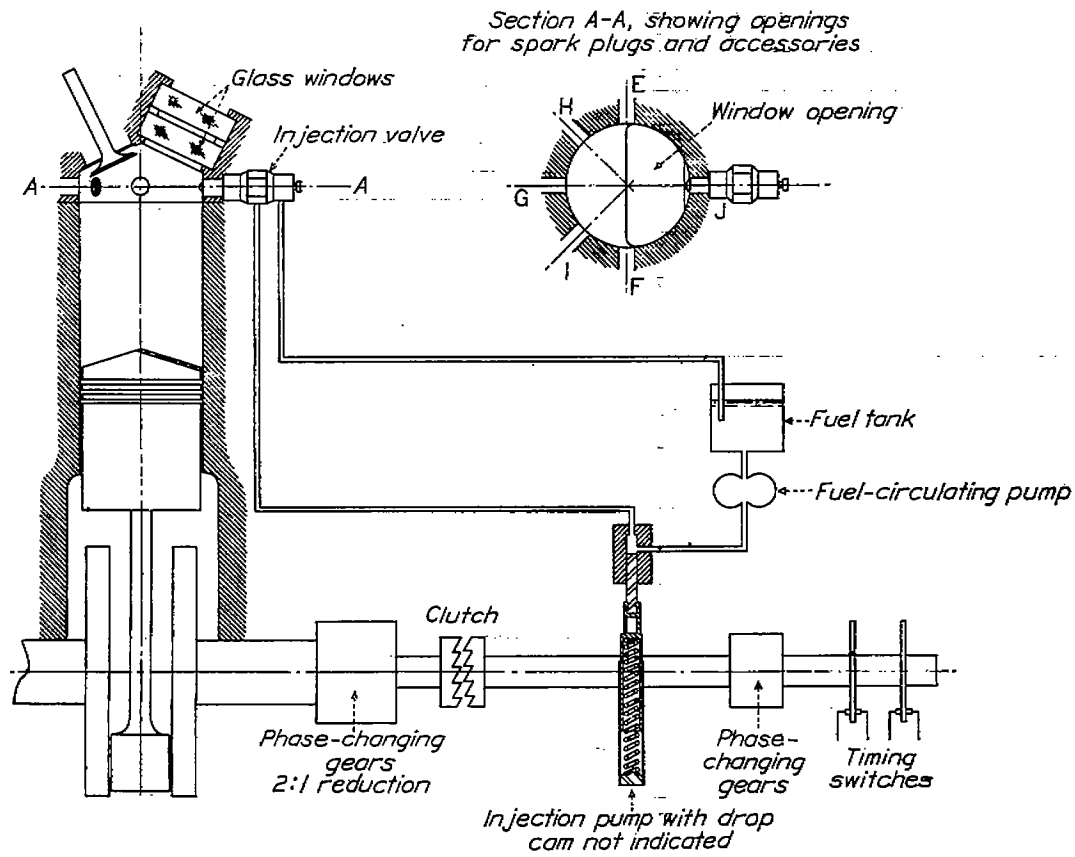


FIGURE I-1.—Old combustion apparatus.

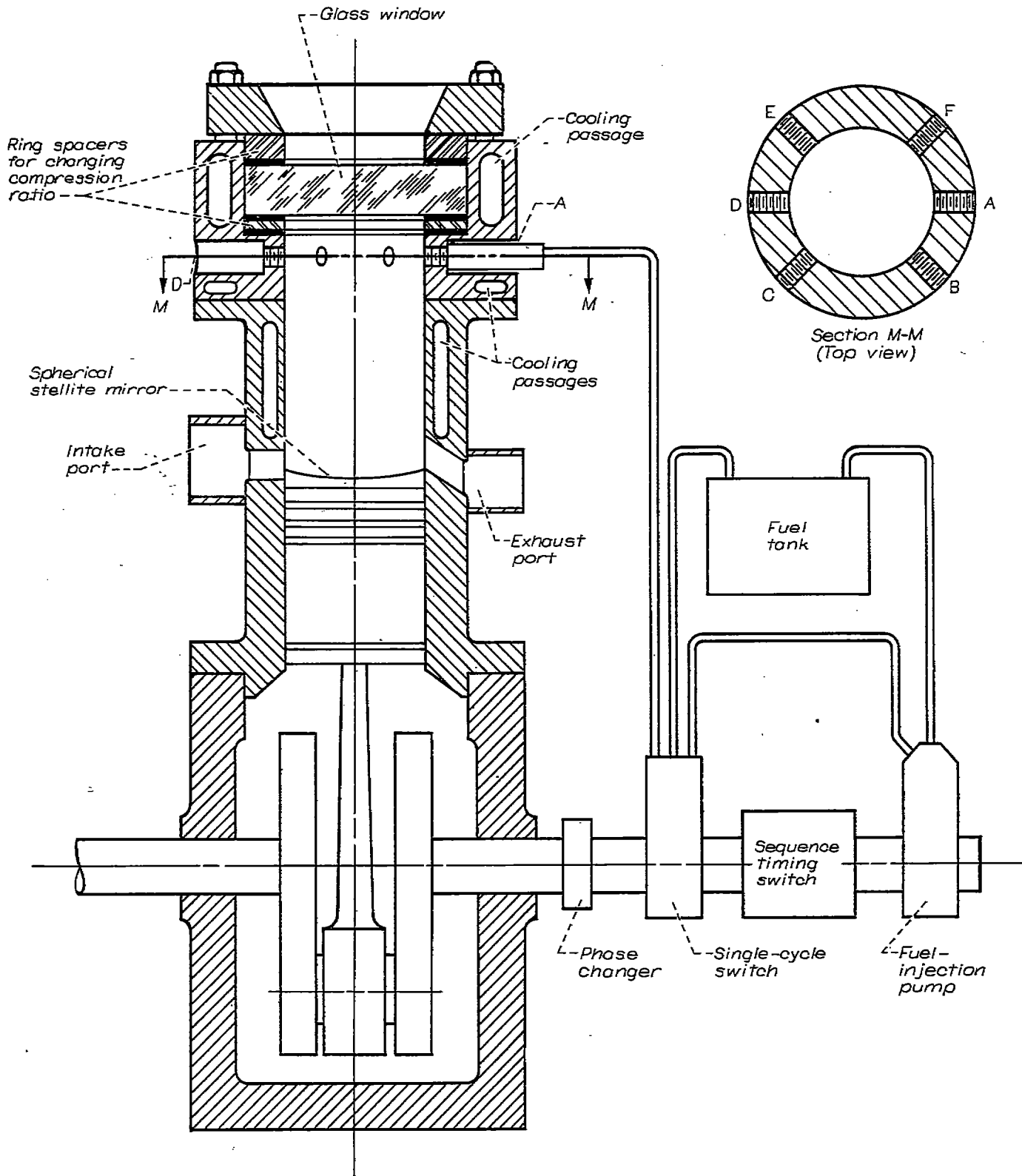


FIGURE I-2.—Full-view combustion apparatus.

REPORT OF FINDINGS OF NACA PHOTOGRAPHIC KNOCK INVESTIGATIONS

Apparatus and operating conditions.—The high-speed motion pictures presented and discussed herein have in part been selected from previously published data (references 5 to 11) obtained with the high-speed and ultra-high-speed motion-picture camera (references 1 to 3) and the NACA combustion apparatus. Most of the work was done with the old combustion apparatus described in references

5 and 46. A small part of the work was done with a newer combustion apparatus. A diagrammatic sketch of the old combustion apparatus is shown in figure I-1; the newer apparatus in figure I-2. The old combustion apparatus is a single-cylinder engine of 5-inch bore and 7-inch stroke, with glass windows in the cylinder head and a glass mirror on the piston top, as shown in the figure. The visible part of the combustion chamber is $4\frac{1}{2}$ inches long, as shown at

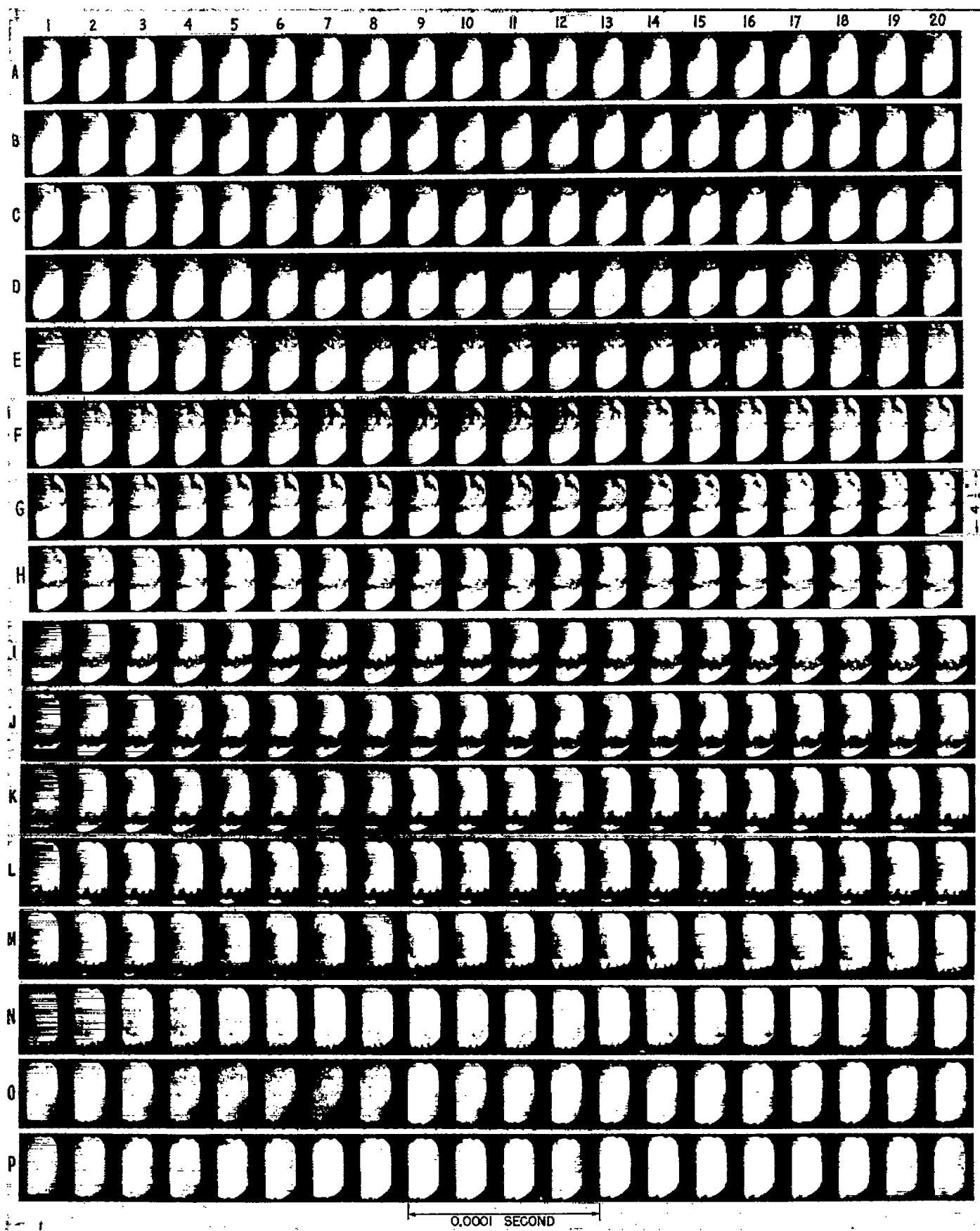


FIGURE I-8.—High-speed photographs of normal nonknocking combustion in spark-ignition engine. Fuel, S-1; compression ratio, 7.0; fuel-air ratio, about 0.08; atmospheric intake; one spark plug; spark timing, 20° B. T. C.

frame G-20 in figure I-3. The newer combustion apparatus (fig. I-2) was designed to provide a view of the entire combustion chamber. This engine has a bore of $4\frac{1}{2}$ inches and a 7-inch stroke. Air for combustion is forced into the cylinder through ports uncovered by the piston at the bottom of its stroke and escapes through other ports on the opposite side of the cylinder. The pressure before the start of compression in this engine is controlled by means of the back pressure applied outside the escape ports.

The optical arrangements for schlieren photography (references 5 and 11) will not be redescribed herein, except to state that with each of the combustion apparatus the schlieren photographs were taken by externally supplied light projected into the combustion chamber through the glass windows and then reflected back out through the glass windows to the high-speed camera by the mirror on the piston top.

In all the investigations in which the combustion apparatus has been used, the engine has been driven by an electric motor and operated under its own power for only one combustion cycle in each run; in each case the entire series of photographs was taken during the single combustion cycle. Solid injection of fuel was used and fuel was injected only for the single power cycle. With the old combustion apparatus the fuel was injected on the inlet stroke; with the newer full-view apparatus it was injected early in the compression stroke. The engines were heated prior to the motoring period and kept hot during the motoring period by the circulation of heated glycerin through the cooling passages of cylinder and head. All of the investigations have been made with glycerin temperature approximately at 250° F leaving the cylinder and head. The investigations have all been made with an engine speed of approximately 500 rpm. Spark timings and spark-plug positions were selected to produce knock at top center with the end gas usually well within the field of view. Other engine operating conditions and the fuels used will be stated in the discussions of the individual tests. Atmospheric intake was always used with the old combustion apparatus.

Normal nonknocking combustion.—Figure I-3 of this paper is a reproduction of figure 3 of the preliminary report (reference 5). This figure shows the normal process of smooth nonknocking combustion. Only one spark plug was used, in E position. (See fig. I-1.) The injection valve was in J position. (See fig. I-1.) The fuel was S-1 reference fuel; spark timing, 20° B. T. C.; compression ratio, 7.0; and fuel-air ratio, approximately 0.08.

Throughout this paper the individual frames of figure I-3 and other figures will be referred to as frame A-1, meaning the first frame of row A, frame D-8, meaning the eighth frame of row D, and so on. The order in which the pictures were taken is from left to right through the first row, frame A-1 through frame A-20, then from left to right through the second row, frame B-1 through B-20, and so on.

In the first few frames of row A of figure I-3 the flame from the igniting spark is just coming into view. A large black spot appears at the upper left-hand corner of each of these frames. This large dark spot is due to an imperfection in the schlieren system and has nothing to do with the combustion. The flame coming into view in these frames is barely visible as a small dark spot at the central upper edge

of each frame. The increase in size of the flame between one frame and the next is extremely small because the time interval involved is only $1/40,000$ second, that is 25 microseconds. The flame very gradually grows larger throughout the first five rows of frames, A to E. In frame E-10 the flame has grown until it covers almost the upper half of the frame as a dark mottled cloud. Although these photographs are actually positive prints, the flame is seen as a dark mottled cloud because of its effect on the externally supplied light. The photographs were taken too fast, and the lens aperture was too small, for the flame to be photographed by the light radiated by it. The burning region appears to scatter the externally supplied light so that it does not get through to the camera lens. The burning region consequently shows up as a dark cloud in contrast with the areas where no combustion is proceeding. The externally supplied light passes through the nonburning areas uninterrupted to the camera lens and causes a fairly uniform white appearance of these areas in the positive prints. For reasons that will be explained it is believed that all of the dark mottling visible in the upper half of frame E-10 is indicative of continuing combustion. In this frame, therefore, the apparent depth of the flame in the direction of flame travel is approximately 2 inches. It is not known to just what extent this apparent depth is real and to what extent it is caused by tonguing of the flame. To explain the apparent depth entirely on the basis of flame tonguing, however, would require a quite illogical assumption that the flame is always much more extensively tongued in the planes that cannot be seen in the photographs than in the plane that is seen in the photographs. (The distance through the combustion chamber in the line of sight from the surface of the mirror on the piston top to the under surface of the inner glass window is approximately 1 in.) The appearance of frame E-10 of figure I-3 is quite typical of this stage of combustion in all photographs taken under the same conditions. The leading edge of the flame as seen in frame E-10 is somewhat irregular but does not show any such pronounced tonguing as would be required to explain the presence of mottling throughout the entire area behind (above) the flame front.

In the frames of rows F, G, and H the flame front slowly advances downward to a position (in frame H-20) about two-thirds of the way across the chamber from the point of ignition. At the same time the dark mottling disappears throughout most of the area behind (above) the flame front, so that in frame H-20 the apparent combustion zone extends only a short distance backward from the flame front. This narrowing of the combustion zone as the flame front travels through the central part of the chamber is also typical of the photographs taken under these conditions. In the frames of rows I to M the flame front slowly completes its travel to the extreme end (lower end) of the combustion chamber. After the flame front reaches the extreme end of the chamber in frame M-20, the mottled combustion zone gradually dissolves in the frames of rows N, O, and P, leaving a clear white field throughout the entire area of the chamber in frame P-20.

It may be noted that the dark spot which was visible in the upper left-hand corners of the early frames of row A is not visible in the frames of row P. This spot, caused by

imperfection of the optical system, moved about because of rocking of the piston at top center and had moved completely out of the field of view in the frames of row P.

From the standpoint of a study of knock, the most important feature of the normal combustion photographs of figure I-3 other than the apparent depth of the combustion zone is the fact that all stages of the combustion process appear slow and smooth. When the photographs are projected on a motion-picture screen the entire process is slowed down so that it resembles the motion of a storm cloud. After the combustion is completed and the mottled zone has faded out the gases in the combustion chamber are very quiescent, a condition contrasting decidedly with the appearance after a knocking combustion.

Nonknocking combustion with preignition from hot spot.—Figure I-4, a reproduction of figure 7 of reference 5, shows a combustion process with the same fuel and the same engine operating conditions as those of figure I-3 but with ignition from a hot spot as well as from the spark plug. The spark plug was again in E position (see fig. I-1), but an electrically heated coil was inserted by means of a special plug at F position (see fig I-1) and the current through this coil was adjusted to such a value that the coil would ignite the fuel-air mixture at an earlier time than the igniting spark at the plug in E position.

When the camera shutter opened for the shot of figure I-4, in the first few frames of row A, the flame from the hot spot had already come well into the field of view. The flame from the spark plug comes into view in the later frames of row E and the earlier frames of row F, visible at the top of each frame as a whitish spot. In this case the flame shows up white by contrast with the dark spot caused by the imperfection of the schlieren system. When the flame gets well out into the white part of the field of view in row J it again shows up as a dark mottled region as in figure I-3. The flame from the spark plug and the flame from the hot spot merge in the frames of rows J and K and the mottled combustion zone very gradually dissolves in the frames of rows L to P. In this case in the frames of row P the dark spot at the upper left-hand corners of the frames, caused by imperfection of the schlieren system, is still visible. Again it has no significance relative to the combustion process.

From examination of the photographs of figure I-4 as stills, as well as from observation of these photographs as a motion picture projected on the screen, it must be concluded that the entire combustion process is just as smooth and gradual as with the normal nonknocking combustion process of figure I-3. After the mottled combustion zone has faded out the gases again appear very quiescent, in contrast with the appearance after a knocking combustion. The photographs of hot-spot ignition clearly show that this type of ignition is not a direct cause of knock.

Preliminary view of knock.—Figure I-5 of this paper is the same as figure 5 of reference 5 and the same as figure 2 of reference 10. The combustion process shown in this

figure involves one of the most violent knocks ever photographed. The engine operating conditions were the same as those for the normal nonknocking combustion process shown in figure I-3. Instead of S-1 fuel, however, a blend consisting of 50 percent S-1 and 50 percent M-2 reference fuels was used.

The flame from the igniting spark comes into view in figure I-5 in the later frames of row C, visible at the top of each frame as a dark mottled cloud. The flame progresses downward through the field of view in the frames of rows D to K in the same smooth gradual manner as in figure I-3. In the frames of rows J and K the flame front becomes much more irregular than in the case of figure I-3, but this irregularity is considered to be no greater than is occasionally observed with nonknocking combustion and is not thought to be significant relative to the knock phenomenon. In the frames of row L and the earlier frames of row M the end gas, the area ahead of (below) the flame front, gradually turns dark. By the time of exposure of frame M-10 the end gas has become so dark that it can no longer be distinguished from the combustion zone behind (above) the spark-ignited flame front. This darkening of the end gas, which occurs gradually throughout the frames of row L and the earlier frames of row M, is believed to be indicative of at least the early stages of an autoignition process. In frame M-10, where no line of demarcation can be discerned between the end gas and the burning gases ignited by the normal flame travel, the photographs at least indicate that the end gas is burning just as truly as the gases behind the flame front. The explosive knock reaction that sets up the knocking gas vibrations, however, has not yet begun to develop in frame M-10. The first evidence of this explosive reaction appears in frame M-11 as a white streak along the lower right edge of the frame and as a slight blurring of the dark combustion zone. In the next frame, M-12, the explosive knock reaction has progressed through the entire field of view and has given a fairly uniform white appearance to the entire field. (The whitened area below the lower right edge of frame M-12 is due to a pocket of gas $\frac{1}{16}$ inch thick between the glass window and the metal surface of the cylinder head. This pocket, caused by the window gasket, is completely explained in reference 5.)

At the time of writing of reference 5 the reaction occurring during the exposure of frames M-11 and M-12 was confidently believed to be the explosive knock reaction because the projected motion pictures clearly showed that the gas vibrations began at the same time as the whitening of the field of view in frames M-11 and M-12. Moreover, a violent explosion could be observed in the motion pictures in the general vicinity of the end gas at the same time that this whitening occurred. A more rigid proof that blurring of the combustion zone such as occurs in frame M-11 of figure I-3 coincides chronologically with the onset of violent gas vibrations will be discussed later in this paper. A discussion of the nature of the reaction occurring in frames M-11 and M-12 will also appear later in the paper.

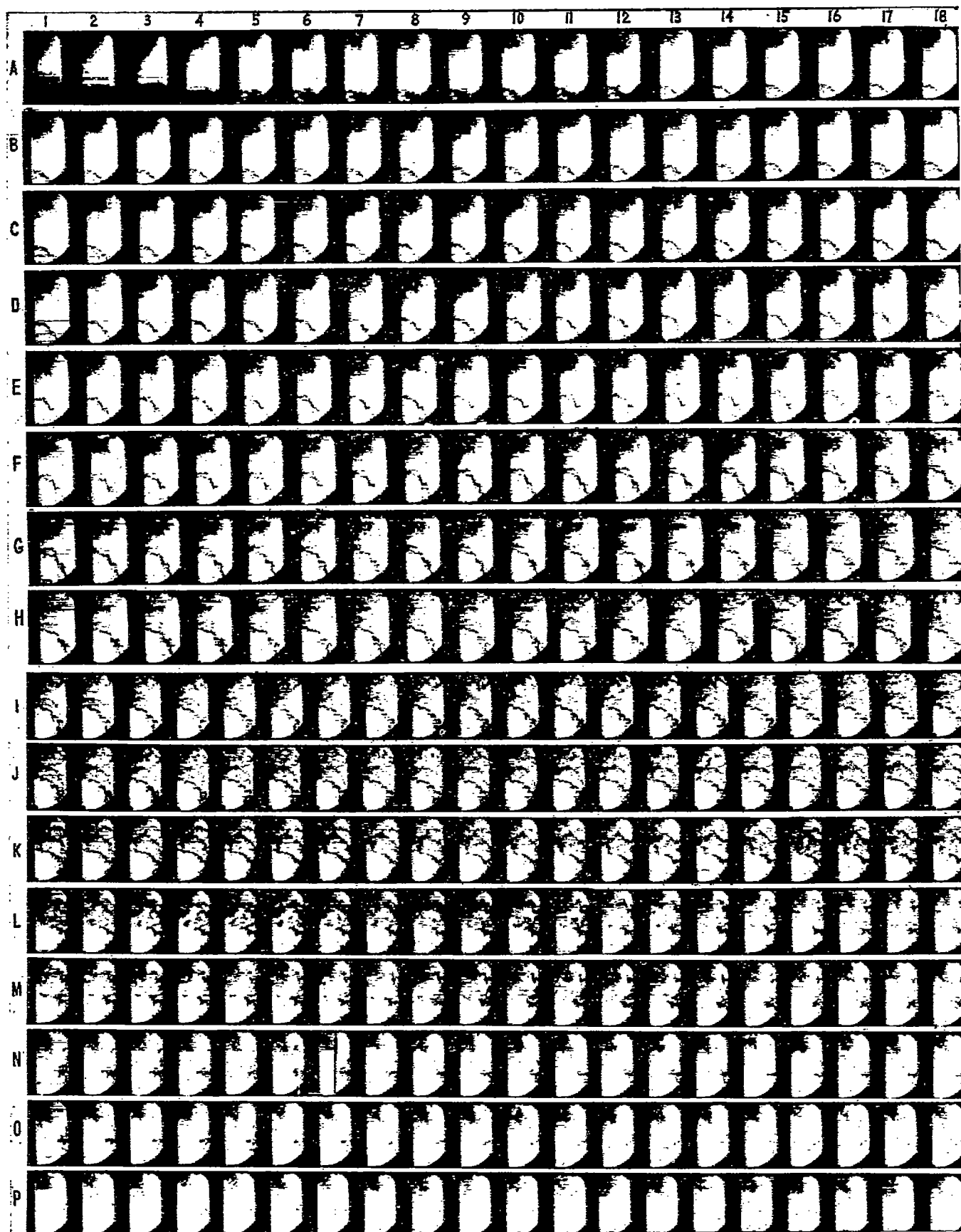


FIGURE I-4.—High-speed photographs of nonknocking combustion in spark-ignition engine with preignition from hot spot. Fuel, S-1; compression ratio, 7.0; fuel-air ratio, about 0.08; atmospheric intake; spark plug at top; hot spot at bottom; spark timing, 20° B. T. C.

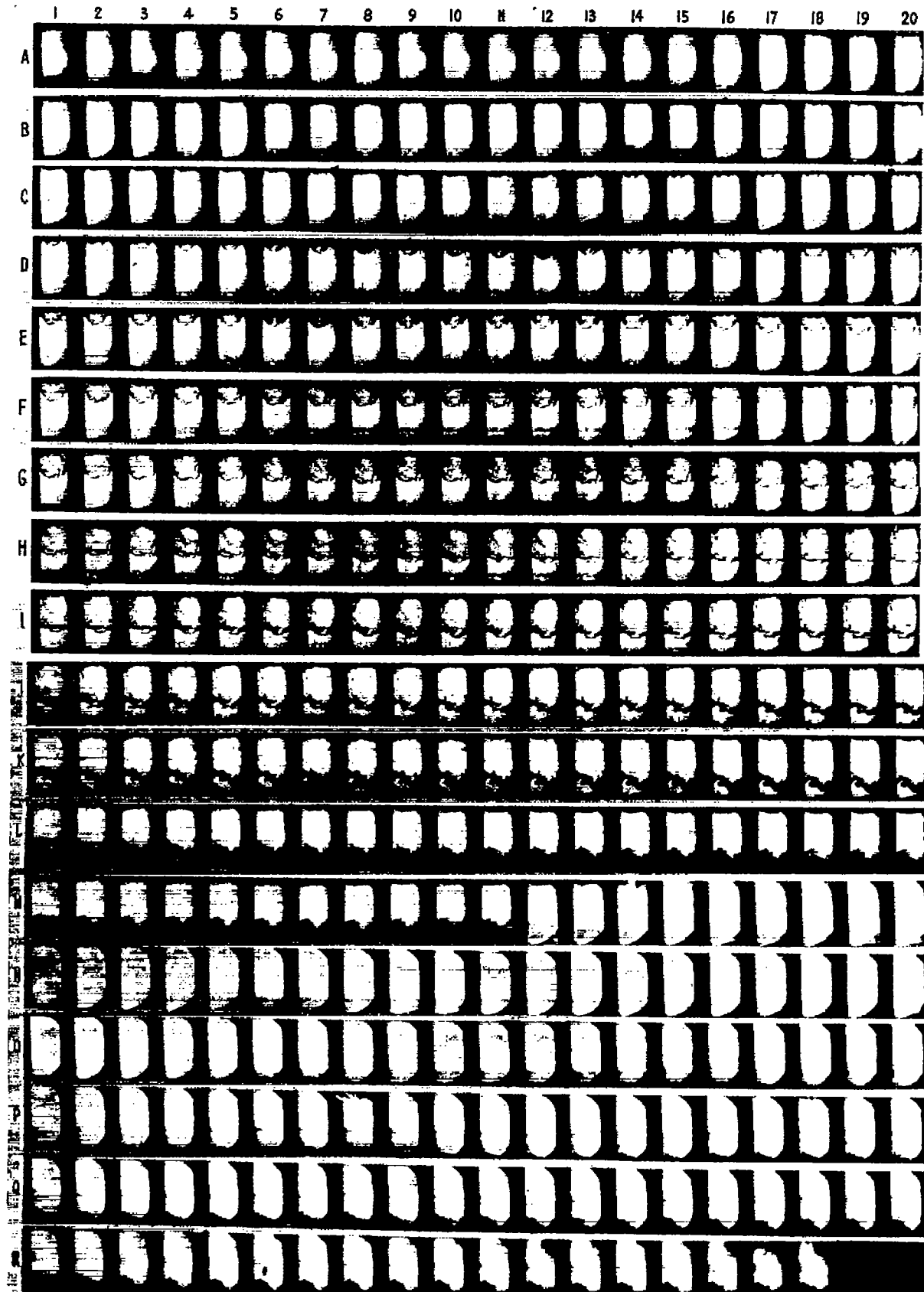


FIGURE 1-5.—High-speed photographs of combustion with violent knock in spark-ignition engine. Fuel, 50 percent S-1 with 50 percent M-2; compression ratio, 7.0; fuel-air ratio, about 0.08 atmospheric intake; one spark plug; spark timing, 20° B. T. C.

As previously mentioned, many readers of reference 5 have been entirely unconvinced that the darkening of the end gas prior to the development of the explosive knock reaction in frames M-11 and M-12 actually is autoignition. This author has held the view that this darkening must be regarded as autoignition because there has seemed to be no satisfactory definition of the distinction between preflame and flame reactions in a gradual process occupying a total time interval of less than 1/1000 second (frames L-1 to M-10). In all human experience with flame the preflame reactions have been separated from the flame reactions by a sudden great increase in the rate of reaction, intensity of light radiation, rate of heat release, and so on. The time interval involved in the actual transition from preflame to flame reactions has never been specified and has, in effect, been regarded as instantaneous because of the absence of any method of measuring the interval. The reaction occurring in frames M-11 and M-12 could be regarded as marking the transition from preflame to flame reactions, but so to regard this reaction would be entirely arbitrary and would be only the result of an illogical extrapolation—an extrapolation in the sense that we think because a sharp dividing line appears to exist between preflame and flame reactions when we "see slowly" a sharp dividing line must also be found to exist when we "see fast."

Qualitatively it could be said that any reaction is proceeding at a very high rate when it produces as much optical change in 1/10,000 second as can be seen between the end gas as it appears in frame M-7 and the end gas as it appears in frame M-10. An investigation is being conducted by G. E. Osterstrom of the NACA technical staff to determine whether the light radiations from the end gas before the explosive knock reaction are sufficient to be measurable. This investigation involves taking simultaneous schlieren photographs and direct flame photographs with a definitely established chronological relationship of the individual frames of one series of photographs to the individual frames of the other series. The preliminary indications are that the radiation from the end gas prior to the explosive knock reaction is sometimes sufficient to photograph at 40,000 frames per second with the high-speed camera. Even if the rate of reaction, intensity of light radiation, and rate of heat release in the end gas could be accurately determined, however, for all of the time intervals covered by frames L-1 to M-10, it would still not be possible to classify the reactions as preflame or flame reactions unless quite arbitrary values were set for these quantities above which the reactions would be regarded as flame reactions.

A possible logical dividing line between preflame and flame reactions on the basis of the thermal theory of autoignition is the condition of more rapid release of heat by the autoigniting gases than normal dissipation of heat from those gases, at constant volume. Another dividing line, based on the chain-reaction theory, is the condition of more rapid formation of chain carriers by chain-branching reactions than destruction of carriers by chain-breaking reactions. Measurements indicate that the normal flame

front did not make any additional progress into the end gas between frames M-1 and M-10 of figure I-5. Furthermore, many photographs have been obtained in which the normal flame front as seen in the projected photographs was actually pushed backward by the end gas a number of frames prior to the development of the explosive knock reaction. Because of this fact, the dividing line on the basis of thermal theory must have been passed at about frame M-1 in figure I-5, so that the end-gas reaction between frames M-1 and M-10 would have to be regarded as flame reaction, unless it is assumed that the end gas is being heated by radiation and conduction from the burning gases more rapidly than the average of the other gases in the chamber including the burning gases themselves. There is no indication, of course, as to where the dividing line based on chain-reaction theory would be drawn relative to the frames of figure I-5.

In view of the necessarily arbitrary nature of any distinction between preflame and flame reactions in frames L-1 to M-10 of figure I-5, the fact that the end gas does sometimes emit sufficient light to photograph by direct flame photography at 40,000 frames per second prior to the explosive knock reaction, and the fact that preknock radiations from the end gas have been photographed at a lower speed by other investigators (reference 46), the reaction visible in the end gas throughout frames L-1 to M-10 of figure I-5 and similar reactions visible in other figures will be referred to throughout this paper as simply "autoignition." The reaction of frames M-11 and M-12 will be shown later to be a detonation wave and may be regarded as autoignition only in the sense that it develops during a process of autoignition and that its development may be influenced by the autoignition process.

The frames following M-12 in figure I-5 show the development of an extremely brilliant, intermittent luminosity reaching peaks in frames M-16, N-1, N-6, O-1, and so on, and the development of an intense smoke cloud in the lower parts of the frames of rows P, Q, and R. The brilliant luminosity and smoke formation will be discussed further under "Chemical Nature of Explosive Knock Reaction." The extremely violent vibration, or bouncing, of the gases that is seen when frames M-12 to R-18 are projected on the screen as a motion picture cannot be seen in visual examination of the photographs in the printed figures. This effect is suggestive of a pot of stiff jelly that has been severely jolted and is characteristic of all of the photographs of knocking combustion obtained with the high-speed camera.

Chronological relation between schlieren photographs and records of cylinder pressure.—In the photographs of figure I-5 the occurrence of knock is very definitely visible in frames M-11 and M-12. In cases of much lighter knocks, however, the occurrence of the knock may be detected in the photographs only as a slight blurring of the dark mottled combustion zone. This blurring is often not visible in the printed reproductions of the photographs, because of inevitable loss of detail, but can be seen on careful inspection of

the original negatives. Inasmuch as the slight blurring of the combustion zone could not be assumed without proof to be identical with the occurrence of knock, one of the early investigations (reference 7) was directed toward the establishment of a definite chronological relationship between this blur and the beginning of the violent gas vibrations associated with knock. Incidental to this relation, some investigation was also made into the chronological relation between the final fadeout of the schlieren combustion pattern and the attainment of peak pressure with nonknocking combustion.

One of the high-speed photographic shots used in the establishment of the chronological relationship is reproduced as figure I-6 of this paper (fig. 11 of reference 7). Three spark plugs were used, in E, F, and G positions (see fig. I-1), a quartz piezoelectric pickup was used in opening J, and the injection valve was in opening H. The spark timing at the plugs in E and F positions was 22° B. T. C. The timing at the plug in G position was earlier (29° B. T. C.) because it was desired to focus the end zone at the diaphragm of the piezoelectric pickup in opening J, and to do so required a

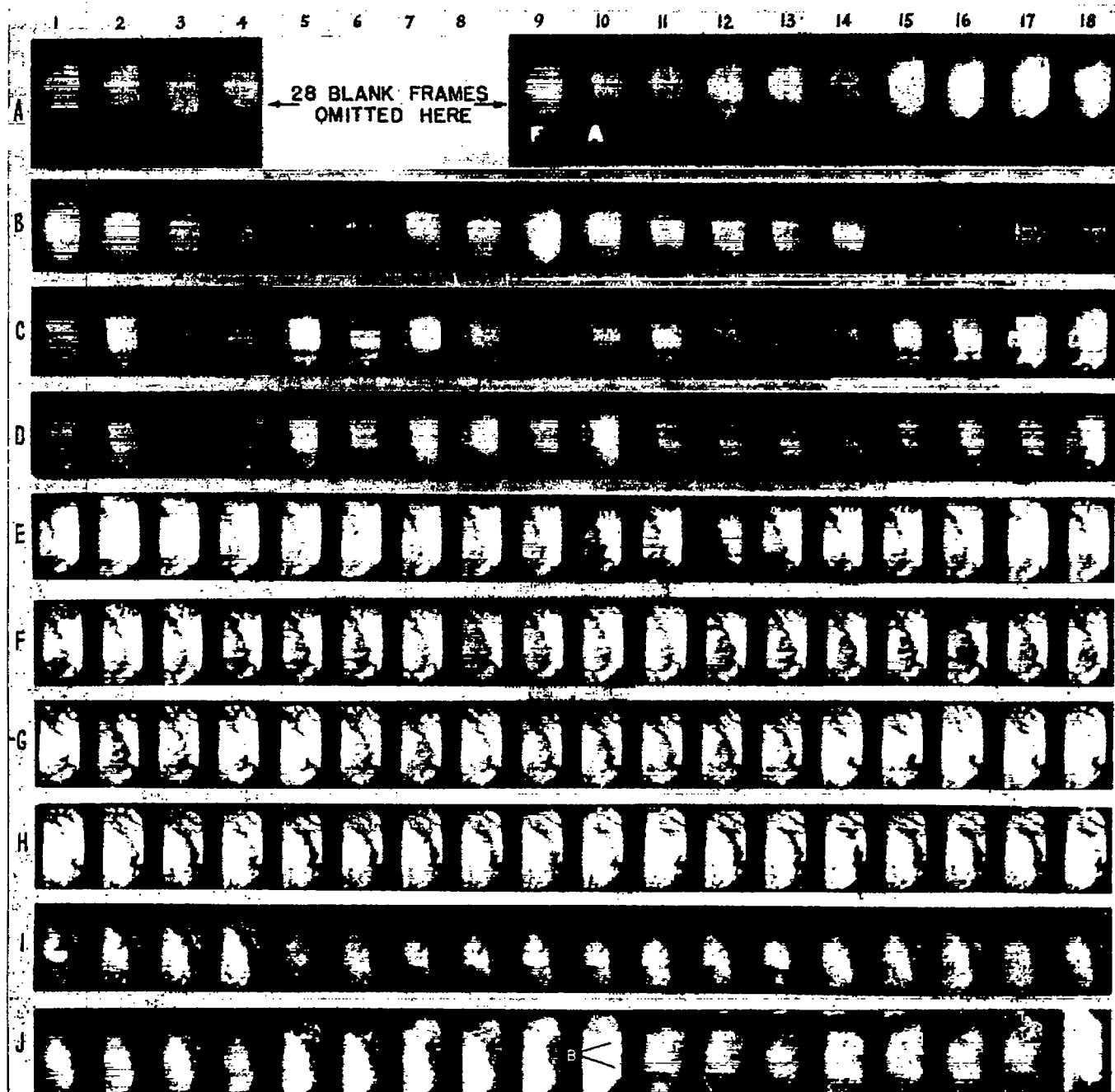


FIGURE I-6.—High-speed photographs of knocking combustion in spark-ignition engine with timing sparks in row A. Fuel, 80 percent S-I with 20 percent M-2; compression ratio, 7.4; fuel-air ratio, about 0.08; atmospheric intake; three spark plugs; spark timing, for left-hand plug, 29° B. T. C., for other two plugs, 22° B. T. C.; B, blurring caused by knock.

much longer travel for the flame from G position than for the flames from E and F positions. The fuel was a blend of 80 percent S-1 and 20 percent M-2 reference fuels; compression ratio 7.4; and fuel-air ratio, approximately 0.08.

The flames from the three igniting sparks come into view in the frames of rows A to E of figure I-6. By the frames of row F the flames have completely merged and have surrounded a small body of end gas in the immediate vicinity of the piezoelectric pickup diaphragm. In the first nine frames of row J autoignition takes place in the end gas, and in frame J-10 knock occurs, as indicated by the blurring and lightening of the combustion zone in the region designated B.

In row A the film perforations are included in the figure. (The perforations were trimmed from the reproductions used for the other rows.) In the taking of the pictures the film was placed around the inside of a drum in a continuous circle consisting of 372 frames. Of the 372 frames, 168 are omitted from the figure after frame J-18 (or before frame A-1) and 28 are omitted as indicated in row A. A specially designed spark plug in the camera produced a timing mark in the perforation strip at frame A-10 at about the time of the beginning of combustion. The same spark plug produced another timing mark at frame A-2, 339½ frames later, after the combustion and knock were completed. These two timing sparks have been used in the determination of the chronological relationship between the photographs of figure I-6 and the corresponding pressure record of figure I-7.

In figure I-7 the trace designated A is an actual photograph of a trace produced on the screen of a cathode-ray oscilloscope during the exposure of the photographs of figure I-6. The horizontal plates were used, as usual, to produce a time sweep. Two independent voltages were applied to the vertical-plate circuit: a small alternating voltage produced by a 4000-cycle-per-second oscillator, and the voltage produced by the piezoelectric pickup in opening J of the cylinder head. The trace designated B in figure I-7 is an actual photograph of the trace produced on another cathode-ray oscilloscope screen during the exposure of the photographs of figure I-6. In the case of trace B, however, only the voltage from the 4000-cycle-per-second oscillator was applied to the vertical-plate circuit.

The electric conduit that supplied the sparking voltages to the spark plug in the camera was coupled capacitatively with the vertical deflection-plate circuits of both oscilloscopes. This coupling produced the breaks designated F in the two oscillograph traces at the time of the first timing spark (see frame A-10 of fig. I-6) and the breaks designated J at the time of the second timing spark (frame A-2 of fig. I-6). The break designated K in figure I-7 was caused by the first shock on the diaphragm of the piezoelectric pickup at the time of beginning of the gas vibrations in the combustion chamber.

The point in the high-speed camera at which the timing marks were produced and the point in the camera at which

the end gas was photographed are separated by a distance of approximately 34½ frames. Because of this separation, necessitated by mechanical considerations, the breaks F in the oscillograph traces of figure I-7 occurred 196½ (not 162) frames before the development of the knocking blur at B in frame J-10 of figure I-6. Likewise, the breaks J in figure I-7 occurred 143 (not 177½) frames after the development of the knocking blur. In trace B of figure I-7, between breaks F and J, 32.8 oscillator cycles were counted (reference 7); there were therefore $\frac{339.5}{32.8}$ or 10.35 motion-picture frames per oscillator cycle. (The second oscilloscope was provided solely because in many cases the disturbances in trace A caused by the knocking gas vibrations were so violent that it was not possible to count oscillator cycles between breaks F and J in trace A.) Nineteen oscillator cycles were counted (reference 7) on trace A of figure I-7 between the break F and the break K; the knocking break K therefore occurred approximately 196½ frames after the first timing spark. This value agrees exactly with the 196½ frames that separated

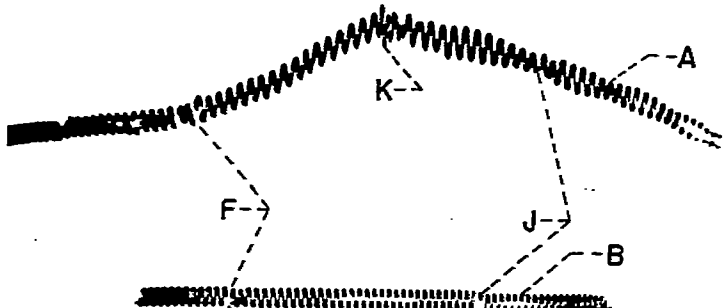


FIGURE I-7.—Composite pressure-time and oscillator trace A and separate oscillator trace B for combustion process of figure I-6. F, breaks caused by first timing spark (frame A-10 of fig. I-6); J, breaks caused by second timing spark (frame A-2 of fig. I-6); K, break caused by start of knock (frame J-10 of fig. I-6); piezoelectric pickup in opening J. (See fig. I-1.)

the first timing spark chronologically from the knocking blur in frame J-10 of figure I-6. (The picture-taking rate is known from camera-acceleration data to be constant within a very small fraction of 1 percent over the period of time involved in the determination, and the frequency of the oscillator output is believed to be similarly constant over the very short time interval involved.)

In eight cases with the end zone in contact with the diaphragm of the piezoelectric pickup the knocking blur was found, by the method used with figures I-6 and I-7, to coincide chronologically with the start of the violent gas vibrations within one-half motion-picture frame. In 16 cases where the end gas was on the opposite side of the chamber from the piezoelectric pickup, the same method indicated that the knocking blur preceded the start of the violent gas vibrations by $4 \pm 1\frac{1}{2}$ motion-picture frames, the value of four motion-picture frames being accounted for by the time required for the knocking disturbance to travel at the speed of sound from the end gas to the diaphragm of the piezoelectric pickup.

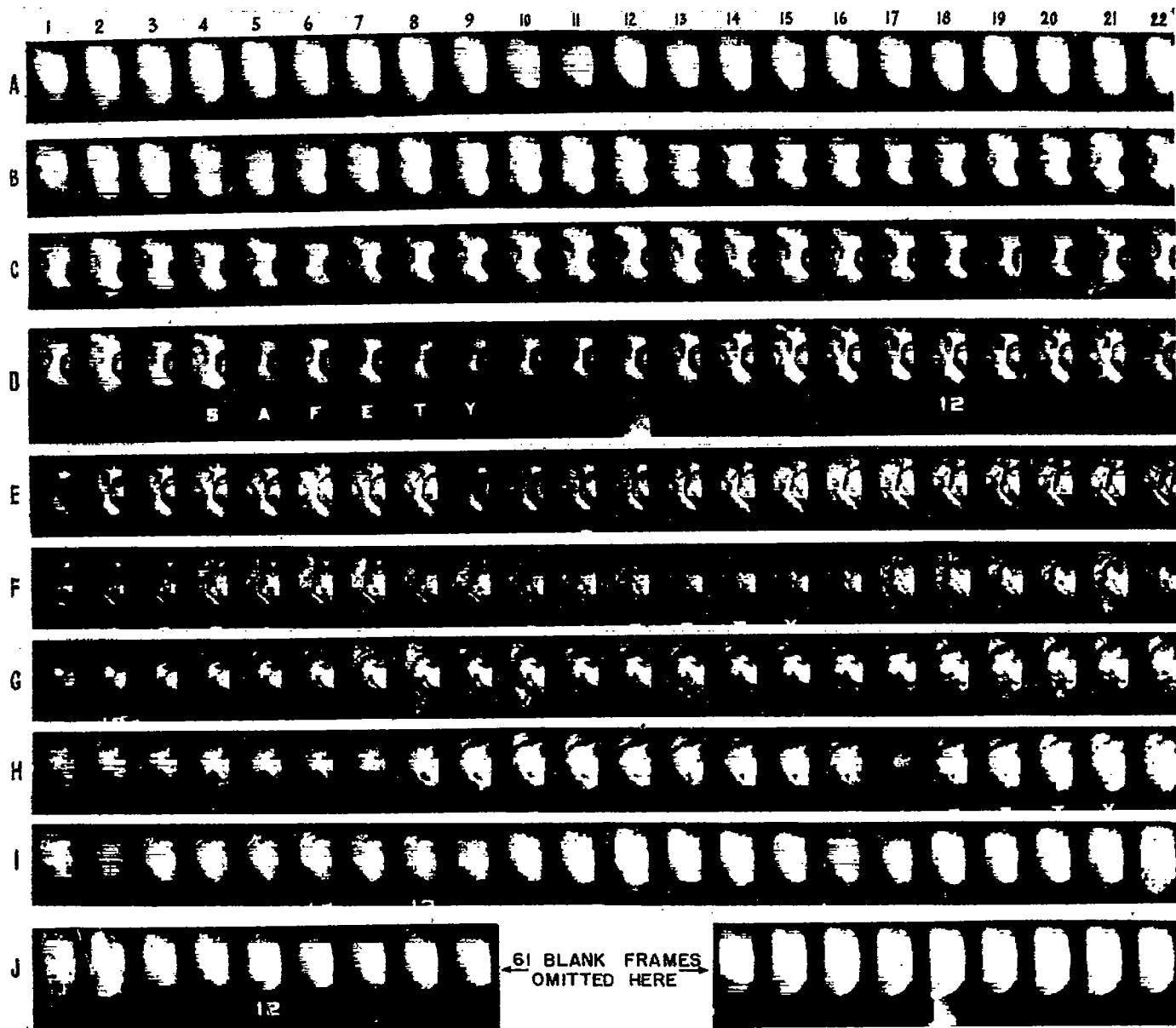


FIGURE I-8.—High-speed photographs of nonknocking combustion in spark-ignition engine with timing sparks in rows D and J. Fuel, S-1; compression ratio, 7.4; fuel-air ratio, about 0.06; atmospheric intake; four spark plugs; spark timing, for left-hand plug, 29° B. T. C., for other three plugs, 22° B. T. C. Frames 1 to 19 selected as point of final fadeout of schlieren pattern.

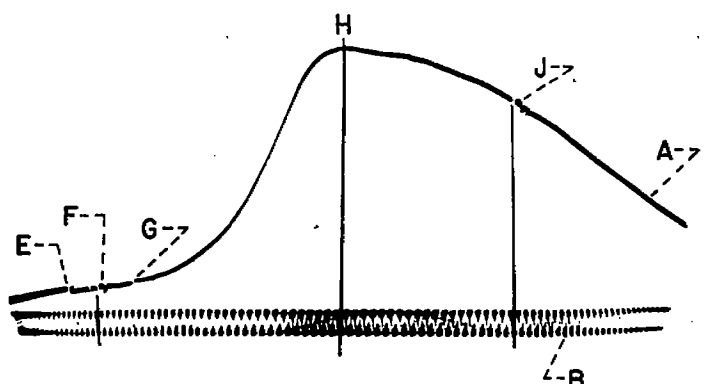


FIGURE I-9.—Pressure-time record A for nonknocking combustion process of figure 8 and separate oscillator trace B. E and G, breaks caused by ignition sparks; F, break caused by first timing spark (frame J-18 of fig. I-8); J, break caused by second timing spark (frame D-12 of fig. I-8); H, point of peak pressure; piezoelectric pickup in opening 1. (See fig. I-1.)

A somewhat similar but less accurate method of determining the chronological relationship is illustrated by figures I-8 and I-9 (same as figs. 15 and 16 of reference 7) as applied to the significance of the mottled combustion pattern in the schlieren pictures. Figure I-8 is a shot of normal nonknocking combustion. Engine operating conditions were the same as with the combustion of figure I-6 except that the piezoelectric pickup was placed in opening 1 (see fig. I-1) and an additional spark plug replaced the piezoelectric pickup at opening J. The fuel was S-1 reference fuel. Ninety-five frames were omitted from figure I-8 after frame J-22 (or before frame A-1), 3 frames were lost at the splice at frame J-2, and 61 frames were omitted as indicated in row J. The first timing spark was exposed before the camera began taking pictures, at frame J-18, and the second timing spark

was exposed 549 frames later, after the camera had ceased taking pictures, at frame D-12.

The first and second timing sparks caused the breaks F and J, respectively, in the pressure-time trace A in figure I-9. With this method the 4000-cycle-per-second oscillator record was not superposed on the pressure-time record. Only one oscilloscope was used. After the pressure-time record was exposed, simultaneously with the exposure of the high-speed photographs, the piezoelectric pickup was immediately disconnected from the vertical-plate circuit of the oscilloscope, the 4000-cycle-per-second oscillator was connected to the vertical-plate circuit, and a second time sweep of the oscilloscope beam was produced, giving the trace B in figure I-9. The trace B was used solely as a measure of the nonlinearity of the time sweep of the oscilloscope. Lines corresponding to constant voltage on the horizontal deflection plates were drawn through trace B from breaks F and J in trace A and also from the point H in trace A, which was considered to be the point of maximum pressure, as shown by trace A. By simple proportionality the point H in trace A of figure I-9 was found to coincide chronologically with the exposure of frame J-4 of figure I-8 (with due allowance for the 34½ frame correction previously mentioned). Upon careful examination of the original negatives of figure I-8, frame I-19 was selected as the point of final fadeout of the

mottled combustion zone; the difference between times of exposure of frames I-19 and J-4 is 250 microseconds, or only 0.75° of crankshaft rotation.

In five cases similar to that of figures I-8 and I-9 the final fadeout of the schlieren combustion pattern in the photographs was found to precede peak pressure by $0.3 \pm 0.7^\circ$ of crankshaft rotation. As explained in reference 7, peak pressure and the fadeout of the schlieren combustion pattern were so close to top center that no correction was required for piston motion. In 47 cases where the method of figures I-8 and I-9 was applied to knocking combustion, with the end zone on the opposite side of the chamber from the piezoelectric pickup, the knocking blur was found to precede the start of the violent gas vibrations by 8 ± 6 motion-picture frames, as compared with $4 \pm 1\frac{1}{2}$ motion-picture frames in the 16 cases in which the method of figures I-6 and I-7 was used. The method of figures I-8 and I-9 is inherently less accurate than that of figures I-6 and I-7, the principal sources of error probably being lack of reproducibility of the time sweep of the oscilloscope and some slight interaction between the vertical- and horizontal-plate circuits of the oscilloscope. The comparison of the two methods indicates that the method of figures I-8 and I-9 is reproducible within $\pm 0.5^\circ$ of crankshaft rotation and that it has a constant error of about 0.6° of crankshaft rotation. Applying the indi-

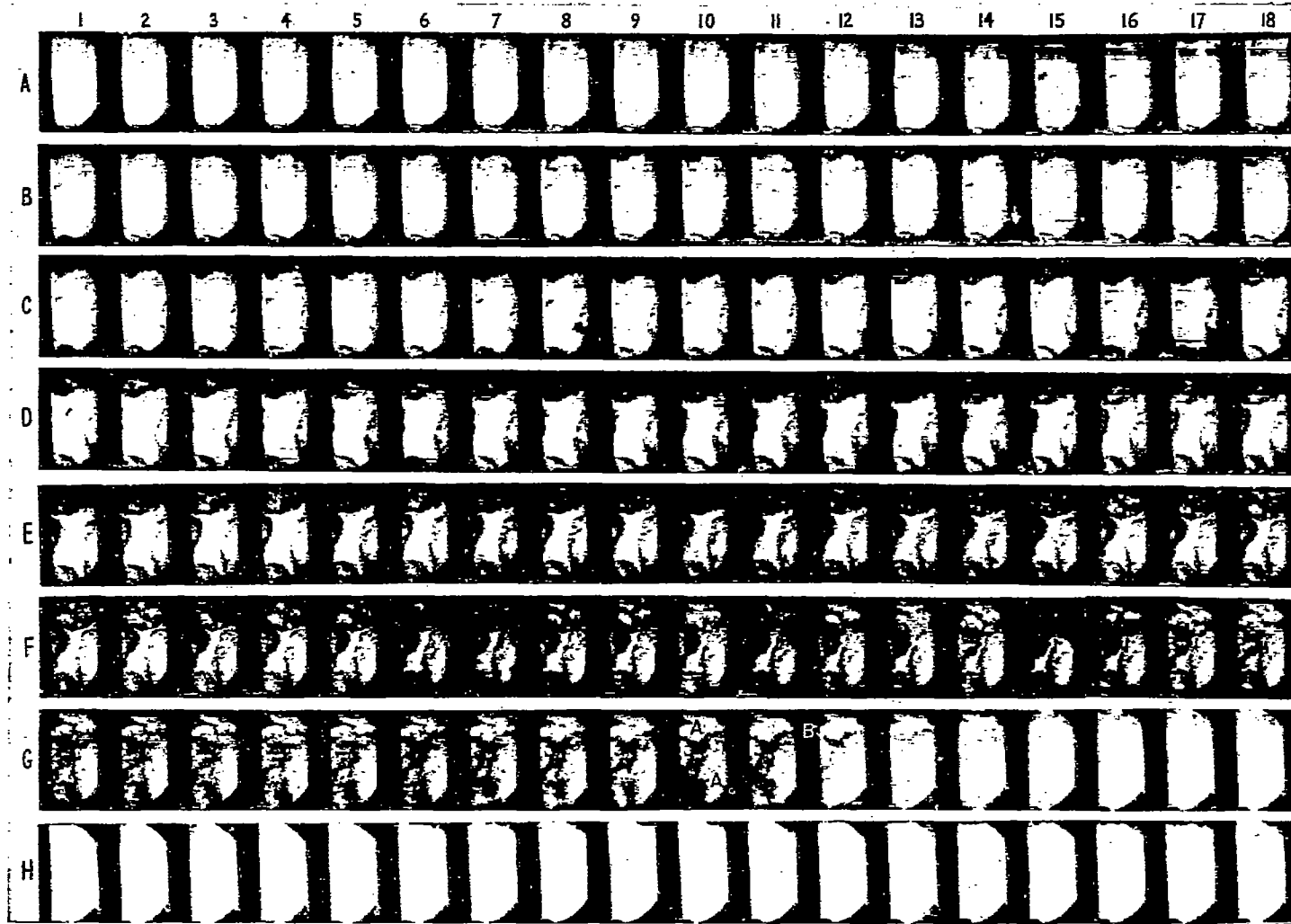


FIGURE I-10.—High-speed photographs of homogeneous end-gas autoignition preceding knock in spark-ignition engine. Fuel, M-2; compression ratio, 7.0; fuel-air ratio, about 0.08; atmospheric intake; four spark plugs; spark timing, for left-hand plug, 27° B. T. C., for other three plugs, 29° B. T. C.; A, regions where burning is complete; S, blurring caused by knock.

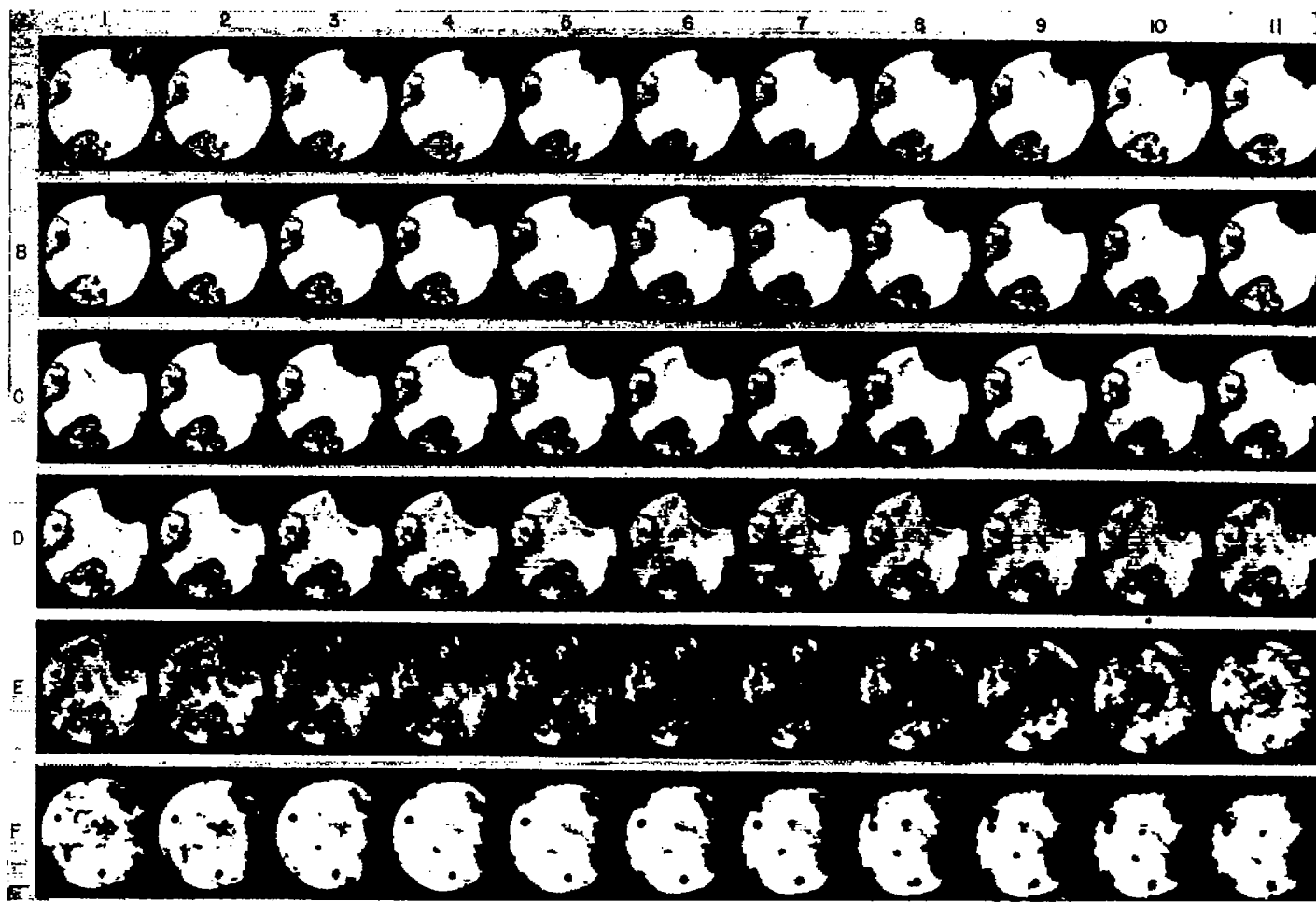


FIGURE I-11.—High-speed photographs of homogeneous autoignition throughout large volume of end gas before knock in spark-ignition engine. Fuel, M-4; compression ratio, 8.7; fuel-air ratio, about 0.17; inlet-air temperature, 445° F; inlet-air pressure, atmospheric; four spark plugs; spark timing, 20° B. T. C.

cated correction for the constant error results in the finding that peak pressure preceded the final fadeout of the mottled combustion zone by $0.3 \pm 0.7^\circ$ of crankshaft rotation. The 0.7° variation from the mean is almost within the demonstrated inaccuracy of the method. It is doubtful whether the point of peak pressure could be selected more accurately than within 0.3° of crankshaft rotation in traces like that of figure I-9.

From the investigation summarized here (reference 7) two conclusions appear justified: first, that the characteristic knocking blur seen in the high-speed photographs does represent the reaction that sets up the violent gas vibrations associated with knock and, second, that the mottled combustion zone does represent continuing combustion, at least so far as the termination of combustion is concerned. The second conclusion as applied to combustion in a constant-volume bomb was previously reached by Lindner (reference 65).

Six types of end-gas autoignition.—The high-speed photographs have revealed six different types of autoignition in the end gas. Some of these types may be interrelated; others seem to be quite distinct. The type of autoignition that will occur under conditions sufficiently severe appears to depend largely upon the fuel used, although the scope of

the investigations has not been sufficient to rule out all other factors entirely as affecting the type of autoignition that will occur. Some other types of autoignition have been followed by the explosive knock reaction in all of the NACA tests where they occurred; other types have been followed by the explosive knock reaction in some cases, in other cases not.

The homogeneous type of autoignition (occurring simultaneously and uniformly throughout the entire body of end gas) is observed in frames L-1 to M-10 of figure I-5 and in frames J-1 to J-9 of figure I-6. This type of autoignition is also well shown in frames G-1 to G-11 of figure I-10, a reproduction of figure 7 of reference 6. (Four spark plugs were used for the combustion process of fig. I-10. The injection valve was in position H of fig. I-1. The fuel was M-2 reference fuel, the spark timing 20° B. T. C. for the plugs in E, F, and J positions and 27° B. T. C. for the plug in G position, compression ratio 7.0, and fuel-air ratio approximately 0.08.) The explosive knock reaction occurs in the area designated B in frame G-12 of figure I-10. The white regions designated A in frame G-10 of the figure are the regions in which combustion is complete; they should not be confused with the end zone which is visible as a white area in frame G-1 but which has become completely dark in frame G-10.

Practically homogeneous autoignition is seen in figure I-11 throughout an end zone very much larger than the end zones of figures I-5, I-6, and I-10. The full-view combustion apparatus was used for the photographs of figure I-11. These photographs were obtained in a recent investigation conducted by H. L. Olsen of the NACA technical staff, as were all photographs of combustion in the full-view apparatus presented later in this paper. Four spark plugs were used in the combustion process for this figure; the flames from three of the plugs made considerable progress through the gases before the first frame of the series was taken, whereas the flame from the fourth spark plug develops very slowly throughout the frames of rows A to D of the figure. The positions of the four spark plugs are shown as B, C, E, and F at frame A-1 of the figure, corresponding to the same lettered positions in figure I-2. The injection valve was in position A (see fig. I-2); the fuel was M-4 reference fuel; spark timing, 20° B. T. C.; compression ratio, approximately 8.7; fuel-air ratio, about 0.17; inlet-air temperature, 445° F; and inlet-air pressure, atmospheric. (Fuel-air ratio was adjusted approximately to maximum knock value; the abnormally high value of 0.17 was required probably because of incomplete fuel vaporization obtained with injection on the compression stroke.)

More than half the total volume of the combustion chamber is involved in the autoignition that developed in the case of figure I-11. The autoignition is first visible as a wisp of mottled gas indicated by the arrow in frame C-1. In all the frames of rows C and D mottling appears throughout the entire area of the end gas, and between frames E-1 and E-7 the entire end gas becomes very dark. The first evidence of the explosive knock reaction appears in frame E-8 and the combustion is completed by frame F-4. The knock in this case was extremely heavy. The pressure-time trace from reference 12 (not reproduced in this paper) indicated a very considerable pressure rise caused by the homogeneous autoignition before the development of the explosive knock reaction.

Homogeneous autoignition has always been followed by the explosive knock reaction in the NACA tests.* In some cases, however, the knock has been quite light in spite of a very large homogeneously igniting end zone, and cases will be presented in which heavy knock has developed in the burning gases alongside of a large end-zone area in which no autoignition has taken place.

A second type of end-gas autoignition, which might be termed "pinpoint" autoignition, is shown in figures I-12 to I-15. Figure I-12 is reproduced from reference 9. In the

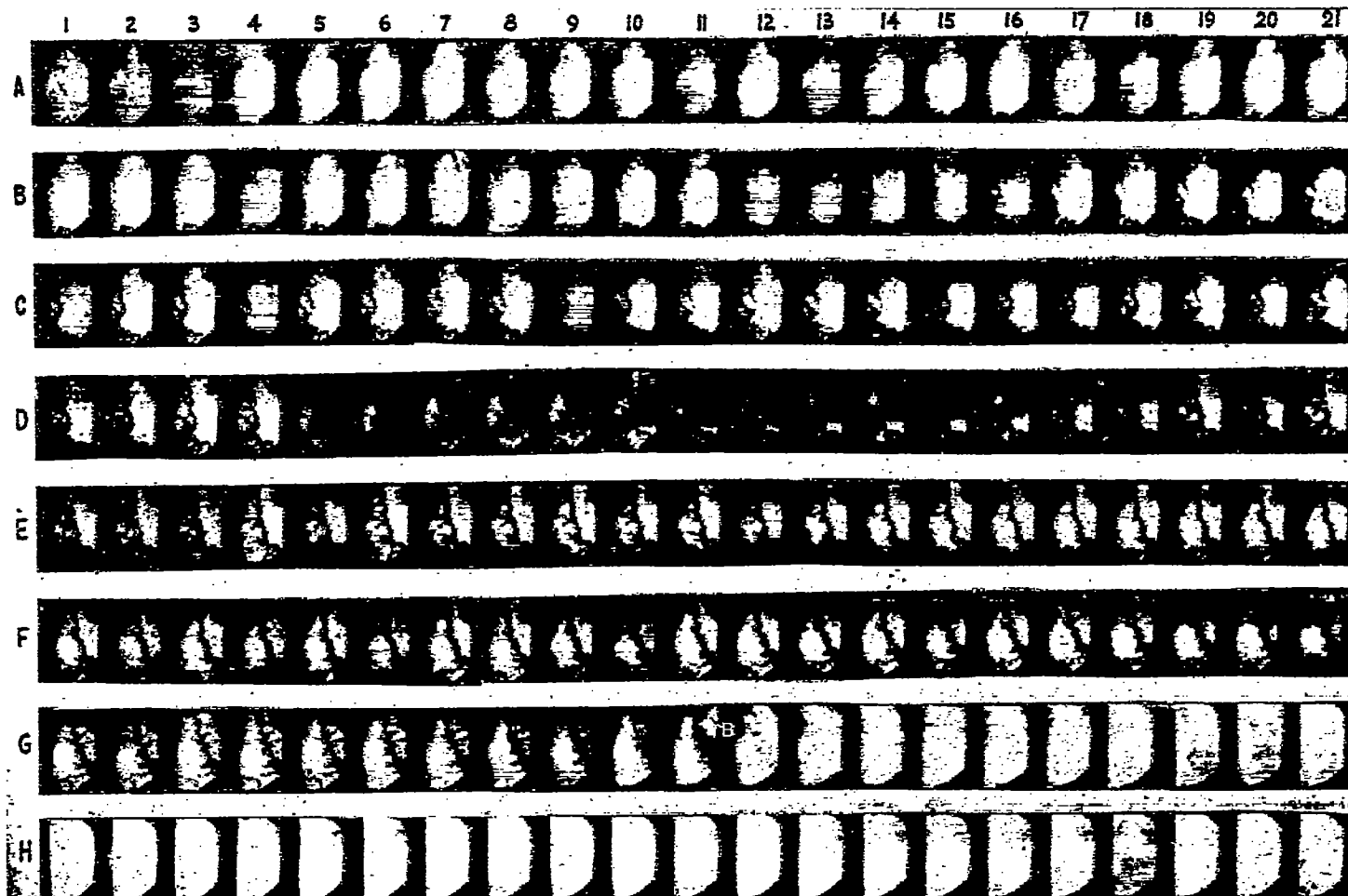


FIGURE I-12.—High-speed photographs of pinpoint end-gas autoignition preceding knock in spark-ignition engine. Fuel, S-1 with 200 ml amyl nitrate per gallon; compression ratio, 7.1; fuel-air ratio, about 0.08; atmospheric intake; two spark plugs; spark timing, at G position (fig. I-1); 27° B. T. C., at F position, 20° B. T. C.; E, luminosity caused by knock.

*Since the writing of this paper a photograph has been obtained by G. E. Osterstrom, NACA, with *n*-heptane fuel, showing homogeneous autoignition throughout a third of the combustion-chamber volume without any evidence of the explosive knock reaction either in the photographs or in the pressure-time record.

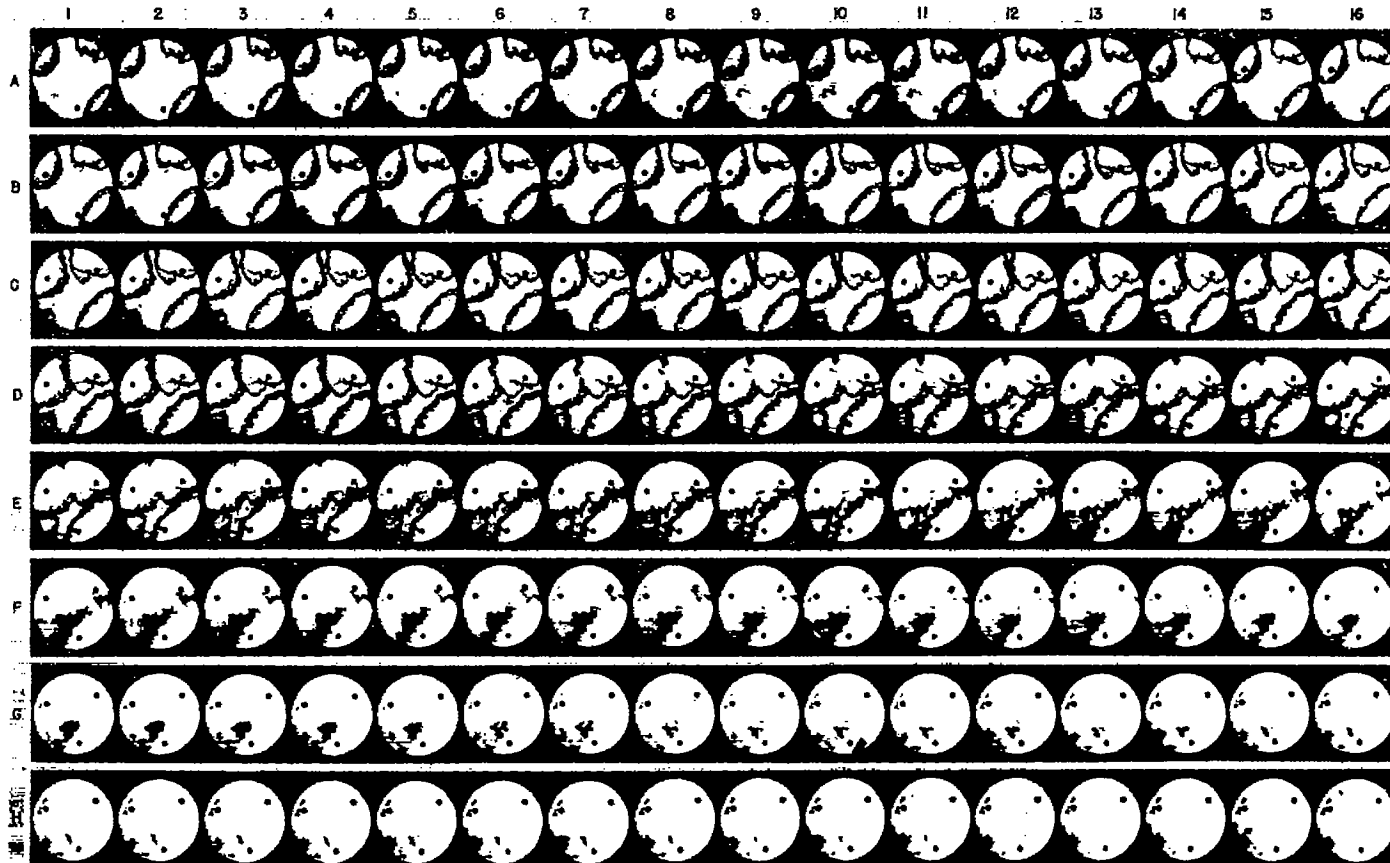


FIGURE 1-13.—High-speed photographs of pinpoint end-gas autoignition without knock in spark-ignition engine. Fuel, benzene; compression ratio, 9.0; inlet-air temperature, 425° F.; inlet-air pressure, atmospheric; four spark plugs; spark timing, 21° B. T. C.

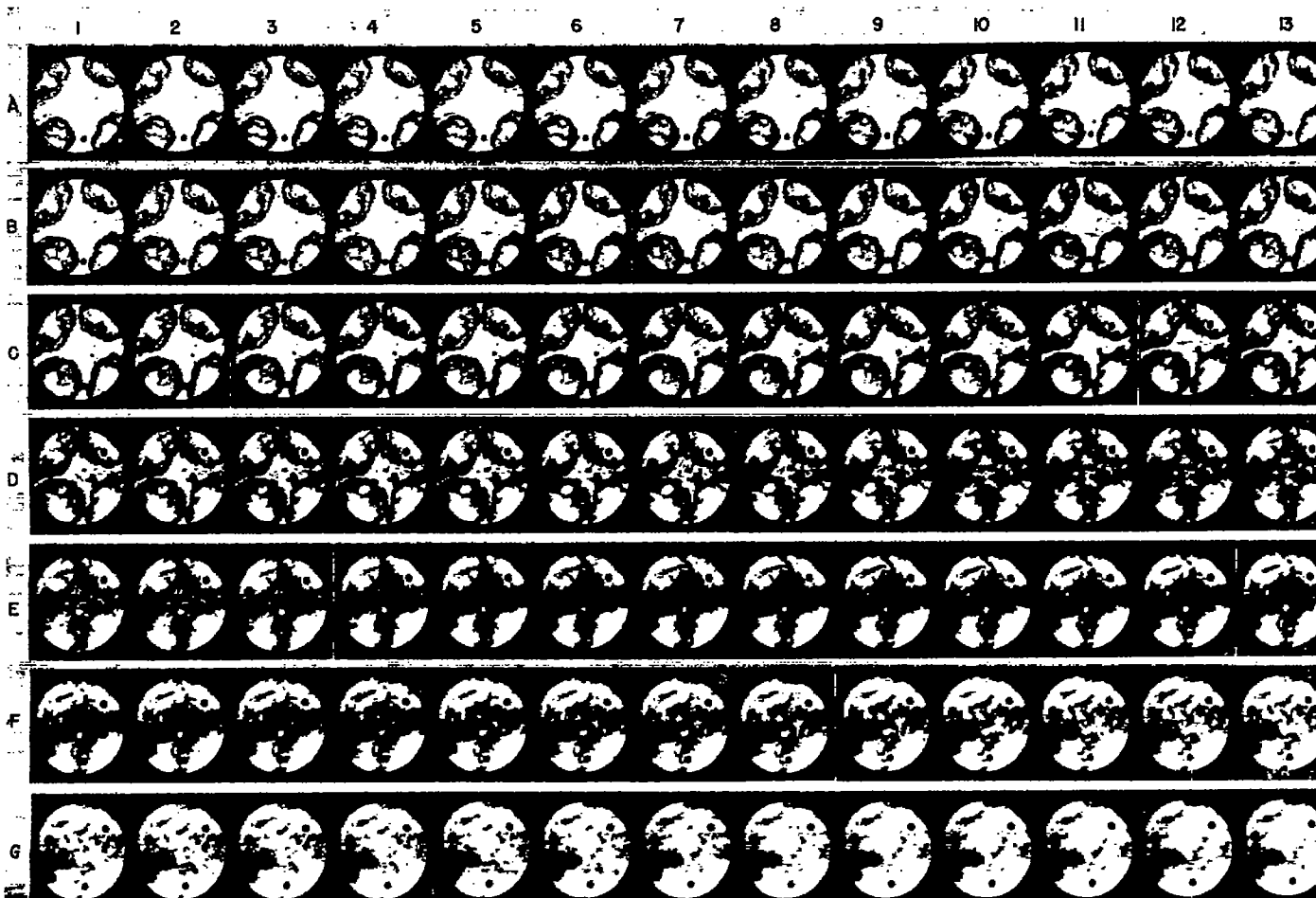


FIGURE 1-14.—High-speed photographs of pinpoint end-gas autoignition followed by very light knock in spark-ignition engine. Fuel, triptane; compression ratio, 9.0; fuel-air ratio, about 0.23; inlet-air temperature, 312° F.; inlet-air pressure, 20 pounds per square inch; four spark plugs; spark timing, 18° B. T. C.

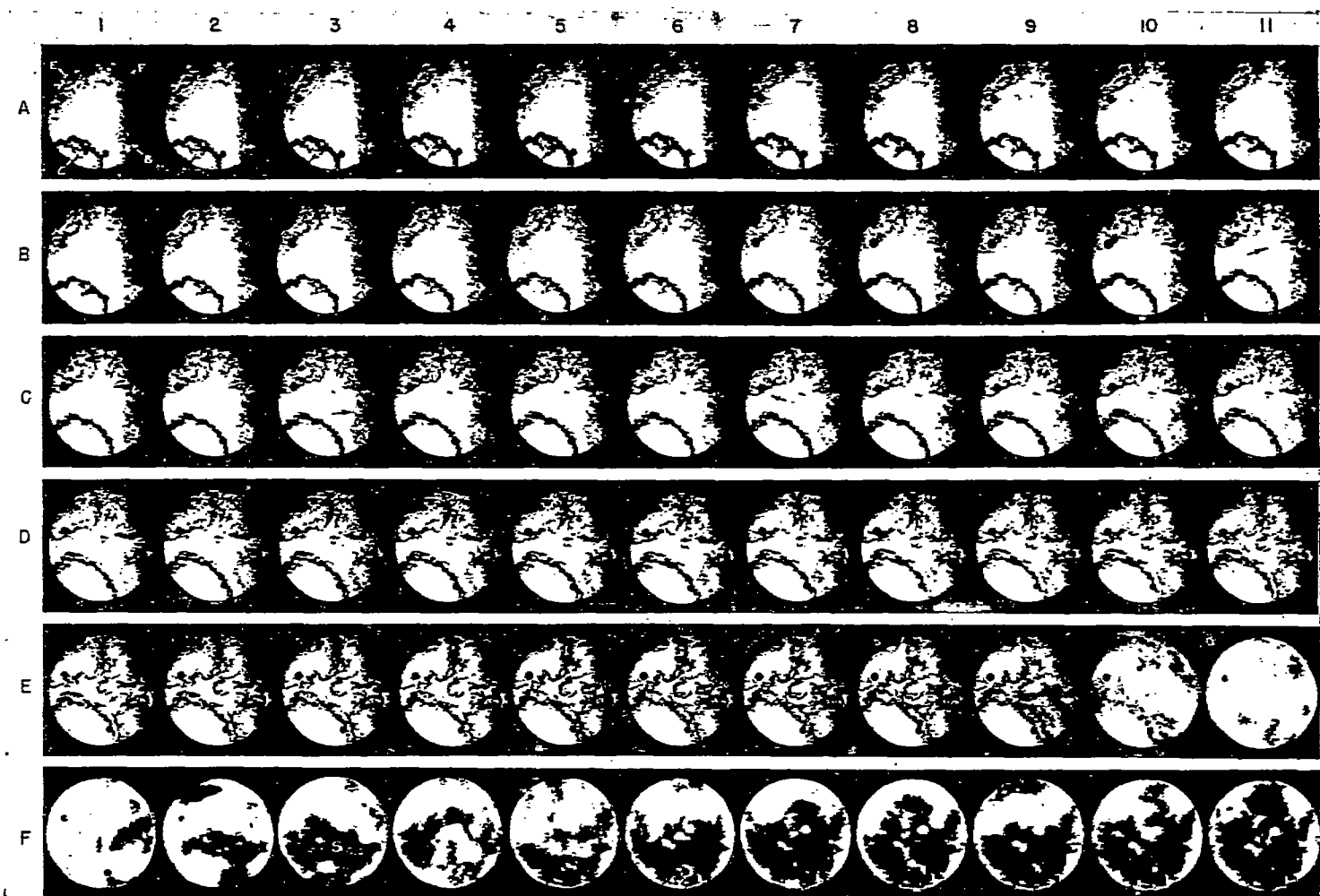
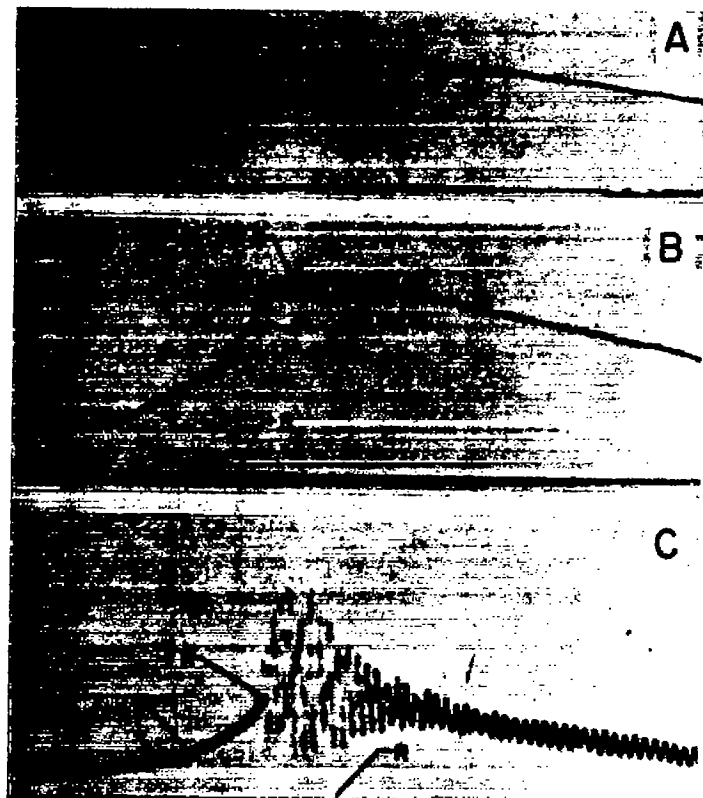


FIGURE I-15.—High-speed photographs of pinpoint end-gas autoignition followed by violent knock in spark-ignition engine. Fuel, S-4; compression ratio, 9.0; fuel-air ratio, about 0.25; inlet-air temperature, 446° F; inlet-air pressure, 18.5 pounds per square inch absolute; four spark plugs; spark timing, 18° B. T. C.

case of figure I-12, taken with the old combustion apparatus, only two spark plugs fired. The spark plug in G position (see fig. I-1) was timed at 27° B. T. C.; that in F position at 20° B. T. C. The injection valve was in H position. The fuel was S-1 reference fuel with admixture of 200 ml amyl nitrate per gallon. The compression ratio was 7.1 and the fuel-air ratio approximately 0.08. The dark frames, D-5 to D-16, in figure I-12 should be disregarded; their appearance was caused by faulty processing of film. The pinpoint autoignition begins to develop in the later frames of row F as very small black dots distributed throughout the end gas. Throughout frames G-1 to G-10 these black dots gradually grow larger until they completely fill the end zone. The explosive knock reaction is first visible at B in frame G-11 and has spread throughout the entire visible part of the chamber in frame G-12. The knock in this case appears to have been violent.

The combustion processes of figures I-13, I-14, and I-15 were fired in the full-view combustion apparatus with four spark plugs timed at 21°, 18°, and 18° B. T. C., respectively. In each case the injection valve was in position A (fig. I-2) and the compression ratio in each case was 9.0. The inlet-air temperatures were 425°, 312°, and 446° F, and the absolute inlet-air pressures atmospheric, 20, and 18.5 pounds per square inch, respectively. The fuel-air ratios for figures I-14 and I-15 were about 0.22 and 0.25, respectively. The

fuel-air ratio for the case of figure I-13 is not known even to an approximation, but it is thought not to be greatly different from the values for the other figures because the flame speeds are of the same order. The fuels for the three cases were benzene, triptane, and S-4 reference fuel, respectively. In each of these three cases the pinpoint autoignition is clearly visible in the end gas (rows D and E of fig. I-13, rows B, C, and D of fig. I-14, and rows B to E of fig. I-15). In many cases the first visibility of the pinpoints is indicated by a small arrow. Careful measurements show that each pinpoint grows at the rate that should be expected if the flame spread out in all directions from a point origin at the same speed as that of the normal flames traveling from the igniting sparks. In the case of benzene (fig. I-13) the pinpoint autoignition does not result in even the slightest gas vibrations. The projected motion pictures appear smooth throughout the entire process. The combustion zone fades out very gradually throughout the frames of rows F, G, and H; this very gradual fadeout is typical of nonknocking combustion and is never seen after occurrence of an explosive knock reaction of any appreciable violence. The pressure-time record (fig. I-16 (a)) shows not the slightest evidence of gas vibration. (All the pressure-time traces of fig. I-16 were obtained from a piezoelectric pickup in position D, fig. I-2.) In the case of triptane (fig. I-14) the development of the pinpoint autoignition and the gradual fadeout



(a) Indicator card for combustion process of figure I-13, showing hot-gas vibrations.
 (b) Indicator card for combustion process of figure I-14, showing light gas vibrations.
 (c) Indicator card for combustion process of figure I-15, showing extremely violent gas vibrations.

Figure I-16.—Pressure-time records.

of the combustion zone is quite similar to the benzene case except that an extremely light knock develops at about frame G-6. The knock at frame G-6 cannot be detected by visual examination of the figure but is seen when the photographs are projected as a motion picture. Also the pressure-time record (fig. I-16 (b)) shows very light gas vibrations starting at the point of peak pressure. In the case of S-4 reference fuel (fig. I-15) the pinpoint autoignition develops in frames B-11 to E-8 and a violent explosive knock reaction develops in frames E-9 and E-10. Upon careful examination unignited end-gas areas may still be seen in frames E-8 and E-9. Some of these unignited end-gas areas still appear white in frame E-10; it appears if the gas in these regions ever burned it did so in a very short interval relative to the photographic exposure time of 25 microseconds. The pressure-time record for the case of S-4 reference fuel (fig. I-16 (c)) shows very violent knock occurring at a time when the heat release from the normal combustion was still rapid.

Figures I-12 to I-16 do not indicate that pinpoint autoignition is in any way related to the explosive knock reaction; this type of autoignition may occur with or without the explosive knock reaction and, as shown by the previous figures, the explosive knock reaction may occur without pinpoint autoignition.

A third type of end-gas autoignition, perhaps fundamentally identical with homogeneous autoignition, is the two-stage type seen in figure I-17. This combustion process was

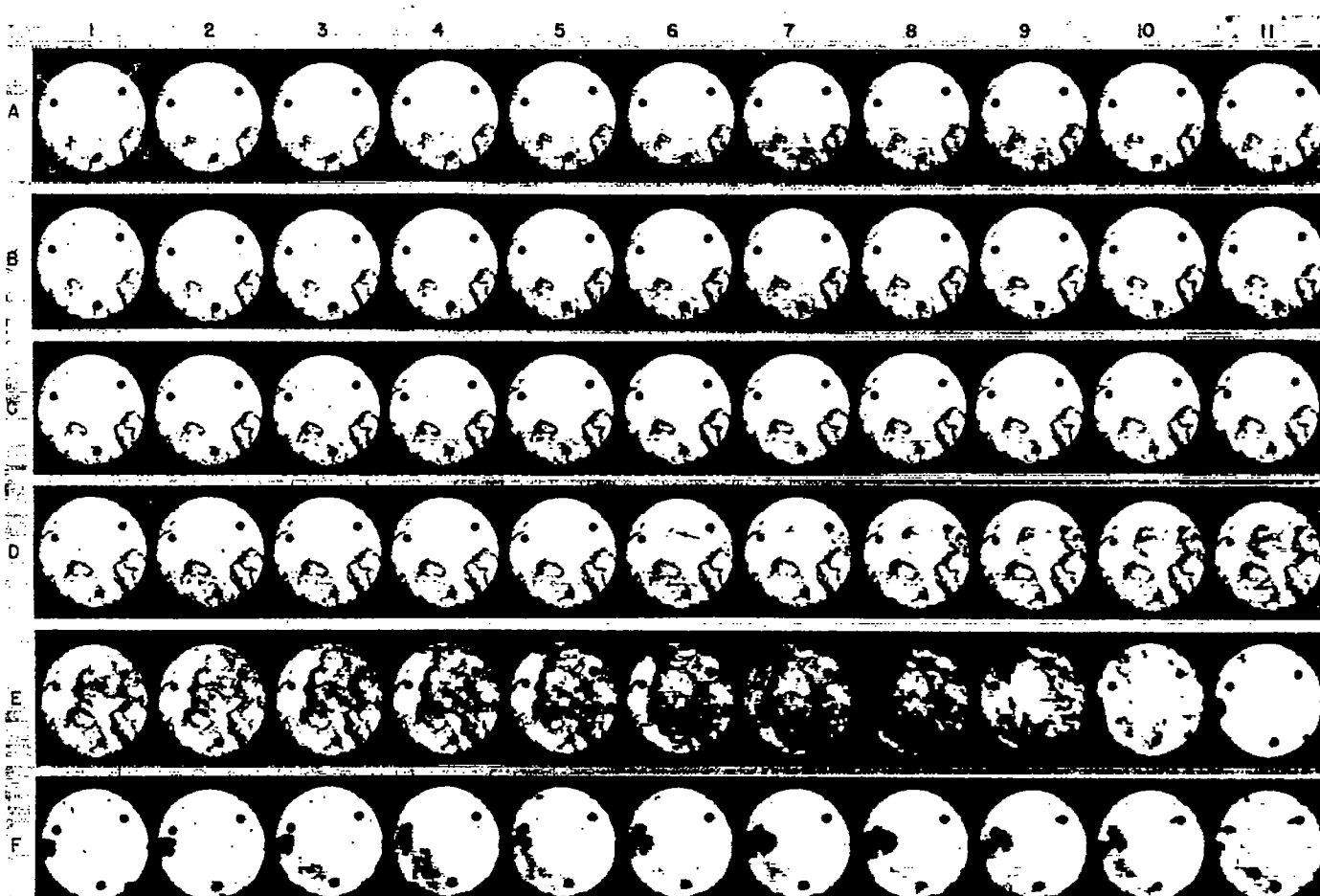


FIGURE I-17.—High-speed photographs of two-stage end-gas autoignition followed by heavy knock in spark-ignition engine. Fuel, M-4; compression ratio, 7.0; inlet air temperature, 768° F; inlet-air pressure, atmospheric; four spark plugs; spark timing, 21° B. T. C.

fired in the full-view combustion apparatus with four spark plugs timed at 21° B. T. C. The injection valve was in position A (fig. I-2); the fuel was M-4 reference fuel; compression ratio, 7.0; inlet-air temperature, 398° F; and inlet-air pressure, atmospheric. The fuel-air ratio is not known but is believed to be quite lean—near the lower limit of flammability. The spark plug at F position (frame A-1) apparently did not fire. The flame from C position is quite indistinct in the frames of rows A and B, but becomes quite sharply defined in rows C and D. The flames from B and E positions are sharply defined throughout rows A to D. The indistinct appearance of the flame from C position in the first two rows of the figure may be an indication that this flame is a borderline case between autoignition and normal propagated flame. A definite case of this type will be presented later in this

secure better photographs of the phenomenon because of the danger of serious damage to the combustion apparatus. This photographic shot was taken just after a series of shots with straight M-4 reference fuel. The M-4 reference fuel was removed from the fuel system and replaced with benzene. The engine operating conditions were then changed to values calculated to produce extensive autoignition with straight benzene fuel. The first combustion cycle after the change of operating conditions resulted in the photographs of figure I-18. It appears that some M-4 fuel was trapped in the injection valve and the actual fuel for the combustion process of this figure was probably either straight M-4 or a blend of M-4 with a small amount of benzene. Four spark plugs were used for this combustion process, timed at 20° B. T. C. The injection valve was in position A (fig. I-2); the compression

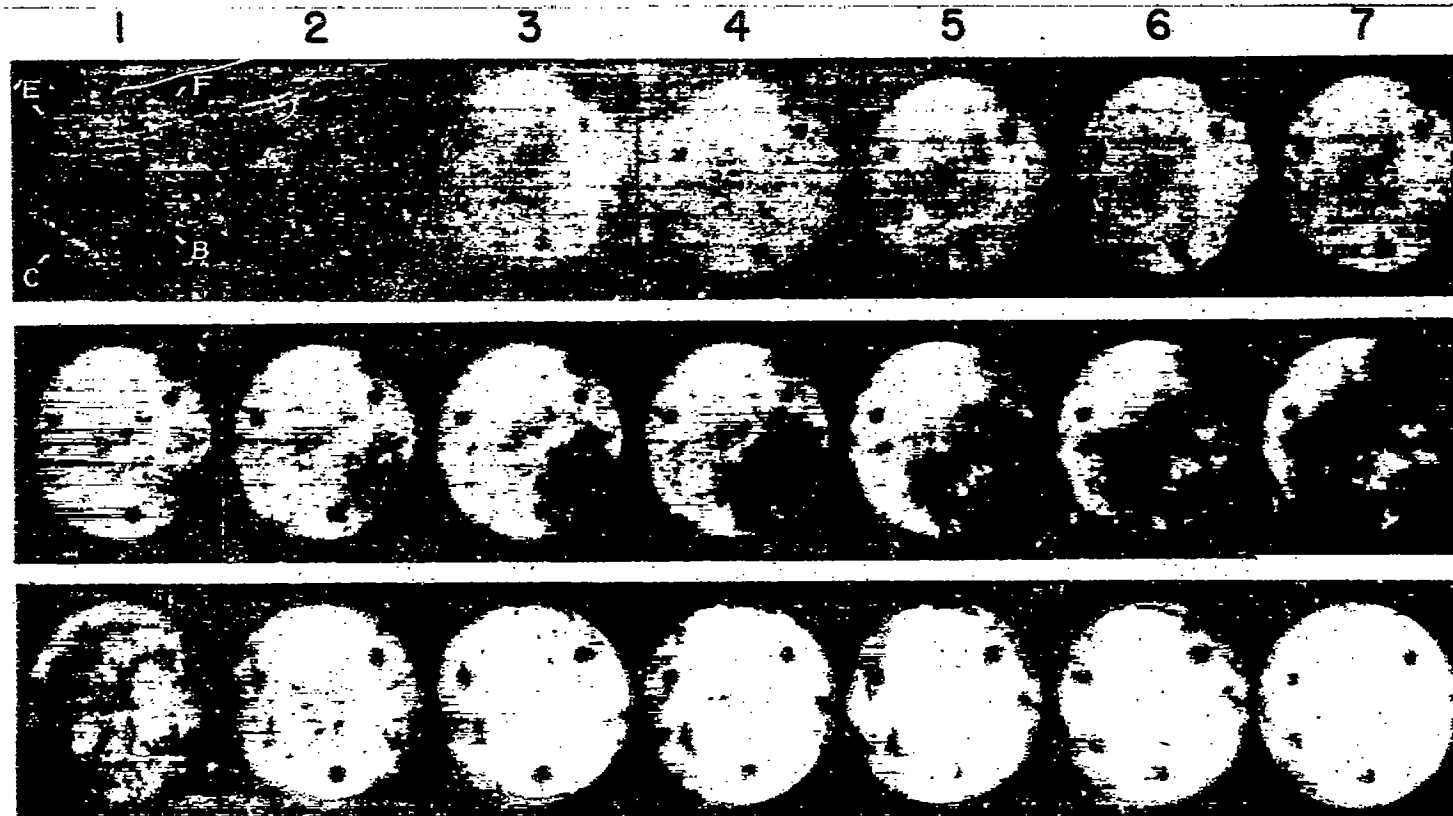


FIGURE I-18.—High-speed photographs of runaway flame preceding violent knock in spark-ignition engine. Fuel, M-4; compression ratio, 9.0; fuel-air ratio, about 0.17; inlet-air temperature, 415° F; inlet-air pressure, 15.5 pounds per square inch absolute; four spark plugs; spark timing, 20° B. T. C.

section. At about frame D-6 in figure I-17 definite autoignition begins to develop as a wisp of mottled gas, indicated by the arrow in this frame. The wisp indicated in frame D-6 serves as a boundary line in the following frames between homogeneously autoigniting gases and nonautoigniting gases. The gases to the right of this wisp autoignite in frames D-7 to E-5. The gases to the left of the wisp show no evidence whatever of autoignition between the frames D-7 and E-5. The gases to the left of the wisp do autoignite, however, in frames E-6 to E-8. The beginning of a violent explosive knock reaction is apparent in frame E-9.

A fourth type of end-gas autoignition appears in figure I-18 as a wild runaway flame. Because of an accident the photographs of this figure were taken under uniquely severe conditions for the fuel used. No attempt was made to

ratio was 9.0; fuel-air ratio, about 0.17; inlet-air temperature, 415° F; and absolute inlet-air pressure, 15.5 pounds per square inch.

Because of the very severe conditions the charge was apparently ready to autoignite at the time the camera shutter opened for the photographs of figure I-18. The entire combustion process, including the explosive knock reaction, took place within 16 motion-picture frames after the camera shutter started to open. For this reason, the frames do not become well illuminated until about the middle of row B, at which time the camera shutter was open sufficiently to produce fair pictures. The spark-plug positions are indicated at frame A-1. At frame A-7 the flames from B and F positions are fairly visible. The flames from C and E positions cannot be seen in the printed reproduction of

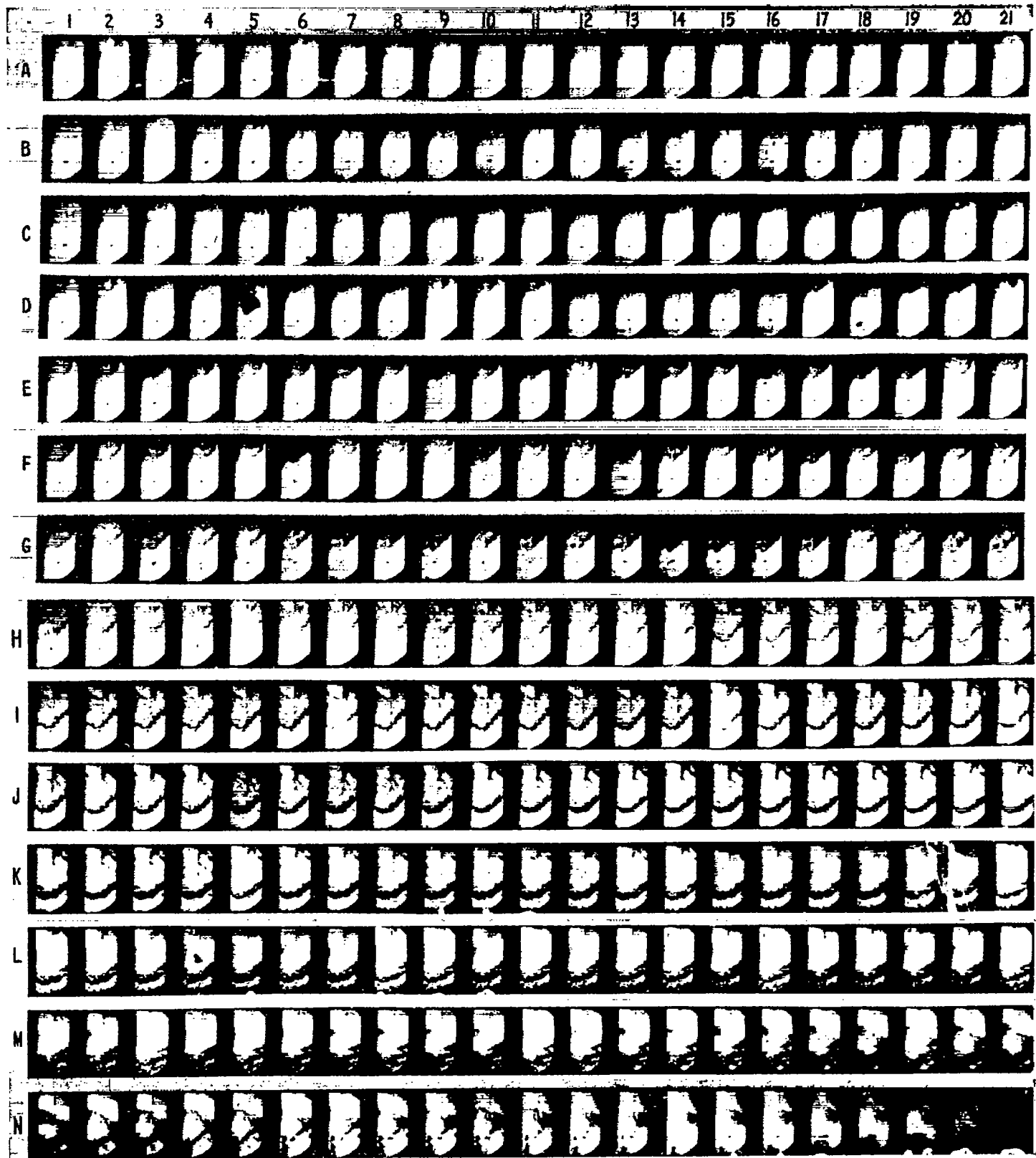


FIGURE I-19. High-speed photographs of development of preknock autoignition flame at far wall of chamber in spark-ignition engine. Fuel, S-2 with 100 ml amyl nitrate per gallon; compression ratio, 7.1; fuel-air ratio, about 0.08; atmospheric intake; one spark plug; spark timing, 20° B. T. C.

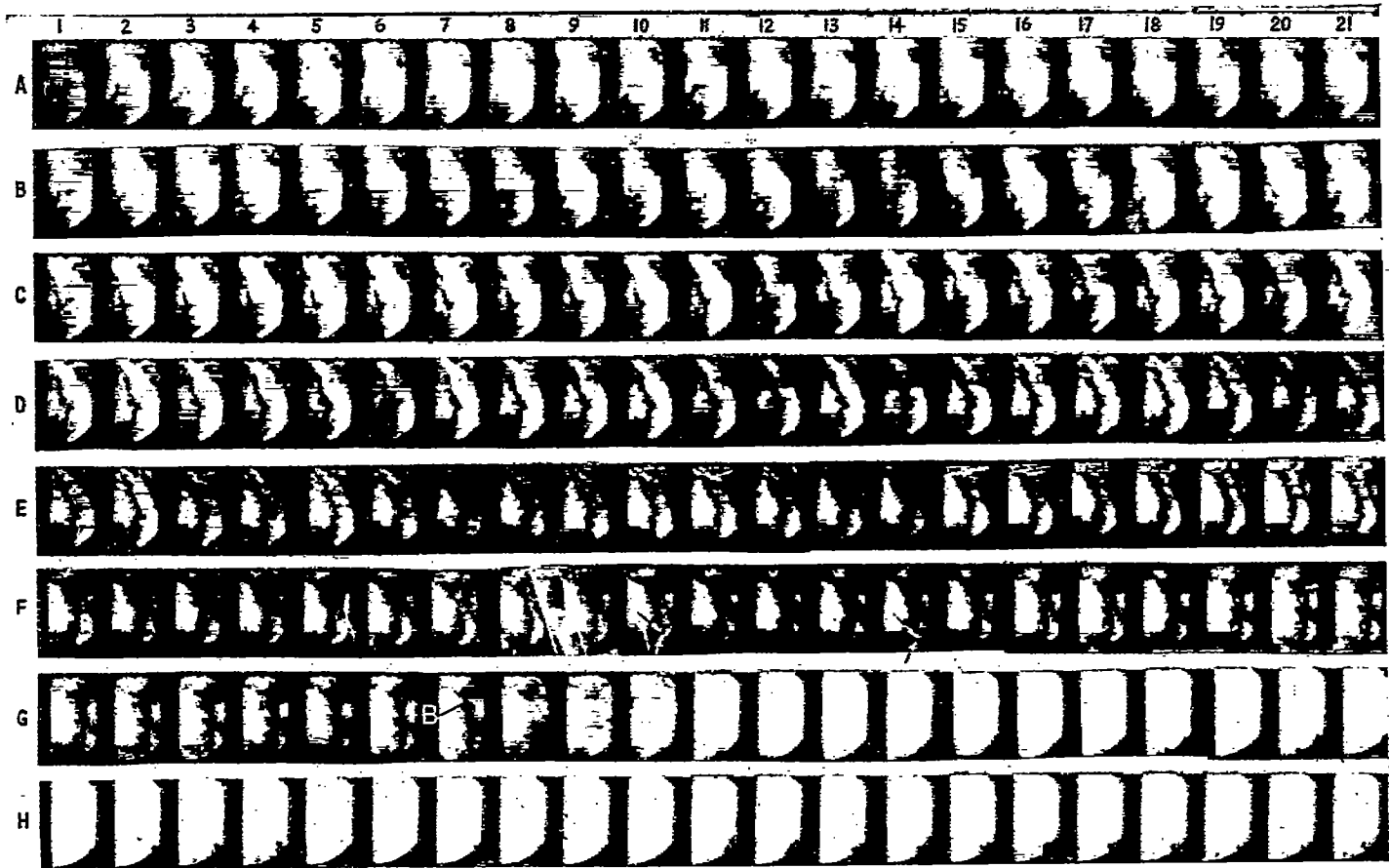


FIGURE I-20.—High-speed photographs of vibratory combustion preceding knock in spark-ignition engine. Fuel, M-2 with 200 ml TEL per gallon; compression ratio, 7.1; fuel-air ratio, about 0.08; atmospheric intake; four spark plugs; spark timing, for left-hand plug, 27° B. T. C., for other three plugs, 20° B. T. C.; B, blurring caused by knock.

frame A-7, but both of these flames can be seen on careful inspection of the original negative. At frame B-1 the flame from B position breaks loose and it travels all the way across the chamber in frames B-1 to C-1 at a speed of 1900 feet per second. The explosive knock reaction occurs after this flame has completed its travel across the chamber at frame C-2, as shown by the sudden whitening of the entire chamber. In frame B-7, after the runaway flame has nearly completed its travel across the chamber, the flame from E position may be clearly seen still apparently under complete control.

When the photographs of figure I-18 are projected as a motion picture the phenomenon seen in row B of the figure has every appearance of a very fast propagated flame. On close inspection of the still photographs, however, it is found that the leading edge of this flame is never sharply defined and the phenomenon appears to be in fact a multistage autoignition process, similar to the phenomenon of figure I-17 but occurring in many more than two stages. This phenomenon is regarded as a borderline case between homogeneous autoignition and a detonation wave. The occurrence of the explosive knock reaction at frame C-2 of the figure will be further discussed in a later section.

A fifth type of end-gas autoignition is shown in figure I-19, same as figure 13 of reference 9. This combustion process

was fired in the old combustion apparatus with one spark plug in E position (fig. I-1) timed at 20° B. T. C. The injection valve was in H position, the fuel was S-2 admixed with 400 ml amyl nitrate per gallon, compression ratio 7.1, and fuel-air ratio about 0.08. In this case the autoignition occurred as a flame developing at the far wall of the chamber and propagating out from the wall to meet the spark-ignited flame. A slight mottling near the far wall of the chamber (lower edge of the chamber as seen in the photographs) develops in the frames of row K of the figure. Also, in the later frames of row K, a few centers of pinpoint autoignition develop near the far wall of the chamber. In the frames of row L additional pinpoints of autoignition develop and a definite flame propagation begins to proceed out from the far wall. This orderly autoignition-flame propagation proceeds throughout the entire end gas in the frames of row M, and in the frames of row N the mottled combustion zone gradually fades out. When the photographs are observed as motion pictures only a very light explosive knock reaction is seen in the frames of row N; this reaction is so light that it cannot be identified as being associated with any particular motion-picture frame. The type of autoignition shown in figure I-19 may be a special case of pinpoint autoignition.

The sixth type of autoignition, an example of which

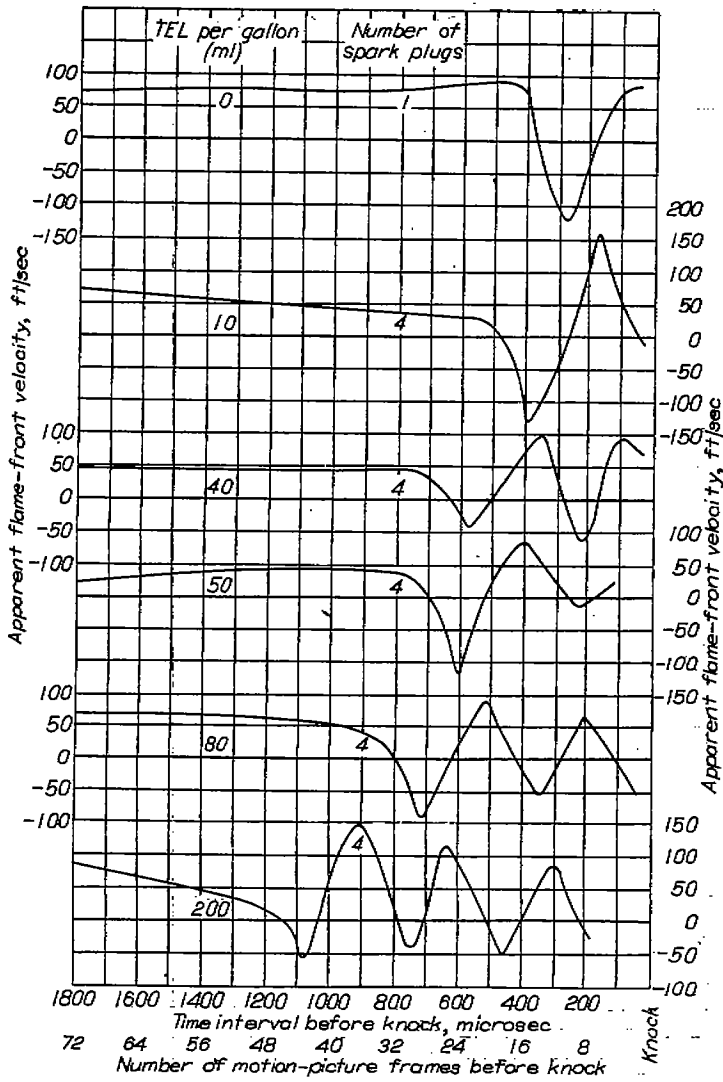


FIGURE I-21.—Apparent flame-front velocities during period of preknock vibration in spark ignition engine.

occurred in the combustion process of figure I-20, is detectable only through the slight preknock vibration which it imparts to the gases. Figure I-20 is a reproduction of figure 2 of reference 9. For this combustion process four spark plugs were used, timed at 20° B. T. C. in E, F, and J positions (fig. I-1) and at 27° B. T. C. in G position. The injection valve was in H position, the compression ratio was 7.1, and the fuel-air ratio about 0.08. The fuel was M-2 reference fuel with an extremely high concentration of tetraethyl lead—200 ml per gallon. Some pinpoint autoignition may be seen in the photographs, originating at centers indicated by the arrows at frames F-10 and F-14. No other visual evidence of autoignition appears, however, and when the explosive knock reaction begins at B in frame G-7 some apparently unignited end gas is still visible at the lower right corner of the chamber. In the original work (reference 9) flame areas were measured on greatly enlarged copies of the individual frames of the figure with a polar planimeter. The results showed that the end gas suddenly expanded at

about frame E-1 of figure I-20, and that between frames E-1 and G-7 at least three cycles of vibration of the gases occurred. The measurements indicated that the amplitude of the vibrations did not increase (in fact, usually diminished)

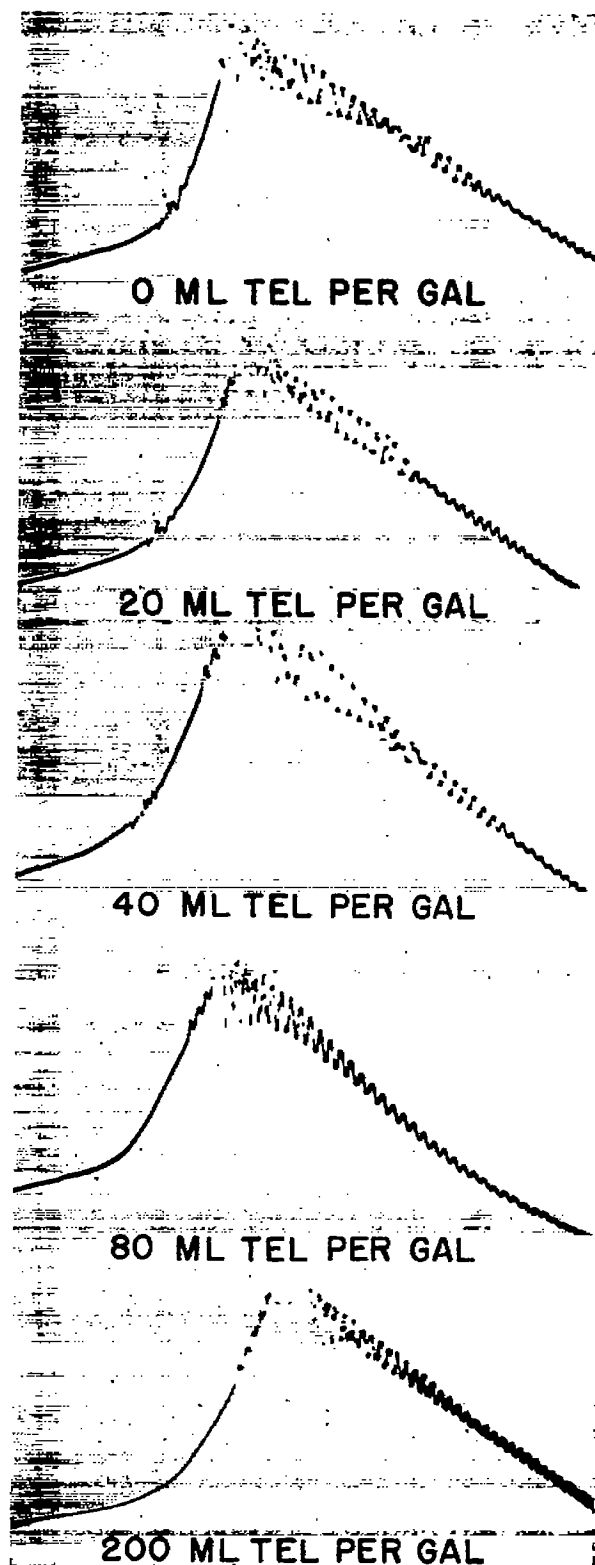


FIGURE I-22.—Actual pressure-time records showing increase in number of cycles of preknock vibration with increasing tetraethyl lead concentration in fuel.

after the first cycle, from which fact it was concluded that a mild explosive reaction occurred in the end gas at about frame E-1. When the photographs of figure I-20 are projected as a motion picture, four cycles of vibration of the gases are easily observed before the explosive knock reaction at frame G-7; they are observed as a backward and forward motion of the flame fronts.

Figure I-21 shows the preknock vibration determined from planimeter measurements of flame areas for different concentrations of tetraethyl lead. A similar variation in number of cycles of preknock vibration with varying tetraethyl lead concentration is shown by the actual pressure-time records of figure I-22, obtained with a piezoelectric pickup in opening I of the cylinder head (fig. I-1). The time interval involved in the preknock vibration was found to increase linearly with the tetraethyl lead concentration up to 200 ml per gallon, the highest concentration used.

Explosive knock reaction without end-gas autoignition.—Many high-speed photographs have been obtained like the ones of figure I-23, in which the end gas appeared to be entirely consumed by the normal flames some time before the occurrence of the explosive knock reaction. This figure is a reproduction of figure 6 of reference 6. Four spark

plugs were used for this combustion, timed at 20° B. T. C. at E, F, and J positions (fig. I-1) and at 27° B. T. C. at G position. The injection valve was at position H, the fuel was a blend of 50 percent 95-octane gasoline with 50 percent M-2 reference fuel, compression ratio 7.0, and fuel-air ratio about 0.08. The last visible end gas disappears, because of normal flame travel, at about frame G-17. The explosive knock reaction occurs at B in frame H-7, 11 frames after the disappearance of the last visible end gas. Other photographs have been obtained in which a mild explosive knock reaction occurred not only after the disappearance of the last visible end gas but even after the entire schlieren combustion pattern had almost faded out (reference 6).

The cases cited are not good proof that the explosive knock reaction can occur without autoignition because of the possible existence of unignited gas pockets in front of or behind the burning gases; such pockets could, of course, not be seen in the photographs. Photographs have been obtained, however, in which unignited end gas may actually be seen at the time the explosive knock reaction occurs and the unignited end gas does not appear to play a part in the explosive knock reaction. Comment has already been made concerning the presence of unignited end gas in one part of

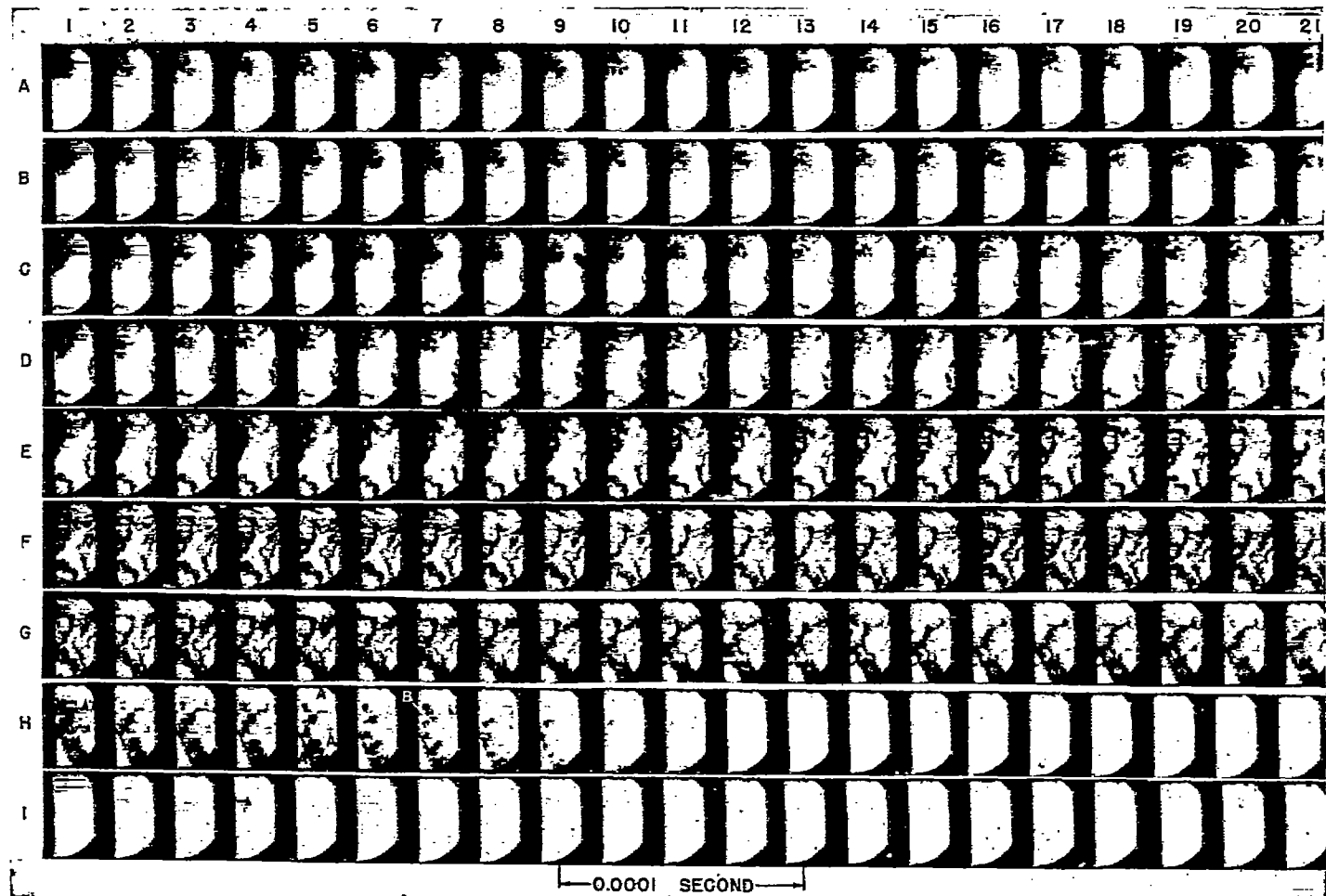


FIGURE I-23.—High-speed photographs showing apparent complete merging of flames before knock in spark-ignition engine. Fuel, 50 percent 95-octane gasoline with 50 percent M-2; compression ratio, 7.0; fuel-air ratio, about 0.08; atmospheric intake; four spark plugs; spark timing, for left-hand plug, 27° B. T. C., for other three plugs, 20° B. T. C.; A, completely burned regions; B, blurring caused by knock.

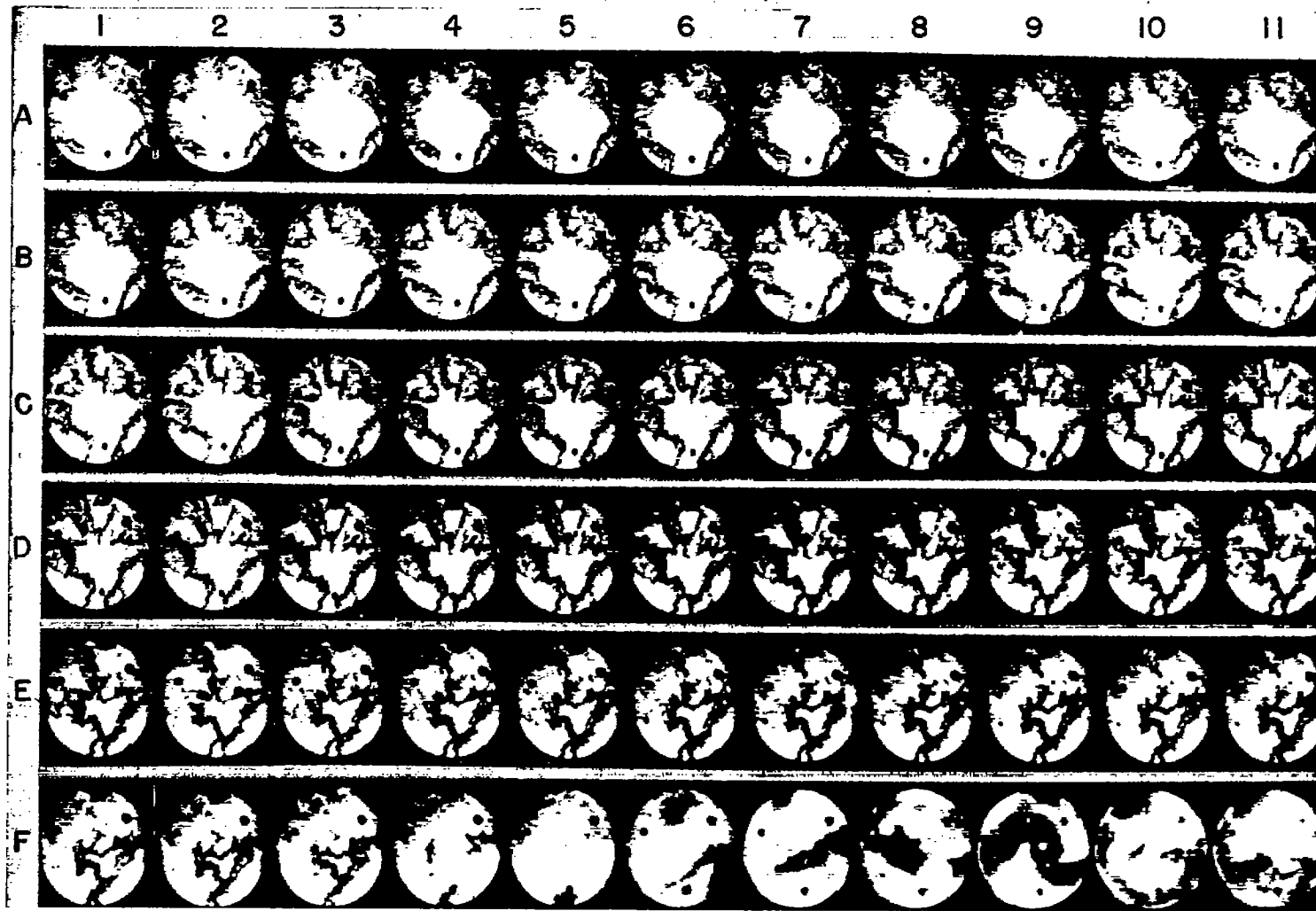


FIGURE I-24.—High-speed photographs of occurrence of violent knock in spark-ignition engine while unignited end gas is still visible. Fuel, S-4; compression ratio, 9.0; fuel-air ratio, about 0.13; inlet-air temperature, 310° F; inlet-air pressure, 15.5 pounds per square inch absolute; four spark plugs; spark timing, 18° B. T. C.

frame G-7 of figure I-20 at the same time that the explosive knock reaction begins in another part of the same frame. A more striking example of this phenomenon appears in figure I-24. Four spark plugs were used in the case of figure I-24, timed at 18° B. T. C. The injection valve was in position A (fig. I-2); the fuel was S-4 reference fuel; compression ratio, 9.0; fuel-air ratio, about 0.13; inlet-air temperature, 310° F; and absolute inlet-air pressure, 15.5 pounds per square inch. In frame F-2 of this figure a fair-sized white unignited end zone is visible, slightly below the center of the chamber, roughly in the shape of a T lying on its side. The explosive knock reaction begins in frame F-3, as indicated by the blurring of the dark mottled combustion zone. This dark mottled combustion zone encroaches somewhat upon the unignited end gas in frame F-3, but most of the end gas visible in frame F-2 remains unignited in frame F-3 in spite of the effect of the explosive knock reaction on the actual combustion zone in frame F-3. Moreover, the end gas that appears white and unignited in frame F-3 still appears white in frames F-4 and F-5, in which the explosive knock reaction is completed. If this body of end gas ever did burn it must have done so in a time interval much shorter than the 25-microsecond exposure time of the individual frames of the figure, or it would have

shown the characteristic dark mottled appearance of burning gas in one of the frames of the figure.

The appearance of frames F-2 to F-5 of figure I-24 indicates that the explosive knock reaction developed in the dark mottled combustion zone and that its effect on the unignited end gas, if it had any such effect, was only incidental. In reference 7 it was concluded that the explosive knock reaction develops only in gases that have been previously ignited either by normal flame travel or by auto-ignition. Photographs were presented in the same paper indicating that the origin of the explosive knock reaction was not necessarily in the same location as the last gas to be ignited.

Physical nature of explosive knock reaction as indicated by high-speed photographs.—From a study of photographs taken at 40,000 frames per second the author of this paper has concluded (reference 10) that the explosive knock reaction is a type of detonation wave traveling through the unburned, or incompletely burned, gases at a speed ranging approximately from one to two times the speed of sound in the burned gases. An example of a detonation wave moving at a speed twice that of sound in the burned gases is found in frames M-11 and M-12 of figure I-5. As previously noted, the explosive knock reaction in this case is first visible as a white streak along the lower right edge of frame M-11

and as a slight blurring of the combustion zone in the same frame. The next frame, M-12, has been rendered white throughout by the knock reaction. As explained in reference 10, it is believed justifiable to disregard the blurring of the mottled combustion zone in frame M-11 and to use the appearances of brilliant luminosity as a measure of the speed of the knock disturbance. On such a basis, the superficial impression obtained from frames M-11 and M-12 of figure I-5 is that the knock disturbance started at the lower right edge of the chamber and spread very rapidly throughout the charge from the point of origin. When the photographs are analyzed, however, with proper allowance for the focal-plane-shutter effect of the camera (reference 1), it is found that the travel of the knock disturbance as shown by frames

tive to the combustion-chamber image as the leading edge of the focal-plane-shutter slit of the camera exposing frame M-12.

Figures I-25 and I-26 are reproductions of portions of a motion-picture animation (reference 12) created for the purpose of demonstrating the manner of exposure of frames M-11 and M-12 of figure I-5. Figure I-25 shows this author's conception of what actually happened during the exposure of the two frames. In this figure the focal-plane shutter is assumed to have been removed from each of the still cameras. The frames of the figure show what would have been seen on the film in each of the two cameras if the film and the image appearing upon it could have been photographed at the rate of about 180,000 frames per second.

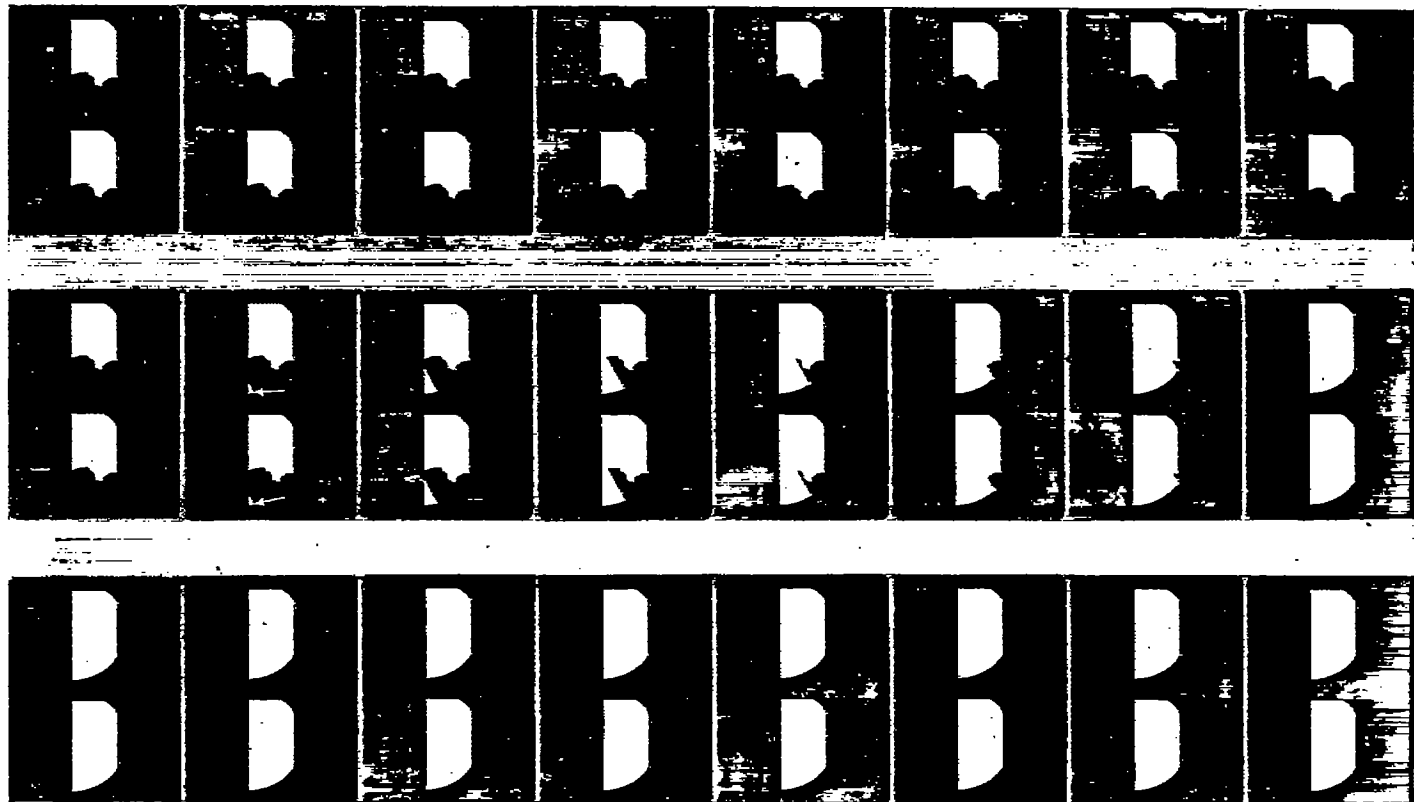


FIGURE I-25.—Animation showing detonation-wave travel as it might appear on film in two still cameras if film and image were photographed at about 180,000 frames per second. Development of detonation wave in frames B-2 to B-8 of this figure corresponds chronologically with exposure of frames M-11 and M-12 of figure I-5.

M-11 and M-12 was actually in a direction opposite to the superficially apparent direction.

An optical effect equivalent to that of the high-speed camera would be obtained if frames M-11 and M-12 of figure I-5 were exposed by two independent still cameras using focal-plane shutters, provided the following three conditions were satisfied: first, the width of the slit aperture in each of the focal-plane shutters must be equal to half the frame spacing, or about $7/10$ the width (not the length) of the combustion chamber as seen in the photographs, second, each focal-plane-shutter slit must travel a distance equal to its own width in $1/40,000$ second in a direction from left to right, as seen in figure I-5 (that is, in the direction away from the previously exposed frames toward the frames yet to be exposed as seen in the figure), and third, the trailing edge of the focal-plane-shutter slit of the camera exposing frame M-11 must at all times be in the same position rela-

The frames are arranged in three rows of eight frames each. Each frame includes two images of the combustion chamber; the lower of the two images is the one seen on the film in the camera exposing frame M-11, the upper of the two images is the one seen on the film in the camera exposing frame M-12. Inasmuch as the focal-plane shutters have been removed from the cameras, and the cameras are still cameras of the most elementary type, the same image appears on the film in both cameras at all times. Throughout the frames of row A and the first frame of row B the film in each camera is being exposed to an image just like that of frame M-10 (fig. I-5). At frame B-2 (fig. I-25) a detonation wave originates at the lower left corner of the visible portion of the chamber as indicated by the two white arrows in this frame. This wave travels across the chamber through the dark mottled combustion zone as seen on the film in each of the two cameras between frames B-2 and B-8. (The

detonation-wave front has been made straight for simplicity of construction of the animation; approximately the same effect would have resulted if the detonation-wave front had been spherical.) The gases behind the detonation-wave front are, of course, incandescent and the entire area that was formerly the dark mottled combustion zone consequently appears brilliant white in all of the frames after the detonation-wave front has completed its travel (frames B-8 to C-8).

Figure I-26 is an animation of the same kind as figure I-25 but shows the motion of the focal-plane shutter in each of the two cameras as well as the progress of the detonation wave. In frame A-1 of figure I-26 the focal-plane-shutter slit that will provide the exposure for the lower photograph (frame M-11 of fig. I-5) may be seen just to the left of the combustion-chamber image as a tall narrow-rectangle. Part of the focal-plane-shutter slit of the upper camera may also be seen in the upper part of frame A-1, with its leading edge exactly in line with the trailing edge of the focal-plane-shutter slit of the lower camera. Throughout the frames of row A the two focal-plane-shutter slits may be seen to move from left to right relative to the combustion-chamber images.

The lower focal-plane-shutter slit begins to pass across the lower combustion-chamber image at frame A-5. In this same frame the trailing edge of the lower focal-plane-shutter slit and the leading edge of the upper focal-plane-shutter

slit are each indicated by a white arrow and will be seen to be in line with each other as in all other frames of the figure. The focal-plane shutters are assumed to be constructed of a dark material that does not reflect light well; the combustion-chamber image consequently appears gray in all areas where it falls on the focal-plane-shutter material. In frames A-5 to A-8, however, part of the light that forms the lower combustion-chamber image passes through the focal-plane-shutter slit and falls on the photosensitive film; this film, being a bright material that reflects light well, causes the part of the image formed upon it to appear brilliant white in the animation. Hence, in frames A-5 to A-8 the brilliant white part of the picture shows the portion of the lower image uncovered by the focal-plane-shutter slit at each instant.

The lower focal-plane-shutter slit continues to pass across the lower combustion-chamber image from left to right in frames B-1 to B-8. At frame B-8 this slit has passed all the way across the lower image and the exposure of that image is completed. The upper focal-plane-shutter slit begins to pass across the upper combustion-chamber image at frame B-2, with its leading edge still exactly in line with the trailing edge of the lower focal-plane-shutter slit. The upper slit completes its travel across the upper combustion-chamber image at frame C-5, at which time the exposure of this image is complete.

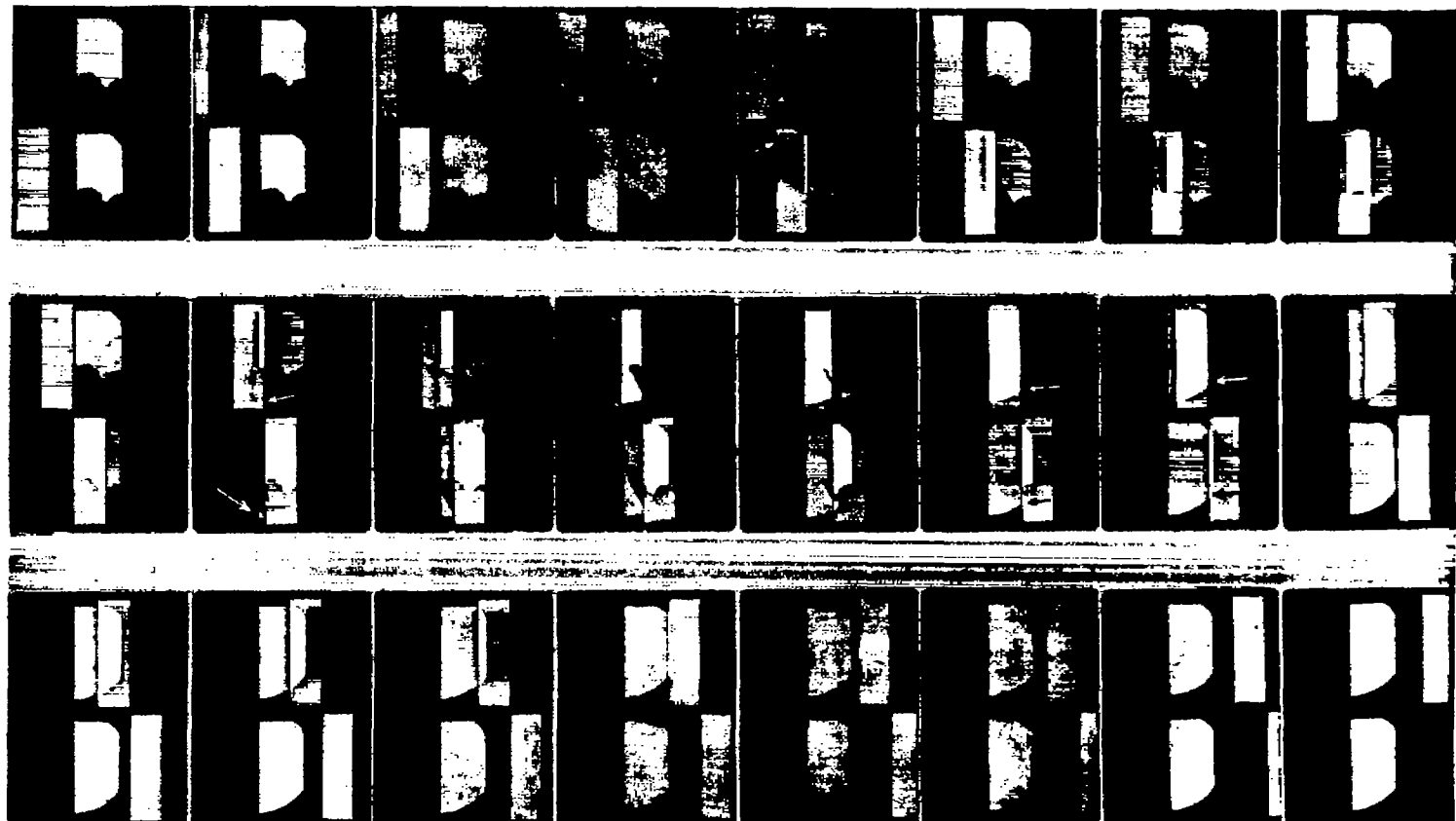


FIGURE I-26.—Animation showing travel of both detonation wave and focal-plane-shutter screen in two still cameras as they might appear if photographed at about 180,000 frames per second. Frames B-2 to B-8 of this figure correspond chronologically with exposure of frames M-11 and M-12 of figure I-5.

In frames B-2 to B-7 of figure I-26 the detonation-wave front may be seen traveling across the upper combustion-chamber image first just a little behind (as indicated by upper white arrow in frame B-2) and later just a little ahead of the leading edge of the upper focal-plane-shutter slit (as indicated by the white arrows in frames B-5, B-6, and B-7), but always quite close to the leading edge of the upper slit. In the same frames (B-2 to B-7) the detonation-wave front may be seen traveling across the lower combustion-chamber image at all times quite close to the trailing edge of the lower focal-plane-shutter slit, first a little behind (as indicated by lower white arrow, frame B-2) and later a little ahead (as indicated by black arrows in frames B-5, B-6, and B-7). As both lower and upper combustion-chamber images (frames M-11 and M-12 of figure I-5) are exposed entirely by light that passes through the upper and lower focal-plane-shutter slits, respectively, during their travel across the images, it is clear from frames B-2 to B-7 of figure I-26 that the upper image (frame M-12 of fig. I-5) when finally developed, will show incandescence over the entire area of the combustion chamber, whereas the lower image (frame M-11 of fig. I-5) will in the main show the same dark mottled combustion zone that is seen in frame M-10 of figure I-5. The only effect the detonation wave will have upon the lower combustion-chamber image (frame M-11 of fig. I-5), as finally developed, will be produced by that part of the detonation wave which travels across the chamber ahead of the trailing edge of the lower focal-plane-shutter slit in frames B-4 to B-7 of figure I-26. Examination of frames B-4 to B-7 shows a very small triangular region of luminosity of gradually increasing size (indicated by black arrows in frames B-5, B-6, and B-7) progressing along the lower right edge of the chamber from left to right. This very small triangular area of luminosity would, in the final developed photograph, produce the white streak along the lower right edge of the chamber, with gradually increasing brilliance toward the right, that is observed in frame M-11 of figure I-5.

In the exposure of frames M-11 and M-12 of figure I-5, the focal-plane-shutter slits moved at a speed of 256 feet per second. The linear dimensions of the actual combustion chamber were 21.5 times as large as those of the combustion-chamber image formed on the film. The detonation wave that produced the effect seen in frames M-11 and M-12 of figure I-5, in the manner illustrated in figures I-25 and I-26, must, therefore, have traveled across the combustion chamber at a speed greater than 6500 feet per second (with due allowance for the fact that the detonation-wave front traveled in a direction at an angle to the direction of motion of the focal-plane shutter.)

If the explosive knock reaction had occurred simultaneously throughout the end gas, as commonly supposed, its luminosity would simply have recorded the relative positions of the trailing edges of the upper and lower focal-plane-shutter slits, consequently the luminosity as seen in frame M-12 of figure I-5 would have extended farther to the left than

the luminosity as seen in frame M-11 by an amount not greater than the width of the focal-plane-shutter slit. The fact that the luminosity visible in frame M-12 extends to the left of the luminosity visible in frame M-11 by an amount greater than the width of the focal-plane-shutter slit precludes the possibility that the luminosity developed simultaneously throughout the chamber. No satisfactory explanation of the appearance of frames M-11 and M-12 of figure I-5 has been advanced other than the explanation illustrated in figures I-25 and I-26. If due consideration is given to the fact that the luminosity visible throughout frame M-12 is quite uniform, and is less than the saturation limit of the photosensitive film, it would seem that each part of frame M-12 must have had about the same exposure to the detonation luminosity and the conditions governing the exposure of the two frames (M-11 and M-12) would, therefore, seem to be mathematically determinate. For these reasons the author believes that the explanation illustrated in figures I-25 and I-26 is the only reasonable explanation of the appearance of these frames.

The effect of the focal-plane shutters of the high-speed camera on apparent velocities of detonation waves is easily shown (reference 10) to comply with the following equation:

$$V = \frac{v V'}{v + V' \cos \alpha}$$

where V is the actual speed of the wave, v the speed of the focal-plane shutter slits, V' the apparent velocity of the wave (progress of the wave between two successive frames, as recorded photographically, divided by nominal time between exposures of the successive frames), and α the angle between the direction of motion of the detonation-wave front and the direction of motion of the focal-plane-shutter slits. (Due regard must be had for the signs of V , V' , and α , as explained in reference 10.) Application of this equation to the case of figure I-27 has given propagation speeds in the neighborhood of 4500 feet per second to the points p_1, p_2, \dots, p_8 from the point of origin of the knock disturbance (calculated to be at the intersection of line C-C with lines C'-C'). (Fig. I-27 is the same as fig. 7 of reference 10. The complete photographic series and complete treatment are presented in the original paper. The complete photographic series of this combustion process also appears as fig. 8 in reference 5. The engine-operating conditions for this figure were the same as for fig. I-4 of the present paper.)

No correcting equation is required to determine the true detonation-wave velocity from figure I-28, because the front of the detonation wave may be located in three successive frames of this figure at points p_{17}, p_{18} , and p_{19} (wave front position indicated by a bright spot at p_{19}) along a line D-D, which is at right angles to the direction of motion of the focal-plane shutter. The complete treatment of this case (reference 10) yields a value between 3250 and 3400 feet per second for the speed of the detonation wave. (Fig. I-28

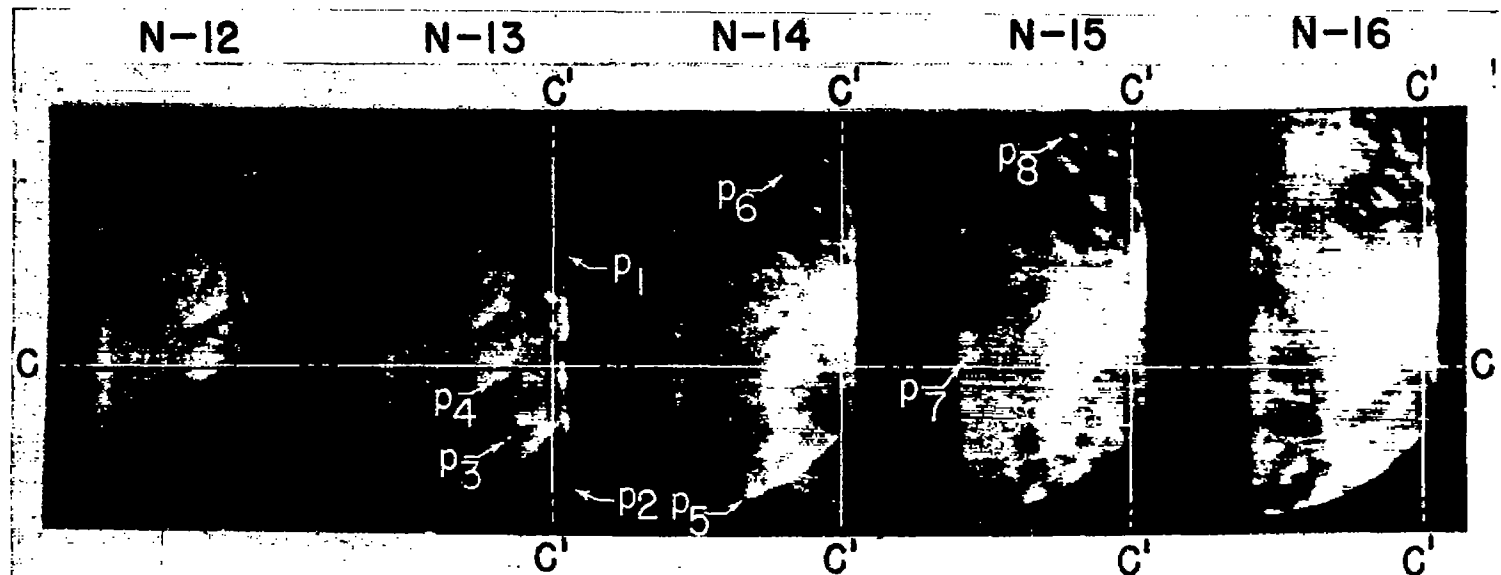


FIGURE I-27.—High-speed photographs of development of incandescent spots caused by detonation wave in knocking spark-ignition engine. Fuel, 50 percent S-1 with 50 percent M-2; compression ratio, 7.0; fuel-air ratio, about 0.08; atmospheric intake; spark plug at top; hot spot at bottom; spark timing, 20° B. T. C.; detonation-wave speed, about 4500 feet per second.

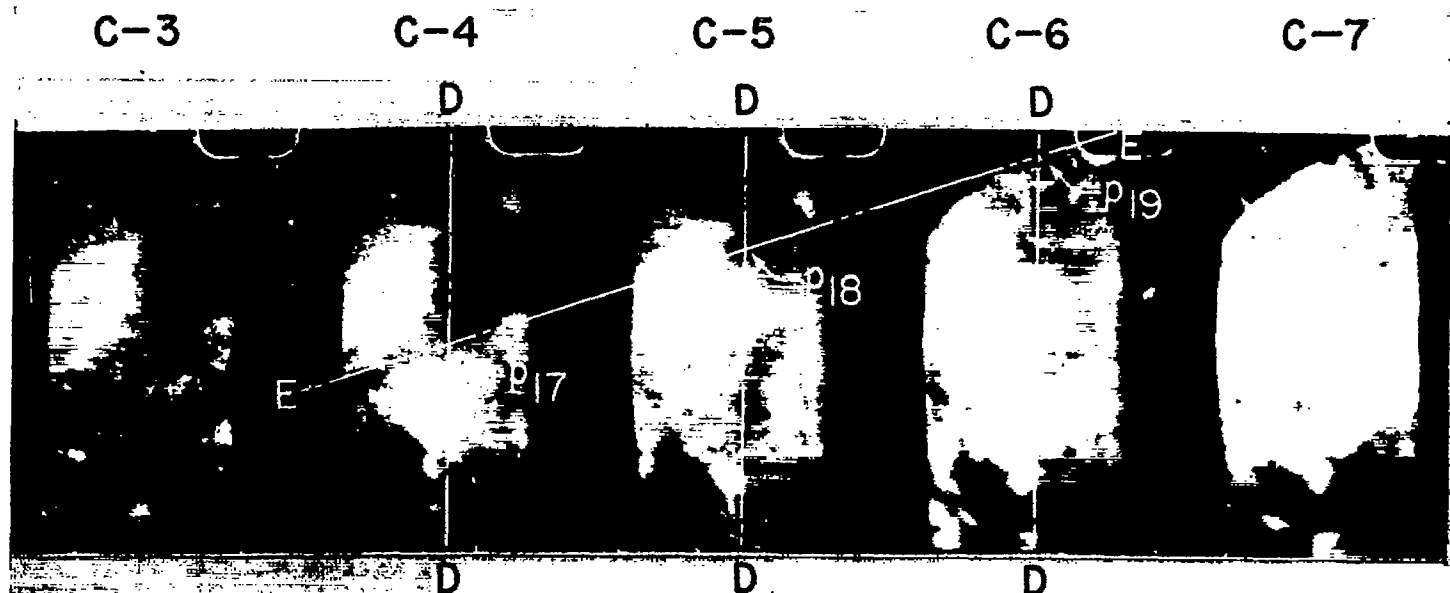


FIGURE I-28.—High-speed photographs of development of luminous area and incandescent spots caused by detonation wave in knocking spark-ignition engine. Fuel, M-1; compression ratio, 7.0; fuel-air ratio, about 0.08; atmospheric intake; four spark plugs; spark timing, for left-hand plug, 27° B. T. C., for other three plugs, 20° B. T. C.; detonation-wave speed, about 3300 feet per second.

is the same as fig. 13 of reference 10. Additional frames of the series are shown in fig. 12 of that paper as well as in fig. 10 of reference 6. The engine-operating conditions were the same as for fig. I-10 of the present paper except that M-1 reference fuel was used.)

Application of the correcting equation to the explosive knock reactions seen in frame G-12 of figure I-10 and frames G-11 and G-12 of figure I-12 has yielded values in the neighborhood of 6000 and 3600 feet per second, respectively (reference 10). The correcting equation, as well as the qualitative treatment illustrated in figures I-25 and I-26,

yields a value of about 7300 feet per second for the reaction that occurred between frames C-1 and C-2 of figure I-18 after the runaway flame had completed its travel across the chamber. Between these two frames the entire combustion chamber changed from a fairly uniform, dark mottled condition to a fairly uniform white condition. (This change was more evident on the original negative than it is in the printed reproduction. The entire series of photographs was badly underexposed and in copying some of the contrast between frames C-1 and C-2 was lost in order that the frames of rows A and B might be brought out more clearly.) A

uniform change throughout the combustion chamber from a dark mottled condition to a white condition between one frame and the next corresponds to an infinite apparent detonation-wave speed, that is, an infinite value of V' . With an infinite value of V' the correcting equation indicates that the actual detonation-wave velocity is equal to the focal-plane shutter velocity, and in the same direction. Consideration of figure I-26 indicates that a uniform change throughout the combustion chamber would be produced if the detonation wave traveled across the chamber in the same direction and at the same speed as the focal-plane-shutter slit rather than at a slight angle to the direction of motion of the slit and at a slightly higher speed. (The white streak along the lower right edge of the chamber in frame M-11 of fig. I-5 would have been absent if the detonation-wave front had not overtaken the trailing edge of the lower focal-plane-shutter slit at about frame C-19 in fig. I-26 and had not traveled across the chamber slightly ahead of this trailing edge in frames C-19 to D-21; the combustion zone would have been uniformly dark in frame M-11 (fig. I-5) and uniformly white in frame M-12.) For the case of figure I-18 the focal-plane-shutter slits traveled at 251 feet per second in a direction approximately opposite to the travel of the runaway flame in frames B-1 to C-1. The actual linear dimensions of the combustion chamber were 29.2 times as great as the dimensions of the combustion-chamber image. The appearance of figure I-18, therefore, indicates that after the runaway flame completed its travel through the end gas in one direction at about 1900 feet per second a detonation wave passed through the gas in the opposite direction at about 7300 feet per second.

Confirmation of detonation-wave aspect of knock by ultra-high-speed photographs.—Only one motion picture of the knock phenomenon taken with the ultra-high-speed camera (reference 3) is available. This one motion picture, however, taken at the rate of 200,000 frames per second, is confirmatory of the conclusions reached from study of the high-speed photographs taken at 40,000 frames per second. It has not been possible to take more than a very few photographic shots with the ultra-high-speed camera because the high-speed rotating part of the camera, operating in a high vacuum, spatters oil on the 94 glass lenses of the camera to such an extent that the lenses become inoperative after only a few runs. Of 5 or 6 shots that were actually taken at 200,000 frames per second, only one happened to be taken at the right time to cover the knock phenomenon. Further developmental work on the ultra-high-speed camera, which is still proceeding, has been directed toward elimination of the oil-spattering problem.

The ultra-high-speed photographs are shown as a series of 20 still pictures in figure I-29. The combustion process for this series of photographs was fired in the old combustion apparatus with one spark plug in G position (fig. I-1), at

27° B. T. C. The injection valve was at opening J (fig. I-1); the fuel was a blend of 70 percent S-3 with 30 percent M-2 reference fuels; compression ratio, 7.0; and fuel-air ratio, about 0.08. Figure I-29 was previously published as figure 4 in reference 11 and was discussed in that paper more extensively than it will be here.

Before frame A-1 of figure I-29 was exposed the flame had traveled all the way across the chamber in the direction of the arrow that has been drawn in this frame. The whitish area in frames A-1 to A-5, designated B in frame A-3, represents the region in which combustion is complete. The dark (nearly black) areas in these frames, designated F in frame A-3, are the dark mottled combustion zone that has become quite familiar in the high-speed photographs of the earlier figures. The series of figure I-29 did not begin early enough to determine whether any autoignition occurred in this combustion process, but at least at the time of exposure of frame A-1 the entire charge was ignited with the exception of possible small pockets in front of or behind the flame. The boundary between the dark and the light areas, designated R in frame A-2 of the figure, is the *rear* edge of the combustion zone—not the flame front.

The ultra-high-speed camera does not have the focal-plane-shutter effect of the high-speed camera, but has in effect a conventional between-the-lens type of shutter. The exposure time of each frame is roughly the same as the time between successive frames, 5 microseconds, although there is a slight overlapping of exposures, as specified in reference 11. The series of figure I-29 is, therefore, truly representative of events as they occurred in the combustion chamber. Examination of frames A-1 to B-1 of the figure reveals no appreciable change of conditions. Frames A-2, A-4, and B-1 are much more sharply defined than frames A-1, A-3, and A-5. This effect, however, is introduced by the camera and has no significance relative to the burning processes. This alternate blurring of frames can be eliminated in further work with the camera. The first significant change in appearance of the photographs occurs in the area designated by the two arrows in frame B-2. This light area is not present in any of the preceding frames. If this area in frame B-2 is compared with the same area in frame B-1, more difference will be noted than in a like comparison of frame B-1 with frame A-1, five frames preceding. In frames B-3 and B-4, the effect of the knock spreads considerably in all directions from the point of origin. The location of the point of origin at the *rear* edge of the combustion zone is strikingly confirmatory of the conclusion reached from study of the 40,000-frame-per-second photographs that the explosive knock reaction apparently originates in the burning gases rather than in the unignited end gas.

Frames B-1 to B-5 of figure I-29 are reproduced in figure I-30. In figure I-30, however, a black line (R_{B-1}) has been drawn in frame B-1 reinforcing the boundary line between

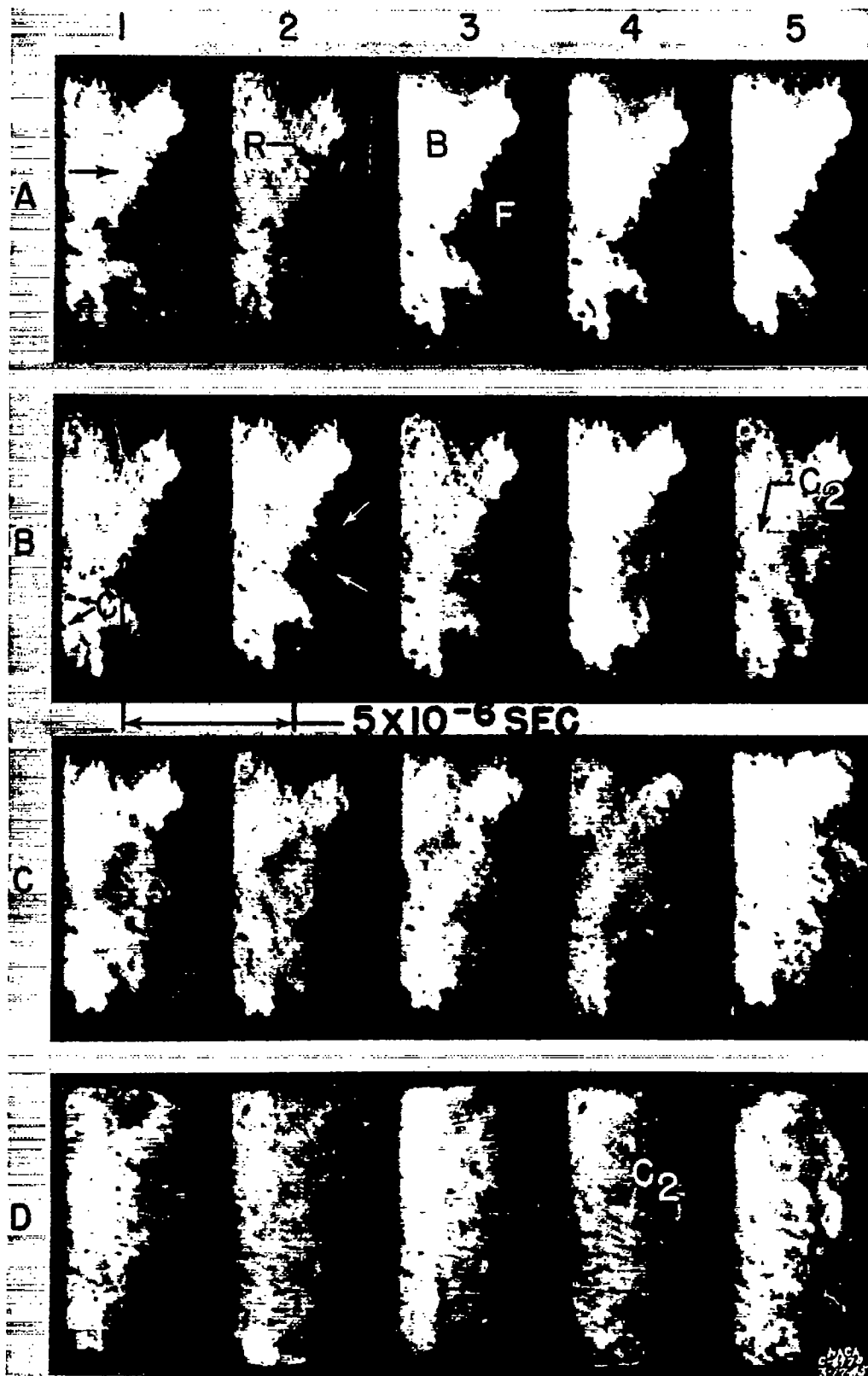


FIGURE I-29.—Ultra-high-speed photographs (200,000 frames per sec) of phenomenon of knock in spark-ignition engine. Fuel, 70 percent S-3 with 30 percent M-2; compression ratio, 7.0; fuel-air ratio, about 0.08; atmospheric intake; one spark plug in G position (fig. I-1); spark timing, 27° B. T. C.

the dark combustion zone on the right and the white burned region on the left. In frames B-2 to B-5 of this figure the same black line has been constructed in each frame, not marking the boundary between burned and unburned as it appears in frames B-2 to B-5 but the boundary as it appeared in frame B-1. In each of the frames B-2 to B-5 two horizontal black lines have been drawn marking the upper and lower extents of the knocking reaction in each frame as indicated by the whitening of the combustion zone to the right of the boundary line R_{B-1} . Distances between the horizontal lines have been designated in each frame as l_2 , l_3 , and so on. Treating the difference between successive values of l as representing the combined upward and downward travel of the knocking disturbance between successive frames (l_1 assumed equal to zero), the following values have been obtained for the speed of the knock disturbance according to the equation:

$$V = \frac{1}{2} \left(\frac{l_2 - l_1}{5 \times 10^{-6}} \right)$$

Frames	Velocity of knocking disturbance (ft/sec)
1 to 2	9200
2 to 3	4200
3 to 4	6900
4 to 5	1200

The average of the first three values is nearly 6800 feet per second, which is of the same order as the higher speeds

determined from the high-speed photographs and the speed of 2000 meters per second determined by Sokolik and Vojinov in reference 18.

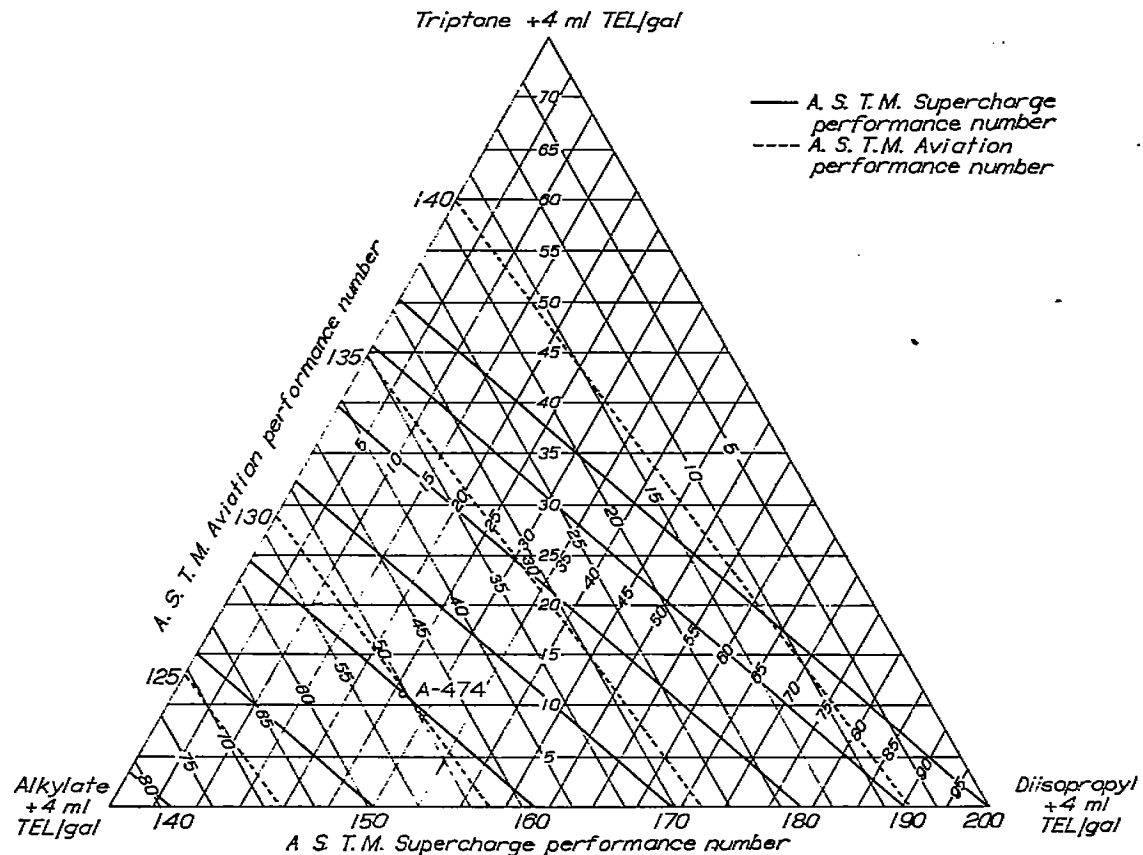
After frame B-4 of figure I-29 the ultra-high-speed photographs no longer show a high speed of propagation of the knock reaction. The portion of the black combustion zone that is still visible in frame B-5 gradually disintegrates throughout the frames of rows C and D, leaving a great many black dots and streaks, which will be discussed later. It is thought either that the areas that still appear black in frame B-5 represent gases that were not in a sufficiently advanced state of combustion to be detonable or that they represent a high concentration of carbon particles resulting from the knock reaction.

Chemical nature of explosive knock reaction.—The high-speed and ultra-high-speed photographs, because of their inherent nature, should not be expected to yield much information concerning the chemical nature of the explosive knock reaction. Two indications have been obtained, however, that may be of the most fundamental importance relative to the chemical nature of the reaction; first, the indication that the reaction results in a definite loss of chemical energy that would otherwise be available, and second, the indication that free carbon is released by the explosive knock reaction. Both of these indications forcibly recall the opinion expressed by Midgley in 1920 (reference 14) that the knocking detonation wave burns only the hydrogen in the hydrocarbon molecule and releases free carbon.

B-1 B-2 B-3 B-4 B-5

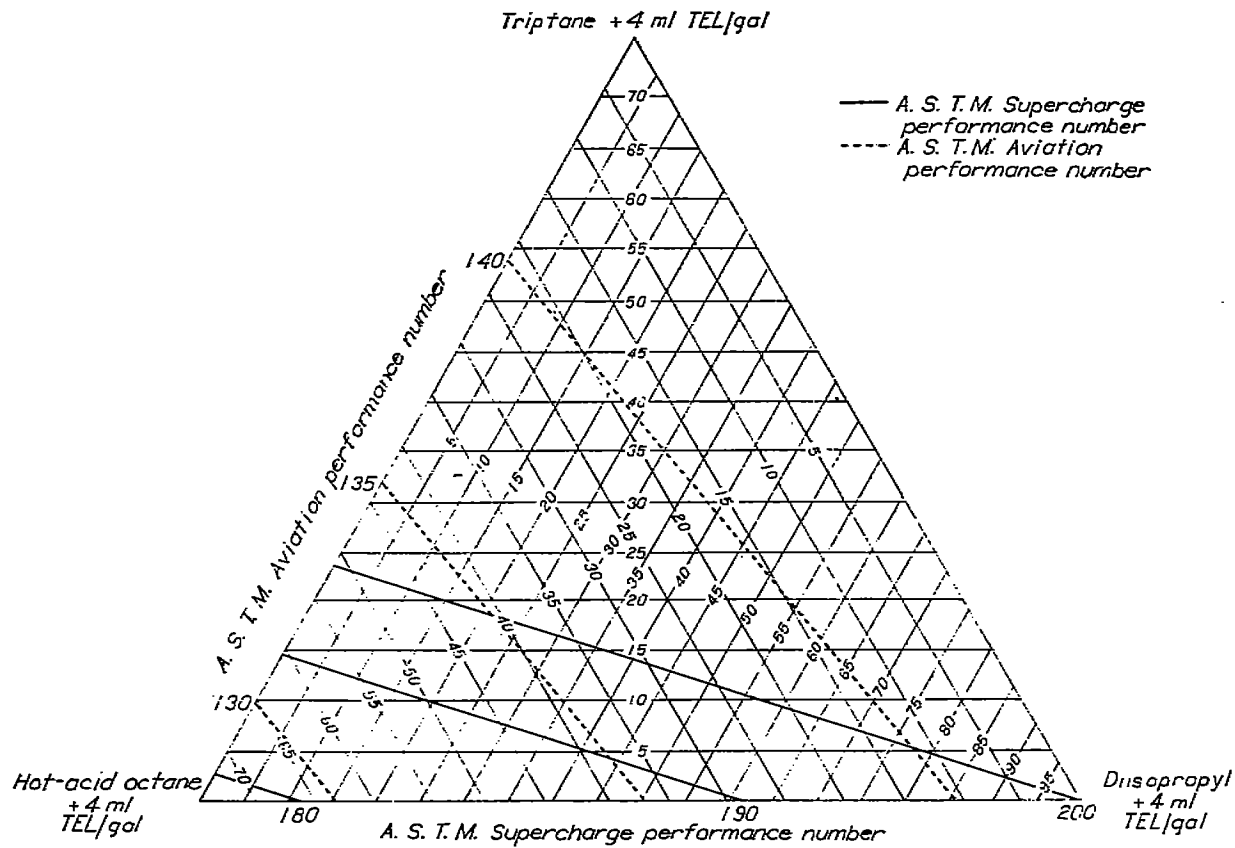


FIGURE I-30.—Frames from figure I-29 outlining actual detonation-wave travel. Detonation-wave speed, about 6800 feet per second both upward and downward from point of origin.



(b) Blends of triptane, aviation alkylate, diisopropyl, and isopentane.

FIGURE VIII-18.—Continued. Blending charts for quaternary blends by A. S. T. M. Aviation and A. S. T. M. Supercharge methods. Reid vapor pressure, approximately 7 pounds per square inch; A. S. T. M. Supercharge fuel-air ratio, 0.1L (Fig. 12 of reference 12.) Percentage isopentane can be determined by subtracting sum of percentages of other components from 100.



(c) Blends of triptane, hot-acid octane, diisopropyl, and isopentane.

FIGURE VIII-18.—Continued. Blending charts for quaternary blends by A. S. T. M. Aviation and A. S. T. M. Supercharge methods. Reid vapor pressure, approximately 7 pounds per square inch; A. S. T. M. Supercharge fuel-air ratio, 0.1L (Fig. 12 of reference 12.) Percentage isopentane can be determined by subtracting sum of percentages of other components from 100.

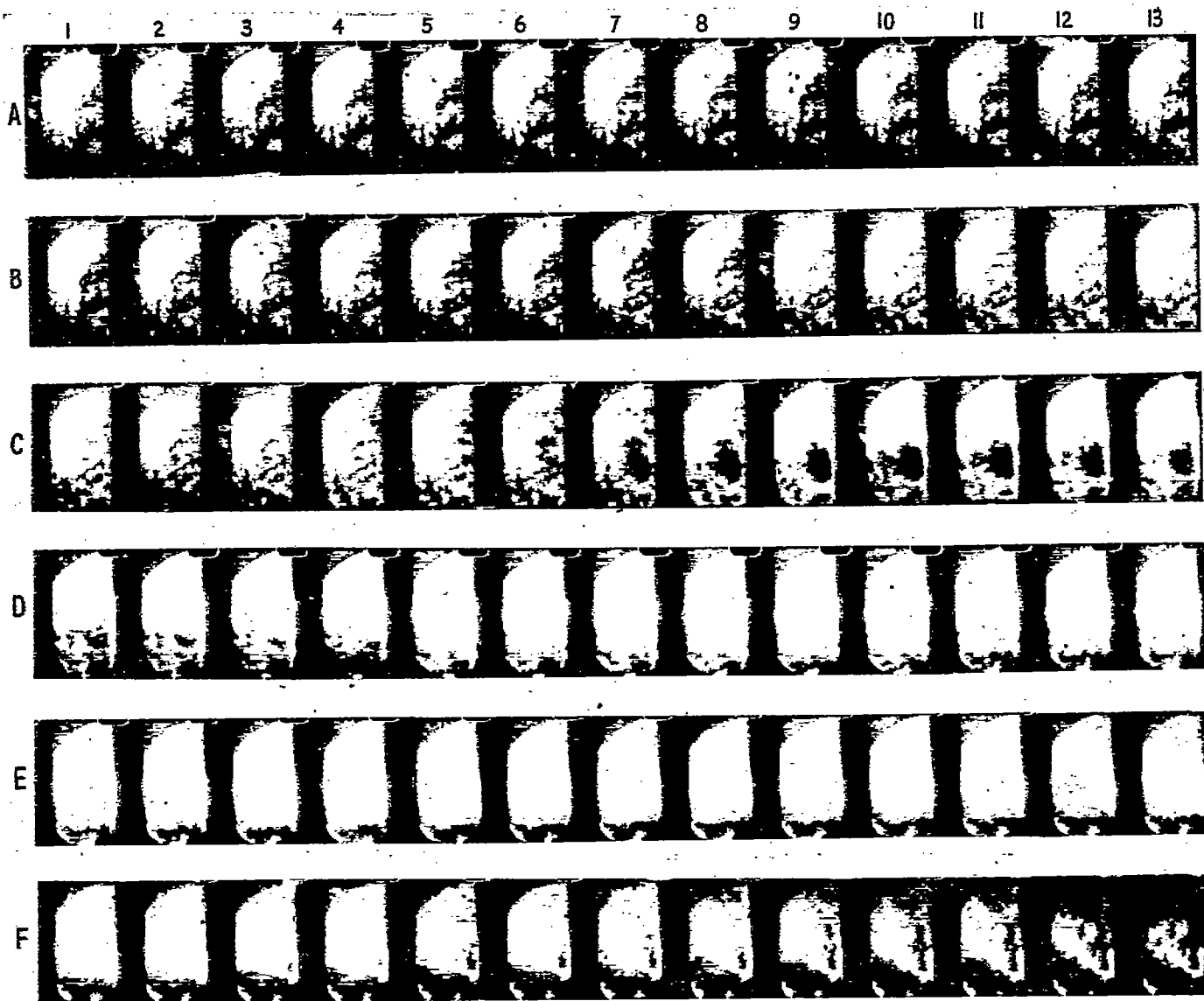


FIGURE I-32.—High-speed photographs showing formation of black carbon cloud immediately after knock in spark-ignition engine and later reversal of carbon cloud from black to white. Fuel, M-1; compression ratio, 7.0; fuel-air ratio, about 0.08; atmospheric intake; four spark plugs; spark timing, for left-hand plug, 27° B. T. C., for other three plugs, 20° B. T. C.

between frames A-1 and C-3. The explosive knock reaction begins at frame C-4, as indicated by blurring of parts of the mottled combustion zone. A large black spot is very evident in frames C-7 to C-13 of the figure. Careful inspection of frames C-5 and C-6 reveals that this black spot was beginning to develop in these frames. Between frames D-1 and D-4 the black spot becomes incandescent; in frame D-4 most of the spot is sufficiently incandescent to match the other parts of the combustion chamber. (Non-uniform illumination of the chamber by the externally supplied light is the probable reason why the lowest 20 percent of the chamber is much less brilliant than the upper parts of the chamber in these frames.) In frames D-5 and D-6 the formerly black spot becomes sufficiently incandescent so that it stands out whiter than the surrounding gases. Between frames D-6 and F-13 parts of this formerly black spot become more and more white as compared with the other gases in the chamber; other parts of the spot apparently cool again and become dark. There is, of course, some gradual change of shape of the spot throughout these frames.

Frames D-6 to about F-8 of figure I-32 have been re-etched

by the engraver to bring out the whiteness of the carbon cloud in contrast with the surrounding gases that are only slightly less white. This re-etching has been done only in order to make the printed reproduction look as nearly as possible like the original untouched photograph in print. Similarly, it was necessary to re-etch several other illustrations to emphasize details that are clearly visible in the photographs but that would have been quite hazy because of the half-tone screen used in the engraving process.

The small spots seen in figures I-27 and I-29, and the large spot in figure I-32, are probably not the only aspect of the free carbon released by the explosive knock reaction. Most of the photographs of heavy knock have shown a very great increase in the general luminosity of the chamber at the time of the explosive knock reaction, amounting in many cases to perhaps a hundredfold increase. This uniform increase in luminosity is probably due to finely divided free carbon. The change is by no means limited to the end gas; it appears to occur throughout the chamber and, if it is concentrated anywhere, it is concentrated at the chamber walls rather than in the end gas. This fact,

together with certain other features of figure I-29 (sec reference 11), suggests that the explosive knock reaction may travel through the burned gases in the same manner as the burning gases; such a revolutionary conclusion probably should not be taken very seriously, however, until considerably more evidence is available.

Summary of findings of NACA photographic knock investigations.—The findings of the NACA photographic knock investigations at speeds of 40,000 and 200,000 frames per second over the period from 1939 to 1946 may be summarized as follows:

1. The photographs have shown that normal nonknocking combustion involves an entirely smooth travel of the flames through the combustion chamber and a smooth gradual fadeout of the combustion zones after completion of the flame travel through the chamber.

2. The photographs have indicated that normal combustion involves a zone of continuing combustion behind the flame front with a depth measured in tenths of an inch; the combustion zone, however, may have a cellular structure.

3. The photographs have shown that preignition from a hot spot is not a direct cause of knock and that the flame from a hot spot is similar to the flame from a spark plug.

4. Vibratory knock has been shown to involve an extremely fast reaction, termed the "explosive knock reaction" herein, which develops suddenly after a period of normal burning. This reaction involves a time interval not greater than 50 microseconds.

5. The explosive knock reaction has been shown to begin within 25 microseconds of the same time as the violent knocking vibrations shown by a piezoelectric pickup placed in the end zone of the combustion chamber.

6. The photographs have indicated that the explosive knock reaction originates only in a portion of gas that is already ignited, either by normal flame travel or by autoignition.

7. The photographs have shown a number of different types of end-gas autoignition, some of which appear always to be followed by the explosive knock reaction and some of which may occur without being followed by the explosive knock reaction. The photographs have also shown cases of the explosive knock reaction not preceded by any form of autoignition.

8. Analysis of the photographs taken at 40,000 frames per second has indicated that the explosive knock reaction is a type of detonation wave traveling, under different conditions, at speeds ranging approximately from 3000 to 6500 feet per second or from about one to two times the speed of sound in the burned gases.

9. The propagation speed of the order of 6500 feet per second for the explosive knock reaction has been confirmed by the one series of photographs obtained at 200,000 frames per second.

10. A definite loss of chemical energy that would otherwise have been available has been shown to result from the explosive knock reaction.

11. The photographs have shown that free carbon is released in both the burning and the burned gases within 10 microseconds after passage of the detonation wave associated with the explosive knock reaction.

The indications of the high-speed and ultra-high-speed photographs do not harmonize with the simple autoignition theory of knock or with the simple detonation-wave theory. They appear rather to support the combined detonation-wave and autoignition theory proposed in the literature discussion that forms the first part of this paper.

REFERENCES

1. Miller, Cearey D.: High-Speed Camera. U. S. Patent Office No. 2,400,885, May 28, 1946.
2. Miller, Cearey D.: The NACA High-Speed Motion-Picture Camera. Optical Compensation at 40,000 Frames per Second. NACA Rep. 856, 1948.
3. Miller, Cearey D.: High-Speed Motion-Picture Camera. U. S. Patent Office No. 2,400,887, May 28, 1946.
4. Miller, Cearey D.: Slow-Motion Study of Injection and Combustion of Fuel in a Diesel Engine. SAE Jour. (Trans.), vol. 53, no. 12, Dec. 1945, pp. 719-733; discussion, pp. 733-735.
5. Rothrock, A. M., Spencer, R. C., and Miller, Cearey D.: A High-Speed Motion-Picture Study of Normal Combustion, Knock, and Preignition in a Spark-Ignition Engine. NACA Rep. 704, 1941.
6. Miller, Cearey D.: A Study by High-Speed Photography of Combustion and Knock in a Spark-Ignition Engine. NACA Rep. 727, 1942.
7. Miller, Cearey D., and Olsen, H. Lowell: Identification of Knock in NACA High-Speed Photographs of Combustion in a Spark-Ignition Engine. NACA Rep. 761, 1943.
8. Brun, Rinaldo J., Olsen, H. Lowell, and Miller, Cearey D.: End-Zone Water Injection as a Means of Suppressing Knock in a Spark-Ignition Engine. NACA RB E4127, 1944.
9. Miller, Cearey D., and Logan, Walter O., Jr.: Preknock Vibrations in a Spark-Ignition Engine Cylinder as Revealed by High-Speed Photography. NACA Rep. 785, 1944.
10. Miller, Cearey D.: Relation between Spark-Ignition Engine Knock, Detonation Waves, and Autoignition as Shown by High-Speed Photography. NACA Rep. 855, 1946.
11. Miller, Cearey D., Olsen, H. Lowell, Logan, Walter O., Jr., and Osterstrom, Gordon E.: Analysis of Spark-Ignition Engine Knock as Seen in Photographs Taken at 200,000 Frames per Second. NACA Rep. 857, 1946.
12. Miller, Cearey D.: Relation of Detonation Wave to Spark-Ignition Engine Knock in Ultra-Slow Motion. NACA Tech. Film, 1946.
13. Clerk, Dugald: Cylinder Actions in Gas and Gasoline Engines. SAE Jour., vol. 8, no. 6, June 1921, pp. 523-539.
14. Midgley, Thomas, Jr.: Combustion of Fuels in the Internal-Combustion Engine. SAE Jour., vol. 7, no. 6, Dec. 1920, pp. 489-497.
15. Maxwell, G. B., and Wheeler, R. V.: Some Flame Characteristics of Motor Fuels. Ind. and Eng. Chem., vol. 20, no. 10, Oct. 1928, pp. 1041-1044.
16. Maxwell, G. B., and Wheeler, R. V.: Flame Characteristics of "Pinking" and "Non-Pinking" Fuels. Part II. Jour. Inst. Petroleum Tech., vol. 15, no. 75, Aug. 1929, pp. 408-415.
17. Egerton, A., Smith, and Ubbelohde, A. R.: Estimation of the Combustion Products from the Cylinder of the Petrol Engine and Its Relation to "Knock". Phil. Trans. Roy. Soc. (London), vol. 234, ser. A, July 30, 1935, pp. 433-521.
18. Sokolik, A., and Voinov, A.: Knocking in an Internal-Combustion Engine. NACA TM 928, 1940.
19. Boerlage, G. D.: Detonation and Autoignition. Some Considerations on Methods of Determination. NACA TM 843, 1937.
20. Draper, C. S.: The Physical Effects of Detonation in a Closed Cylindrical Chamber. NACA Rep. 498, 1934.
21. Withrow, Lloyd, and Rassweiler, Gerald M.: Engine Knock. The Auto. Eng., vol. XXIV, no. 322, Aug. 1934, pp. 281-284.
22. Grinstead, C. E.: Sound and Pressure Waves in Detonation. Jour. Aero. Sci., vol. 6, no. 10, Aug. 1939, pp. 412-417.
23. Rothrock, A. M., Miller, Cearey D., and Spencer, R. C.: Slow Motion Study of Normal Combustion, Preignition, and Knock in a Spark-Ignition Engine. NACA Tech. Film 14, 1940.

24. Leary, W. A., and Taylor, E. S.: The Significance of the Time Concept in Engine Detonation. NACA ARR, Jan. 1943.

25. Ricardo, H. R.: Paraffin as Fuel. The Auto. Eng., vol. IX, no. 2, Jan. 1919, pp. 2-5.

26. Woodbury, C. A., Lewis, H. A., and Canby, A. T.: The Nature of Flame Movement in a Closed Cylinder. SAE Jour., vol. VIII, no. 3, March 1921, pp. 209-218.

27. Mallard, et Le Chatelier: Recherches expérimentales et théoriques sur la combustion des mélanges gazeux explosifs. Deuxième mémoire sur la vitesse de propagation de la flamme dans les mélanges gazeux. Ann. des Mines, T. IV, Sér. 8, 1883, pp. 296-378.

28. Withrow, Lloyd, and Rassweiler, Gerald M.: Slow Motion Shows Knocking and Non-Knocking Explosions. SAE Jour., vol. 39, no. 2, Aug. 1938, pp. 297-303, 312.

29. Serruys, Max: Mécanique appliquée.—Calcul d'une limite supérieure de la durée de la détonation dans les moteurs à explosion et explication de la présence d'une lacune dans les diagrammes fournis par certains manographes électriques. Comptes Rendus, T. 197, Mai 30, 1932, pp. 1894-1896.

30. Serruys, Max: Mécanique appliquée.—Enregistrement des manifestations piezométriques consécutives au cognement dans les moteurs à explosion. Comptes Rendus, T. 197, Nov. 27, 1933, pp. 1296-1298.

31. Dixon, Harold B.: The Initiation and Propagation of Explosions. Jour. Chem. Soc. Trans. (London), vol. XCIX, pt. I, 1911, pp. 588-598.

32. Dixon, Harold B., Bradshaw, Laurence, and Campbell, Colin: The Firing of Gases by Adiabatic Compression. Part 1. Photographic Analysis of the Flame. Jour. Chem. Soc. Trans. (London), vol. CV, pt. II, 1914, pp. 2027-2035.

33. Withrow, Lloyd, and Boyd, T. A.: Photographic Flame Studies in the Gasoline Engine. Ind. and Eng. Chem., vol. 23, no. 5, May 1931, pp. 539-547.

34. Rassweiler, Gerald M., and Withrow, Lloyd: Emission Spectra of Engine Flames. Ind. and Eng. Chem., vol. 24, no. 5, May 1932, pp. 528-538.

35. Boyd, T. A.: Engine Flame Researches. SAE Jour., vol. 45, no. 4, Oct. 1939, pp. 421-432.

36. Withrow, Lloyd, and Rassweiler, Gerald M.: Spectroscopic Studies of Engine Combustion. Ind. and Eng. Chem., vol. 23, no. 7, July 1931, pp. 769-776.

37. Rassweiler, Gerald M., and Withrow, Lloyd: Spectrographic Detection of Formaldehyde in an Engine Prior to Knock. Ind. and Eng. Chem., vol. 25, no. 12, Dec. 1933, pp. 1359-1366.

38. Rassweiler, Gerald M., and Williams, Lloyd: Two Knocks in a Single Explosion. The Auto. Eng., vol. XXIV, no. 324, Oct. 1934, pp. 385-388.

39. Duchene, R.: Combustion of Gaseous Mixtures. NACA TM 694, 1932.

40. Anon.: The Chemical Background for Engine Research, R. E. Burk, and Oliver Grummitt, eds. Vol. 2. Interscience Pub., Inc. (New York), 1943, pp. 165-234.

41. Schnauffer, Kurt: Engine-Cylinder Flame-Propagation Studied by New Methods. SAE Jour., vol. 34, no. 1, Jan. 1934, pp. 17-24.

42. Hastings, Charles E.: Ionization in the Knock Zone of Internal-Combustion Engine. NACA TN 774, 1940.

43. Schnauffer, Kurt: Das Klopfen von Zündermotoren. VDI Zeitschr., Bd. 75, Nr. 15, April 11, 1931, S. 455-456.

44. Souders, Mott, Jr., and Brown, Geo. Granger: Gaseous Explosions. VIII—Effect of Tetraethyl Lead, Hot Surfaces, and Spark Ignition on Flame and Pressure Propagation. Ind. and Eng. Chem., vol. 21, no. 12, Dec. 1929, pp. 1261-1268.

45. Boerlage, G. D., Broeze, J. J., van Driel, H., and Peletier, L. A.: Detonation and Stationary Gas Waves in Petrol Engines. Engineering, vol. CXLIII, no. 3712, March 5, 1937, pp. 254-255.

46. Rothrock, A. M., and Spencer, R. C.: A Photographic Study of Combustion and Knock in a Spark-Ignition Engine. NACA Rep. 622, 1938.

47. Hunn, J. V., and Brown, George Granger: Gaseous Explosions. VI—Flame and Pressure Propagation. Ind. and Eng. Chem., vol. 20, no. 10, Oct. 1928, pp. 1032-1040.

48. Kirkby, William Anthony, and Wheeler, Richard Vernon: Explosives in Closed Cylinders. Part I. Methane-Air Explosions in a Long Cylinder. Part II. The Effect of the Length of Cylinder. Jour. Chem. Soc. Trans. (London), pt. 2, 1928, pp. 3203-3214.

49. Lorentzen, Jørgen: Zur Erklärung des Klopfens in den Vergasermotoren und der Wirkung der Antiklopfmittel. Zeitschr. f. angew. Chem., Jahrg. 44, Nr. 7, Feb. 14, 1931, S. 130-136.

50. Wawrziniok: Pressure Rise, Gas Vibrations and Combustion Noises During the Explosion of Fuels. NACA TM 711, 1933.

51. Köchling, A.: Versuche zur Aufklärung des Klopfvorganges. VDI Zeitschr., Bd. 82, Nr. 39, Sept. 24, 1938, S. 1126-1134.

52. Maxwell, G. B., and Wheeler, R. V.: Flame Characteristics of "Pinking" and "Non-Pinking" Fuels. Jour. Inst. Petroleum Tech., vol. 14, April 1928, pp. 175-189.

53. Payman, W., and Titman, H.: Explosion Waves and Shock Waves. III—Initiation of Detonation in Mixtures of Ethylene and Oxygen and of Carbon Monoxide and Oxygen. Proc. Roy. Soc. (London), vol. 152, no. 876, ser. A, Nov. 1, 1935, pp. 418-445.

54. Stevens, F. W.: Constant Pressure Bomb. NACA Rep. 176, 1923.

55. Stevens, F. W.: The Gaseous Explosive Reaction—The Effect of Inert Gases. NACA Rep. 280, 1927.

56. Stevens, F. W.: The Gaseous Explosive Reaction—The Effect of Pressure on the Rate of Propagation of the Reaction Zone and upon Rate of Molecular Transformation. NACA Rep. 372, 1930.

57. Stevens, F. W.: The Rate of Flame Propagation in Gaseous Explosive Reactions. Jour. Am. Chem. Soc., vol. 48, no. 7, July 1926, pp. 1896-1906.

58. Stevens, F. W.: The Gaseous Explosive Reaction—A Study of the Kinetics of Composite Fuels. NACA Rep. 305, 1929.

59. Lewis, Bernard, and von Elbe, Guenther: On the Question of "Afterburning" in Gas Explosions. Jour. Chem. Phys., vol. 2, no. 10, Oct. 1934, pp. 659-664.

60. Randolph, D. W., and Silsbee, F. B.: Flame Speed and Spark Intensity. NACA Rep. 187, 1924.

61. Withrow, Lloyd, Lovell, W. G., and Boyd, T. A.: Following Combustion in the Gasoline Engine by Chemical Means. Ind. and Eng. Chem., vol. 22, no. 9, Sept. 1930, pp. 945-951.

62. Rassweiler, Gerald M., and Withrow, Lloyd: Motion Pictures of Engine Flames Correlated with Pressure Cards. SAE Jour., vol. 42, no. 5, May 1938, pp. 185-204.

63. Rassweiler, Gerald M., Withrow, Lloyd, and Cornelius, Walter: Engine Combustion and Pressure Development. SAE Jour., vol. 46, no. 1, Jan. 1940, pp. 25-48.

64. Withrow, Lloyd, and Cornelius, Walter: Effectiveness of the Burning Process in Non-Knocking Engine Explosions. SAE Jour., vol. 47, no. 6, Dec. 1940, pp. 526-545.

65. Linder, Werner: Mehrfachfunkenaufnahmen von Explosionsvorgängen nach der Toeplerschen Schlierenmethode. Forschungsarbeiten auf dem Gebiete des Ingenieurwesens, Heft 326, 1930, S. 1-18.

66. Marvin, Charles F., Jr., and Best, Robert D.: Flame Movement and Pressure Development in an Engine Cylinder. NACA Rep. 399, 1931.

67. Marvin, Charles F., Jr., Caldwell, Frank R., and Steele, Sydney: Infrared Radiation from Explosions in a Spark-Ignition Engine. NACA Rep. 486, 1934.

68. Flock, Ernest F., Marvin, Charles F., Jr., Caldwell, Frank R., and Roeder, Carl H.: Flame Speeds and Energy Considerations for Explosions in a Spherical Bomb. NACA Rep. 682, 1940.

69. Lewis, Bernard, and von Elbe, Guenther: Stability and Structure of Burner Flames. Jour. Chem. Phys., vol. 11, Feb. 1943, pp. 75-97.

70. Shelkin, K. I.: On Combustion in a Turbulent Flow. NACA TM 1110, 1947.

71. Boerlage, G. D., and van Dyck, W. J. D.: Causes of Detonation in Petrol and Diesel Engines. R. A. S. Jour., vol. XXXVIII, no. 288, Dec. 1934, pp. 953-986.

72. Dreyhaupt, Fritz: Up-to-Date Summary of Question of Detonation. The Engineers' Digest, vol. III, no. 12, Dec. 1942, pp. 407-414.

CHAPTER II

CORRELATIONS OF KNOCK-LIMITED PERFORMANCE DATA

If mechanical limitations are disregarded, the power output of an engine can be increased by varying any one of several operating conditions until the knock limit of the fuel is reached. Once this limit is encountered, further efforts to increase the power will result in overheating of the engine and prolonged operation under these knocking conditions may result in damage to the engine. For these reasons, much research has been conducted to extend knowledge of the nature of knock and, through application of this knowledge, to eliminate knock as an obstacle to greater engine power.

Knock itself is fundamentally related to the following events that occur in the engine cylinder after induction of the fuel-air charge:

1. The fuel-air mixture (charge) is taken into the cylinder at a given temperature and pressure.
2. Compression of the charge begins as the piston moves upward. During this compression the volume occupied by the charge decreases, the pressure increases, and the temperature increases. The total temperature increase includes the temperature rise resulting from an amount of heat transferred from the hot cylinder walls.
3. Ignition of the charge takes place at some point before the piston reaches top center.
4. From the point of ignition the burning charge moves across the cylinder and the flame front compresses the unburned portion of the charge, as illustrated in figure II-1. The arcs emanating from the spark represent progressive positions of the flame front.
5. The density and the temperature in the unburned portion of the charge increase as the flame front progresses.

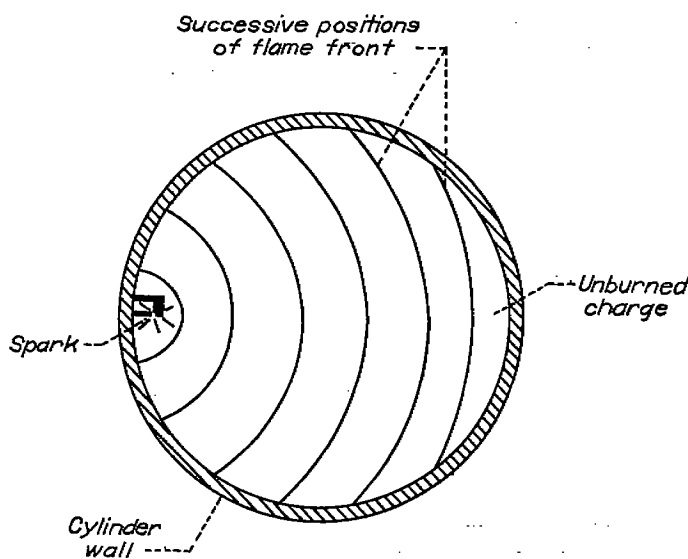


FIGURE II-1.—Schematic diagram of travel of flame front across

6. For a given fuel, a unique combination of density and temperature may occur and at this point the unburned portion of the charge will spontaneously ignite (ch. I) with considerable violence to produce the phenomenon called knock.

Rothrock and Biermann (reference 1) assume density and temperature to be the physical properties of the combustion gas that determine whether or not the fuel will knock. For each gas density, a gas temperature exists at which the unburned portion of the charge ahead of the flame front will ignite spontaneously. This combination of density and temperature may or may not be reached, depending upon the controlled and uncontrolled factors of engine operation. These factors are listed in reference 1 as follows:

- Chemical composition of fuel
- Fuel-air ratio
- Exhaust-gas dilution
- Humidity
- Compression ratio
- Inlet-air temperature
- Inlet-air pressure
- Wall temperature of combustion chamber and cylinder
- Spark advance
- Engine speed
- Engine dimensions
- Combustion-chamber form

If, as pointed out in reference 1, many combinations of density and temperature exist at which a fuel will knock, it is impossible to express the knock limit of a fuel adequately by testing that fuel at only one set of engine operating conditions. Each fuel must be tested under a variety of conditions in order to establish the absolute relation between knock-limited density and temperature. This relation will be the same regardless of the engine in which it is determined.

SYMBOLS

The following symbols are used in this chapter:

a, b	coefficients in specific-heat (constant volume) equation for charge
c	specific heat of mixture at constant volume, $\text{Btu}/(\text{lb})/\text{° F}$
f	fuel-air ratio
F_1, F_2, F_3	functions
H	heat content per pound of mixture, $\text{Btu}/(\text{lb})$
i	intake cycles per minute
J	mechanical equivalent of heat, $778 \text{ (ft-lb)}/\text{Btu}$
K	constant
m	molecular weight of charge
n	moles of gas present in cylinder

P	pressure, (lb)/(sq in.)
R	universal gas constant, (ft-lb)/(mole)(°R)
r	compression ratio
T	temperature, °R
T'	mean temperature throughout combustion chamber just before knock, °R
ΔT	temperature rise of cylinder contents due to constant-volume burning, °F
V_c	clearance volume, (cu in.)
V_d	displacement volume, (cu in.)
V_s	specific volume, (cu ft/lb)
W	gas flow, (lb)/cycle
Z	factor replacing $\frac{\rho_c}{T_c^{\gamma-1}}$
γ	ratio of specific heats
η_{com}	combustion efficiency
ρ	density, (lb)/(cu in.)
Subscripts:	
b	burned mixture at top center
c	compression
e	effective
k	in knocking zone (end gas) immediately preceding knock
0	inlet air

CORRELATIONS BASED UPON END-GAS CONDITIONS

The last portion of the charge to burn, which under proper conditions of density and temperature ignites spontaneously, is commonly designated the end gas. The space occupied by this gas is called the end zone. From the conventional thermodynamic equations, expressions are derived in reference 1 for determination of the end-gas density and temperature. The compression of the fresh charge admitted to the cylinder occurs in two steps: (1) the charge is adiabatically compressed by the piston until ignition takes place; and (2) the unburned charge ahead of the flame front is assumed to be adiabatically compressed by both the piston and the flame front until knock occurs, or

Step (1):

$$\frac{T_0}{T_c} = \left(\frac{P_0}{P_c} \right)^{\frac{1}{\gamma}}$$

Step (2):

$$\frac{T_c}{T_k} = \left(\frac{P_c}{P_k} \right)^{\frac{1}{\gamma}}$$

where

T_0, P_0 inlet-air temperature and pressure, respectively
 T_c, P_c temperature and pressure, respectively, after compression by piston
 T_k, P_k temperature and pressure, respectively, in knocking zone immediately preceding knock
 γ ratio of specific heat at constant pressure to specific heat at constant volume

Combining steps 1 and 2 yields

$$T_k = T_0 \left(\frac{P_k}{P_0} \right)^{\frac{1}{\gamma}} \quad (1)$$

This equation expresses the temperature in the knocking zone. The expression for density of the unburned charge ahead of the flame front is given by the equation

$$K_{\rho_k} = \frac{P_0}{T_0} \left(\frac{P_k}{P_0} \right)^{\frac{1}{\gamma}} \quad (2)$$

where

ρ_k gas density in knocking zone immediately preceding knock

K constant

Equations (1) and (2) are the same as those of reference 2, except that density has been used instead of pressure.

These equations show that if an engine is operated at conditions of incipient knock and P_k is measured, the density and the temperature may be calculated. Accurate measurements of P_k , however, are very difficult; therefore, the calculations as well as experimentation can be simplified by expressing the density and the temperature in terms of more easily determined factors. For example, equation (2) can be written

$$K_{\rho_k} = \frac{P_0}{T_0} \left(\frac{P_k}{P_c} \frac{P_c}{P_0} \right)^{\frac{1}{\gamma}}$$

If P_c and T_c are the compression pressure and temperature, respectively, and T' is the mean temperature throughout the combustion chamber just before knock occurs, the density ρ_k is expressed by

$$K_{\rho_k} = \frac{P_0}{T_0} \frac{T'}{T_c} \left(\frac{P_c}{P_0} \right)^{\frac{1}{\gamma}}$$

Because

$$T' = T_c + \frac{H}{c_v} = T_0 r^{\gamma-1} + \frac{H}{c_v}$$

and

$$\left(\frac{P_c}{P_0} \right)^{\frac{1}{\gamma}} = r$$

where

H heat content per pound of mixture
 c_v specific heat of mixture at constant volume
 r compression ratio of engine

then

$$K_{\rho_k} = \frac{r P_0}{T_0} \left(1 + \frac{H}{c_v T_0 r^{\gamma-1}} \right)^{\frac{1}{\gamma}} \quad (3)$$

Similarly,

$$T_k = T_0 r^{\gamma-1} \left(1 + \frac{H}{c_v T_0 r^{\gamma-1}} \right)^{\frac{1}{\gamma}} \quad (4)$$

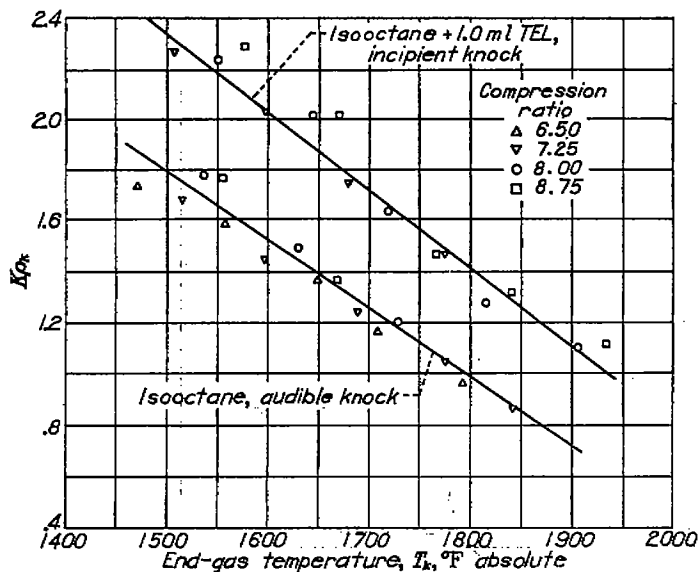


FIGURE II-2.—Effect of estimated end-gas temperature on maximum permissible density factor for leaded and unleaded isoctane in flat-disk combustion chamber. Engine speed, 2500 rpm; improved cooling in cylinder head; fuel-air ratio, 0.081. (Fig. 2 of reference 1.)

In the evaluation (reference 1) of equations (3) and (4), c_s was estimated as 0.25 Btu per pound per °F, γ as 1.29, and H as 1160 Btu per pound of mixture. The quantity H was estimated by the following expression:

$$H = \frac{18,000 \eta_{\text{com}} f}{1+f}$$

where

η_{com} combustion efficiency

f fuel-air ratio

The combustion efficiencies used in reference 1 were obtained from reference 3.

The application of the foregoing relations is illustrated in figure II-2. These data were obtained at an engine speed of 2500 rpm and a fuel-air ratio of 0.081. Although the data represent several compression ratios and several inlet-air temperatures, a single curve is obtained for each fuel. For the range of values examined in reference 1, the value of

$\left(1 + \frac{H}{c_s T_0 r^{\gamma-1}}\right)^{\frac{1}{\gamma}}$ at an inlet-air temperature of 120° F varied from a value of 3.82 at a compression ratio of 6.5 to a value of 3.62 at a compression ratio of 8.75. It was therefore assumed that the density factor (equation (3)) could be expressed by rP_0/T_0 . Similarly, the end-gas temperature T_k could be expressed by $T_0 r^{\gamma-1}$. In reference 1, $r^{\gamma-1}$ is also eliminated from the term for T_k because the data justified the omission. Proper consideration of equation (3), however, does not support the elimination of $r^{\gamma-1}$ from equation (4).

The omission of the terms $r^{\gamma-1}$ and $\left(1 + \frac{H}{c_s T_0 r^{\gamma-1}}\right)^{\frac{1}{\gamma}}$ from equation (4) permits the use of T_0 in place of T_k . A comparison of several fuels on this basis is shown in figure II-3. The curves for the fuels tend to converge at high inlet-air tempera-

tures, which indicates that for some temperature it is conceivable that this particular group of fuels might have the same knock-limited performance. This trend is due to the similarity of the fuels used. As will be shown later in this chapter, the curves for various fuels are not ordinarily so similar.

Because the density and temperature relations vary with fuel-air ratio (reference 1), Taylor, Leary, and Diver (reference 4) obtained additional data to improve the accuracy of the expressions in reference 1 and specifically to investigate further the influence of fuel-air ratio. In addition, an effort is made to determine the effect of exhaust-gas dilution on the compression ratio for incipient detonation. As a further refinement of the end-gas conditions, allowance is made for variation of specific heats and chemical equilibrium of the charge before and after combustion with temperature, pressure, and fuel-air ratio. The procedure used for computing end-gas temperatures in reference 4 is as follows:

A point is first selected on the compression stroke of an indicator diagram and the specific volume V_s of the charge is computed. The temperature T_0 is then computed from the following relation:

$$T_0 = \frac{P_0 V_s}{R}$$

where

R gas constant, 1544/m

m molecular weight of charge

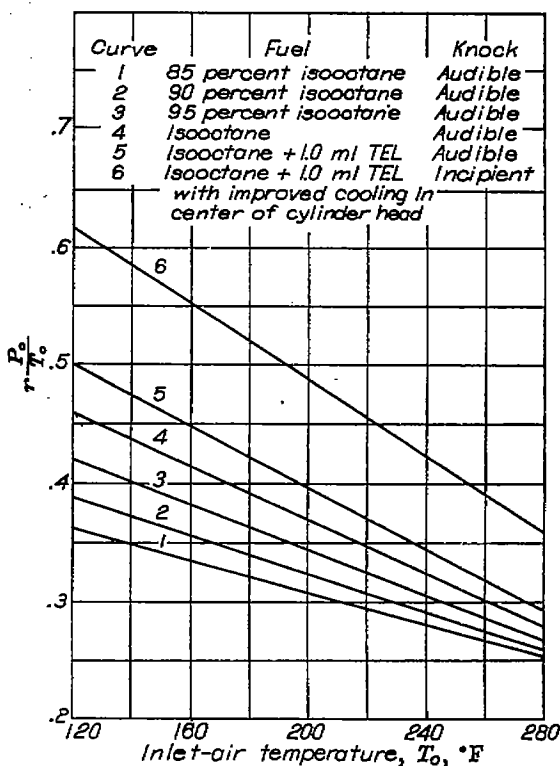


FIGURE II-3.—Effect of inlet-air temperature on maximum permissible density factor for series of fuel blends in flat-disk combustion chamber. Engine speed, 2500 rpm; fuel-air ratio, 0.081. (Fig. 4 of reference 1.)

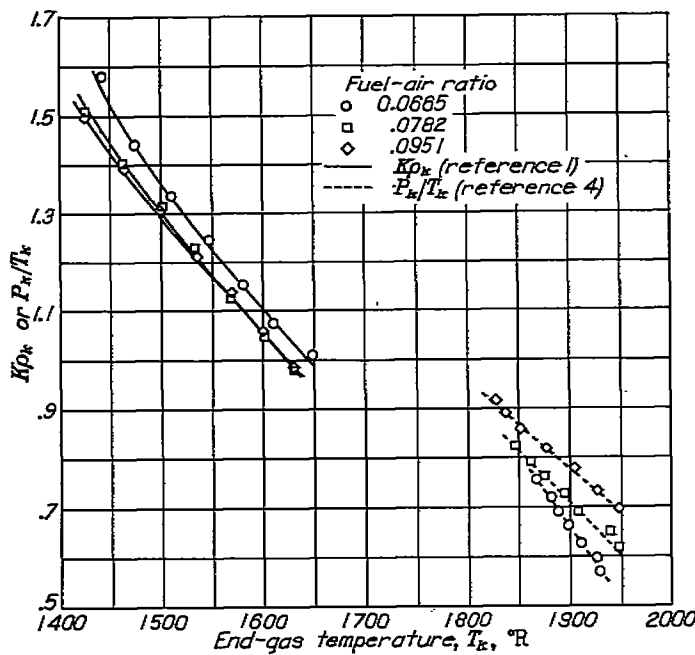


FIGURE II-4.—Comparison of effect of end-gas temperature on maximum permissible end-gas density as determined by methods of references 1 and 4. (Fig. 24 of reference 4.)

The end-gas temperature T_k is calculated from the equation for T_k taken from reference 5.

$$\log T_k = \log T_0 + \frac{R}{(a+J)J} \log \frac{P_k}{P_0} - \frac{b}{2.30(a+J)} (T_k - T_0) \quad (5)$$

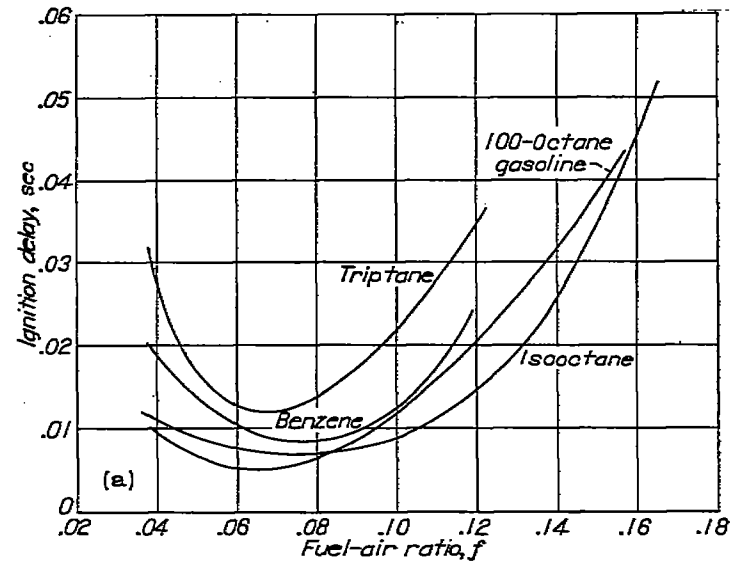
where

a, b coefficients in specific-heat equation at constant volume for charge

J mechanical equivalent of heat, 778(ft-lb)/Btu

A comparison of the end-gas calculations from references 1 and 4 is shown in figure II-4. The results of these references are in agreement as to the variation of end-gas density with end-gas temperature, but the order of variation of end-gas density with fuel-air ratio at any given end-gas temperature is reversed by the two methods of calculation. An additional analysis by Rothrock cited in reference 4 attributes the apparent reversal of the effect of the fuel-air ratio to the difference between the measured maximum pressures of reference 4 and the computed maximum pressures of reference 1.

The studies of reference 4 were made at constant engine speed and therefore do not consider the effect of time or rate of combustion on knock. In a subsequent investigation, Leary and Taylor (reference 6) attempt to explain the significance of time in engine detonation by the use of indicator diagrams obtained during knock tests. As a result of these studies, the investigators conclude that higher maximum permissible pressures can be used in an engine if the rate of compression of the end gas is increased. This conclusion led to the development of an experimental com-

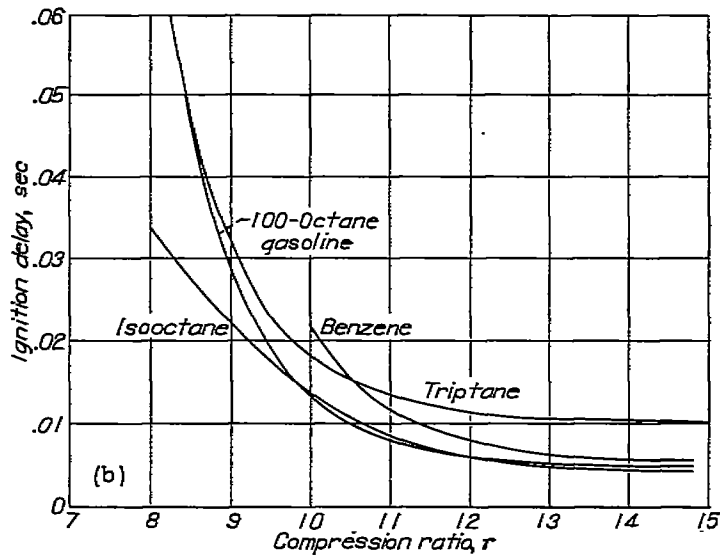


(a) Variable fuel-air ratio. Compression ratio, 11.7. (Fig. 32 of reference 8.)

FIGURE II-5.—Comparison of isoctane, 100-octane gasoline, triptane, and benzene with respect to variation in ignition delay. Initial pressure, 14.7 pounds per square inch absolute; initial temperature, 149° F; compression time, approximately 0.006 second.

pression machine (reference 7) for use in studies of fuel knocking characteristics.

The first results obtained in the compression machine are reported in reference 8 as an explanation of differences in knocking characteristics of fuels. Ignition delay as a function of fuel-air ratio is shown in figure II-5 (a) for four fuels. When the curves for isoctane (2,2,4-trimethylpentane) and 100-octane gasoline are compared, the ignition delay of the gasoline is seen to be greater than that of isoctane at fuel-air ratios greater than 0.085. The reverse is true at fuel-air ratios below 0.085. On the basis of these results, it is suggested (reference 8) that the knock-limited



(b) Variable compression ratio. Fuel-air ratio, stoichiometric. (Fig. 33 of reference 8.)

FIGURE II-5.—Concluded. Comparison of isoctane, 100-octane gasoline, triptane, and benzene with respect to variation in ignition delay. Initial pressure, 14.7 pounds per square inch absolute; initial temperature, 149° F; compression time, approximately 0.006 second.

performance of these fuels may be similar; that is, iso-octane would be higher than 100-octane gasoline at low fuel-air ratios but lower than gasoline at high fuel-air ratios. This belief was confirmed by supercharged knock tests. If ignition delay were the only criterion of knock, it could be concluded from figure II-5 (a) that triptane (2,2,3-trimethylbutane) has the highest antiknock performance with benzene next in order; however, the authors of reference 8 contend that this result may not be true inasmuch as the pressure-time curve during the delay period is also of considerable importance.

Ignition delay as a function of compression ratio is shown in figure II-5 (b). The delay period decreases as the compression ratio increases. The ignition delays for triptane are higher than those of iso-octane and 100-octane gasoline over the entire range of compression ratios. Benzene has ignition delays greater than those of triptane at compression ratios below 10.5, but over the entire compression-ratio range the pressure-time records of reference 8 for benzene always indicate a smoother reaction than that of triptane. From this relation it may be surmised that the high-antiknock characteristics of benzene are attributable to the slow pressure rise during combustion of the end gas rather than to the long ignition delay periods.

The correlations of end-gas conditions proposed in references 1 and 4 do not account for variations of fuel-air ratio (fig. II-4); consequently, the end-gas density-temperature relations are rederived in reference 9 with this factor taken into consideration. The following equations are proposed in reference 9:

The density of the charge after adiabatic compression by the piston is

$$\rho_c = \frac{W}{V_c} \quad (6)$$

where

ρ_c density after compression

W weight of gas induced per cycle

V_c clearance volume

The temperature of the charge after compression is

$$T_c = T_0 r^{\gamma-1} \quad (7)$$

The state of the gases before burning in the cylinder when the piston is at top center may be expressed by the ideal gas equation,

$$P_c V_c = n R T_c \quad (8)$$

where

P_c compression pressure

n moles of gas present in cylinder

R universal gas constant

The state of the gases at top center after burning is

$$P_b V_c = n R T_b \quad (9)$$

where

P_b pressure of burned mixture at top center

T_b temperature of burned mixture at top center

Combining equations (8) and (9) gives

$$\frac{P_b}{P_c} = \frac{T_b}{T_c} \quad (10)$$

The end gas is adiabatically compressed during constant-volume combustion

$$\frac{P_{k,e}}{P_c} = \left(\frac{T_{k,e}}{T_c} \right)^{\frac{1}{\gamma-1}} \quad (11)$$

and

$$\frac{\rho_{k,e}}{\rho_c} = \left(\frac{T_{k,e}}{T_c} \right)^{\frac{1}{\gamma-1}} \quad (12)$$

where

$P_{k,e}$ effective end-gas pressure at instant before knock

$T_{k,e}$ effective end-gas temperature at instant before knock

$\rho_{k,e}$ effective end-gas density at instant before knock

The term "effective" was used in reference 9 in referring to the end-gas quantities (subscript k,e) inasmuch as these quantities are based upon an idealized air-cycle analysis and are therefore not the same as the actual values.

As the flame front moves across the cylinder, the unburned gas (assumed to be small) is compressed and knock occurs just before completion of combustion of the entire charge.

In equation (11), P_b can be substituted for $P_{k,e}$

$$\frac{P_b}{P_c} = \left(\frac{T_{k,e}}{T_c} \right)^{\frac{1}{\gamma-1}} \quad (13)$$

Combining equations (10) and (13) yields

$$T_{k,e} = T_c \left(\frac{T_b}{T_c} \right)^{\frac{1}{\gamma-1}} \quad (14)$$

however,

$$T_b = T_c + \Delta T \quad (15)$$

where

ΔT temperature rise of cylinder contents due to constant-volume burning

Therefore,

$$T_{k,e} = T_c \left(1 + \frac{\Delta T}{T_c} \right)^{\frac{1}{\gamma-1}} \quad (16)$$

In reference 9, a relation is assumed to exist between effective end-gas density and effective end-gas temperature at the incipient-knock condition; this relation includes the effects of variations of fuel-air ratio, compression ratio, and inlet-air temperature:

$$\rho_{k,e} = F_1(T_{k,e}) \quad (17)$$

Combining equations (12) and (17) yields

$$\rho_c \left(\frac{T_{k,e}}{T_c} \right)^{\frac{1}{\gamma-1}} = F_1(T_{k,e}) \quad (18)$$

or

$$\frac{\rho_c}{T_c^{\gamma-1}} = \frac{F_1(T_{k,e})}{T_{k,e}^{\gamma-1}} = F_2(T_{k,e}) \quad (19)$$

Replacing $T_{k,e}$ by its equivalent in equation (16) and letting Z equal $\rho_c/T_c^{\gamma-1}$ gives

$$Z = F_2 \left[T_c \left(1 + \frac{\Delta T}{T_c} \right)^{\frac{\gamma-1}{\gamma}} \right] \quad (20)$$

The constant-volume temperature rise during burning ΔT is dependent upon factors such as fuel-air ratio and pressure and temperature of the charge before burning. Of these factors, fuel-air ratio is the most important one affecting ΔT ; therefore, ΔT is considered (reference 9) to be a function of fuel-air ratio alone. At some reference fuel-air ratio, ΔT can be taken as a constant. In reference 9, a fuel-air ratio of 0.08 is selected. A representative value (4040° F) of ΔT is chosen from reference 10 to be used in the correlation of the experimental data of reference 9.

The constant-volume temperature rise due to combustion becomes

$$\Delta T = 4040 F_3(f) \quad (21)$$

where f is fuel-air ratio.

Substituting this value of ΔT into equation (20) gives

$$Z = F_2 \left\{ T_c \left[1 + \frac{4040 F_3(f)}{T_c} \right]^{\frac{\gamma-1}{\gamma}} \right\} \quad (22)$$

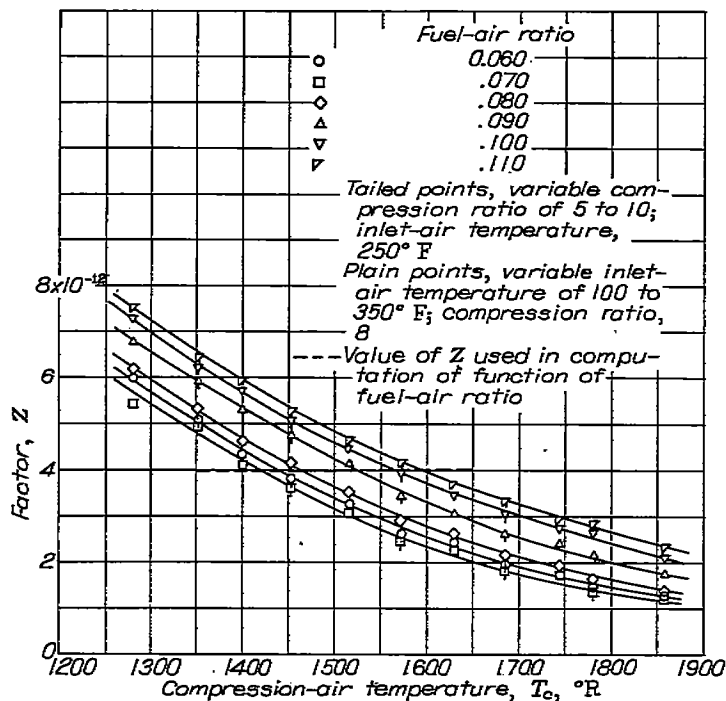


FIGURE II-6.—Effect of compression-air temperature and fuel-air ratio on knock-limited values of factor Z for AN-F-28 fuel in CFR engine. Engine speed, 1800 rpm; coolant temperature, 250° F; spark advance, 30° B. T. C. (Fig. 4 of reference 9; data calculated from reference 10.)

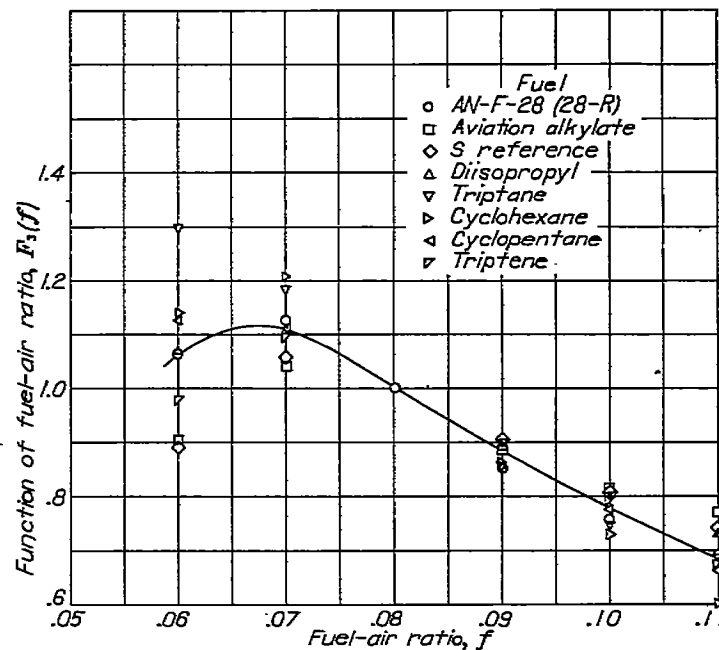


FIGURE II-7.—Effect of fuel-air ratio on function of fuel-air ratio for eight fuels in supercharged CFR engine. (Fig. 5 of reference 9.)

By use of equations (6), (7), (12), (16), and (21), the following expressions may be written for $T_{k,e}$ and $\rho_{k,e}$:

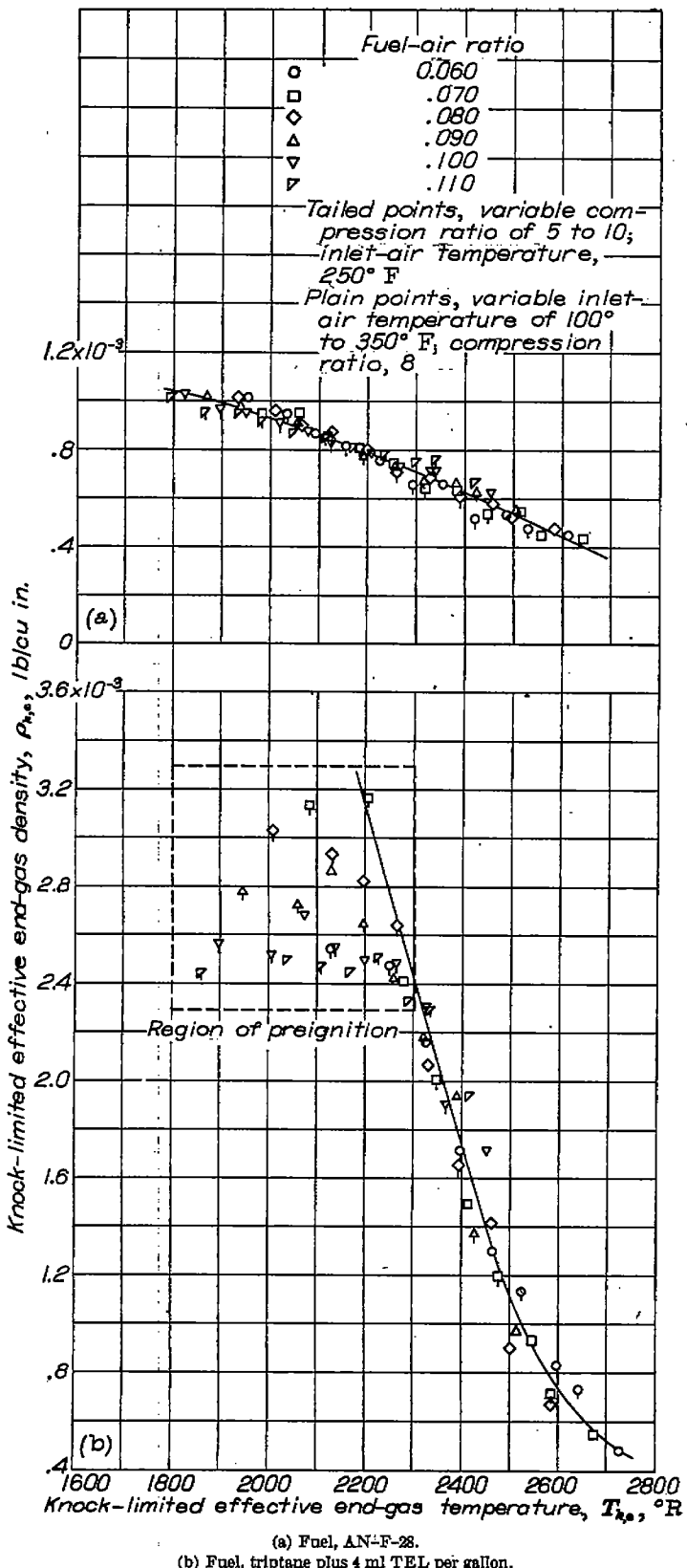
$$T_{k,e} = T_0 r^{\gamma-1} \left[1 + \frac{4040 F_3(f)}{T_0 r^{\gamma-1}} \right]^{\frac{1}{\gamma}} \quad (23)$$

$$\rho_{k,e} = \frac{W}{V_c r} \left(\frac{T_{k,e}}{T_0} \right)^{\frac{1}{\gamma-1}} \quad (24)$$

Equations (23) and (24) can be solved for $T_{k,e}$ and $\rho_{k,e}$ if $F_3(f)$ is known. The utility of these equations for correlation of engine variables depends upon whether a single curve results between $T_{k,e}$ and $\rho_{k,e}$, when T_0 , r , or f is varied and also upon the accuracy with which $F_3(f)$ can be evaluated.

In order to determine $F_3(f)$, values of Z are computed (reference 9) from experimental data obtained in a CFR test engine with AN-F-28 (28-R), a 100/130 grade aviation gasoline. The values of Z are computed from $\rho_c/T_c^{\gamma-1}$, and a constant γ of 1.4 is used. The computed values are then plotted against T_c as shown in figure II-6. The experimental data upon which this figure is based covered a range of compression ratios from 5 to 10 at a constant inlet-air temperature of 250° F and a range of inlet-air temperatures from 100° to 350° F at a compression ratio of 8. A constant engine speed of 1800 rpm, a coolant temperature of 250° F, and a spark advance of 30° B. T. C., were maintained in all cases.

At constant Z (fig. II-6), a new value of T_c exists for each fuel-air ratio and the right side of equation (22) is constant regardless of fuel-air ratio; consequently, the following equation may be written:



(a) Fuel, AN-F-28.
(b) Fuel, triptane plus 4 ml TEL per gallon.

FIGURE II-8.—Variation of knock-limited effective end-gas density with knock-limited effective end-gas temperature for changes in fuel-air ratio, inlet-air temperature, and compression ratio. Inlet-air pressure varied to maintain incipient knock. (Fig. 6 of reference 9; data calculated from reference 12.)

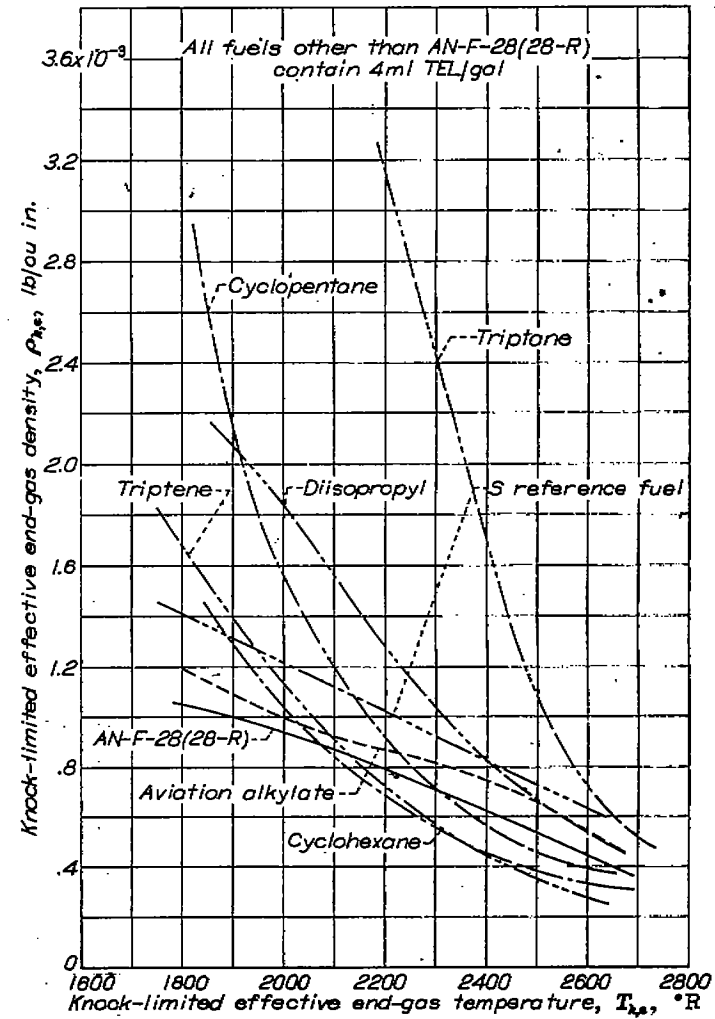


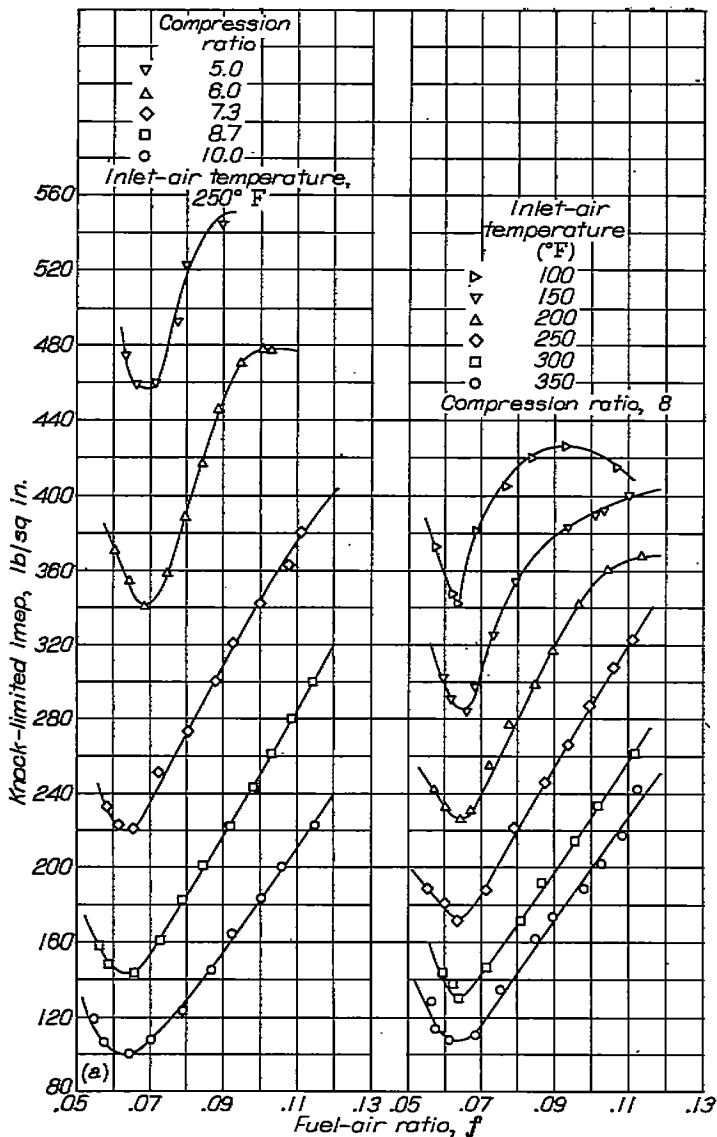
FIGURE II-9.—Effect of change in knock-limited effective end-gas temperature on knock-limited effective end-gas density for eight fuels. (Fig. 8 of reference 9.)

$$T_c \left[1 + \frac{4040 F_s(f)}{T_c} \right]^{\frac{1}{\gamma}} = T_{c,0.08} \left(1 + \frac{4040}{T_{c,0.08}} \right)^{\frac{1}{\gamma}} \quad (25)$$

The left side of this equation applies for any fuel-air ratio, whereas the right side applies only to the previously mentioned reference fuel-air ratio of 0.08, where $F_s(f)$ has been taken as 1.0. By substitution of different values of T_c from figure II-6 into the left side and the value of T_c for a fuel-air ratio of 0.08 in the right side of equation (25) it is possible to solve for $F_s(f)$.

Values of $F_s(f)$ are determined in reference 9 for seven other fuels and the results are plotted in figure II-7. The curve on this figure represents the mean of the data. Obviously the relation between $F_s(f)$ and f varies with the fuel used and for this reason the use of the mean curve is not recommended unless data for a specific fuel are unavailable.

By means of the $F_s(f)$ curves (fig. II-6) for each fuel, values of $T_{k,e}$ and $\rho_{k,e}$ are calculated (reference 9) from



(a) Knock-limited indicated mean effective pressure. (Fig. 7 of reference 12.)

FIGURE II-10.—Effect of compression ratio and inlet-air temperature on knock-limited performance of diisopropyl plus 4 ml TEL per gallon.

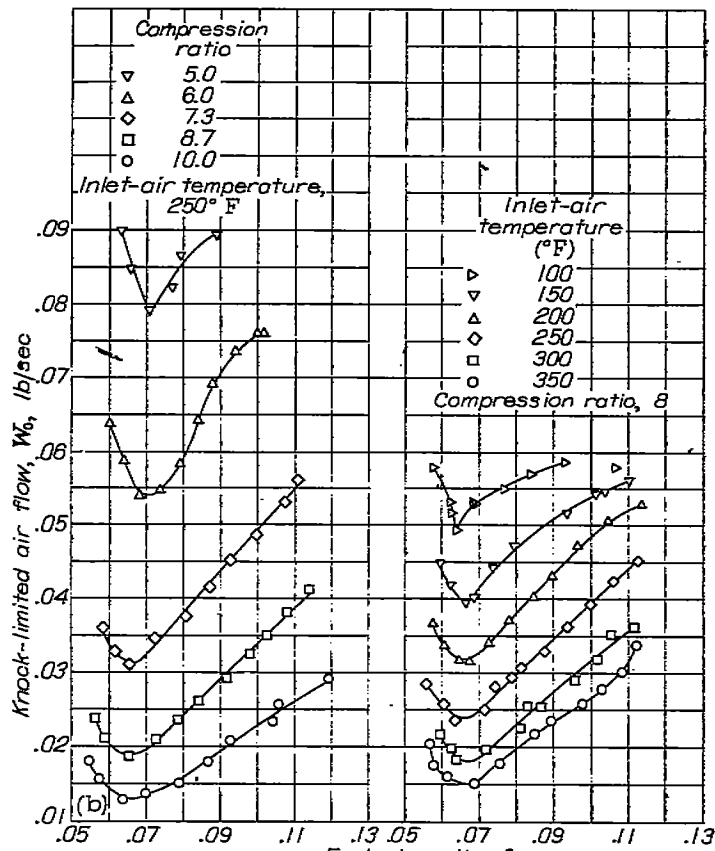
equations (23) and (24). In general, the correlations were quite satisfactory, as illustrated by figure II-8 (a). The poorest correlation was found for triptane (fig. II-8 (b)), particularly at low values of $T_{k,e}$; however, good correlation could not be expected in this case because of the tendency of the fuel to preignite. (See ch. IV.) A comparison of the knock-limited effective density-temperature curves for the fuels investigated is presented in figure II-9.

In order to determine the accuracy of the curves of $T_{k,e}$ against $\rho_{k,e}$, the authors of reference 9 calculated the knock-limited air flow W_a (equation (24)) from $T_{k,e}$ — $\rho_{k,e}$ curves based upon the mean and individual $F_3(f)$ curves of fig-

ure II-7. The results of this comparison are presented in the following table:

Fuel	Mean error in calculated knock-limited charge flow (percent)			
	Individual $F_3(f)$	Mean $F_3(f)$	Variable inlet-air temperature	
			Individual $F_3(f)$	Mean $F_3(f)$
AN-F-28 (28-R).....	3.5	4.2	4.6	5.5
Aviation alkylate.....	2.9	6.4	3.9	5.4
S reference.....	2.7	7.6	3.7	7.0
Diisopropyl.....	3.7	5.0	4.0	3.0
Triptane.....	8.6	24.4	6.6	22.4
Cyclopentane.....	7.3	7.2	7.5	8.6
Cyclohexane.....	5.1	7.4	7.2	9.0
Triptene.....	6.0	8.5	6.2	6.6

As would be expected, the least error in the calculated air flow resulted from use of the curves of $T_{k,e}$ against $\rho_{k,e}$ based upon the individual $F_3(f)$ curves. Diisopropyl at variable compression-ratio conditions and cyclopentane at variable inlet-air-temperature conditions appear to be exceptions, but the difference in mean error is small between the air flows computed from individual or mean $F_3(f)$ curves.



(b) Knock-limited air flow.

FIGURE II-10.—Concluded. Effect of compression ratio and inlet-air temperature on knock-limited performance of diisopropyl plus 4 ml TEL per gallon.

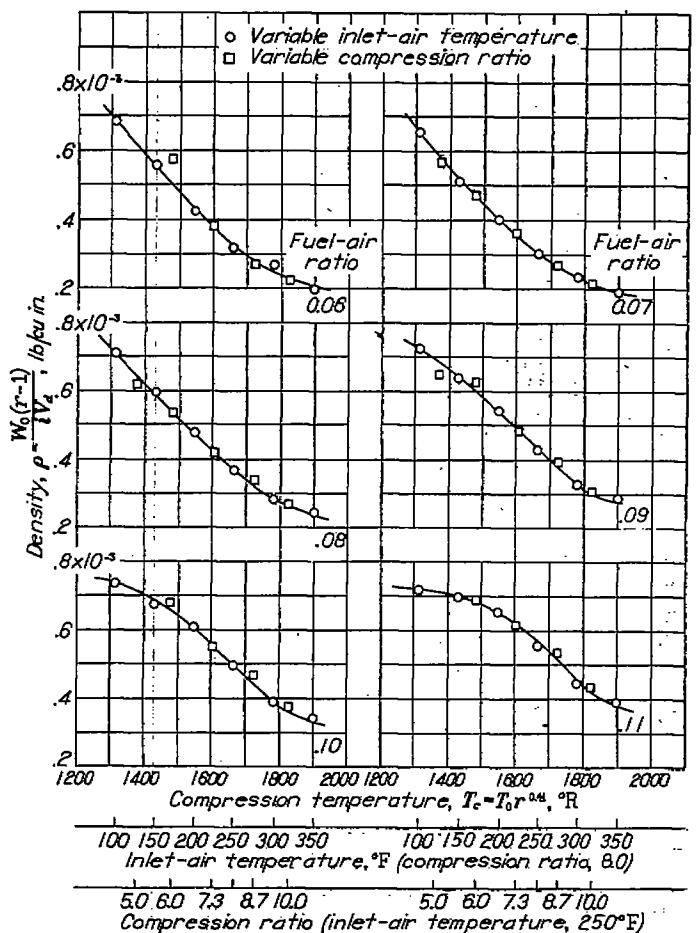


FIGURE II-11.—Effect of compression temperature on knock-limited compression-air density for diisopropyl plus 4 ml TEL per gallon. (Fig. 16 of reference 12.)

CORRELATIONS BASED UPON COMPRESSION CONDITIONS

The calculation of end-gas temperatures and densities described in the foregoing section is sufficiently complicated and uncertain to make it desirable to use some simple method of data correlation. One such method, based upon compression conditions, is proposed in reference 11. The method does not correlate all the variables of engine operation such as spark advance, engine speed, or fuel-air ratio, but is useful in explaining the effects of compression ratio and inlet-air temperature on fuel performance.

In this method, a relation is assumed to exist between compression conditions before ignition occurs and end-gas conditions after ignition occurs; therefore, calculated compression densities and temperatures may be used in place of end-gas densities and temperatures.

The compression density may be calculated as follows:

$$\rho_c = \frac{W_0}{i V_c} = \frac{W_0(r-1)}{i V_d} \quad (26)$$

where

W_0 inlet-air flow, (lb/min)
 i intake cycles per minute

V_c clearance volume, (cu in.)
 V_d displacement volume, (cu in.)

The calculation of compression temperature (reference 11) neglects the effects of fuel vaporization, heat transfer to the cylinder walls, fuel-air ratio, and preflame reactions; however, the correlations obtained with an adiabatic-compression formula justify these omissions.

$$T_c = T_0 r^{1/4} \quad (27)$$

In order to verify this method of correlation, knock-limited performance data were obtained for a number of fuels in references 11 and 12. These data resulted from tests in which all operating conditions except compression ratio were held constant. The tests were then repeated with all variables except inlet-air temperature constant. An illustration of the engine data for a single fuel is presented in figure II-10. Compression densities and temperatures calculated from data in these figures are shown in figure II-11. Comparisons of several fuels (reference 13) are shown in figure II-12.

The curves shown in these figures illustrate the relative sensitivities of fuels to changes of temperature and compression ratio and also may be used to describe the popular terms "mild" and "severe" conditions. For example (fig. II-12 (a)), an increase in compression ratio or inlet-air temperature causes an increase in compression temperature and a decrease in knock-limited performance as indicated by the low compression densities. Any combination of engine operating variables, such as spark advance, inlet-air temperature, compression ratio, and engine speed, that tends to produce exceptionally low knock-limited compression densities, is commonly termed a "severe" condition. Conversely, "mild" conditions tend to produce high knock-limited compression densities.

The type of curve shown in figure II-12 (a) has also been used to express the term "temperature sensitivity." Although no universally accepted definition of temperature sensitivity has been devised, the authors of reference 12 suggest that the compression-density—temperature plot offers a more generally applicable definition than any other yet devised. The slope of the curve of compression density plotted against compression temperature would offer a measurement of temperature sensitivity. Calculations of these slopes for the fuels investigated in reference 12 indicated that the temperature sensitivities of isoctane, aviation gasoline, an aviation alkylate, and diisopropyl (2,3-dimethylbutane) were very nearly independent of engine conditions. The temperature sensitivity of triptane decreased as the severity of the engine conditions decreased; the temperature sensitivities of cyclopentane, cyclohexane, triptene, (2,3,3-trimethylbutene-1), and toluene increased as the severity of the engine conditions decreased.

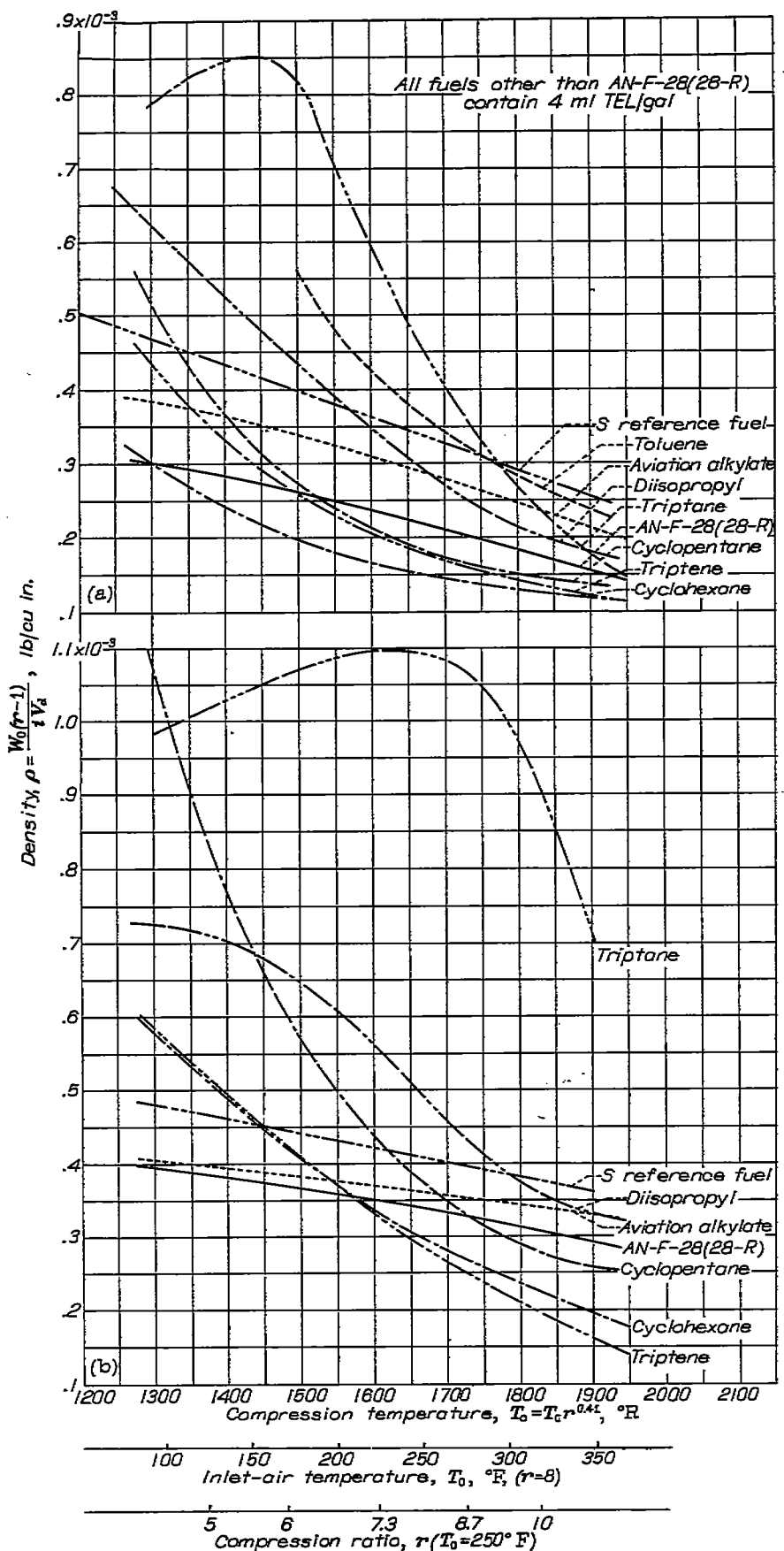


FIGURE II-12.—Temperature-density relations for various fuels in CFR engine. Engine speed, 1800 rpm; coolant temperature, 250° F; spark advance, 30° B. T. C. (Fig. 7 of reference 13.)

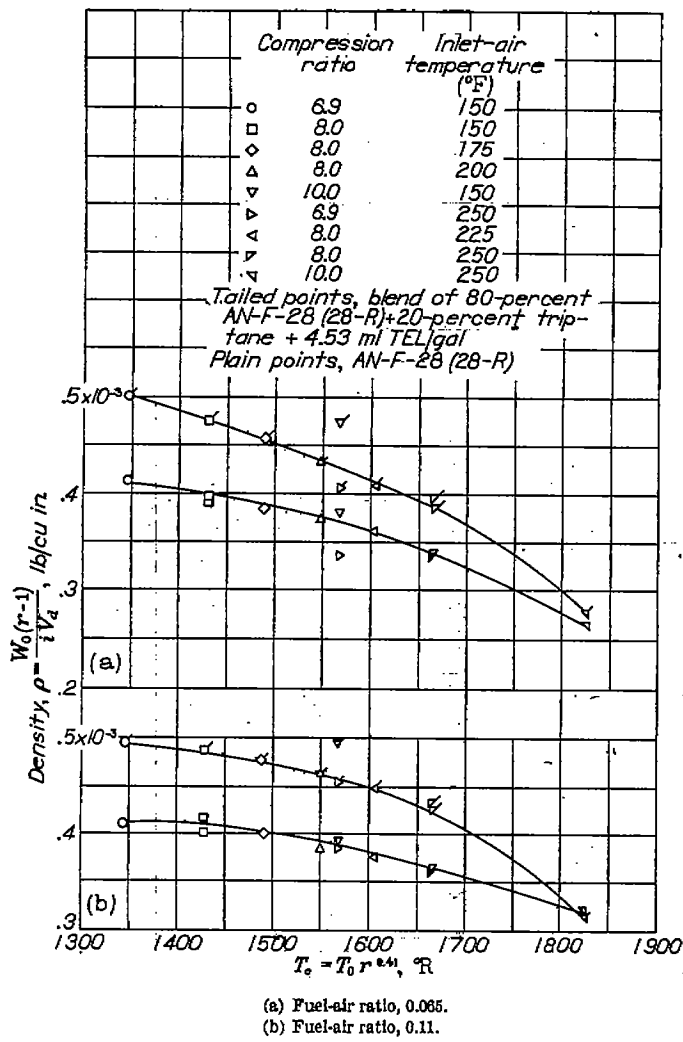


FIGURE II-13.—Temperature-density relations for two fuels in R-2600 cylinder. Engine speed, 2100 rpm; spark advance, 20° B. T. C.; rear spark-plug-bushing temperature, 450° F. (Fig. 8 of reference 13.)

The data presented in figure II-12 were obtained in a CFR engine that is designed to permit variation of compression ratio. In order to determine if the compression-density—temperature correlation would hold for full-scale engines, similar tests were made in an experimental engine employing a single cylinder from an aircraft engine. The compression ratio was varied by using pistons of different displacement in the cylinder. The results of these runs (reference 13) are shown in figure II-13.

Inasmuch as the correlation is satisfactory for full-scale engines (fig. II-13), the experimental evaluation of engines or fuels can be minimized. For example, investigation of the effect of compression ratio on knock-limited performance

in full-scale multicylinder engines is impractical because of the cost, time, and effort involved in changing pistons. Curves like those of figure II-13, however, can be established with relative ease by varying inlet-air temperature. From the curve so established, the effect of compression ratio on knock-limited compression density can be calculated from assumed compression temperatures.

Although the simplicity of the compression-density—temperature correlation is greater than that of the end-gas correlations presented in the preceding section of this chapter, the end-gas method has the obvious advantage of compensating for variations in fuel-air ratio as well as for compression ratio and inlet-air temperature.

REFERENCES

1. Rothrock, A. M., and Biermann, Arnold E.: The Knocking Characteristics of Fuels in Relation to Maximum Permissible Performance of Aircraft Engines. NACA Rep. 655, 1939.
2. Serruys, Max: La combustion detonante dans les moteurs à l'explosion. Pub. No. 103, Pub. Sci. et Tech. du Ministère de l'Air, 1937.
3. Gerrish, Harold C., and Voss, Fred: Mixture Distribution in a Single-Row Radial Engine. NACA TN 583, 1936.
4. Taylor, E. S., Leary, W. A., and Diver, J. R.: Effect of Fuel-Air Ratio, Inlet Temperature, and Exhaust Pressure on Detonation. NACA Rep. 699, 1940.
5. Goodenough, G. A.: Principles of Thermodynamics. Henry Holt and Co., 4th ed., 1931.
6. Leary, W. A., and Taylor, E. S.: The Significance of the Time Concept in Engine Detonation. NACA ARR, Jan. 1943.
7. Leary, W. A., Taylor, E. S., Taylor, C. F., and Jovellanos, J. U.: A Rapid Compression Machine Suitable for Studying Short Ignition Delays. NACA TN 1332, 1948.
8. Leary, W. A., Taylor, E. S., Taylor, C. F., and Jovellanos, J. U.: The Effect of Fuel Composition, Compression Pressure, and Fuel-Air Ratio on the Compression-Ignition Characteristics of Several Fuels. NACA TN 1470, 1948.
9. Tower, Leonard K., and Alquist, Henry E.: Correlation of Effects of Fuel-Air Ratio, Compression Ratio, and Inlet-Air Temperature on Knock Limits of Aviation Fuels. NACA TN 2066, 1950.
10. Hershey, R. L., Eberhardt, J. E., and Hottel, H. C.: Thermodynamic Properties of the Working Fluid in Internal-Combustion Engines. SAE Jour. (Trans.), vol. 39, no. 4, Oct. 1936, pp. 409-424.
11. Evvard, John C., and Branstetter, J. Robert: A Correlation of the Effects of Compression Ratio and Inlet-Air Temperature on the Knock Limits of Aviation Fuels in a CFR Engine—I. NACA ACR E5D20, 1945.
12. Alquist, Henry E., O'Dell, Leon, and Evvard, John C.: A Correlation of the Effects of Compression Ratio and Inlet-Air Temperature on the Knock Limits of Aviation Fuels in a CFR Engine—II. NACA ARR E6E13, 1946.
13. Barnett, Henry C.: An Evaluation of the Knock-Limited Performance of Triptane. NACA MR E6B20, 1946.

CHAPTER III

ANTIKNOCK PERFORMANCE SCALES

For many years the efforts of investigators in the field of fuel research have been directed toward the development of suitable scales for measuring the knocking characteristics of fuels. As a result of these efforts, a number of scales have been studied, but only a few have passed beyond the stage of tentative acceptance. The emphasis in this development has generally been placed upon one objective—that the method permit the assignment of a numerical antiknock value to each fuel and that the rating so determined be reasonably constant regardless of the engine or operating condition used.

The achievement of this objective has been hindered because the many fuels suitable for aviation use vary widely in their response to changes in engine conditions and also because the rating scales currently used are unsatisfactory for rating fuels in the high performance range. As a result of these difficulties, attention has been turned in recent years to the problem of establishing a rating scale that will permit determination of ratings for high-performance fuels. An effort has been made in these studies to select reference fuels that will respond to changes in engine conditions in a manner similar to that of service fuels. The material in this chapter is given in greater detail in reference 1.

DEVELOPMENT OF FUEL-RATING SCALES

Octane scale.—One of the earliest and the most enduring knock-rating scales is the familiar octane-number scale proposed by Edgar (reference 2) in 1927. This scale is based on two reference fuels, iso-octane (2,2,4-trimethylpentane) and *n*-heptane, suggested because iso-octane knocked less and *n*-heptane more than any other fuels then known. In this system, iso-octane is arbitrarily assigned a rating (octane number) of 100 and *n*-heptane, a rating of 0. The characteristic shape of curves representing the octane scale is shown in figure III-1 from data obtained in the A. S. T. M. Supercharge engine (A. S. T. M. designation D909-47T).

The octane scale is restricted to the determination of ratings for fuels producing knock-limited power equal to or less than that of iso-octane and equal to or greater than that of *n*-heptane. At the lower end of the scale, the limitation offers no serious obstacle because interest in fuels with greater knocking tendencies than *n*-heptane is purely academic. On the other hand, the upper or iso-octane end of the scale offers a very serious obstacle inasmuch as many pure hydrocarbons and commercial blending stocks are known to exceed the knock-limited power output of iso-octane.

In addition to being limited in use to fuels having antiknock values between those of *n*-heptane and iso-octane, the octane scale fails to provide numerical ratings that remain

constant from engine to engine or from one condition to another. That is, a fuel having an octane number of 80 in one engine may have an octane number of 90 in another engine. Investigation has shown, however, that the ratings of paraffinic fuels, with the exception of certain highly branched isomers, tend to remain more nearly constant from engine to engine than do widely different types of hydrocarbon within the range of performance covered by the octane scale (reference 3). This fact can be attributed to the differences in sensitivities of various fuels to changes in operating conditions. Inasmuch as the rating fuels (iso-octane and *n*-heptane) are paraffinic, these fuels would be expected to respond to changes in operating conditions in much the same manner as a paraffinic test fuel. If, on the other hand, the test fuel contains large concentrations of aromatic, cycloparaffinic, or olefinic compounds, the response to variations in operating conditions would differ greatly from the behavior of the paraffinic rating fuels.

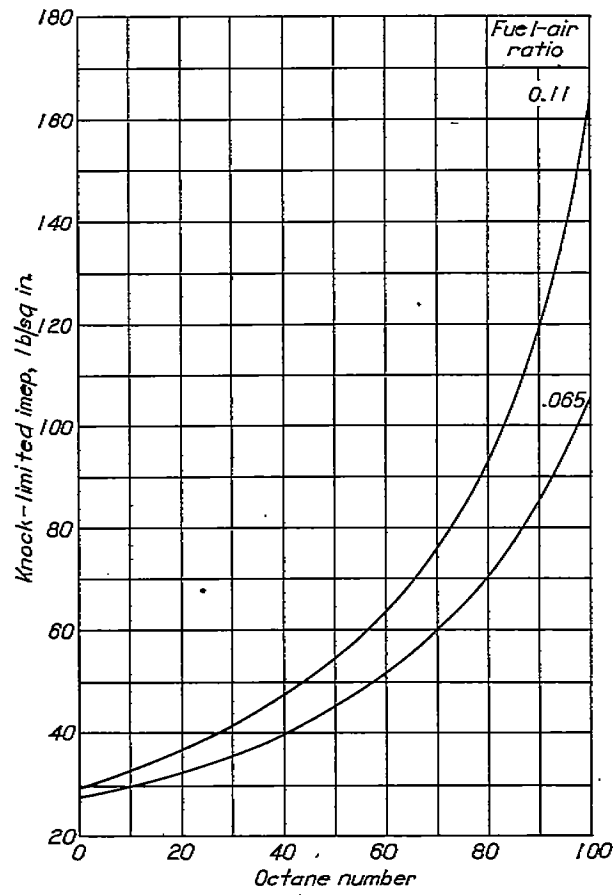


FIGURE III-1.—Octane scale determined on A. S. T. M. Supercharge engine at standard conditions. Compression ratio, 7.0; engine speed, 1500 rpm; inlet-air temperature 225° F; coolant temperature, 375° F; spark advance, 45° B. T. C. (Fig. 1 of reference 1.)

Lead scale.—When fuels with knock ratings that exceeded the upper limit of the octane scale were first considered for service use, it became apparent that the octane scale was no longer adequate for rating aviation fuels; consequently, the search began for a performance scale that would accommodate the high-performance fuels used in modern aircraft power plants. In order to meet this problem, it was decided that fuels exceeding the performance of iso-octane should be matched against iso-octane to which had been added a given amount of tetraethyl lead. (See fig. III-2.) The procedure for rating fuels by the lead scale is the same as that used for the octane scale; that is, the knock intensity of the test fuel is determined in a standard engine at standard conditions and the knocking tendencies of blends of iso-octane and tetraethyl lead are compared with those of the test fuel until one blend is found to give a knock intensity equal to that of the test fuel.

Performance-number scale.—Neither the octane scale nor the lead scale permitted the assignment of a numerical rating indicative of the power output of a fuel, and in an effort to circumvent this difficulty a scale of performance numbers was adopted. The performance scale (fig. III-3) represents an approximate average of the knock-limited performance as determined in several different engines at differ-

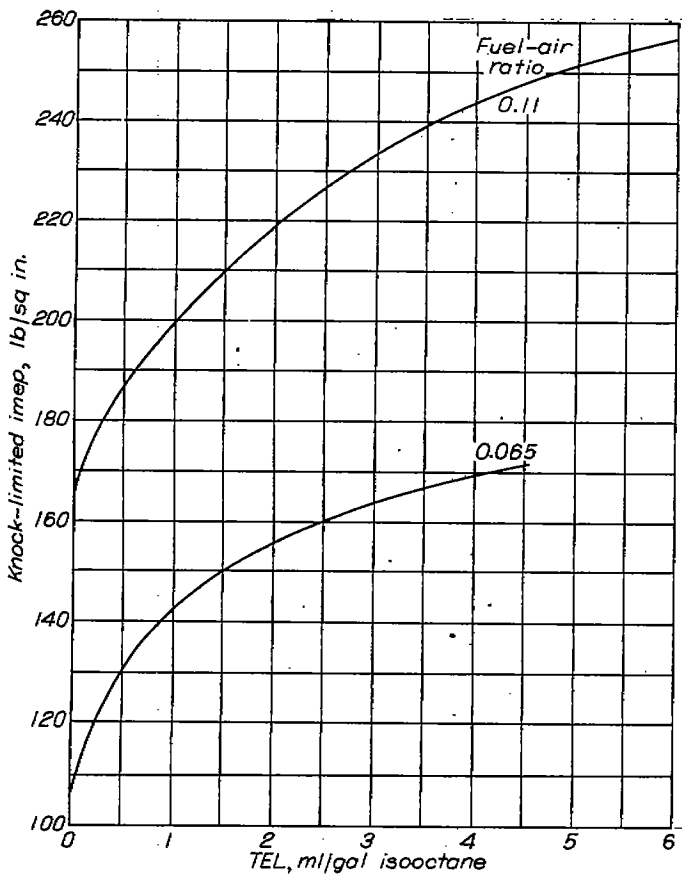


FIGURE III-2.—Lead rating scale determined on A. S. T. M. Supercharge engine at standard conditions. Compression ratio, 7.0; engine speed, 1800 rpm; inlet-air temperature, 225° F; coolant temperature, 375° F; spark advance, 45° B. T. C. (Fig. 2 of reference 1.)

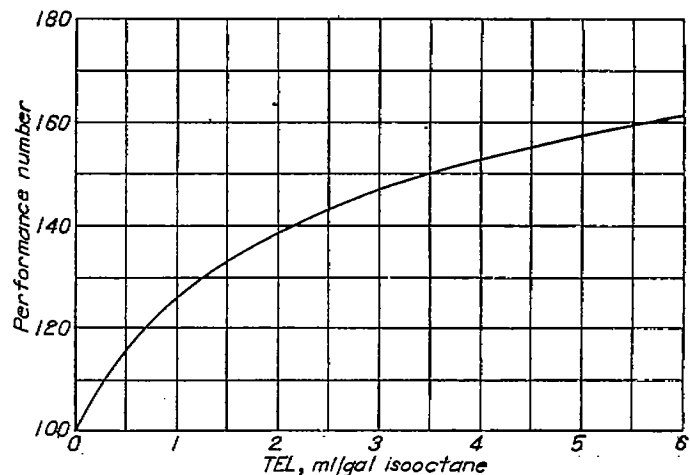


FIGURE III-3.—Performance-number scale. (Fig. 3 of reference 1.)

ent operating conditions for iso-octane containing various amounts of tetraethyl lead. Although empirically determined, this scale has proved useful in expressing fuel ratings and in correlating performance of fuels in different engines, but it still does not provide an absolute measure of power output.

The performance-number scale does not alter the procedure for rating fuels by use of leaded iso-octane (lead scale) but does change the method of reporting the rating. For example, if a test fuel is found to give knock-limited performance equal to iso-octane plus 2.0 ml TEL per gallon in any engine at any condition, its rating is reported as 138 performance number. (See fig. III-3.)

The performance scale as originally adopted was intended for use only with fuels having ratings above an octane number of 100 by the A. S. T. M. Supercharge method. General acceptance of the scale soon led to expression of ratings by the A. S. T. M. Aviation method (A. S. T. M. designation D614-47T) in terms of performance numbers and later resulted in extension of the scale below a performance number of 100.

Proposed rating scales.—One limitation of the octane scale and the lead scale is that the service fuels containing an approximately constant amount of tetraethyl lead (3.0 to 4.6 ml/gal) must be matched against unleaded rating fuels or against rating fuels having variable concentrations of lead. This limitation is inherently related to the problem of fuel sensitivity to changes in operating conditions in that tetraethyl lead affects the sensitivity of the fuel to which it is added.

In order to minimize this effect on fuel ratings, investigators in the field have proposed rating scales in which the reference fuels contain a constant amount of tetraethyl lead in the range of concentrations found in service fuels. Some of these schemes recommend the addition of a third component, such as an aromatic, in the reference fuel blend in order to produce reference fuels having sensitivities more nearly equal to service fuels.

EVALUATION OF PROPOSED FUEL-RATING SCALES

On the basis of studies made by the Coordinating Research Council (reference 4), it was proposed that triptane (2,2,3-trimethylbutane) and *n*-heptane be adopted as the reference fuels for a new rating scale. Both fuels were to contain 3.78 ml TEL per gallon. The studies on which this proposal was based were conducted in A. S. T. M. Aviation and A. S. T. M. Supercharge fuel-rating engines at standard operating conditions. In order to extend the data of the Coordinating Research Council beyond standard operating conditions, an investigation of the proposed rating scale over a range of engine conditions was conducted by the NACA and is reported in reference 1. The results of this investigation of triptane and *n*-heptane were compared with results obtained under similar test conditions for current rating scales and other proposed scales.

The effects of varying engine conditions were simulated by varying inlet-air temperature from 100° to 300° F in the A. S. T. M. Supercharge engine. The combinations of reference fuels investigated were:

1. Isooctane and *n*-heptane
2. Isooctane (containing 0 to 6 ml TEL/gal)
3. Isooctane and *n*-heptane (both containing 3.78 ml TEL/gal)

TABLE III-1.—SERVICE AND SERVICE-TYPE FUELS *

Fuel	Nominal performance grade lean/rich ^b
AN-F-26	76/88
AN-F-28 (28-R)	100/130
Special blend number 1 (SB-1) (22 percent benzene+34 percent virgin base stock+43 percent alkylate+4 ml TEL/gal)	100/140
AN-F-33 (33-R)	115/145
Special blend number 2 (SB-2) (43 percent diisopropyl+12 percent virgin base stock+45 percent alkylate+4 ml TEL/gal)	120/150
Special blend number 3 (SB-3) (34 percent diisopropyl+12.5 percent hot-acid octane+41.5 percent alkylate+12 percent isopentane+4 ml TEL/gal)	130/160
Special blend number 4 (SB-4) (55 percent diisopropyl+8 percent triptane+29 percent alkylate+8 percent isopentane+4 ml TEL/gal)	135/175
Special blend number 5 (SB-5) (62 percent diisopropyl+19 percent triptane+11 percent alkylate+8 percent isopentane+4 ml TEL/gal)	140/200
RAFD-52 (45 percent S reference fuel+45 percent diisopropyl+10 percent isopentane+4.6 ml TEL/gal)	146/175
RAFD-53 (45 percent S reference fuel+45 percent triptane+10 percent isopentane+4.6 ml TEL/gal)	153/192

* Reproduced from reference 1.

^b Lean ratings by A. S. T. M. Aviation method are intended to be indicative of "cruise" performance. Rich ratings by A. S. T. M. Supercharge method are intended to be indicative of take-off performance. (See reference 5.)

4. Triptane and *n*-heptane (both containing 3.78 ml TEL/gal)
5. Triptane and iso-octane (both containing 3.78 ml TEL/gal)

In order to compare the merits of the various rating scales, several service and service-type fuels were included in the investigation. (See table III-1.) In choosing these particular fuels and blends, an effort was made to cover a wide range of performance numbers both rich and lean. Inspection properties for these fuels are presented in table III-2.

Although complete knock-limited mixture-response curves were obtained in the A. S. T. M. Supercharge engine, the analysis of results presented (reference 1) is restricted to two fuel-air ratios, 0.065 and 0.11. Examples of data at these two fuel-air ratios are shown in figure III-4.

The points on the curves in these figures are cross-plotted from mixture-response curves.

Antiknock ratings made by the A. S. T. M. Aviation method for the various reference-fuel blends are presented in table III-3.

Comparisons among various reference scales.—In figure III-5 the various reference scales are compared at standard A. S. T. M. Aviation and A. S. T. M. Supercharge operating conditions. It is seen in figure III-5 (a) that for A. S. T. M. Aviation conditions the data for leaded blends of isooctane and *n*-heptane fall on a 45° line, which indicates that the A. S. T. M. Aviation (lean) rating of isooctane containing 3.78 ml TEL per gallon is equal to that of triptane containing the same quantity of tetraethyl lead. Conversely, data at A. S. T. M. Supercharge (rich) conditions (fig. III-5 (b)) show that for equal knock-limited indicated mean effective pressures more isooctane is required than triptane in leaded blends with *n*-heptane. In figure III-5 (b) it is shown that between 80 and 84 percent triptane in a blend with *n*-heptane (leaded) would be required to equal the upper limit (161) of the current performance scale.

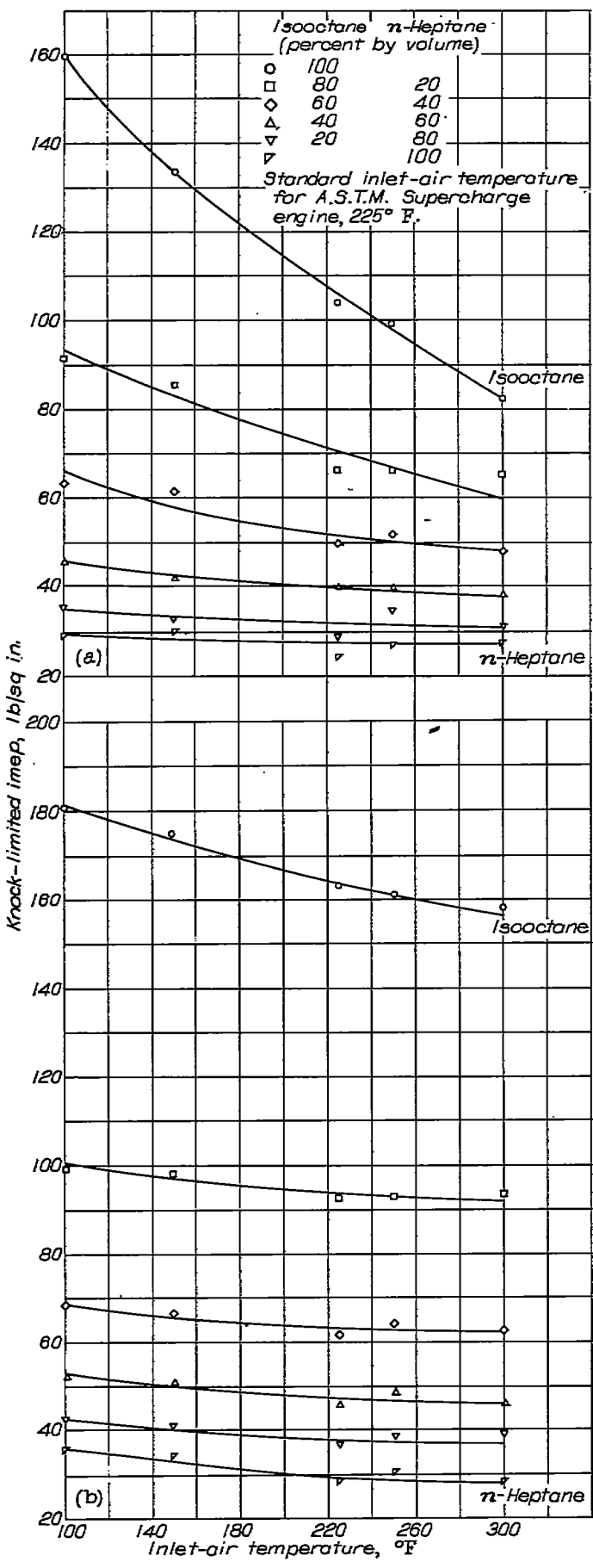
An additional observation can be made from figure III-5: namely, that for A. S. T. M. Aviation conditions the two-component reference-fuel systems with constant tetraethyl-lead concentrations are related by straight lines, whereas at A. S. T. M. Supercharge conditions definite curvature is obtained.

TABLE III-2.—INSPECTION DATA FOR SERVICE AND SERVICE-TYPE FUELS *

Fuel designation	AN-F-26	AN-F-28 (28-R)	AN-F-33 (33-R)	SB-1	SB-2	SB-3	SB-4	SB-5	RAFD-52	RAFD-53
A. S. T. M. distillation:										
Initial boiling point, (°F)	136	104	96	122	122	106	124	122	120	140
10 percent evaporated, (°F)	180	145	134	136	144	124	136	136	142	163
40 percent evaporated, (°F)	120	192	197	143	160	160	148	144	160	183
50 percent evaporated, (°F)	190	209	217	152	170	170	152	148	168	190
90 percent evaporated, (°F)	236	278	274	224	242	240	224	190	204	200
End point, (°F)	320	333	339	342	350	340	342	290	236	232
Residue, percent	0.9	0.9	1.0	0.8	1.0	1.0	1.2	0.9	1.0	0.4
Loss, percent	1.1	—	1.0	1.2	1.3	0.5	1.2	0.6	1.0	0.06
TEL content, (ml/gal)	4.95	4.36	4.83	4.02	4.17	4.39	4.11	3.98	4.52	4.69
Copper dish gum, (mg/100 ml)	6.9	2.9	5	10.1	0.8	6.3	1.5	18.6	1.1	3.3
Freezing point, (°F)	< -76	< -76	< -76	-36.4	< -76	< -76	< -76	< -76	< -76	< -76
Hydrogen-carbon ratio	0.177	0.174	0.182	0.156	0.192	0.189	0.194	0.191	0.197	0.188
Net heat of combustion, (Btu/lb)	19,103	18,700	18,900	18,517	19,196	18,155	19,350	18,266	19,247	19,373

* Table II of reference 1.

113637-53-84



(a) Fuel-air ratio, 0.065

(b) Fuel-air ratio, 0.11.

FIGURE III-4.—Variation of knock-limited performance of unleaded blends of isooctane and n-heptane with inlet-air temperature. Compression ratio, 7.0; engine speed, 1800 rpm; inlet-air temperature, 225° F; coolant temperature 373° F; spark advance, 45° B. T. C.; fuel-air ratio, 0.11. (Fig. 5 of reference 1.)

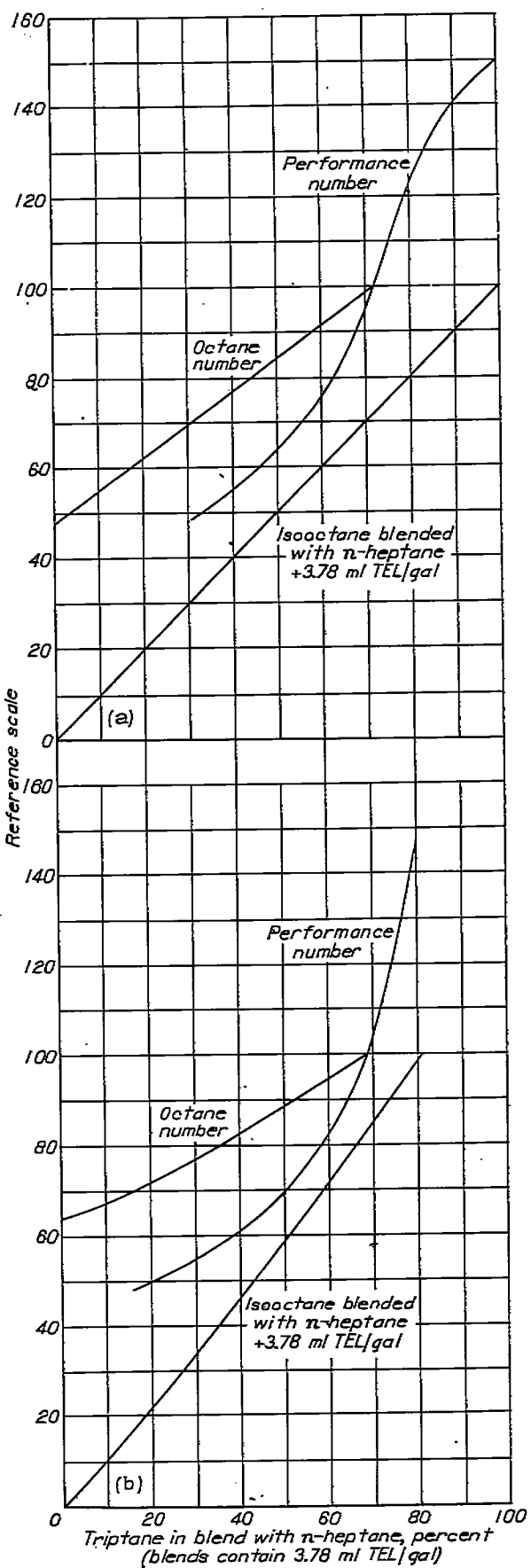
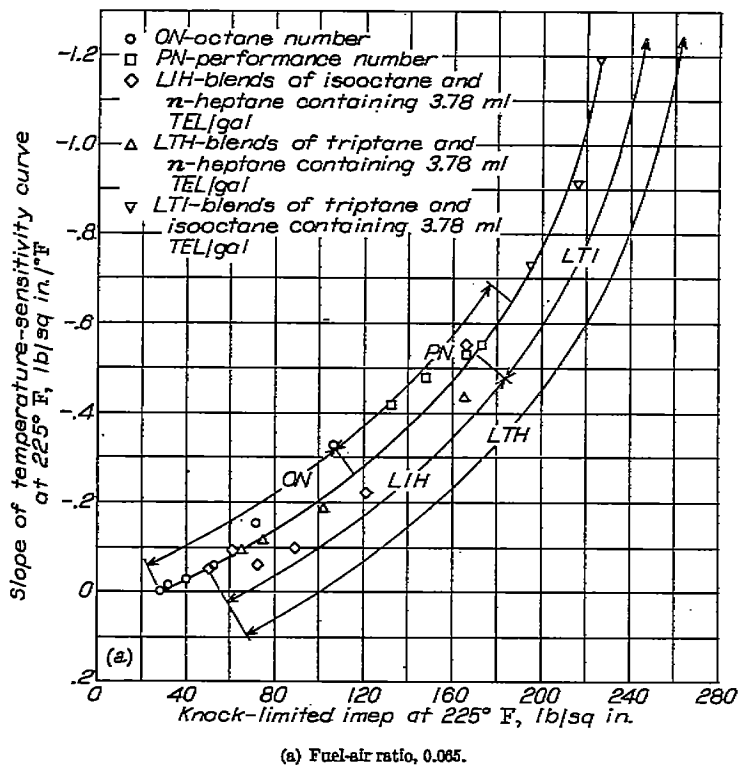
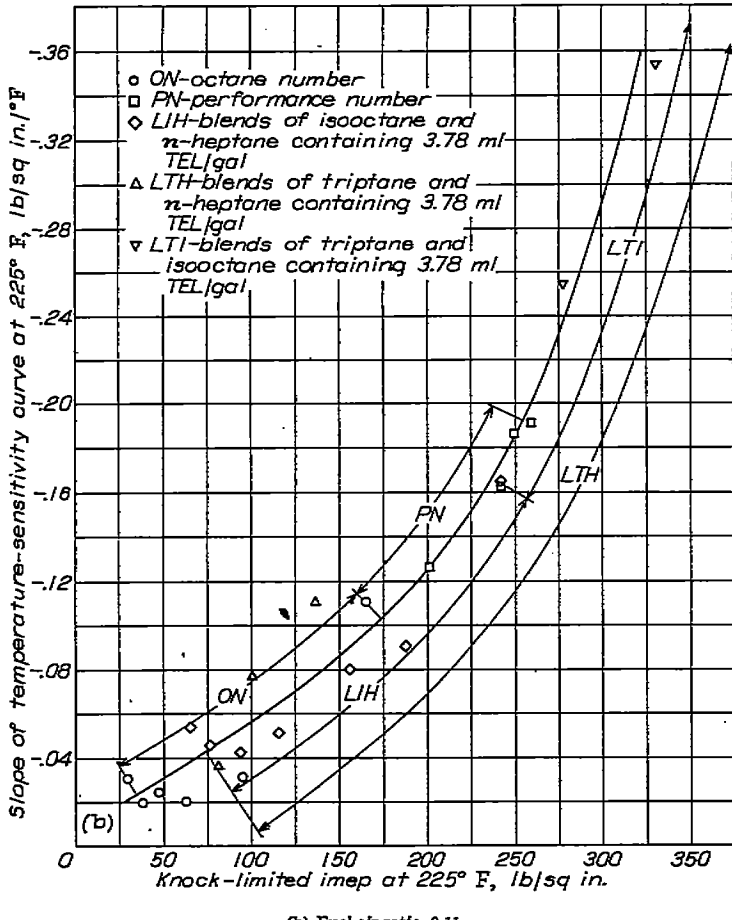
(a) Engine, A. S. T. M. Aviation.
(b) Engine, A. S. T. M. Supercharge; fuel-air ratio, 0.11.

FIGURE III-5.—Relations among various rating scales. Compression ratio, 7.0; engine speed, 1800 rpm; inlet-air temperature, 225° F; coolant temperature 373° F; spark advance, 45° B. T. C.; fuel-air ratio, 0.11. (Fig. 15 of reference 1.)



(a) Fuel-air ratio, 0.065.



(b) Fuel-air ratio, 0.11.

FIGURE III-6.—Variation of temperature sensitivity with knock-limited performance for various reference-fuel blends in A. S. T. M. Supercharge engine. Compression ratio, 7.0; engine speed, 1800 rpm; inlet-air temperature, 225°F; coolant temperature, 375°F; spark advance, 45° B. T. C. (Fig. 16 of reference 1.)

TABLE III-3.—A. S. T. M. AVIATION RATINGS FOR REFERENCE-FUEL BLENDS

Composition, percent by volume ^b			A. S. T. M. Aviation Rating	
<i>n</i> -Heptane	Isooctane	Triptane	Octane number or Isooctane+TEL	Performance number
100	0	—	47	—
80	20	—	60	—
60	40	—	76.8	54
50	50	—	85.3	65.5
20	80	—	14	105
0	100	—	8.78	161.3
—	80	20	4.0	152.5
—	60	40	4.0	152.5
—	40	60	4.0	152.5
—	20	80	4.4	154.5
—	0	100	3.6	150.5
20	—	20	62	—
60	—	40	76.8	54.5
40	—	60	90.8	75.3
20	—	80	.85	123

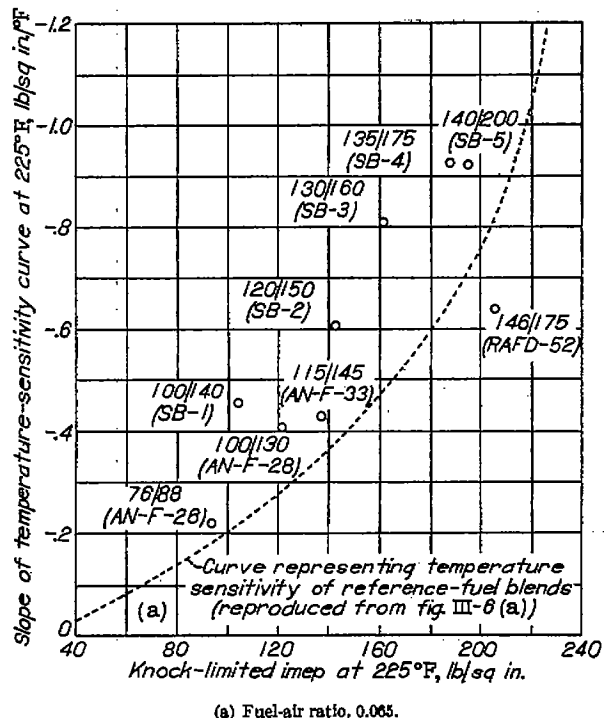
^a Table III of reference 1.^b All blends contained 3.78 ml TEL/gal.

Temperature sensitivity of reference fuels.—As a measure of the temperature sensitivity of the reference-fuel combinations, the slopes of curves similar to those in figure III-4 for all the reference-fuel combinations were computed at an inlet-air temperature of 225°F (standard A. S. T. M. Supercharge conditions) and plotted against the knock-limited mean effective pressures at the same temperature. These plots were made for fuel-air ratios of 0.065 and 0.11 and are shown in figure III-6. A single curve was drawn through each set of points (lean and rich) to illustrate the variation of temperature sensitivity with knock-limited performance for the various reference-fuel blends. The different portions of the curve determined by individual reference-fuel combinations are also indicated on figure III-6.

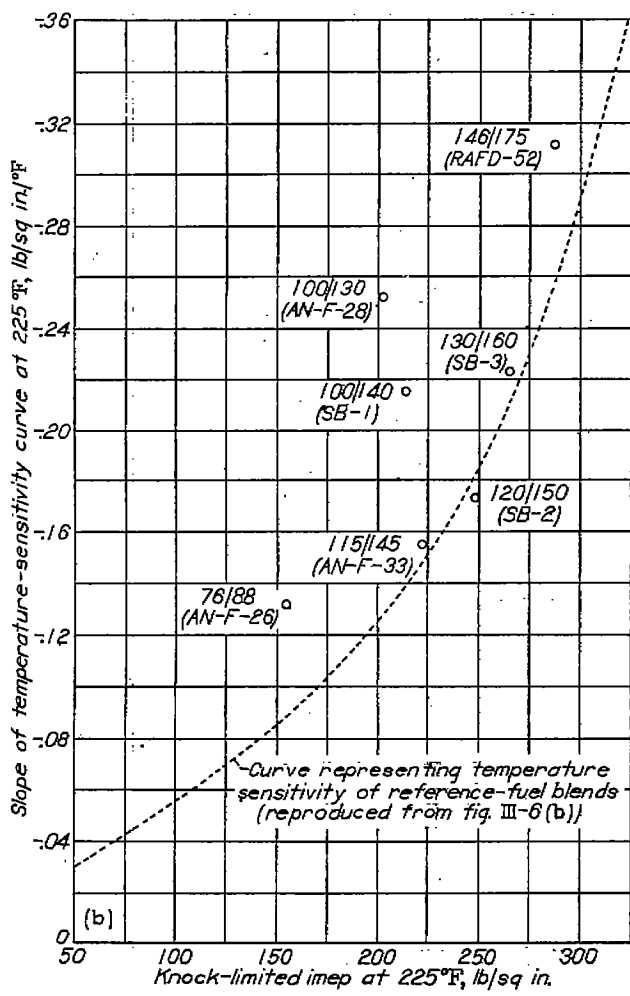
Above the upper limit of the current performance-number scale (fig. III-6), the sensitivity increases rapidly as the knock-limited indicated mean effective pressure increases. If this trend is generally true for service-type fuels, it is apparent from this figure that such fuels having high knock limits should be matched against leaded blends of triptane and isoctane or triptane and *n*-heptane in order to have reference fuels and service fuels of comparable sensitivity. For lower performance fuels, however, any of the reference scales indicated would be suitable from sensitivity considerations.

Temperature sensitivity of service-type fuels.—The effects of inlet-air temperature on the knock-limited performance of the service-type fuels (table III-1) were also investigated in the A. S. T. M. Supercharge engine. The slopes of the temperature-sensitivity curves (reference 1) were computed at 225°F and plotted in the same manner described for figure III-6. The result is shown in figure III-7 with the curves from figure III-6 reproduced for comparison.

The points representing service fuels (fig. III-7) lie primarily above the curves established for the reference fuels. This divergence is attributed to the fact that the service fuels are blends containing a number of different components; whereas the reference-fuel blends are composed of only two components. Insofar as a perfect rating scale is concerned, the ideal condition would be for the service-fuel data to fall directly on the reference-fuel curve.



(a) Fuel-air ratio, 0.065.



(b) Fuel-air ratio, 0.11.

FIGURE III-7.—Comparison among the temperature sensitivities of reference-fuel blends and service-type fuels in A. S. T. M. Supercharge engine. Compression ratio, 7.0; engine speed, 1800 rpm; inlet-air temperature, 225° F; coolant temperature, 375° F; spark advance, 45° B. T. C. (Fig. 18 of reference 1.)

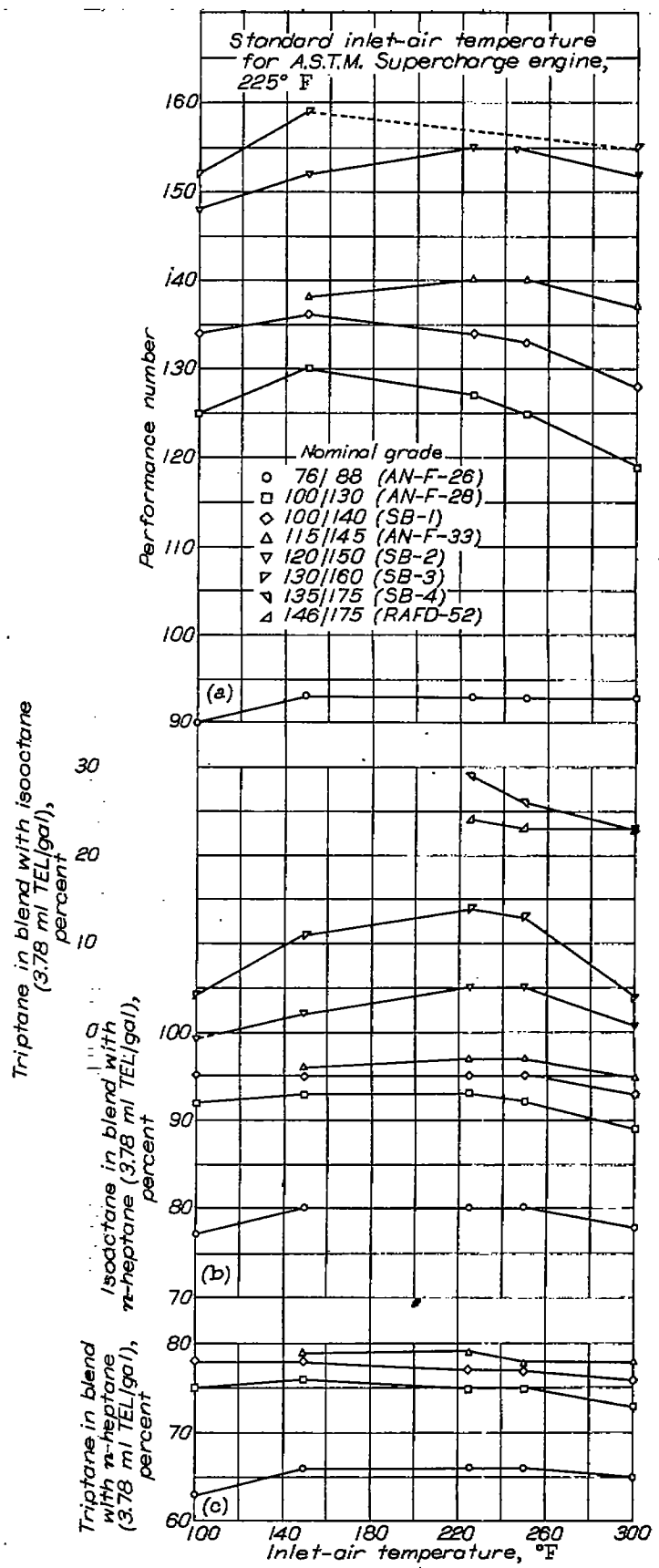


FIGURE III-8.—Effect of inlet-air temperature on antiknock ratings of service-type fuels in A. S. T. M. Supercharge engine at rich fuel-air ratio. Compression ratio, 7.0; engine speed, 1800 rpm; coolant temperature, 375° F; spark advance, 45° B. T. C.; fuel-air ratio, 0.11. (Fig. 20 of reference 1.)

TABLE III-4.—A. S. T. M. AVIATION AND A. S. T. M. SUPERCHARGE RATINGS OF SERVICE AND SERVICE-TYPE FUELS IN TERMS OF SEVERAL REFERENCE-FUEL COMBINATIONS *

Fuel designation and nominal grade	Rating scale ^b	A. S. T. M. Aviation rating ^c	A. S. T. M. Supercharge rating at fuel-air ratio of 0.065					A. S. T. M. Supercharge rating at fuel-air ratio of 0.11				
			Inlet-air temperature, °F					Inlet-air temperature, °F				
			100°	150°	225°	250°	300°	100°	150°	225°	250°	300°
AN-F-26 (76/88)	Imep ON PN LIH LTH LTI	91 76 60 60 60	134 95 85 72 60	114 94 82 69 58	94 95 85 64 56	88 95 85 61 55	79 97 90 55 53	159 97 90 77 63	163 98 93 80 66	156 98 93 80 66	152 98 93 80 66	145
AN-F-26 (100/130)	Imep ON PN LIH LTH LTI	101 72 72 72	180 112 86 72	154 110 84 71	121 110 81 68	111 109 87 67	92 109 87 62	216 125 92 75	214 130 93 78	202 127 93 75	195 125 92 75	180
SB-1 (100/140)	Imep ON PN LIH LTH LTI	99.3 88 71 71 71	184 114 87 73	148 107 83 69	104 97 72 61	95 99 72 59	83 100 95 56	231 184 134 78	226 186 134 78	212 134 95 77	207 133 95 77	193
AN-F-33 (116/145)	Imep ON PN LIH LTH LTI	115 95 77 77 77	220 133 95 80	178 128 91 76	137 120 89 73	126 121 87 72	107 122 81 70	— — — —	229 138 96 79	222 140 97 79	218 140 97 78	205
SB-2 (120/150)	Imep ON PN LIH LTH LTI	121 79 79 79	277 157 — 7	212 148 99 —	143 125 91 75	131 125 89 74	109 124 83 70	260 148 99 —	257 152 — 2	249 155 — 5	244 155 — 5	231
SB-3 (130/160)	Imep ON PN LIH LTH LTI	124 88 88 88	292 166 — 16	235 166 — 9	162 147 99 78	143 139 95 77	118 135 90 74	270 152 — 4	270 159 — 11	265 159 — 14	258 159 — 13	235
SB-4 (135/175)	Imep ON PN LIH LTH LTI	141 91 91 91	— — — 24	262 — — 15	189 — — 9	165 160 — 77	126 146 — 77	— — — —	— — — —	298 — — 29	286 — — 26	261
SB-5 (140/200)	Imep ON PN LIH LTH LTI	143 92 92 92	— — — 27	267 — — 20	195 — — 16	173 155 100 80	133 — — 2	— — — —	— — — —	— — — 24	— — — 23	269
RAFD-52 (146/175)	Imep ON PN LIH LTH LTI	147 96 96 96	— — — 15	247 — — 29	205 — — 31	188 — — 6	137 — — —	— — — —	— — — —	267 — — 24	279 — — 23	262
RAFD-53 (153/192)	Imep ON PN LIH LTH LTI	147 96 96 96	— — — —	— — — —	246 — — —	169 — — 32	147 — — 16	— — — —	— — — —	— — — —	— — — —	312 — — 60

* Table IV of reference 1.

b Imep, knock-limited indicated mean effective pressure; ON, octane number; PN, performance number; LIH, blend of isoctane and *n*-heptane containing 3.78 ml TEL/gal; LTH, blend of triptane and *n*-heptane containing 3.78 ml TEL/gal; LTI, blend of triptane and isoctane containing 3.78 ml TEL/gal.

c Octane numbers and performance numbers obtained by the standard A. S. T. M. Aviation rating procedure. Ratings in terms of other scales estimated from fig. III-5(a).

Because this situation is improbable, the next best solution must be for reference-fuel blends and service fuels to have sensitivities of approximately the same magnitude at the same knock-limited performance levels. The attainment of this characteristic can be approached by the use of either the joint reference scale, leaded triptane-isoctane and leaded isoctane-*n*-heptane, or by the leaded triptane-*n*-heptane scale (fig. III-7).

In evaluating the merits of a rating scale, however, three factors other than temperature sensitivity must be considered, namely that the scale should:

(1) Be a continuous scale

(2) Involve a minimum number of reference fuels

(3) Cover the complete range of knock-limited performance likely to be encountered with a variety of service fuels.

In figures III-6 and III-7, it has been shown that both the leaded triptane-*n*-heptane scale and the joint scale of leaded isoctane-*n*-heptane and leaded triptane-isoctane have the last of these characteristics. Only the leaded triptane-*n*-heptane scale, however, possesses the first two characteristics as well; consequently, this scale appears to be the most practical choice. The problem of availability of reference fuels is obviously important but is beyond the scope of the investigation reported in reference 1.

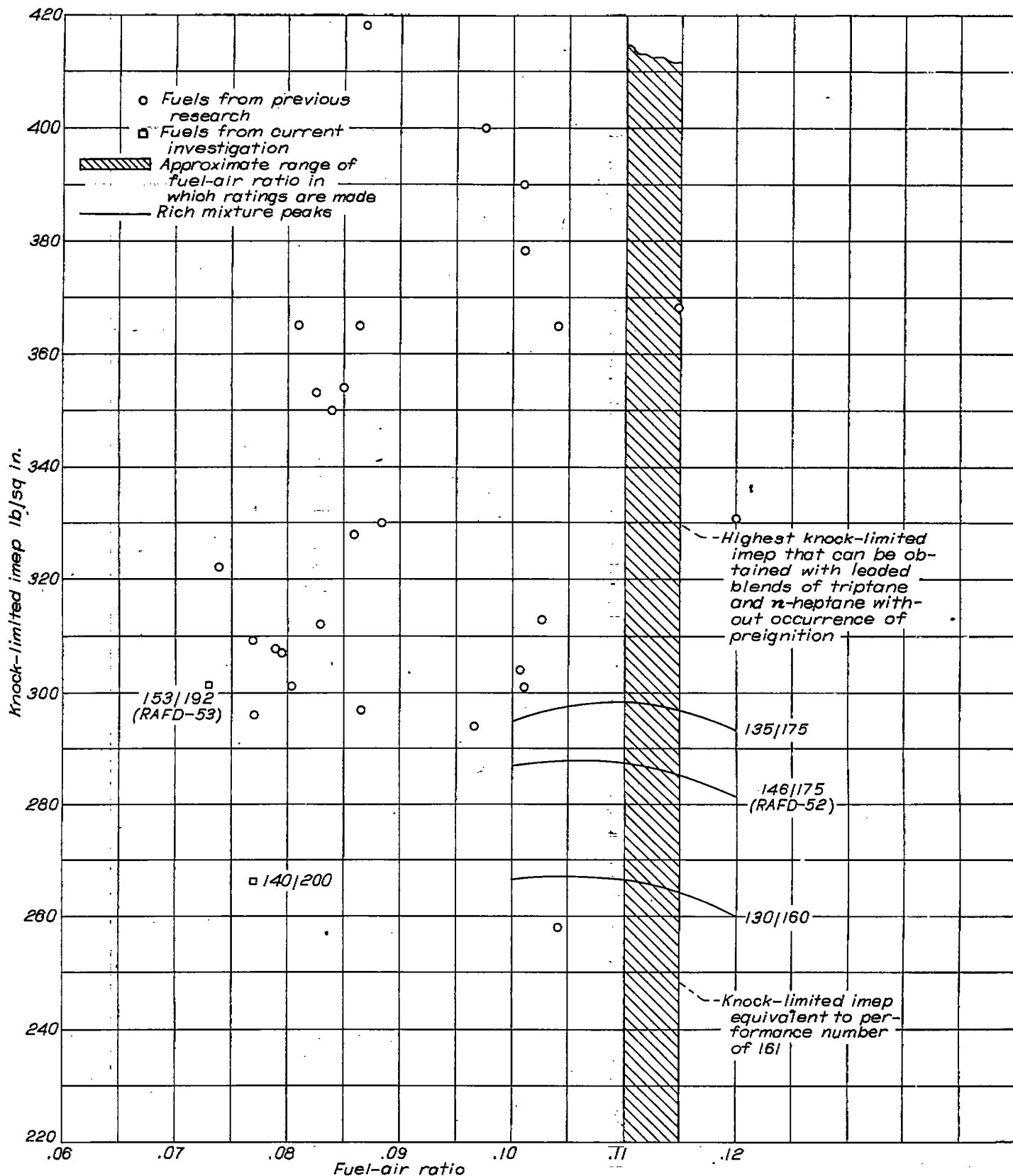


FIGURE III-9.—Maximum knock-limited mean effective pressures attainable for various fuels by A. S. T. M. Supercharge method without encountering preignition. Compression ratio, 7.0; engine speed, 1800 rpm; inlet-air temperature, 225° F; coolant temperature, 875° F; spark advance, 45° B. T. C. (Fig. 21 of reference 1.)

Ratings of service-type fuels.—The 10 service-type fuels were assigned ratings in terms of the 5 reference scales examined in this investigation. These ratings are given in table III-4 for standard A. S. T. M. Aviation conditions and for A. S. T. M. Supercharge conditions at five inlet-air temperatures and two fuel-air ratios. The ratings in this table were determined for comparing the constancy of the assigned ratings by the different rating scales over a range of conditions established by varying inlet-air temperature. This comparison is presented in figure III-8 for the A. S. T. M. Supercharge engine at a fuel-air ratio of 0.11.

These figures alone cannot serve as a basis for choosing the best reference scale because the constancy of an assigned rating from one set of operating conditions to another is largely dependent upon the relative sensitivities of reference fuels and test fuels previously discussed.

Limitations of reference scales.—In the preceding discussion, it has been stated that in many cases knock-limited indicated mean effective pressures were not obtained for some of the higher-performance service-type and reference fuels investigated in the A. S. T. M. Supercharge engine. The attainment of complete data for high-performance fuels was hampered throughout the investigation by the tendency of these fuels to preignite in the A. S. T. M. Supercharge engine. The engine operator at all times obtained as much of the mixture-response curve as possible before the start of preignition (see ch. IV); for some fuels, however, points richer than a fuel-air ratio of about 0.08 could not be taken. Inasmuch as the peaks of the curves were not obtained, ratings could not be made in the fuel-air-ratio range characteristic of the standard A. S. T. M. Supercharge method.

Preignition occurred with the high-performance fuels regardless of the condition of the engine; changing the type of spark plug failed to prevent preignition.

Preignition was encountered so frequently that early data obtained in the NACA laboratories were examined in order to define the range of indicated mean effective pressure in which preignition is likely to occur in the A. S. T. M. Supercharge engine. The results of this study are presented in figure III-9, together with data from the present investigation. Each point on this plot represents the richest point of a mixture-response curve that could be obtained before the occurrence of preignition. It is seen in figure III-9 that with several fuels it was possible to reach preignition-free performance at indicated mean effective pressures greater than 400 pounds per square inch; however, a number of fuels preignited at levels below 400 down to about 258 pounds per square inch. In most cases, the limiting fuel-air ratios were leaner than the fuel-air-ratio range in which A. S. T. M. Supercharge ratings are usually made.

Inasmuch as preignition imposes a very real limit on an A. S. T. M. Supercharge rating scale at a rich fuel-air ratio, the maximum indicated mean effective pressures that can be obtained with current and proposed reference scales are indicated in figure III-9. The difference between scales is about 75 pounds per square inch indicated mean effective pressure; the adoption of either reference scale utilizing triptane as one of the components will thus extend the range in which "direct-match" ratings can be made by about 75 pounds per square inch. Even then there will be some fuels (as indicated by preignition test points in fig. III-9) that cannot be rated in this range. In fact, only three of the five service-type fuels exceeding a performance number of 161 could be rated (shown as solid lines between fuel-air ratios of 0.10 and 0.12 in fig. III-9). The remaining two fuels having performance numbers over 161 preignited at fuel-air ratios leaner than 0.08 (indicated by the square data points on fig. III-9).

If the A. S. T. M. Aviation and A. S. T. M. Supercharge engines are to continue in use as the standard fuel-rating engines, the advantages to be gained by the adoption of new reference-fuel systems utilizing triptane are clearly questionable, as pointed out by the authors of reference 1. The present scale of performance numbers has been shown to permit ratings for fuels up to a performance number of 161 in the A. S. T. M. Aviation engine; triptane plus 3.78 ml TEL per gallon, which represents the maximum performance of either of the proposed reference-fuel combinations, permits ratings only up to a performance number of 151. Moreover, in the A. S. T. M. Supercharge engine the tendencies of many high-performance service-type fuels and high-performance reference-fuel blends to preignite makes the advantage of extending the range in which ratings can be made in this engine somewhat uncertain.

REFERENCES

1. Barnett, Henry C., and Clarke, Thomas G.: An Evaluation of Proposed Reference Fuel Scales for Knock Rating. NACA TN 1619, 1948.
2. Edgar, Graham: Measurement of Knock Characteristics of Gasoline in Terms of a Standard Fuel. Ind. and Eng. Chem., vol. 19, no. 1, Jan. 1927, pp. 145-146.
3. Wear, Jerrold D., and Sanders, Newell D.: Experimental Studies of Knock-Limited Blending Characteristics of Aviation Fuels. II—Investigation of Leaded Paraffinic Fuels in an Air-Cooled Cylinder. NACA TN 1374, 1947.
4. Brooks, Donald B.: Development of Reference Fuel Scales for Knock Rating. SAE Jour. (Trans.), vol. 54, no. 8, Aug. 1946, pp. 394-402.
5. Anon.: ASTM Manual of Engine Test Methods for Rating Fuels. A. S. T. M. (Philadelphia), 1948.

CHAPTER IV

PREIGNITION

Over a period of years research directed toward increasing engine power has been paralleled by research in engine cooling. This pattern of investigation arises from the occurrence of mechanical failures in engine cylinders when certain established temperature limits are exceeded. Opinions vary as to the principal danger of high cylinder temperatures; however, final cylinder failure obviously results from high temperatures, high pressures, or both (reference 1). The initial cause of failure may be knock, preignition, or failure of sealing devices, such as piston rings and valves, but the sequence in which the events leading up to failure occur will vary with operating conditions, design features, and fuel.

In an effort to clarify the exact roles played by these factors in service operation, this chapter presents a discussion of NACA investigations in which the characteristics of preignition are studied and the relation of preignition and knock to engine temperatures is analyzed.

CHARACTERISTICS OF PREIGNITION

Preignition and knock.—A hot spot in an engine cylinder may cause ignition of the fuel-air charge in the cylinder prior to ignition by the spark plug. This phenomenon is known as preignition. Preignition and knock are separate phenomena, as indicated by Rothrock and Biermann (reference 2). If, as suggested by this investigation, the occurrence of knock depends upon the density and the temperature of the last portion of the charge to burn, it is reasonable to assume that preignition which causes the end gas to burn nearer top center also tends to promote fuel knock, whereas preignition which causes the end gas to burn well before top center may lessen the possibility of fuel knock. In reference 1, this theory is thus concluded to provide one explanation of why preignition is often accompanied by knock and why, in other cases, in which preignition may be severe enough to cause immediate engine failure, fuel knock may not be present. A specific case of this nature is reported in reference 3.

Run-away and stable preignition.—Run-away and stable preignition are defined by Hundere and Bert (reference 4) in terms of the rate of increase of the hot-spot temperature and the required temperature for surface ignition. If, for example, the hot-spot temperature increases much more rapidly than the required surface temperature for ignition, run-away preignition occurs. When this situation exists, the ignition of the fuel-air charge may advance more and more until ignition takes place in the intake duct; a backfire then occurs.

On the other hand, stable preignition is obtained when the required surface temperature for ignition increases more rapidly than the actual hot-spot temperature. A point is then reached where the required temperature and the actual temperature are equal, and stable ignition occurs. In this case, the ignition system may be inoperative and the engine will operate normally; ignition is then accomplished solely by the hot spot in the cylinder.

Preignition characteristics vary with fuel type; for some fuels, such as benzene, preignition may become severe enough to wreck an engine cylinder so quickly that no appreciable increase in temperature or decrease in engine output can be observed.

EFFECTS OF ENGINE VARIABLES ON PREIGNITION

An investigation reported by Corrington and Fisher (reference 5) was undertaken to obtain information on the behavior of an engine during preignition operation. Spark plugs of various heat ranges were used as sources of preignition in most of the tests of reference 5. In some cases, however, preignition was excited by exhaust valves. A valve having a badly corroded head was installed in place of the Nichrome coated valves normally employed; cold-operating spark plugs were used.

Preignition was excited at various fuel-air ratios, power levels, engine speeds, and mixture temperatures.

The investigation reported in reference 5 was made in a single, liquid-cooled engine cylinder. The setup consisted of a multicylinder engine block mounted in such a manner that any one cylinder could be used. Details of the installation and the methods of instrumentation are described in references 5 and 6.

Reproducibility of preignition runs.—Cylinder design and the location and heat capacity of the preignition source are factors that influence the behavior of an engine during preignition operation. Reproducibility of preignition data will be imperfect, however, even if these factors and all operating conditions are held constant. For the studies in which spark plugs initiated preignition (reference 5), the cause of irreproducibility was the time required for the preignition to advance from normal spark timing to a point about 60° B. T. C. On occasional cycles, a run would start with ignition a few degrees early. The ignition time became earlier as the cycles with early ignition occurred more frequently. Cylinder temperature rose slowly during this period of operation. When the ignition time had advanced to about 60° B. T. C., the preignition process was greatly accelerated and successive runs were fairly reproducible. The time required was 30 to 60 seconds for preignition to become advanced to this critical value (60° B. T. C.). It is suggested in reference 5 that this variation in time to reach the critical value may result either from changes in condition of the spark plug due to deposits and corrosion or errors in setting the engine conditions.

Typical preignition runs.—Data from typical preignition runs are shown in figure IV-1. The location of the zero point on the abscissa has no significance inasmuch as the curves were adjusted on the time scale so that the points coincided where preignition became rapidly accelerated. This arrangement eliminates the period of poor reproducibility from consideration.

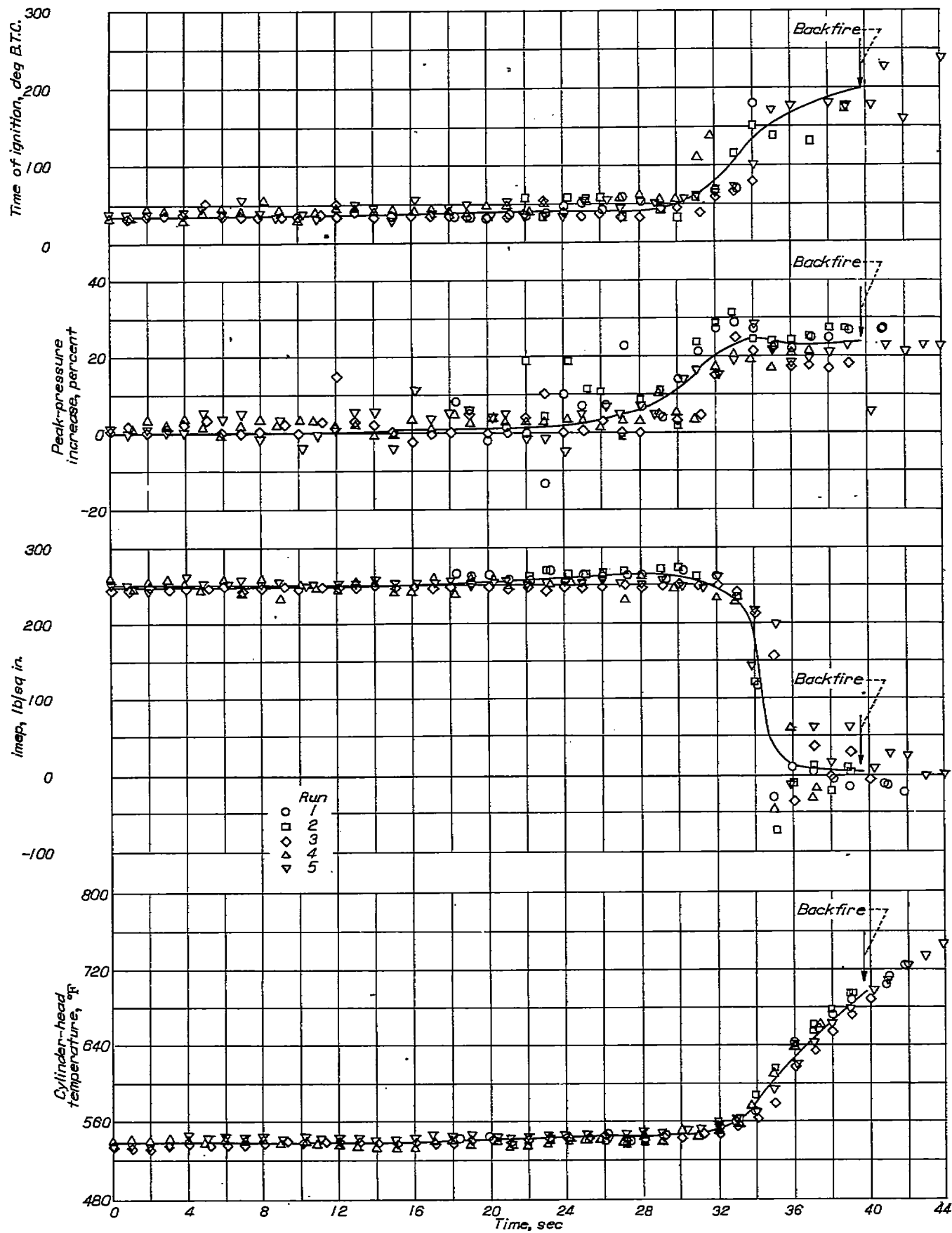


FIGURE IV-1.—Typical preignition runs indicating reproducibility of data in full-scale single-cylinder engine. Compression ratio, 6.65; engine speed, 3000 rpm; mixture temperature, 175° F. coolant temperature, 260° F; spark advance: inlet, 28° B. T. C.; outlet, 84° B. T. C.; fuel-air ratio, 0.070; preignition source, spark plug in exhaust side. (Fig. 4 of reference 5.)

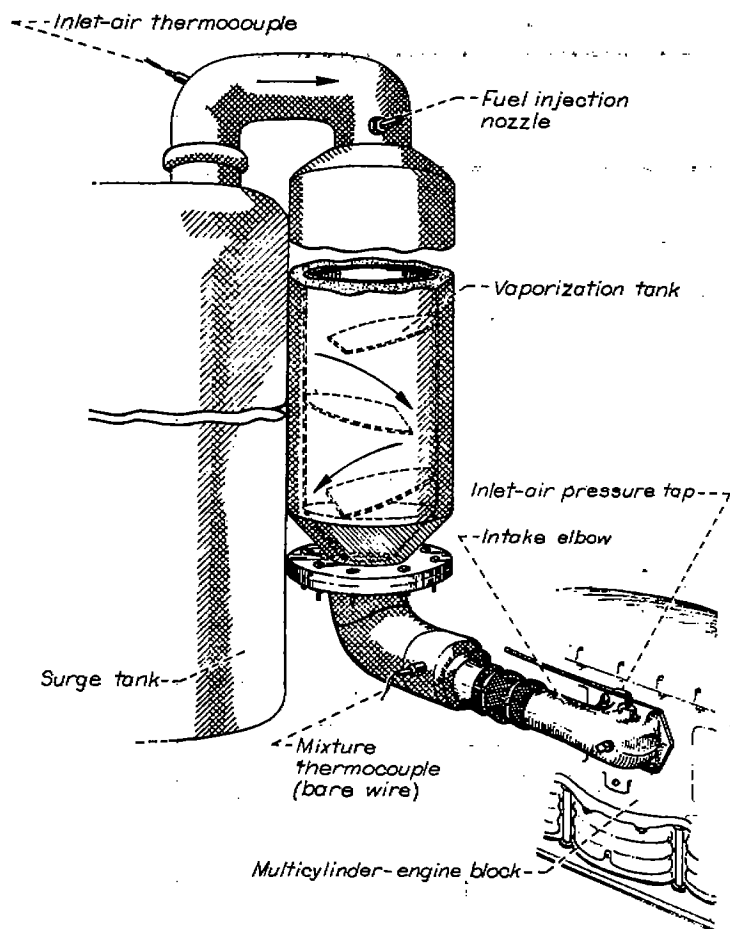


FIGURE IV-2.—Full-scale single-cylinder test-engine induction system. (Fig. 2 of reference 5.)

The curves in figure IV-1 represent the averages of the individual runs and may be considered typical of engine operation during preignition at a given set of conditions. All curves discussed in succeeding paragraphs have been obtained in the same manner from several runs at each operating condition.

The preignition run in figure IV-1 was terminated by backfiring, as was true for most of the runs conducted in reference 5. Backfiring occurs when the time of ignition is considerably earlier than that at which the intake valves close (118° B. T. C.). The flame cannot pass into the induction system unless a pressure rise occurs sufficient to slow down or to reverse the flow through the intake valves.

After a backfire, the fuel-air charge in the vaporization tank (fig. IV-2) burned and the resulting pressure rise caused reversal of the air flow at the tank entrance. Because the fuel was injected at this point, the flame burned out quickly. Combustion in the cylinder was reestablished after about 1 second, but the preignition source was sufficiently hot to cause early ignition again. Backfiring continued at intervals until a change in the operating conditions cooled the preignition source.

At high power output and fuel-air ratios leaner than 0.095, preignition caused backfiring. Preignition was stable at richer mixtures and ignition occurred near bottom center.

Effect of fuel-air ratio on preignition.—Fuel-air ratio, because of its influence on combustion temperatures and rate

of burning, is one of the important variables to be considered during preignition operation. The effect of fuel-air ratio on preignition is illustrated in figure IV-3. As seen in figure IV-3, the time of ignition at the lean fuel-air ratio (0.070) advanced to about 220° B. T. C. (40° B. B. C.) about 7 seconds after the start of the rapidly advancing preignition period. The time of ignition at the start of this period was about 48° B. T. C. At the rich fuel-air ratio (0.099), the time of ignition advanced less rapidly than at the lean fuel-air ratio and became stable at about 150° to 160° B. T. C. No backfire occurred at the rich fuel-air ratio.

The increase in peak pressure was about 20 percent at the lean fuel-air ratio and 25 percent at the rich fuel-air ratio; according to reference 5, however, these increases are in doubt because of scatter in the experimental data.

The power output (fig. IV-3) dropped sharply during the period of preignition. During the same period the cylinder-head temperatures increased sharply. As pointed out in reference 5, the piston temperature might be expected to follow curves similar to those shown for the cylinder-head temperature with the possibility that the temperature rise might be even greater.

Effect of power output on preignition.—The effect of engine power level on preignition is shown in figure IV-4. In order to obtain these data, it was necessary (reference 5) to use spark plugs of three different heat ranges. The results of these tests indicate that the time before backfiring increased as the power level decreased. This result is consistent with the decrease in cyclic temperatures as the power decreased, as indicated by the cylinder-head temperatures (fig. IV-4). The percentage increase in peak cylinder pressures increased as the power level decreased.

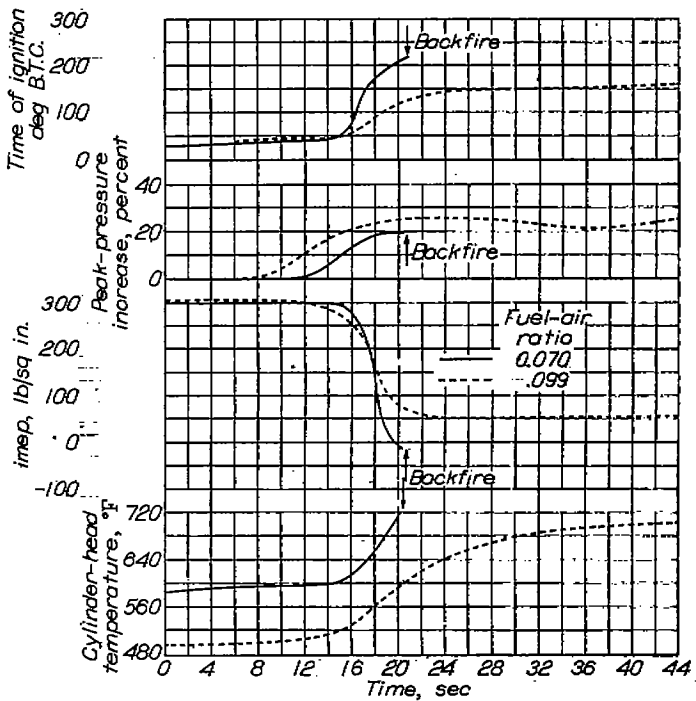


FIGURE IV-3.—Effect of fuel-air ratio on engine behavior during preignition. Compression ratio, 6.65; engine speed, 3000 rpm; mixture temperature, 175° F; coolant temperature, 250° F; spark advance: inlet, 28° B. T. C.; outlet, 34° B. T. C.; preignition source, spark plug in exhaust side. (Fig. 5 of reference 5.)

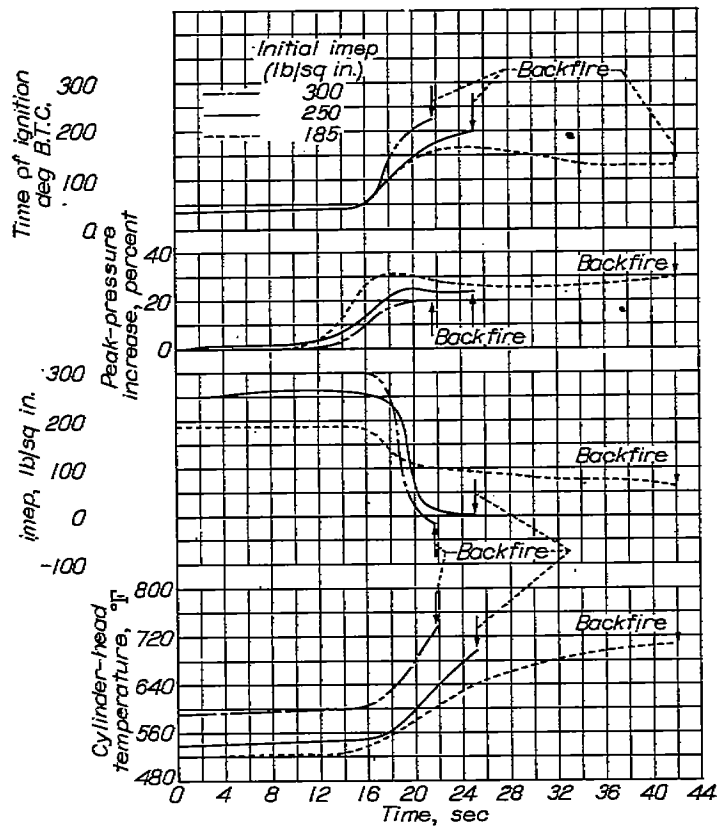


FIGURE IV-4.—Effect of power output on engine behavior during preignition. Compression ratio, 6.65; engine speed, 3000 rpm; mixture temperature, 175° F; coolant temperature, 250° F; spark advance: inlet, 28° B. T. C.; outlet, 34° B. T. C.; fuel-air ratio, 0.070; preignition source, spark plug in exhaust side. (Fig. 6 of reference 5.)

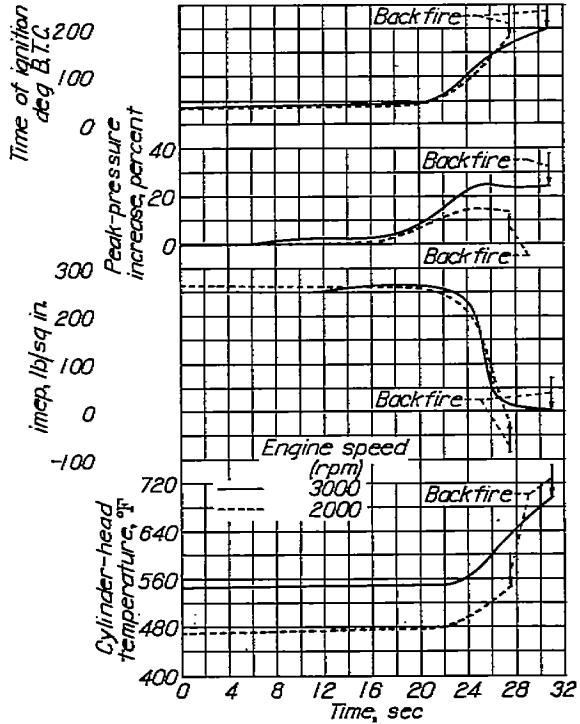


FIGURE IV-5.—Effect of engine speed on engine behavior during preignition. Compression ratio, 6.65; mixture temperature, 175° F; coolant temperature, 250° F; spark advance: inlet, 28° B. T. C.; outlet, 34° B. T. C.; fuel-air ratio, 0.070; preignition source, spark plug in exhaust side. (Fig. 8 of reference 5.)

Effect of engine speed on preignition.—Preignition data obtained at two engine speeds are shown in figure IV-5.

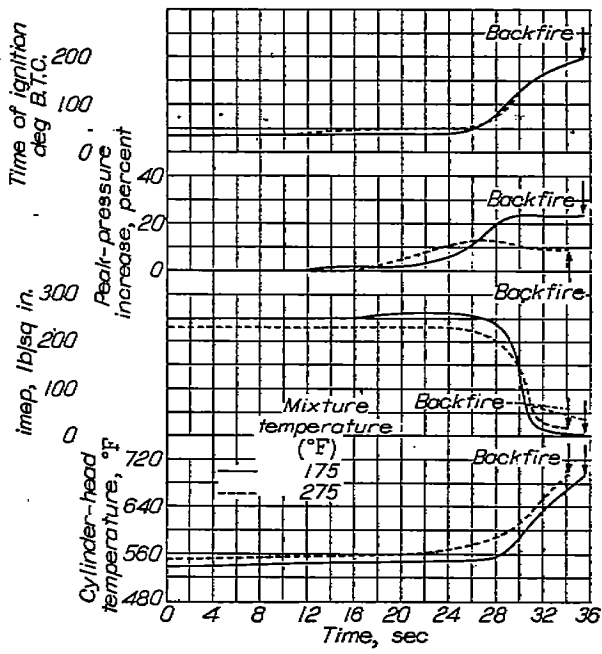


FIGURE IV-6.—Effect of mixture temperature on engine behavior during preignition. Compression ratio, 6.65; engine speed, 3000 rpm; coolant temperature, 250° F; spark advance: inlet, 28° B. T. C.; outlet 34° B. T. C.; fuel-air ratio 0.070; preignition source, spark plug in exhaust side. (Fig. 9 of reference 5.)

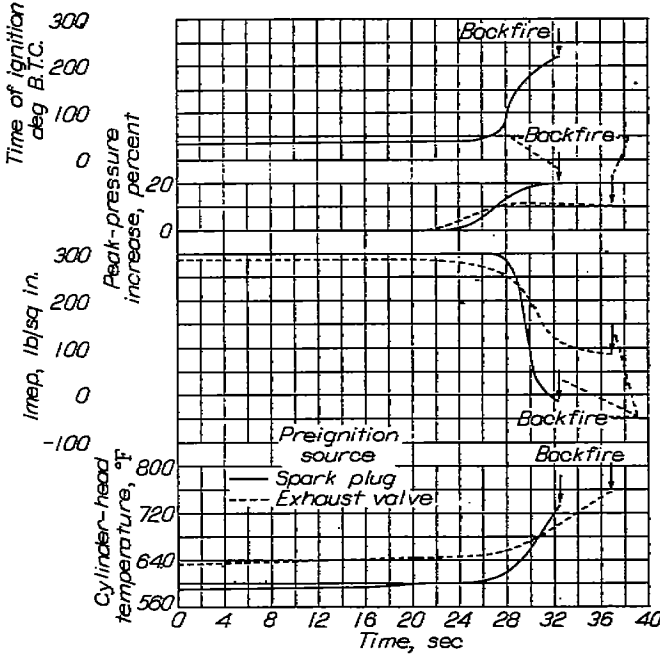
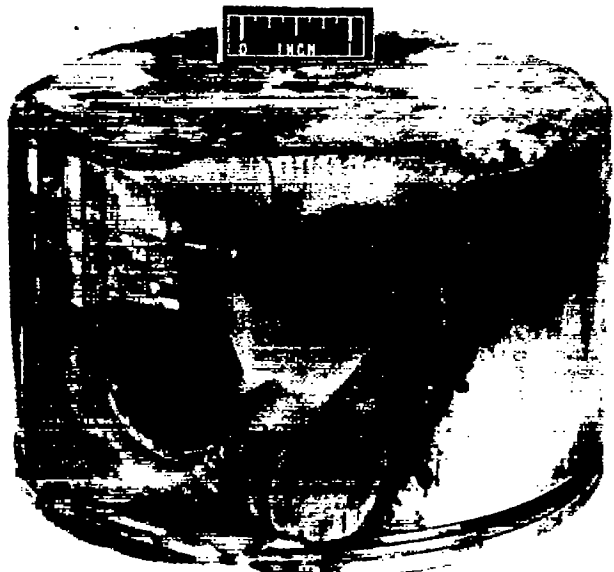


FIGURE IV-7.—Effect of preignition source on engine behavior during preignition. Compression ratio, 6.65; engine speed, 3000 rpm; mixture temperature, 175° F; coolant temperature, 250° F; spark advance: inlet, 28° B. T. C.; outlet, 34° B. T. C.; fuel-air ratio, 0.070. (Fig. 10 of reference 5.)

These two runs were made at about the same power level. Backfires were encountered in both cases at about the same time of ignition (195° B. T. C.).

The peak cylinder pressure increased about 15 and 25 percent at engine speeds of 2000 and 3000 rpm, respectively. This difference can be partly explained by the increase in the heat transferred per cycle at the lower engine speed. (See reference 5.) The cylinder-head-temperature rise (fig. IV-5) was less at the lower speed because backfiring occurred sooner.

Effect of mixture temperature on preignition.—Little difference was found in the preignition behavior of the engine that could be attributed to the influence of mixture temperature (fig. IV-6). At a mixture temperature of 175° F, the peak pressures were higher than at 275° F. The time-of-ignition curve at 275° F is incomplete because of difficulties with instrumentation. (See reference 5.)



(a) Piston failure. Clearance between top of piston skirt and cylinder barrel, 0.004 inch less than normal; imep, 271 pounds per square inch; fuel-air ratio, 0.098.

FIGURE IV-8.—Exhaust-side view of pistons after preignition runs. (Fig. 12 of reference 5.)



(b) Piston failure. Clearance between top of piston skirt and cylinder barrel, normal (0.021 in.); imep, 364 pounds per square inch; fuel-air ratio, 0.094.

FIGURE IV-8.—Continued. Exhaust-side view of pistons after preignition runs. (Fig. 12 of reference 5.)



(c) Piston failure. Clearance between top of piston skirt and cylinder barrel, 0.005 inch greater than normal; imep, 364 pounds per square inch; fuel-air ratio, 0.094.

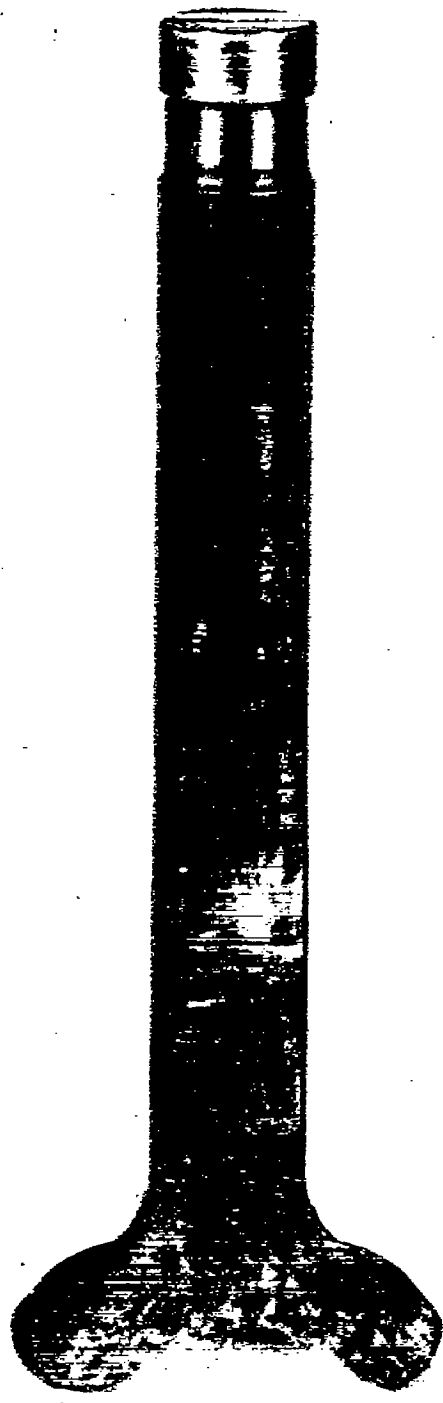
FIGURE IV-8.—Continued. Exhaust-side view of pistons after preignition runs. (Fig. 12 of reference 5.)



(d) Undamaged piston. Clearance between top of piston skirt and cylinder barrel, 0.013 inch greater than normal; imep, 392 pounds per square inch.

FIGURE IV-8.—Concluded. Exhaust-side view of pistons after preignition runs. (Fig. 12 of reference 5.)

Effect of ignition source on preignition.—In order to evaluate the effect of ignition source on preignition, two runs were made that employed a hot spark plug in one case and a hot exhaust valve in the other. The resulting data are shown in figure IV-7. Preignition advanced more slowly with the exhaust valve as the source; however, backfire was



(a) Exhaust valve after run of figure IV-8 (b). (Fig. 14 of reference 5.)

FIGURE IV-9.—Damage to engine components during piston failures in preignition runs.

encountered sooner when the spark plug initiated the preignition. The peak-pressure increase and the power decrease were greater when the spark plug served as the source of preignition.

Types of failure caused by preignition.—Typical examples of piston failures are shown in figure IV-8. These failures occurred in runs with reduced piston cooling and at generally

higher power levels than those of the runs described in the preceding paragraphs.

The first failure (fig. IV-8 (a)) resulted from a run in which the clearance between piston and cylinder was about 0.004 inch less than normal (0.021 in.) for the engine. In this case the piston seized and the side of the piston melted. With normal clearance (fig. IV-8 (b)) a higher power level was necessary to cause failure. This failure differed from the failure shown in figure IV-8 (a) in that local melting took place in the center of the piston crown. The failure shown in figure IV-8 (c) resulted from a run with the clearance 0.005 inch greater than normal. More local melting in the center of the piston crown was found with this clearance than was found in the run with normal clearance (fig. IV-8 (b)). In the last run (fig. IV-8 (d)), the clearance was increased 0.013 inch greater than normal and seizure and subsequent failure were not experienced at the power level investigated.

Examples of failures to other cylinder parts are shown in figure IV-9. The exhaust valve (fig. IV-9 (a)) burned during the run in which the piston failure in figure IV-8 (b) was encountered. The valve failure is attributed (reference 5) to particles of aluminum or other substance lodging between the valve and the valve seat. The cylinder barrel (fig. IV-9 (b)) was damaged when the piston shown in figure IV-8 (c) failed. The hot gases caused burning through the barrel into the coolant passage.



(b) Cylinder barrel after run of figure IV-8 (c). (Fig. 15 of reference 5.)

FIGURE IV-9.—Concluded. Damage to engine components during piston failures in preignition runs.

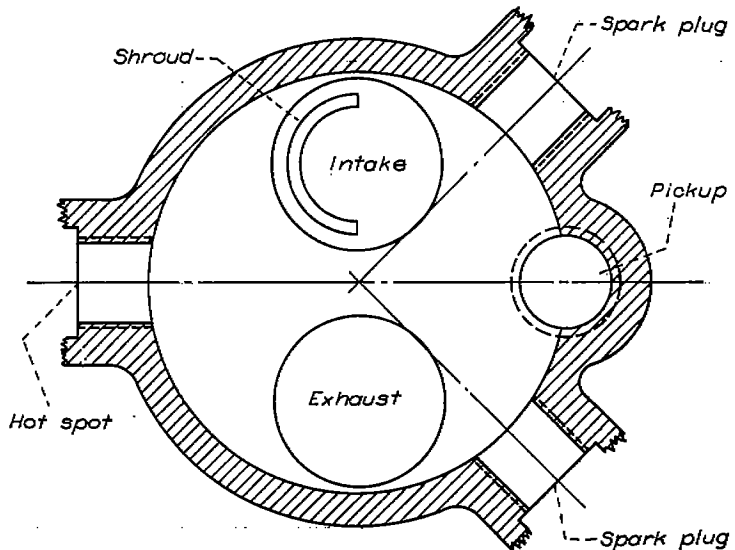
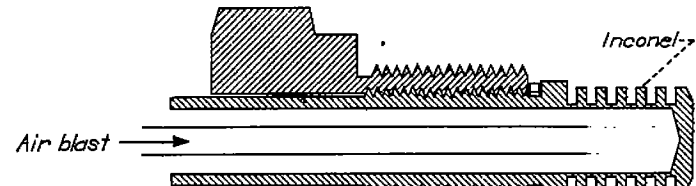
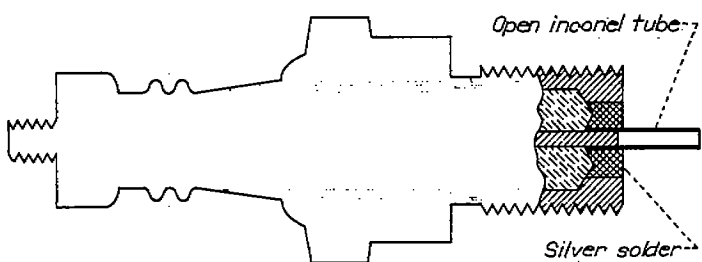


FIGURE IV-10.—Diagram of CFR cylinder used in small-scale engine studies of fuel preignition limits. (Fig. 1 of reference 10.)



(a)



(b)

(a) Flinned hot spot. (Fig. 2 of reference 10.)

(b) Open-tube hot spot. (Fig. 3 of reference 10.)

FIGURE IV-11.—Hot spots employed in preignition studies.

PREIGNITION CHARACTERISTICS OF FUELS

The nature of preignition and the behavior of an engine during preignition operation has been discussed; the influence of fuels on preignition is now considered. The fundamental relations that govern the preignition of fuels are studied in references 7 to 9. The results as cited by Male and Evvard (reference 10) indicate that the hot-spot "threshold" temperature required to produce preignition is relatively insensitive to fuel composition. The ability of a fuel to heat an engine hot spot to the preignition temperature by normal or surface combustion, however, was found dependent upon

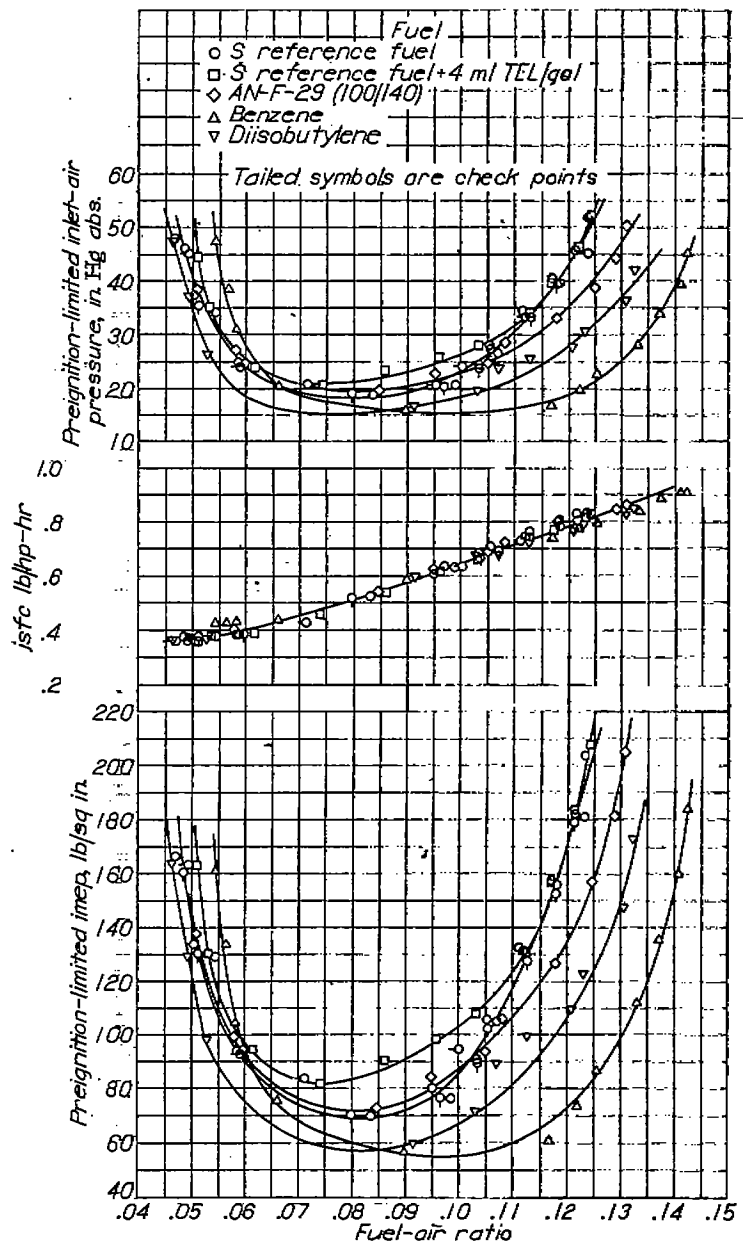


FIGURE IV-12.—Preignition limits of fuels in supercharged CFR engine. Compression ratio, 7.0; engine speed, 1800 rpm; inlet-air temperature, 100° F; coolant temperature, 250° F; spark advance, 32° B. T. C.; preignition source, finned hot spot. (Fig. 4 of reference 10.)

fuel composition, operating conditions, and design of engine and hot spot.

The investigation reported in reference 10 was intended to demonstrate the preignition-limited performance of several fuels. A later investigation reported by Male (reference 11) illustrates how the preignition-limited performance of fuels is affected by engine operating conditions. Both these investigations were conducted on small-scale engines.

Preignition limits of several fuels.—For the study of preignition-limited performance of fuels (reference 10), a supercharged CFR engine with an aluminum piston and a sodium-cooled exhaust valve were used. The intake valve was shrouded (180° shroud) and was installed as shown in figure IV-10. According to reference 10, the shrouded valve aids in isolating the effects of knock.

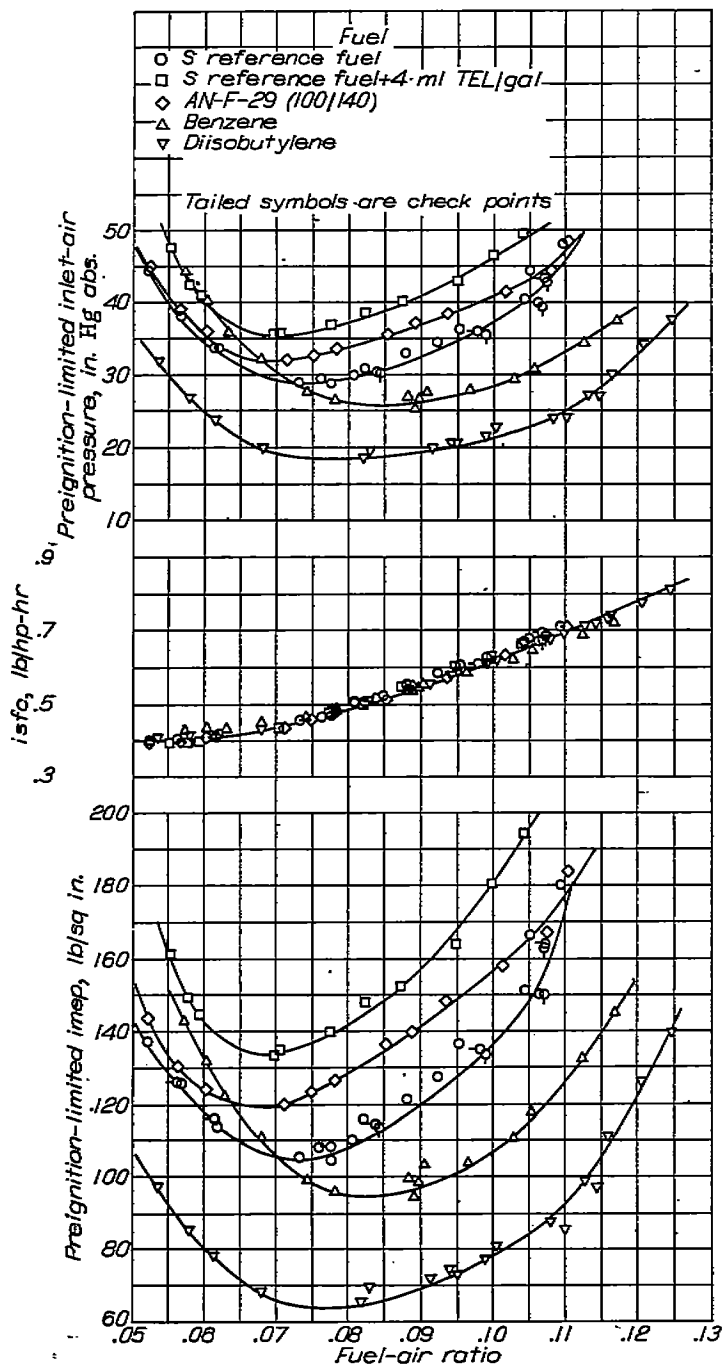


FIGURE IV-13.—Preignition limits of fuels in supercharged CFR engine. Compression ratio, 7.0; engine speed, 1800 rpm; inlet-air temperature, 225° F; coolant temperature, 250° F; spark advance, 20° B. T. C.; preignition source, open-tube hot spot. (Fig. 5 of reference 10.)

This fact is substantiated by unpublished data showing that a shrouded intake valve decreases the sensitivity of thermal-plug temperatures to knock. In order to follow the changing pressure diagram during preignition and to detect knock, a magnetostriction pickup unit was used in conjunction with a cathode-ray oscilloscope. The position of this pickup unit is shown in figure IV-10. (See reference 10.)

The two types of hot spot used in reference 10 are shown in figure IV-11. For tests in which the finned hot spot (fig. IV-11 (a)) was used, the inlet-air temperature was 100° F and the spark advance was 32° B. T. C. The inlet-air

temperature was 225° F and the spark advance 20° B. T. C. for the tests in which the open-tube hot spot (fig. IV-11 (b)) was used.

Preignition-limited performance data for five fuels at two sets of engine conditions are shown in figures IV-12 and IV-13. In general, the curves of preignition-limited indicated mean effective pressure have similar shapes with the minimum power points occurring at fuel-air ratios richer than stoichiometric. Between fuel-air ratios of about 0.070 to 0.085 the relative performance of the fuels in order of decreasing performance was

S reference fuel + 4 ml TEL/gal
 AN-F-29 (100/140 grade)
 S reference fuel
 Benzene
 Diisobutylene

The over-all spread in indicated mean effective pressure for the five fuels was greater in figure IV-13 than in figure IV-12. This difference and the change in order of benzene and diisobutylene at mixtures richer than 0.085 is attributed (reference 10) to differences in the hot spots, or conditions, or both.

In figures IV-12 and IV-13, the reproducibility of preignition data is demonstrated by check points on the curve for unleaded S reference fuel. The deviations of the data points from the faired curve are about the same as those found in determinations of knock-limited performance.

At constant inlet-air pressures, the maximum thermal-plug temperatures were determined for the fuels (reference 10). This step was considered necessary because the ability of a fuel to increase general engine temperatures might affect the preignition characteristics of the fuel. Preignition-limited fuel-air ratios (fig. IV-12) and thermal-plug temperatures at corresponding inlet-air pressures are shown in the following table:

Fuel	Inlet-air pressure, in. Hg abs					
	20		30		40	
	Thermal-plug temperature * (° F)	Preignition-limited fuel-air ratio ^b	Thermal-plug temperature * (° F)	Preignition-limited fuel-air ratio ^b	Thermal-plug temperature * (° F)	Preignition-limited fuel-air ratio ^b
Benzene	561	0.123	669	0.135	761	0.141
Diisobutylene	541	.106	649	.128	735	.133
S reference fuel	529	.093	631	.110	715	.118
AN-F-29	537	.089	641	.114	728	.125
S reference fuel + 4 ml TEL	529	-----	631	.108	715	.118

* Observed at fuel-air ratio for maximum thermal-plug temperature.

^b Data taken from fig. IV-12.

It was concluded (reference 10) from these data that thermal-plug temperatures do not offer a dependable basis for establishing fuel preignition ratings. This conclusion was drawn from the investigations of S reference fuel in which it was found that the same thermal-plug temperatures were obtained with and without tetraethyl lead, although the preignition-limited-performance curves were different (fig. IV-12).

The presence of tetraethyl lead in S reference fuel appears (fig. IV-12) to increase the preignition-limited performance. A similar investigation in which triptane was used showed the same trend (fig. IV-14). Also shown in figure IV-14 is a curve representing the preignition-limited performance of AN-F-28 (28-R) aviation gasoline. The preignition-limited performance of this fuel is very nearly the same as that of triptane containing 4 ml TEL per gallon. This result is of interest inasmuch as the knock-limited performance of triptane is considerably greater than that of AN-F-28 fuel under most operating conditions. (See ch. II.) A curve for S reference fuel is included in figure IV-14 for comparison. This curve was determined at the time of the triptane and AN-F-28 runs and is slightly different from the S reference fuel curves in figures IV-12 and IV-13.

Preignition limits of aromatic amines.—The effects of six aromatic amines on the preignition-limited performance of AN-F-28 (28-R) fuel were investigated in reference 12.

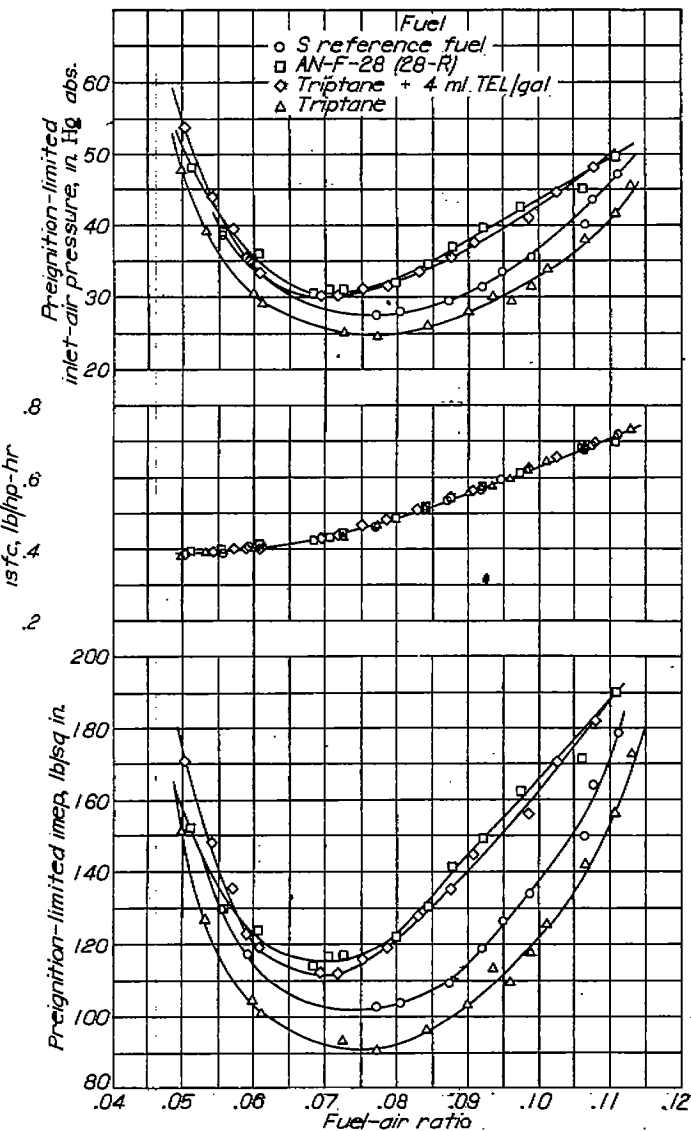


FIGURE IV-14.—Comparison of preignition limits of triptane (leaded and unleaded) with preignition limits of other fuels in supercharged CFR engine. Compression ratio, 7.0; engine speed, 1800 rpm; inlet-air temperature, 225° F; coolant temperature, 250° F; spark advance, 20° B. T. C.; preignition source, open-tube hot spot. (Fig. 6 of reference 10.)

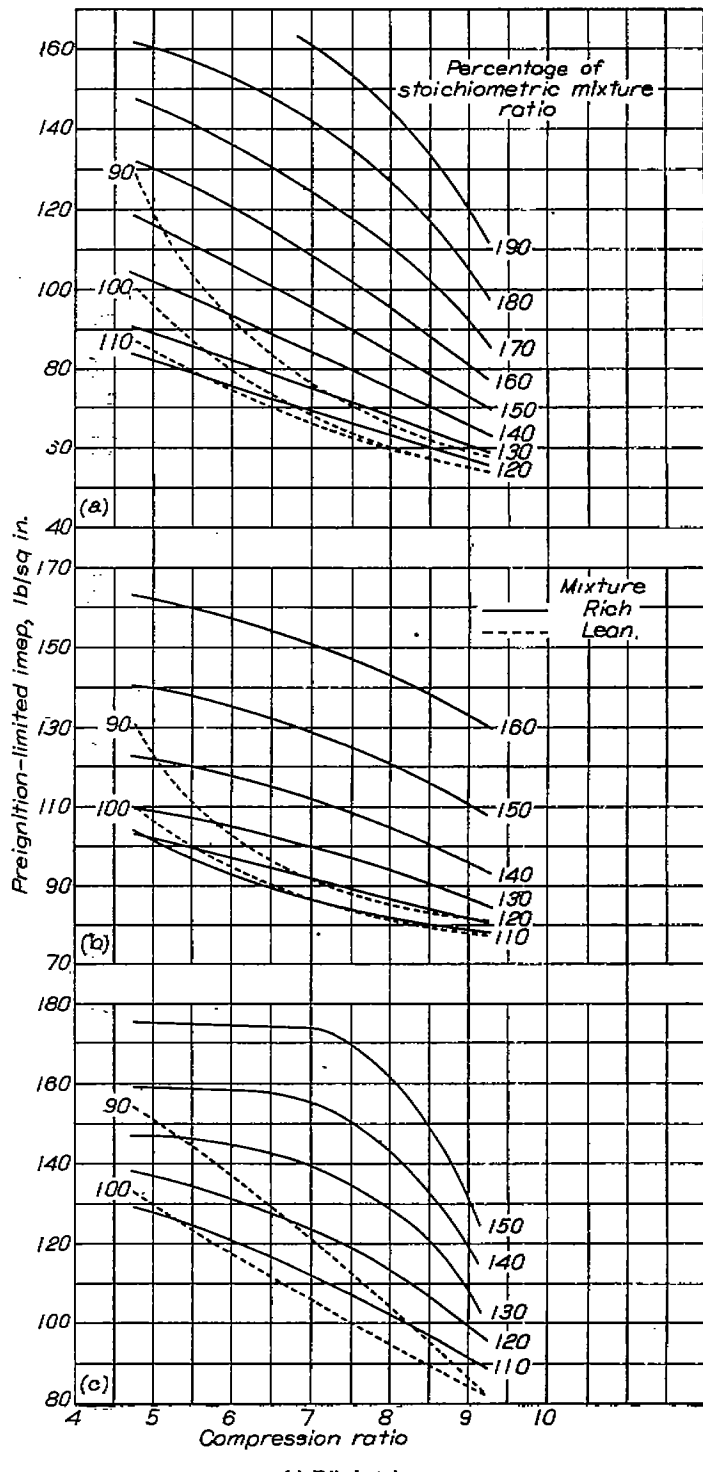


FIGURE IV-15.—Effect of compression ratio on preignition limits in supercharged CFR engine. Engine speed, 1800 rpm; inlet-air temperature, 225° F; coolant temperature, 250° F; spark advance, 20° B. T. C.; preignition source, open-tube hot spot. (Fig. 14 of reference 11.)

In this study, blends of AN-F-28 (28-R) fuel containing 2 percent by weight of the following amines were prepared and tested: xylidines, cumidines, N-methylxylidines, N-methylcumidines, N-methylaniline, and N-methyltoluidines. A CFR engine was used for these experiments. Pertinent details of the setup have been mentioned in connection with the runs shown in figures IV-12 to IV-14. A more complete description is presented in reference 11.

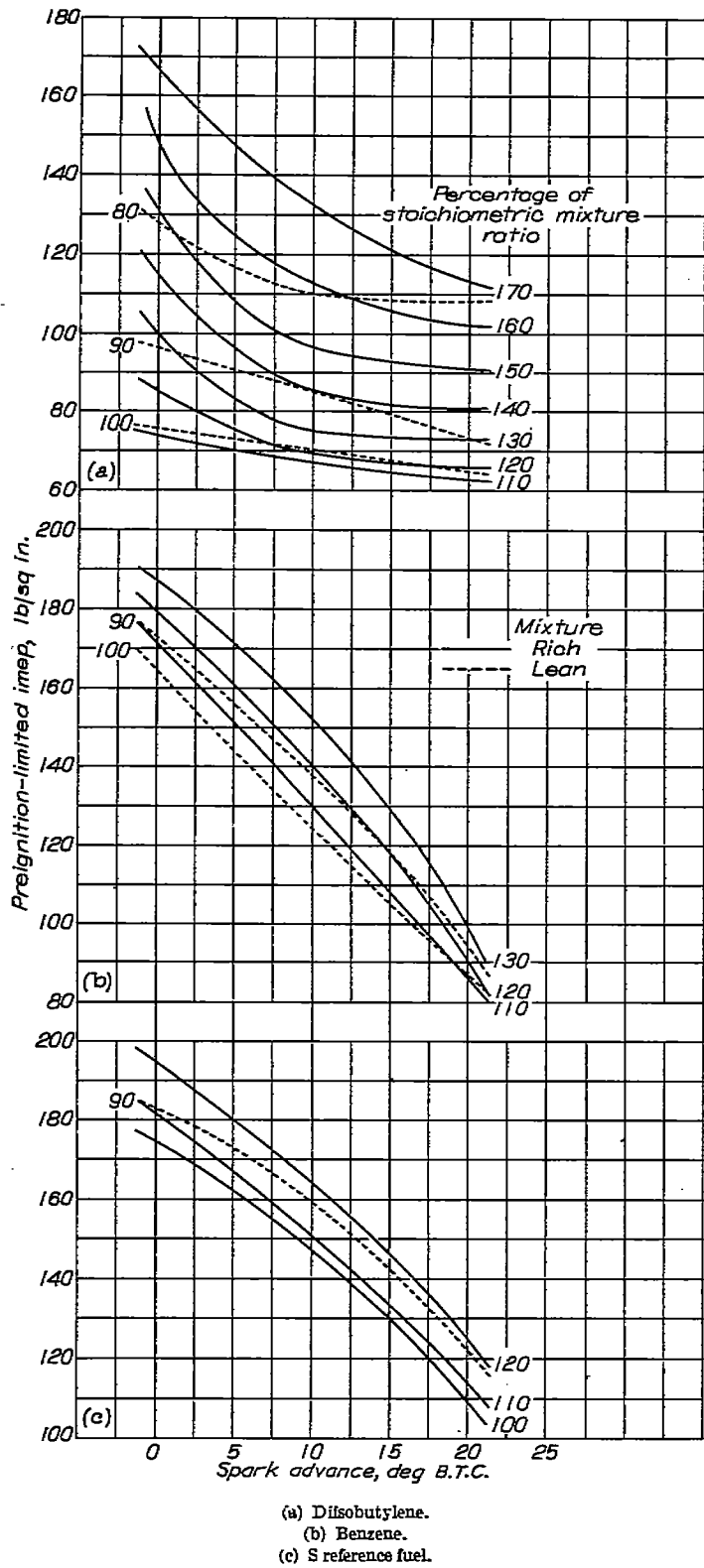


FIGURE IV-16.—Effect of spark advance on preignition limits in supercharged CFR engine. Compression ratio, 7.0; engine speed, 1800 rpm; inlet-air temperature, 225° F; coolant temperature, 250° F; preignition source, open-tube hot spot. (Fig. 15 of reference 11.)

The results of the investigation of reference 12 are presented in the following table in the form of ratios of preignition-limited indicated mean effective pressures of the six blends to that of AN-F-28 (28-R) fuel. This basis of comparison was chosen in order to eliminate effects of day-to-day variations in performance of the engine as well as differences arising from changes in the hot spot.

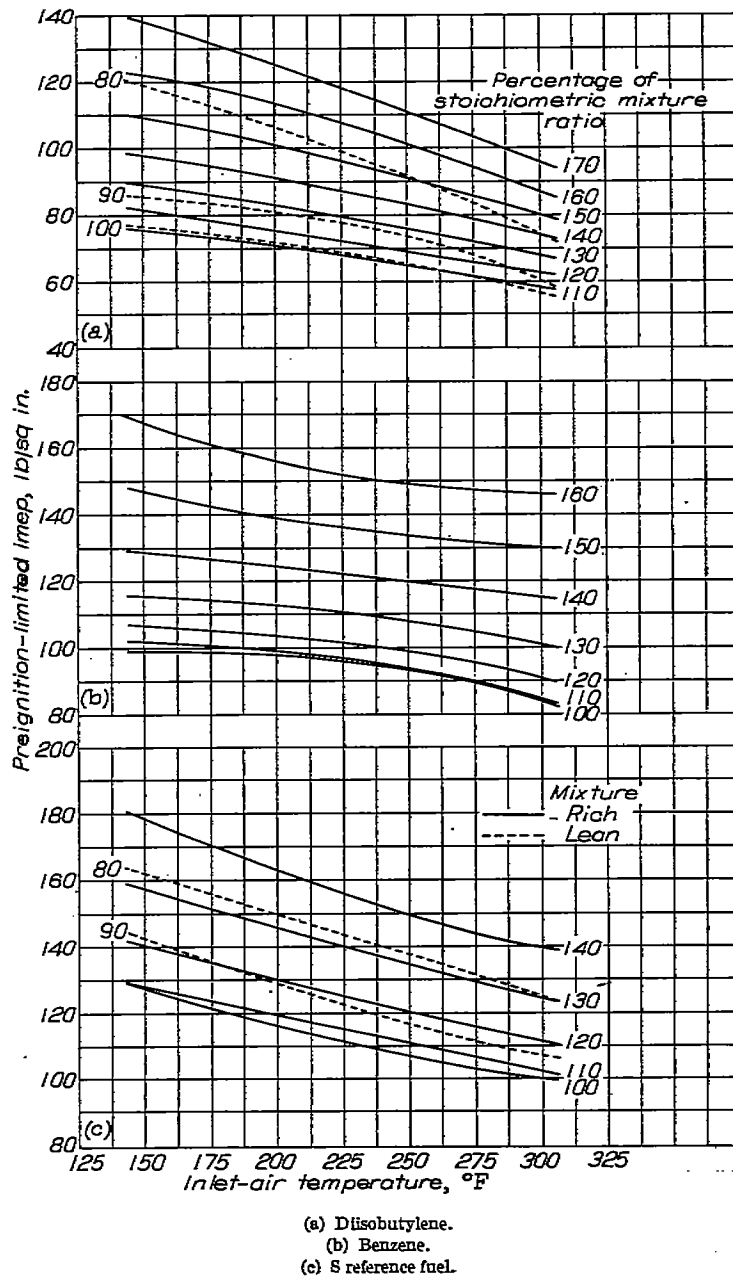


FIGURE IV-17.—Effect of inlet-air temperature on preignition limits in supercharged CFR engine. Compression ratio, 7.0; engine speed, 1800 rpm; coolant temperature, 250° F; spark advance, 20° B. T. C.; preignition source, open-tube hot spot. (Fig. 16 of reference 11.)

Aromatic amine added to AN-F-28 (28-R) (2 percent by weight)	Fuel-air ratio				
	0.06	0.07	0.08	0.09	0.10
imep ratio *					
None	1.00	1.00	1.00	1.00	1.00
N-methylaniline	1.02	.98	.99	.99	1.01
N-methyltoluidines	.91	.92	.94	.97	.98
Xylylidines	.96	.95	.96	1.00	1.02
N-methylxylylidines	.93	.93	.93	.99	1.00
Oumidines	.98	.91	.91	.91	.91
N-methylcumidines	.92	.90	.96	.97	.99

* Ratio of imep of blend to imep of 28-R fuel.

Of the aromatic amines examined in reference 12, N-methylaniline and N-methylxylylidines had the highest preignition limits; however, within the experimental accuracy of these tests, the preignition limits of these two aromatic amines appear to be equal to the preignition limit

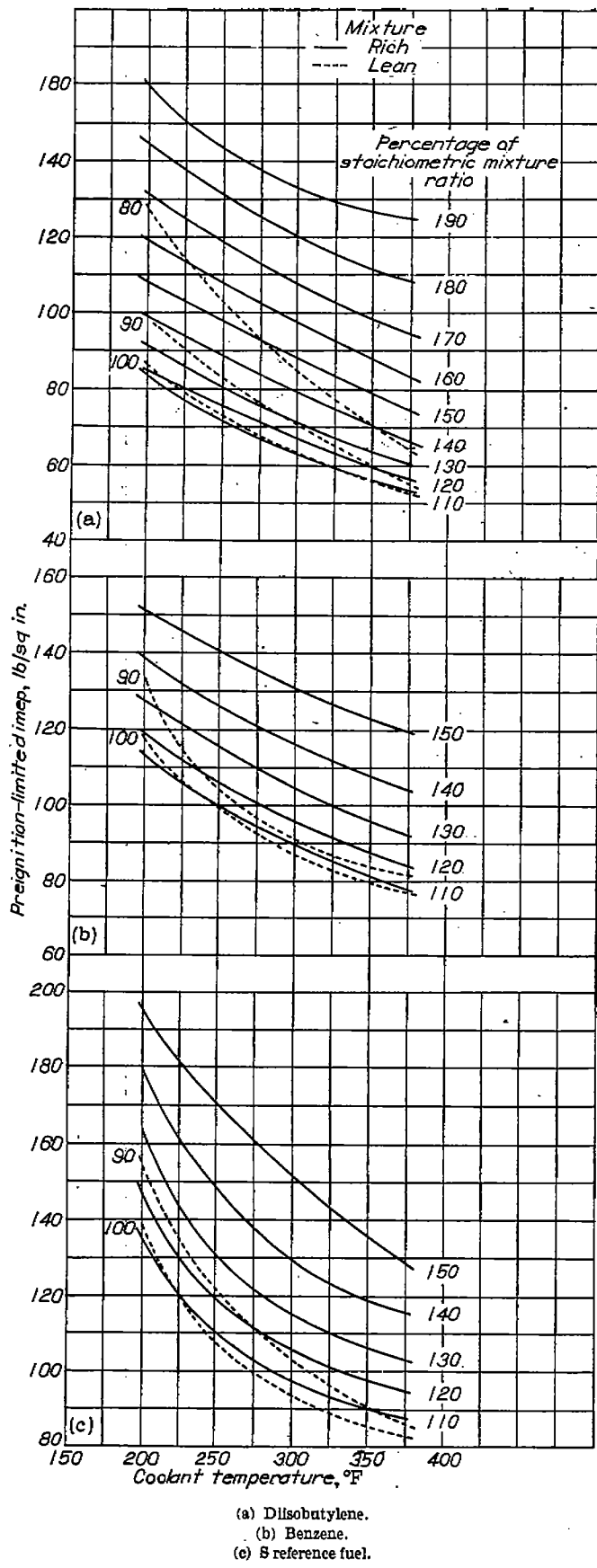


FIGURE IV-18.—Effect of coolant temperature on preignition limits in supercharged CFR engine. Compression ratio, 7.0; engine speed, 1800 rpm; inlet-air temperature, 22° F; coolant temperature, 25° F; spark advance, 20° B. T. C.; preignition source, open-tube hot spot. (Fig. 17 of reference 11.)

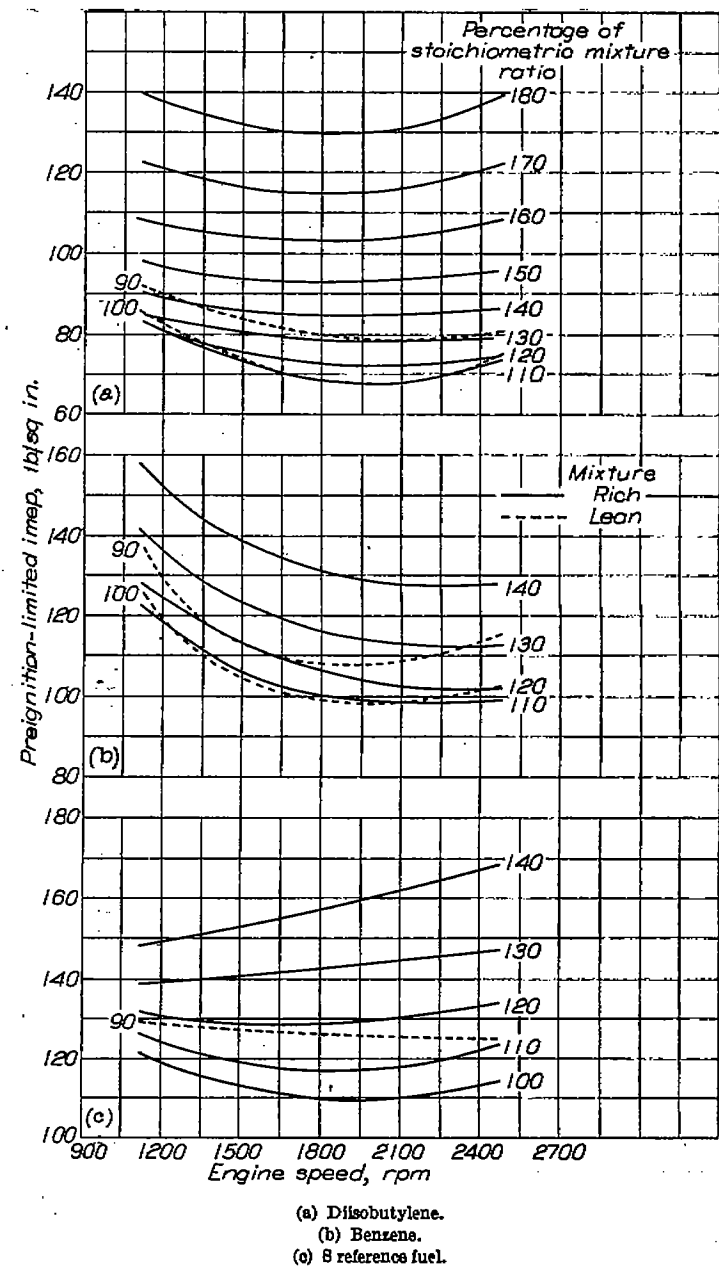


FIGURE IV-19.—Effect of engine speed on preignition limits in supercharged CFR engine. Compression ratio, 7.0; inlet-air temperature, 22° F; coolant temperature, 25° F; spark advance, 20° B. T. C.; preignition source, open-tube hot spot. (Fig. 18 of reference 11.)

of the base fuel, AN-F-28 (28-R). At lean fuel-air ratios, the remaining aromatic amines lowered the preignition limit of AN-F-28 (28-R) fuel about 2 to 10 percent. At rich fuel-air ratios, the cumidines lowered the preignition limit of AN-F-28 (28-R) fuel about 9 percent, whereas the other aromatic amines had little or no effect on the base fuel.

EFFECT OF ENGINE VARIABLES ON PREIGNITION-LIMITED PERFORMANCE

The influence of engine operating variables on preignition-limited performance is illustrated in reference 11. The study was made in a supercharged CFR engine; the following three fuels were used: S reference fuel, diisobutylene, and benzene. The hot spot was an open-tube type. (See fig. IV-11 (b).)

Effect of compression ratio on preignition limit.—The variation of preignition-limited indicated mean effective pressure with compression ratio is shown in figure IV-15. For the three fuels examined, the preignition-limited performance decreased as the compression ratio increased. At the stoichiometric fuel-air ratio, this change for the fuels varied between approximately 7 and 12 pounds per square inch per unit change in compression ratio. The decrease in preignition limits may be attributed to the increase in cyclic temperatures as the compression ratio is increased.

Effect of spark advance on preignition limit.—In figure IV-16, the preignition-limited indicated mean effective pressure is seen to decrease as the spark was advanced. Among the fuels this decrease was about 0.5 to 4 pounds per square inch per degree of spark advance at stoichiometric mixtures. The magnitude of this spread in indicated mean effective pressure among the fuels results from the fact that the sensitivity of diisobutylene to changes of spark advance is so different from the sensitivity of the other fuels (fig. IV-16).

Effect of inlet-air temperature on preignition limit.—The effect of inlet-air temperature on preignition-limited performance is illustrated in figure IV-17. The slopes of the curves for the three fuels are very similar. At stoichiometric mixtures, the decrease in preignition-limited indicated mean effective pressure in these experiments was about 0.1 to 0.3 pound per square inch per °F. Here again the decrease in preignition limits can be attributed to increased cyclic temperatures.

Effect of coolant temperature on preignition limit.—The effect of coolant temperature on preignition limits of the three fuels was determined by using three different coolants in an evaporative cooling system. The coolants used were water, ethylene glycol, and a mixture of water and ethylene glycol. The results of these tests are shown in figure IV-18.

As shown in figure IV-18, the preignition-limited performance decreased as the coolant temperature was increased; however, as emphasized in reference 11, the effect is not solely a temperature effect but includes also the effect of

differences in heat-transfer characteristics of the three coolants.

Effect of engine speed on preignition limit.—The results of runs in which the effect of engine speed on preignition-limited performance were investigated are shown in figure IV-19. Many of these curves, especially those near stoichiometric mixtures, pass through a minimum. At the stoichiometric mixture, minimum values of preignition-limited indicated mean effective pressure were found at engine speeds between 1500 and 2100 rpm.

REFERENCES

1. Biermann, Arnold E., and Corrington, Lester C.: Relation of Preignition and Knock to Allowable Engine Temperatures. NACA ARR 3G14, 1943.
2. Rothrock, A. M., and Biermann, Arnold E.: The Knocking Characteristics of Fuels in Relation to Maximum Permissible Performance of Aircraft Engines. NACA Rep. 655, 1939.
3. MacCoul, Neil: Power Loss Accompanying Detonation. SAE Jour., vol. 44, no. 4, April 1939, pp. 154-160.
4. Hundere, A., and Bert, J. A.: Preignition and Its Deleterious Effects in Aircraft Engines. SAE Quart. Trans., vol. 2, no. 4, Oct. 1948, pp. 546-562.
5. Corrington, Lester C., and Fisher, William F.: Effect of Preignition on Cylinder Temperatures, Pressures, Power Output, and Piston Failures. NACA TN 1637, 1948.
6. Waldron, C. D., and Biermann, A. E.: Method of Mounting Cylinder Blocks of In-Line Engines on CUE Crankcases. NACA RB E4G27, 1944.
7. Serruys, Max: Experimental Study of Ignition by Hot Spot in Internal Combustion Engines. NACA TM 873, 1938.
8. Spencer, R. C.: Preignition Characteristics of Several Fuels under Simulated Engine Conditions. NACA Rep. 710, 1941.
9. Alquist, Henry E., and Male, Donald W.: Trends in Surface-Ignition Temperatures. NACA ARR E4I25, 1944.
10. Male, Donald W., and Evvard, John C.: Preignition-Limited Performance of Several Fuels. NACA Rep. 811, 1945.
11. Male, Donald W.: The Effect of Engine Variables on the Preignition-Limited Performance of Three Fuels. NACA TN 1131, 1946.
12. Male, Donald W.: The Effect of Six Aromatic Amines on the Preignition-Limited Performance of 28-R Aviation Fuel in a CFR Engine. NACA MR E5E12a, 1945.

CHAPTER V

HYDROCARBONS AND ETHERS AS ANTIKNOCK BLENDING AGENTS

Improvements in aircraft power plants during the past 30 years have resulted in demands for fuels of increasingly high antiknock performance. This trend has necessitated a thorough investigation of possible high-antiknock compounds that may or may not occur naturally in petroleum. The task of surveying an endless procession of possible fuel-blending agents has fallen to the petroleum industry and interested research groups. Through the combined efforts of the organizations concerned, a large quantity of data has been amassed. These data permit an accurate appraisal of the merits of many chemical compounds heretofore given little more than cursory consideration as fuel-blending agents.

As a participant in this field of research, the NACA in 1937 sponsored a project by the National Bureau of Standards for the preparation of 1-liter quantities of selected paraffins and olefins. The engine evaluation of the antiknock qualities of these compounds was first conducted under the sponsorship of the American Petroleum Institute (API) and the results of this work have been reported by Lovell (reference 1). In addition, the API has sponsored a synthesis program conducted at the laboratories of Ohio State University. All these programs have been continued up to the present and were augmented during 1942-47 by additional synthesis and engine evaluation at the NACA Lewis laboratory.

The synthesis project at the National Bureau of Standards has been devoted to compounds in the paraffinic and olefinic classes; the synthesis project at the NACA Lewis laboratory has been devoted to compounds in the aromatic and ether classes; and the synthesis program at Ohio State University has been devoted to compounds in these and other classes.

The engine evaluation of pure compounds sponsored by the API was conducted in laboratories of the General Motors Corp. and the Ethyl Corp. The engine evaluation of blends reported in this chapter was conducted at the NACA Lewis laboratory.

Results of the NACA study of paraffins, olefins, aromatics, and ethers are published in a number of reports (references 2 to 14); each report contains data for several compounds on factors such as blending characteristics, temperature sensitivity, lead response, and relation between molecular structure and antiknock ratings. In the succeeding sections of this chapter the effects of molecular structure on these factors of performance are discussed.

ENGINES AND EXPERIMENTAL CONDITIONS

The engine evaluation of the antiknock characteristics of organic compounds was conducted in four test engines: (1) a CFR engine conforming to specifications for the A. S. T. M. Aviation method (D614-47T) for rating fuels; (2) CFR engine conforming to specifications for the A. S. T. M. Supercharge method (D909-47T) for rating fuels; (3) an engine having a displacement of 17.6 cubic inches (about half that of a CFR engine) and popularly known as the 17.6

engine; and (4) a full-scale air-cooled aircraft cylinder mounted on a CUE crankcase.

The 17.6 and A. S. T. M. Supercharge engines were equipped with dual fuel systems, one line for the "warm-up fuel" and one for the test fuel. Knocking was detected in both engines by means of a cathode-ray oscilloscope in conjunction with a magnetostriction pickup unit.

The full-scale single-cylinder test engine was fitted with baffles and cooling air was directed toward the cylinder in order to simulate cooling conditions in flight. Further details of the full-scale installation are given in reference 2.

Pertinent operating conditions for the various engines are presented in table V-1. The 17.6 engine was operated at two inlet-air temperatures, 100° and 250° F, in order to obtain an indication of the sensitivity of fuels to changes in temperature. When the inlet-air temperature was varied, all other conditions were held the same as shown in table V-1.

TABLE V-1.—ENGINE OPERATING CONDITIONS

Condition	Engine				
	17.6	A. S. T. M. Aviation	A. S. T. M. Super- charge	Full-scale single cylinder	
				Simulated take-off	Simulated cruise
Compression ratio.....	7.0	Variable	7.0	7.3	7.3
Inlet-air temperature, °F.....	100 250	125	226	260	210
Inlet-mixture temperature, °F.....		220			
Inlet-air pressure.....	Variable	Atmospheric	Variable	Variable	Variable
Fuel-air ratio.....	Variable	0.67	Variable	Variable	Variable
Speed, rpm.....	1800	1200	1900	2600	2000
Spark advance, deg B. T. C.....	30	35	45	20/20	20/20
Coolant temperature, °F.....	212	874	875	85	85
Cooling-air temperature, ^b , °F.....					

^a Approximate.

^b Cooling-air flow was determined by running engine at brake mean effective pressure of 140 lb/sq in. and fuel-air ratio of 0.10 and by adjusting air flow until temperature of rear spark-plug bushing was 365° F.

The conditions shown in table V-1 for the A. S. T. M. Aviation and A. S. T. M. Supercharge engines are standard for these engines when antiknock ratings are being determined. As indicated in table V-1, the A. S. T. M. Aviation engine is a nonsupercharged engine in which the compression ratio is varied in order to determine the knock limit of a given fuel at a lean fuel-air ratio with all conditions other than compression ratio held reasonably constant. On the other hand, the A. S. T. M. Supercharge engine is operated with all conditions except inlet-air pressure and fuel-air ratio held constant. Knock limits are determined by varying the manifold pressure until knocking occurs. Although the fuel-air ratio can be varied for this engine, antiknock ratings are made at a rich fuel-air ratio, usually about 0.11. The A. S. T. M. Aviation method (lean ratings) may thus be indicative of fuel performance at cruise conditions; whereas the A. S. T. M. Supercharge method (rich ratings) may be indicative of take-off performance.

The full-scale engine conditions were proposed by the Coordinating Research Council in an effort to standardize full-scale single-cylinder experimental engine operation throughout the country. During the early stages of the NACA investigation, fuels were investigated in the full-scale single-cylinder engine (quantity permitting), but these methods were later abandoned when it became apparent that the small-scale engine adequately described the fuel performance.

COMPOUNDS INVESTIGATED

The compounds investigated included 13 branched paraffins, 5 branched olefins, 27 aromatics, and 22 ethers. The paraffins and olefins examined were in the C₆ to C₉ molecular-weight range; the aromatics were in the C₆ to C₁₂ range; and the ethers were in the C₄ to C₁₁ range.

The individual compounds, together with physical properties determined by the National Bureau of Standards or the NACA Lewis Laboratory, are listed in table V-2.

TABLE V-2.—PHYSICAL PROPERTIES

(a) Paraffins and olefins.*

Paraffins and olefins	Formula	Freezing point (°C)	Boiling point		Density at 20° C (gram/ml)	Refractive index n_D^{20}
			(°F)	(°C)		
Paraffins						
2-Methylbutane	C ₅ H ₁₂	-159.890	82.14	27.854	0.61967	1.35373
2,2-Dimethylbutane	C ₆ H ₁₄	-69.73	121.54	49.743	0.64917	1.36876
2,3-Dimethylbutane		-128.41	138.38	57.900	.66164	1.37495
2,2,3-Trimethylbutane	C ₇ H ₁₆	-24.96	171.57	80.871	0.69002	1.38946
2,3-Dimethylpentane			163.62	88.79	.69112	1.38200
2,2,3-Trimethylpentane	C ₈ H ₁₈	-112.27	229.72	109.844	0.71605	1.40295
2,2,3,3-Trimethylpentane		-100.70	238.57	114.763	.72020	1.40762
2,3,4-Trimethylpentane		-109.210	236.25	113.470	.71905	1.40422
2,2,3,3-Tetramethylpentane	C ₉ H ₂₀	-9.9	284.41	140.23	0.7566	1.4234
2,2,3,4-Tetramethylpentane		-121.6	271.42	133.01	.7390	1.4146
2,2,4,4-Tetramethylpentane		-66.54	232.10	122.28	.7198	1.40683
2,3,3,4-Tetramethylpentane		-102.1	236.77	141.54	.7547	1.4220
2,4-Dimethyl-3-ethylpentane			278.11	136.73	.7379	1.4137
Olefins						
2,3-Dimethyl-2-pentene	C ₇ H ₁₄	-119	207	97	0.728	1.421
2,3,4-Trimethyl-2-pentene	C ₈ H ₁₆		241.27	116.28	0.7434	1.4275
2,4,4-Trimethyl-1-pentene		-93.5	214.59	101.44	.7150	1.4086
2,4,4-Trimethyl-2-pentene		-106.4	220.84	104.91	.7212	1.4180
3,4,4-Trimethyl-2-pentene			234	112	.739	1.423

*Data from reference 15.

(b) Aromatics.

Aromatic	Formula	Freezing point (°C)	Boiling point		Density at 20° C (gram/ml)	Refractive index n_D^{20}
			(°F)	(°C)		
Benzene	C ₆ H ₆	5.49	176.2	80.1	0.8789	1.5012
Methylbenzene	C ₇ H ₈	-95.014	231.1	110.6	0.8670	1.4967
Ethylbenzene	C ₈ H ₁₀	-95.026	278.8	136.0	0.8872	1.4960
1,2-Dimethylbenzene		-25.34	291.9	144.4	.8799	1.5052
1,3-Dimethylbenzene		-48.31	282.4	159.1	.8642	1.4971
1,4-Dimethylbenzene		13.26	261.1	138.4	.8810	1.4960
<i>n</i> -Propylbenzene	C ₈ H ₁₂	-69.61	318.7	159.3	0.8620	1.4920
Isopropylbenzene		-68.16	306.3	152.4	.8621	1.4913
1-Methyl-2-ethylbenzene		-80.94	329.2	105.1	.8507	1.5045
1-Methyl-3-ethylbenzene		-65.62	322.3	161.3	.8645	1.4985
1-Methyl-4-ethylbenzene		-68.60	323.8	162.0	.8811	1.4951
1,2,3-Trimethylbenzene		-25.97	349.0	176.1	.8945	1.5137
1,2,4-Trimethylbenzene		-44.23	336.7	169.3	.8758	1.5048
1,3,5-Trimethylbenzene		-44.55	328.8	164.9	.8650	1.4990
<i>n</i> -Butylbenzene	C ₁₀ H ₁₄	-88.19	361.8	183.2	0.8603	1.4898
Isobutylbenzene		-51.87	342.0	172.2	.8527	1.4880
<i>sec</i> -Butylbenzene		-75.73	343.9	173.3	.8620	1.4900
<i>tert</i> -Butylbenzene		-57.96	336.6	169.2	.8605	1.4925
1-Methyl-4-isopropylbenzene		-68.39	351.0	177.2	.8568	1.4906
1,2-Diethylbenzene		-32.05	361.8	183.2	.8797	1.5032
1,3-Diethylbenzene		-84.64	358.9	181.6	.8643	1.4955
1,4-Diethylbenzene		-43.31	362.7	183.7	.8621	1.4948
1,3-Dimethyl-5-ethylbenzene		-84.43	362.5	183.6	.8647	1.4980
1-Methyl-3- <i>tert</i> -butylbenzene	C ₁₁ H ₁₆	-41.53	372.6	189.2	0.8658	1.4945
1-Methyl-4- <i>tert</i> -butylbenzene		-52.73	378.7	192.6	.8612	1.4919
1-Methyl-3,5-diethylbenzene		-74.01	363.1	200.6	.8633	1.4960
1,3,5-Triethylbenzene	C ₁₂ H ₁₈	-68.44	420.6	215.9	0.8620	1.4957

TABLE V-2.—PHYSICAL PROPERTIES—Concluded

(e) Ethers.

Ether	Formula	Freezing point (°C)	Boiling point		Density at 20°C (gram/ml)	Refractive index n_D^{20}
			(°F)	(°C)		
Methyl <i>tert</i> -butyl ether	C_4H_9O	-109.00	130.3	54.63	0.7403	1.3689
Ethyl <i>tert</i> -butyl ether	$C_5H_{11}O$	-94.44	161.5	71.93	.7355	1.3766
Isopropyl <i>tert</i> -butyl ether	$C_6H_{13}O$	-88.10	189.4	87.42	.7113	1.3900
Methyl phenyl ether (anisole)	C_6H_5O	-37.16	308.5	153.63	.9939	1.5170
Ethyl phenyl ether (phenetole)	C_7H_9O	-29.49	337.9	169.95	.9651	1.5076
Methyl <i>p</i> -tolyl ether (<i>p</i> -methylanisole)	$C_7H_{11}O$	-32.20	350.0	176.69	.9701	1.5123
<i>o</i> -Methylanisole	C_6H_5O	-34.21	341.3	171.81	.9756	1.5178
<i>m</i> -Methylanisole	C_6H_5O	-66.05	349.8	176.53	.9716	1.5187
<i>p</i> - <i>tert</i> -Butylanisole	$C_7H_{13}O$	-19.11	433.7	223.18	.9353	1.5030
<i>n</i> -Propyl phenyl ether	$C_7H_{15}O$	-27.09	372.8	189.31	.9476	1.5012
Isopropyl phenyl ether	$C_8H_{17}O$	-33.05	350.1	176.73	.9405	1.4975
<i>tert</i> -Butyl phenyl ether	$C_8H_{19}O$	-18.38	369	187	.9247	1.4560
Methyl benzyl ether	C_7H_9O	-53.11	337.8	169.9	.9030	1.5019
Isopropyl benzyl ether	$C_8H_{11}O$	-67.18	379	193	.9214	1.4859
Methyl methallyl ether	C_4H_8O	-113.15	162.3	60.86	.7772	1.3941
Isopropyl methallyl ether	$C_5H_{10}O$	-217.8	103.20	.7753	1.4012	
<i>tert</i> -Butyl methallyl ether	$C_6H_{12}O$	-85.69	237	114	.7853	1.4063
Dimethallyl ether	C_5H_8O	-57.72	273.9	134.40	.8131	1.4285
Phenyl methallyl ether	C_7H_9O	-63.82	410	210	.0634	1.5157
Methyl cyclopropyl ether	C_4H_6O		109.8	43.20	.7639	1.3799
Methyl cyclopentyl ether	$C_5H_{10}O$	-135.03	221.7	106.39	.8025	1.4203
Methyl cyclohexyl ether	$C_6H_{12}O$	-74.39	272.0	138.35	.8756	1.4346

* Approximate value (decomposed on atmospheric boiling).

BASE FUELS

Inasmuch as limited quantities of the compounds were available, all tests were conducted on blends rather than on the pure compound. By this procedure, considerable information could be obtained with a relatively small quantity of a given compound. The pure fuels were investigated in blends with two base fuels, one of which was S reference fuel. The other was a blend of 85 percent (by volume) S reference fuel and 15 percent M reference fuel. This blend contained 4.0 ml TEL per gallon. For all practical purposes, S reference fuel is pure isoctane and M reference fuel is a straight-run stock of about 20 octane number (A. S. T. M. Motor method). Use of this base blend was discontinued during the investigation and a blend of 87½ percent S reference fuel and 12½ percent *n*-heptane was substituted. This blend, too, contained 4.0 ml TEL per gallon.

The performance rating of the leaded blend of S and M reference fuels was about 113/108, whereas the rating of the leaded blend of S reference fuel and *n*-heptane was about 120/112.

PRESENTATION OF DATA

The antiknock performance data for all blends and base fuels are presented in appendix A, tables A-1 to A-8. In many cases the performance values have been adjusted to compensate for differences in the base blend used. Where these adjustments have been made, the values will obviously disagree with values reported in references 2 to 14; however, for the purposes herein, the data as a whole have been placed on a more uniform basis.

The previously mentioned adjustments, in effect, permit treatment of the data as if only two base fuels had been used, namely, isoctane (leaded and unleaded) and a leaded blend of isoctane and *n*-heptane.

RELATION BETWEEN MOLECULAR STRUCTURE AND ANTIKNOCK CHARACTERISTICS

A large part of past research relating to molecular structure and antiknock behavior has been summarized by Lovell (reference 1) and by Lovell and Campbell (reference 16).

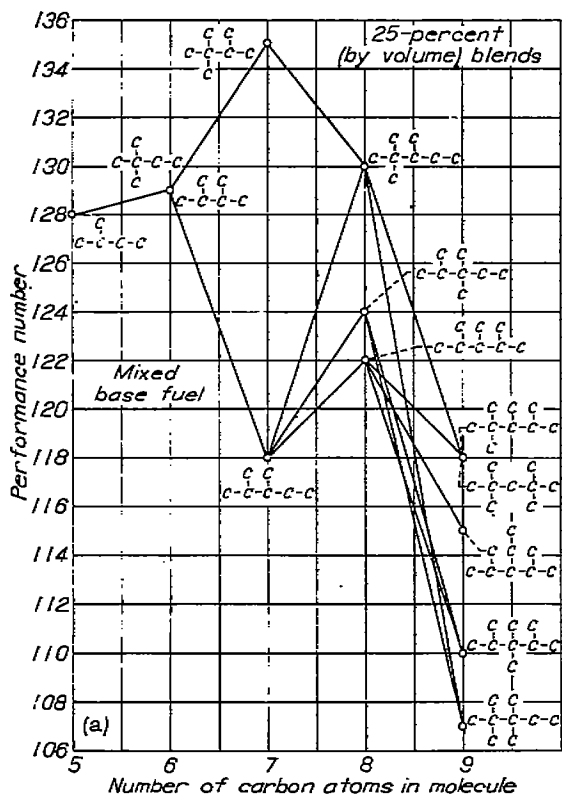
In both these investigations, an attempt was made to secure generalizations that would assist in the prediction of relative antiknock values from molecular structures. The past studies have on the whole been very successful in this respect. As this particular phase of fuel research has progressed, however, the basic knowledge of engine performance has advanced; consequently, exceptions to these generalizations can and do exist by virtue of differences in engines and engine operating conditions. That is, the relative antiknock characteristics of a given group of fuels can be changed considerably by altering the engine or experimental conditions.

As a result, the concept of "severe" and "mild" engine conditions has been devised as an aid in evaluating the merits of different fuels. A severe condition is one in which controlled conditions such as inlet-air temperature, coolant temperature, compression ratio, spark advance, and engine speed combine in their effects to make a fuel knock more readily. (See ch. II.) In reference 14, the various engine operating conditions used in the NACA investigation of ethers are aligned into a relative order of severity. This same order of severity is used in the present discussion and is presented in table V-3.

TABLE V-3.—DEGREE OF SEVERITY OF VARIOUS OPERATING CONDITIONS

Engine	Mixture condition	Degree of severity
A. S. T. M. Aviation	Lean	Severe.
Full-scale take-off	do	Moderate to severe.
A. S. T. M. Supercharge	Rich	Moderate.
Full-scale take-off	do	Do.
Full-scale cruise	Lean	Do.
17.6 (inlet-air temperature, 250° F.)	do	Do.
Full-scale cruise	Rich	Moderate to mild.
17.6 (inlet-air temperature, 250° F.)	do	Do.
17.6 (inlet-air temperature, 100° F.)	Lean	Do.
17.6 (inlet-air temperature, 100° F.)	Rich	Mild.

Because of this so-called severity concept, any statement to the effect that one fuel performs better than another fuel has little significance unless it is true for all operating conditions or restricted to one operating condition. For this reason, the emphasis in an investigation of the type reported



(a) Engine, A. S. T. M. Aviation.

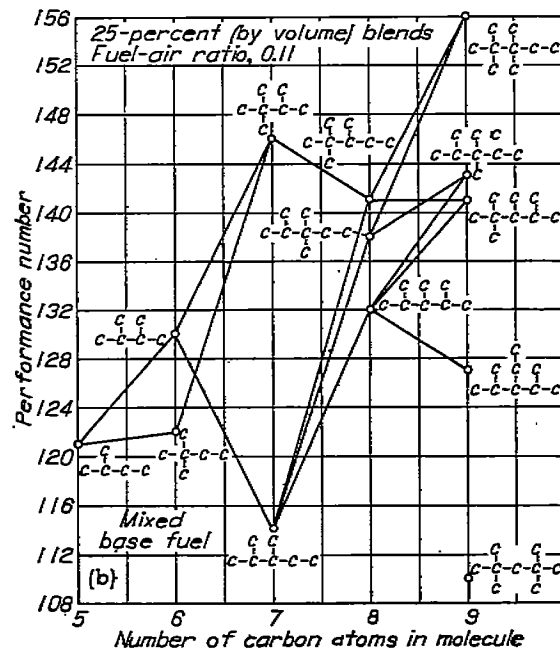
FIGURE V-1.—Knock-limited performance of paraffins in blend with mixed base fuel consisting of 87.5 percent isooctane and 12.5 percent *n*-heptane+4 ml TEL per gallon.

herein must be placed upon the trends in the relation between structure and knock rating that appear to apply under most conditions.

Paraffins.—Data were obtained for 13 paraffinic hydrocarbons in leaded blends with the mixed base fuel. Inasmuch as the quantities of hydrocarbon were somewhat limited, all the paraffins were compared only at the 25-percent (by volume) concentration level and only at standard A. S. T. M. Aviation and A. S. T. M. Supercharge conditions (appendix A, table A-1 (a)). The data for these blends are shown in figure V-1.

This figure illustrates the relation between molecular structure and antiknock performance for the paraffins investigated. The lines joining the various data points are shown merely to define the paths followed by compounds in an homologous series. An increase of one carbon atom on the abscissa of these figures is equivalent to a molecular-weight increase equal to the molecular weight of a CH_2 group.

At the A. S. T. M. Aviation conditions (fig. V-1 (a)),

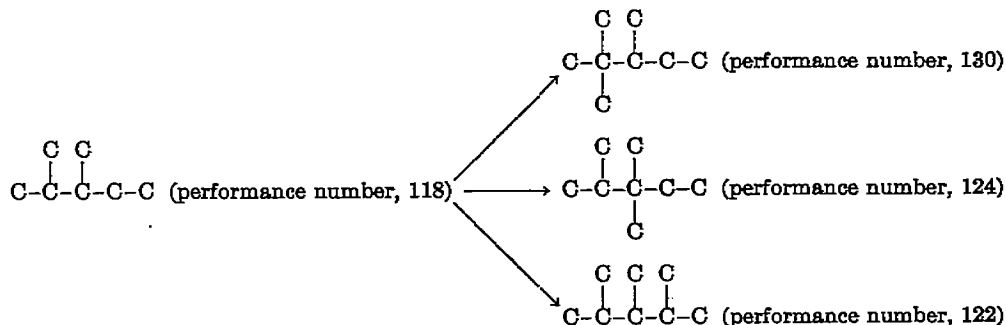


(b) Engine, A. S. T. M. Supercharge.

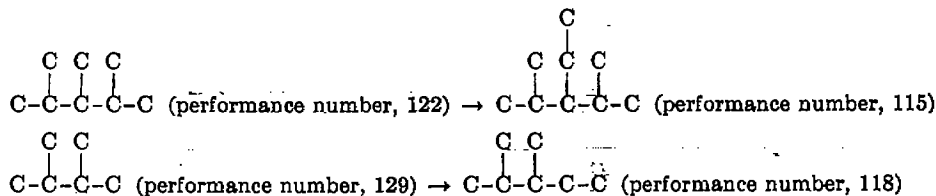
FIGURE V-1.—Concluded. Knock-limited performance of paraffins in blend with mixed base fuel consisting of 87.5 percent isooctane and 12.5 percent *n*-heptane+4 ml TEL per gallon.

seven of the paraffinic hydrocarbons raised the knock-limited performance of the base fuel. The increases varied between 2 and 15 performance numbers with 2,2,3-trimethylbutane (triptane) having the highest rating. This result indicates that under severe conditions, represented by the A. S. T. M. Aviation (lean) method, triptane has outstanding antiknock characteristics.

Insofar as the effect of molecular structure on antiknock characteristics is concerned, three trends have been emphasized (references 1 and 16). The first trend is concerned with centralization of the molecule. For example, 2,2,3,3-tetramethylbutane is a more centralized or compact molecule than 2,2,3-trimethylpentane and should therefore have a higher antiknock rating. The second trend shows the effect of adding methyl (CH_3) groups to a molecule in order to form successive members of an homologous series. The addition of a methyl group to increase the branching tends to produce a compound having a higher antiknock rating; however, the position in which the group is added to the molecule will influence the rating of the new compound. This effect, based on A. S. T. M. Aviation antiknock ratings for the blends examined in the present investigation, is illustrated as follows:



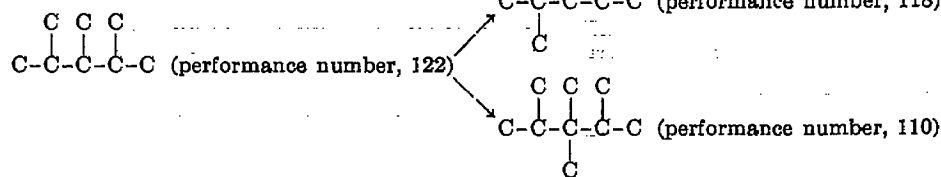
The third trend is concerned with the increase in length of a carbon side chain or the primary carbon chain of a molecule. The effect of such an addition is to decrease the antiknock rating as illustrated by the following examples:



In general, the trends reported in references 1 and 16 and discussed in the preceding paragraph (fig. V-1 (a)) appear to be valid at mild or moderate engine operating conditions. At severe operating conditions, however, exceptions do occur as regards centralization of the molecule or increased branching in the molecule.

At the A. S. T. M. Supercharge conditions, which, as indicated in table V-3, are of moderate severity, the NACA data (fig. V-1 (b)) agree substantially with the results found by Lovell (reference 1). In this case (fig. V-1 (b)), 12 of the 13 paraffinic hydrocarbons investigated raised the knock-limited performance of the base fuel; the increases were in the range of 2 to 44 performance numbers. The antiknock rating of the blend containing 2,2,3,3-tetramethylpentane was the highest obtained and the triptane blend was next.

In order to illustrate the fact that increased centralization of the molecule does not always result in high antiknock values, the A. S. T. M. Aviation ratings are plotted against the A. S. T. M. Supercharge ratings for five nonanes blended with the mixed base fuel in figure V-2. If, in this figure, 2,2,3,3-tetramethylpentane is considered the most compact molecule and 2,2,4,4-tetramethylpentane the least compact, then it is apparent (because the correlating line has a negative slope) that increasing compactness may improve antiknock performance under one set of conditions and depreciate antiknock performance at other conditions. As previously mentioned, the addition of methyl groups, that is, increased branching, does not always result in improved performance. This fact is illustrated by the following A. S. T. M. Aviation ratings:



It is emphasized, however, that these exceptions appear to exist at severe operating conditions as exemplified by the A. S. T. M. Aviation engine.

Olefins.—Five olefins were examined in leaded blends with the mixed base fuel at standard A. S. T. M. Aviation and A. S. T. M. Supercharge conditions (appendix A, table A-1 (a)). The concentration of olefin in each blend was 25 percent by volume.

The data obtained are somewhat limited insofar as the relation between molecular structure and antiknock value is concerned; however, comparisons can be made with references 1 and 16 to determine further the consistency of trends noted by previous investigators. Lovell (reference 1) found that for branched aliphatic compounds if the parent paraffin hydrocarbon had a high antiknock value the introduction of a double bond would decrease the antiknock value. This

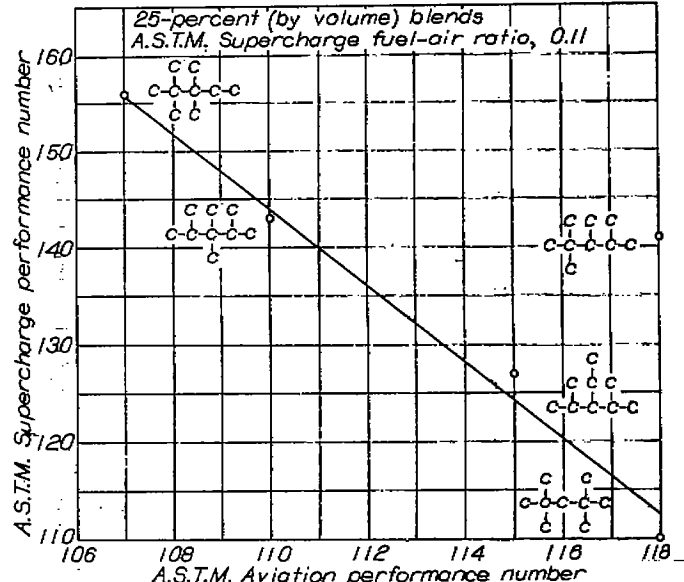
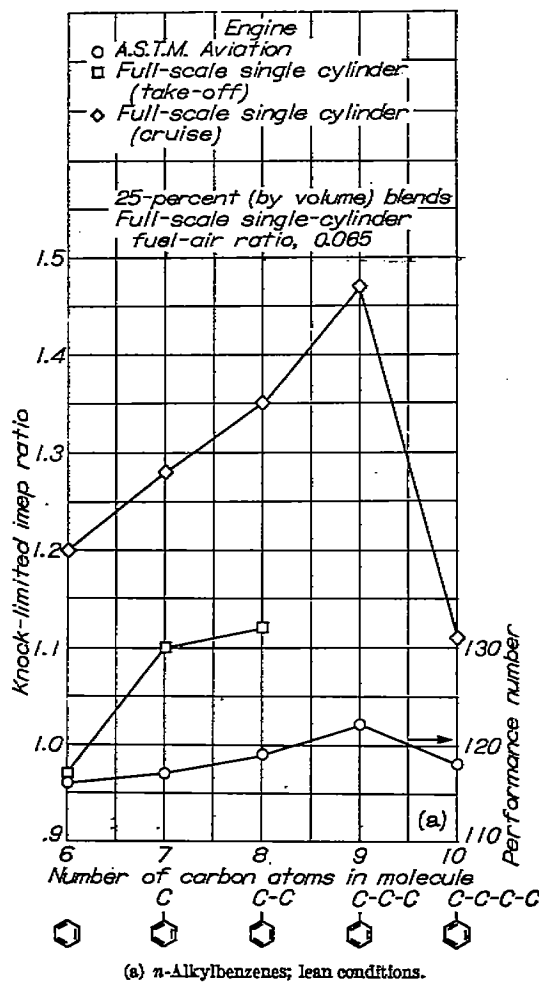


FIGURE V-2.—Relation between A. S. T. M. Supercharge and A. S. T. M. Aviation performance numbers of nonanes in blend with mixed base fuel consisting of 87.5 percent isooctane and 12.5 percent *n*-heptane + 4 ml TEL per gallon.

trend is supported by the following data from the present investigation (appendix A, table A-1 (a)):

Paraffin	Performance number of 25-percent blend *		Olefin	Performance number of 25-percent blend *	
	A. S. T. M. Aviation	A. S. T. M. Supercharge		A. S. T. M. Aviation	A. S. T. M. Supercharge
$\text{C}-\text{C}-\text{C}-\text{C}-\text{C}$	118	114	$\text{O}-\text{C}=\text{C}-\text{C}-\text{C}$	100	117
$\text{C}-\text{C}-\text{C}-\text{C}-\text{C}$	122	132	$\text{C}-\text{C}-\text{C}-\text{C}-\text{C}$	101	104
$\text{C}-\text{C}-\text{C}-\text{O}-\text{C}$	130	141	$\text{C}-\text{C}-\text{C}-\text{O}-\text{C}$	106	109

* All blends were leaded to 4 ml TEL/gal.

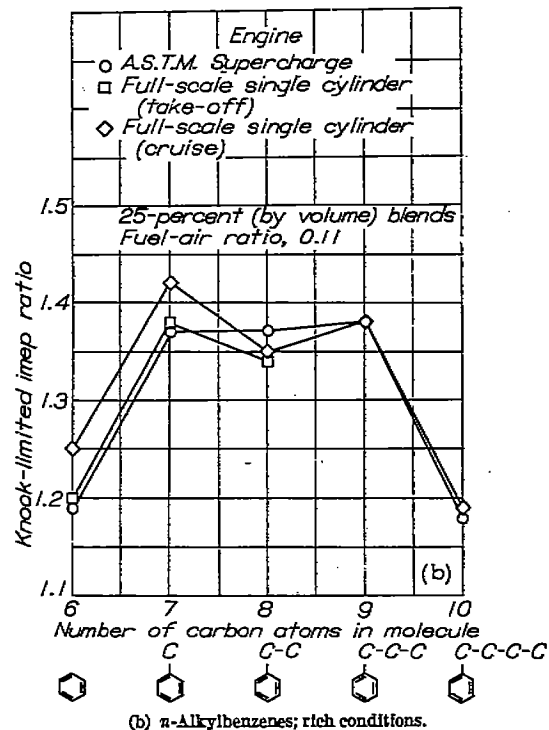
(a) *n*-Alkylbenzenes; lean conditions.FIGURE V-3.—Continued. Knock-limited performance of aromatics in blend with mixed base fuel consisting of 87.5 percent isoctane and 12.5 percent *n*-heptane+4 ml TEL per gallon.

In the foregoing examples, the double bond in the olefin appeared in the 2 position and, with one exception, the ratings for the olefins are lower than those of the corresponding paraffins. The one exception is shown for the A. S. T. M. Supercharge ratings of 2,3-dimethylpentane and 2,3-dimethyl-2-pentene where the olefin has an antiknock rating three performance numbers higher than the paraffin.

Of the five olefins investigated, only two, 2,4,4-trimethyl-1-pentene and 2,4,4-trimethyl-2-pentene, indicate the effect of the position of the double bond on antiknock performance. For the engines and the conditions examined (appendix A, tables A-1 (a) and A-5 (a)), the ratings of these two compounds appear to be the same at the more severe conditions. At milder conditions, the 2,4,4-trimethyl-2-pentene has lower ratings than 2,4,4-trimethyl-1-pentene. This trend is contrary to the trend found for straight-chain olefins but is in agreement with data for branched-chain olefins (reference 1).

Aromatics.—The most complete set of antiknock performance data obtained in the present investigation resulted from engine studies made with 27 aromatic hydrocarbons in blends with selected base fuels. On the basis of these data, the relations between molecular structure and antiknock value and the influence of engine operating conditions on these relations for the aromatics can be readily seen.

The relation between structure and antiknock performance for a series of *n*-alkylbenzenes at a lean fuel-air ratio

(b) *n*-Alkylbenzenes; rich conditions.FIGURE V-3.—Continued. Knock-limited performance of aromatics in blend with mixed base fuel consisting of 87.5 percent isoctane and 12.5 percent *n*-heptane+4 ml TEL per gallon.

is shown in figure V-3 (a). In this figure it was necessary to use performance numbers for the A. S. T. M. Aviation engine, inasmuch as knock-limited indicated mean effective pressures are not measured on this engine. The first three carbon atoms added to the side chains of the aromatic compounds successively increased the blend knock limits. The addition of a fourth carbon atom to the side chain caused a sharp drop in performance at the full-scale single-cylinder cruise condition and a slight drop in the A. S. T. M. Aviation engine.

More specifically, the data in figure V-3 (a) indicate that, for the full-scale single-cylinder cruise condition, the 25-percent benzene blend has a knock limit 20 percent higher than the base fuel; toluene is 28 percent higher; ethylbenzene, 35 percent higher; *n*-propylbenzene, 47 percent higher; whereas, *n*-butylbenzene is only 11 percent better than the base fuel. At the other experimental conditions (fig. V-3 (a)), the trends are the same but the magnitude of the increases is less. In fact, under simulated full-scale take-off conditions the benzene blend is lower in performance than the base fuel, which is represented by the ratio 1.0. In the A. S. T. M. Aviation engine, the base fuel has a performance number of 120 and, with the exception of *n*-propylbenzene, all the aromatic blends have performance numbers lower than 120. This depreciation in performance is characteristic of aromatics at conditions as severe as those encountered in the A. S. T. M. Aviation engine.

Figure V-3 (b) is similar to figure V-3 (a) except that the fuel-air ratio is rich and the A. S. T. M. Supercharge (rich) rating method has replaced the A. S. T. M. Aviation (lean) rating method. The trends shown are somewhat different from those in figure V-3 (a), but the similarity between the A. S. T. M. Supercharge data and the full-scale data is apparent. At the conditions investigated, the first addition

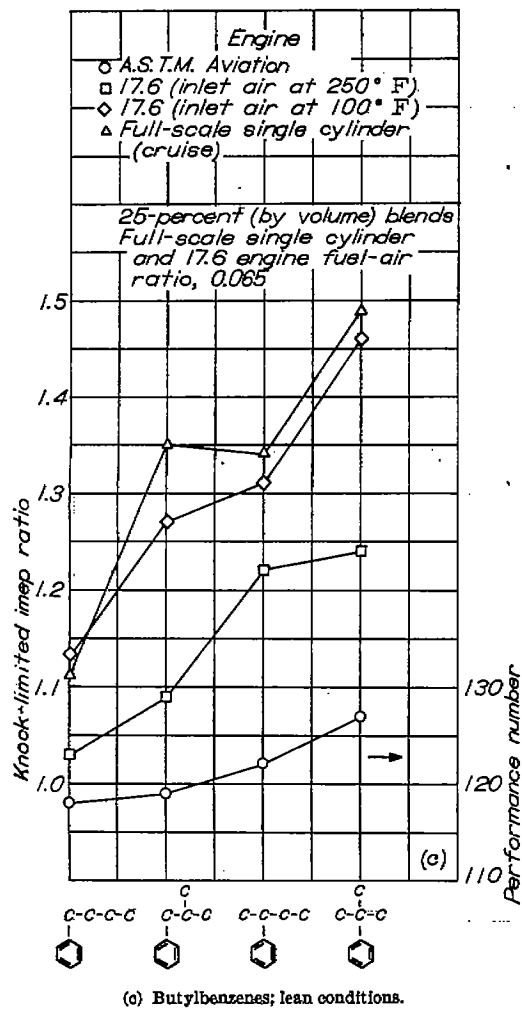


FIGURE V-3.—Continued. Knock-limited performance of aromatics in blend with mixed base fuel consisting of 87.5 percent isoctane and 12.5 percent *n*-heptane+4 ml TEL per gallon.

of a carbon atom to the benzene ring produces a sharp improvement in performance; the next addition results in a decrease except for the A. S. T. M. Supercharge data, which are unchanged; the next addition slightly increases the performance; and the addition of the fourth carbon atom to the side chain results in a very sharp decrease in knock limit, as found at the lean conditions (fig. V-3 (a)).

The change in performance accompanying changes in molecular weight in an homologous series is illustrated in figures V-3 (a) and V-3 (b). The effect of different isomeric structures on performance when the molecular weight is unchanged is shown in figure V-3 (c). For this example, the four butylbenzenes, *n*-butylbenzene, isobutylbenzene, *sec*-butylbenzene, and *tert*-butylbenzene, were chosen. At the two 17.6 engine conditions and the A. S. T. M. Aviation condition, changing from the normal to the iso, the secondary, and the tertiary structures progressively improves the performance. Under simulated full-scale cruise conditions, the isobutylbenzene is slightly better than the *sec*-butylbenzene, but the small difference in antiknock value is probably insignificant.

Data for the four butylbenzenes at a rich fuel-air ratio are

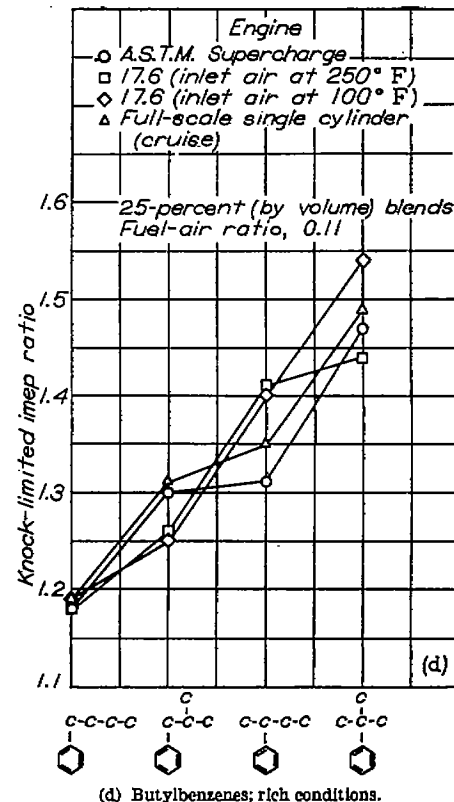


FIGURE V-3.—Continued. Knock-limited performance of aromatics in blend with mixed base fuel consisting of 87.5 percent isoctane and 12.5 percent *n*-heptane+4 ml TEL per gallon.

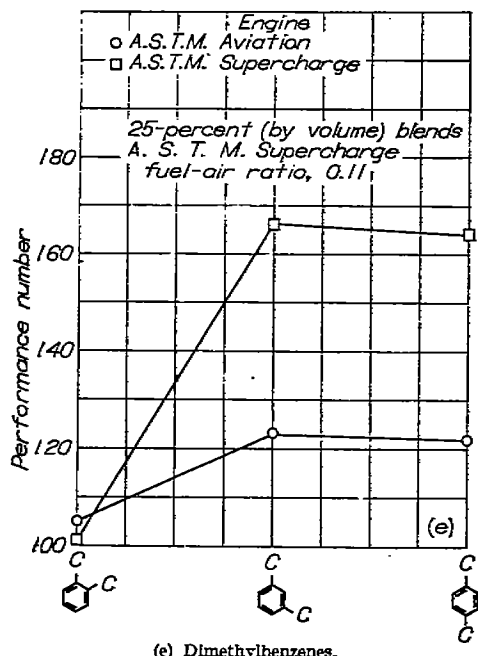
presented in figure V-3 (d). The trends shown in this figure are similar to those found in figure V-3 (c).

Generally speaking, in figures V-3 (a) to V-3 (d), the trends in performance of the aromatic blends in the standard A. S. T. M. Aviation and A. S. T. M. Supercharge engines were similar to those in the other engines. This similarity among engines, however, is not always observed over wide ranges of operating conditions. Nevertheless, the comparison of performance characteristics of the organic compounds throughout the remainder of this chapter will be based primarily upon the A. S. T. M. Aviation and A. S. T. M. Supercharge engine data because these data were obtained in engines currently accepted as standards for rating fuels.

The knock-limited performance of dimethylbenzenes (xylenes) is illustrated in figure V-3 (e). In both engines, the 1,3-dimethylbenzene blend gave higher performance than either 1,2- or 1,4-dimethylbenzene. The 1,4-dimethylbenzene has an antiknock rating only slightly less than that of 1,3-dimethylbenzene but still considerably higher than that of 1,2-dimethylbenzene.

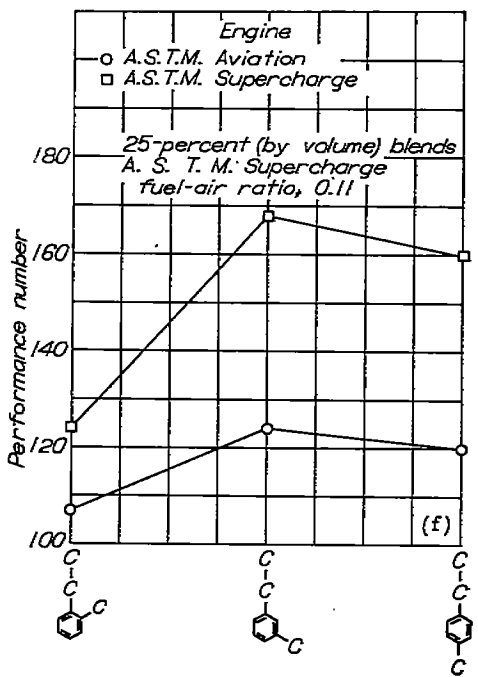
The trends shown in figure V-3 (f) for the methylethylbenzenes are the same as those shown in figure V-3 (e) for the dimethylbenzenes; that is, 1-methyl-3-ethylbenzene is appreciably better than 1-methyl-2-ethylbenzene and slightly better than the 1-methyl-4-ethylbenzene. A similar result was obtained for the diethylbenzenes (fig. V-3 (g)).

The antiknock performance of disubstituted compounds is illustrated in figures V-3 (e) to V-3 (g). Figure V-3 (h) illustrates antiknock trends for trisubstituted compounds.



(e) Dimethylbenzenes.

FIGURE V-3.—Continued. Knock-limited performance of aromatics in blend with mixed base fuel consisting of 87.5 percent isooctane and 12.5 percent *n*-heptane+4 ml TEL per gallon.

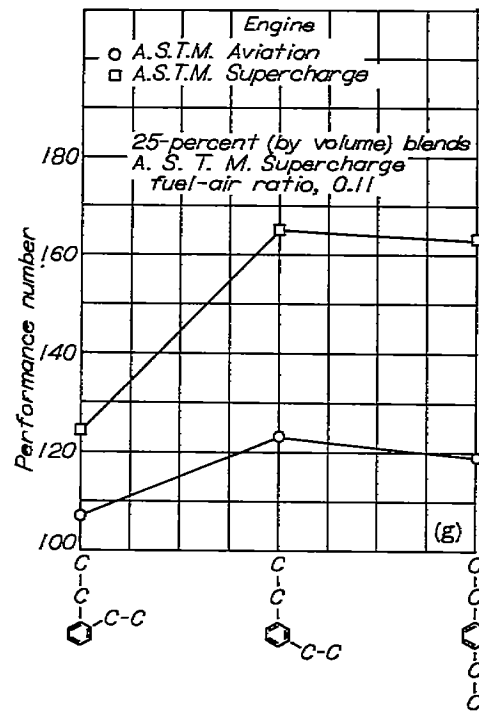


(f) Methylethylbenzenes.

FIGURE V-3.—Continued. Knock-limited performance of aromatics in blend with mixed base fuel consisting of 87.5 percent isooctane and 12.5 percent *n*-heptane+4 ml TEL per gallon.

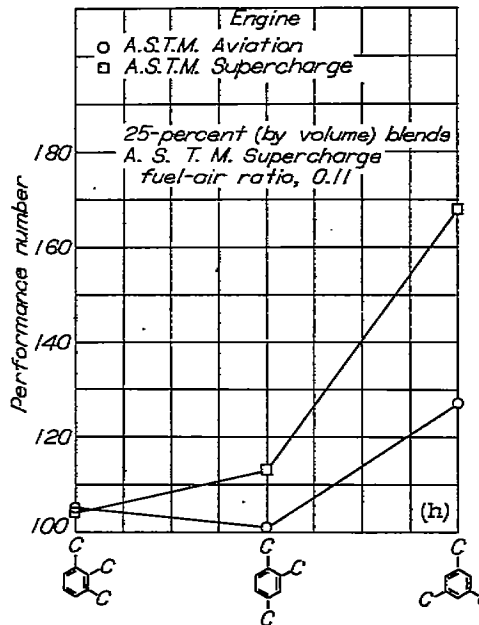
The 1,2,4-trimethylbenzene blend has a slightly higher knock limit than the 1,2,3-trimethylbenzene blend in the A. S. T. M. Supercharge engine but has a slightly lower knock limit in the A. S. T. M. Aviation engine. The 1,3,5-trimethylbenzene is considerably better than either of the other trimethylbenzenes.

The relative antiknock characteristics of all the aromatic hydrocarbons examined are presented in figure V-3 (i) at



(g) Diethylbenzenes.

FIGURE V-3.—Continued. Knock-limited performance of aromatics in blend with mixed base fuel consisting of 87.5 percent isooctane and 12.5 percent *n*-heptane+4 ml TEL per gallon.



(h) Trimethylbenzenes.

FIGURE V-3.—Continued. Knock-limited performance of aromatics in blend with mixed base fuel consisting of 87.5 percent isooctane and 12.5 percent *n*-heptane+4 ml TEL per gallon.

A. S. T. M. Aviation lean conditions. About 15 aromatics improved the knock-limited performance of the base fuel. These particular blends fall within a range about seven performance numbers above the base fuel. From these data at lean conditions, 1,3,5-trimethylbenzene and *tert*-butylbenzene appear to be the most desirable aromatics in the 25-percent blends investigated.

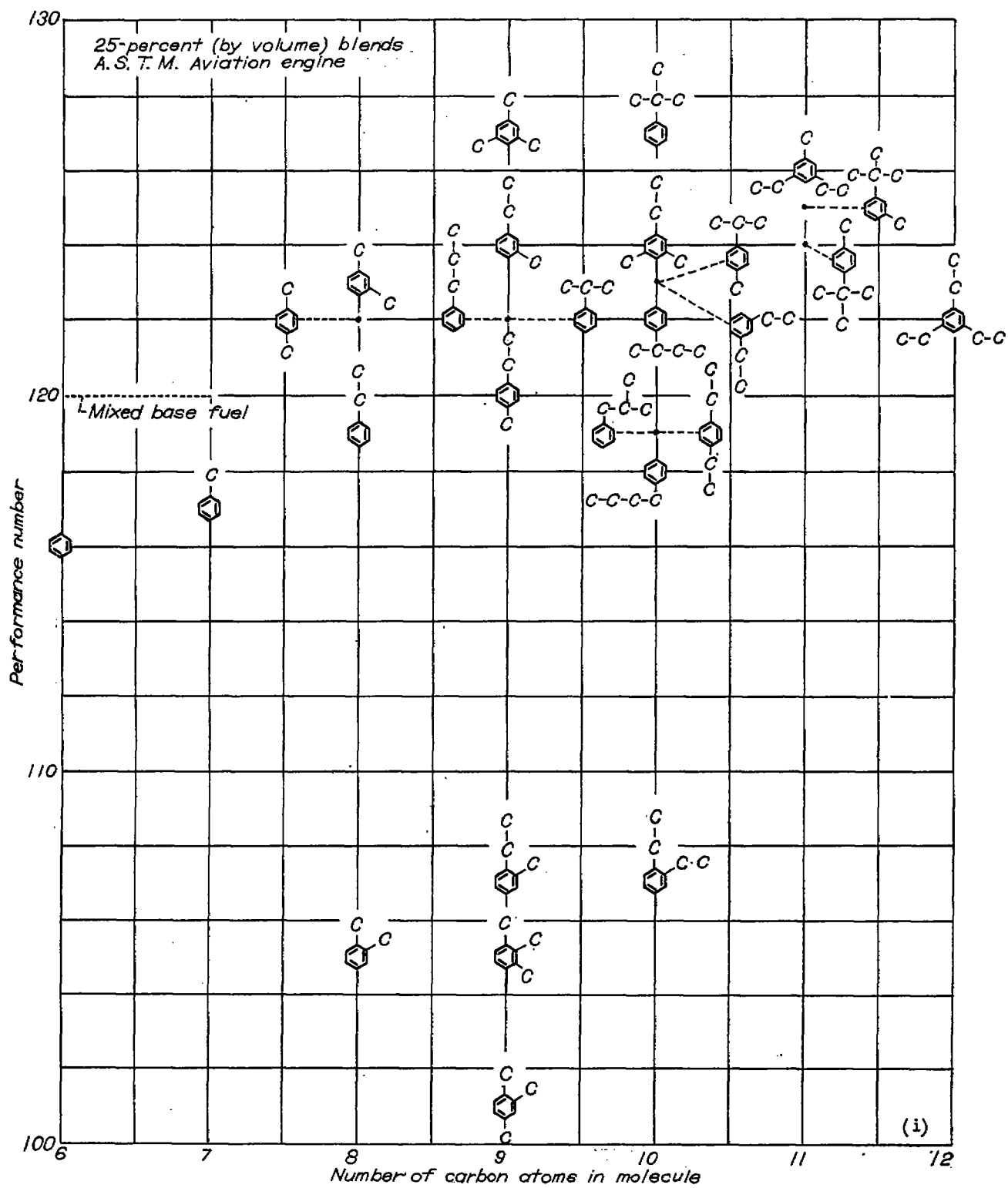


FIGURE V-3.—Continued. Knock-limited performance of aromatics in blend with mixed base fuel consisting of 87.5 percent isoctane and 12.5 percent *n*-heptane + 4 ml TEL per gallon.

The aromatic blends are compared at A. S. T. M. Supercharge rich conditions in figure V-3 (j). In contrast to the A. S. T. M. Aviation data (fig. V-3 (i)), the 25-percent addi-

tions of aromatics to the base fuel caused considerable improvement in A. S. T. M. Supercharge performance, from a performance number of 112 for the base fuel to about 176

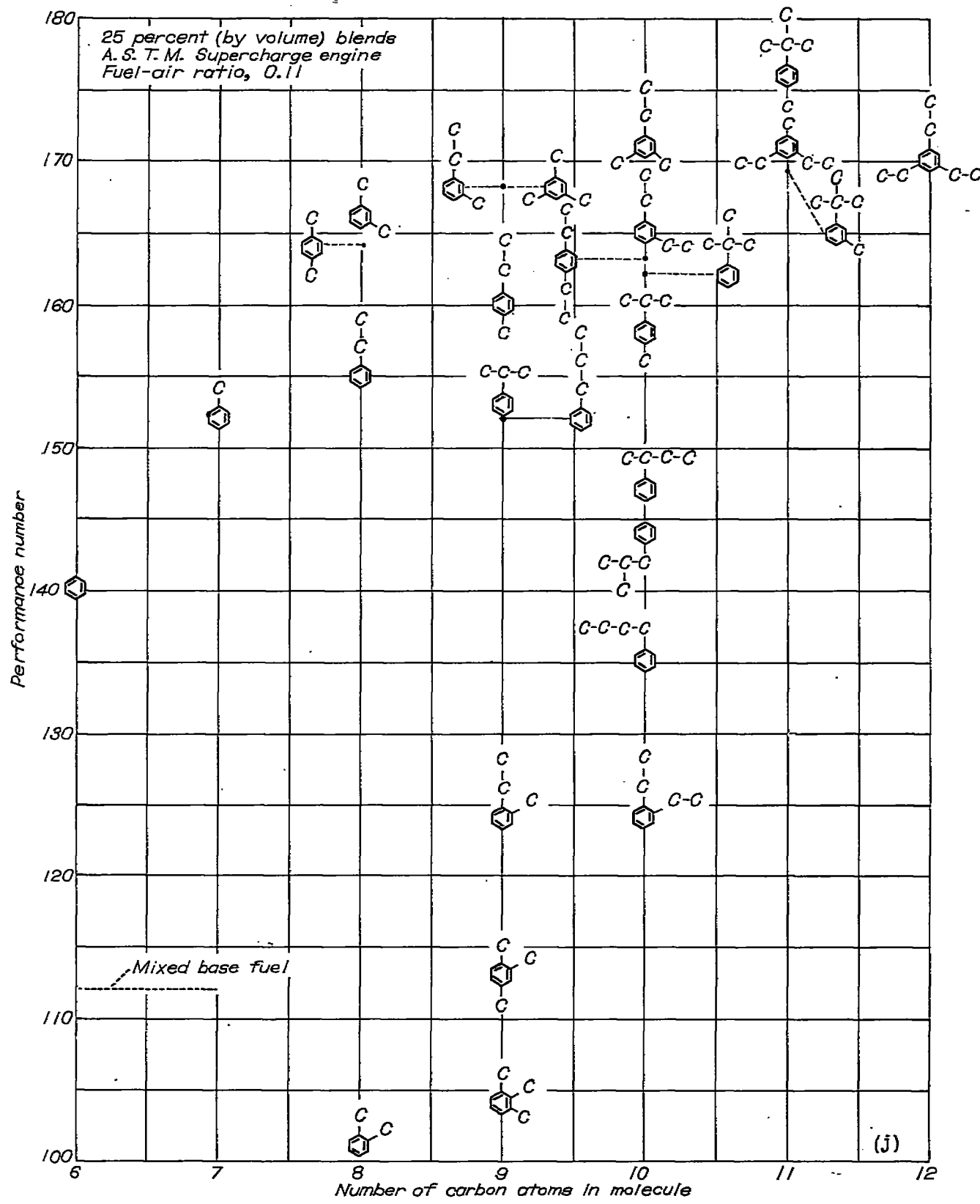
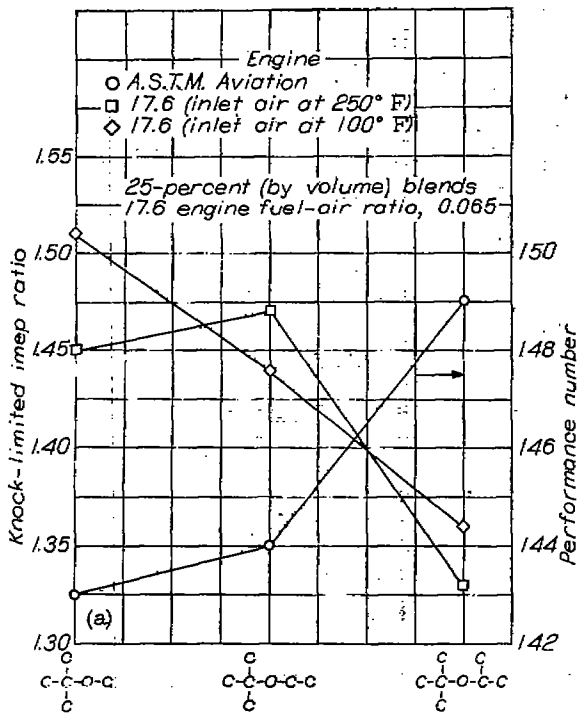
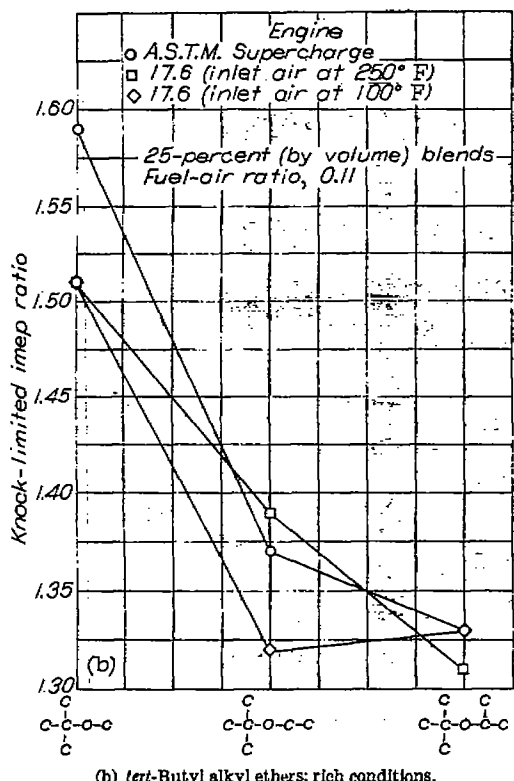
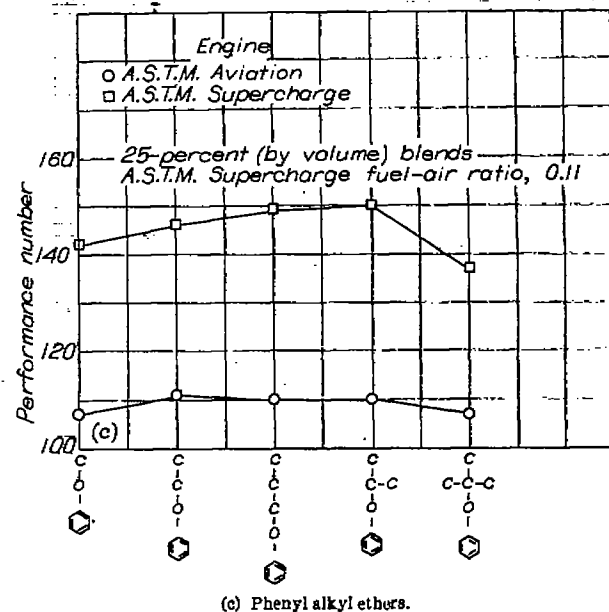


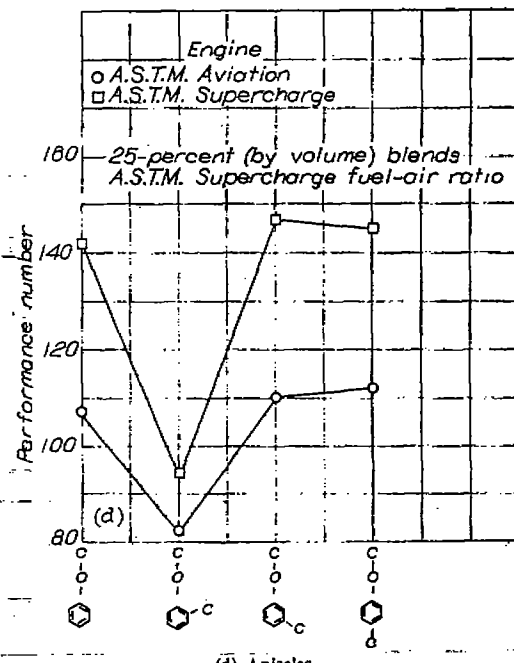
FIGURE V-3.—Concluded. Knock-limited performance of aromatics in blend with mixed base fuel consisting of 87.5 percent isoctane and 12.5 percent *n*-heptane+4 ml TEL per gallon.

(a) *tert*-Butyl alkyl ethers; lean conditions.FIGURE V-4.—Knock-limited performance of ethers in blend with mixed base fuel consisting of 87.5 percent isooctane and 12.5 percent *n*-heptane+4 ml TEL per gallon.(b) *tert*-Butyl alkyl ethers; rich conditions.FIGURE V-4.—Continued. Knock-limited performance of ethers in blend with mixed base fuel consisting of 87.5 percent isooctane and 12.5 percent *n*-heptane+4 ml TEL per gallon.

for the best aromatic. These results are consistent with results obtained by other investigators in that aromatics in fuel blends generally offer considerable advantage at rich fuel-air ratios but only moderate improvement or even depreciation at lean fuel-air ratios under severe operating conditions. The 1,3,5-trimethylbenzene and *tert*-butylbenzene blends, which have good antiknock characteristics at A.S.T.M.



(c) Phenyl alkyl ethers.

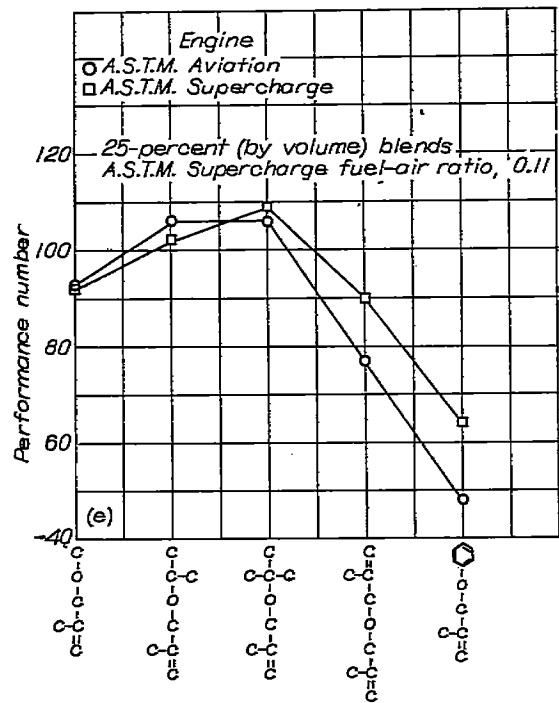
FIGURE V-4.—Continued. Knock-limited performance of ethers in blend with mixed base fuel consisting of 87.5 percent isooctane and 12.5 percent *n*-heptane+4 ml TEL per gallon.

(d) Anisoles.

FIGURE V-4.—Continued. Knock-limited performance of ethers in blend with mixed base fuel consisting of 87.5 percent isooctane and 12.5 percent *n*-heptane+4 ml TEL per gallon.

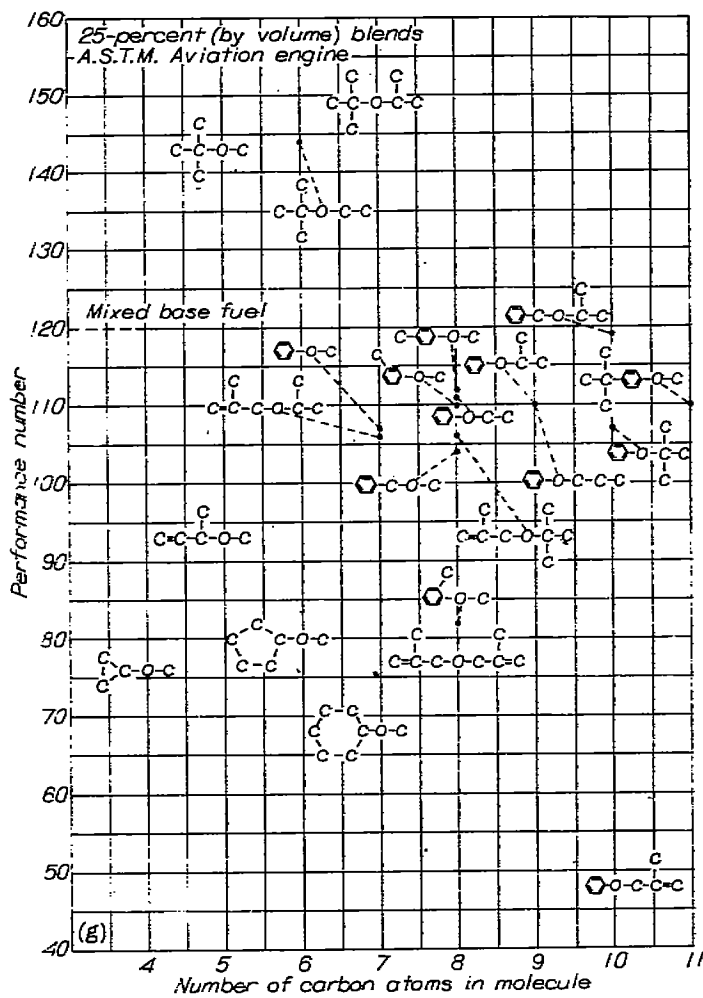
Aviation conditions (fig. V-3 (i)), were still relatively high in performance at rich conditions (fig. V-3 (j)) but were exceeded by other aromatics. Among these high-performance aromatics were 1,3-dimethyl-5-ethylbenzene, 1-methyl-3,5-diethylbenzene, 1-methyl-4-*tert*-butylbenzene, and 1,3,5-triethylbenzene.

In the aromatic data just discussed, only one trend appears worthy of mention, namely, that meta structural arrangements are equal to or slightly better than para arrangements in antiknock performance and both arrangements are considerably better than the ortho structural arrangement. In one case (fig. V-3 (j)), however, the para arrangement was better than the meta arrangement as shown by comparison of 1-methyl-3-*tert*-butylbenzene and 1-methyl-4-*tert*-butylbenzene. Essentially the same trend



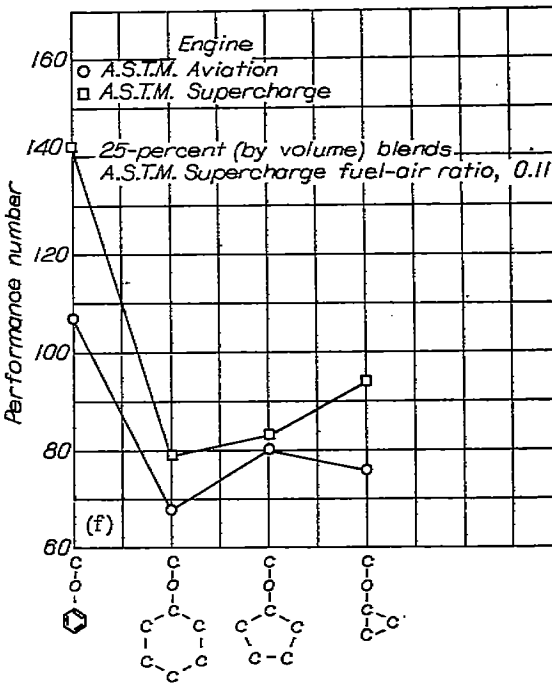
(e) Methallyl ethers.

FIGURE V-4.—Continued. Knock-limited performance of ethers in blend with mixed base fuel consisting of 87.5 percent isoctane and 12.5 percent *n*-heptane+4 ml TEL per gallon.



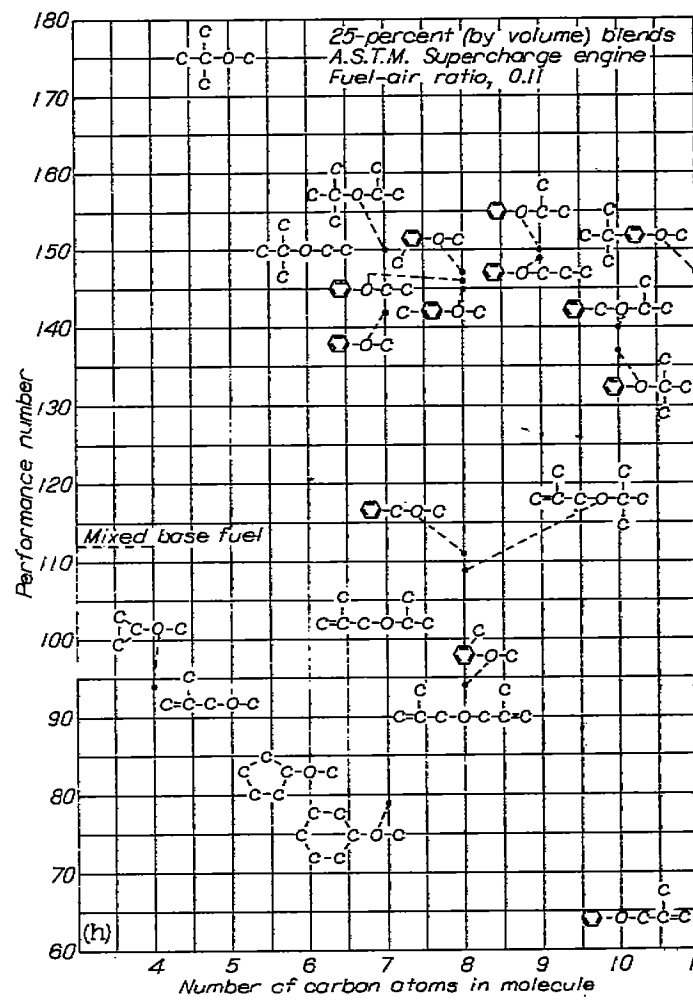
(g) Ethers; lean conditions.

FIGURE V-4.—Continued. Knock-limited performance of ethers in blend with mixed base fuel consisting of 87.5 percent isoctane and 12.5 percent *n*-heptane+4 ml TEL per gallon.



(f) Anisole and three methyl cycloalkyl ethers.

FIGURE V-4.—Continued. Knock-limited performance of ethers in blend with mixed base fuel consisting of 87.5 percent isoctane and 12.5 percent *n*-heptane+4 ml TEL per gallon.



(h) Ethers; rich conditions.

FIGURE V-4.—Continued. Knock-limited performance of ethers in blend with mixed base fuel consisting of 87.5 percent isoctane and 12.5 percent *n*-heptane+4 ml TEL per gallon.

is reported in reference 1 for the relation among ortho, meta, and para compounds.

For the paraffins (fig. V-1), increasing the length of the primary carbon chain resulted in a decrease in the antiknock performance; however, for the aromatics (fig. V-3 (a) and V-3 (b)), an increase in length of a carbon side chain is beneficial up to a certain point, but further additions to the side chain are detrimental to the antiknock performance.

Ethers.—The antiknock characteristics of three alkyl ethers are illustrated in figures V-4 (a) and V-4 (b) for lean and rich fuel-air ratios, respectively. At lean conditions (fig. V-4 (a)) in the A. S. T. M. Aviation engine, isopropyl *tert*-butyl ether was appreciably higher in antiknock value than either methyl or ethyl *tert*-butyl ether. Ethyl *tert*-butyl ether appears to be slightly higher than methyl *tert*-butyl ether in this engine. In the 17.6 engine (fig. V-4 (a)) at both conditions, the results obtained for the three alkyl ethers were directly opposite to those found in the A. S. T. M. Aviation engine. Methyl *tert*-butyl ether was equal to or better than ethyl *tert*-butyl ether and both were appreciably better than isopropyl *tert*-butyl ether. This trend was found also at the rich conditions shown in figure V-4 (b).

The antiknock characteristics of five phenyl alkyl ethers are shown in figure V-4 (c). In both engines methyl phenyl ether and *tert*-butyl phenyl ether gave the lowest performance numbers. The remaining three ethers were about equal in performance in both engines. A comparison of figures V-4 (a) and V-4 (c) shows that the phenyl alkyl ethers investigated have considerably poorer antiknock characteristics than do the *tert*-butyl alkyl ethers at A. S. T. M. Aviation conditions.

The effects of ortho, meta, and para structural arrangements on the antiknock performance of phenyl alkyl ethers are illustrated in figure V-4 (d). The basic ether for this particular example is methyl phenyl ether (anisole), which is shown on the left side of the figure. The addition of a carbon atom to the benzene ring to form *o*-methylanisole caused a decrease in performance. Adding a carbon atom in the meta or para position to form *m*-methylanisole and *p*-methylanisole slightly increased the antiknock performance. In each engine, *m*-methylanisole and *p*-methylanisole were about equal in performance number and both were considerably better than *o*-methylanisole. This result was similar to that obtained for the aromatics (figs. V-3 (e) to V-3 (g)).

Several ethers containing olefinic radicals are shown in figure V-4 (e). Isopropyl methallyl ether and *tert*-butyl methallyl ether blends had the highest performance numbers of this group of compounds and phenyl methallyl ether the lowest. At A. S. T. M. Aviation and A. S. T. M. Supercharge conditions, phenyl methallyl ether was the poorest of the 22 ethers examined.

Hydrogenating the benzene nucleus of anisole to give methyl cyclohexyl ether is shown in figure V-4 (f) to produce a large drop in performance number. Of the three methyl cycloalkyl ethers shown, all of which were relatively low, methyl cyclopropyl ether was the highest at A. S. T. M. Supercharge conditions and methyl cyclopentyl ether was highest at A. S. T. M. Aviation conditions.

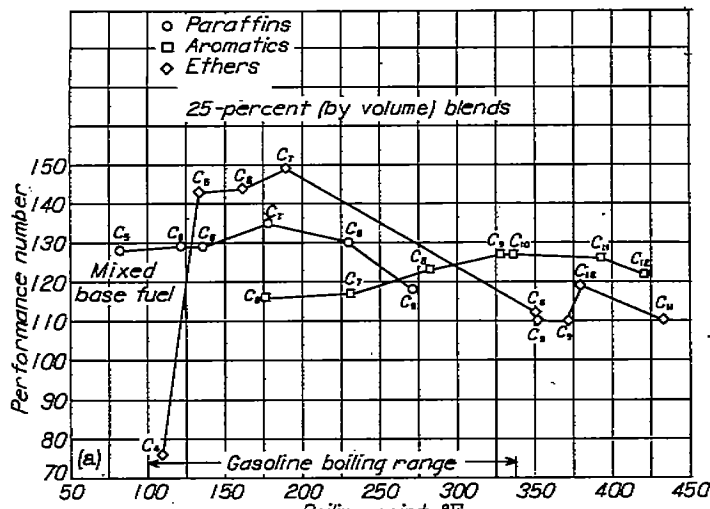
The relative antiknock characteristics of all the ethers investigated are presented in figure V-4 (g) at A. S. T. M. Aviation (lean) conditions. Under these conditions only the three *tert*-butyl alkyl ethers raised the knock limit of the base fuels. The maximum improvement in performance number was 29 and was obtained with isopropyl *tert*-butyl ether.

The antiknock characteristics of all the ethers investigated are compared in figure V-4 (h) at A. S. T. M. Supercharge (rich) conditions. Twelve of the ethers improved the performance of the base fuel; the greatest increase in knock-limited performance, about 63 performance numbers, was obtained with methyl *tert*-butyl ether. Comparison of figures V-4 (g) and V-4 (h) clearly shows that nine of the phenyl alkyl ethers have much better antiknock characteristics at rich mixtures than at lean mixtures. It is also apparent that the methyl cycloalkyl ethers show little promise as antiknock blending agents at the A. S. T. M. Aviation and A. S. T. M. Supercharge conditions.

Comparison of classes of compounds.—As a matter of interest, the isomers having the highest antiknock ratings in figures V-1, V-3 (i), V-3 (j), V-4 (g), and V-4 (h) have been plotted in figure V-5. The performance numbers have been plotted against boiling points in order to illustrate the most promising antiknock compounds in the boiling range of commercial gasolines. Comparison of the curves in figure V-5 is not strictly valid, inasmuch as all the isomers in a given group of compounds have not been studied. Within the limitations of the investigation, however, these two figures do illustrate how the antiknock characteristics of the better paraffins, aromatics, and ethers compare.

When the boiling range of aviation gasoline is assumed to be 100° to 338° F, it is seen (fig. V-5 (a)) that for A. S. T. M. Aviation lean conditions the C₅ and C₆ paraffins have the highest performance numbers in the boiling range from 80° to 120° F. In the boiling range between 130° and about 300° F, the ethers have the highest performance numbers. Above 300° F the highest performance numbers were obtained with the aromatic blends.

At A. S. T. M. Supercharge conditions (fig. V-5 (b)), the paraffin blends had the highest performance numbers in the range of boiling temperatures from 80° to 120° F. Above 120° F the ethers had the highest antiknock ratings up to a boiling temperature of 220° F. At higher boiling temperatures the aromatics exhibited superior antiknock characteristics.



(a) Engine, A. S. T. M. Aviation.

FIGURE V-5.—Comparison of isomers having highest antiknock values in blend with mixed base fuel consisting of 87.5 percent isoctane and 12.5 percent *n*-heptane+4 ml TEL per gallon.

BLENDING CHARACTERISTICS

In the preceding section, the discussion of structural trends was based on studies in which 25 percent of a given compound was blended with a selected base fuel. On the basis of such studies, it can be concluded that one compound is better than another or that all compounds align themselves in an order of antiknock performance that is influenced by engine operating conditions. This situation is complicated, however, in that the relative order of antiknock value of a series of compounds at a fixed engine condition is influenced by the concentration of the compound in the blends upon which such an investigation is based. In other words, one compound could be better than another if both were compared in 25-percent blends but the reverse could be true if both were compared in 50-percent blends.

Blending characteristics of various potential aviation-fuel blending agents have been the subject of considerable investigation. A portion of the more recent findings in such studies is reported in references 17 to 20. The results of these investigations show conclusively that compounds differ radically in their blending behavior as regards antiknock performance.

Paraffins.—The blending characteristics of paraffinic fuels at rich fuel-air ratios may be expressed by the following equation (see chapter VIII):

$$\frac{1}{P_b} = \frac{N_1}{P_1} + \frac{N_2}{P_2} + \frac{N_3}{P_3} + \dots \quad (1)$$

where

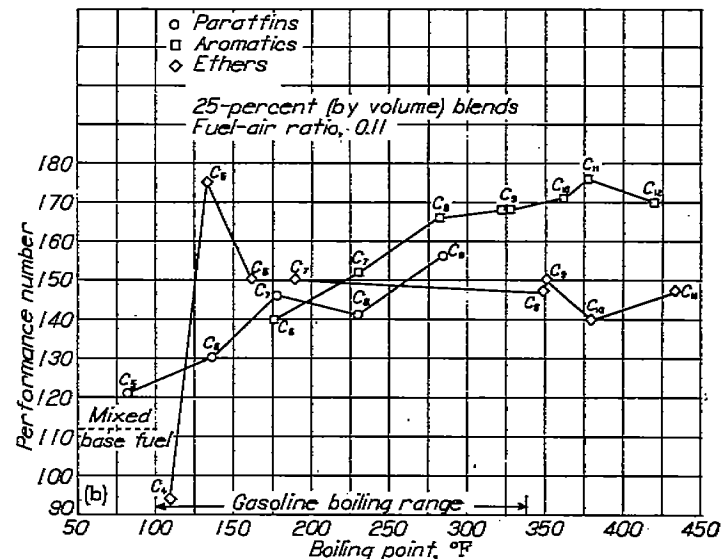
N_1, N_2, N_3, \dots mass fractions of components 1, 2, 3, . . . , respectively, in blend

P_b knock-limited indicated mean effective pressure of blend
 P_1, P_2, P_3, \dots knock-limited indicated mean effective pressures of components 1, 2, 3, . . . , respectively

The application of this equation to data in the present investigation is illustrated in figure V-6 (a) for the A. S. T. M. Supercharge engine. The ordinate of this figure is a reciprocal scale and the abscissa is linear. For the fuels shown, 2,2,3,4-tetramethylpentane, 2,3,3,4-tetramethylpentane, and 2,2,3-trimethylbutane, the blending relation with the base fuel is linear up to a concentration of 50 percent added paraffin. Knock-limited indicated mean effective pressures (fig. V-6 (a)) for 2,2,3,4-tetramethylpentane and 2,3,3,4-tetramethylpentane are from reference 12. Similar data for 2,2,3-trimethylbutane are from reference 11.

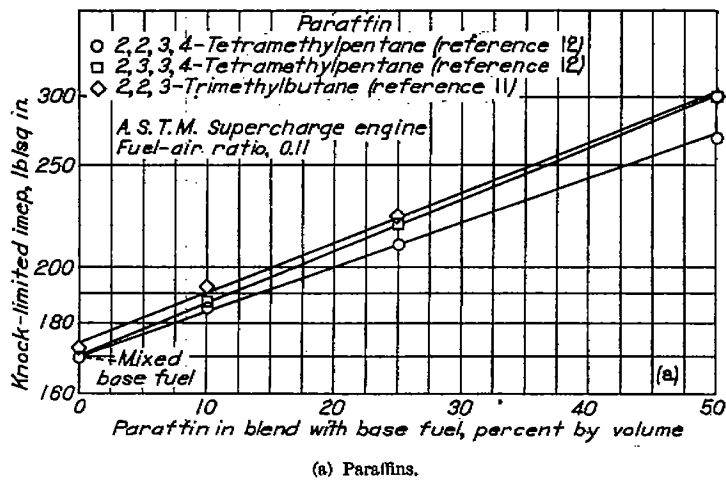
Although data for these fuels at lean fuel-air ratios are not shown herein, an examination of such data indicated that the blending relation is nonlinear. The authors of reference 17 attribute this fact to the variation of the end-gas temperature from one blend to another. That is, for a system in which a paraffinic blending agent is blended with a paraffinic base stock, the relation between the reciprocal of the knock-limited performance and the composition will be linear if the end-gas temperature, or a wall temperature closely related to the end-gas temperature, is held constant for each blend tested.

Olefins.—Blending data for two olefins (reference 12) are shown in figure V-6 (b) for the A. S. T. M. Supercharge engine operating at a rich fuel-air ratio. In this case, olefinic



(b) Engine, A. S. T. M. Supercharge.

FIGURE V-5.—Concluded. Comparison of isomers having highest antiknock values in blend with mixed base fuel consisting of 87.5 percent isoctane and 12.5 percent *n*-heptane+4 ml TEL per gallon.



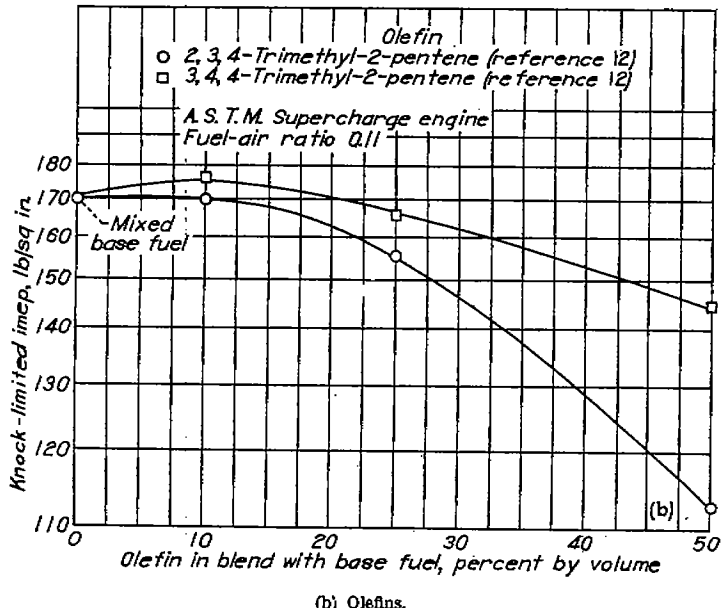
(a) Paraffins.

FIGURE V-6.—Knock-limited performance of blends with mixed base fuel consisting of 87.5 percent isoctane and 12.5 percent n-heptane + 4 ml TEL per gallon.

blending agents are blended with a paraffinic base fuel and the resulting relation between the reciprocal of the knock-limited performance and composition is nonlinear. The blending equation (1) is based upon one assumption, that for the equation to apply the blends should be tested at a constant percentage of excess of fuel or air. The differences between stoichiometric fuel-air ratios for olefins and paraffins, however, do not appear sufficiently great to explain the nonlinearity of this blending curve.

Aromatics.—The blending relations for the aromatic hydrocarbons (fig. V-6 (c)), like those of the olefins (fig. V-6 (b)), were found to be nonlinear in the A. S. T. M. Supercharge engine at rich mixtures. With the exception of 1,2-dimethylbenzene and 1,2,4-trimethylbenzene, all the aromatics increased the knock-limited performance of the base fuel at the concentration investigated.

It has previously been mentioned that the concentration level at which compounds are examined may have considerable effect on the relative order of antiknock rating, as shown



(b) Olefins.

FIGURE V-6.—Continued. Knock-limited performance of blends with mixed base fuel consisting of 87.5 percent isoctane and 12.5 percent n-heptane + 4 ml TEL per gallon.

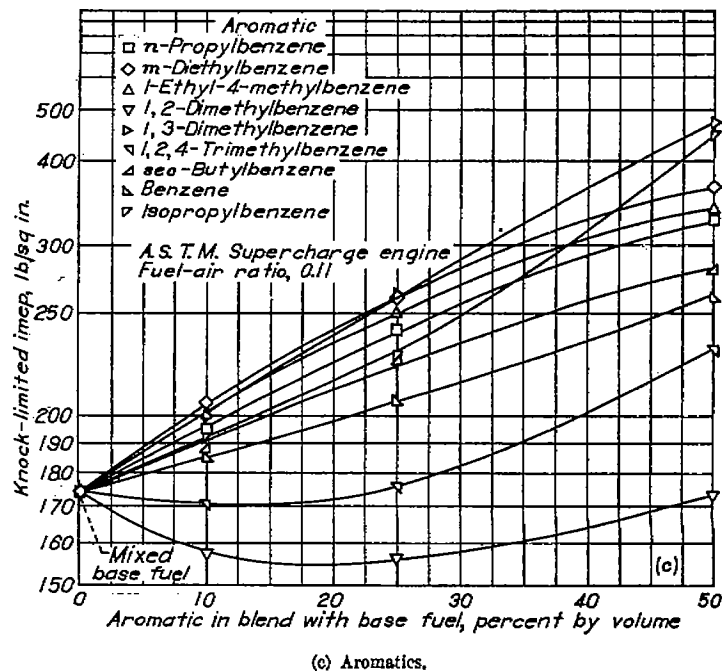
in figure V-6 (c) for isopropylbenzene. For example, a blend of 50 percent by volume of isopropylbenzene has the second highest antiknock rating of the aromatics investigated; at concentrations below 35 percent by volume, however, the performance of isopropylbenzenes is exceeded by that of 1,3-dimethylbenzene, 1,3-diethylbenzene, 1-ethyl-4-methylbenzene, and *n*-propylbenzene.

This result can perhaps be seen a little more clearly in figure V-7 (b), in which the blending data for the A. S. T. M. Supercharge engine are illustrated by a bar chart. The hydrocarbons are listed on this chart in order of decreasing antiknock rating, as determined by the 50-percent blends. At lower concentrations, however, the bars indicate a different order of rating.

At A. S. T. M. Aviation conditions (fig. V-7 (a)), the variation of knock-limited performance with composition was found to be different from that obtained at A. S. T. M. Supercharge conditions (figs. V-6 (c) and V-7 (b)). For example, the data presented in figure V-7 (a) indicate that the knock-limited performance of the base fuel is decreased as the concentration of aromatic is increased. Moreover, in figure V-7 (a) the aromatics do not rate in the same order at all concentrations.

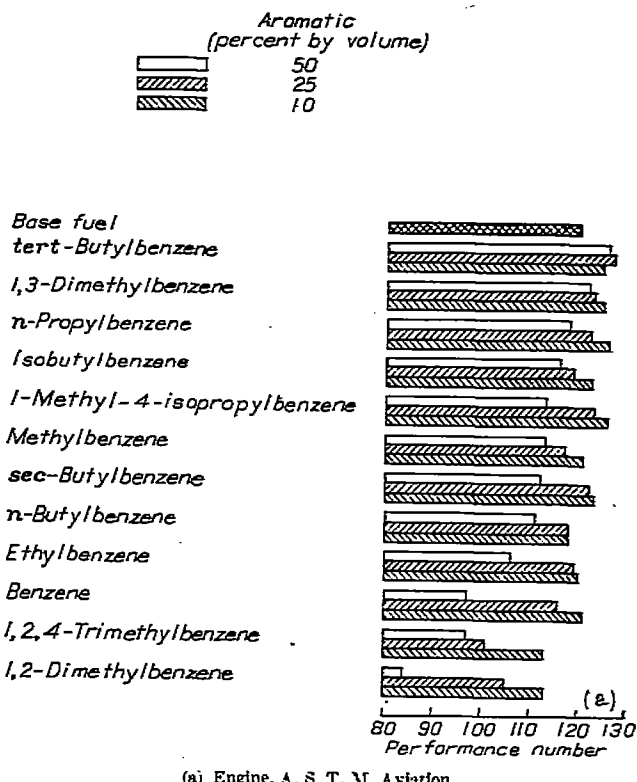
Ethers.—Blending data for six ethers determined at A. S. T. M. Supercharge conditions are shown in figure V-8 (b). Methyl *tert*-butyl ether and ethyl *tert*-butyl ether have the highest antiknock characteristics of the six ethers at all concentrations. Isopropyl *tert*-butyl ether is also better than the three aromatic ethers at a concentration of 50 percent; however, at concentrations below about 20 percent, isopropyl *tert*-butyl ether is lower than any of the other ethers.

The ethers shown in figure V-8 (b), like the olefins and aromatics, do not follow the reciprocal blending relation defined by equation (1).



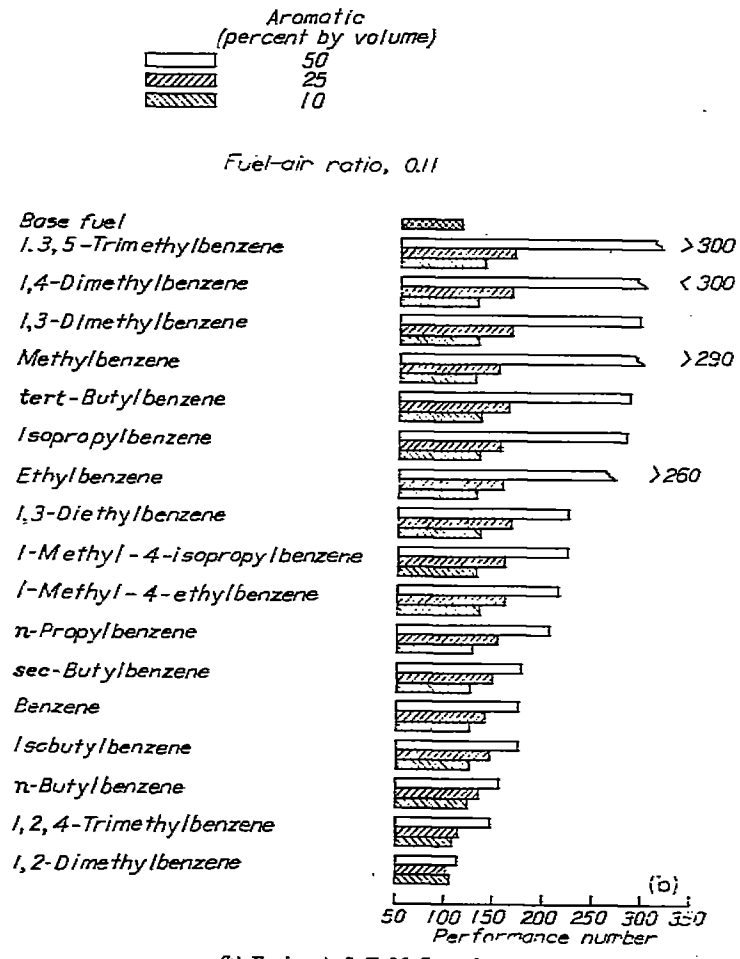
(c) Aromatics.

FIGURE V-6.—Concluded. Knock-limited performance of blends with mixed base fuel consisting of 87.5 percent isoctane and 12.5 percent n-heptane + 4 ml TEL per gallon.



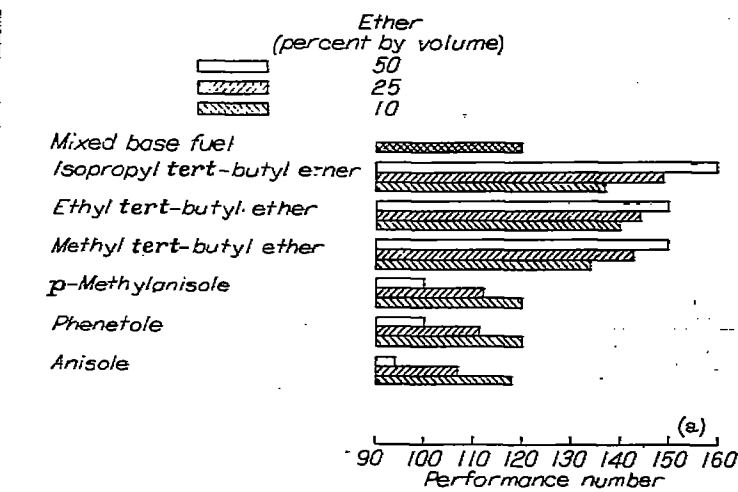
(a) Engine, A. S. T. M. Aviation.

FIGURE V-7.—Comparison of knock-limited performance of aromatic blends with mixed base fuel consisting of 87.5 percent isoctane and 12.5 percent *n*-heptane+4 ml TEL per gallon.



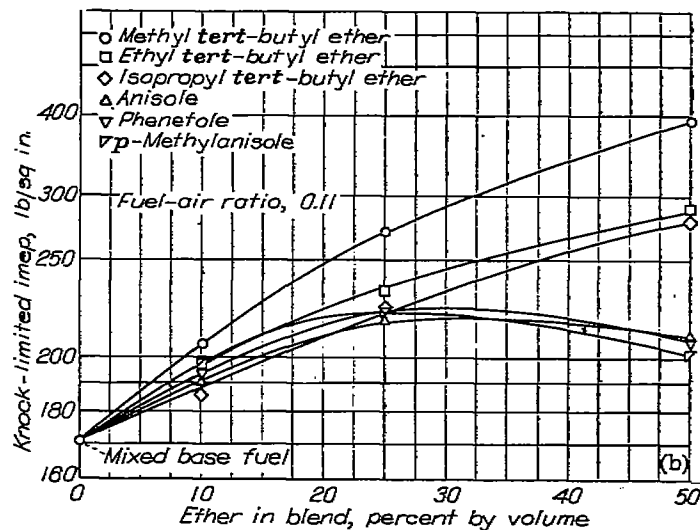
(b) Engine, A. S. T. M. Supercharge.

FIGURE V-7.—Concluded. Comparison of knock-limited performance of aromatic blends with mixed base fuel consisting of 87.5 percent isoctane and 12.5 percent *n*-heptane+4 ml TEL per gallon.



(a) Engine, A. S. T. M. Aviation.

FIGURE V-8.—Comparison of knock-limited performance of ether blends with mixed base fuel consisting of 87.5 percent isoctane and 12.5 percent *n*-heptane+4 ml TEL per gallon.



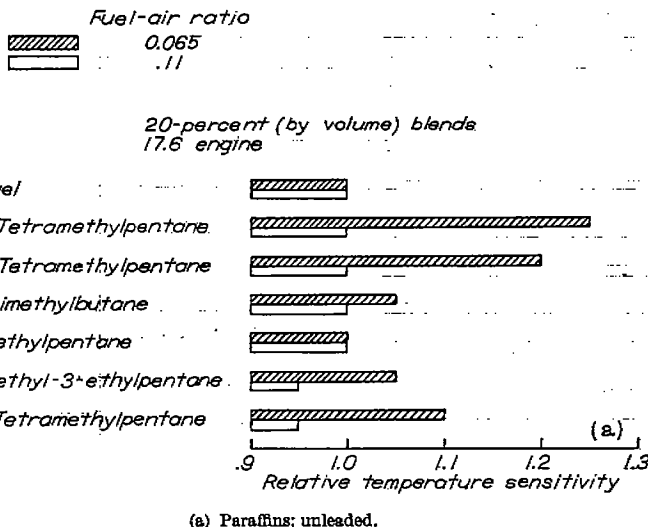
(b) Engine, A. S. T. M. Supercharge.

FIGURE V-8.—Concluded. Comparison of knock-limited performance of ether blends with mixed base fuel consisting of 87.5 percent isoctane and 12.5 percent *n*-heptane+4 ml TEL per gallon.

The blending relations for the ethers in figure V-8 (b) were investigated at A. S. T. M. Aviation conditions and the results obtained are presented in figure V-8 (a). At these conditions, the three *tert*-butyl alkyl ethers all improved the knock-limited performance of the base fuel; the improvement became greater as concentration was increased. On the other hand, the three aromatic ethers decreased the performance of the base fuel; the decrease became greater as the concentration was increased.

TEMPERATURE SENSITIVITY

In order to determine the effects of changes of inlet-air temperature on knock-limited performance, most of the hydrocarbons and ethers were evaluated in the 17.6 engine at inlet-air temperatures of 100° and 250° F. These tests were made with each compound in 20-percent-by-volume blends with isoctane. The final blends were evaluated at both temperatures in the unleaded state and with 4 ml TEL per gallon. (See appendix A, tables A-3 and A-4, respectively.) The greatest portion of the temperature-sensitivity studies of this investigation was conducted on blends with



(a) Paraffins; unleaded.

FIGURE V-9.—Temperature sensitivity of blends with isooctane. Compression ratio, 7.0; engine speed, 1800 rpm; coolant temperature, 212° F; spark advance, 30° B. T. C.

isooctane. A few experiments, however, were made in which the compounds were blended with the mixed base fuel. (See appendix A, table A-5.)

The term "temperature sensitivity" has been given several definitions by investigators in the field of fuel research; however, none of these definitions has been wholly satisfactory. Perhaps the data offering the most scientific approach to such a definition are reported in references 21 to 24, but the emphasis in these references is placed upon engine severity rather than the more restricted idea of temperature sensitivity; that is, engine severity is a more inclusive term that considers other factors of engine performance such as compression ratio, spark advance, engine speed, and cooling, as well as inlet-air temperature.

Considerable experimental data are required in order to evaluate fully the engine severity as described in references 21 to 24 and in most cases during the present investigation the available quantities of the pure fuels were too small for

extensive studies. For this reason, the sensitivity studies of these fuels to changes of engine conditions were restricted merely to measurements of the effect of inlet-air temperature on knock-limited performance. In so doing it was necessary to establish arbitrarily a definition for temperature sensitivity. This term is defined by the following equation:

$$\text{Relative temperature sensitivity} = \frac{\begin{cases} \text{knock-limited imep of blend (inlet air at 100° F)} \\ \text{knock-limited imep of base fuel (inlet air at 100° F)} \end{cases}}{\begin{cases} \text{knock-limited imep of blend (inlet air at 250° F)} \\ \text{knock-limited imep of base fuel (inlet air at 250° F)} \end{cases}}$$

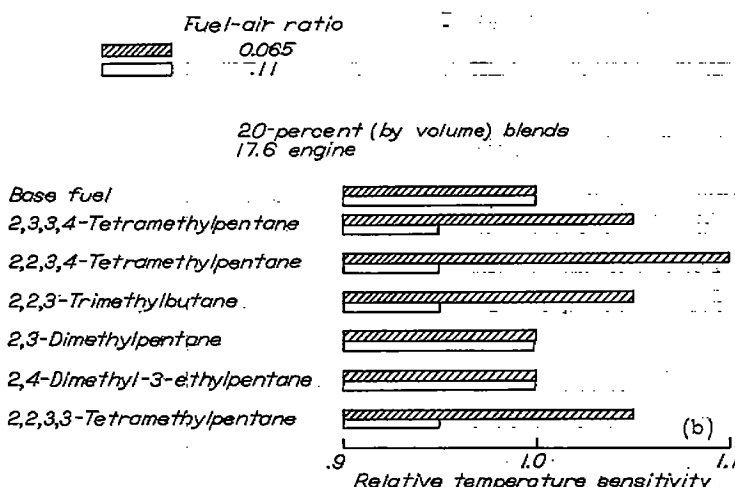
The term "relative" is used in this definition as the equation essentially describes the temperature sensitivity of the blend relative to that of the base fuel. This definition is the same as that used in references 5 to 11 and 13. The base fuels used in this study were paraffins and do not show high temperature sensitivity.

Temperature sensitivities computed by this equation for all the compounds in the present investigation are presented in appendix A, table A-6. In the discussion of temperature sensitivity in the following paragraphs and in the subsequent discussion of lead susceptibility, it should be remembered that the data were obtained over a long period of time and reproducibility errors therefore exist. Although no extensive reproducibility data were obtained, a few such runs indicated that relative temperature sensitivities computed by the equation and relative lead susceptibilities computed by a similar equation may be in error by ± 0.05 .

Paraffins.—The temperature sensitivities of unleaded and leaded paraffinic fuel blends in the 17.6 engine at two fuel-air ratios are compared in figures V-9 (a) and V-9 (b). Of the paraffinic blending agents investigated (references 12 and 13), the three nonanes, 2,3,3,4-tetramethylpentane, 2,2,3,4-tetramethylpentane, and 2,2,3,3-tetramethylpentane, appear to be most sensitive to changes of inlet-air temperature at the lean fuel-air ratio in unleaded blends (fig. V-9 (a)). At the rich fuel-air ratio, however, the differences in temperature sensitivities among the paraffins are small.

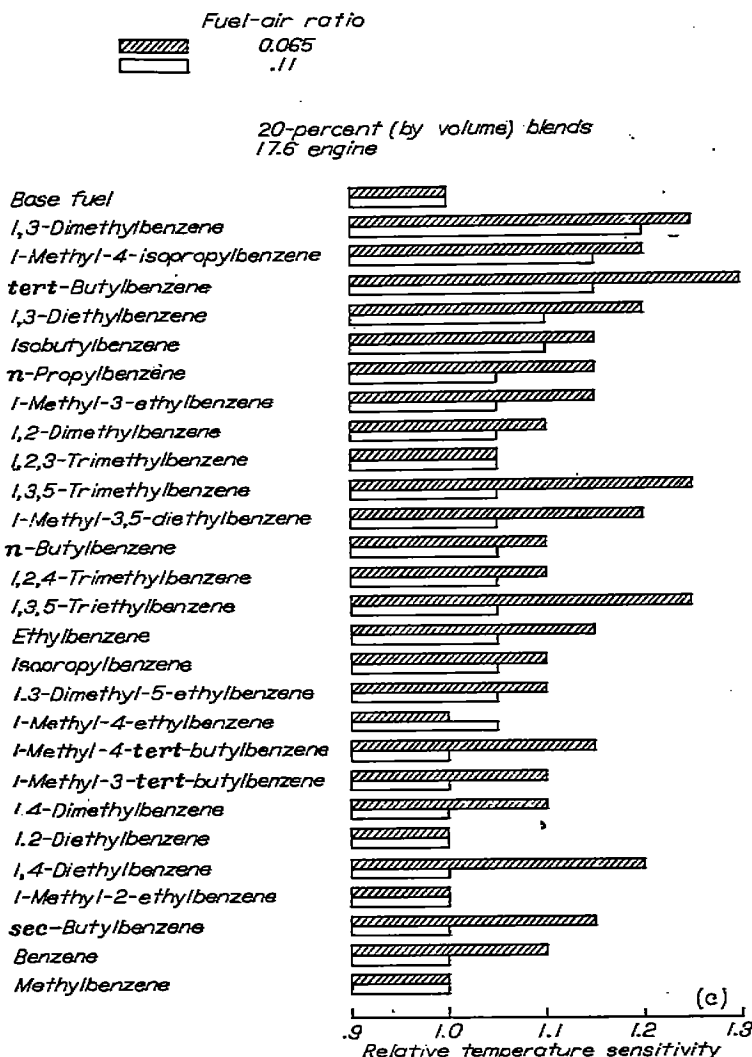
In figures V-9 (a) and V-9 (b), the paraffins are listed in the same order. Inspection of these plots illustrates that tetraethyl lead affects temperature sensitivity. For example, in figures V-9 (a) and V-9 (b) the order of temperature sensitivities of the various paraffins is obviously different at both fuel-air ratios.

As previously mentioned, a few of the compounds in this investigation were examined in blends with the mixed base fuel. In the investigation of reference 13, paraffinic and olefinic blending agents in blends with the mixed base fuel were subjected to variations of compression ratio. When these data are computed in the manner explained in references 23 and 24, it is possible to compare over a reasonably wide range the influence of engine severity on knock-limited performance. This effect is determined by computation of compression-air densities and compression temperatures at the knock limit; the main assumption is that these factors are related in some manner to end-gas densities and temperatures that cannot be directly measured (reference 21). The



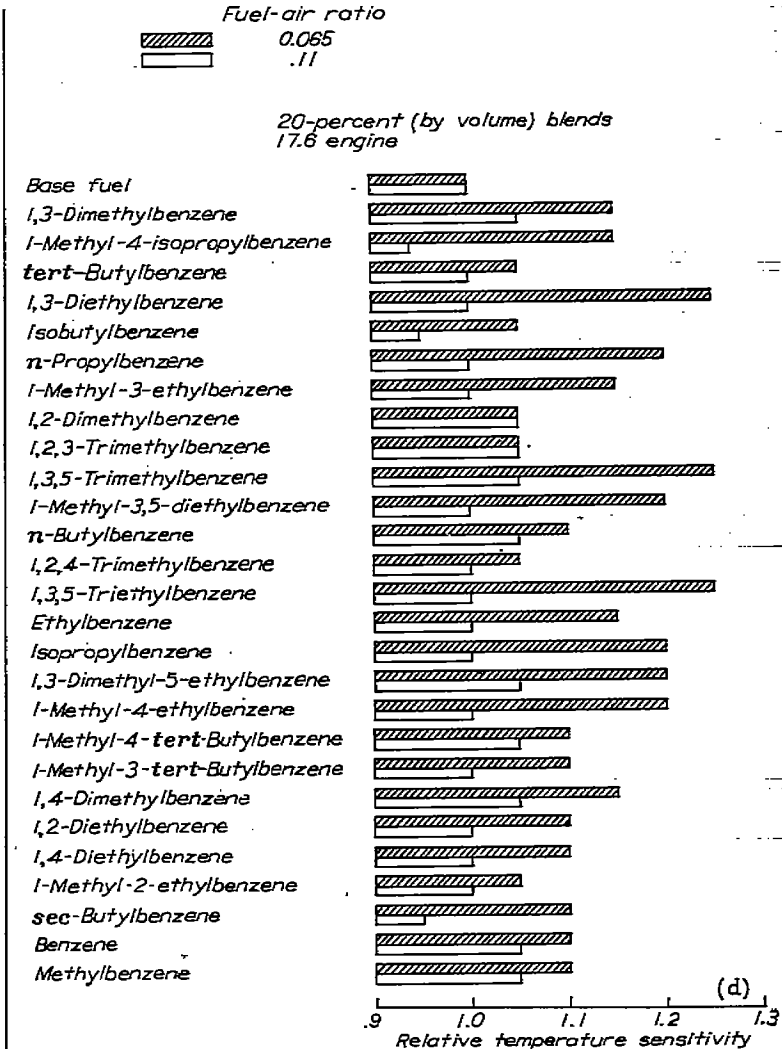
(b) Paraffins; leaded to 4 ml TEL per gallon.

FIGURE V-9.—Continued. Temperature sensitivity of blends with isooctane. Compression ratio, 7.0; engine speed, 1800 rpm; coolant temperature, 212° F; spark advance, 30° B. T. C.



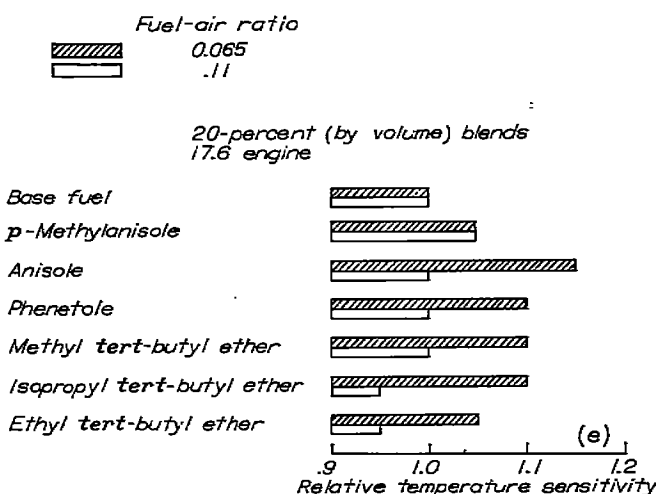
(c) Aromatics; unleaded.

FIGURE V-9.—Continued. Temperature sensitivity of blends with isoctane. Compression ratio, 7.0; engine speed, 1800 rpm; coolant temperature, 212° F; spark advance, 30° B. T. C.



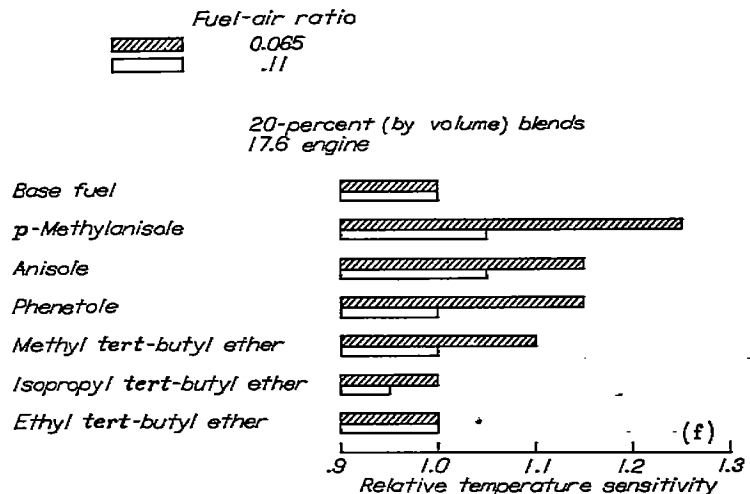
(d) Aromatics; leaded to 4 ml TEL per gallon.

FIGURE V-9.—Continued. Temperature sensitivity of blends with isoctane. Compression ratio, 7.0; engine speed, 1800 rpm; coolant temperature, 212° F; spark advance, 30° B. T. C.



(e) Ethers; unleaded.

FIGURE V-9.—Continued. Temperature sensitivity of blends with isoctane. Compression ratio, 7.0; engine speed, 1800 rpm; coolant temperature, 212° F; spark advance, 30° B. T. C.



(f) Ethers; leaded to 4 ml TEL per gallon.

FIGURE V-9.—Concluded. Temperature sensitivity of blends with isoctane. Compression ratio, 7.0; engine speed, 1800 rpm; coolant temperature, 212° F; spark advance, 30° B. T. C.

compression-air densities and temperatures are calculated by the following equations:

$$\rho_c = \frac{W_0(r-1)}{iV_d} \quad (2)$$

$$T_c = T_0 r^{\gamma-1} \quad (3)$$

where

ρ_c compression-air density, pounds per cubic inch

W_0 intake-air flow, pounds per minute

r compression ratio

i intake cycles per minute

V_d engine displacement volume, cubic inches

T_c compression-air temperature, °R

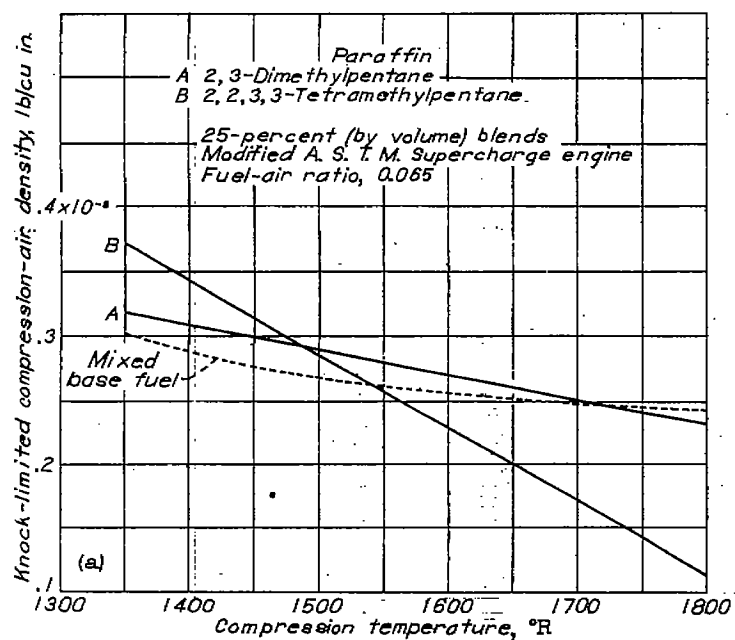
T_0 intake-air temperature, °R

γ ratio of specific heat of charge at constant pressure to that at constant volume (assumed to be 1.4)

Although the data in reference 13 were determined by varying the compression ratio, it is apparent from the equation of compression temperature that the effect of varying the compression ratio is equivalent to that of varying the intake-air temperature.

The sensitivities of two paraffinic fuels (reference 13) are shown in figures V-10 (a) and V-10 (b) at two fuel-air ratios in a modified A. S. T. M. Supercharge engine. The two paraffin blends are more sensitive than the base fuel to changes of compression ratio or intake-air temperature, as indicated by the slopes of the curves in figures V-10 (a) and V-10 (b). The two paraffin blends had lower knock limits than the base fuel at severe conditions (high compression temperatures), but higher limits at mild conditions (low compression temperatures).

Olefins.—Plots similar to those in figures V-10 (a) and V-10 (b) are shown in figures V-10 (c) and V-10 (d) for



(a) Paraffins; lean conditions.

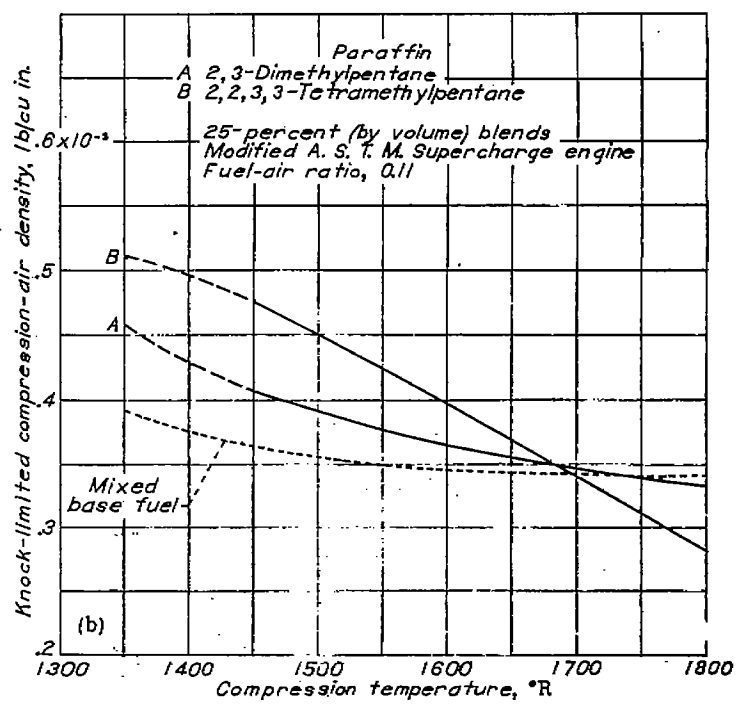
FIGURE V-10.—Effect of compression temperature on compression-air density for blends with mixed base fuel consisting of 87.5 percent isoctane and 12.5 percent *n*-heptane+4 ml TEL per gallon. Compression ratio, variable; engine speed, 1800 rpm; inlet-air temperature, 250° F.; coolant temperature, 250° F.; spark advance, 30° B. T. C.

three olefins in blends with the mixed base fuel (reference 13). At both fuel-air ratios, the three olefin blends were more sensitive to a change of engine severity than the base fuel. At the severe conditions the three olefin blends had lower knock limits than did the base fuel, but at milder conditions the olefin blends had higher knock limits.

Aromatics.—The temperature sensitivities of aromatic blends determined in the 17.6 engine are shown in figures V-9 (c) and V-9 (d). The aromatics are listed in figure V-9 (c) in the order of decreasing sensitivity at the rich fuel-air ratio. As in the case of paraffins (figs. V-9 (a) and V-9 (b)), the sensitivities were inconsistent from one fuel-air ratio to another. Moreover, the sensitivities were influenced by tetraethyl lead.

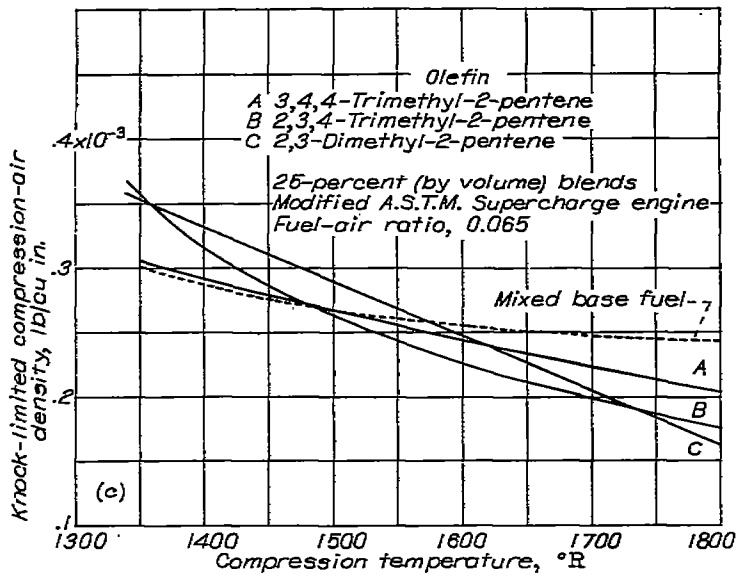
The most sensitive aromatics at the rich fuel-air ratio (fig. V-9 (c)) were 1,3-dimethylbenzene, 1-methyl-4-isopropylbenzene, and *tert*-butylbenzene; whereas at the lean fuel-air ratio, a number of aromatics had high sensitivities. In leaded blends (fig. V-9 (d)), the differences in relative temperature sensitivity among the aromatics were not great at the rich fuel-air ratio, but at a lean fuel-air ratio appreciable differences occurred. At the lean fuel-air ratio, a number of the aromatics had sensitivities 20 to 25 percent greater than the sensitivity of the base fuel.

It has been shown herein that 1,3,5-trimethylbenzene and *tert*-butylbenzene had higher performance numbers than the other aromatics investigated at the lean condition of the A. S. T. M. Aviation method (fig. V-3 (i)). For this reason the temperature sensitivities of these two aromatics are of particular interest. These two aromatics in unleaded blends have temperature sensitivities equal to or greater than sensitivities of the other aromatics investigated at the lean fuel-



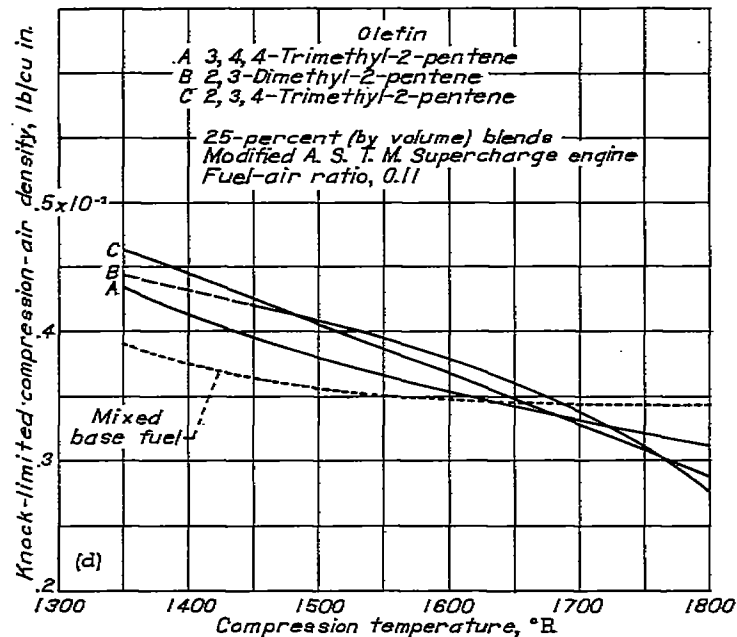
(b) Paraffins; rich conditions.

FIGURE V-10.—Continued. Effect of compression temperature on compression-air density for blends with mixed base fuel consisting of 87.5 percent isoctane and 12.5 percent *n*-heptane+4 ml TEL per gallon. Compression ratio, variable; engine speed, 1900 rpm; inlet-air temperature, 250° F.; coolant temperature, 250° F.; spark advance, 30° B. T. C.



(c) Olefins; lean conditions.

FIGURE V-10.—Continued. Effect of compression temperature on compression-air density for blends with mixed base fuel consisting of 87.5 percent isoctane and 12.5 percent n -heptane+4 ml TEL per gallon. Compression ratio, variable; engine speed, 1800 rpm; inlet-air temperature, 250° F; coolant temperature, 250° F; spark advance, 30° B. T. C.

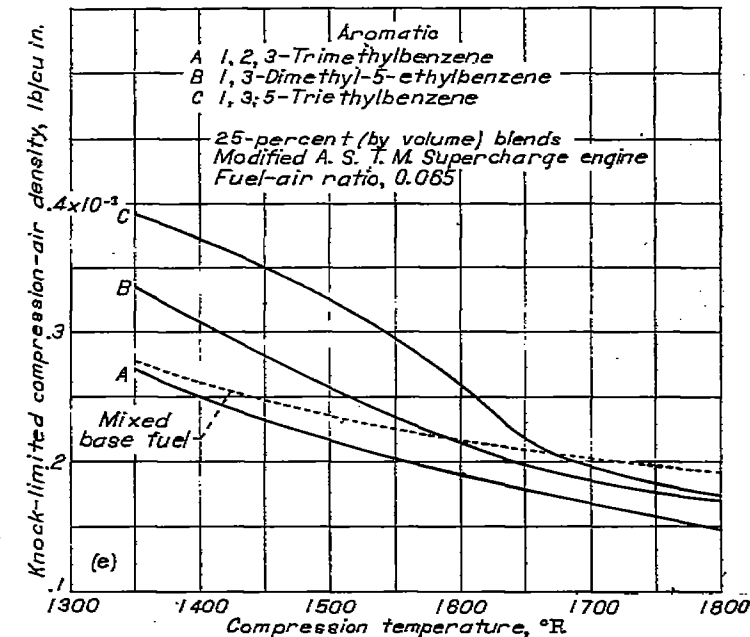


(d) Olefins; rich conditions.

FIGURE V-10.—Continued. Effect of compression temperature on compression-air density for blends with mixed base fuel consisting of 87.5 percent isoctane and 12.5 percent n -heptane+4 ml TEL per gallon. Compression ratio, variable; engine speed, 1800 rpm; inlet-air temperature, 250° F; coolant temperature, 250° F; spark advance, 30° B. T. C.

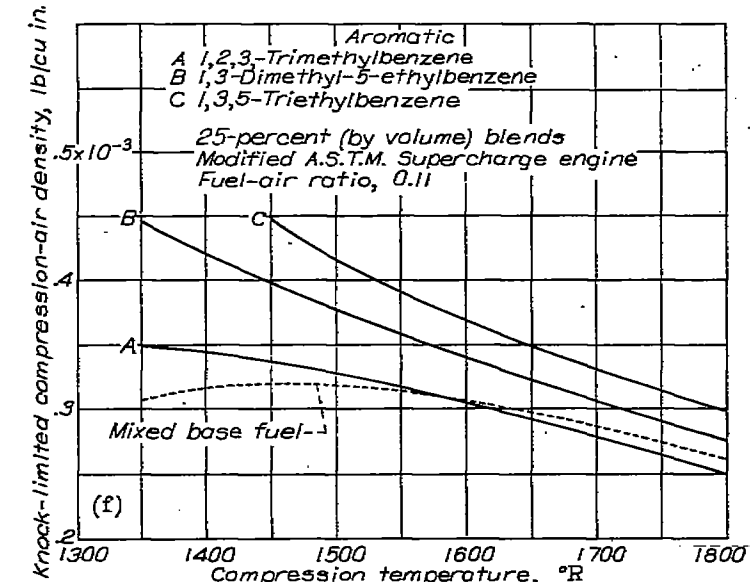
air ratio (fig. V-9 (c)). On the other hand, the leaded blends shown in figure V-9 (d) indicate that the temperature sensitivity of *tert*-butylbenzene is reduced considerably, whereas 1,3,5-trimethylbenzene is still quite sensitive.

Similarly, among the better aromatics at A. S. T. M. Supercharge conditions (fig. V-3 (j)) were 1,3-dimethyl-5-ethylbenzene, 1-methyl-3,5-diethylbenzene, 1-methyl-4-*tert*-



(e) Aromatics; lean conditions.

FIGURE V-10.—Continued. Effect of compression temperature on compression-air density for blends with mixed base fuel consisting of 87.5 percent isoctane and 12.5 percent n -heptane+4 ml TEL per gallon. Compression ratio, variable; engine speed, 1800 rpm; inlet-air temperature, 250° F; coolant temperature, 250° F; spark advance, 30° B. T. C.



(f) Aromatics; rich conditions.

FIGURE V-10.—Concluded. Effect of compression temperature on compression-air density for blends with mixed base fuel consisting of 87.5 percent isoctane and 12.5 percent n -heptane+4 ml TEL per gallon. Compression ratio, variable; engine speed, 1800 rpm; inlet-air temperature, 250° F; coolant temperature, 250° F; spark advance, 30° B. T. C.

butylbenzene, and 1,3,5-triethylbenzene. As indicated in figure V-9 (c) for unleaded blends at a rich fuel-air ratio, these four aromatics show only moderate temperature sensitivity varying between 1.0 and 1.05. In leaded blends (fig. V-9 (d)) and at a rich fuel-air ratio, the four aromatics still exhibited only moderate temperature sensitivity varying between 1.0 and 1.05.

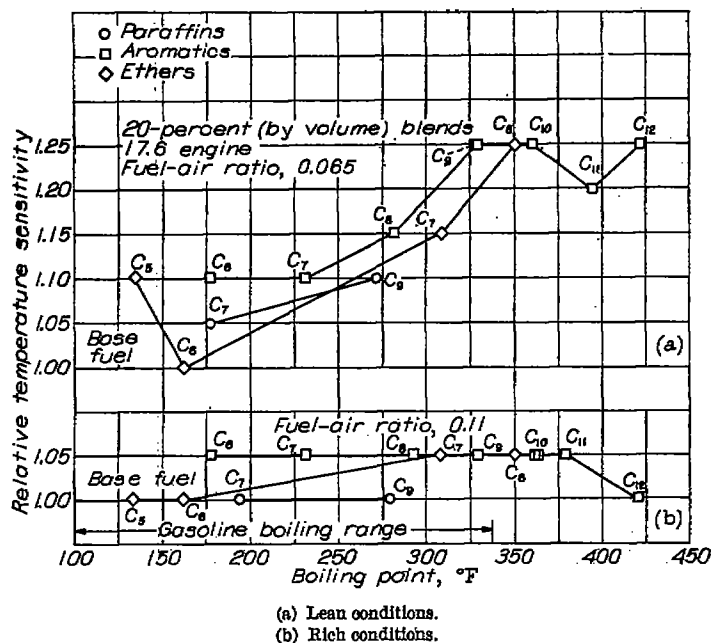


FIGURE V-11.—Comparison of isomers having highest temperature sensitivities in blend with isoctane. Compression ratio, 7.0; engine speed, 1800 rpm; coolant temperature, 212° F; spark advance, 30° B. T. C.

Compression-air density-temperature relations were determined for several aromatics and are reported in reference 10. The relation obtained for three of the aromatics is presented in figures V-10 (e) and V-10 (f) in order to illustrate the nature of the results. As indicated by the slopes of the curves in these figures, the sensitivities of the aromatic blends are somewhat greater than the sensitivity of the base fuel.

Ethers.—Temperature sensitivities determined for six ethers are shown in figures V-9 (e) and V-9 (f). The ethers (unleaded blends) are listed in figure V-9 (e) in the order of decreasing sensitivity at the rich fuel-air ratio (0.11); at this fuel-air ratio the three aromatic ethers appear to be more

sensitive to temperature changes than do the *tert*-butyl alkyl ethers, with the possible exception of methyl *tert*-butyl ether. At the lean fuel-air ratio (0.065), anisole appears to be the most sensitive of the ethers; however, with consideration for the estimated reproducibility of these data there may be little real difference in the sensitivities of the six ethers shown.

In leaded blends (fig. V-9 (f)), the aromatic ethers are perhaps more temperature-sensitive than the *tert*-butyl alkyl ethers with the possible exception of methyl *tert*-butyl ether at the lean fuel-air ratio. At the rich fuel-air ratio, anisole and *p*-methylanisole show the highest sensitivities; however, the experimental accuracy may minimize the apparent differences shown on the figures.

Comparison of classes of compounds.—The temperature sensitivities of the various classes of compounds are compared in figure V-11. The procedure used in preparing these plots was the same as that used for figure V-5.

In figure V-11 at two fuel-air ratios, the low-boiling ethers have the greatest temperature sensitivities in the boiling range of 100° to 175° F. Above 175° F the aromatics are more sensitive than the other classes examined. In the boiling range from 300° to 350° F, however, the ethers have temperature sensitivities comparable to those of the aromatics.

LEAD SUSCEPTIBILITY

Lead susceptibilities of the various organic compounds investigated were determined in the 17.6 engine by comparing unleaded blends (20 percent by volume) with blends containing 4 ml TEL per gallon. Data were obtained at two inlet-air temperatures, 100° and 250° F. (See appendix A, table A-7.)

Lead susceptibility, or lead response, is usually defined as the increase in octane number or power output resulting from the addition of a given quantity of tetraethyl lead to a fuel. For the present investigation, however, lead susceptibility is

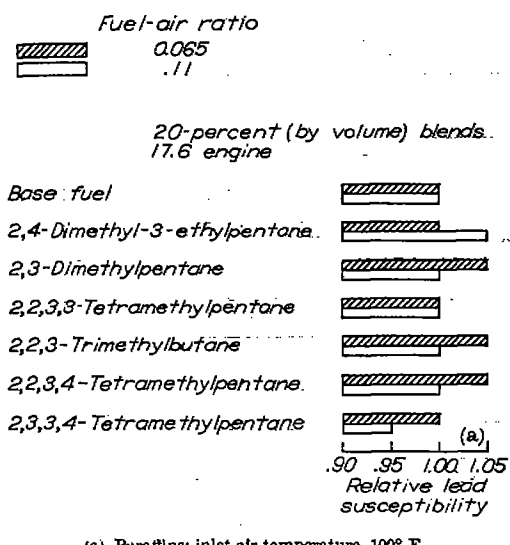


FIGURE V-12.—Lead susceptibility (4 ml TEL/gal) of blends with isoctane. Compression ratio, 7.0; engine speed, 1800 rpm; coolant temperature, 212° F; spark advance, 30° B. T. C.

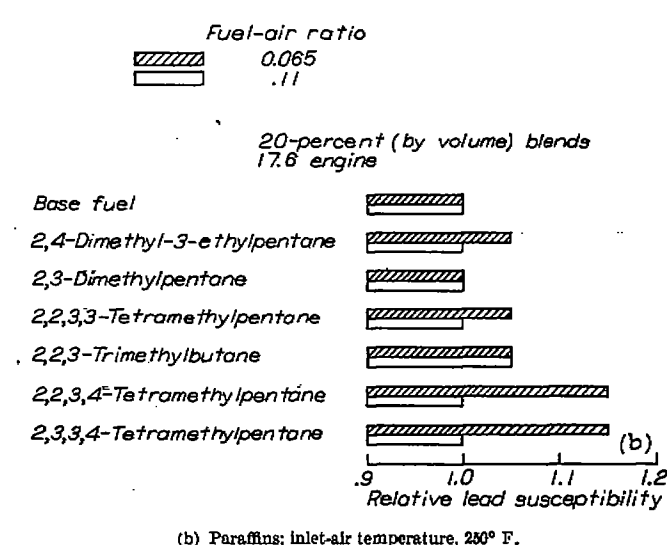


FIGURE V-12.—Continued. Lead susceptibility (4 ml TEL/gal) of blends with isoctane. Compression ratio, 7.0; engine speed, 1800 rpm; coolant temperature, 212° F; spark advance, 30° B. T. C.

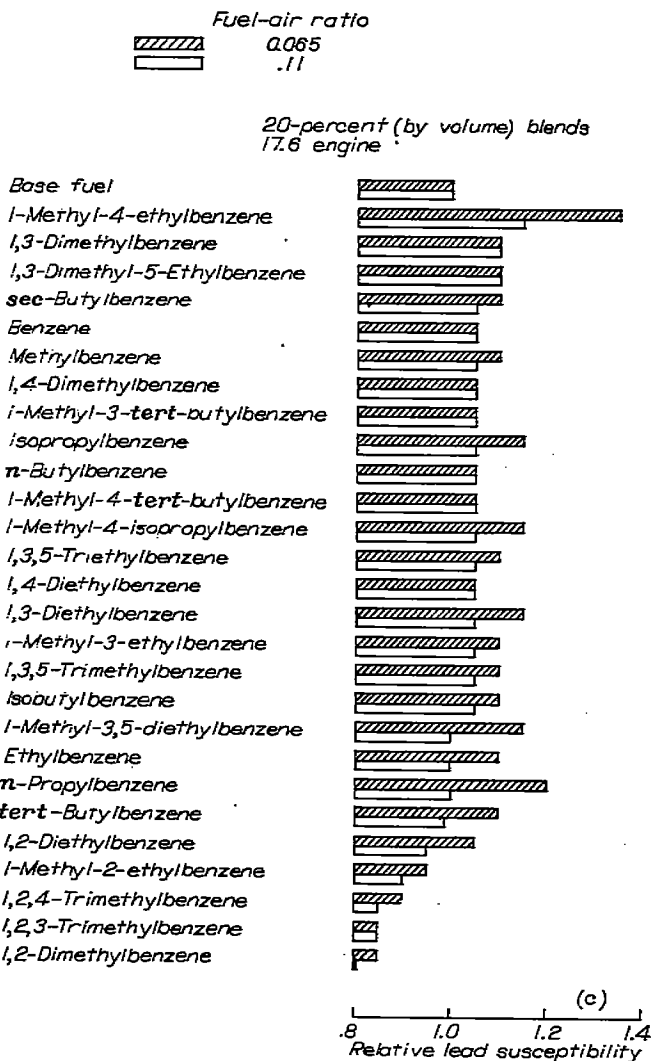


FIGURE V-12.—Continued. Lead susceptibility (4 ml TEL/gal) of blends with isoctane. Compression ratio, 7.0; engine speed, 1800 rpm; coolant temperature, 212° F; spark advance, 30° B. T. C.

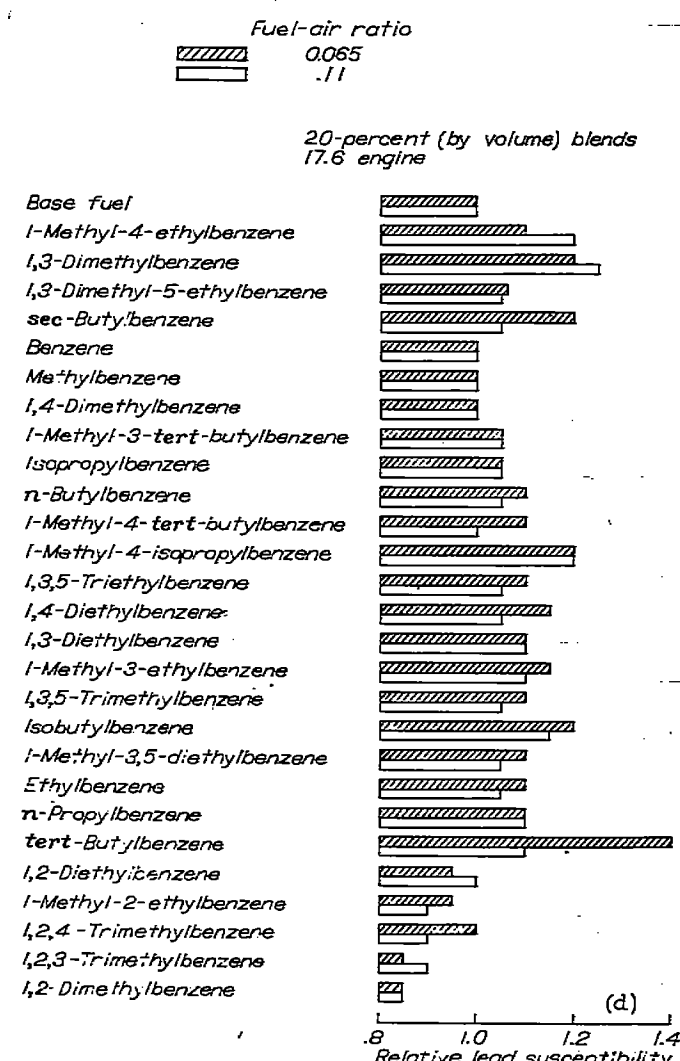


FIGURE V-12.—Continued. Lead susceptibility (4 ml TEL/gal) of blends with isoctane. Compression ratio, 7.0; engine speed, 1800 rpm; coolant temperature, 212° F; spark advance, 30° B. T. C.

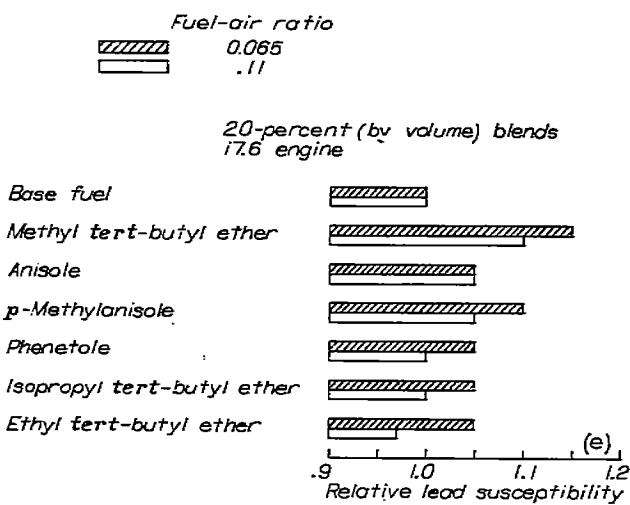


FIGURE V-12.—Continued. Lead susceptibility (4 ml TEL/gal) of blends with isoctane. Compression ratio, 7.0; engine speed, 1800 rpm; coolant temperature, 212° F; spark advance, 30° B. T. C.

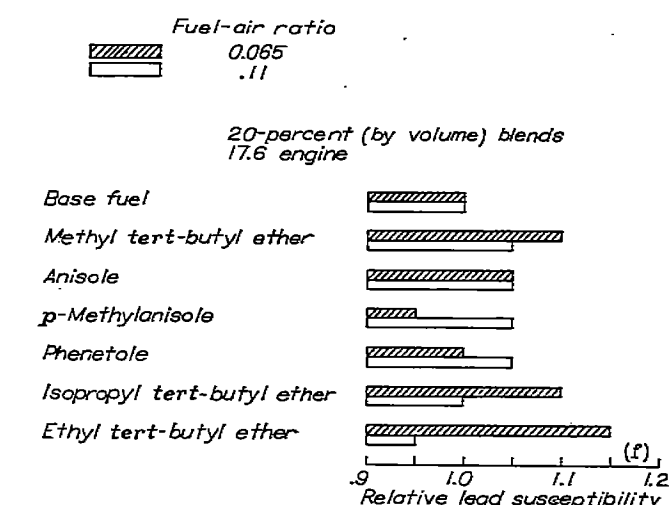


FIGURE V-12.—Concluded. Lead susceptibility (4 ml TEL/gal) of blends with isoctane. Compression ratio, 7.0; engine speed, 1800 rpm; coolant temperature, 212° F; spark advance, 30° B. T. C.

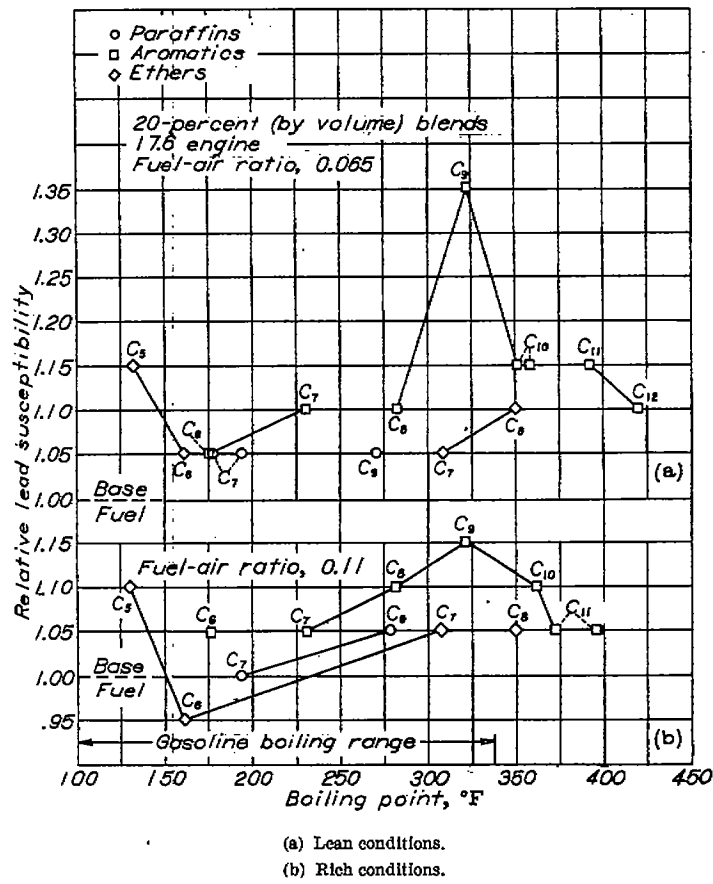


FIGURE V-13.—Comparison of isomers having highest lead susceptibility in blends with isoctane. Compression ratio, 7.0; engine speed, 1800 rpm; inlet-air temperature, 100° F; coolant temperature, 212° F; spark advance, 30° B. T. C.

expressed in a manner similar to that used for temperature sensitivity:

$$\text{Relative lead susceptibility} = \begin{cases} \frac{\text{knock-limited imep of blend} + 4 \text{ ml TEL/gal}}{\text{knock-limited imep of base fuel} + 4 \text{ ml TEL/gal}} \\ \frac{\text{knock-limited imep of blend} + 0 \text{ ml TEL/gal}}{\text{knock-limited imep of base fuel} + 0 \text{ ml TEL/gal}} \end{cases}$$

As in the foregoing discussion of temperature sensitivity, the estimated accuracy of these ratios is about ± 0.05 .

Paraffins.—The lead susceptibilities of six paraffinic blends are shown in figures V-12 (a) and V-12 (b). In figure V-12 (a) (inlet-air temperature, 100° F), the fuels are arranged in order of decreasing response at the rich mixture. At this condition, 2,4-dimethyl-3-ethylpentane exhibits the greatest susceptibility to tetraethyl lead, but at the lean fuel-air ratio, 2,3-dimethylpentane, 2,2,3-trimethylbutane, and 2,2,3,4-tetramethylpentane have the best response. The lead susceptibility is appreciably influenced by fuel-air ratio.

In figure V-12 (b) (inlet-air temperature, 250° F), the fuels are listed in the same order as that of figure V-12 (a), but little or no difference in lead susceptibility is apparent at the rich fuel-air ratio except in the case of 2,2,3-trimethylbutane. At the lean fuel-air ratio, 2,2,3,4-tetramethylpentane and 2,3,3,4-tetramethylpentane had the highest lead susceptibilities.

Olefins.—A limited amount of data was obtained in the 17.6 engine to show the lead susceptibility of olefins in 20-

percent-by-volume blends with isoctane. (See appendix A, table A-7 (a).) For convenience, a portion of these data is summarized in the following table:

Olefin	Lead susceptibility of 20-percent olefin blends relative to isoctane			
	Inlet-air temperature (°F)			
	250	100	Fuel-air ratio	
	0.065	0.11	0.065	0.11
2,3-dimethyl-2-pentene	0.95	1.00	1.00	0.95
2,3,4-trimethyl-2-pentene	1.05	1.05	1.05	1.05
3,4,4-trimethyl-2-pentene	1.00	1.00	1.05	1.00

Aromatics.—In figures V-12 (c) and V-12 (d), the lead susceptibilities of aromatic blends are shown. The blends in figure V-12 (c) are listed in order of decreasing response at the rich fuel-air ratio. At this ratio, the data indicate that 1-methyl-4-ethylbenzene is the aromatic most susceptible to additions of tetraethyl lead. This particular aromatic also had the greatest response at the lean fuel-air ratio. From figures V-12 (c) and V-12 (d), lead susceptibility is obviously affected by fuel-air ratio.

At the higher inlet-air temperature (fig. V-12 (d)), the trend in lead susceptibility differs from that observed at 100° F (fig. V-12 (c)) for the aromatics. For the rich fuel-air ratio (fig. V-12 (d)), three of the aromatics, 1-methyl-4-ethylbenzene, 1,3-dimethylbenzene, and 1-methyl-4-isopropylbenzene, appear to be the most susceptible. At the lean fuel-air ratio, however, *tert*-butylbenzene is considerably more susceptible than the other aromatics.

Ethers.—Lead susceptibilities of the ether blends are presented in figures V-12 (e) and V-12 (f). At an inlet-air temperature of 100° F (fig. V-12 (e)), methyl *tert*-butyl ether and *p*-methyl anisole have the greatest lead susceptibilities at the lean fuel-air ratio. At the rich fuel-air ratio, methyl *tert*-butyl ether has the highest susceptibility with anisole and *p*-methyl anisole next.

At an inlet-air temperature of 250° F (fig. V-12 (f)), the three *tert*-butyl alkyl ethers have the highest susceptibilities at the lean fuel-air ratio. The three aromatic ethers and methyl *tert*-butyl ether exhibit the highest susceptibilities at the rich fuel-air ratio.

Comparison of classes of compounds.—In figure V-13, the lead susceptibilities are plotted against boiling points for the isomers having highest lead susceptibilities in each class of compounds. At both lean (fig. V-13 (a)) and rich (fig. V-13 (b)) fuel-air ratios, the low-boiling ethers appear to be most susceptible to tetraethyl lead in the boiling range from 125° to 160° F. Above 160° F, the aromatics show the greatest lead response.

CONCLUDING REMARKS

On the basis of an investigation of the type reported herein, it is difficult to draw any specific conclusions, inasmuch as antiknock characteristics are influenced by many

factors. The relative order of antiknock ratings of a series of compounds is influenced by engine conditions, by the tetraethyl lead content, and by the concentration of blending agent in the base fuel with which a comparison is made. With consideration for these factors, *tert*-butylbenzene, methyl and ethyl *tert*-butyl ethers, 2,2,3-trimethylbutane, and several nonanes were among the best compounds in their respective organic classes. This selection was based upon temperature sensitivity and lead susceptibility as well as antiknock value.

In an effort to generalize the data obtained in this investigation, the subsequent conclusions are expressed in terms of the relation of various performance factors to the gasoline boiling range as influenced by the classes of organic compounds investigated. Furthermore, these conclusions must necessarily be restricted to the limitations of this investigation and therefore cannot be applied without exception.

Antiknock ratings.—In the low-boiling gasoline range, the highest antiknock ratings are among the more volatile paraffins and ethers. In the intermediate gasoline range, the ethers excel; in the high-boiling range the aromatics have the highest antiknock ratings.

Temperature sensitivity.—In the low-boiling gasoline range, the data are incomplete as regards temperature sensitivity, but there are indications that the volatile ethers are more sensitive to temperature changes than are the paraffins or aromatics. In the intermediate and high-boiling ranges of gasoline, the aromatics are more sensitive to temperature than the paraffins and the ethers. Moreover, the aromatics that have the highest antiknock ratings are also sensitive to temperature.

Lead susceptibility.—In the low-boiling gasoline range, the data are incomplete as regards lead susceptibility, but there are indications that the more volatile ethers are more susceptible to additions of tetraethyl lead than are the paraffins and the aromatics. In the intermediate and high-boiling ranges of gasoline, the aromatics show greater lead susceptibility than either the paraffins or the ethers.

REFERENCES

1. Lovell, Wheeler G.: Knocking Characteristics of Hydrocarbons. *Ind. and Eng. Chem.*, vol. 40, no. 12, Dec. 1948, pp. 2388-2438.
2. Jones, Anthony W., and Bull, Arthur W.: Knock-Limited Performance of Pure Hydrocarbons Blended with a Base Fuel in a Full-Scale Aircraft-Engine Cylinder. I—Eight Paraffins, Two Olefins. *NACA ARR E4E25*, 1944.
3. Bull, Arthur W., and Jones, Anthony W.: Knock-Limited Performance of Pure Hydrocarbons Blended with a Base Fuel in a Full-Scale Aircraft-Engine Cylinder. II—Twelve Aromatics. *NACA ARR E4I09*, 1944.
4. Jones, Anthony W., Bull, Arthur W., and Jonash, Edmund R.: Knock-Limited Performance of Pure Hydrocarbons Blended with a Base Fuel in a Full-Scale Aircraft-Engine Cylinder. III—Four Aromatics, Six Ethers. *NACA ARR E6B14*, 1946.
5. Meyer, Carl L., and Branstetter, J. Robert: The Knock-Limited Performance of Fuel Blends Containing Aromatics. I—Toluene, Ethylbenzene, and *p*-Xylene. *NACA ARR E4J05*, 1944.
6. Branstetter, J. Robert, and Meyer, Carl L.: The Knock-Limited Performance of Fuel Blends Containing Aromatics. II—Iso-propylbenzene, Benzene, and *o*-Xylene. *NACA ARR E5A20*, 1945.
7. Meyer, Carl L., and Branstetter, J. Robert: The Knock-Limited Performance of Fuel Blends Containing Aromatics. III—1,3,5-Trimethylbenzene, *tert*-Butylbenzene, and 1,2,4-Trimethylbenzene. *NACA ARR E5D16*, 1945.
8. Meyer, Carl L., and Branstetter, J. Robert: The Knock-Limited Performance of Fuel Blends Containing Aromatics. IV—Data for *m*-Diethylbenzene, 1-Ethyl-4-methylbenzene, and *sec*-Butylbenzene Together with a Summarization of Data for 12 Aromatic Hydrocarbons. *NACA ARR E5D16a*, 1945.
9. Meyer, Carl L., and Branstetter, J. Robert: The Knock-Limited Performance of Fuel Blends Containing Aromatics. V—*n*-Propylbenzene, *n*-Butylbenzene, Isobutylbenzene, *m*-Xylene, and 1-Isopropyl-4-methylbenzene. *NACA ARR E6C05*, 1946.
10. Drell, I. L., and Alquist, H. E.: Knock-Limited Performance of Fuel Blends Containing Aromatics. VI—10 Alylkbenzenes. *NACA TN 1994*, 1949.
11. Branstetter, J. Robert: Comparison of the Knock-Limited Performance of Triptane with 23 Other Purified Hydrocarbons. *NACA MR E5E15*, 1945.
12. Jonash, Edmund R., Meyer, Carl L., and Branstetter, J. Robert: Knock-Limited Performance Tests of 2,2,3,4-Tetramethylpentane, 2,3,3,4-Tetramethylpentane, 3,4,4-Trimethyl-2-pentene, and 2,3,4-Trimethyl-2-pentene in Small-Scale and Full-Scale Cylinders. *NACA ARR E6C04*, 1946.
13. Genco, R. S., and Drell, I. L.: Knock-Limited Performance of Several Branched Paraffins and Olefins. *NACA TN 1616*, 1948.
14. Drell, I. L., and Branstetter, J. R.: Knock-Limited Performance of Blends Containing Ethers. *NACA TN 2070*, 1950.
15. Rossini, Frederick K., Pitzer, Kenneth S., Taylor, William J., Ebert, Joan P., Kilpatrick, John E., Beckett, Charles W., Williams, Mary G., and Werner, Helene G.: Selected Values of Properties of Hydrocarbons. Circular C461, NBS, Nov. 1947.
16. Lovell, Wheeler G., and Campbell, John M.: Knocking Characteristics and Molecular Structure of Hydrocarbons. The Science of Petroleum, vol. IV, Oxford Univ. Press (London), 1938, pp. 3004-3023.
17. Sanders, Newell D., Hensley, Reece V., and Breitwieser, Roland: Experimental Studies of the Knock-Limited Blending Characteristics of Aviation Fuels. I—Preliminary Tests in an Air-Cooled Cylinder. *NACA ARR E4I28*, 1944.
18. Wear, Jerrold D., and Sanders, Newell D.: Experimental Studies of the Knock-Limited Blending Characteristics of Aviation Fuels. II—Investigation of Leaded Paraffinic Fuels in an Air-Cooled Cylinder. *NACA TN 1374*, 1947.
19. Drell, I. L., and Wear, J. D.: Experimental Studies of the Knock-Limited Blending Characteristics of Aviation Fuel. III—Aromatics and Cycloparaffins. *NACA TN 1416*, 1947.
20. Hensley, Reece V., and Breitwieser, Roland: Knock-Limited Blending Characteristics of Benzene, Toluene, Mixed Xylenes, and Cumene in an Air-Cooled Cylinder. *NACA MR E5B03*, 1945.
21. Rothrock, A. M., and Biermann, Arnold E.: The Knocking Characteristics of Fuels in Relation to Maximum Permissible Performance of Aircraft Engines. *NACA Rep. 655*, 1939.
22. Taylor, E. S., Leary, W. A., and Diver, J. R.: Effect of Fuel-Air Ratio, Inlet Temperature, and Exhaust Pressure on Detonation. *NACA Rep. 699*, 1940.
23. Evvard, John C., and Branstetter, J. Robert: A Correlation of the Effects of Compression Ratio and Inlet-Air Temperature on the Knock Limits of Aviation Fuels in a CFR Engine—I. *NACA ACR E5D20*, 1945.
24. Alquist, Henry E., O'Dell, Leon, and Evvard, John C.: A Correlation of the Effects of Compression Ratio and Inlet-Air Temperature on the Knock Limits of Aviation Fuels in a CFR Engine—II. *NACA ARR E6E13*, 1946.

CHAPTER VI

AROMATIC AMINES AS FUEL ADDITIVES

In addition to those fuel components that may be classified in the broad category of blending agents, there are other compounds known as fuel additives. These compounds are generally distinguished by their chemical dissimilarity to the constituents normally found in petroleum and by their pronounced effect, when present in even small concentrations, on certain fuel characteristics. An optimum concentration of additive for over-all fuel performance can usually be found that best satisfies all requirements of the fuel; that is, the concentration of additive that will yield maximum improvement in a given fuel characteristic may have a deleterious effect on another equally important characteristic so that a compromise must be made.

By far the most important of the fuel additives are the so-called antiknock *dopes*. Tetraethyl lead (ch. VII), one of the most widely publicized additives in use today, is known primarily for its knock-suppressing qualities. The critical shortages of tetraethyl lead and the high-antiknock blending agents during World War II stimulated the search for other compounds that might be of value as antiknock agents. The NACA participated in this search for new antiknock additives, and a summarization of that survey of the aromatic amines is presented in this chapter.

Although the studies of the NACA placed greatest emphasis on the antiknock qualities of the aromatic amines, other properties were investigated to determine the useful concentrations that could be employed. These properties included low-temperature solubility measurements and determinations of the gasoline-water distribution coefficients. In addition, new methods of analysis were devised to determine the quantities of amines present in prepared fuels. Such analytical methods are necessary for purposes of fuel inspection because the use of additives is controlled by specifications.

ANTIKNOCK EVALUATION OF AROMATIC AMINES

Engines and test conditions.—Two small-scale engines and one full-scale single-cylinder test engine were used in the evaluation of the antiknock characteristics of aromatic amines. One small-scale engine was a CFR engine that conformed to the A. S. T. M. Supercharge method for knock rating except for the fuel system and the method of knock detection. The fuel system was arranged so that fuel was circulated through a primary pump, a fuel cooler, and back into the injection pump gallery. Knock was detected by a magnetostriction pickup unit in conjunction with a cathode-ray oscilloscope. Incipient detonation was taken as the criterion of knock.

As pointed out in chapter II, antiknock behavior at one condition of engine operation does not afford a satisfactory basis for estimation of performance at another condition or in another engine. For this reason, the following three sets of conditions were chosen for the small-scale engine evaluation of the aromatic amines.

	Inlet-air temperature (° F)	Spark advance (° B. T. C.)	Coolant temperature (° F)
A. S. T. M. Supercharge standard conditions	225	45	375
Condition A	250	30	250
Condition B	150	30	250

The engine speed of 1800 rpm and compression ratio of 7.0 were held constant throughout the investigation.

Of these three sets of conditions, the A. S. T. M. Supercharge condition is considered to be the most severe by virtue of the advanced spark and high coolant temperature; condition A is somewhat milder; and condition B is the mildest of the three. Additional runs were made in the second CFR engine, which was equipped to conform to specifications of the A. S. T. M. Aviation method for knock rating.

At each of these conditions, 2-percent (by weight) blends of the aromatic amines were examined with AN-F-28 (28-R) fuel as the base fuel. In order to eliminate reproducibility errors, the straight base fuel and the base fuel containing amine were compared on the same day. The selection of 2 percent amine as the only concentration to be investigated was determined primarily by the quantities of amines available.

The full-scale engine investigation was conducted in an air-cooled aircraft cylinder mounted on a Cooperative Universal Engine (CUE) crankcase. The auxiliary apparatus used in these tests was similar to that described in reference 1 except that a heat exchanger was installed in the cooling-air line to control the cooling-air temperature; the exhaust system was so modified that the engine could be operated either at atmospheric or reduced exhaust pressure.

The cooling-air flow was determined for each run by operating the engine at a brake mean effective pressure of 140 pounds per square inch and a fuel-air ratio of 0.10 and by adjusting the damper valve in the cooling-air line until a rear-spark-plug-bushing temperature of 365° F was reached. The cooling-air pressure drop across the cylinder was maintained constant for each run.

Mixture-response curves were determined at two operating conditions: (1) simulated cruise conditions recommended by the Coordinating Research Council (CRC), which specify an engine speed of 2000 rpm, an inlet-air temperature of 210° F, a spark advance of 20° B. T. C., and atmospheric exhaust pressure; and (2) a modification of these CRC conditions that consisted of an advance spark setting of 30° B. T. C. and a reduced exhaust pressure of 15 inches of mercury absolute. The exhaust pressure of 15 inches of mercury was chosen in view of earlier test results (reference 2) in which a critical relation was shown to exist between manifold and exhaust pressures and knock-limited power in the lean region where the manifold pressure is within 10 and -5 inches

TABLE VI-1.—ANTIKNOCK EFFECTIVENESS OF AROMATIC AMINE ADDITIONS TO AN-F-28 (28-R) FUEL IN SMALL-SCALE (CFR) ENGINE CYLINDER

Aromatic amine (2-percent addition to 28-R fuel)	Relative power	$\frac{\text{imep of aromatic amine plus 28-R}}{\text{imep of 28-R}}$										A. S. T. M. Aviation ratings ^b	
		Fuel-air ratio											
		0.062		0.07		0.09		0.11		Condition			
		Condition	Condition	Condition	Condition	Condition	Condition	Condition	Condition	Condition	Condition		
	A. S. T. M. Supercharge	A	B	A. S. T. M. Supercharge	A	B	A. S. T. M. Supercharge	A	B	A. S. T. M. Supercharge	A	B	
1 Base fuel (28-R)	1.00	1.00	1.00	1.00	1.00	1.00	1.00	1.00	1.00	1.00	1.00	1.00	
2 Aniline	1.00	1.03	1.13	1.07	1.07	1.15	1.03	1.12	1.15	1.09	1.11	1.14	
3 N-Methylaniline	.93	1.11	1.10	.99	1.15	1.13	1.05	1.15	1.11	1.14	1.12	1.10	
4 N-Ethylaniline	.91	1.09	1.04	.97	1.04	1.04	1.04	1.05	1.05	1.01	1.04	1.04	
5 N-Propylaniline	1.03	1.00	1.03	.98	1.06	1.06	.96	1.03	1.04	1.02	1.02	1.06	
6 N-Isopropylaniline	.96	.96	1.01	.95	.95	.99	.96	1.00	1.01	1.01	1.04	1.01	
7 N-Butylaniline	.91	1.00	1.03	.90	.94	1.01	.91	1.00	1.01	1.01	1.01	1.01	
8 N- <i>tert</i> -Butylaniline	.97	1.02	1.01	.84	1.00	1.01	.97	1.00	1.01	1.02	.99	1.02	
9 N,N-Dimethylaniline	-----	.98	1.01	-----	.98	1.00	-----	.98	.99	-----	.99	1.00	
10 N,N-Diethylaniline	-----	1.00	1.01	-----	.98	.98	-----	1.00	.99	1.00	1.03	1.01	
11 o-Toluidine	.88	1.03	1.01	.92	1.03	1.04	.99	1.06	1.10	1.07	1.09	1.15	
12 m-Toluidine	.98	1.15	1.09	.96	1.16	1.09	1.05	1.08	1.10	1.09	1.06	1.11	
13 p-Toluidine	1.03	1.08	1.02	1.06	1.13	1.11	1.09	1.18	1.12	1.11	1.14	1.11	
14 o-Ethylaniline	1.00	1.01	1.04	1.00	1.03	1.01	.92	1.05	1.04	1.00	1.04	1.07	
15 p-Ethylaniline	.97	1.10	1.12	.97	1.13	1.12	1.04	1.12	1.14	1.09	1.13	1.12	
16 o-Isopropylaniline	.92	.99	1.00	.98	1.03	.98	.90	1.01	1.06	.97	1.01	1.05	
17 p-Isopropylaniline	1.00	1.09	1.16	1.00	1.03	1.16	1.02	1.11	1.13	1.11	1.16	1.12	
18 p- <i>tert</i> -Butylaniline	1.06	1.02	1.09	1.03	1.02	1.11	1.08	1.07	1.08	1.11	1.12	1.10	
19 2,4-Xyldidine	.93	1.04	1.13	.92	1.03	1.14	.99	1.12	1.13	1.09	1.12	1.12	
20 2,3-Xyldidine	.98	1.01	1.12	.81	1.07	1.12	.97	1.10	1.09	1.10	1.07	1.11	
21 2,6-Xyldidine	.95	1.04	1.07	1.00	1.08	1.11	1.06	1.10	1.10	1.07	1.15	1.12	
22 2,4-Diethylaniline	.87	.98	1.04	.92	.92	1.04	.93	1.03	1.03	.98	1.06	1.03	
23 2-Methyl-5-isopropylaniline	.86	1.10	1.11	.86	1.00	1.12	.95	1.07	1.12	1.11	1.11	1.12	
24 2,4,6-Trimethylaniline	.88	1.16	1.06	.92	1.07	1.05	.98	1.08	1.08	1.05	1.10	1.11	
25 N-Methyl-o-toluidine	.97	1.07	1.08	.95	1.07	1.07	.95	1.10	1.09	1.02	1.11	1.14	
26 N-Methyl-p-toluidine	.98	1.13	1.16	.91	1.07	1.05	1.20	1.19	1.19	1.18	1.15	1.15	
27 N-Methyl-p-ethylaniline	.97	1.14	1.13	.98	1.18	1.16	1.06	1.14	1.12	1.14	1.15	1.13	
28 N-Methyl-p-isopropylaniline	.95	1.15	1.11	1.05	1.17	1.14	1.08	1.14	1.12	1.15	1.11	1.14	
29 N-Methyl-p- <i>tert</i> -Butylaniline	1.00	1.11	1.12	.91	1.13	1.14	1.02	1.16	1.10	1.14	1.12	1.10	
30 N-Ethyl-p-toluidine	1.00	1.04	1.07	.98	1.06	1.08	.99	1.04	1.07	1.02	1.04	1.08	
31 N-Isopropyl-p-toluidine	.89	.99	1.00	.87	.99	1.00	.88	1.01	1.03	.96	1.02	1.03	
32 N-Isopropyl-p-isopropylaniline	1.00	1.00	1.00	.99	1.02	1.03	1.00	1.01	1.02	1.00	1.08	1.03	
33 N-Methyl-2,4-xyldidine	.98	1.07	1.08	1.00	1.08	1.09	1.00	1.09	1.06	1.04	1.15	1.04	
34 N,N-Dimethyl-1,2-methyl-5-isopropylaniline	.97	.97	1.01	.95	.97	.98	.94	.98	.99	.97	.99	1.00	
35 N,N-Dimethyl-2,4,6-trimethylaniline	.97	1.04	.98	.95	.98	.96	.88	.96	.97	.94	.97	.98	
36 N,N-Dimethyl-p-phenylenediamine	.97	1.12	----	.89	1.13	----	.99	1.18	----	1.16	1.16	----	
37 N,N'-Dimethyl-p-phenylenediamine	1.15	1.15	----	1.11	1.13	1.19	1.22	1.17	1.19	1.16	1.17	1.14	
38 N,N-Diethyl-p-phenylenediamine	.98	1.11	1.10	.89	1.11	1.19	1.10	1.17	1.19	1.16	1.17	1.14	
39 Diphenylamine	1.10	1.11	1.10	1.07	1.08	1.08	1.09	1.10	1.11	1.11	1.15	1.10	
40 Methyl diphenylamine	1.00	1.06	1.16	1.10	1.01	1.04	1.04	1.01	1.00	1.01	1.01	1.07	
41 o-Methoxyaniline	.76	1.00	1.00	.74	.91	1.01	.80	1.01	1.03	.99	1.03	1.04	

^a Data from references 2 to 6.^b Performance numbers.

c 1.76 percent amine added.

mercury of the exhaust pressure. The spark advance of 30° B. T. C. was chosen because of the interest in aircraft-engine operation at advanced spark under cruise conditions.

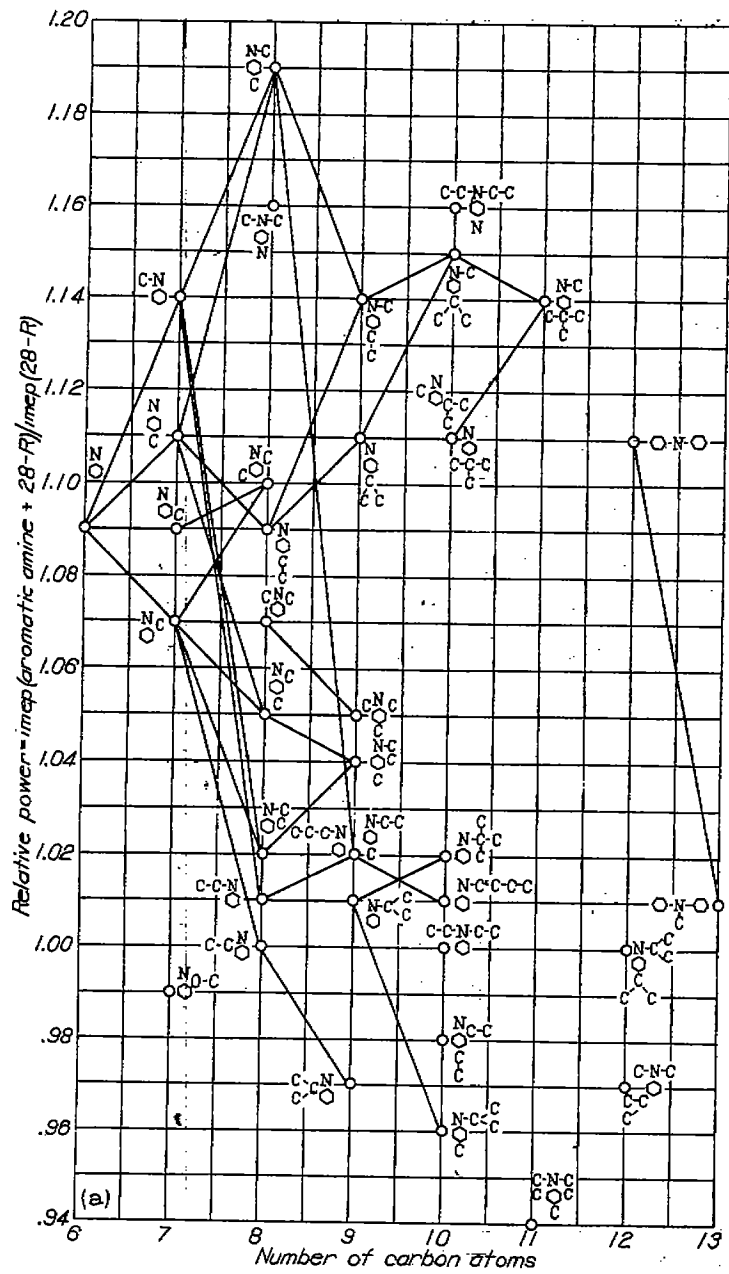
In the full-scale engine studies, 2-percent (by weight) amine blends with AN-F-28 fuel were also used.

Knock-limited performance.—In order to present the most reliable comparison of the many amines examined, the antiknock ratings of all blends are expressed as power ratios (references 3 to 7). The small-scale engine results shown in table VI-1 (except for A. S. T. M. Aviation results) are therefore expressed as the quotient of the knock-limited indicated mean effective pressure (imep) of the amine blend divided by the knock-limited indicated mean effective pressure of the base fuel (AN-F-28). By this method the

influence of day-to-day variations in engine reproducibility is reduced to a minimum because each blend was examined on the same day as the base fuel.

The data from table VI-1 have been plotted in figure VI-1 to illustrate the relations that exist between antiknock effectiveness and molecular structure. Because the A. S. T. M. Supercharge method is a rich-mixture rating method, only the data at a fuel-air ratio of 0.11 have been considered in this analysis.

Fuel sensitivity (ch. II) is an obstacle to the development of any rigid generalizations between chemical structure and performance. For example, in figure VI-1 (a) at A. S. T. M. Supercharge conditions, it is seen that 15 aromatic amines have antiknock values equal to or greater than aniline. At condition A (fig. VI-1 (b)), 17 aromatic amines are equal to

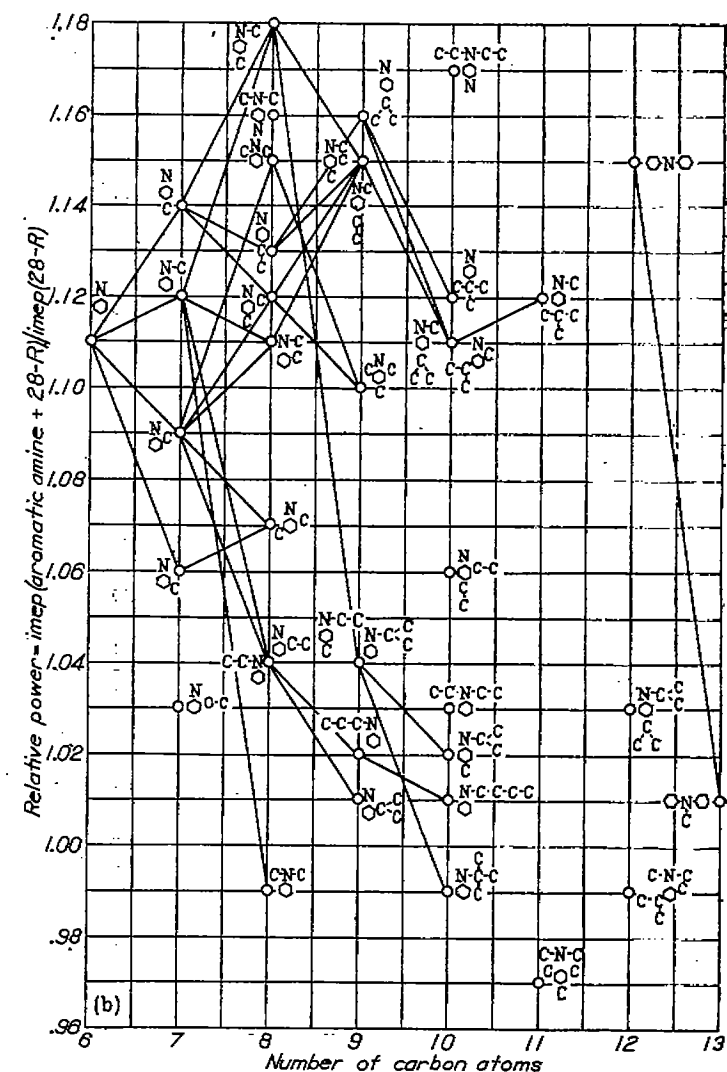


(a) A. S. T. M. Supercharge standard conditions.

FIGURE VI-1.—Antiknock effectiveness of 2-percent aromatic amine blends with AN-F-28 (28-R) fuel. Fuel-air ratio, 0.11.

or greater than aniline, but at condition B (fig. VI-1 (c)), only 5 compounds are equal to or greater than aniline. Purely from consideration of nominal engine operating conditions it will be recalled that the A. S. T. M. Supercharge condition is probably the most severe, with condition B the mildest, and condition A intermediate. It is obvious, then, that some risk is involved in a statement that any single amine is always better than aniline. In fact, N-methyl-*p*-toluidine is the only compound that did exceed aniline in antiknock value at all three conditions, and at condition B the margin of superiority was, for all practical purposes, negligible.

On the basis of the data contained in figures VI-1, however, two generalizations can be made with regard to

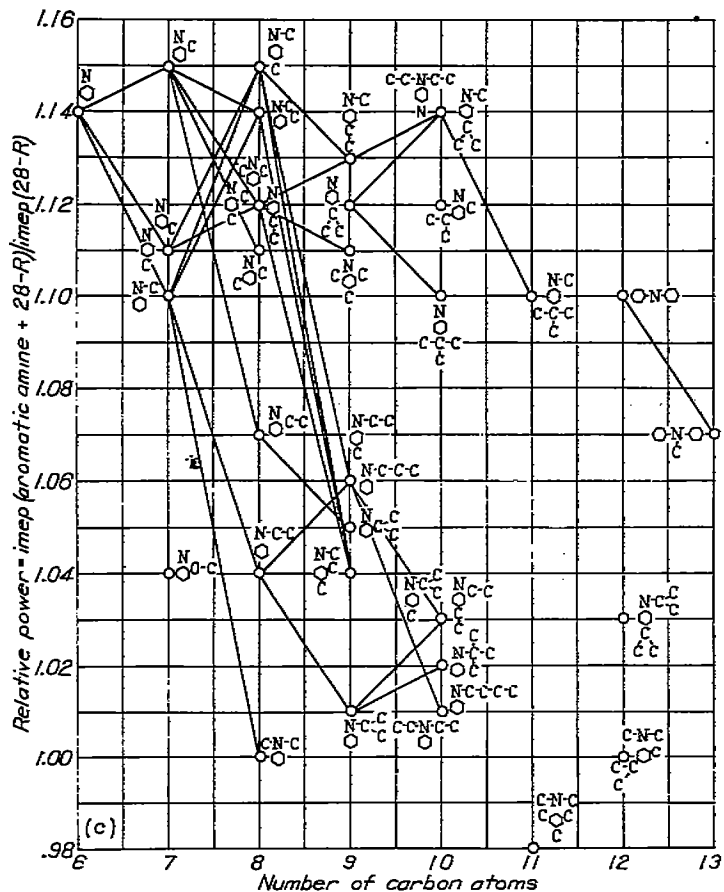


(b) A. S. T. M. Supercharge modified A conditions.

FIGURE VI-1.—Continued. Antiknock effectiveness of 2-percent aromatic amine blends with AN-F-28 (28-R) fuel. Fuel-air ratio, 0.11.

structural trends. The first of these is as follows: When one hydrogen atom in the $-NH_2$ group of any given primary aromatic amine is replaced by an alkyl group, the greatest increase or least decrease in antiknock value from that of the primary amine will result when the alkyl substituent is a methyl radical ($-CH_3$). This statement is supported by the following data:

Aromatic amine	Relative Power		
	A. S. T. M. Supercharge	Condition A	Condition B
Aniline			
N-Methylaniline	1.09	1.11	1.14
N-Ethylaniline	1.14	1.19	1.10
N-Propylaniline	1.01	1.04	1.04
N-Butylaniline	1.02	1.02	1.06
N-Isopropylaniline	1.01	1.01	1.01
N- <i>tert</i> -Butylaniline	1.02	1.04	1.01
<i>p</i> -Toluidine			
N-Methyl- <i>p</i> -toluidine	1.11	1.14	1.11
N-Ethyl- <i>p</i> -toluidine	1.19	1.19	1.15
N-Isopropyl- <i>p</i> -toluidine	1.02	1.04	1.06
<i>p</i> -Isopropylaniline			
N-Methyl- <i>p</i> -isopropylaniline	1.11	1.16	1.12
N-Isopropyl- <i>p</i> -isopropylaniline	1.15	1.11	1.14
	1.00	1.08	1.03



(c) A. S. T. M. Supercharge modified B conditions.

FIGURE VI-1.—Concluded. Antiknock effectiveness of 2-percent aromatic amine blends with AN-F-28 (28-R) fuel. Fuel-air ratio, 0.11.

For each of these three series of compounds, the antiknock values of the three primary amines considered as bases (aniline, *p*-toluidine, and *p*-isopropylaniline) were increased more by the substitution of a methyl radical for one of the hydrogen atoms attached to the nitrogen than by substitution of any other radical. For the two cases where the performance decreased (*N*-methylaniline at condition B and *N*-methyl-*p*-isopropylaniline at condition A), the decrease in performance was less with the methyl radical than with any of the other radicals examined.

The influence of replacing a hydrogen atom attached to the nitrogen with an aromatic radical was investigated for only one compound; however, in this one case the aromatic radical appeared approximately equal in effectiveness to a methyl radical, as shown by the following table:

Aromatic amine	Relative Power		
	A. S. T. M. Supercharge	Condition A	Condition B
Aniline	1.09	1.11	1.14
<i>N</i> -Methylaniline	1.14	1.12	1.10
Diphenylamine	1.11	1.15	1.10

The second generalization of the data can be made with reference to hydrogen substitutions on the aromatic ring: *The addition of an alkyl radical to the aromatic ring of an aromatic amine is more effective insofar as antiknock value is concerned when the addition is made in the para position rather*

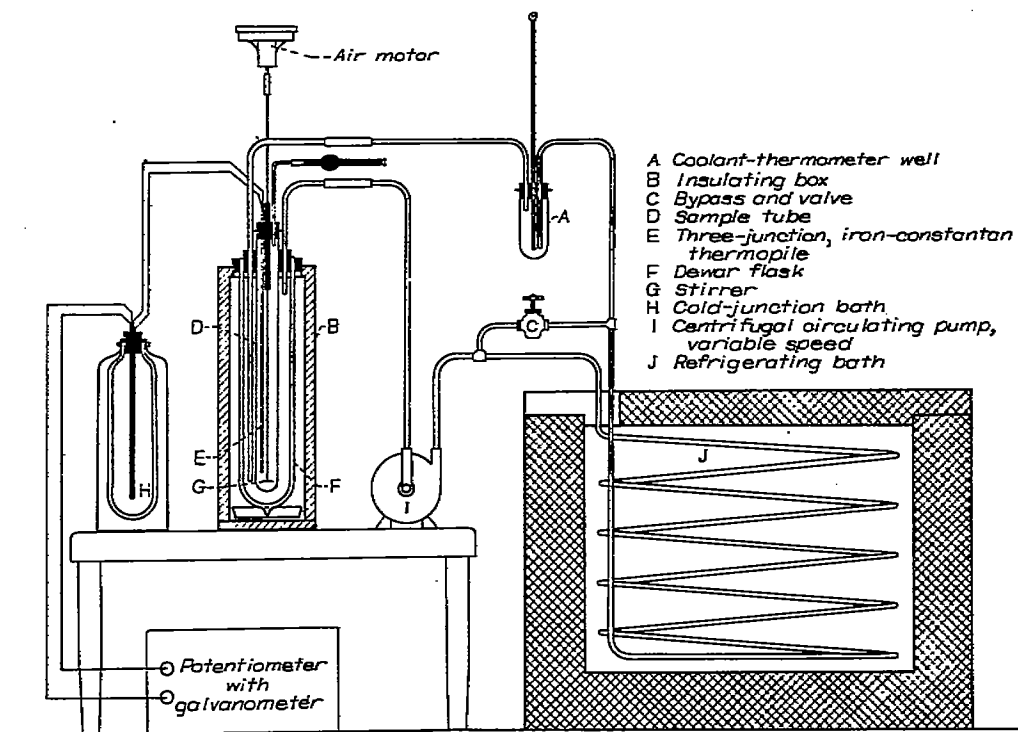


FIGURE VI-2.—Apparatus for determination of cloud point. (Fig. 1 of reference 9.)

TABLE VI-2.—ANTIKNOCK EFFECTIVENESS OF AROMATIC-AMINE ADDITIONS TO AN-F-28 (28-R) FUEL IN A FULL-SCALE AIR-COOLED AIRCRAFT ENGINE CYLINDER

For each compound there are two rows of values. The first row is imep, lb/sq in.; the second is imep ratio, which is the ratio of the imep of 98 percent 28-R fuel plus 2 percent aromatic amine to the imep of 28-R.

Aromatic amine (2-percent addition to 28-R)	Relative power (engine speed, 2000 rpm; inlet-air temperature, 210° F; compression ratio, 7.3)									
	Spark advance, 20° B. T. C.; exhaust pressure, 20±0.5 in. Hg abs.					Spark advance, 30° B. T. C.; exhaust pressure, 15 in. Hg abs.				
	Fuel-air ratio					Fuel-air ratio				
	0.065	0.07	0.08	0.09	0.10	0.065	0.07	0.08	0.09	0.10
Base fuel (28-R)	141 1.00	155 1.00	209 1.00	235 1.00	253 1.00	166 1.00	179 1.00	203 1.00	226 1.00	236 1.00
N-Methylxylidines (mixed isomers)	164 1.16	163 1.26	222 1.06	236 1.06	233 1.12	173 1.04	184 1.03	209 1.03	232 1.03	249 1.06
N-Methylcumidines (mixed isomers)	195 1.38	208 1.34	245 1.17	272 1.16	290 1.18	182 1.10	194 1.08	220 1.08	245 1.08	259 1.10
N-Methyltoluidines (75 percent <i>p</i> , 25 percent <i>o</i>)	195 1.38	216 1.30	244 1.17	275 1.17	288 1.14	178 1.07	187 1.05	204 1.01	239 1.06	260 1.10
Xylidines (mixed isomers)	172 1.22	192 1.24	230 1.10	257 1.09	280 1.11	173 1.04	184 1.03	214 1.05	237 1.05	257 1.09
Cumidines (from refinery cumene—mixed isomers)	184 1.30	200 1.29	237 1.13	267 1.09	282 1.11	173 1.04	188 1.05	215 1.06	232 1.03	260 1.06
N-Methylaniline	192 1.36	210 1.36	240 1.15	269 1.14	290 1.15	181 1.09	190 1.06	218 1.07	240 1.06	262 1.11

* Reference 8.

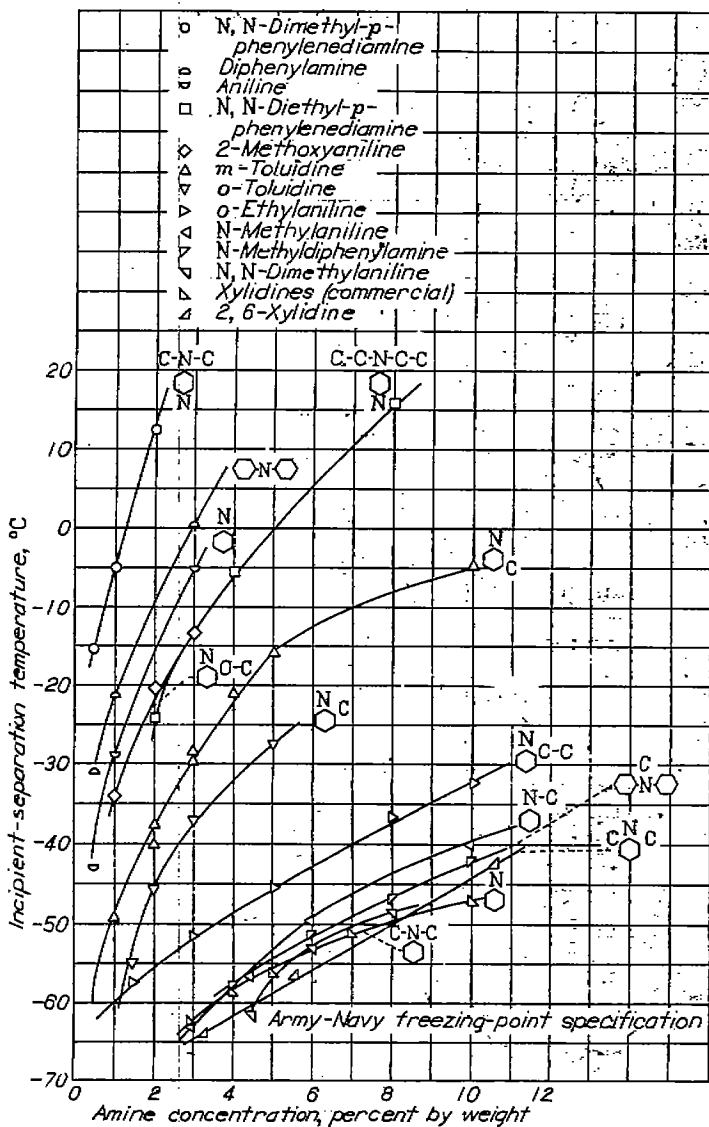


FIGURE VI-3.—Solubility of aromatic amines in grade .65 base stock with aromatic hydrocarbons extracted. (Fig. 2 of reference 9.)

than in the *ortho* or *meta* positions. This statement is based on the following data:

Aromatic amine	Relative Power		
	A. S. T. M. Supercharge	Condition A	Condition B
Aniline	1.09	1.11	1.14
<i>o</i> -Toluidine	1.07	1.09	1.15
<i>m</i> -Toluidine	1.09	1.08	1.11
<i>p</i> -Toluidine	1.11	1.14	1.11
N-Methylaniline	1.14	1.12	1.10
<i>N</i> -Methyl- <i>o</i> -toluidine	1.02	1.11	1.14
<i>N</i> -Methyl- <i>p</i> -toluidine	1.18	1.18	1.15
Aniline	1.09	1.11	1.14
<i>o</i> -Ethylaniline	1.00	1.04	1.07
<i>p</i> -Ethylaniline	1.08	1.13	1.12
Aniline	1.09	1.11	1.14
<i>o</i> -Isopropylaniline	1.07	1.01	1.05
<i>p</i> -Isopropylaniline	1.11	1.16	1.12

The small number of A. S. T. M. Aviation ratings (table VI-1) does not justify inclusion as supporting data for the foregoing generalizations. It is interesting to note, however, that the addition of diphenylamine improved the performance of the base fuel by 15 performance numbers more than any of the other aromatic amines for which A. S. T. M. Aviation ratings were obtained.

One additional observation to be made from the data of table VI-1 concerns the replacement by alkyl radicals of both hydrogen atoms attached to the nitrogen, that is,



As shown by the following comparisons, the replacement of one hydrogen atom by an alkyl radical is more effective for maintaining or improving the antiknock value of the starting compound than replacement of both hydrogen atoms:

Aromatic amine	Relative Power		
	A. S. T. M. Supercharge	Condition A	Condition B
Aniline	1.09	1.11	1.14
N-Methylaniline	1.14	1.12	1.10
N,N-Dimethylaniline	—	.99	1.00
Aniline	1.09	1.11	1.14
N-Ethylaniline	1.01	1.04	1.04
N,N-Diethylaniline	1.00	1.03	1.01

Suitable quantities of the pure aromatic amines used in the small-scale engine studies were not available for the full-scale engine investigation (reference 8); therefore, a few isomeric mixtures were examined. The results of these tests are presented in table VI-2.

The data show that all the aromatic amines increased the knock-limited performance of the base fuel at both full-scale engine conditions throughout the fuel-air ratio range. At both sets of engine conditions and lean and rich fuel-air ratios, the blends of N-methylecumidines, N-methyltoluidines, and N-methylaniline were about equal in knock-limited performance, and all three were superior to the other blends tested.

When the severity of the test conditions was changed by advancing the spark and reducing the exhaust pressure, contrary effects were noted for the several blends. In every case the rich-mixture (fuel-air ratio, 0.10) knock-limited performance of the several fuels was decreased by the change of conditions. The lean-mixture (fuel-air ratio, 0.065) performance of 28-R fuel and the blend containing N-methyl-xylidines was increased, whereas the blend containing xylidines remained about the same. The percentage improvement in the knock-limited performance of the base fuel resulting from addition of the amines was less at the condition of advanced spark and reduced exhaust pressure than at the other condition.

PHYSICAL PROPERTIES OF AROMATIC AMINES

Of the physical properties examined in the NACA investigation of aromatic amines, low-temperature solubility and gasoline-water distribution coefficients received the greatest attention. The low-temperature solubility characteristics are of primary importance because of specification requirements that the additives must remain in solution at the lowest temperatures encountered in service. Current fuel specifications limit the freezing point to a maximum of -76°F (-60°C). Gasoline-water distribution coefficients are of interest because of the wide usage of water-distribution storage systems. In such systems the additive may be extracted from the fuel by diffusion when fuel and water are in intimate contact.

Physical properties, other than low-temperature solubility and gasoline-water distribution coefficients, were determined for the amines examined and are presented in table VI-3.

Low-temperature solubility.—Solubilities of 42 aromatic amines in blends with gasoline were measured at temperatures as low as -85°F (-65°C) and at concentrations as high as 10 percent by weight (reference 9). The solubilities of aromatic amines are appreciably affected by the compo-

TABLE VI-3.—PHYSICAL PROPERTIES OF AROMATIC AMINES *

Aromatic amine	Boiling range ^b ($^{\circ}\text{C}$)	Index of refraction ^c n_D^{20}	Density (grams/ml)
Aniline	184-184.5	1.5853	1.0220
N-Methylaniline	195-196	1.5704	.9850
N-Ethylaniline	203-204	1.5638	.9807
N-Propylaniline	220.5-223.5	1.5425	.9438
N-Butylaniline	240.0-240.5	1.5339	.9323
N-Isopropylaniline	206.5-209	1.5404	.9374
N- <i>tert</i> -Butylaniline	95 at 16 mm	1.5270	.9244
N,N-Dimethylaniline	192.5-193.5	1.5580	.9564
N,N-Diethylaniline	215-217	1.5418	.9347
<i>o</i> -Toluidine	198.5-201.5	1.5718	.9859
<i>m</i> -Toluidine	202.5-203.5	1.5674	.9893
<i>p</i> -Toluidine	204.5-214.4	1.5570	.9610
N-Methyl- <i>p</i> -toluidine	209-211	1.5646	.9763
N-Methyl- <i>o</i> -toluidine	206.5-207.5	1.5600	.9608
N-Methyltoluidines (80 percent <i>p</i> , 40 percent <i>o</i>)	208.5-215	1.5590	.9638
N-Methyltoluidines (80 percent <i>p</i> , 20 percent <i>o</i>)	210-213	1.5590	.9638
N-Ethyl- <i>p</i> -toluidine	217-220	1.5439	.9441
N-Isopropyl- <i>p</i> -toluidine	222-223	1.5319	.9238
<i>o</i> -Ethylaniline	211	1.5602	.9610
<i>p</i> -Ethylaniline	216	1.5547	.9672
N-Methyl- <i>p</i> -ethylaniline	227.5	1.5455	.9455
N-Methyl- <i>o</i> -ethylaniline, mixed isomers (from chloroethylenes)	222.5-230.5	1.5493	.9503
<i>p</i> - <i>tert</i> -Butylaniline	96.5-98.0 at 5-6 mm	1.5888	.9446
<i>o</i> -Isopropylaniline	219-220	1.5434	.9643
<i>p</i> -Isopropylaniline	225.5-226.5	1.5432	.9514
N-Methyl- <i>p</i> -isopropylaniline	240	1.5390	.9347
N-Isopropyl- <i>p</i> -isopropylaniline	246-247	1.5209	.9075
2,4,5-Trimethylaniline	110.0 at 15 mm	1.5502	.9615
Cumidines (from synthetic cumenes)	225-226	1.5448	.9535
Cumidines (from refinery cumenes)	220-241	1.5434	.9531
N-Methylcumidines (from bromocumenes)	237.5-241.5	1.5390	.9366
N-Methyl- <i>p</i> - <i>tert</i> -butylaniline	245.5-249.5	1.5348	.9305
<i>o</i> -Methoxyaniline	224-225	1.5760	1.0631
Xyliidines (commercial)	216-219.5	1.5601	.9771
2,4-Xyliidine	216.0-216.5	1.5591	.9751
2,5-Xyliidine	216	1.5596	.9755
N-Methyl-2,4-xylidine	221-222	1.5542	.9532
N-Methylxyliidines (from bromoxylenes)	220-227	1.5540	.9585
2,4-Diethylaniline	241-242	1.5433	.9511
2-Methyl-3-isopropylaniline	240-242	1.5408	.9435
N,N-Dimethyl-2-methyl-4-isopropylaniline	84 at 5 mm	1.5124	.9028
N,N-Dimethyl-2,4,6-trimethylaniline	213.5	1.5116	.9066
Pseudocumidine (technical)	226-241	1.5538	.9720
Diphenylamine	52.0-53.5	—	—
<i>o</i> -Phenylenediamine	140.0-142.0	—	—
N-Methyl- <i>p</i> -phenylenediamine	121 at 5 mm	1.621	—
N,N-Dimethyl- <i>p</i> -phenylenediamine	108-111 at 4-6 mm	—	—
N,N-Dimethyl- <i>p</i> -phenylenediamine	117 at 2.5 mm	—	—
N,N-Dimethyl- <i>p</i> -phenylenediamine	117 at 1 mm	—	—
N-Methyldiphenylamine	295-296	1.6224	1.0527

* Table I of reference 9.

^b Boiling range at 760 mm Hg except where noted.

^c Melting point measured for this solid rather than boiling range.

sition of gasoline to which the addition is made; therefore, three different base gasolines were used:

1. Grade 65 gasoline from which aromatic hydrocarbons were successively extracted with 10-percent fuming sulfuric acid and silica gel.

2. Extracted grade 65 gasoline to which was added 15 percent by volume of an aromatic mixture of 5 parts xylene, 2 parts cumene, and 1 part toluene.

3. Different batches of typical current aviation gasoline, AN-F-28 (Amendment 2) fuel containing 12 to 20 percent aromatic hydrocarbons by volume.

The apparatus for determination of low-temperature solubilities of the amines is shown in figure VI-2. Briefly, the procedure used in reference 9 to determine the solubility consisted in slowly cooling and stirring the gasoline-amine sample in the sample tube until the amine separated as a cloud from the gasoline; the temperature at which the cloud formed was recorded. The sample was then slowly warmed until the amine went into solution and the cloud disappeared; the temperature was again recorded. These two temperatures were averaged to give the incipient-separation temperature or cloud point. Cloud points were reproducible to within $\pm 1.5^{\circ}\text{C}$.

TABLE VI-4.—SOLUBILITY OF AROMATIC AMINES
IN THREE AVIATION FUELS AT -60°C *

[Percentages by weight]

Aromatic amine	Aromatic-free grade 65	Aromatic-free grade 65 plus 15 percent by volume aromatics	AN-F-28
Aniline	<0.5	0.5	>10
N-Methylaniline	3.6	12 (-62°C)	>10
N-Ethylaniline	>10	>10	>10
N-Propylaniline	>10	>10	>10
N-Isopropylaniline	>10	>10	>10
N-tert-Butylaniline	>10	>10	>10
N,N-Dimethylaniline	4.7	9.8	8.3
N,N-Diethylaniline	>10	>10	>10
<i>o</i> -Toluidine	1.3	4.2	4.4
<i>m</i> -Toluidine	<0.5	2.6	3.6
N-Methyl- <i>p</i> -toluidine	>10	>10	>10
N-Methyl- <i>o</i> -toluidine	>10	>10	>10
N-Methyltoluidines (from chlorotoluenes)	>10	>10	>10
N-Ethyl- <i>p</i> -toluidine	>10	>10	>10
N-Isopropyl- <i>p</i> -toluidine	>10	>10	>10
<i>o</i> -Ethylaniline	0.9	>10	>10
N-Methyl- <i>p</i> -ethylaniline	>10	>10	>10
N-Methylethylaniline, mixed isomers (from chloroethylbenzenes)	>10	>10	>10
<i>o</i> -Isopropylaniline	>10	>10	>10
N-Methyl- <i>p</i> -isopropylaniline	>10	>10	>10
N-Isopropyl- <i>p</i> -isopropylaniline	>10	>10	>10
Cumidines (from synthetic cumenes)	>10	>10	>10
Cumidines (from refinery cumenes)	>10	>10	>10
N-Methylecumidines (from bromocumenes)	>10	>10	>10
N-Methyl- <i>p</i> -tert-butylaniline	>10	>10	>10
2-Methoxyaniline	<0.5	<0.5	>10
Xylylne (commercial) (reference 10)	3.7	10	>10
2,6-Xylylne	4.6	11.1	9.1
N-Methyl-2,4-xylylne	>10	>10	>10
2,4-Diethylaniline	>10	>10	>10
2-Methyl-5-isopropylaniline	>10	>10	>10
N,N-Dimethyl-2-methyl-5-isopropylaniline	>10	>10	>10
N,N-Dimethyl-2,4,6-trimethylaniline	>10	>10	>10
Pseudocumidine (technical)	>10	>10	>10
Diphenylamine	<0.5	<0.5	>10
p-Phenylenediamine	<0.5	<0.5	>10
N-Methyl- <i>p</i> -Phenylenediamine	<0.5	<0.5	>10
N,N-Dimethyl- <i>p</i> -Phenylenediamine	<0.5	<0.5	>10
N,N-Diethyl- <i>p</i> -Phenylenediamine	<0.5	<0.5	>10
N,N-Dimethyl- <i>p</i> -Phenylenediamine	<0.5	<0.5	>10
N-Methyldiphenylamine	3.3	>10	>10

* Table II of reference 9.

* Aromatic mixture consisted of five parts xylene, two parts cumene, and one part toluene.

* Solubility at room temperature.

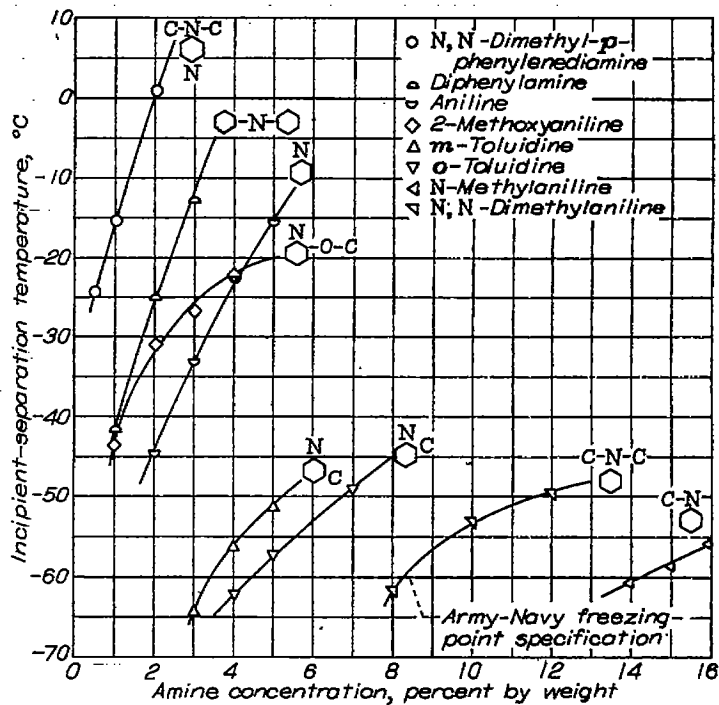


FIGURE VI-3.—Solubility of aromatic amines in AN-F-28, Amendment-2, fuel. (Fig. 4 of reference 9.)

The solubilities of the amines in the aromatic-free gasoline, in the gasoline of 15-percent aromatic content, and in the AN-F-28 fuel are presented in figures VI-3, VI-4, and VI-5, respectively. The amines that were soluble to at least 10 percent by weight at -76°F (-60°C) in each of the gasolines are

- N-Ethylaniline
- N-Propylaniline
- N-Isopropylaniline
- N-tert-Butylaniline
- N,N-Diethylaniline
- N-Methyl-*p*-toluidine
- N-Methyl-*o*-toluidine
- N-Methyltoluidines (from chlorotoluenes)
- N-Ethyl-*p*-toluidine
- N-Isopropyl-*p*-toluidine
- N-Methyl-*p*-ethylaniline
- N-Methylethylaniline, mixed isomers (from chloroethylbenzenes)
- o*-Isopropylaniline
- p*-Isopropylaniline
- N-Methyl-*p*-isopropylaniline
- N-Isopropyl-*p*-isopropylaniline
- Cumidines (from synthetic cumenes)
- Cumidines (from refinery cumenes)
- N-Methylecumidines (from bromocumenes)
- N-Methyl-*p*-tert-butylaniline
- N-Methyl-2,4-xylylne
- N-Methylxylylne (from bromoxylenes)
- 2,4-Diethylaniline
- 2-Methyl-5-isopropylaniline
- N,N-Dimethyl-2-methyl-5-isopropylaniline
- N,N-Diethyl-2,4,6-trimethylaniline
- Pseudocumidine (technical)

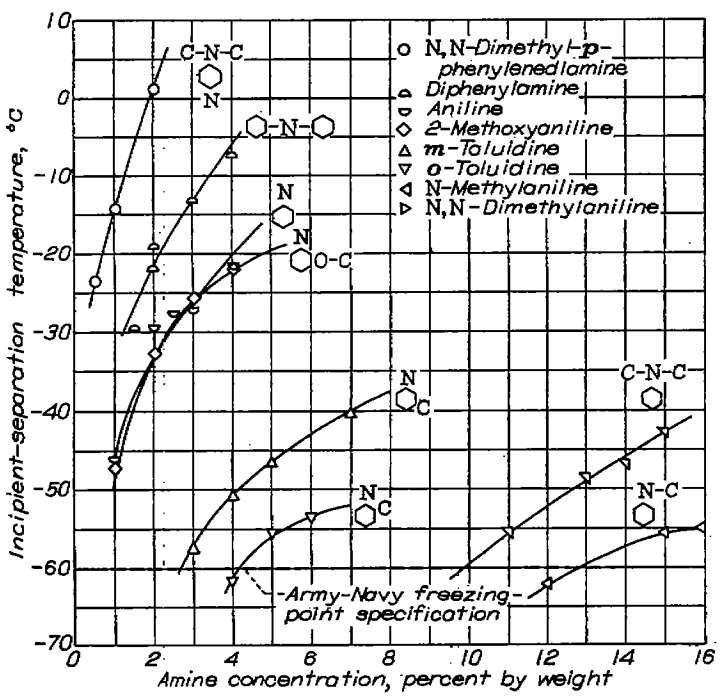


FIGURE VI-4.—Solubility of aromatic amines in blend of 85 percent extracted grade 65 base stock and 15 percent (by volume) of aromatic mixture consisting of 5 parts xylene, 2 parts cumene, and 1 part toluene. (Fig. 3 of reference 9.)

At room temperature, N-methyl-*p*-phenylenediamine and *p*-phenylenediamine were less than 0.5 percent (by weight) soluble in the test gasoline; no additional solubility data were taken for these compounds. At room temperature, N,N'-dimethyl-*p*-phenylenediamine was soluble to the extent of 1 to 2 percent by weight but was too unstable to permit accurate measurement of solubility by the method employed. N,N-Diethyl-*p*-phenylenediamine was tested only in the aromatic-free gasoline.

When figures VI-3 and VI-4 are compared, it is seen that composition of the base fuel greatly influenced the solubilities of the amines. The addition of 15 percent aromatics to the aromatic-free gasoline approximately doubled or tripled the amine solubility. Solubilities in AN-F-28 fuel (fig. VI-5) were about the same as those in the gasoline containing 15 percent aromatics. Representative samples of AN-F-28 fuel contained 12 to 20 percent (by volume) aromatics.

A summary of the solubilities of the amines at -76° F (-60° C) in the different test gasolines is presented in table VI-4. The results were obtained by interpolating or extrapolating the experimental data. The data obtained for commercial xylidines (reference 10) are included for comparison.

The solubility of an aromatic amine in the aromatic-free gasoline at -76° F (-60° C) may be taken as an indication of the maximum concentration in which the amine could be added to current aviation fuels on the basis of solubility alone. The aromatic hydrocarbons present in most of the wartime aviation fuels provided a margin of safety in preventing this concentration of amine from separating at -76° F (-60° C).

Gasoline-water distribution coefficients.—If a fuel containing an additive such as an aromatic amine is stored in contact with water for an extended period of time, a certain amount of the additive will be extracted by the water. An analysis of a fuel-storage system in which this extraction might occur was made by Olson and Tischler (reference 11) in order to develop an expression from which the loss of amine to water could be approximated. Storage systems of this type have been variously termed "overwater storage systems, water-displacement storage systems, and aqua storage systems."

As pointed out in reference 11, it is unlikely that a single expression can be written for use under all conditions encountered in practice, but certain assumptions permit a mathematical derivation of an equation that covers a wide range of situations. In the operation of a tank utilizing the water-displacement principle, fuel is removed from the tank by adding water at the bottom of the tank. Fuel is added to the tank by removal of storage water from the tank. Two phases, one of gasoline and one of water, exist in the tank, which is full of liquid at all times.

The following assumptions are made in reference 11 in determining the expressions for concentration of additive in fuel stored over water at any volume of fuel:

1. When equilibrium conditions are reached, the distribution law applies to the additive; namely, the ratio between the concentrations of the additive in the two phases of the gasoline-water system is constant at constant temperature.

The ratio is described as the distribution coefficient and defined as

$$K = \frac{\text{additive concentration in gasoline phase}}{\text{additive concentration in water phase}}$$

This constant must be experimentally determined for each additive. It varies with temperature of the fuel and water and with the nature of the fuel. Any variation in the distribution coefficient caused by additive concentration may be assumed negligible in the range of concentrations produced by the distribution process.

2. The volume of the additive itself, when present to the extent of 2 or 3 percent or less, is negligible by comparison with the volumes of gasoline and water. The equilibrium concentration is the minimum concentration of additive in the fuel at the volume in question.

The following symbols are used in the analysis of reference 11:

<i>K</i>	gasoline-water distribution coefficient (experimentally determined)
<i>X</i>	concentration of additive in gasoline before addition or removal of portion of fuel
<i>X'</i>	concentration of additive in gasoline after addition or removal of portion of fuel (at equilibrium)
<i>V</i>	volume of storage tank
<i>V_g</i>	volume of fuel in tank before addition or removal of portion of fuel
<i>V_{g'}</i>	volume of fuel in tank after addition or removal of portion of fuel
<i>V_w</i>	volume of water in tank before addition or removal of portion of fuel
<i>V_{w'}</i>	volume of water in tank after addition or removal of portion of fuel
<i>V_f</i>	volume of fuel added or withdrawn ($V_f = V_{g'} - V_g$)
<i>Y</i>	concentration of additive in water added or withdrawn
<i>Z</i>	concentration of additive in fuel added or withdrawn

Because the manner in which an overwater-storage system is operated is one of the most important variables influencing the additive concentration in the stored fuel, two cases representing two very different operating procedures have been studied:

Case 1.—The first case applies to successive additions or withdrawals of fuel stored in contact with water when an appreciable period of time has elapsed between each addition or withdrawal.

In order to approximate this situation it is assumed that during the actual addition or withdrawal of fuel, no additive is transferred between the gasoline and water phases but that equilibrium distribution of additive between the two phases is attained during the period between successive additions or withdrawals of fuel. This assumption is based on the slowness of the rate of diffusion of additive between the two phases. The following equation will agree more closely with the actual situation the longer the period between additions or withdrawals of fuel:

$$(XV_f + ZV_f) + \left(\frac{XV_g}{K} - YV_f \right) = X'(V_g + V_f) + \frac{X'}{K}(V_w - V_f) \quad (1)$$

This equation may be expressed in words as follows:

(Quantity of additive in gasoline after addition or withdrawal of fuel but before equilibrium) + (quantity of additive in water after addition or withdrawal of fuel but before equilibrium) = (quantity of additive in gasoline after equilibrium) + (quantity of additive in water after equilibrium).

Expanding and collecting terms gives

$$X' = \frac{KXV_s + KZV_f + X V_w - KYV_f}{KV_s + KV_f + V_w - V_f} \quad (2)$$

If fuel is displaced from the tank by fresh water, $Z = X$, $Y = 0$, $V_s' = V_s + V_f$ and $V_w' = V_w - V_f$. Then

$$X' = X \left(\frac{V_w + KV_s'}{V_w' + KV_s'} \right) \quad (3)$$

Case 2.—The second case applies to successive small withdrawals of fuel over an appreciable length of time. For this approximation, equilibrium distribution of additive is assumed to exist between gasoline and water at all times. An equation of this sort permits evaluation of additive concentration under circumstances where withdrawals of fuel have been small, compared with the tank capacity, but very numerous. Equation (4) may thus be considered as the result of applying the equations of case 1 to an infinite number of steps, with equilibrium established between each step.

Let $\Delta X = X' - X$, $\Delta V_s = V_s' - V_s$, and $\Delta V_w = V_w' - V_w$

Then,

$$X' V_s' + \frac{X' V_w'}{K} = X' - \Delta Y (V_s' - \Delta V_s) + \left(\frac{X' - \Delta X}{K} \right) (V_w' - \Delta V_w) + (X' - \Delta X) \Delta V_s \quad (4)$$

or, in words,

(Quantity of additive in fuel stored over water) + (quantity of additive in water) = (quantity of additive in stored fuel before removal of small increment) + (quantity of additive in water before addition of increment of fresh water) + (quantity of additive removed in small increment of fuel).

By removing second-order differentials, equation (4) can be expanded and simplified:

$$-X' \Delta V_w = (KV_s' + V_w') \Delta X \quad (5)$$

But $-\Delta V_w = \Delta V_s$ and $V_w' = V - V_s'$; therefore,

$$\frac{\Delta X}{X'} = \frac{\Delta V_s}{V_s'(K-1) + V} \quad (6)$$

By integration from any concentration X and volume V_s to X' and V_s' ,

$$X' = X \left[\frac{V_s'(K-1) + V}{V_s(K-1) + V} \right]^{\frac{1}{K-1}} \quad (7)$$

TABLE VI-5.—STORAGE-SYSTEM INVESTIGATION

Sample taken	May 27	June 7	June 19	July 3	July 13 1943
Fuel in tank before removal of batch, gal.	8105	8105	6105	2105	1105
Water in tank before removal of batch, gal.	16,895	16,895	16,895	22,895	23,895
Fuel removed, gal.		2000	4000	1000	1105
(Fuel placed in storage system)					
Xyldines, grams/100 ml (electrometrically)	1.05 .98	(*)	{ 0.94 .826 .826 } .82	0.825 .83	0.815 .82 (*)
Mean 1.01	0.900	0.896	0.825	0.806	
Equilibrium concentration, X' (equation (2))					

* Analysis indicated under each date is prior to removal from the storage tank of the quantity of fuel indicated under that date.

^b Sample was inadvertently mixed with some xyldine-free fuel.

^c The fuel stored over water gave a negligible decrease in knock rating when compared with the original batch of fuel.

^d Sample calculation for run on June 7: Because the tank contained no fuel prior to the addition of the 8105 gallons on May 27, $V_s = 0$, $X = 0$, and $Y = 0$; therefore, from equation (2)

$$X' = \frac{(17)(1.01)(8105)}{(17)(8105) + 25,000 - 8105}$$

= 0.900 (equilibrium concentration attained on standing).

^e Sample calculation for run on June 19: In this case, $Z = X$ and $Y = 0$. Equation (2) therefore becomes equation (3) and

$$X' = 0.900 \left(\frac{(16,895 + (17)(6105))}{(16,895 + (17)(6105))} \right) = 0.886$$

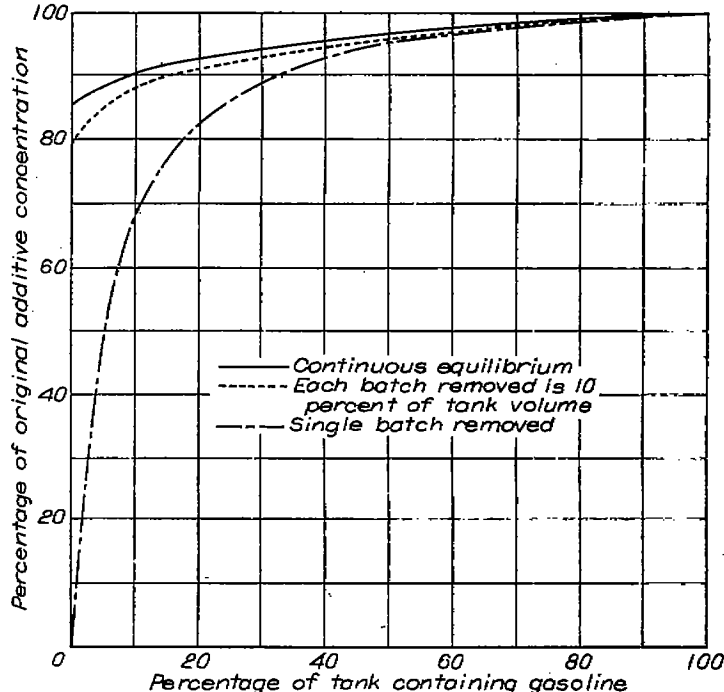


FIGURE VI-6.—Additive concentration in gasoline stored over water for distribution coefficient of 20. (Fig. 1 of reference 11.)

In full-scale, overwater-storage tests of xyldine-blended fuel, 8105 gallons of aviation fuel were stored in a tank of 25,000-gallon capacity and immediately sampled and analyzed. The stored fuel (containing xyldines) was sampled and analyzed periodically, and part of the fuel was removed. This process is a batch process; therefore, equation (2) is applicable. This test provides an evaluation of the equation for the particular conditions.

With the assumption of an average temperature of 65° F for the tank contents and fuel displacement with fresh water,

a volume distribution coefficient of 17 was selected for xylidines (reference 12). The results of the full-scale, water-system test and the equilibrium concentration calculated from equation (2) are compared in table VI-5. The calculated results agree well with the experimental data for this particular test.

Normally anticipated additive concentration in fuel stored over water is shown in figure VI-6 for three different types of tank operation. A volume distribution coefficient of 20 is assumed, inasmuch as experimental values range from 13 to 26 for xylidines (reference 12).

The topmost curve of figure VI-6 represents fuel displaced

from a full tank in successive small increments over a period of time sufficiently long for equilibrium to exist continuously. Equation (7) applies for this case. The second curve illustrates the variation in concentration to be expected if fuel is displaced from a full tank in successive quantities with equilibrium existing between withdrawals. Equation (2) applies for this case. The lower curve illustrates the concentration to be expected if fuel is displaced from a full tank in a single, fairly rapid operation with equilibrium established only after the withdrawal; it also illustrates the change in concentration resulting from the addition of a batch of fuel to a tank containing additive-free water.

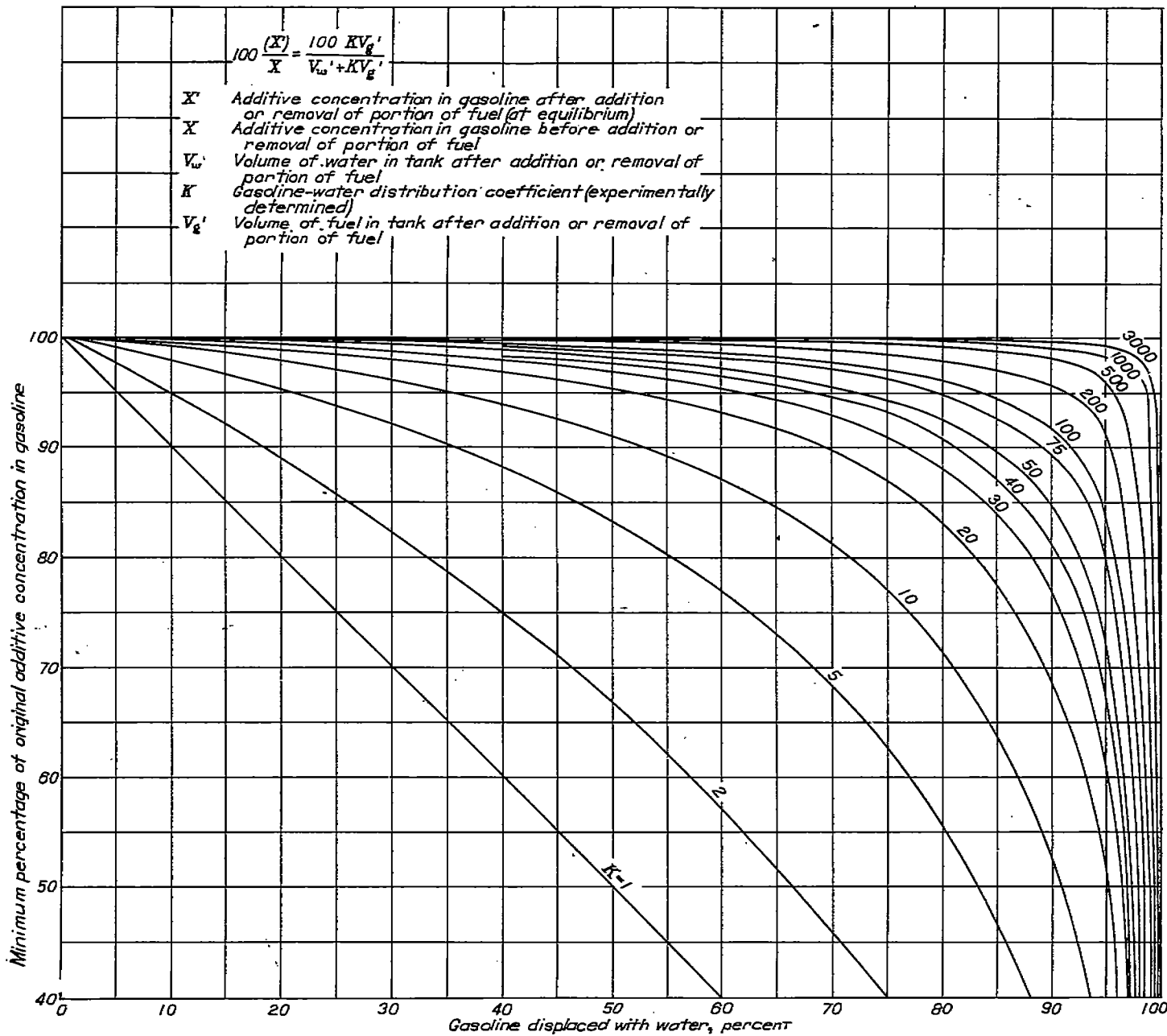


FIGURE VI-7.—Maximum possible loss of additive from fuel stored over water. A value for distribution coefficient is required for particular system, but plot is independent of original concentration of additive, nature of fluids, or temperature. (Fig. 2 of reference 13.)

Generally speaking, the loss of an additive, such as xylidines, with a distribution coefficient of about 20 will not be severe. The greatest loss will occur when the tank contains a ratio of xylidine-free water to fuel greater than about 4:1 (reference 11).

It is emphasized that the equations presented in the foregoing paragraphs apply only to the extent that the assumptions hold for a particular application. In practice, factors such as temperature, varying gasoline-water interface area, and frequency and quantity of additions or withdrawals will influence the results.

As previously stated, the evaluation of loss of additive to water in a water-displacement fuel-storage system is dependent on the distribution coefficient K for the particular additive under consideration. Olson, Tischler, and Goodman (reference 13), and Goodman and Howard (reference 14) have determined distribution coefficients for 45 aromatic amines.

The base gasoline used in determining the distribution coefficients was an aromatic-extracted grade 65 gasoline to which was added 15 percent (by volume) of an aromatic-hydrocarbon mixture consisting of five parts xylene, two parts cumene, and one part toluene. Blends of 1, 3, and 6 percent (by weight) aromatic amine in this base fuel were examined. Earlier data on xylidines (reference 12) show that temperature is the most significant variable affecting the distribution coefficient; consequently, measurements were made at 40° and 100° F. The distribution coefficients for the amines are shown in table VI-6.

The effect of the distribution coefficient in loss of additive to water in a water-displacement system is illustrated in figure VI-7 (reference 13). This figure was prepared by use of the previously discussed equations (reference 11) and is independent of the original additive concentration, the nature of the two fluids, or the temperature. Figure VI-7 shows the minimum possible additive concentration in the fuel remaining in the tank after part of the fuel is displaced from a full tank with amine-free water. The greatest amine loss will occur if the fuel is removed in a single batch; however, this seldom occurs in practice. A lower loss of additive than indicated in figure VI-7 will result if removal of the stored fuel is stepwise.

Methods of analysis for aromatic amines.—For a period of about 2 years the NACA used spectrophotometric measurements of the ultraviolet absorption of aromatic amines in the analysis for presence of amines in gasoline and water. This method of analysis has been reported in detail by

Tischler and Howard (references 15 and 16). The spectrophotometric method is more accurate than titration methods and has proved to be applicable to quantitative determination in hydrocarbon solutions of all monoaryl amines tested in the NACA laboratories.

REFERENCES

1. Jones, Anthony W., and Bull, Arthur W.: Knock-Limited Performance of Pure Hydrocarbons Blended with a Base Fuel in a Full-Scale Aircraft-Engine Cylinder. I—Eight Paraffins, Two Olefins. NACA ARR E4E25, 1944.
2. Cook, Harvey A., Held, Louis F., and Pritchard, Ernest I.: The Influence of Exhaust Pressure on Knock-Limited Performance. NACA MR E5A05, 1945.
3. Branstetter, J. Robert: Knock-Limited Performance of Blends of AN-F-28 Fuel Containing 2 Percent Aromatic Amines—I. NACA MR, April 1944.
4. Alquist, Henry E., and Tower, Leonard K.: Knock-Limited Performance of Blends of AN-F-28 Fuel Containing 2 Percent Aromatic Amines—II. NACA MR, June 1944.
5. Alquist, Henry E., and Tower, Leonard K.: Knock-Limited Performance of Blends of AN-F-28 Fuel Containing 2 Percent Aromatic Amines—III. NACA MR, August 1944.
6. Alquist, Henry E., and Tower, Leonard K.: Knock-Limited Performance of Blends of AN-F-28 Fuel Containing 2 Percent Aromatic Amines—IV. NACA MR E4L21, 1944.
7. Alquist, Henry E., and Tower, Leonard K.: Knock-Limited Performance of Blends of AN-F-28 Fuel Containing 2 Percent Aromatic Amines—V. NACA MR E5H06, 1945.
8. Jones, Anthony W., Bull, Arthur W., and Jonash, Edmund R.: Knock-Limited Performance of Six Aromatic Amines Blended with a Base Fuel in a Full-Scale Aircraft-Engine Cylinder. NACA MR E5D04, 1945.
9. Kelly, Richard L.: The Low-Temperature Solubility of 42 Aromatic Amines in Aviation Gasoline. NACA MR E5K09, 1945.
10. Olson, Walter T.: The Low-Temperature Solubility of Technical Xylidines in Aviation Gasoline. NACA MR, June 1943.
11. Olson, Walter T., and Tischler, Adelbert O.: Loss of Xylidines in Overwater Storage of Xylidine-Blended Fuel. NACA MR, March 1944.
12. Tischler, Adelbert O., Slabey, Vernon A., and Olson, Walter T.: Gasoline-Water Distribution Coefficients of Xylidines. NACA MR, June 1943.
13. Olson, Walter T., Tischler, Adelbert O., and Goodman, Irving A.: Gasoline-Water Distribution Coefficients of 27 Aromatic Amines. NACA MR, Aug. 1944.
14. Goodman, Irving A., and Howard, J. Nelson: Suitability of 18 Aromatic Amines for Overwater Storage When Blended with Aviation Gasoline. NACA MR E5F20a, 1945.
15. Tischler, Adelbert O.: Quantitative Analysis for Aromatic Amines in Aviation Fuels by Ultraviolet Spectrophotometry. NACA ARR E5H27, 1945.
16. Tischler, Adelbert O., and Howard, J. Nelson: Ultraviolet Absorption Spectra of Aromatic Amines in Isooctane and in Water. NACA ARR E5H27a, 1945.

TABLE VI-6.—DISTRIBUTION COEFFICIENTS OF AROMATIC AMINES

Aromatic amine	Original concentration in fuel (percent by weight)	Temperature, ° F					
		40			100		
		Concentration in water at equilibrium (percent by weight)	Distribution coefficient on weight basis K_{wt}	Distribution coefficient on volume basis K_{vol}	Concentration in water at equilibrium (percent by weight)	Distribution coefficient on weight basis K_{wt}	Distribution coefficient on volume basis K_{vol}
Aniline	1 3 6	0.405 1.200 2.173	1.48 1.53 1.84	1.08 1.12 1.35	0.287 .860 1.557	2.50 2.57 2.84	1.76 1.81 2.07
N-Methylaniline	1 3 6	0.041 .112 .195	23 26 30	17 19 22	0.029 .076 .141	34 39 41	24 27 29
N-Ethylaniline	1 3 6	0.014 .043 .074	70 69 80	51 51 53	0.009 .026 .050	110 115 120	73 80 85
N-Propylaniline	1 3 6	0.003 .009 .019	300 330 320	220 240 230	0.002 .007 .013	500 400 480	350 250 320
N-Butylaniline	1 3 6	0.002 .005 .009	500 600 700	370 440 500	0.001 .004 .007	1000 800 900	700 550 630
N-Isopropylaniline	1 3 6	0.016 .043 .099	62 62 60	45 45 44	0.012 .034 .064	82 87 93	54 61 65
N- <i>tert</i> -Butylaniline	1 3 6	0.010 .026 .043	100 120 140	73 88 105	0.005 .014 .028	200 210 260	140 160 150
N, N-Dimethylaniline	1 3 6	0.003 .009 .017	300 330 350	220 240 260	0.003 .003 .014	300 370 430	210 260 300
N, N-Diethylaniline	1 3 6	0.0005 .001 .0015	2000 3000 4000	1500 2000 3000	0.0003 .0006 .0003	3000 5000 5000	2000 4000 6000
<i>o</i> -Toluidine	1 3 6	0.150 .415 .705	5.68 6.24 7.62	4.18 4.53 5.03	0.096 .267 .450	9.4 10.3 11.6	6.6 7.2 8.2
<i>m</i> -Toluidine	1 3 6	0.154 .410 .717	5.51 6.37 7.47	4.04 4.66 5.47	0.104 .282 .505	8.6 9.7 11.0	5.7 6.8 7.7
<i>p</i> -Toluidine	1 3 6	0.196 .571	4.12 4.30	8.02 3.15	0.123 .382 .569	7.2 7.8 9.7	5.1 5.4 6.8
N-Methyl- <i>p</i> -toluidine	1 3 6	0.020 .055 .099	49 54 60	36 40 44	0.013 .036 .066	76 82 90	54 58 63
N-Methyl- <i>o</i> -toluidine	1 3 6	0.021 .046 .073	47 66 76	34 43 56	0.011 .029 .051	94 105 115	66 74 80
N-Methyltoluidines (60 percent <i>p</i> -, 40 percent <i>o</i> -)	1 3 6	0.029 .074 .120	24 40 46	25 29 34	0.020 .051 .091	49 53 65	35 41 45
N-Methyltoluidines (80 percent <i>p</i> -, 20 percent <i>o</i> -)	1 3 6	0.022 .053 .091	45 56 66	33 41 45	0.015 .038 .064	65 79 93	46 56 65
N-Ethyl- <i>p</i> -toluidine	1 3 6	0.004 .010 .017	250 300 350	150 220 260	0.003 .008 .015	200 270 400	210 260 250
N-Isopropyl- <i>p</i> -toluidine	1 3 6	0.007 .020 .035	140 150 170	105 110 125	0.005 .014 .022	200 210 270	140 150 190
<i>o</i> -Ethylaniline	1 3 6	0.054 .146 .244	13 20 24	13 15 18	0.032 .078 .162	30 33 39	21 23 27
<i>p</i> -Ethylaniline	1 3 6	0.067 .171 .293	14 17 20	10 12 15	0.040 .105 .150	24 28 33	17 20 23

TABLE VI-6.—DISTRIBUTION COEFFICIENTS OF AROMATIC AMINES—Continued

Aromatic amine	Original concentration in fuel (percent by weight)	Temperature, °F					
		40			100		
		Concentration in water at equilibrium (percent by weight)	Distribution coefficient on weight basis K_{ws}	Distribution coefficient on volume basis K_{vol}	Concentration in water at equilibrium (percent by weight)	Distribution coefficient on weight basis K_{ws}	Distribution coefficient on volume basis K_{vol}
N-Methylethylaniline	1	0.006	155	115	0.005	200	140
	3	.017	180	130	.011	270	190
	6	.030	200	145	.026	240	170
N-Methyl-p-ethylaniline	1	0.006	160	115	0.003	300	210
	3	.015	200	145	.010	300	210
	6	.028	210	155	.018	330	230
p- <i>tert</i> -Butylaniline	1	0.008	120	88	0.005	200	140
	3	.021	140	105	.014	210	150
	6	.035	170	125	.027	220	155
o-Isopropylaniline	1	0.021	47	34	0.010	100	70
	3	.053	58	41	.030	100	70
	6	.090	66	48	.053	115	80
p-Isopropylaniline	1	0.021	47	34	0.012	82	58
	3	.048	62	45	.033	90	63
	6	.077	77	56	.059	100	70
N-Methyl-p-Isopropylaniline	1	0.003	300	220	0.001	1000	700
	3	.006	500	370	.004	800	550
	6	.009	700	500	.008	800	550
2,4,6-Trimethylaniline	1	0.013	78	56	0.007	140	100
	3	.036	92	60	.021	140	100
	6	.065	91	67	.040	150	105
Cumidines (from synthetic cumene)	1	0.021	47	34	0.013	76	54
	3	.059	61	37	.037	80	56
	6	.100	69	43	.066	90	63
N-Methylecumidines	1	0.009	110	81	0.003	300	210
	3	.020	160	110	.010	300	210
	6	.036	170	125	.019	320	230
2-Methoxyaniline	1	0.183	4.48	3.28	0.120	6.8	4.8
	3	.491	5.15	3.77	.350	7.6	5.4
	6	.846	6.21	4.54	.632	8.6	6.1
Xyldines (technical)	1	0.050	19	14	0.033	29	20
	3	.143	20	15	.063	35	25
	6	.260	22	16	.157	37	28
2,4-Xyldine	1	0.063	18	13	0.031	31	22
	3	.142	20	15	.069	32	24
	6	.257	22	16	.170	34	24
2,5-Xyldine	1	0.048	20	15	0.029	33	23
	3	.132	22	16	.066	34	24
	6	.226	26	19	.149	39	27
2,6-Xyldine	1	0.063	15	11	0.040	24	17
	3	.173	16	12	.109	27	19
	6	.290	20	15	.190	31	23
N-Methyl-2,4-xyldine	1	0.009	110	81	0.005	200	140
	3	.018	165	120	.012	260	175
	6	.028	210	155	.017	350	250
N-Methylxyldines	1	0.010	100	73	0.006	200	140
	3	.021	140	105	.013	230	160
	6	.039	150	110	.024	250	175
2,4-Diethylaniline	1	0.005	200	145	0.003	300	210
	3	.014	210	155	.008	370	260
	6	.026	230	170	.014	430	300
2-Methyl-5-Isopropylaniline	1	0.008	120	88	0.006	200	140
	3	.023	130	95	.014	210	150
	6	.037	160	115	.026	230	160
Pseudocumidine (technical)	1	0.036	27	20	0.022	45	32
	3	.103	28	21	.060	49	34
	6	.172	34	25	.108	55	39

Standard water solutions of the following amines could not be prepared because of the very low water solubility of the amine:

N-Methyl-p-*tert*-butylaniline
N-Isopropyl-p-isopropylaniline
N,N-Dimethyl-2-methyl-5-isopropylaniline
N,N-Dimethyl-2,4,6-trimethylaniline
Diphenylamine
N-Methyl-diphenylamine.

^a Data from references 18 and 14.

^b Density of gasoline solution at 40° F, 0.732 gram/ml.

^c Values for K_{vol} were computed by multiplying corresponding K_{ws} values by density of gasoline solution.

^d Density of gasoline solution at 100° F, 0.704 gram/ml.

CHAPTER VII

TETRAETHYL LEAD AS A FUEL ADDITIVE

For years tetraethyl lead $Pb(C_2H_5)_4$ has been considered the most effective practical additive for suppressing knock in conventional spark-ignition engines. In comparison with the additive-type compounds discussed in chapter VI, tetraethyl lead is considerably more effective. An investigation reported by Calingaert (reference 1) indicates that the knock-suppressing tendency of tetraethyl lead is 118 times greater than that of aniline.

On the basis of cost and antiknock effectiveness alone, tetraethyl lead is far more desirable than any known blending agent, because so little is required in a fuel to equal the antiknock effectiveness of a much larger volume of blending agent. Deleterious effects may, however, occur in engines when fuels containing high concentrations of tetraethyl lead are used. These harmful effects have necessitated strict regulations on the quantity that can be tolerated in fuels for various types of service.

In general, fuels used in commercial aviation contain smaller quantities of tetraethyl lead than those used in military aircraft. At the outbreak of World War II, Army-Navy aviation-fuel specifications permitted tetraethyl lead in quantities less than 3.0 ml per gallon. This limit was later raised to 4.0 ml per gallon; as critical shortages of more desirable blending agents occurred, the limit was again raised to 4.6 ml per gallon. Upon one occasion during the war, continued shortages of fuel stocks and the need for much higher performance fuels resulted in considerable experimentation with fuels containing 6.0 ml per gallon.

PROCESS OF LEAD-DEPOSIT ACCUMULATIONS ON AIRCRAFT-ENGINE SPARK PLUGS

As noted in reference 2, one of the disadvantages of tetraethyl lead as an antiknock agent for aircraft fuels is its characteristic of depositing, either as metallic lead or as a compound, on combustion-chamber surfaces during engine operation. Such deposits on spark plugs cause ignition failures both by bridging the electrode gaps and by forming conducting paths across the insulator surfaces and are suspected of lowering preignition ratings of spark plugs (ch. IV) and contributing to erosion of spark-plug electrodes. For these reasons lead deposition on spark plugs constitutes a flying hazard, increases time and cost of engine maintenance, and limits the use of tetraethyl lead in fuels.

The investigation described in reference 2 illustrates the characteristics of the progressive build-up of spark-plug deposits. In order to determine the progressive accumulation of deposit on spark plugs, each spark plug was weighed periodically throughout a series of test runs in a CFR engine at constant operating conditions. Additional runs were made in a single cylinder of a full-scale liquid-cooled aircraft engine. Three different types of spark plug, designated A, B, and C, were used.

Variation of deposition with time.—The results of a deposit test in the CFR engine for a type A spark plug are shown in figure VII-1. The condition of large total deposit was simulated without the necessity of excessive operating periods by increasing the tetraethyl lead content of the fuel to 34 ml per gallon.

The accumulation of deposit increases with operating time (fig. VII-1), but the rate of deposition decreases. After completion of this test, an effort was made to operate the engine with the coated spark plug, but the test was unsuccessful because of short circuiting.

Effect of power level on deposition.—Operating conditions affect the accumulation of deposits on spark plugs, as illustrated in figure VII-2. Failure of the spark plug during the low-power run occurred shortly after 14 hours of operation because of the formation of a small bead of lead deposit

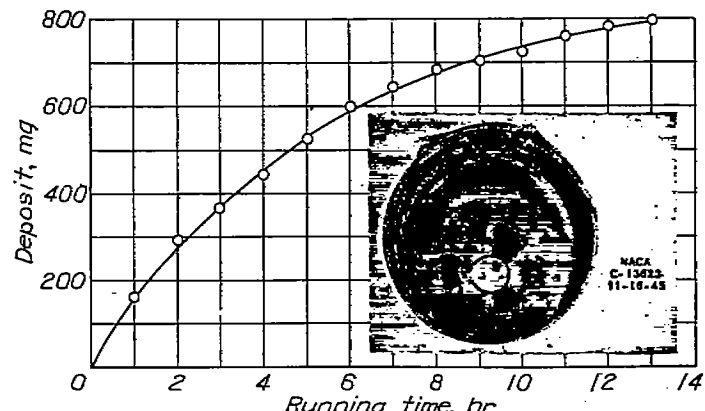


FIGURE VII-1.—Lead deposition for type A spark plug in CFR engine with AN-F-28 fuel leaded to 34 ml TEL per gallon. Compression ratio, 6.65; engine speed, 1800 rpm; imep, 82 pounds per square inch; fuel-air ratio, 0.10; inlet-air temperature, 85° F; coolant temperature, 212° F; spark advance, 45° B. T. C. (Fig. 1 of reference 2.)

on an electrode gap. A photograph of the spark plug in this case is shown in figure VII-3.

Accumulation of deposit masses.—Spark-plug deposition for a type B spark plug in the full-scale single-cylinder test engine is shown in figure VII-4 (reference 2). The spark plug was located in the exhaust position and the engine was operated under simulated cruise conditions. The fuel contained 18 ml TEL per gallon. During this test the condition of the plug was photographically recorded at various time intervals (fig. VII-5). As shown in these photographs, the deposit existed during operation in the form of molten globules, which changed position. The changes in position are attributed to the influence of gravitation and molecular forces and forces arising from gas flow in the combustion chamber (reference 2). The concentration of deposit near the lowest point of the spark-plug cavity became more pronounced as the deposit increased.

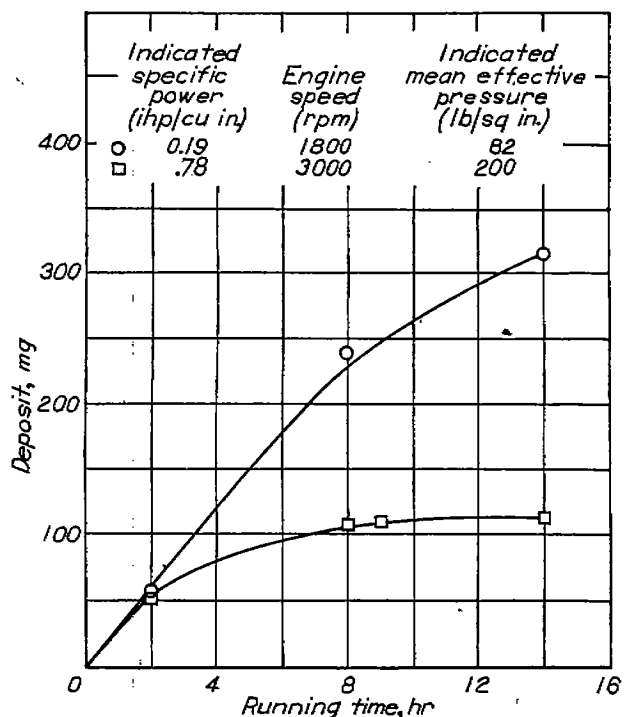


FIGURE VII-2.—Effect of power level on lead deposition for type C spark plug in CFR engine with AN-F-28 fuel leaded to 4.6 ml TEL per gallon. Compression ratio, 6.65; fuel-air ratio, 0.10; inlet-air temperature, 90° F; coolant temperature, 212° F; spark advance, 45° B. T. C. (Fig. 2 of reference 2.)



FIGURE VII-3.—Type C spark plug with lead in left gap. Failure of plug occurred after 14 hours operation at low power in CFR engine. (Fig. 3 of reference 2.)

As pointed out in reference 2, observation of deposits on many spark plugs indicates that these deposits may vary considerably in characteristics and appearance under different conditions. Consequently, no particular deposit can be considered typical. Deposits similar to those in figure VII-5 have been observed on badly fouled spark plugs from service engines.

Deposit losses.—From the data discussed in the foregoing paragraphs, it was concluded (reference 2) that the manner in which the rate of deposition varies (figs. VII-1, VII-2, and VII-4) suggests that the net rate is the result of deposition (possibly at constant rate) and loss of deposit at a rate

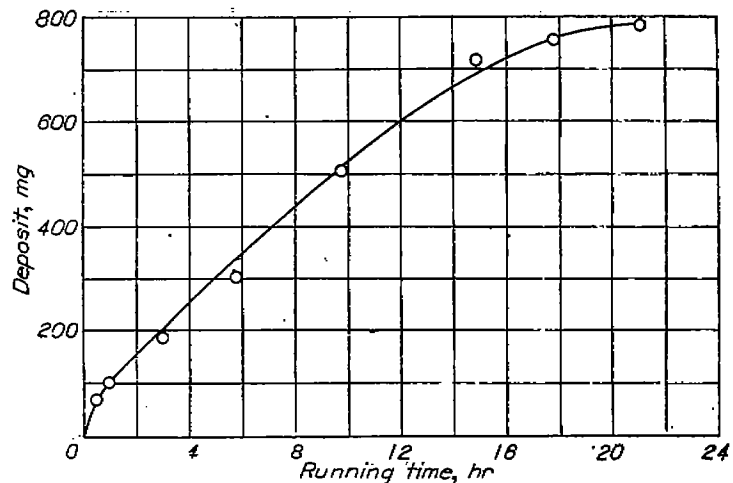


FIGURE VII-4.—Lead deposition for type B spark plug in exhaust position of liquid-cooled aircraft cylinder with AN-F-28 fuel leaded to 18 ml TEL per gallon. Engine speed, 2000 rpm; inlet-air pressure, 30 inches of mercury absolute; fuel-air ratio, 0.10; inlet-air temperature, 85° F; coolant temperature, 250° F. (Fig. 4 of reference 2.)

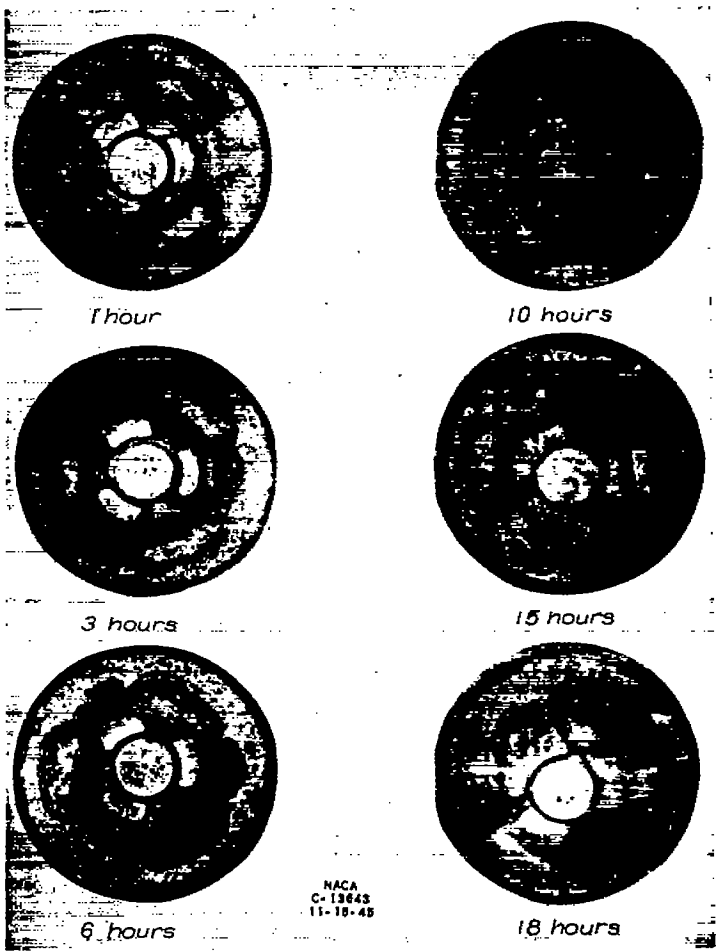


FIGURE VII-5.—Accumulation of lead deposits on type B spark plug in exhaust position of liquid-cooled aircraft cylinder. (Fig. 5 of reference 2.)

that increases as the total deposit increases. In order to test this conclusion, a spark plug was operated in the CFR engine on S reference fuel containing 6 ml TEL per gallon.

After 7½ hours of operation, the deposit weight was found to be 159 milligrams. The spark plug was then replaced without cleaning and operated for 1 hour under the same conditions but with unleaded S reference fuel. At the end of 1 hour the deposit weight had decreased to 112 milligrams, a decrease of 30 percent. A similar test on another spark plug resulted in a 35-percent weight loss.

Significance of deposit weights.—A spark plug may fail electrically when a deposit of sufficient electric conductance to prevent sparking is formed between the spark-plug shell, or a ground electrode, and the center electrode. A very small quantity of deposit may cause failure if the deposit directly bridges the electrode gap. (See fig. VII-3.) There is evidence, however, that gap bridging is not the most common type of failure of spark plugs incorporating large nickel or tungsten electrodes. In the more usual case of failure by conduction along deposits on the insulator, relatively large quantities of deposit are necessary before short circuiting occurs. The amount, distribution, and conductivity of the deposit determine the path of short circuiting. From the photographic evidence in figure VII-5 it was concluded (reference 2) that, aside from certain concentrating influences such as the force of gravity and large temperature differences, the deposit distribution is primarily a matter of chance. The amount of deposit and the chemical or physical properties of the deposit can then be considered as factors determining the probability of failure. The actual failure, however, is dependent upon the distribution of deposit.

ETHYLENE DIBROMIDE IN TETRAETHYL LEAD FLUID

One of the principal causes of exhaust-valve failure in reciprocating engines has been found to be corrosion and collapse of the valve crown at excessively high operating temperatures (reference 3). Analysis of deposits on exhaust valves has shown conclusively that all the lead present in the fuel has not been properly scavenged from the cylinder. This fact supports the conclusion of Banks (reference 4) and Hives and Smith (reference 5) that hot corrosion of exhaust valves is a result of the action of lead oxide deposited on the valve head during operation with leaded fuel.

In order to minimize the undesirable lead deposits, ethylene dibromide is added to the tetraethyl lead before addition to the fuel. The ethylene dibromide reacts with lead in the cylinder during combustion to form volatile compounds that may be easily scavenged with the exhaust gases. The mixture of ethylene dibromide and tetraethyl lead (and small quantities of dye and kerosene) prior to addition to the fuel is called tetraethyl lead fluid. The fluid currently used in aircraft fuels contains 0.96 gram of ethylene dibromide per ml TEL. This quantity of ethylene dibromide is the amount theoretically required to combine with all the lead in the

mixture. Such a mixture of the dibromide and tetraethyl lead is popularly known as a 1-T (one-theory) mix.

An investigation (reference 6) was conducted to determine the influence of excess ethylene dibromide on the degree of valve-crown corrosion occurring during engine operation. The effects resulting from use of 1-T and 2-T mixes were compared. Because the use of excess ethylene dibromide could conceivably reduce the knock-limited performance of the leaded fuel, studies of knock-limited performance were included.

Effect on exhaust-valve corrosion.—Results of valve-corrosion tests in a full-scale air-cooled aircraft cylinder are summarized in the following table (reference 6):

Fuel	TEL (ml/gal)	Mix	Length of run (hr)	Weight loss of valve		
				Total (grams)	Rate (gram/hr)	Rate (percentage of loss with 1-T mix)
	4.53	1-T 2-T	22 16½	5.18 1.97	0.235 .119	100 51
	6.0	1-T 2-T	18 18	3.17 .53	0.176 .029	100 16

*AN-F-28 (28-R) was used as base fuel. This fuel contained about 4.53 ml TEL/gal.

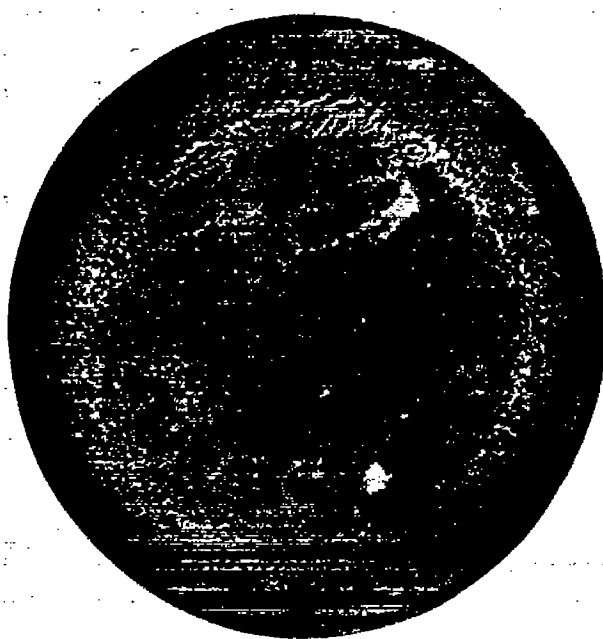
For the tests in which the concentration of tetraethyl lead was 4.53 ml per gallon, the exhaust-valve temperature was held at approximately 1200° F. When the concentration was increased to 6.0 ml per gallon, however, the combustion-air inlet temperature was reduced to 95° F as compared with 150° F for the test with the fuel of lower tetraethyl lead concentration. This change caused a lower exhaust-valve temperature and probably accounts for the reduction in amount of valve corrosion in the test of fuel with 6.0 ml TEL per gallon.

Comparative photographs of the valves from the tests just described are shown in figures VII-6 and VII-7.

Effect on lead deposition.—Because of corrosion of the valve crown it was difficult to determine quantitatively the effect of ethylene dibromide on deposits. (See reference 6.) For this reason, the measurement of deposits was confined to the piston crown and the spark plugs. In the test with the fuel containing 4.53 ml TEL per gallon, the rate of lead deposition on the piston crown with the 2-T mix was about 73 percent of the rate during the test with the 1-T mix.

The effect of ethylene dibromide on spark-plug deposits was also determined for fuel containing 6.0 ml TEL per gallon; these results are shown in the following table:

Spark plug	Mix	Weight of deposit (gram)	Reduction in deposit (percent)
Front.....	1-T 2-T	0.083 .021	0 75
Rear.....	1-T 2-T	0.109 .014	0 87



(a) Valve after 22 hours of operation with 1-T mix.



(b) Valve after 18 1/2 hours of operation with 2-T mix.

NACA
C-7178
10-25-44

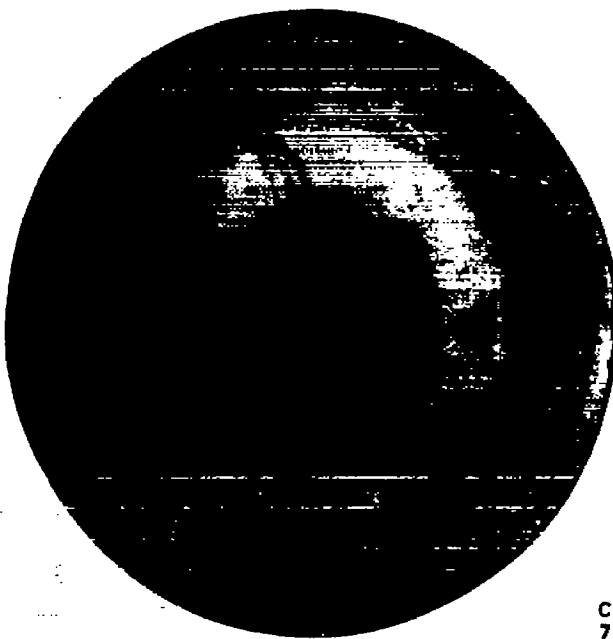
FIGURE VII-6.—Effect of excess ethylene dibromide on exhaust valves in air-cooled aircraft cylinder with fuel leaded to 4.53 ml TEL per gallon. (Fig. 1 of reference 6.)

Effect on knock-limited power.—When the ethylene dibromide concentration was increased to the equivalent of a 2-T mix, there was apparently no effect on the knock limit over the range of conditions investigated in the full-scale air-cooled cylinder (fig. VII-8). (See references 6 and 7.)

Other tests were made to evaluate the effects of ethylene dibromide on knock-limited power in a CFR test engine operating at conditions specified for the A. S. T. M. Supercharge method; the results are presented in table VII-1.



(a) Valve after 18 hours operation with 1-T mix.



(b) Valve after 18 hours operation with 2-T mix.

NACA
C-5546
7-3-44

FIGURE VII-7.—Effect of excess ethylene dibromide on exhaust valves in air-cooled aircraft cylinder with fuel leaded to 6.0 ml TEL per gallon. (Fig. 2 of reference 6.)

TABLE VII-1.—EFFECT OF ETHYLENE DIBROMIDE IN LEADED AND UNLEADED S REFERENCE FUEL ON KNOCK-LIMITED POWER

[Where two values are given in the table for the same determination, the second value was obtained from a check run.]

Leaded S reference fuel				
Ethylene dibromide in S reference fuel +6 ml TEL (ml/gal)	Relative power ^a			
	Fuel-air ratio			
	0.062	0.070	0.090	0.110
2.67 (1-T).....	1.00	1.00	1.00	1.00
0 (0-T).....	0.98	1.00	1.01 1.01	1.00
4.01 (1.5-T).....	1.01 .99	1.01 1.00	1.01 .98	1.01 1.00
5.34 (2-T).....	0.92	0.91	0.94 .95	0.95 .93
Unleaded S reference fuel				
Ethylene dibromide in unleaded S reference fuel (ml/gal)	Relative power ^b			
	Fuel-air ratio			
	0.062	0.070	0.090	0.110
0.....	1.00	1.00	1.00	1.00
2.67.....	0.98	0.96	0.94 .96	0.97 .98
5.34.....	0.97	0.92	0.92 .94	0.97 .96

^aimep (S+6 ml TEL+test concentration of ethylene dibromide)

^bimep (S+6 ml TEL+2.67 ml ethylene dibromide (1-T))

imep (S+test concentration of ethylene dibromide)

imep (S)

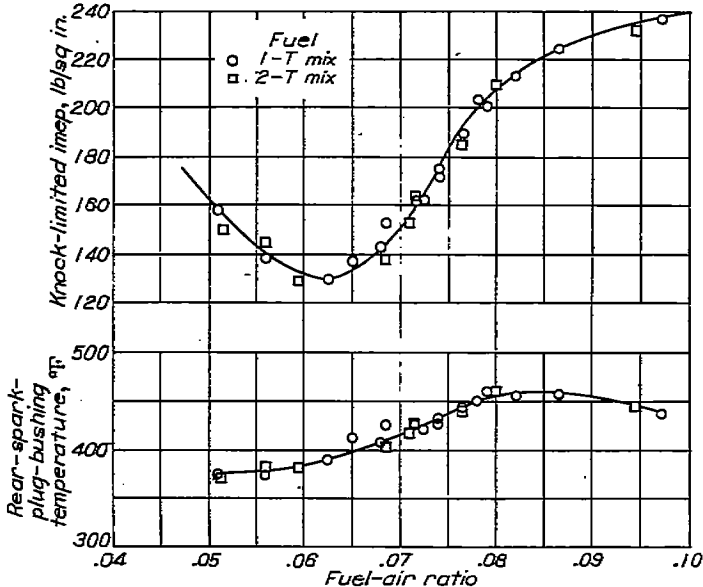


FIGURE VII-8.—Effect of excess ethylene dibromide on knock-limited performance in air-cooled aircraft cylinder. Engine speed, 2200 rpm; inlet-air temperature, 250° F; spark advance, 20° B. T. O. (Fig. 8 of reference 6.)

Increasing the ethylene dibromide concentration from 0 to 5.34 ml per gallon decreased the knock-limited power of the leaded and unleaded S reference fuel about the same amount, 6 to 9 percent depending upon the fuel-air ratio. Changing the concentration of ethylene dibromide from 0 to 2.67 to 4.01 ml per gallon had no effect on the knock-limited performance of the leaded fuel; however, a change of 0 to 2.67 ml per gallon decreased the knock-limited power of the unleaded fuel a maximum of about 6 percent.

LEAD SUSCEPTIBILITY

The lead susceptibility or lead response of a fuel is defined as the increase in knock-limited performance of the fuel resulting from the addition of a given quantity of tetraethyl lead. In 1943 the NACA conducted an analysis of existing data on pure hydrocarbon fuels to determine the manner in which the lead susceptibility is influenced by fuel type, engine type, and engine operating conditions. This analysis (references 8 and 9) was based on data obtained from the American Petroleum Institute (API) Hydrocarbon Research Project.

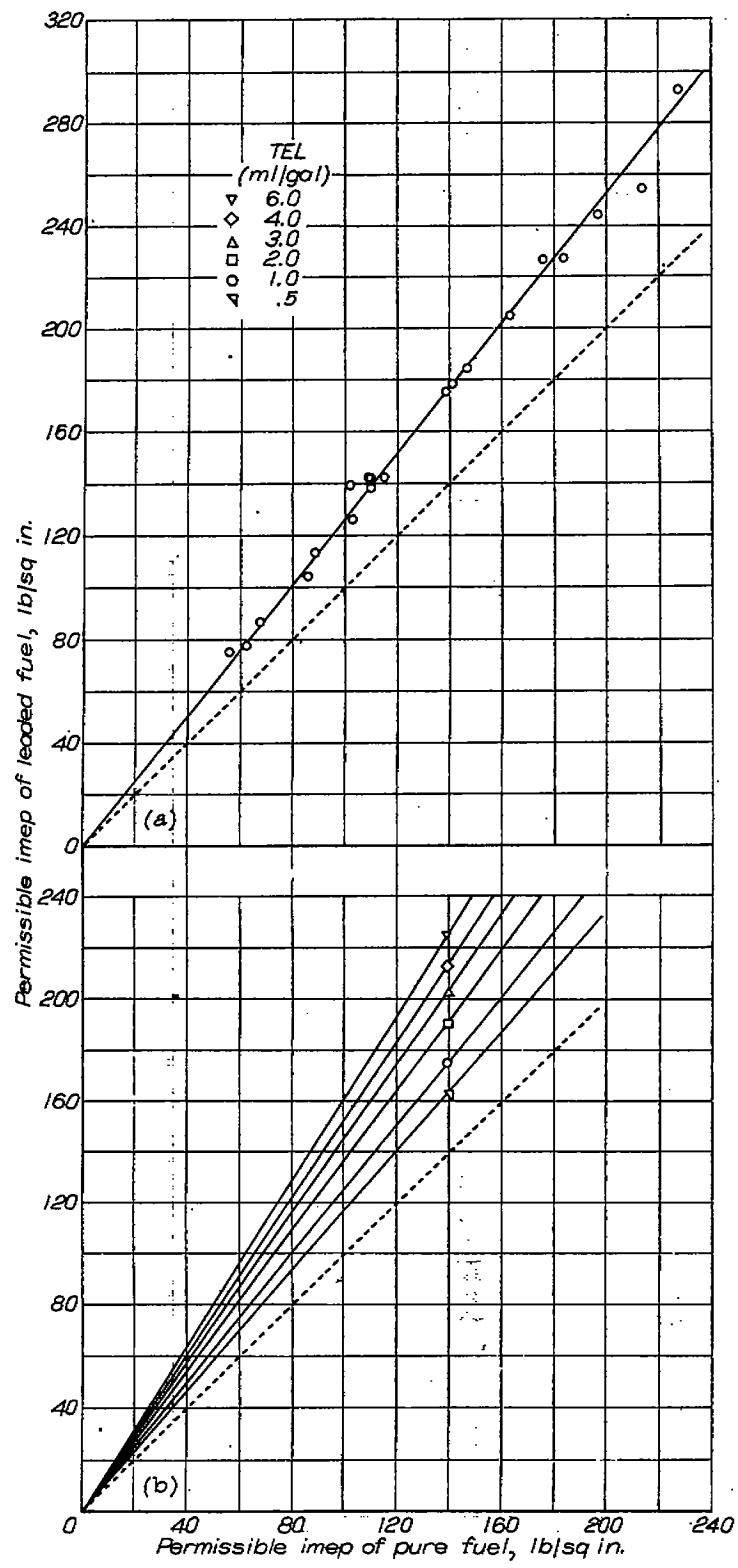
DATA FROM SUPERCHARGED ENGINES

In cooperation with the API, the Ethyl Corporation investigated the lead susceptibility of many pure compounds. These data were determined in a small-scale engine having a displacement of 17.6 cubic inches.

Paraffins.—Examination of the Ethyl Corp. data demonstrated that the lead susceptibility could be represented as a straight line by plotting the knock-limited indicated mean effective pressures of the pure fuels against the knock-limited indicated mean effective pressures of the leaded fuels (reference 8). By this method, data for paraffinic fuels were plotted as shown in figure VII-9 (a). It is obvious in this figure that the fuel which has the highest permissible indicated mean effective pressure in the pure state has the greatest lead response. The percentage increase in indicated mean effective pressure for 1.0 ml TEL, however, is constant regardless of the permissible indicated mean effective pressure. Heron and Beatty (reference 10) found this fact to be true for 6.0-ml additions of tetraethyl lead.

The susceptibility of isoctane to various quantities of tetraethyl lead is shown in figure VII-9 (b). Because it was believed that the lead susceptibility of all paraffins might be represented by a chart similar to figure VII-9 (b), a later investigation (reference 9) was made with blends of two paraffinic fuels (S and M reference fuels) containing up to 8.0 ml TEL per gallon. This study was made in a supercharged CFR engine modified as described in reference 11.

Data from reference 9 are plotted in figure VII-10. These plots are based on results reported by Heron and Beatty (reference 10) which indicate that for supercharged tests a linear relation exists between the reciprocal of the knock-limited indicated mean effective pressures and blend composition. (See chapter VIII.)



(a) Paraffins. (Fig. 10 of reference 8.)

(b) Isooctane (2,2,4-trimethylpentane). (Fig. 11 of reference 8.)

FIGURE VII-9.—Lead susceptibility of various fuels in 17.6 engine. Compression ratio, 5.6; engine speed, 900 rpm; approximate fuel-air ratio, 0.07; inlet-air temperature, 225° F; coolant temperature, 300° F.

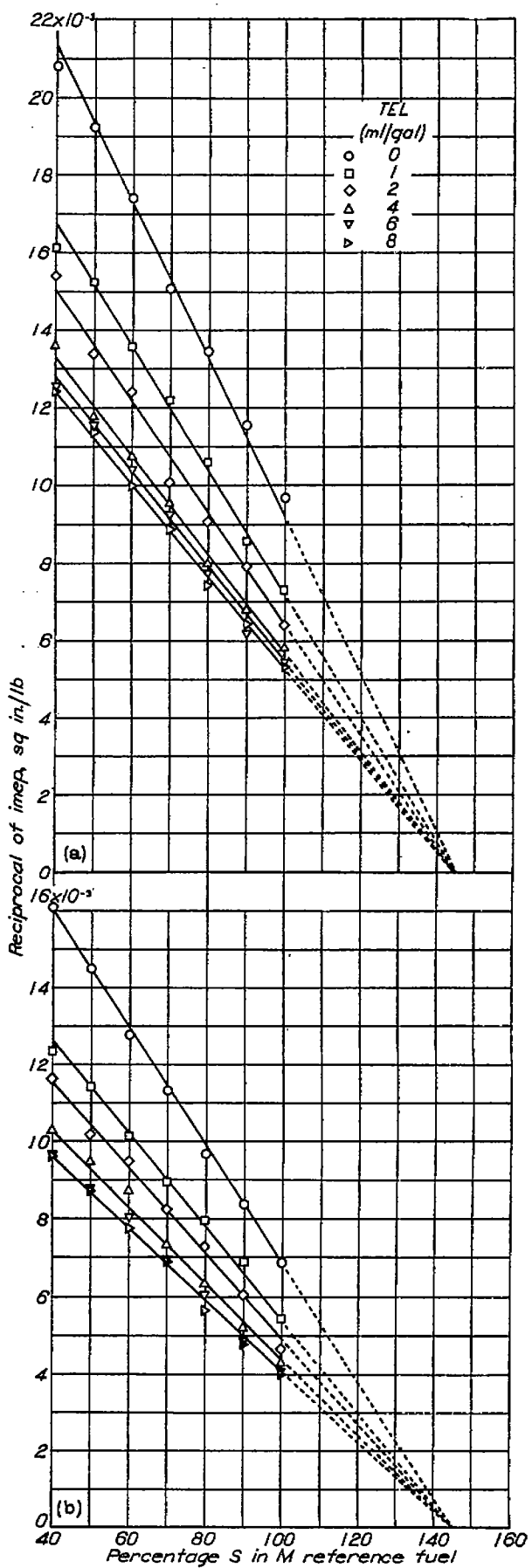
The lines of constant tetraethyl lead concentration in these figures can be represented by the equation of an equilateral hyperbola:

$$P(A-N) = B \quad (1)$$

where

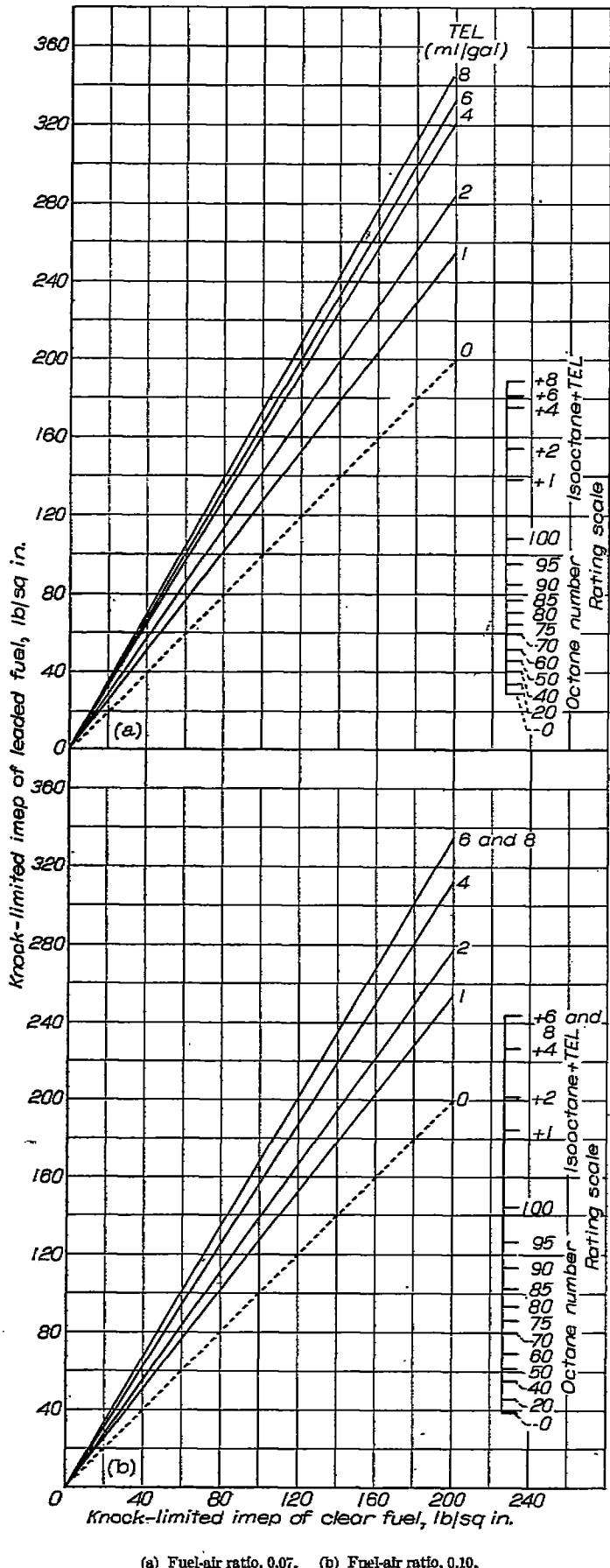
P knock-limited indicated mean effective pressure

A constant



(a) Fuel-air ratio, 0.07. (b) Fuel-air ratio, 0.10.

FIGURE VII-10.—Lead susceptibility of blends of S and M reference fuels in CFR engine. Compression ratio, 7.0; engine speed, 2000 rpm; inlet-air temperature, 250° F; coolant temperature, 250° F; spark advance, 35° B. T. C. (Fig. 6 of reference 9.)



(a) Fuel-air ratio, 0.07. (b) Fuel-air ratio, 0.10.

FIGURE VII-11.—Lead susceptibility of paraffinic fuels in CFR engines. Compression ratio, 7.0; engine speed, 2000 rpm; inlet-air temperature, 260° F; coolant temperature, 260° F; spark advance, 35° B. T. C. (Fig. 7 of reference 9.)

N volume percentage of S reference fuel in M reference fuel
 B slope

The asymptotes of the hyperbola represented by equation (1) are zero and A . The constant A is independent of tetraethyl lead concentration and fuel-air ratio and is equal to 145 (the intersection of the curves with the abscissa).

In figures VII-11, the data from figure VII-10 have been converted to plots of the knock-limited indicated mean effective pressure of the clear fuel against the knock-limited indicated mean effective pressure of the leaded fuel. This type of plot has an advantage over that of figure VII-10 in that the lead susceptibility can be represented by a linear elation without the use of a reciprocal scale.

A scale representing antiknock ratings in terms of octane numbers and leaded iso-octane has been added to figure VII-11. This scale corresponds to the ordinate values of knock-limited indicated mean effective pressure; that is, a 90-octane fuel whether clear or leaded (fig. VII-11(a)) has a knock-limited indicated mean effective pressure of 85 pounds per square inch under the conditions presented. With the addition of this scale, the chart may be used to obtain either the knock-limited indicated mean effective pressure or the octane rating of a paraffinic fuel containing various quantities of tetraethyl lead. Only the unleaded fuel need be tested in order to estimate the lead response for any concentration of tetraethyl lead.

The estimation of lead susceptibility according to the foregoing procedure is of value in the study of paraffinic fuels in which the quantity of fuel available for testing is limited. In such cases the rating of the clear fuel can be determined by a standard rating method such as the A. S. T. M. Supercharge rating method, and the rating of the test fuel plus various amounts of tetraethyl lead can be approximated from a chart previously established for the selected rating method.

Cycloparaffins and olefins.—Insufficient data exist to establish definitely the susceptibilities of the cycloparaffins (fig. VII-12 (a)) and olefins (fig. VII-12 (b)). When figures VII-9, VII-12 (a), and VII-12 (b) are compared, the order of lead response for the paraffins, cycloparaffins, and olefins is found to be as follows:

Hydrocarbons	Percentage increase IMEP					
	(ml TEL/gal)					
	1.0	2.0	3.0	4.0	5.0	6.0
Paraffins	26	36	46	51	57	61
Cycloparaffins	23	—	—	—	—	—
• Olefins	14	—	—	—	—	—

* Percentage increase in IMEP for olefins was estimated from diisobutylene.

DATA FROM NONSUPERCHARGED ENGINES

The relation between critical compression ratio and A. S. T. M. Motor method octane number can be represented by the equation for a hyperbola. (See fig. VII-13.) The curve in this figure was calculated from figure 1 of reference 12, which shows the relation between height of compression chamber and A. S. T. M. Motor method octane number.

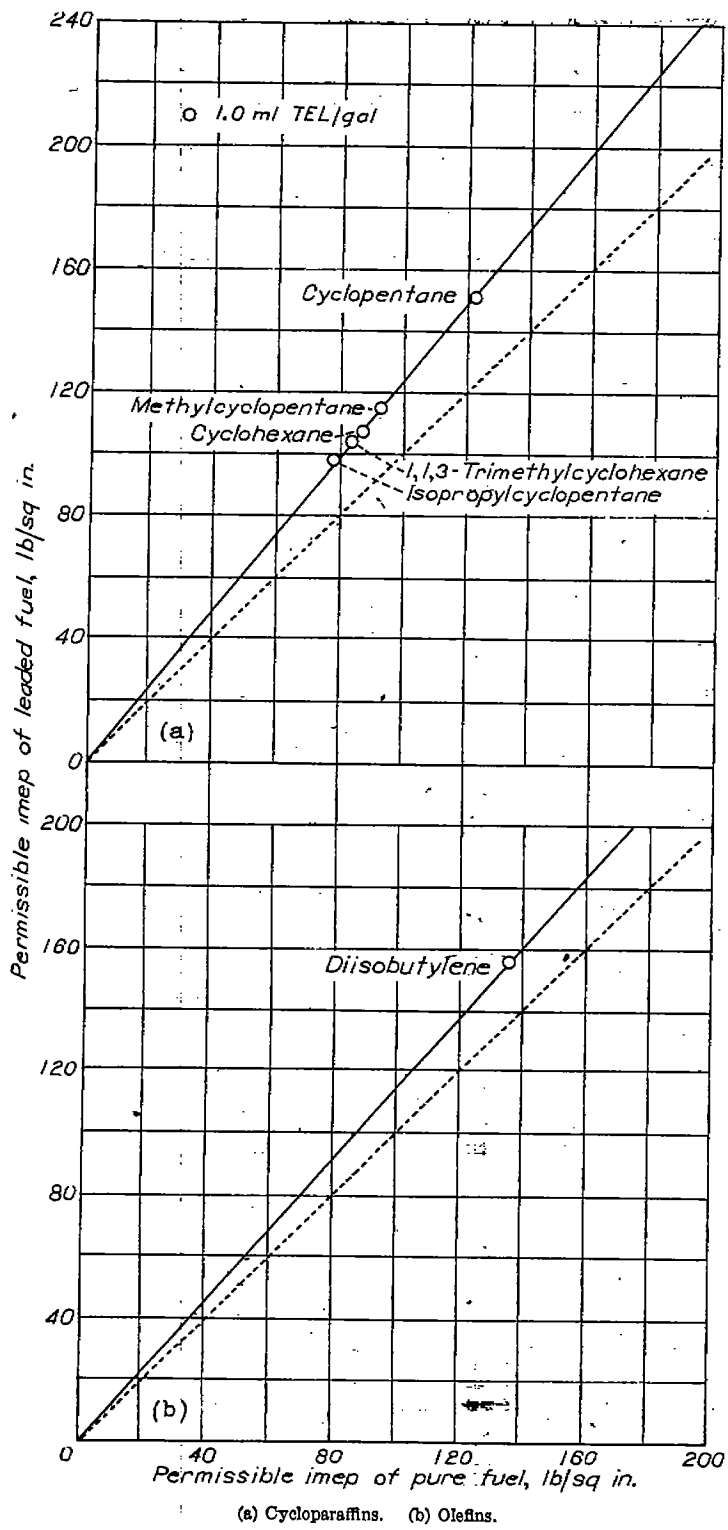


FIGURE VII-12.—Lead susceptibility of various fuels in 17.6 engine. Compression ratio, 5.6; engine speed, 900 rpm; approximate fuel-air ratio, 0.07; inlet-air temperature, 225° F; coolant temperature, 300° F. (Fig. 18 of reference 8.)

The equation for the curve in figure VII-13 is

$$(R - 3.3)(125 - N_1) = 125 \quad (2)$$

where

R critical compression ratio

N_1 A. S. T. M. Motor method octane number

The asymptotes for the curve are critical compression ratio, 3.3 and A. S. T. M. Motor method octane number, 125. As

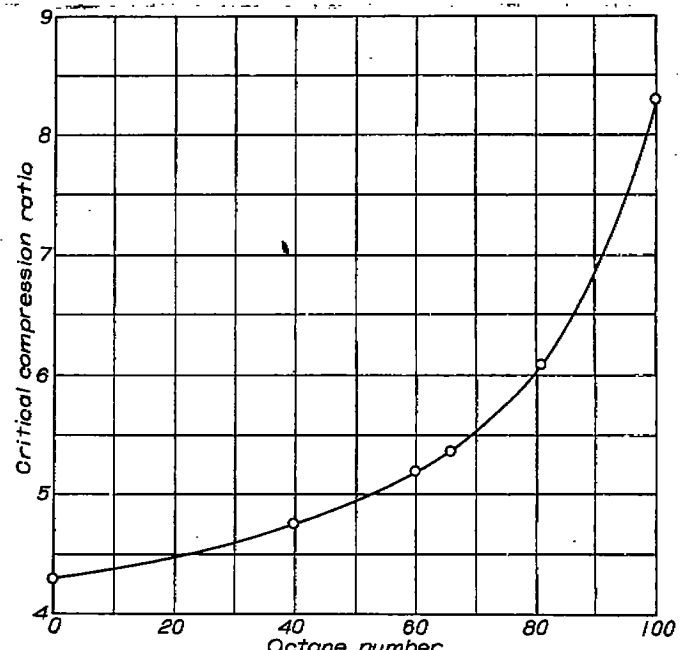


FIGURE VII-13.—Variation of critical compression ratio with octane number for A. S. T. M. Motor method. (Fig. 3 of reference 8.)

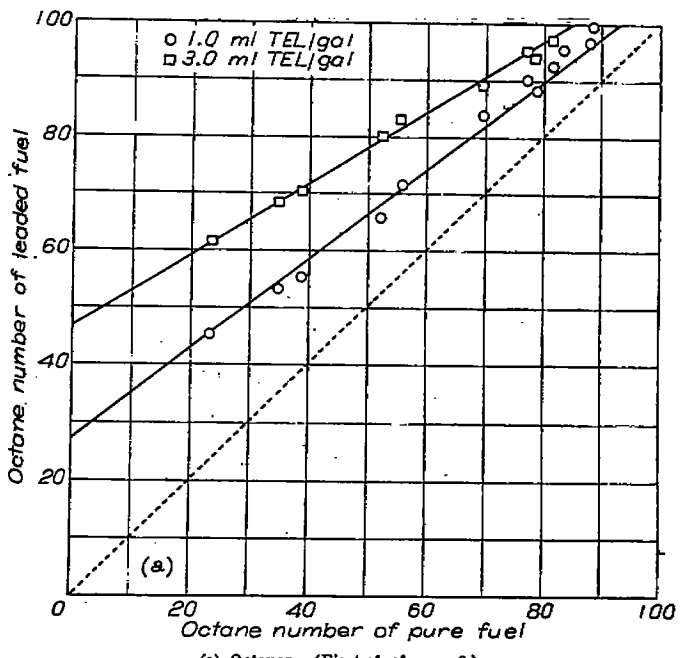
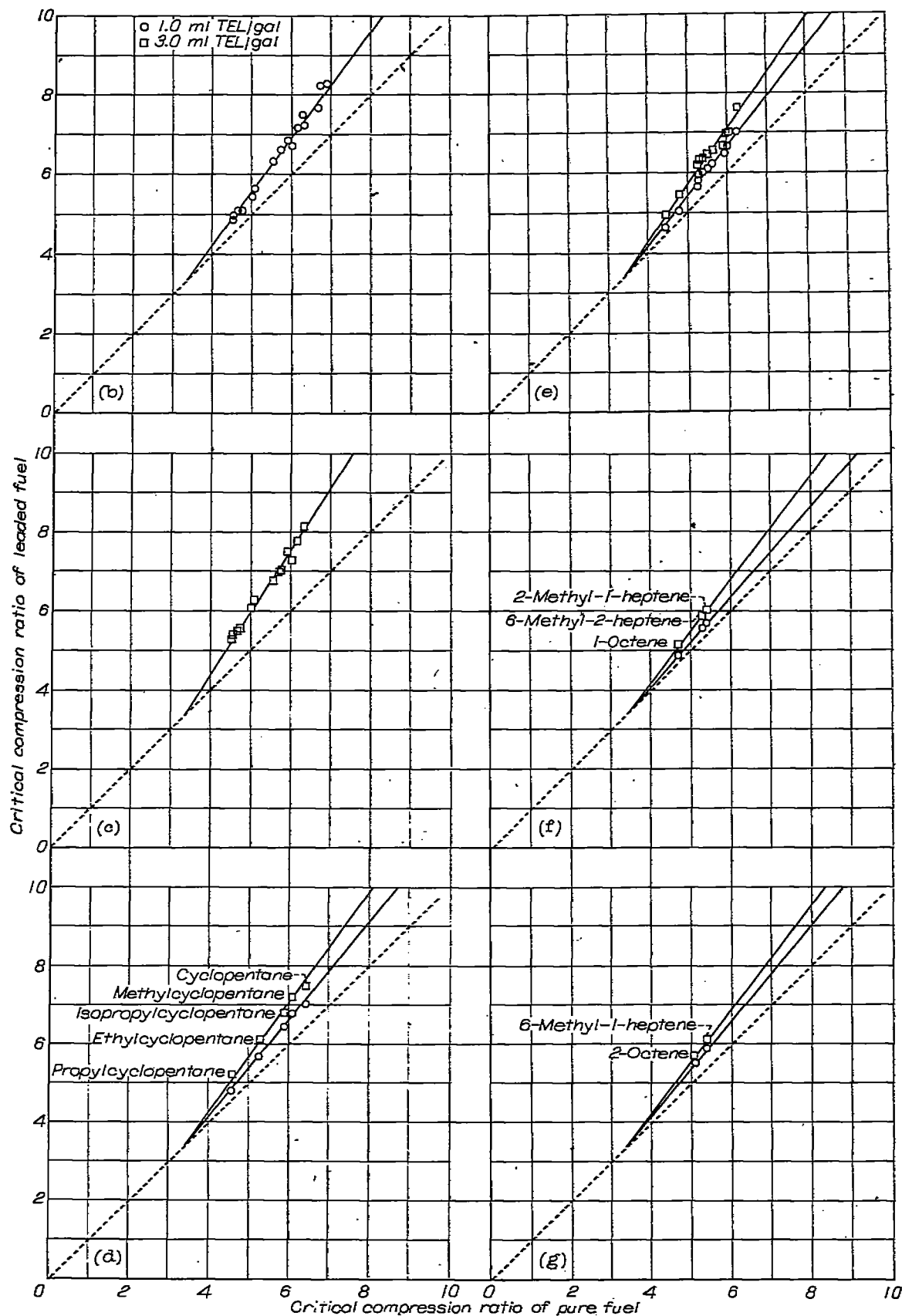


FIGURE VII-14.—Lead susceptibility of various fuels based on A. S. T. M. Motor ratings.

pointed out in reference 8, these asymptotes will vary with engine operating conditions.

The curve just discussed is related to a linear method used by Heron and Beatty (reference 10) to express lead susceptibility (gain of octane number per ml TEL). The method is illustrated in figure VII-14 (a) for data obtained by the API. The relation between figures VII-13 and VII-14 (a) may be shown by extending the lines in figure VII-14 (a) until they intersect. This intersection occurs at an octane number of 125. If both scales of figure VII-14 (a) were converted to critical compression ratios, the point of intersection of the curves would be at a compression ratio of 3.3. These two points of intersection are the asymptotes of figure VII-13.



(b) Paraffins. Tetraethyl lead content, 1.0 ml per gallon. (Fig. 19 of reference 8.)

(c) Paraffins. Tetraethyl lead content, 3.0 ml per gallon. (Fig. 20 of reference 8.)

(d) Cyclopentane derivatives. (Fig. 21 of reference 8.)

(e) Cyclohexane derivatives. (Fig. 22 of reference 8.)

(f) Octanes. (Fig. 23 of reference 8.)

(g) Octenes. (Fig. 24 of reference 8.)

Figure VII-14.—Concluded. Lead susceptibility of various fuels based on A. S. T. M. Motor method ratings.

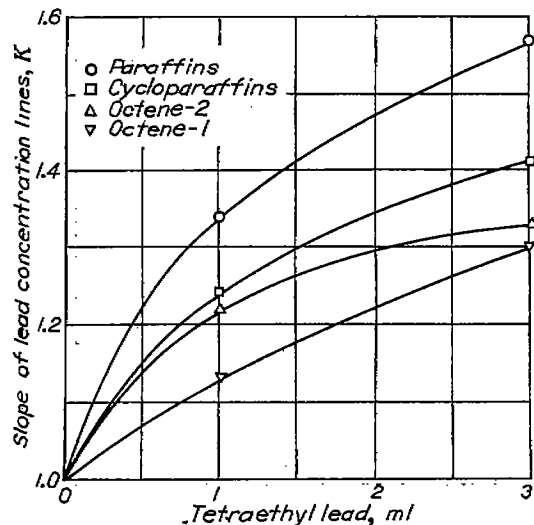
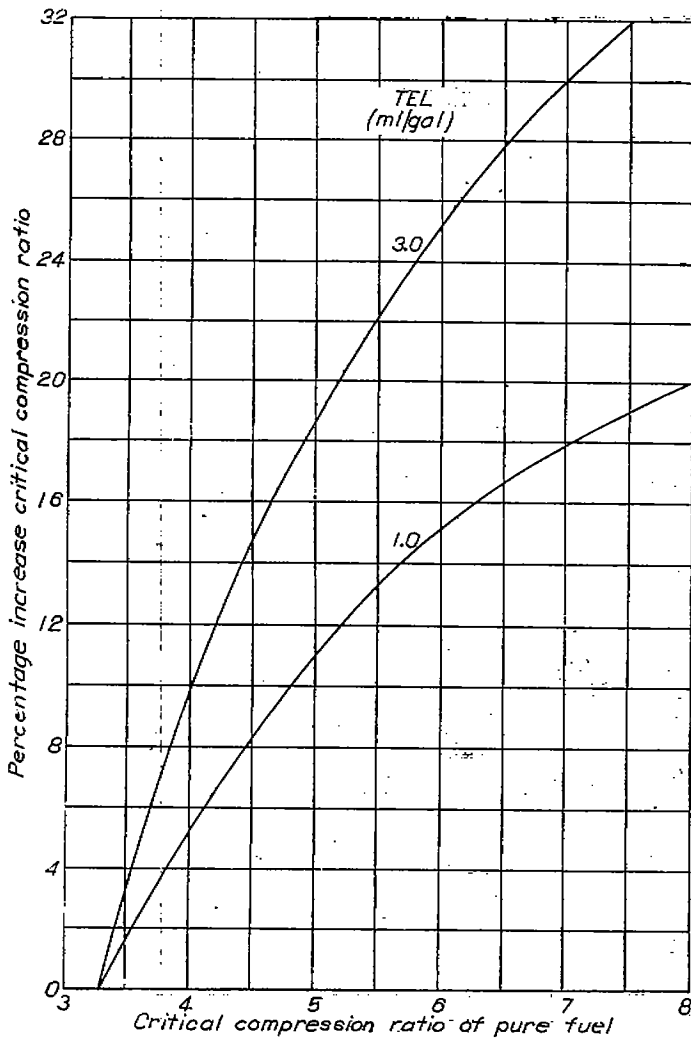
FIGURE VII-15.—Variation of K with tetraethyl lead concentration. (Fig. 25 of reference 8.)

FIGURE VII-16.—Variation of compression ratio with tetraethyl lead concentration. (Fig. 26 of reference 8.)

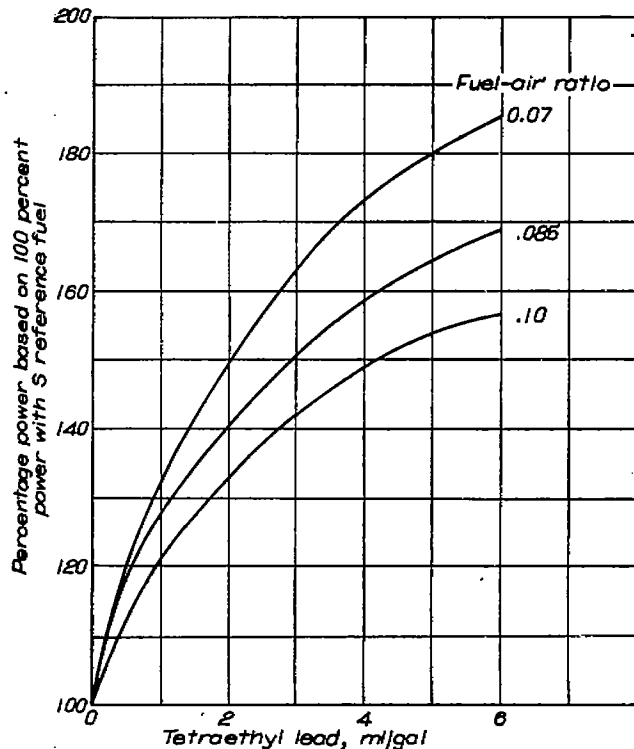


FIGURE VII-17.—Variation of power increase with tetraethyl lead concentration for reference fuel as determined by A. S. T. M. Supercharge method. (Fig. 10 of reference 9.)

By the use of critical compression ratios, an analysis similar to that used for supercharged test engine data has been made (reference 8). As shown in figures VII-14 (b) and VII-14 (c), the lead response of the paraffins may be represented by single straight lines for 1.0 and 3.0 ml TEL, respectively. The equation for these straight lines of constant tetraethyl lead concentration is

$$R_1 = KR - 3.3 (K-1) \quad (3)$$

where

R_1 critical compression ratio of leaded fuel

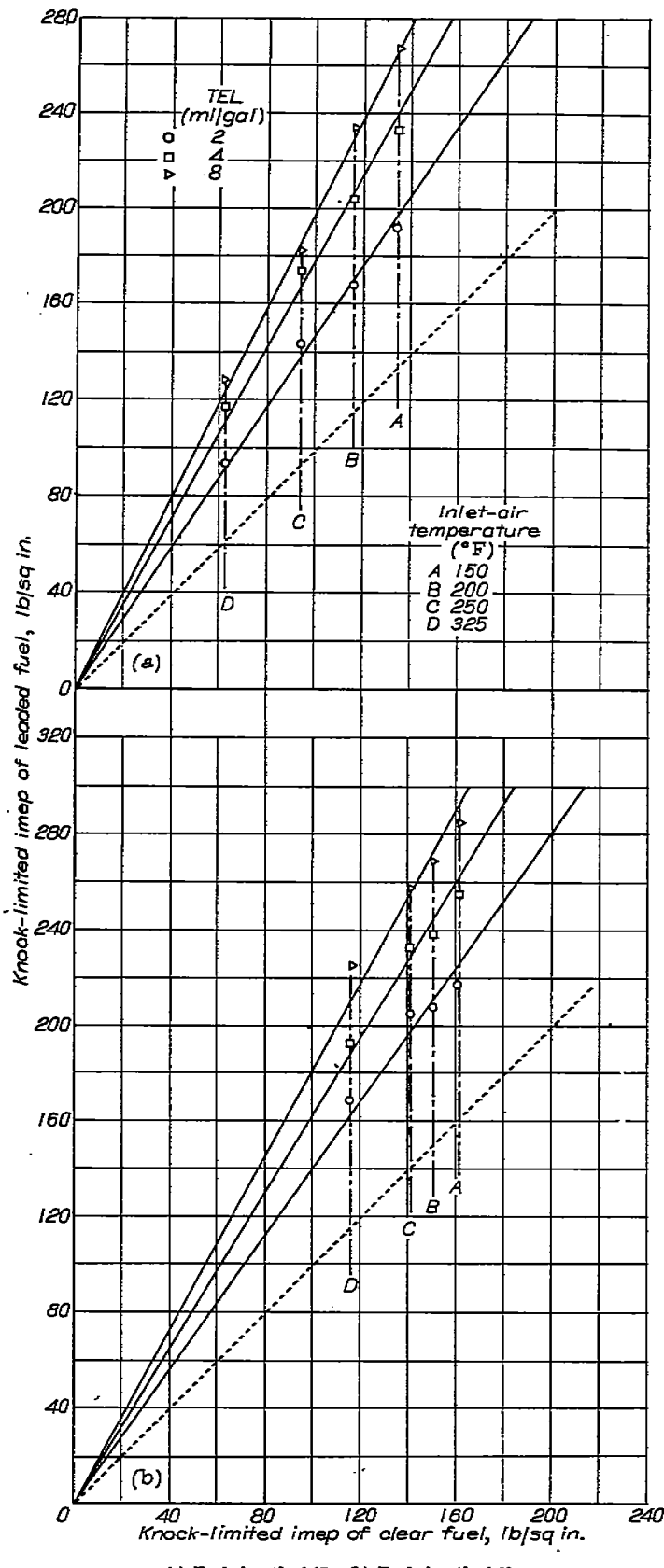
R critical compression ratio of pure fuel

K slope of line of constant tetraethyl lead concentration

The cycloparaffins (figs. VII-14 (d) and VII-14 (e)) may also be represented by single straight lines. The lead susceptibility of the olefins (figs. VII-14 (f) and VII-14 (g)) is apparently affected by the position of the double bond and therefore a single line cannot be used to represent the class as a whole.

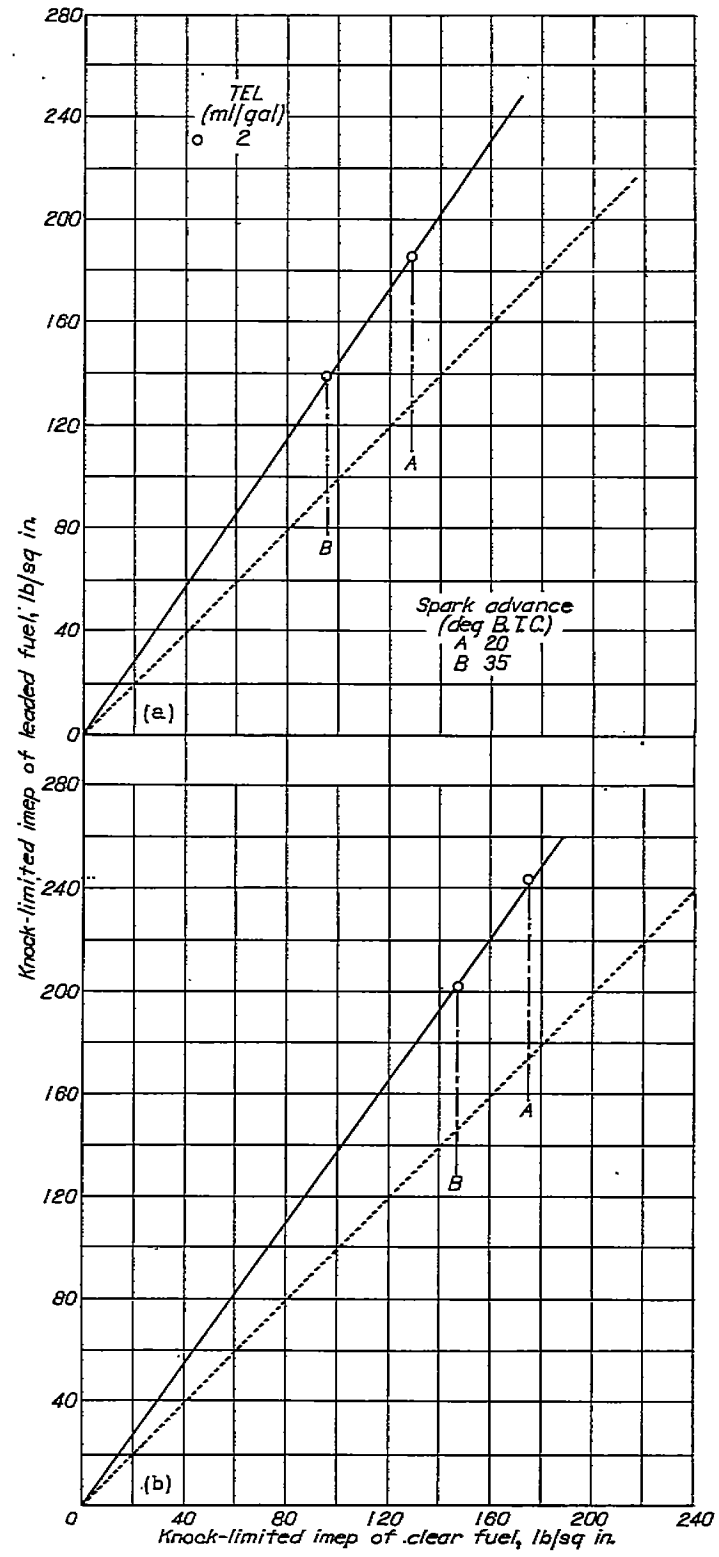
For each class of hydrocarbons a different value of K will be obtained (equation (3)). The values of K determined for the data presented in this analysis are as follows:

Hydrocarbon	Slopes of lead susceptibility curves	
	For 1.0 ml	For 3.0 ml
Paraffins	1.34	1.57
Cycloparaffins	1.24	1.41
Octene-2	1.22	1.33
Octene-1	1.18	1.30



(a) Fuel-air ratio, 0.07. (b) Fuel-air ratio, 0.10.

FIGURE VII-18.—Effect of inlet-air temperature on lead susceptibility of S reference fuel in CFR engine. Compression ratio, 7.0; engine speed, 2000 rpm; coolant temperature, 250° F; spark advance, 35° B. T. C. (Fig. 11 of reference 9.)



(a) Fuel-air ratio, 0.07. (b) Fuel-air ratio, 0.10.

FIGURE VII-19.—Effect of spark advance on lead susceptibility of S reference fuel in CFR engine. Compression ratio, 7.0; engine speed, 2000 rpm; inlet-air temperature, 250° F; coolant temperature, 250° F. (Fig. 12 of reference 9.)

Because K is the slope of the line of constant tetraethyl lead concentration, it is necessary to determine the lead response of only one compound in a particular hydrocarbon classification in order to estimate the lead response of other compounds of the same type from their pure ratings. The variation of K with tetraethyl lead concentration is shown in figure VII-15.

Unlike supercharged data in which the percentage increase in power is constant for a given quantity of tetraethyl lead regardless of the pure fuel rating, the percentage increase in critical compression ratio for a given quantity of tetraethyl lead varies with the pure fuel ratings. This variation is illustrated for the paraffins by the curves in figure VII-16.

EFFECTS OF ENGINE CONDITIONS ON LEAD SUSCEPTIBILITY

Fuel-air ratio.—The effects of fuel-air ratio on lead susceptibility are readily seen in figure VII-17. Curves from the standard reference fuel framework for the A. S. T. M. Supercharge rating engine were used in preparing this plot. It is emphasized that the effects shown will vary considerably from one engine or condition to another.

Inlet-air temperature.—The lead susceptibility from tests at different inlet-air temperatures is presented in figure VII-18 at two different fuel-air ratios. For the range of inlet-air temperatures examined, the lead susceptibility of S reference fuel was constant; that is, the percentage increase of knock-limited indicated mean effective pressure caused by the addition of a given amount of tetraethyl lead was the same regardless of the inlet-air temperature.

Spark advance.—Tests made on S reference fuel clear and with 2 ml TEL per gallon at spark advances of 20° and 35°

B. T. C. are shown in figure VII-19. These data indicate that the lead susceptibility of S reference fuel is independent of variations of spark advance.

REFERENCES

1. Calingaert, George: Anti-Knock Compounds. Vol. IV, pt. IV, sec. 42 of The Science of Petroleum. Univ. Press (Oxford), 1938, pp. 3024-3029.
2. Sloop, J. L., Kinney, George R., and Rowe, William H.: Process of Lead-Drop Accumulations on Aircraft-Engine Spark Plugs. NACA MR E5K27, 1945.
3. Mulcahy, B. A., and Zipkin, M. A.: Tests of Improvements in Exhaust-Valve Performance Resulting from Changes in Exhaust-Valve and Port Design. NACA ARR E5G26, 1945.
4. Banks, F. R.: Some Problems of Modern High-Duty Aero Engines and Their Fuels. Jour. Inst. Petroleum Technologists, vol. 23, no. 160, Feb. 1937, pp. 63-137; discussion, pp. 138-177.
5. Hives, E. W., and Smith, F. L.: High-Output Aircraft Engines. SAE Jour. (Trans.), vol. 46, no. 3, March 1940, pp. 106-117.
6. Mulcahy, B. A., and Zipkin, M. A.: The Effects of an Increase in the Concentration of Ethylene Dibromide in a Leaded Fuel on Lead Deposition, Corrosion of Exhaust Valves, and Knock-Limited Power. NACA ARR E5E04a, 1945.
7. Kinney, George R., and Niemi, Richard O.: The Effect of Ethylene Dibromide on the Knock-Limited Performance of Leaded and Nonleaded S Reference Fuel. NACA MR E6B12, 1946.
8. Barnett, Henry C.: Lead Susceptibility of Paraffins, Cyclo-paraffins, and Olefins. NACA ARR 3E26, 1943.
9. Barnett, Henry C., and Imming, Harry S.: The Effect of Engine Conditions on the Lead Susceptibility of Paraffinic Fuels. NACA ARR E4J02, 1944.
10. Heron, S. D., and Beatty, Harold A.: Aircraft Fuels. Jour. Aero. Sci., vol. 5, no. 12, Oct. 1938, pp. 463-479.
11. Imming, Harry S.: The Effect of Piston-Head Temperature on Knock-Limited Power. NACA ARR E4G13, 1944.
12. Smittenberg, J., Hoog, H., Moerbeek, B. H., and v. d. Zijden, M. J.: Octane Ratings of a Number of Pure Hydrocarbons and Some of Their Binary Mixtures. Jour. Inst. Petroleum, vol. 26, no. 200, June 1940, pp. 294-300.

CHAPTER VIII

ANTIKNOCK BLENDING CHARACTERISTICS OF FUELS

For many years it has been known that all hydrocarbons do not exhibit the same antiknock blending characteristics. Lovell and Campbell (reference 1) illustrated this fact, and Smittenberg *et al* (reference 2) likewise clearly demonstrated that the antiknock characteristics of fuel blends depend upon the nature of the components in the blend.

An investigation was initiated in 1943 by Sanders (reference 3) to ascertain the possibility of developing a method for predicting the knock limits of fuel blends under supercharged and nonsupercharged engine operating conditions. In the original phases of this analysis, results of critical-compression-ratio (nonsupercharged) rating methods rather than results of supercharged methods were emphasized because more complete data were available and the analysis required was more detailed.

SYMBOLS

The following symbols are used in this chapter:

A, B	constants characteristic of fuels
a, b, c	constants
F	$=N_1(B_1R_1-B_2R_2)+B_2R_2$
G	$=N_1(B_1-B_2)+B_2=N_1B_1+(1-N_1)B_2$
H	height of compression chamber, inches
k	quantity of knock-producing agent generated per unit mass
N	mass fraction
P	knock-limited indicated mean effective pressure
R	compression ratio
W, X, Y	constants in hyperbolic blending relation
β	blending constant
ρ	density
Subscripts:	
a	value of subscript 1 at asymptote
b	blend
cr	critical
d	pertaining to knock agent produced under conditions at which blend will knock
i	isoctane
m	pertaining to knock-producing agent at condition of incipient knock
t	total
$1, 2, 3, \dots$	pertaining to components 1, 2, 3... in fuel blend

DERIVATIONS OF BLENDING EQUATIONS

The derivations developed in reference 3 require a clear understanding of the principles of knock testing by supercharged and nonsupercharged methods. In supercharged engine tests, all conditions except inlet-air pressure and fuel-air ratio are held constant. Fuel-air ratio may or may not be constant depending upon the operating technique employed. Inlet-air pressure is increased until a predetermined

standard knock intensity is observed. The knock-limited indicated mean effective pressure or the density of air in the cylinder charge may be used as a measure of the knock limit of the fuel being tested.

In nonsupercharged engine tests, all conditions except compression ratio are held constant. The compression ratio is increased until the standard knock intensity is reached. The compression ratio at this intensity is the measure of the knock limit and is generally termed critical compression ratio. Changes of inlet-air pressure do not affect any of the cyclic temperatures; however, an increase of compression ratio increases the temperature at the end of compression, the combustion temperature, and the end-gas temperature. The primary difference between nonsupercharged and supercharged engine methods thus lies in the fact that knock limits in nonsupercharged engines are measured at varying end-gas temperatures, whereas in supercharged engines knock limits are determined at the same end-gas temperature. (See reference 4.)

In order to derive the desired blending equations, certain assumptions were made in reference 3 regarding the mechanism of knock:

(1) Knock results from the reaction of some intermediate products during combustion, and the nature of these products as well as the reaction between them is the same regardless of the fuel used. This assumption is introduced in order that the knocking properties of fuels may be treated as additive properties.

(2) Knock occurs when the mass of knock-producing agents per unit volume reaches a given value at any end-gas temperature.

(3) At any one end-gas temperature and for any one fuel component, the mass per unit volume of the knock-producing agent evolved by that component is directly proportional to the mass of the component per unit volume; or, as stated in reference 3, a unit mass of a particular component will generate a certain mass of knock-producing agent regardless of the other components in the blend.

(4) In order to consider the differences in knock limits of the blend components, it is assumed that for any one end-gas temperature, the mass per unit volume of the knock-producing agents is a function of the molecular structure of the fuel.

(5) During combustion the temperature increase for all fuels or blends under consideration is the same. On the basis of this assumption it is possible to relate fuel knock limits to engine compression density and temperature instead of end-gas density and temperature. Many hydrocarbons of interest fulfill this condition, but some classes of fuels, such as alcohols and ethers, do not (reference 3).

The initial step in the derivation of the desired equation is justified by assumptions (1) and (2).

$$\rho_m = \rho_1 + \rho_2 + \rho_3 + \dots \quad (1)$$

where

ρ_m

mass per unit volume of knock-producing agent at condition of incipient knock

$\rho_1, \rho_2, \rho_3, \dots$ mass per unit volume of knock agent produced by each component under conditions at which the blend will knock

It has been stated previously that the end-gas temperatures are constant for supercharged-engine tests but vary with the critical compression ratio of the fuel in nonsupercharged-engine tests; therefore, from assumptions (3) and (4) the following relations hold for supercharged tests:

$$\rho_1 = k_1 \rho_t N_1$$

$$\rho_2 = k_2 \rho_t N_2$$

$$\rho_3 = k_3 \rho_t N_3$$

where

N_1, N_2, N_3 mass fractions of components 1, 2, 3, respectively, in fuel blend

ρ_t total mass of fuel per unit volume

k_1, k_2, k_3 quantity of knock-producing agent generated per unit mass by components 1, 2, 3, respectively

When the pure compound 1 is tested, the knock-limited density of fuel in the charge is $\rho_{t,1}$ and

$$\rho_m = \rho_1 = k_1 \rho_{t,1} \quad (2)$$

Therefore,

$$k_1 = \frac{\rho_m}{\rho_{t,1}}$$

and

$$\rho_1 = \frac{\rho_m}{\rho_{t,1}} \rho_{t,1} N_1$$

Similarly,

$$\rho_2 = \frac{\rho_m}{\rho_{t,2}} \rho_{t,2} N_2$$

and

$$\rho_3 = \frac{\rho_m}{\rho_{t,3}} \rho_{t,3} N_3$$

Substituting these values of $\rho_1, \rho_2, \rho_3, \dots$ in equation (1) yields

$$\rho_m = \frac{\rho_m}{\rho_{t,1}} \rho_{t,1} N_1 + \frac{\rho_m}{\rho_{t,2}} \rho_{t,2} N_2 + \frac{\rho_m}{\rho_{t,3}} \rho_{t,3} N_3 + \dots$$

and

$$\frac{1}{\rho_t} = \frac{N_1}{\rho_{t,1}} + \frac{N_2}{\rho_{t,2}} + \frac{N_3}{\rho_{t,3}} + \dots \quad (3)$$

As limited by the assumptions, equation (3) is a blending equation applicable to supercharged-engine data. Because the compression ratio and fuel-air ratio must be the same for the various components in a given application of this equation, knock-limited inlet-air densities may be used instead of the fuel densities for values of $\rho_t, \rho_{t,1}, \rho_{t,2}, \rho_{t,3}, \dots$. With this substitution, equation (3) may be expressed in words as

follows: The reciprocal of the knock-limited inlet-air density of a fuel blend tested by a supercharged-engine method is the weighted average of the reciprocals of the knock-limited inlet-air densities of the pure components.

Indicated mean effective pressure is proportional to inlet-air density; therefore, it can be substituted in equation (3) for density:

$$\frac{1}{P_b} = \frac{N_1}{P_1} + \frac{N_2}{P_2} + \frac{N_3}{P_3} + \dots \quad (3b)$$

where

P_b knock-limited indicated mean effective pressure of fuel blend

P_1, P_2, P_3 knock-limited indicated mean effective pressures of components 1, 2, 3, respectively, when tested individually

For nonsupercharged tests, the charge density at the end of compression is proportional to the compression ratio. By use of an equation similar to equation (2), ρ_t was related to the compression ratio instead of the mass of fuel per unit volume (reference 3). The value of k_1 , however, varies with compression ratio because the compression temperature varies with compression ratio. In order to account for the variation of k_1 , the following relation was assumed (reference 3) between ρ_t and compression ratio R :

$$\rho_t = (A_1 + B_1 R) N_1 \quad (4)$$

where

A_1, B_1 constants characteristic of fuel 1

Similarly,

$$\rho_2 = (A_2 + B_2 R) N_2$$

and

$$\rho_3 = (A_3 + B_3 R) N_3$$

where

A_2, B_2, A_3, B_3 constants characteristic of fuels 2 and 3

Substituting these values in equation (1) gives

$$\rho_m = N_1 (A_1 + B_1 R) + N_2 (A_2 + B_2 R) + N_3 (A_3 + B_3 R) + \dots \quad (5)$$

The value of A_1 may be determined by letting $N_1=1, N_2=0, N_3=0$, and $R=R_{1,cr}$ where $R_{1,cr}$ is the critical compression ratio of fuel 1 when tested individually.

$$\rho_m = A_1 + B_1 R_{1,cr}$$

$$A_1 = \rho_m - B_1 R_{1,cr}$$

Likewise,

$$A_2 = \rho_m - B_2 R_{2,cr}$$

and

$$A_3 = \rho_m - B_3 R_{3,cr}$$

Substituting in equation (5) gives

$$R = \frac{N_1 B_1 R_{1,cr} + N_2 B_2 R_{2,cr} + N_3 B_3 R_{3,cr} + \dots}{N_1 B_1 + N_2 B_2 + N_3 B_3 + \dots} \quad (6)$$

As limited by the assumptions, equation (6) is the blending equation applicable to nonsupercharged-engine data.

In this equation B_1 , B_2 , B_3 . . . are defined as blending constants and each fuel has a blending constant that is independent of the other fuels in the blend and is determined by the critical compression ratio of the fuel and the rate of change of knock limit with inlet-air temperature.

For two-component blends, $N_2=1-N_1$ and equation (6) may be written as

$$R = \frac{N_1(B_1 R_{1,cr} - B_2 R_{2,cr}) + B_2 R_{2,cr}}{N_1(B_1 - B_2) + B_2} \quad (7)$$

Equation (7) is the equation of an equilateral hyperbola asymptotic to

$$N = \frac{B_2}{B_2 - B_1} = N_{a,1}$$

and

$$R = \frac{B_1 R_1 - B_2 R_2}{B_1 - B_2} = R_a$$

where

$N_{a,1}$ value of N_1 at asymptote

R_a value of R at asymptote

The asymptotic form of equation (7) is

$$(R - R_a)(N_a - N_1) = N_a(R_2 - R_a) \quad (8)$$

According to reference 3, it is unnecessary to know the absolute values of the constants in equations (6) and (7), but the relative values must be known; that is, one component may be assigned an arbitrary value of the constant, thereby fixing the values of the constants for all other components tested at the same conditions. Values of B for other components may be found by determining the critical compression ratio of the pure component and of one blend of the component with another component for which the blending constant is known. With these values the equation can be solved for the value of the unknown blending constant. When the relative values of B have been determined for all compounds, the knock limits of all blends may be computed from the blending equation.

GRAPHICAL SOLUTION OF BLENDING EQUATION FOR NONSUPERCHARGED-ENGINE DATA

A graphical method was suggested in reference 3 for determination of the blending characteristics of fuels when tested in nonsupercharged engines. Equation (7) may be put into the following form:

$$F = RG \quad (9)$$

where

$$F = N_1(B_1 R_1 - B_2 R_2) + B_2 R_2$$

and

$$G = N_1(B_1 - B_2) + B_2 = N_1 B_1 + (1 - N_1) B_2$$

If R is held constant, F is proportional to G . In figure VIII-1, the value of F has been plotted against the value of G for values of R between 2 and 15. Inasmuch as G is actually the weighted average value of B_1 and B_2 , the abscissa of

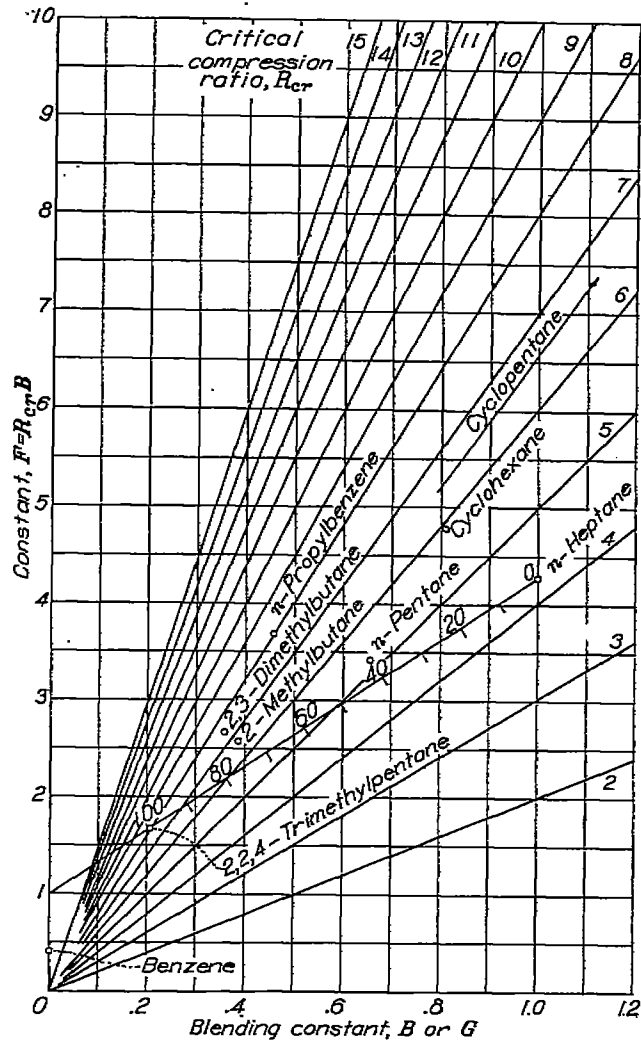


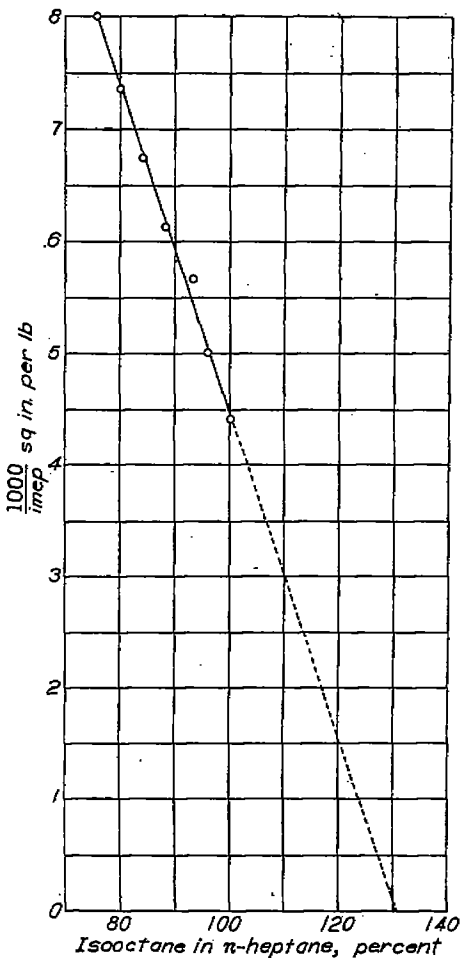
FIGURE VIII-1.—Blending chart for A. S. T. M. Motor method. (Fig. 1 of reference 3.)

figure VIII-1 has been marked G or B . All potential fuel components whose critical compression ratios and blending constants are known may be plotted on this chart.

A straight line joining the points for any two components represents all blends of the two components. This relation is true because F and G are linear functions of N_1 and, consequently, F is a linear function of G . A point representing any blend of the two components divides the line in the same ratio as that in which the components exist in the blend. For example, a blend containing 60 percent 2,2,4-trimethylpentane (isoctane) and 40 percent n -heptane will be on the line joining the points for the two components and will be 60 percent of the distance from n -heptane to 2,2,4-trimethylpentane.

EXPERIMENTAL VERIFICATION OF BLENDING EQUATIONS

Heron and Beatty (reference 5) have shown that if the reciprocal of the knock-limited indicated mean effective pressures of blends of isoctane and n -heptane is plotted against the percentage of isoctane in the blends, a straight line will result. This fact substantiates equation (3) for supercharged-engine data. The data obtained in reference 5 are shown in figure VIII-2 (a).



(a) 17.6 engine. Compression ratio, 5.6; engine speed, 900 rpm; inlet-air temperature, 225° F; coolant temperature, 300° F; spark advance, 20° B. T. C. (Fig. 2 of reference 3.)

FIGURE VIII-2.—Effect of blend composition on knock-limited performance.

Further verification of this relation is presented in figure VIII-2 (b), which shows data for S and M reference fuel blends investigated in reference 3.

Data obtained in references 2 and 6 were used in reference 3 for verification of the blending equation developed for nonsupercharged engine tests. The blending equation for n-heptane and isooctane under A. S. T. M. Motor method conditions is shown in reference 2 to be

$$N_t = \left(\frac{1.369 - H}{1.954 - H} \right) 179 \quad (10)$$

where

N_t isooctane in blend, percent

H height of compression chamber, inches

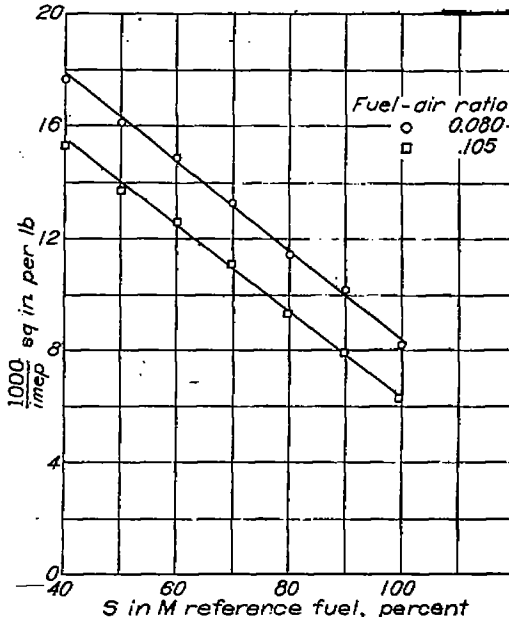
The value of N_t is given on a volumetric basis in reference 2 but, since the densities of the two components are about the same, N may be used as the mass fraction. The length of the engine stroke was 4.5 inches; therefore, the relation between R and H can be expressed as follows:

$$R = \frac{4.5 + H}{H} \quad (11)$$

Combining equations (10) and (11) gives

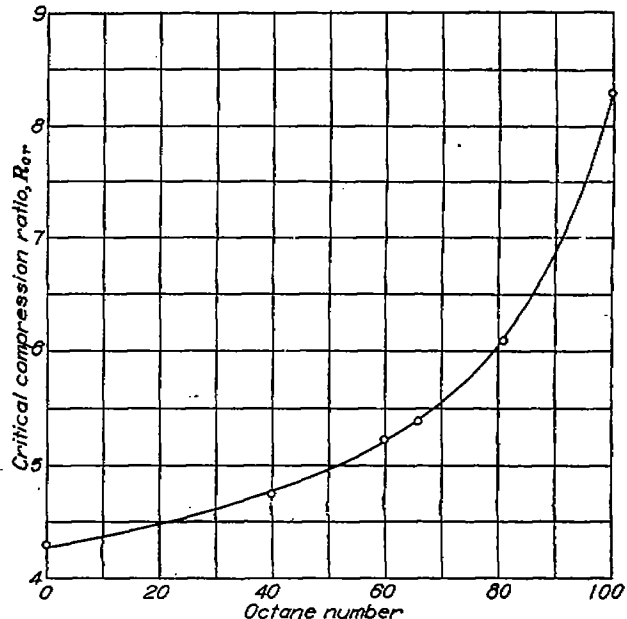
$$(R - 3.3)(125 - N_t) = 125 \quad (12)$$

The equilateral hyperbola represented by equation (12) is asymptotic to $R = 3.3$ and $N_t = 125$. The relation between R and N_t is shown in figure VIII-3(a). Inasmuch as the



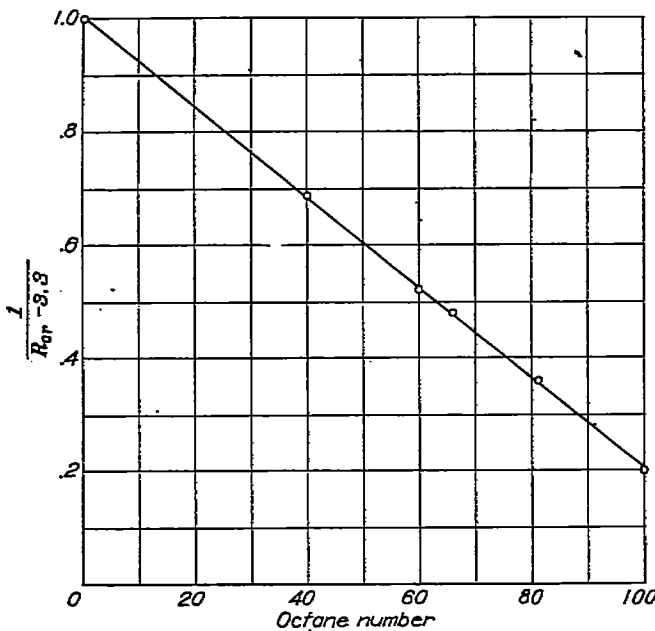
(b) CFR engine. Compression ratio, 7.0; engine speed, 2000 rpm; inlet-air temperature, 250° F; coolant temperature, 250° F; spark advance, 35° B. T. C. (Fig. 3 of reference 3.)

FIGURE VIII-2.—Concluded. Effect of blend composition on knock-limited performance.



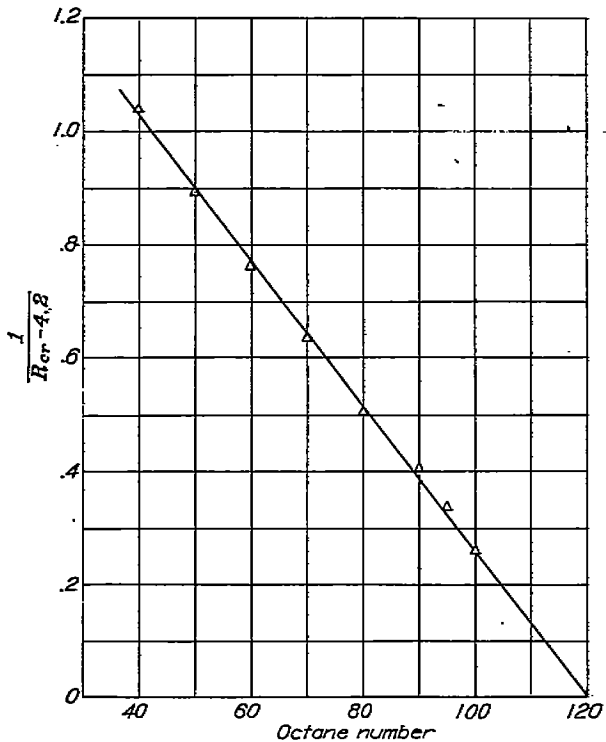
(a) A. S. T. M. Motor method. (Fig. 4 of reference 3.)

FIGURE VIII-3.—Blending characteristics of 2,2,4-trimethylpentane and n-heptane.



(b) A. S. T. M. Motor method; reciprocal plot. (Fig. 5 of reference 3.)

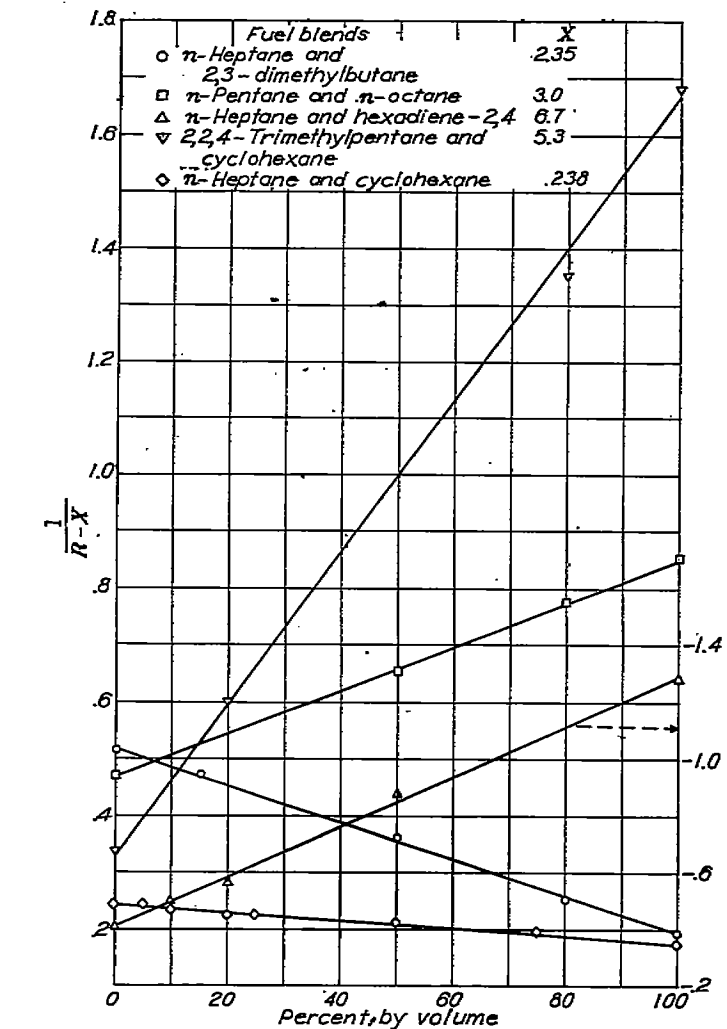
FIGURE VIII-3.—Continued. Blending characteristics of 2,2,4-trimethylpentane and n-heptane.



(c) A. S. T. M. Research method; reciprocal plot. (Fig. 6 of reference 3.)

FIGURE VIII-3.—Concluded. Blending characteristics of 2,2,4-trimethylpentane and n-heptane.

components of this system are n-heptane and iso-octane, N is equivalent to octane number. (See ch. III.) The curve in figure VIII-3(a) is drawn from equation (12), whereas the data points shown are taken directly from reference 2. The data from figure VIII-3(a) were replotted (reference 3)

FIGURE VIII-4.—Verification of hyperbolic blending relation for knock ratings of fuel blends by A. S. T. M. Motor method. (Fig. 7 of reference 3.) Equation of hyperbola: $(R-X)(Y-N)=W$.

as shown in figure VIII-3(b) as confirmation of the hyperbolic blending relation.

Similar data for the A. S. T. M. Research method were reported by Brooks (reference 6) and are plotted in figure VIII-3(c). Here again the relation is linear, but the intercepts are 120 and 1.53 as compared with 125 and 1.0 for the A. S. T. M. Motor method shown in figure VIII-3(b). The equation for the A. S. T. M. Research method data is

$$(R-4.2)(120-N)=78.3 \quad (13)$$

From the foregoing comparison of the A. S. T. M. Motor and Research methods, it was concluded (reference 3) that the asymptotes of the blending hyperbola change with changing engine conditions.

Blending relations for other two-component blending systems are shown in figure VIII-4. The data for these systems were taken from reference 2. Three two-component systems investigated in reference 2 did not follow the hyperbolic relation. These systems are shown in figure VIII-5.

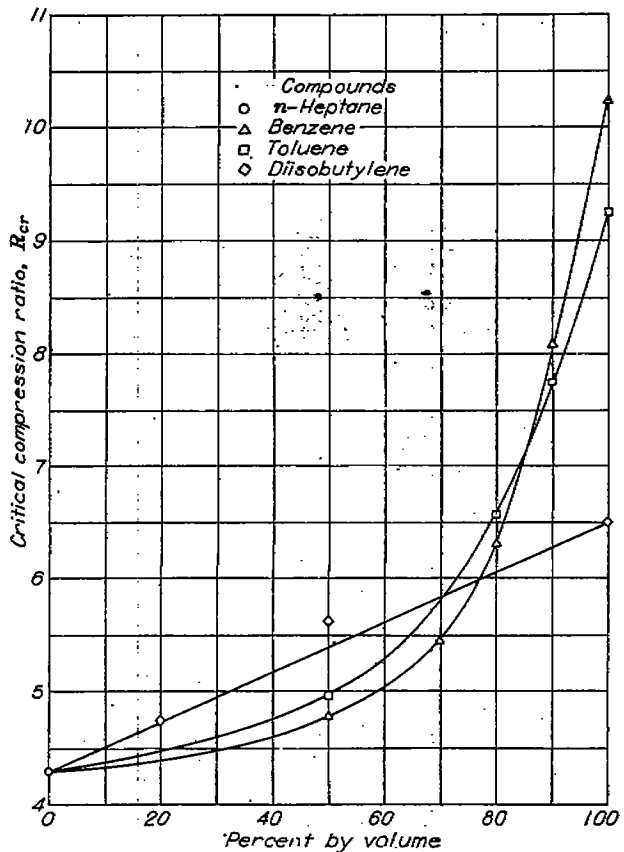


FIGURE VIII-5.—Blending characteristics of diisobutylene, benzene, and toluene in *n*-heptane by A. S. T. M. Motor method. (Fig. 6 of reference 3.)



FIGURE VIII-6.—View of combustion chamber showing location of thermocouple in end zone. (Fig. 1 of reference 8.)

In connection with the system of blends of *n*-heptane and benzene (fig. VIII-5), it was found that up to a concentration of 90 percent benzene a hyperbolic relation is valid, but the value for pure benzene does not follow the relation (reference 3). In explanation of this discrepancy it should be noted that the authors of reference 2 expressed the belief that the knock rating of pure benzene might be in error.

In order to illustrate the invariance of the blending constant, a series of calculations was made involving several hydrocarbons (reference 3). The constants evolved in these calculations have been plotted on figure VIII-1. Values for cyclopentane and *n*-propylbenzene were computed from data reported in reference 7.

APPLICABILITY OF EQUATIONS TO DIFFERENT BLENDING AGENTS AND ADDITIVES

The preliminary data used in support of the derivation developed in the foregoing pages were admittedly meager; consequently, an extensive investigation was initiated to determine the general applicability of the blending equation. In the course of this investigation a number of fuels of various types were studied under different engine operating conditions in supercharged engines. The results of this investigation are reported in the succeeding paragraphs.

Paraffins.—The base fuels used in this phase of the study were an alkylate blending agent and a virgin base gasoline. The blending agents examined were:

- Triptane (2,2,3-trimethylbutane)
- Isopentane (2-methylbutane)
- Diisopropyl (2,3-dimethylbutane)
- Neohexane (2,2-dimethylbutane)
- Hot-acid octane

All blending agents and base stocks contained 4.0 ml TEL per gallon. Inspection data for these fuels are included in appendix A, table A-9. (See references 8 and 9.)

The experimental studies of these fuels were made in a single air-cooled aircraft cylinder mounted on a CUE crankcase. This apparatus is described in detail in reference 9 with the exception of a special thermocouple embedded in the cylinder head about $\frac{1}{16}$ inch from the combustion-chamber wall at a position estimated to be very near the exhaust end zone (fig. VIII-6). The temperature at this thermocouple was held constant by means of an automatic potentiometer regulator that controlled cooling-air flow across the cylinder. This instrumentation is consistent with the assumption made in reference 3 that for the blending equation to be applicable to supercharged engine data the cyclic and end-gas temperatures must be held constant.

In figure VIII-7, a portion of the data determined in the investigation of reference 8 is shown. The ordinate scales of these figures are inverted reciprocal scales. When plotted in this manner, the data should fall on a straight line if the results are applicable to equation (3b). It is apparent in these figures that the paraffinic fuels examined, with the

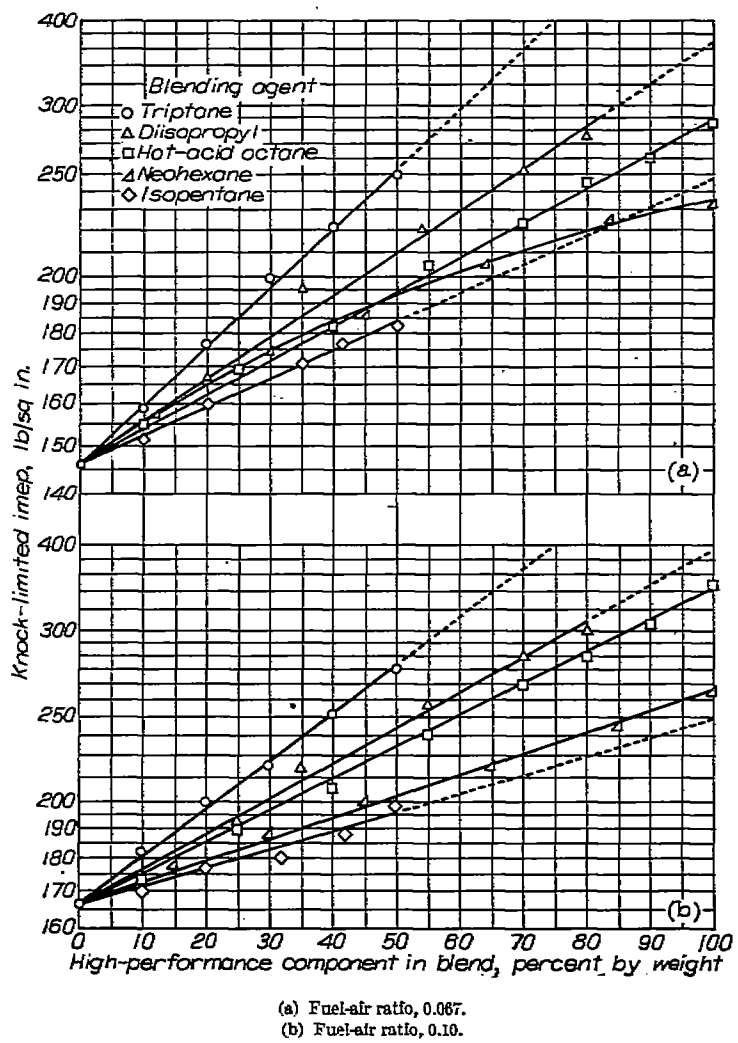
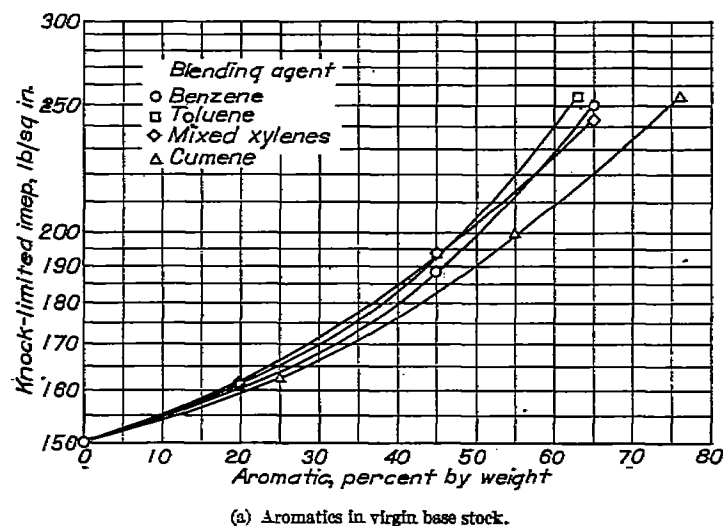


FIGURE VIII-7.—Blending characteristics of paraffins in virgin base stock leaded to 4 ml TEL per gallon in full-scale air-cooled aircraft cylinder. Compression ratio, 7.7; engine speed, 2000 rpm; spark advance, 20° B. T. C.; inlet mixture temperature, 350° F; exhaust back pressure, atmospheric. (Data taken from reference 8.)

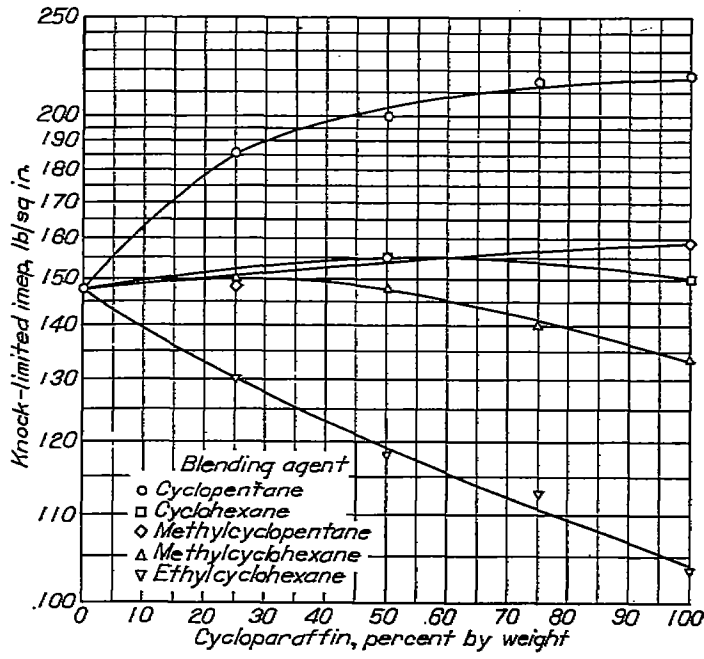
exception of neohexane at the lean fuel-air ratio, are in accord with the blending equation for supercharged-engine data.

These data were obtained at a spark advance of 20° B. T. C., a condition considered to be relatively mild; consequently, additional tests were made at a more severe condition (spark advance, 30° B. T. C.). The results of these advanced spark studies are essentially the same as those shown in figure VIII-7; that is, the relation between the reciprocal indicated mean effective pressure and composition was linear. In this case, however, data for neohexane followed the relation at both lean and rich mixtures. (See reference 8.)

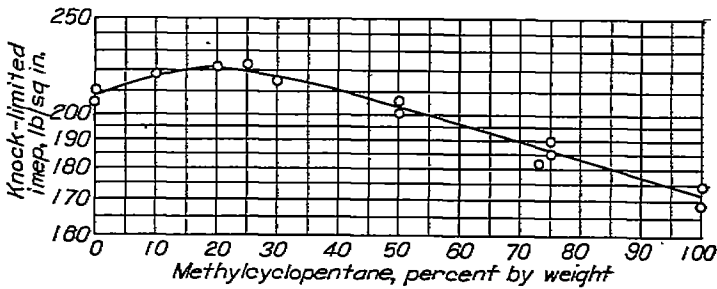
Aromatics.—Experimental verification of the blending relation for aromatic fuels proved to be difficult inasmuch as pure aromatics have exceptionally high knock limits and are prone to preignite. (See reference 10.) Despite these obstacles, however, a reasonable quantity of data was obtained to determine the limitations of this class of compounds. In pursuing this phase of the investigation, no effort was made to attain the knock limit of the pure aromatics. Instead, each aromatic was blended with a paraffinic base stock and the concentration was increased until the power level was con-



(a) Aromatics in virgin base stock.



(b) Cycloparaffins in virgin base stock.



(c) Methylcyclopentane in aviation kerosene.

FIGURE VIII-8.—Blending characteristics of various fuels leaded to 4 ml TEL per gallon in full-scale air-cooled aircraft cylinder. Compression ratio, 7.8; engine speed, 2250 rpm; spark advance, 20° B. T. C.; inlet mixture temperature, 240° F; end-zone temperature, 400° F; exhaust back pressure, 16 inches of mercury absolute; fuel-air ratio, 0.10. (Data taken from reference 10.)

sidered too high to warrant further increases. Results of these tests are shown in figure VIII-8 (a). Here it is seen that the relation between composition and reciprocal indicated mean effective pressure is nonlinear.

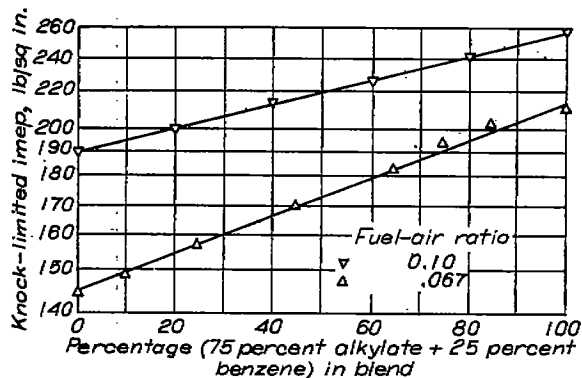


FIGURE VIII-9.—Blending characteristics of benzene, virgin base stock, and aviation alkylate in full-scale air-cooled aircraft cylinder. Concentration of benzene in all blends, 25 percent by volume; compression ratio, 7.7; engine speed, 2000 rpm; spark advance, 20° B. T. C.; inlet mixture temperature, 240° F; end-zone temperature, 350° F. (Fig. 3 (b) of reference 11.)

A modification of equation (3b) is proposed in reference 9 in order to account for fuel components that do not follow the linear blending relations.

$$P_b = \frac{P_1 N_1 B_1 + P_2 N_2 B_2 + P_3 N_3 B_3 + \dots}{N_1 B_1 + N_2 B_2 + N_3 B_3 + \dots} \quad (14)$$

Another form of equation (14) is (reference 9)

$$\frac{N_1 \beta_1 + N_2 \beta_2 + N_3 \beta_3 + \dots}{P_b} = \frac{N_1 \beta_1}{P_1} + \frac{N_2 \beta_2}{P_2} + \frac{N_3 \beta_3}{P_3} + \dots \quad (15)$$

$\beta_1, \beta_2, \beta_3, \dots$ blending constants related to constants B_1, B_2, B_3, \dots by the following equations:

$$\beta_1 = P_1 B_1$$

$$\beta_2 = P_2 B_2$$

$$\beta_3 = P_3 B_3$$

Both equations (14) and (15) are equal to equation (3b) when $\beta_1 = \beta_2 = \beta_3$ or $P_1 B_1 = P_2 B_2 = P_3 B_3$.

Performance data for aromatic fuels were employed (reference 10) to determine the validity of equation (15). From the analysis it was concluded that the equation does not apply over the entire range of composition; that is, the blending constant β for a given aromatic varies somewhat.

From a practical point of view, however, marketed aviation fuels seldom contain concentrations of aromatics in excess of 25 percent (generally much less), and for a limited range of concentration it is believed that equation (15) may be useful. Evidence to support this belief is shown in figure VIII-9.

It is seen in this figure that the blending relations are linear for a 25-percent concentration of benzene in blends of alkylate and virgin-base stock. Similar results were obtained with toluene, mixed xylenes, and cumene (reference 11). On the basis of figure V-6 (c) described in chapter V it is doubtful if the relations would be linear for concentrations much greater than 25 percent.

Cycloparaffins.—The results of tests with cycloparaffinic fuels are shown in figure VIII-8 (b). As in the case of the

aromatic fuels, the cycloparaffinic fuels examined failed to follow the blending relation in the form of either equation (3b) or equation (15).

One result of unusual interest was found in the cycloparaffinic investigation of reference 10. (See fig. VIII-8 (c).) In this figure it is seen that methylecyclopentane, when blended with alkylate, produced intermediate blends having higher knock limits than either of the pure components. This was also true for other cycloparaffins in blends with different base stocks. (See reference 10.)

Special additives.—The influence of special additives (for example, tetraethyl lead and xylidines) on the applicability of the blending equation is discussed in reference 9. In brief, the effect of such additives is essentially the same as the effect of low concentrations of aromatics mentioned in connection with figure VIII-9. That is, the blending equation applies so long as the concentration of such additives in the major blend components is constant.

PREPARATION OF BLENDING CHARTS

In the preceding sections of this chapter, a blending equation has been described and its limits of applicability have been shown by experimental data. The remainder of this chapter is devoted to an analysis that will illustrate the practical use of this equation. Specifically, the purpose of this analysis is to illustrate the preparation of performance charts from which blends of any desired lean and rich antiknock ratings can be selected. These charts are based entirely upon the A. S. T. M. Aviation (lean) and A. S. T. M. Supercharge (rich) knock rating methods. Experimental data upon which the charts are based may be found in appendix A, table A-10. (See reference 12.)

Performance numbers.—The scale of performance numbers for fuel knock rating terminates at 161. (See ch. III.) It was therefore necessary to extrapolate the scale in order to evaluate blends that would have antiknock ratings in excess of 161 by the A. S. T. M. Supercharge method. This extrapolation was made by plotting the performance numbers against knock-limited indicated mean effective pressures from a reference-fuel framework given in reference 13. The rating scale thus developed is shown in figure VIII-10. Although a definite break in this curve occurs at a performance number of 130, the curve appears to be linear between 130 and 160. On the assumption that this linear relation is true, a straight line was drawn through the points at 130 and 161 and extended to a performance number of 200.

Ternary blends.—As an example of the preparation of a performance chart, consider first that it is desired to know the A. S. T. M. Aviation and the A. S. T. M. Supercharge performance numbers of all possible ternary blends of hot-acid octane, an aviation alkylate, and a virgin base stock. A plot of composition against the reciprocal of the knock-limited indicated mean effective pressure for binary blends of any two of these fuels will result in a straight line. The three binary combinations of these materials are shown in figure VIII-11.

In the next operation, lines of constant performance number are drawn on the plot (shown as dashed lines on fig. VIII-11). These lines are established by reading values of indicated mean effective pressure at equal increments of performance number in figure VIII-10. The data as shown in figure VIII-11 comprise the basic information needed to establish A. S. T. M. Supercharge rating lines on the final chart for multicomponent blends.

For convenience in relating composition and knock-limited performance of ternary fuel blends, all performance charts in this investigation were prepared on triangular coordinate paper. The equation of a straight line on triangular coordinate paper is of the form

$$a = bN_1 + cN_2 + N_3$$

where

a, b, c constants

N_1, N_2, N_3 concentration of components 1, 2, and 3 in

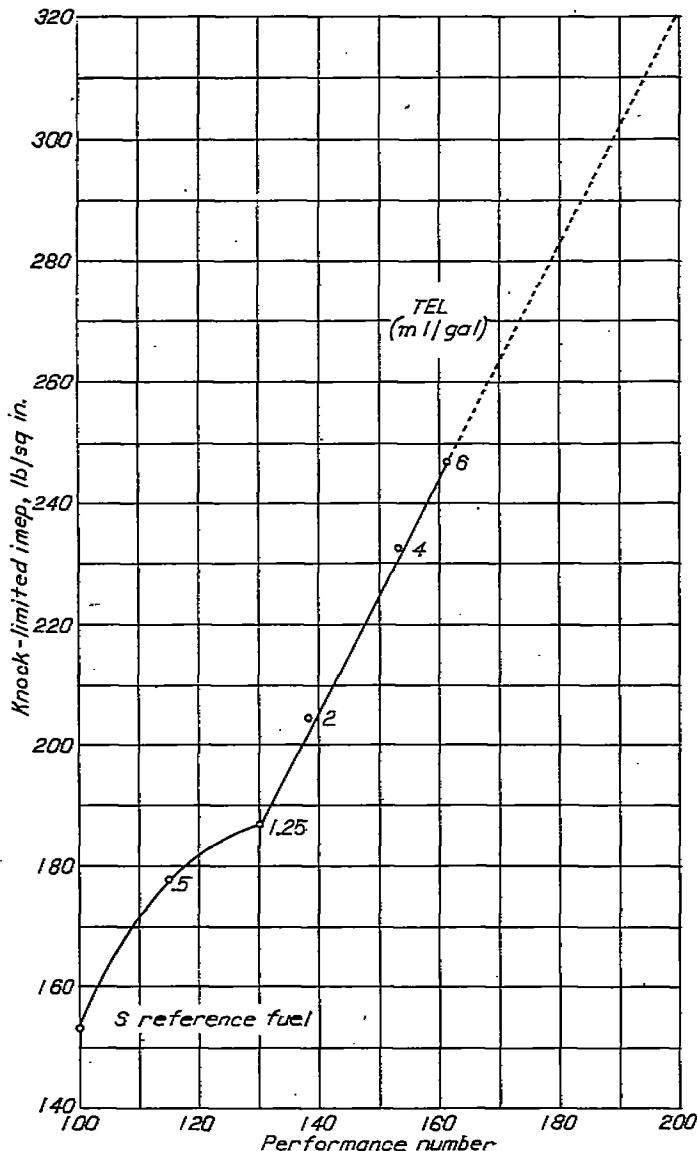


FIGURE VIII-10.—Relation between performance number and knock-limited indicated mean effective pressure by A. S. T. M. Supercharge method. Fuel-air ratio, 0.11. (Fig. 1 of reference 12.)

ternary blend. Any equation relating knock-limited performance and blend composition that can be reduced to this form can be represented by a straight line of constant performance on triangular coordinate paper. Equation (3b) can be reduced to this form by multiplying through by any one of the performance values P_1 , P_2 , or P_3 .

The performance chart for the system of hot-acid octane, aviation alkylate, and virgin base stock is shown in figure VIII-12 (a). Lines of constant performance number in this figure were determined by noting the intersections of the constant performance lines (fig. VIII-11) with the blending lines. For example, the 150-performance-number line in figure VIII-11 intersects the blending line of hot-acid octane and aviation alkylate at a composition of 32 percent hot-acid octane and 68 percent alkylate and intersects the blending line of hot-acid octane and virgin base stock at a composition

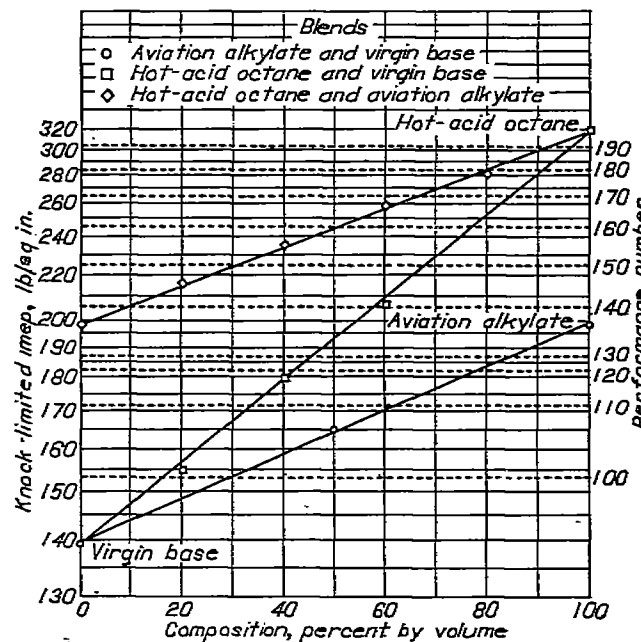
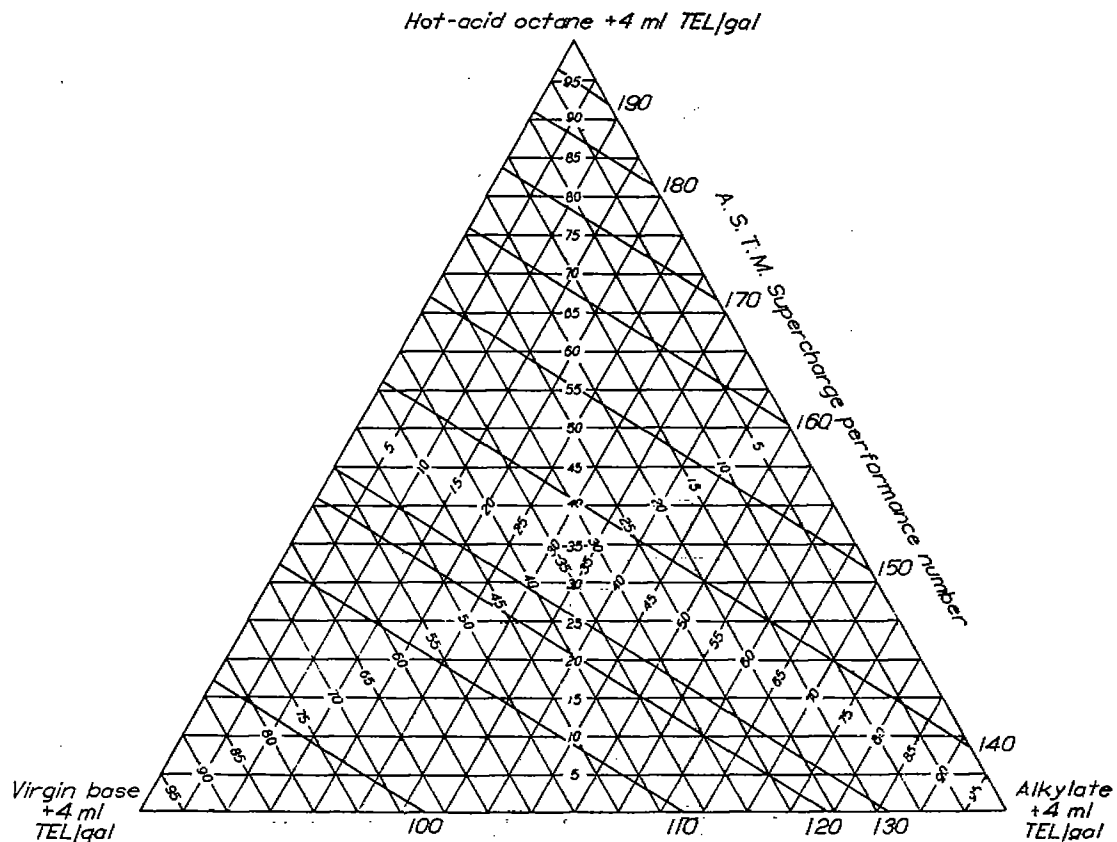


FIGURE VIII-11.—A. S. T. M. Supercharge blending characteristics of hot-acid octane, aviation alkylate, and virgin base stock leaded to 4 ml TEL per gallon. Fuel-air ratio, 0.11. (Fig. 2 of reference 12.)

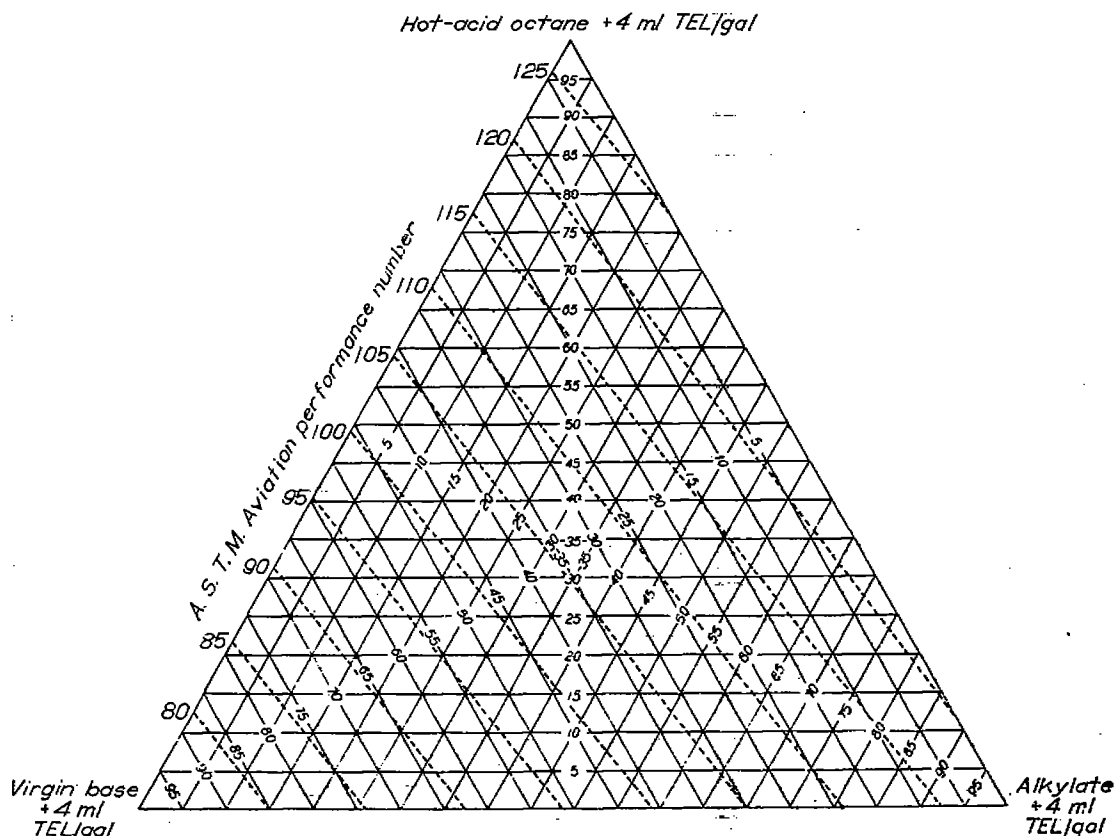
of 67 percent hot-acid octane and 33 percent virgin base stock. These two compositions were plotted on figure VIII-12 (a) and joined by a straight line. Any point on this line represents a blend of hot-acid octane, alkylate, and virgin base stock that will give a performance number of 150 in the A. S. T. M. Supercharge engine at a fuel-air ratio of 0.11. All other lines in figure VIII-12 (a) were established in the same manner.

The lines in figure VIII-12 (a) are parallel, which is true when curves of the type shown in figure VIII-11 are linear. On the basis of data presented earlier in this chapter it appears that most paraffinic fuels do blend linearly. Even though certain constituents, such as the aromatics or ethers, do not blend linearly in combination with paraffinic base fuels, the procedure just outlined for the preparation of performance-number charts is not altered. In such cases,



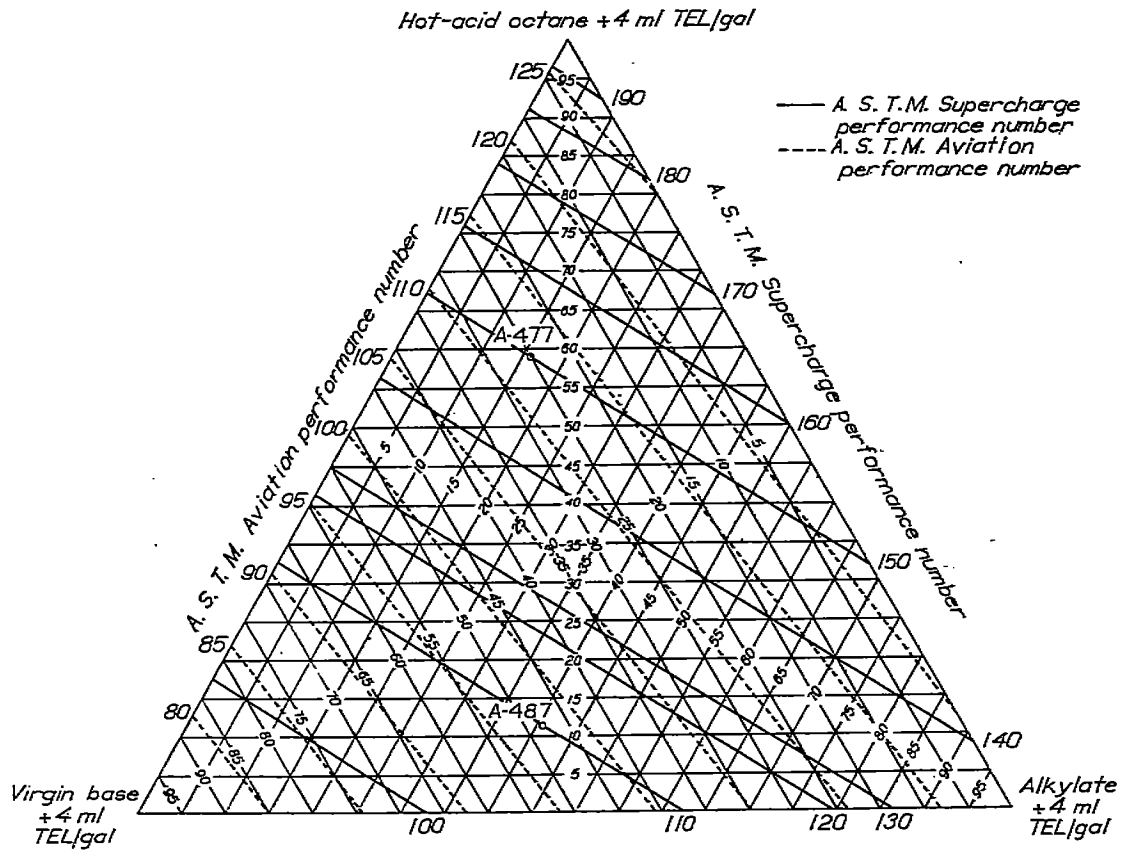
(a) A. S. T. M. Supercharge method. (Fig. 3 of reference 12.)

FIGURE VIII-12.—Blending charts for hot-acid octane, aviation alkylate, and virgin base stock.



(b) A. S. T. M. Aviation method. (Fig. 5 of reference 12.)

FIGURE VIII-12.—Continued. Blending charts for hot-acid octane, aviation alkylate, and virgin base stock.



(c) A. S. T. M. Supercharge and A. S. T. M. Aviation methods. (Fig. 6 of reference 12.)

FIGURE VIII-12.—Concluded. Blending charts for hot-acid octane, aviation alkylate, and virgin base stock.

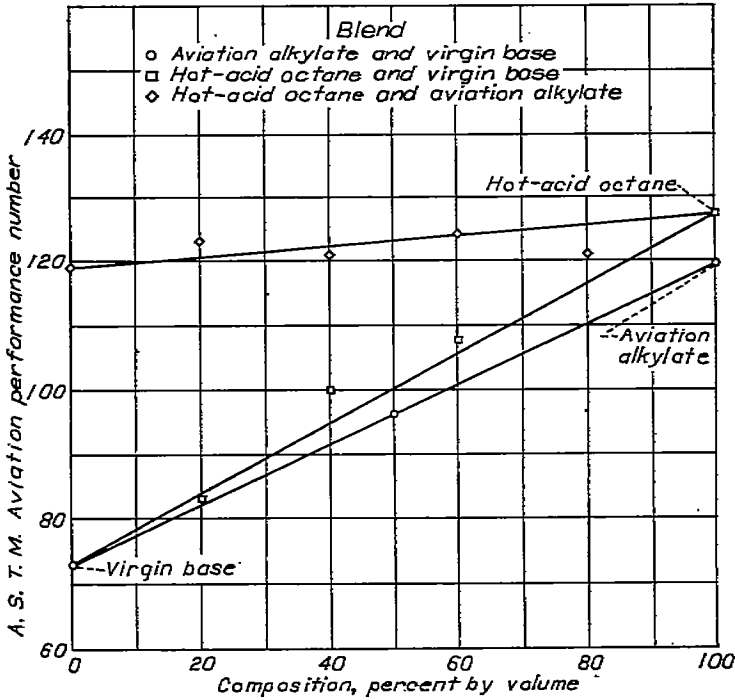


FIGURE VIII-13. A. S. T. M. Aviation blending characteristics of hot-acid octane, aviation alkylate, and virgin base stock leaded to 4 ml TEL per gallon. (Fig. 4 of reference 12.)

however, the charts prepared are subject to some error that arises from the assumption that curves of constant performance number on triangular coordinate paper are linear. Moreover, a nonlinear relation in a plot of the type shown in figure VIII-11 results in a variation of slope with performance number on the final triangular plot.

The procedure used for determining the lines of constant A. S. T. M. Aviation performance numbers for blends of the same fuels used in preparing figure VIII-12 (a) differs from that used for A. S. T. M. performance in that performance numbers are plotted directly against composition on linear coordinate paper and an estimated "best" curve is drawn through the data points to determine the binary blending relations shown in figure VIII-13. There is nothing to justify the use of this empirical method for dealing with A. S. T. M. Aviation ratings other than the fact that the end result agrees reasonably well with the experimental results. One or two exceptions to this method will be pointed out later.

The composition at the intersections of a given constant performance line with the blending lines (fig. VIII-13) were plotted on triangular coordinate paper and joined by straight lines. The resulting performance lines are shown in figure VIII-12 (b). The final chart (fig. VIII-12 (c)) was obtained by superimposing figure VIII-12 (b) on figure VIII-12 (a). Additional charts are shown in appendix B, figures B-1 and B-2 for other blending agents and base stocks. (All blends contained 4 ml TEL/gal.)

In appendix B, figure B-1 (e) represents the system of blends for cumene, virgin base, and alkylate; the lines showing A. S. T. M. Supercharge performance numbers were determined by plotting peak knock-limited-power values rather than power values at a fuel-air ratio of 0.11. This deviation from the procedure used for all other charts was necessitated by the fact that most of the mixture-response

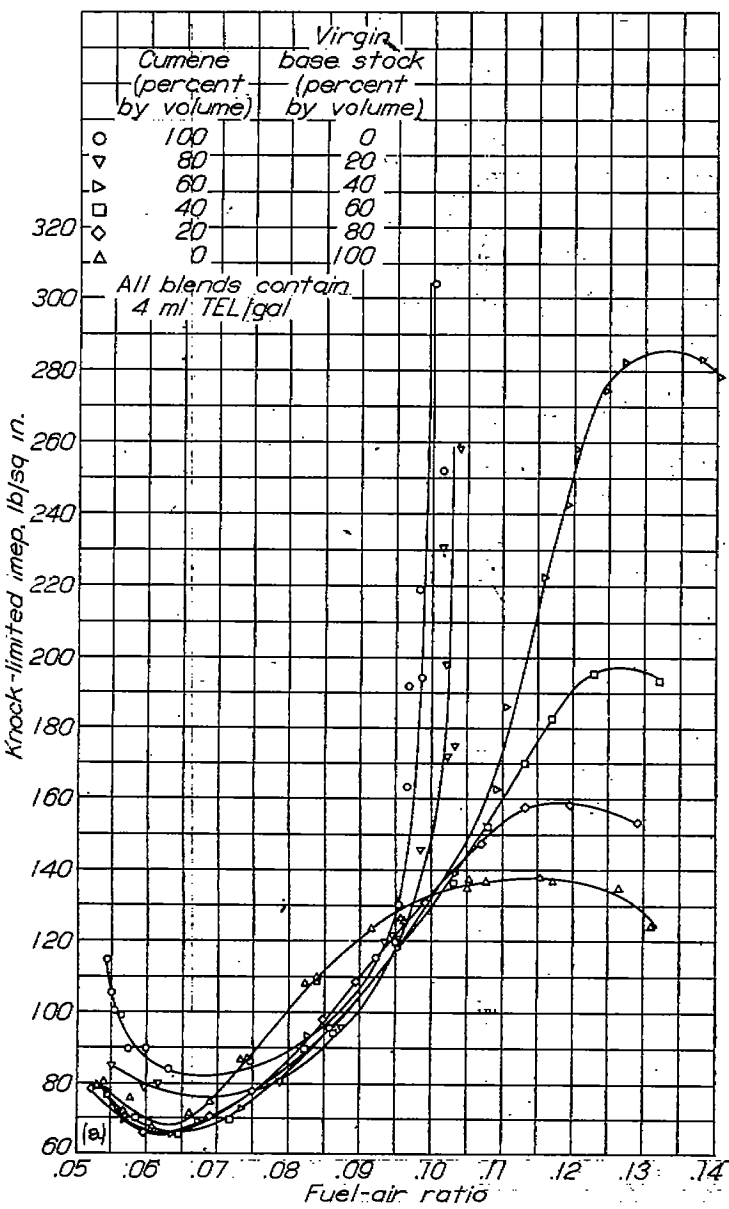


FIGURE VIII-14.—A. S. T. M. Supercharge mixture-response curves for blends of cumene and virgin base stock leaded to 4 ml TEL per gallon. (Fig. 9 (a) of reference 12.)

curves for the cumene blends intersected at fuel-air ratios between 0.10 and 0.11. (See fig. VIII-14.) The fuel-air ratio for peak-knock-limited power varied between 0.115 and 0.132 for the cumene blends. No chart was prepared for blends of cumene, aviation alkylate, and one-pass catalytic stock because rich-mixture peaks were not obtained for a sufficient number of the binary blends of cumene and one-pass catalytic stock.

For the charts representing blends of xylenes (appendix B, figs. B-1 (f) and B-2 (g)), A. S. T. M. Aviation performance lines were omitted. This omission arises from the fact that the curve of composition against performance number for binary blends of xylenes and aviation alkylate passed through a minimum. (See fig. VIII-15.)

In general, data obtained on the A. S. T. M. Aviation engine for the aromatic blends could not be handled with complete satisfaction by the empirical procedure previously

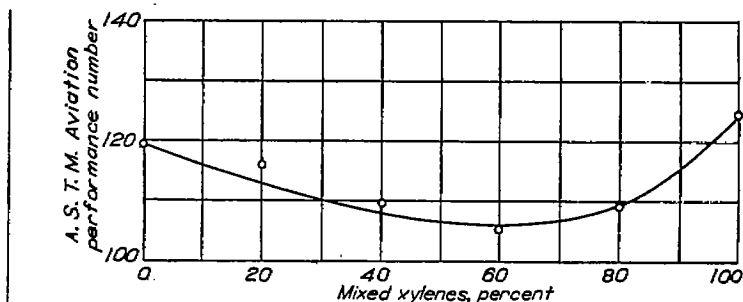


FIGURE VIII-15.—A. S. T. M. Aviation blending characteristics of mixed xylenes and aviation alkylate. (Fig. 10 of reference 12.)

explained. For this reason the accuracy of the lines of constant A. S. T. M. Aviation performance shown for the aromatic-paraffinic systems is questionable.

Quaternary blends.—The performance charts presented in the preceding section are of interest primarily from consideration of maximum knock-limited performance attainable with various combinations of fuel blending agents and base stocks. On the other hand, producers of aviation fuel are interested in the maximum knock-free power attainable with a finished blend that meets physical-property specifications for aviation fuels. Accordingly, several charts have been prepared to illustrate how physical properties might be taken into consideration. In these examples the only physical property considered is the Reid vapor pressure. Current aviation fuel specifications preclude the use of fuels having vapor pressures in excess of 7 pounds per square inch.

In order to prepare these charts, adjustments in Reid vapor pressures of the main components were made by adding isopentane, which in the pure state has a vapor pressure of about 20 pounds per square inch. The addition of isopentane to adjust the vapor pressure of the components in a system such as that shown in figure VIII-16 will necessarily affect the maximum knock-free power attainable because of the performance rating of isopentane relative to the ratings of the other components in the system, as shown in table VIII-1.

TABLE VIII-1.—A. S. T. M. AVIATION AND A. S. T. M. SUPERCHARGE PERFORMANCE RATINGS AND REID VAPOR PRESSURES FOR VARIOUS AVIATION-FUEL COMPONENTS

Blending agent	Reid vapor pressure (lb/sq in.)	Performance number*	
		A. S. T. M. Aviation	A. S. T. M. Supercharge ^b
Isopentane	19.6	133	114
Neohexane	9.7	161	159
Methyl tert-butyl ether	8.8	>161	>200
Diisopropyl	7.4	142	202
Virgin base stock	6.9	78	94
Alkylate	4.7	119	137
Benzene	3.5	68	>200
Triptane	3.0	149	>200
Hot-acid octane	2.7	127	197
Toluene	1.1	118	>200
Mixed xylenes	.5	124	>200
Cumene	.3	85	>200

* Performance numbers are for pure blending agent containing 4 ml TEL/gal.

^b Performance numbers over 161 are extrapolated (fig. VIII-10). Ratings are for fuel-air ratio of 0.11.

^c Extrapolated from experimental data for blends containing up to 60 percent isopentane.

^d Assumed to be the same as the rating for unleaded benzene.

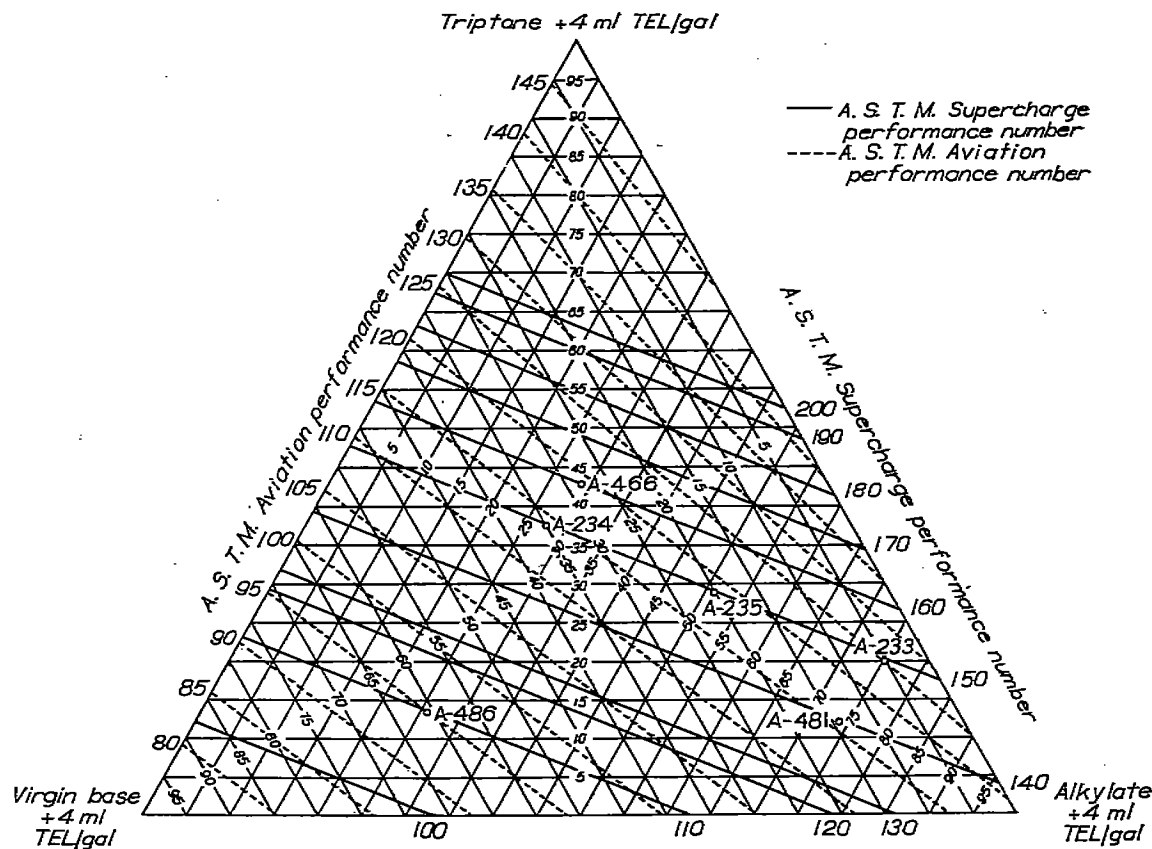


FIGURE VIII-16.—Blending chart for triptane, aviation alkylate, and virgin base stock by A. S. T. M. Aviation and A. S. T. M. Supercharge methods. (Fig. 7 (a) of reference 12.) A. S. T. M. Supercharge fuel-air ratio, 0.11.

In figure VIII-16, for example, a blend of 58.5 percent triptane, 30.5 percent alkylate, and 11 percent virgin base stock has a lean-rich performance-number rating of 135/200 and a Reid vapor pressure of approximately 3.5 pounds per square inch. In order to obtain the same performance (135/200) with a blend of triptane, alkylate, and virgin base stock that has been isopentanized to a Reid vapor pressure of 7 pounds per square inch (maximum permitted), a blend of 55 percent triptane, 17 percent alkylate, 7 percent virgin base stock, and 21 percent isopentane could be used. The addition of isopentane has thus effectively decreased the quantity of triptane needed to obtain the 135/200 performance rating. Isopentane has better performance characteristics than the alkylate or the virgin base stock used, as well as a higher Reid vapor pressure than the other three constituents in the blend. (See table VIII-1.)

It must be emphasized that the preceding example is given merely as an illustration of a fuel characteristic other than antiknock quality that must be considered for a finished fuel blend. This example is not intended to imply that the preparation of fuel blends with Reid vapor pressures adjusted to meet specifications will necessarily produce blends that will meet all other pertinent specifications.

Several performance charts for quaternary blends containing isopentane were prepared for comparison with the

charts previously described for ternary blends. In each of the quaternary systems the vapor pressure was adjusted to 7 pounds per square inch. Three assumptions were made in the preparation of these charts:

(1) The relation between composition and Reid vapor pressure is linear for binary blends of isopentane with another paraffinic fuel.

(2) The relation between composition and the reciprocal of the A. S. T. M. Supercharge (rich) knock-limited indicated mean effective pressure is linear for binary blends of isopentane with another paraffinic fuel.

(3) The relation between composition and the A. S. T. M. Aviation performance number is linear for binary blends of isopentane with another paraffinic fuel.

On the basis of the available data, assumption (3) appears to be valid for only a few cases. For this reason the A. S. T. M. Aviation performance lines on the charts for quaternary blends may be in error.

As an example of the preparation of the performance chart for a quaternary system, assume that it is desired to isopentanize the blends represented by figure VIII-16. The first step in this problem is to determine the amount of isopentane to be added to each of the pure components to obtain a Reid vapor pressure of 7 pounds per square inch and to determine the resultant lean and rich performance-

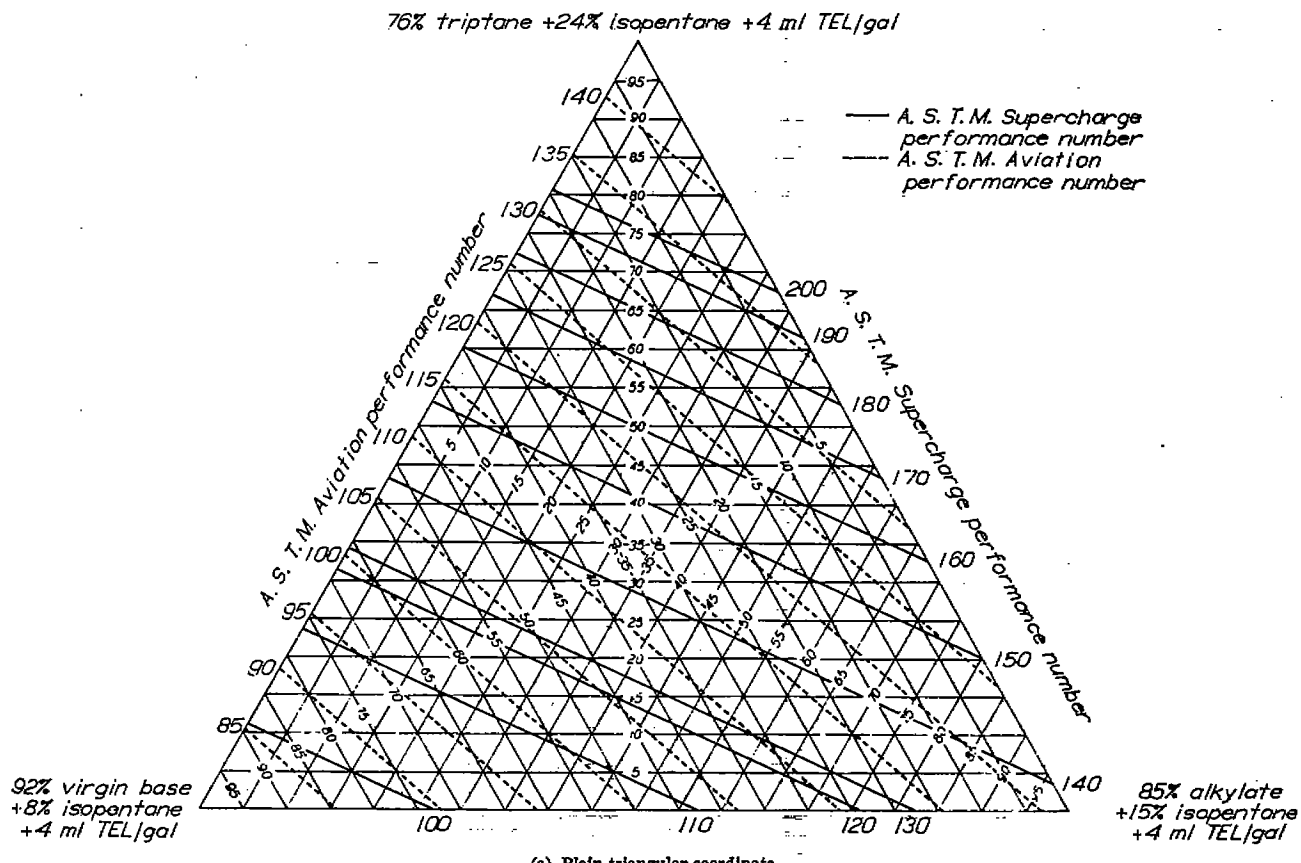


FIGURE VIII-17.—Blending charts for triptane, aviation alkylate, virgin base stock, and isopentane by A. S. T. M. Aviation and A. S. T. M. Supercharge methods. Reid vapor pressure, approximately 7 pounds per square inch; A. S. T. M. Supercharge fuel-air ratio, 0.11. (Fig. 11 of reference 12.)

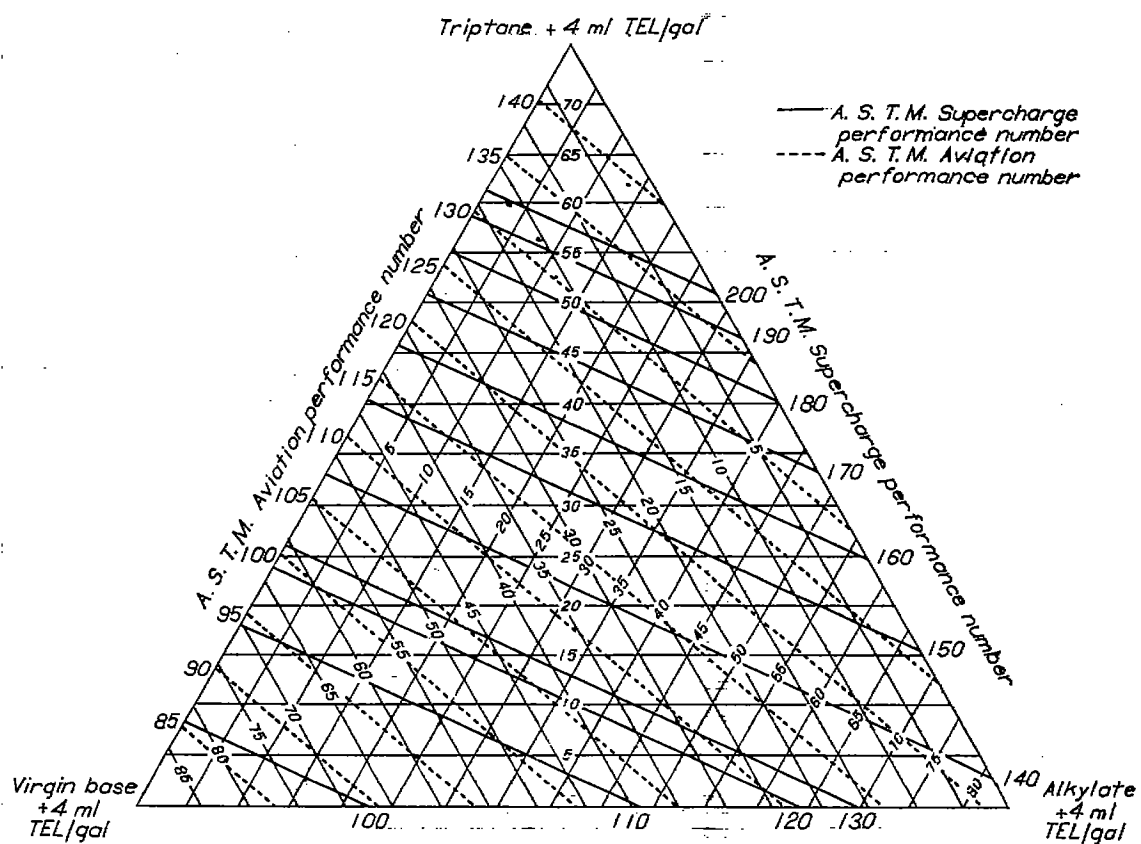


FIGURE VIII-17.—Concluded. Blending charts for triptane, aviation alkylate, virgin base stock, and isopentane by A. S. T. M. Aviation and A. S. T. M. Supercharge methods. Reid vapor pressure, approximately 7 pounds per square inch; A. S. T. M. Supercharge fuel-air ratio, 0.11. (Fig. 11 of reference 12.) Percentage isopentane can be determined by subtracting sum of percentages of other components from 100.

number ratings for these blends. This information as determined from the foregoing assumptions and table VIII-1 is presented in the following table:

Fuel blend	A. S. T. M. Aviation performance number	A. S. T. M. Supercharge in- dicated mean effective pressure (lb/sq in.)
76 percent triptane + 24 percent isopentane + 4 ml TEL/gal	145	455
85 percent alkylate + 15 percent isopentane + 4 ml TEL/gal	121	200
92 percent virgin base + 8 percent isopentane + 4 ml TEL/gal	78	142

The triangular chart shown in figure VIII-17 (a) was obtained by treating these three blends (all of which have Reid vapor pressures of 7 lb/sq in.) as separate components by the procedure used in preparing figure VIII-16. Any point on figure VIII-17 (a) represents the A. S. T. M. Aviation and the A. S. T. M. Supercharge performance number of a quaternary blend. The actual quantity of each component in the blend, however, cannot be readily determined from the chart because the percentages given on the altitudes of the triangle show only the amounts of the binary blends at the vertexes. For this reason, the grid of the chart was so adjusted, as shown in figure VIII-17 (b), that the quantity of any one of the four components in the blend could be read directly from the chart.

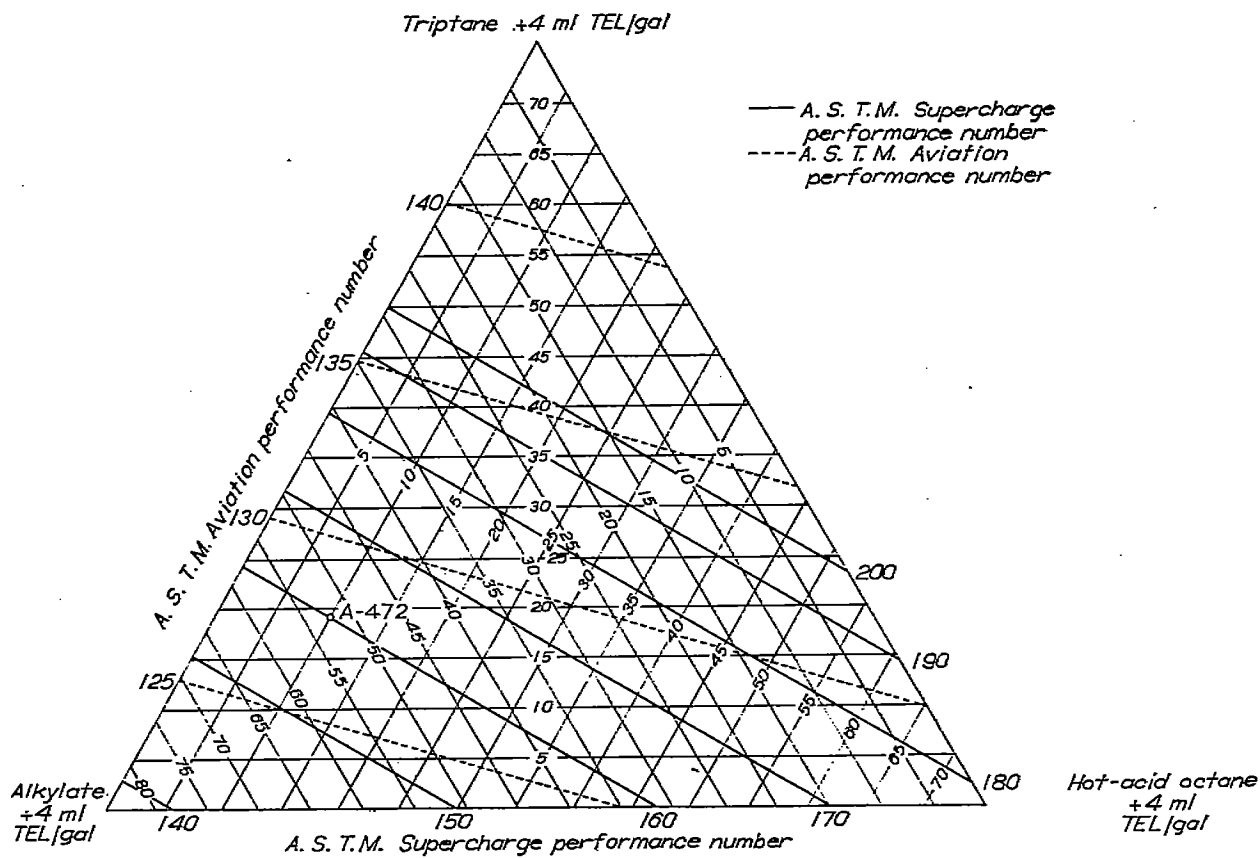
As an illustration of the method for determining the com-

position of a fuel in figure VIII-17 (b), suppose that it is desired to prepare a blend of triptane, aviation alkylate, virgin base stock, and isopentane having a lean-rich rating of 130/180. The concentrations of triptane, alkylate, and virgin base in the blend having the desired rating can be read directly from the altitudes of the triangle in the manner used in previous charts. These concentrations are 48, 19, and 13 percent, respectively. The concentration of isopentane can be determined by subtracting the sum of the percentages of the other components from 100.

Performance charts for other quaternary systems are presented in figure VIII-18. The experimental value for the Reid vapor pressure of diisopropyl (table VIII-1) is 7.4; however, in preparing figures VIII-18 (b) to VIII-18 (d), a value of 7.0 was assumed for this fuel.

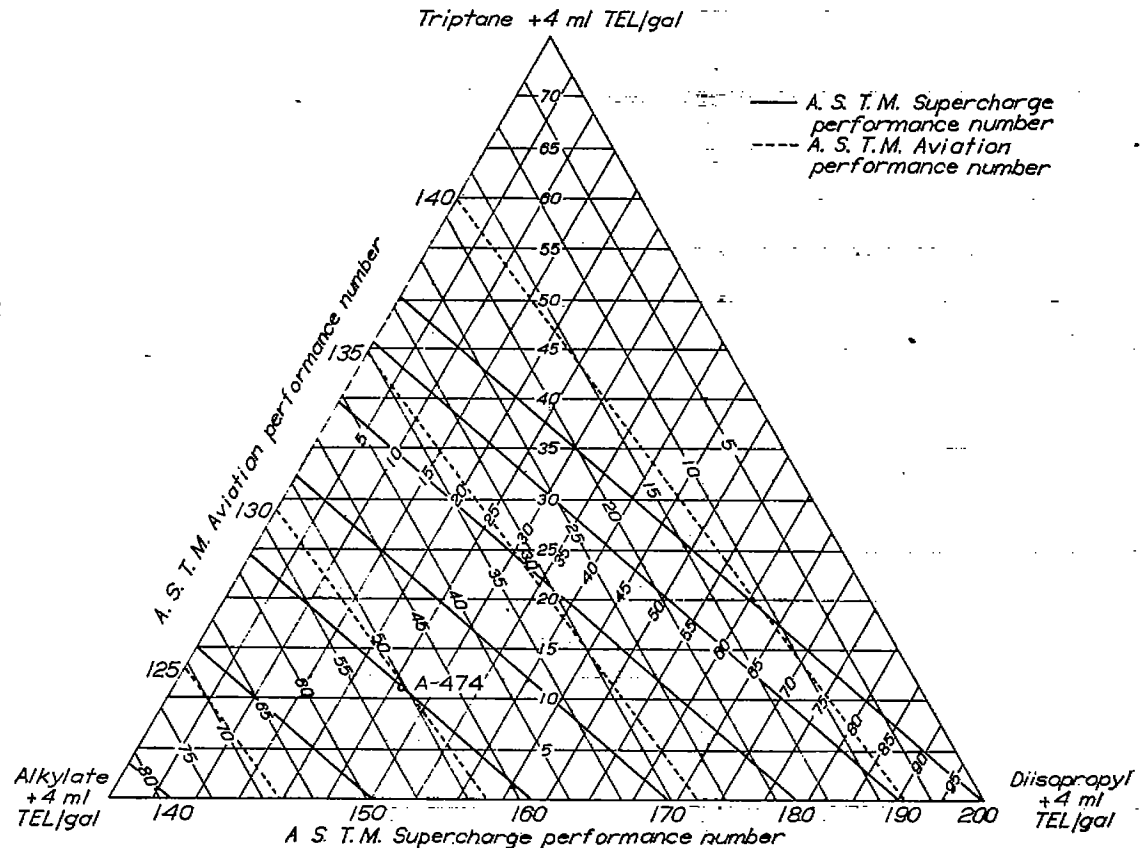
Accuracy of performance charts.—The accuracy of the charts was determined by selecting ternary or quaternary blends from the various charts and testing these blends by the standard A. S. T. M. Aviation and A. S. T. M. Supercharge procedures. Inasmuch as the rich ratings shown on the charts were estimated at a fuel-air ratio of 0.11, the check ratings were determined at this same fuel-air ratio.

The check blends tested are shown with their ratings in table VIII-2. These blends are also shown on the various charts (appendix B and figs. VIII-12 (c), VIII-16, and VIII-18 (a) to VIII-18 (c)) by the symbols. The fuel numbers shown adjacent to each of the symbols on the charts correspond to the fuel numbers given in this table.



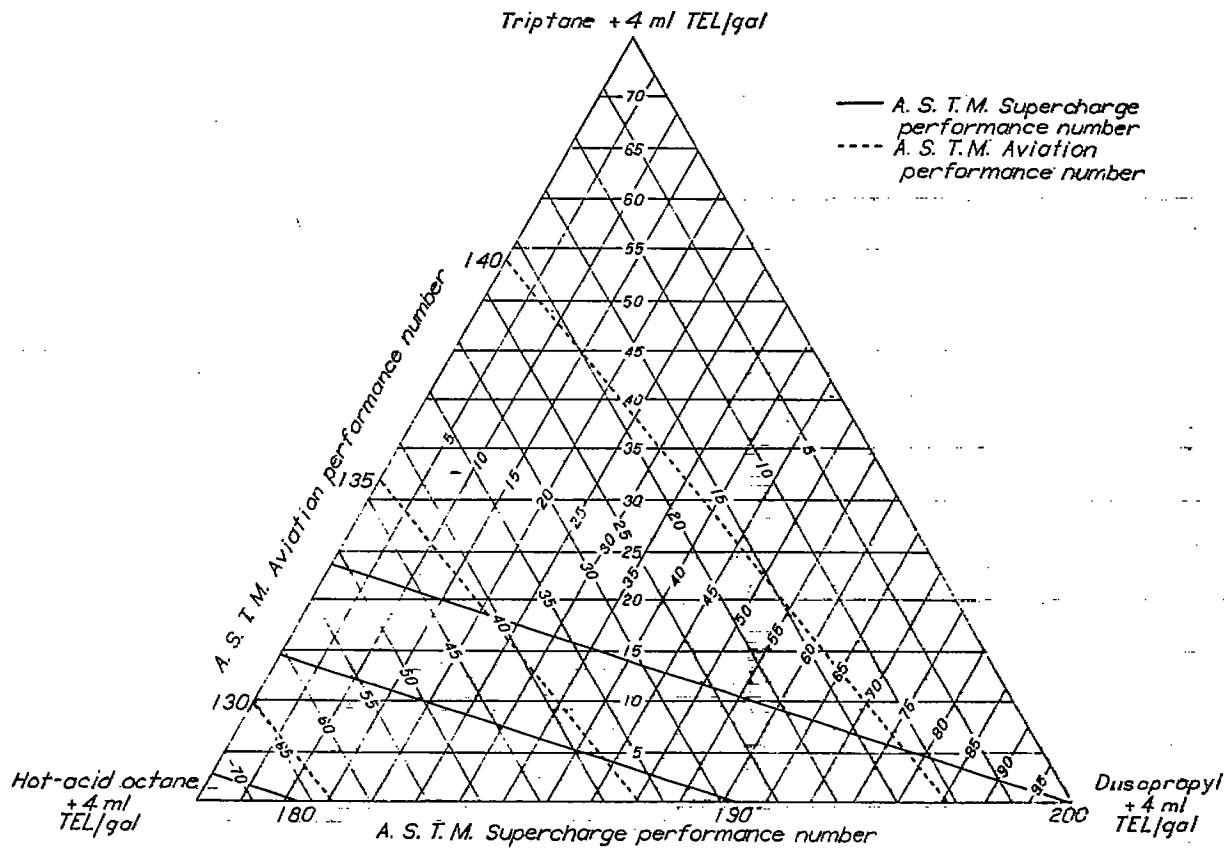
(a) Blends of triptane, aviation alkylate, hot-acid octane, and isopentane.

FIGURE VIII-18.—Blending charts for quaternary blends by A. S. T. M. Aviation and A. S. T. M. Supercharge methods. Reid vapor pressure, approximately 7 pounds per square inch; A. S. T. M. Supercharge fuel-air ratio, 0.11. (Fig. 12 of reference 12.) Percentage isopentane can be determined by subtracting sum of percentages of other components from 100.



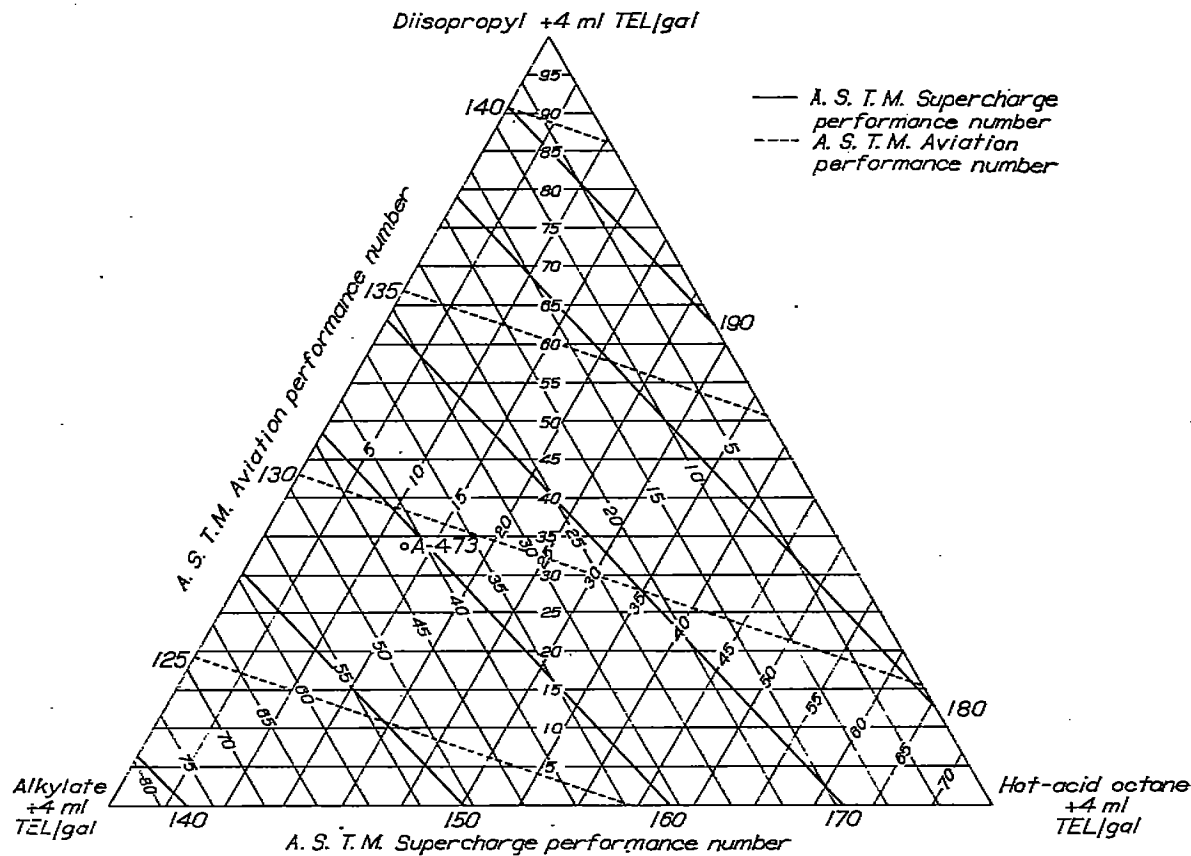
(b) Blends of triptane, aviation alkylate, diisopropyl, and isopentane.

FIGURE VIII-18.—Continued. Blending charts for quaternary blends by A. S. T. M. Aviation and A. S. T. M. Supercharge methods. Reid vapor pressure, approximately 7 pounds per square inch; A. S. T. M. Supercharge fuel-air ratio, 0.11. (Fig. 12 of reference 12.) Percentage isopentane can be determined by subtracting sum of percentages of other components from 100.



(c) Blends of triptane, hot-acid octane, diisopropyl, and isopentane.

FIGURE VIII-18.—Continued. Blending charts for quaternary blends by A. S. T. M. Aviation and A. S. T. M. Supercharge methods. Reid vapor pressure, approximately 7 pounds per square inch; A. S. T. M. Supercharge fuel-air ratio, 0.11. (Fig. 12 of reference 12.) Percentage isopentane can be determined by subtracting sum of percentages of other components from 100.



(d) Blends of diisopropyl, aviation alkylate, hot-acid octane, and isopentane.

FIGURE VIII-18.—Concluded. Blending charts for quaternary blends by A. S. T. M. Aviation and A. S. T. M. Supercharge methods. Reid vapor pressure, approximately 7 pounds per square inch; A. S. T. M. Supercharge fuel-air ratio, 0.11. (Fig. 12 of reference 12.) Percentage isopentane can be determined by subtracting sum of percentages of other components from 100.

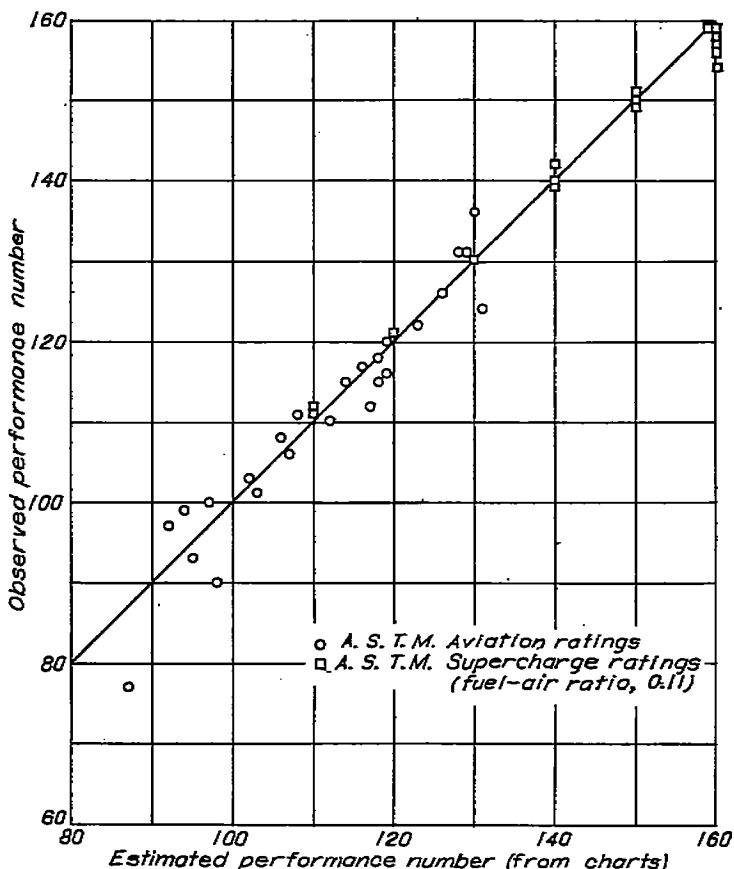


FIGURE VIII-19.—Comparison of estimated and observed knock-limited performance ratings determined by A. S. T. M. Aviation and A. S. T. M. Supercharge methods. A. S. T. M. Supercharge fuel-air ratio, 0.11. (Fig. 13 of reference 12.)

All the data in table VIII-2 are presented in figure VIII-19 to show the relation between estimated and observed performance numbers. For the 25 blends shown in figure VIII-19, the average deviation from the match line was 3.1 performance numbers for the lean ratings and 1.5 for the rich ratings.

In consideration of the accuracy of the charts it must be emphasized that the previously mentioned discrepancies noted in the lean ratings of binary blends containing aromatics are responsible for some of the large deviations in table VIII-2.

Discussion of performance charts.—The performance charts prepared in connection with this chapter can be used for certain general comparisons of paraffins, aromatics, and ethers. In figure VIII-16, for example, at the point representing a blend of 80 percent aviation alkylate, 20 percent virgin base stock, and 4 ml TEL per gallon, the lean-rich rating is 110/122. If a straight line is followed from this point toward the triptane vertex until 20 percent triptane has been added, the rating becomes 118/145. The addition of 20 percent triptane to the base blend has thus increased the lean rating of the base blend by 8 performance numbers and the rich rating by 23. If, however, the chart for benzene (appendix B, fig. B-1 (d)) with the same base stocks is examined, it is seen that a 20-percent addition of benzene changes the rating of the starting blend from 110/122 to 106/146. The addition of 20 percent benzene has therefore decreased the lean rating by 4 performance numbers, whereas

TABLE VIII-2.—A. S. T. M. AVIATION AND A. S. T. M. SUPERCHARGE PERFORMANCE RATINGS OF TERNARY AND QUATERNARY FUEL BLENDS

[The following abbreviations are used throughout the table: VBS for virgin base stock; alkylate for aviation alkylate; one-pass stock for one-pass catalytic stock; and MTB ether for methyl *tert*-butyl ether]

Fuel	Fuel composition ^a	Performance numbers			
		A. S. T. M. Aviation ratings		A. S. T. M. Supercharge ratings ^b	
		Estimated	Observed	Estimated	Observed
Ternary blends					
A-477	59% hot-acid octane+25% VBS+16% alkylate	112	110	150	149
A-487	11% hot-acid octane+48% VBS+41% alkylate	98	90	150	111
A-233	20% triptane+5% VBS+75% alkylate	128	126	150	151
A-235	20% triptane+20% VBS+51% alkylate	119	120	150	151
A-234	38% triptane+35% VBS+27% alkylate	114	115	150	150
A-466	43% triptane+28% VBS+29% alkylate	119	116	150	158
A-421	12% triptane+14% VBS+74% alkylate	116	117	140	142
A-486	13% triptane+61% VBS+26% alkylate	95	93	110	112
A-478	43% diisopropyl+12% VBS+45% alkylate	123	122	150	150
A-524	34% diisopropyl+52% VBS+14% alkylate	103	101	120	121
A-483	58% neohexane+14% VBS+30% alkylate	131	124	140	140
A-523	12% neohexane+42% VBS+45% alkylate	102	103	110	111
A-482	28% benzene+34% VBS+42% alkylate	97	100	140	139
A-522	47% benzene+41% VBS+12% alkylate	87	77	160	164
A-484	14% toluene+54% VBS+32% alkylate	92	97	130	130
A-521	23% toluene+17% VBS+60% alkylate	107	106	160	156
A-520	33% MTB ether+55% VBS+12% alkylate	106	108	160	154
A-539	6% MTB ether+50% VBS+35% alkylate	94	99	110	111
A-470	66% hot-acid octane+13% one-pass stock+32% alkylate	118	118	160	159
A-471	35% triptane+48% one-pass stock+20% alkylate	108	111	160	159
A-480	20% triptane+18% one-pass stock+64% alkylate	117	112	150	150
A-555	39% diisopropyl+24% one-pass stock+37% alkylate	118	115	150	150
Quaternary blends					
A-472	19% triptane+10% hot-acid octane+52.5% alkylate+18.5% isopentane	126	131	160	157
A-474	11.5% triptane+25.5% diisopropyl+50.5% alkylate+12.5% isopentane	130	136	160	159
A-473	34% diisopropyl+12.5% hot-acid octane+41.5% alkylate+12% isopentane	129	131	159	159

^a Each fuel contains approximately 4 ml TEL/gal.

^b Ratings made at fuel-air ratio of 0.11.

the rich rating has been increased by 24. From this comparison it follows that in this example the aromatic (benzene) and the paraffin (triptane) are equally effective for increas-

ing the A. S. T. M. Supercharge (rich) performance but that triptane is more effective than benzene for improving lean performance.

REFERENCES

1. Lovell, Wheeler G., and Campbell, John M.: Knocking Characteristics and Molecular Structure of Hydrocarbons. The Science of Petroleum, vol. IV, Oxford Univ. Press (London), 1938, pp. 3004-3023.
2. Smittenberg, J., Hoog, H., Moerbeek, B. H., and v. d. Zijden, M. J.: Octane Ratings of a Number of Pure Hydrocarbons and Some of Their Binary Mixtures. Jour. Inst. Petroleum, vol. 26, no. 200, June 1940, pp. 294-300.
3. Sanders, Newell D.: A Method of Estimating the Knock Rating of Hydrocarbon Fuel Blends. NACA Rep. 760, 1943.
4. Rothrock, A. M.: Fuel Rating—Its Relation to Engine Performance. SAE Jour. (Trans.), vol. 48, no. 2, Feb. 1941, pp. 51-65.
5. Heron, S. D., and Beatty, Harold A.: Aircraft Fuels. Jour. Aero. Sci., vol. 5, no. 12, Oct. 1938, pp. 463-470.
6. Brooks, Donald B.: Effect of Altitude on Knock Rating of CFR Engines. Res. Paper 1475, Nat. Bur. of Standards Jour. Res., vol. 28, no. 6, June 1942, pp. 713-734.
7. Doss, M. P.: Physical Constants of the Principal Hydrocarbons. The Texas Company, 3d ed., 1942.
8. Wear, Jerrold D., and Sanders, Newell D.: Experimental Studies of the Knock-Limited Blending Characteristics of Aviation Fuels. II—Investigation of Leaded Paraffinic Fuels in an Air-Cooled Cylinder. NACA TN 1374, 1947.
9. Sanders, Newell D., Hensley, Reece V., and Breitwieser, Roland: Experimental Studies of the Knock-Limited Blending Characteristics of Aviation Fuels. I—Preliminary Tests in an Air-Cooled Cylinder. NACA ARR E4I28, 1944.
10. Drell, I. L., and Wear, J. D.: Experimental Studies of the Knock-Limited Blending Characteristics of Aviation Fuels. III—Aromatics and Cycloparaffins. NACA TN 1416, 1947.
11. Hensley, Reece V., and Breitwieser, Roland: Knock-Limited Blending Characteristics of Benzene, Toluene, Mixed Xylene and Cumene in an Air-Cooled Cylinder. NACA MR E5B03, 1945.
12. Barnett, Henry C.: Estimation of F-3 and F-4 Knock-Limited Performance Ratings for Ternary and Quaternary Blends Containing Triptane or Other High-Antiknock Aviation-Fuel Blending Agents. NACA Rep. 904, 1948. (Formerly MR E5A29.)
13. Imming, Harry S., Barnett, Henry C., and Genco, Russell S.: F-3 and F-4 Engine Tests of Several High-Antiknock Components of Aviation Fuel. NACA MR E4K27, 1944.

CHAPTER IX

FUEL VOLATILITY

A number of problems arise from the influence of fuel volatility on engine and aircraft performance. Among these are vapor lock, mixture distribution, ease of starting, cold weather operation, and vaporization loss. In order to permit reasonable control of these factors, fuel specifications include provisions for regulation of volatility. The particular limits established on the volatility characteristics of fuels are based on numerous laboratory investigations and considerable service experience. Some of the laboratory researches on volatility characteristics of fuel are described in this chapter.

MIXTURE DISTRIBUTION

In multicylinder engines an important requisite of good performance is uniform distribution of the fuel-air charge to the individual cylinders. However, design factors relating to engine induction systems (for example, intake manifolds, carburetors, and superchargers) tend to make the problem of distribution one of varying significance with each particular engine. Aside from the undesirable effect on general engine operation, nonuniform distribution increases fuel consumption and cooling requirements and decreases over-all knock limits. For a given engine and a fuel of given volatility, the mixture distribution is affected by over-all fuel-air ratio of the engine, engine speed, supercharger gear ratio, charge weight flow or engine power, throttle setting, and combustion-air inlet temperature. The investigation of reference 1 illustrates the degree to which these engine variables may affect mixture distribution.

Distribution of fuel-air mixture to the various cylinders was determined by exhaust-gas analysis (reference 2) by an improved sampling technique reported by Cook and Olson (reference 3). The engine used was an 18-cylinder, double-row, radial air-cooled engine installed on a test stand and fitted with a flight cowling. (See fig. IX-1.) The engine was equipped with a single-stage supercharger with low and high gear ratios of 7.6 and 9.45, respectively. Additional installation details may be found in reference 1.

The carburetor-deck pressure was maintained atmospheric and the throttle setting was varied to maintain fixed power for the tests in which the over-all fuel-air ratio, the engine speed, the power, or the intake-air temperature was varied. (See reference 1.) The results therefore show the effect of both the variable under investigation and the associated variation of throttle setting and are representative of normal sea-level performance. When the engine power and speed were varied, one of the most important influences on mixture-distribution changes was the variation in throttle angle resulting from atmospheric carburetor-deck pressure. During the tests of varying throttle setting, the carburetor-deck pressure was changed to maintain constant power; operation at altitude was thereby simulated.

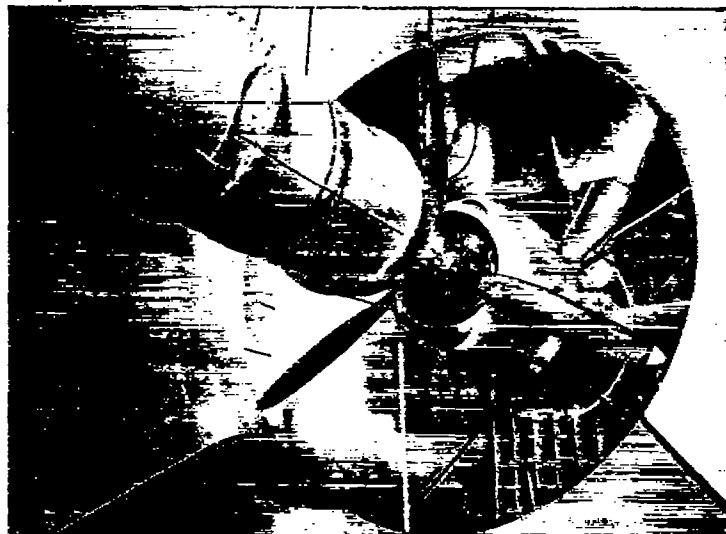


FIGURE IX-1.—Installation of test engine and cowling. (Fig. 1 of reference 1.)

Effect of over-all fuel-air ratio on mixture distribution.—In figure IX-2 the influence of over-all fuel-air ratio on distribution is illustrated. It is readily seen in this figure that the distribution is best at lean fuel-air ratios. The difference between the richest and the leanest cylinders at an over-all fuel-air ratio of 0.101 is reduced from 0.032 to 0.003 at an over-all fuel-air ratio of 0.059. This general trend was found to be true at all operating conditions, although the magnitude of the differences varied. The trend is attributed to the fact that more nearly complete fuel evaporation occurs at low fuel flows where the irregularities of distribution caused by the concentration of fuel droplets are reduced. (See reference 1.)

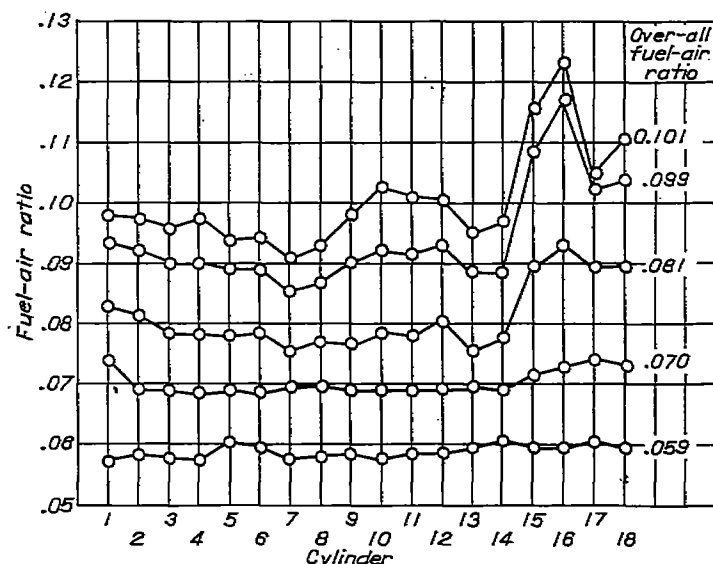
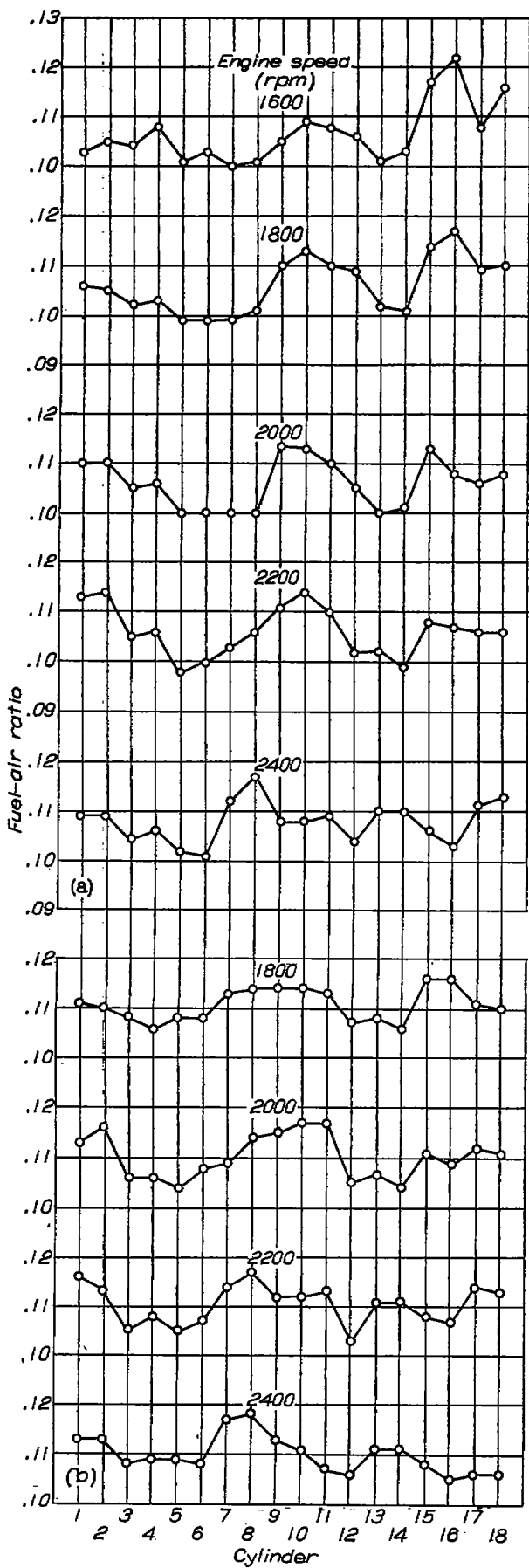


FIGURE IX-2.—Variation of mixture distribution with over-all fuel-air ratio. Engine speed, 1600 rpm; engine power, 800 brake horsepower; low supercharger gear ratio. (Fig. 7 (a) of reference 1.)



(a) Engine power, 800 brake horsepower; over-all fuel-air ratio, 0.108.

(b) Engine power, 1000 brake horsepower; over-all fuel-air ratio, 0.110.

FIGURE IX-3.—Variation of mixture distribution with engine speed. (Fig. 9 of reference 1.)

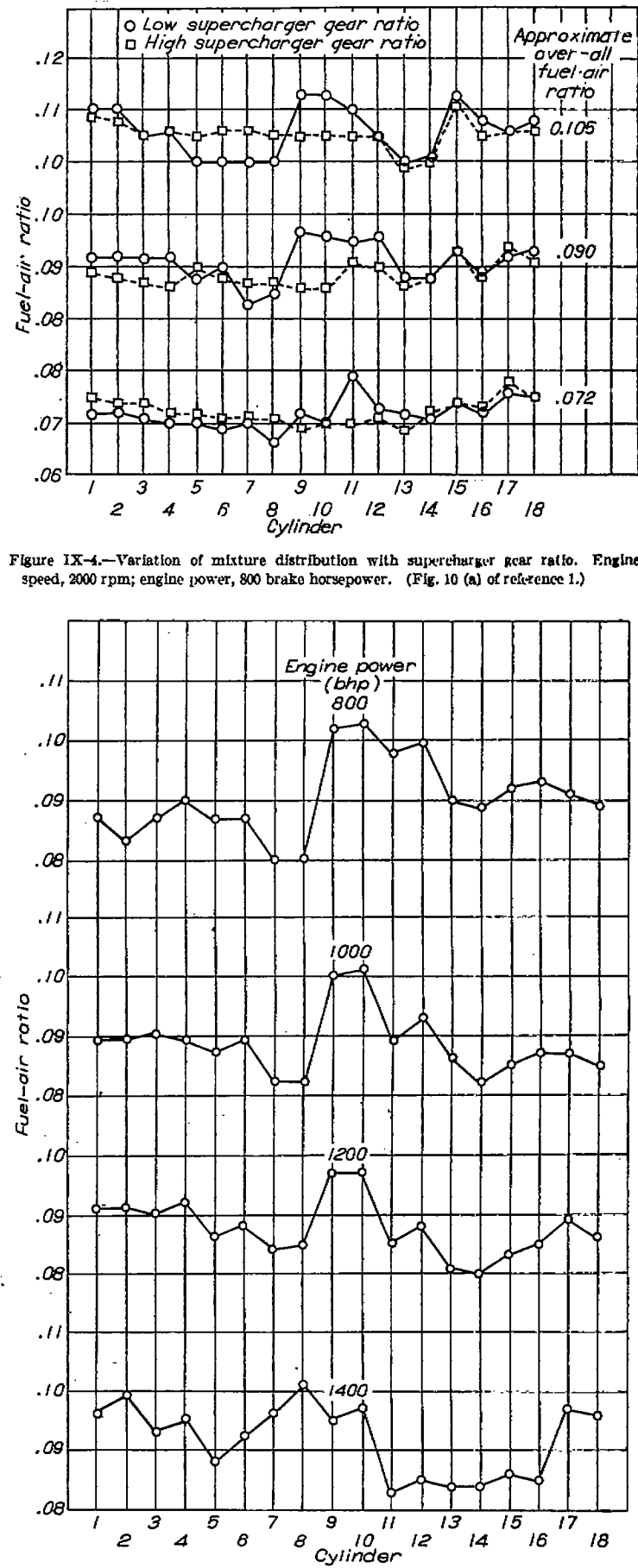


Figure IX-4.—Variation of mixture distribution with supercharger gear ratio. Engine speed, 2000 rpm; engine power, 800 brake horsepower. (Fig. 10 (a) of reference 1.)

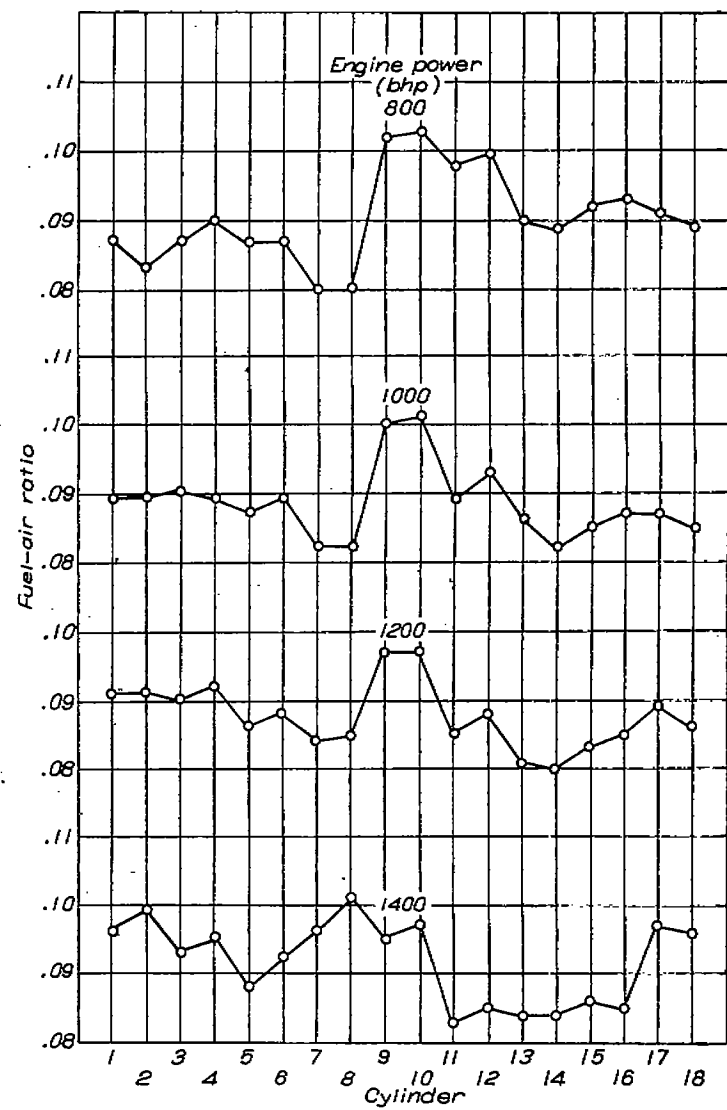


FIGURE IX-5.—Variation of mixture distribution with engine power. Engine speed, 2200 rpm; over-all fuel-air ratio, 0.089; low supercharger gear ratio. (Fig. 11 (b) of reference 1.)

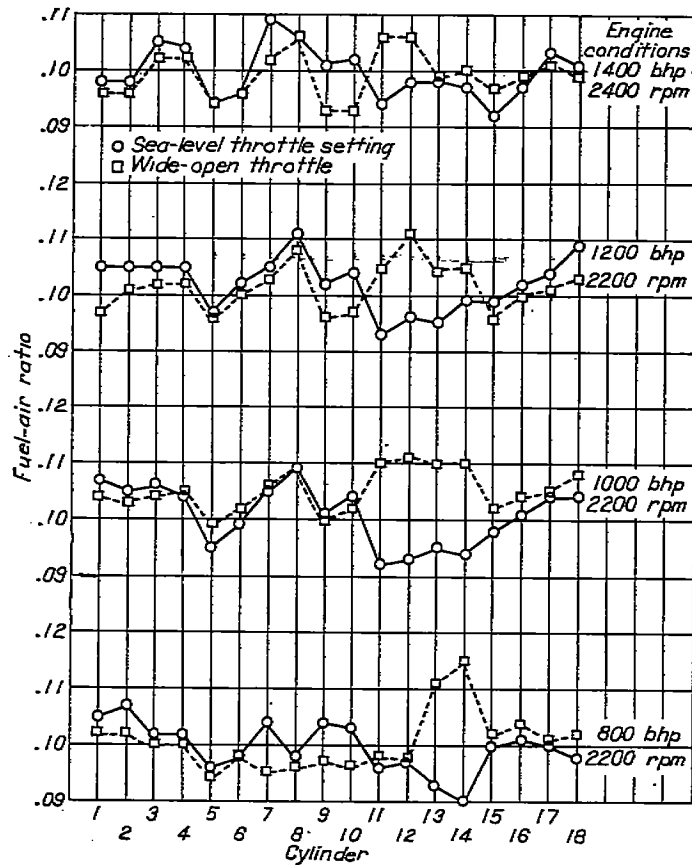


FIGURE IX-6.—Variation of mixture distribution with throttle setting. Over-all fuel-air ratio, 0.100; low supercharger gear ratio. (Fig. 12 (a) of reference 1.)

Effect of engine speed on mixture distribution.—The results of tests at low supercharger gear ratio indicated that the variation of mixture strength between the richest and the leanest cylinders is not appreciably affected by changes of engine speed between 1600 and 2400 rpm (fig. IX-3) despite the accompanying variation in throttle angles. The general shape of the distribution patterns does vary somewhat. For example, in figure IX-3 two peaks may be seen occurring in the neighborhood of cylinders 10 and 16 at low engine speed. The peak near cylinder 16 is diminished whereas that near cylinder 10 becomes more prominent as the speed increases. At high speeds each of the maximum points tends to move to the adjacent cylinder in a direction opposite that of the impeller rotation, that is, from cylinders 10 and 16 to cylinders 8 and 14, respectively.

Effect of supercharger gear ratio on mixture distribution.—The effect of supercharger gear ratio on mixture distribution is shown in figure IX-4. At the high supercharger gear ratio, the mixture distribution was considerably improved over the distribution at low gear ratio. It was suggested in reference 1 that the more nearly uniform mixture distribution at the higher impeller speeds was due to the higher combustion-air temperature and the resulting better evaporation of the fuel passing through the supercharger as well as from the more thorough mixing at the diffuser entrance. It should be recalled, however, that in the preceding discussion no effect on mixture distribution was found when the impeller speed was increased by increasing engine speed at constant supercharger gear ratio.

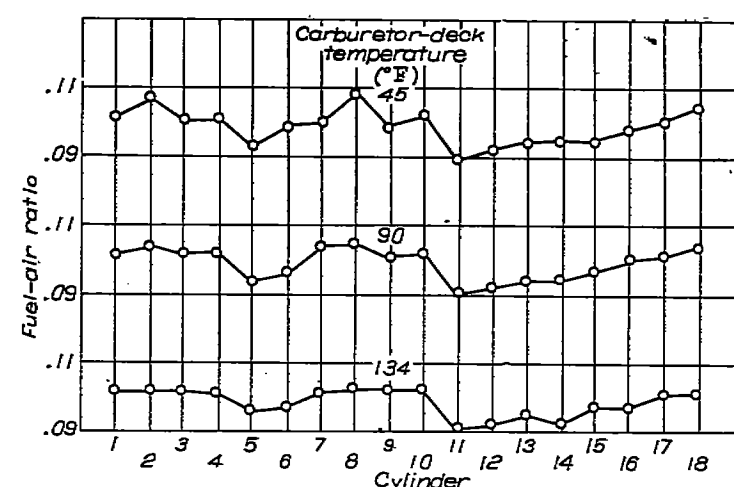


FIGURE IX-7.—Variation of mixture distribution with carburetor-deck temperature. Engine speed, 2200 rpm; engine power, 1000 brake horsepower; approximate over-all fuel-air ratio, 0.100; low supercharger gear ratio. (Fig. 14 of reference 1.)

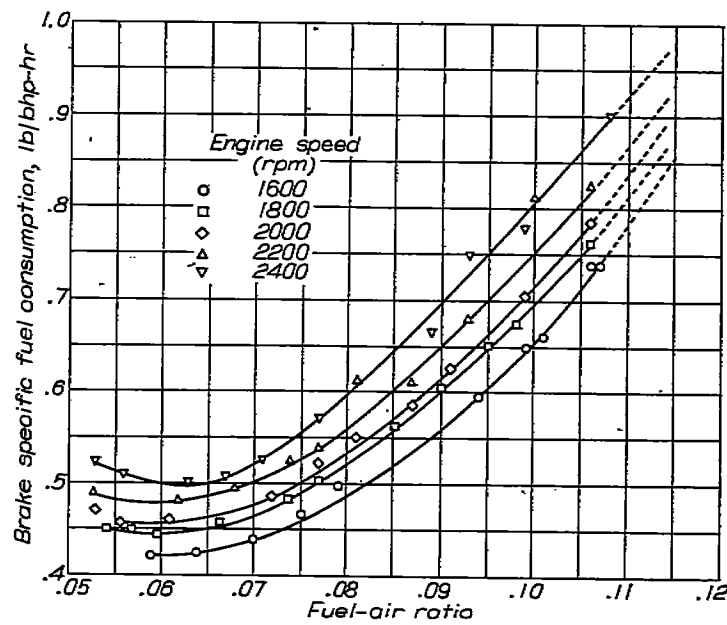


FIGURE IX-8.—Effect of fuel-air ratio on fuel consumption at various engine speeds. Engine power, 800 brake horsepower; low supercharger gear ratio. (Fig. 17 of reference 1.)

Effect of variation of power on mixture distribution.—Mixture-distribution curves for various values of brake horsepower are shown in figure IX-5 for an over-all fuel-air ratio of 0.089. The differences in mixture strength between the richest and leanest cylinder are not greatly affected by power level. Similar results were obtained at over-all fuel-air ratios leaner and richer than 0.089.

Effect of throttle setting on mixture distribution.—Tests were conducted at different throttle settings to determine the change in mixture distribution. The results obtained at one fuel-air ratio are shown in figure IX-6. The most significant differences in the distribution pattern were observed at the low power conditions. At 800 brake horsepower, for example, cylinder 14, the leanest cylinder at sea-level throttle setting, became the richest cylinder at wide-open throttle.

Although the mixture distribution patterns were different at the various power levels and throttle settings, no trend of improvement in distribution was apparent.

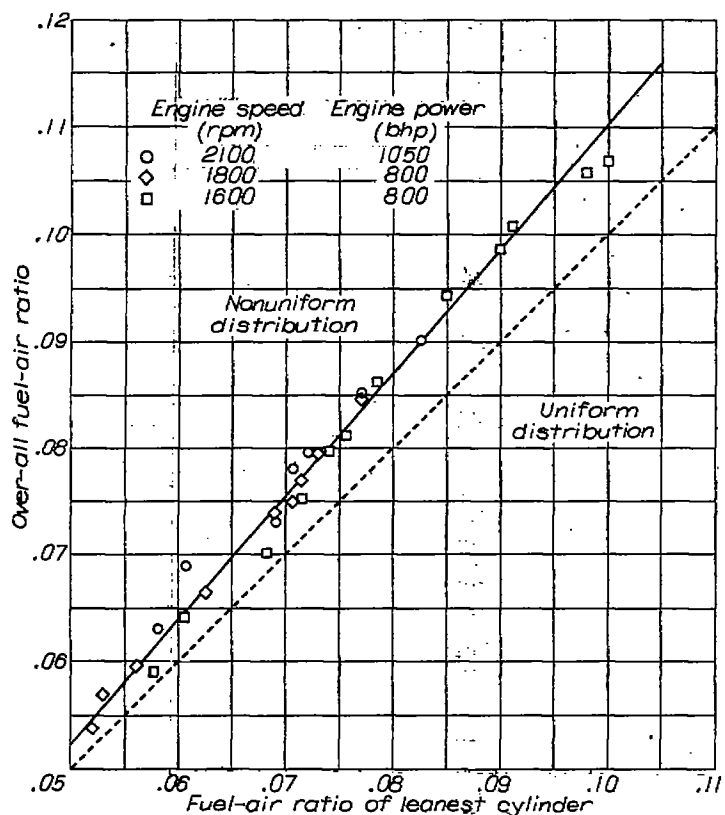


FIGURE IX-9.—Relation between over-all fuel-air ratio and fuel-air ratio of leanest cylinder. (Fig. 18 of reference 1.)

Effect of combustion-air temperature on mixture distribution.—Mixture distribution patterns for carburetor-deck temperatures of 45°, 90°, and 134° F are shown in figure IX-7. The general shapes of the curves in this figure are similar, but the differences between the richest and leanest cylinders decrease with increasing carburetor-deck temperature. This trend may be attributed to increased fuel evaporation at the higher temperatures and the resulting better mixing of fuel and air.

Effect of mixture distribution on fuel consumption.—In a multicylinder engine, operation with nonuniform distribution results in higher fuel consumption. The relation between brake specific fuel consumption and fuel-air ratio (fig. IX-8) is such that the over-all brake specific fuel consumption for nonuniform mixture distribution is necessarily greater than that for uniform distribution. Calculations (reference 1) indicated, however, that the difference is more pronounced when the poor distribution is obtained at a lean over-all fuel-air ratio. If mixture distribution is uniform, the brake specific fuel consumption of the entire engine is the same as that of each cylinder inasmuch as the fuel-air ratio for each cylinder is equal to that of the engine average.

If the extent to which the over-all fuel-air ratio may be reduced is (because of detonation or cooling) determined by the leanest cylinder, the effect of nonuniform mixture distribution is important. The relation between the fuel-air ratio of the leanest cylinder and the over-all fuel-air ratio is presented in figure IX-9. Also shown is the curve representing uniform distribution. At any given value of the abscissa

the difference between the two curves represents the increase in over-all fuel-air ratio required by nonuniform distribution to attain a given value of fuel-air ratio for the leanest cylinder.

Inasmuch as the mixture distribution is more nearly uniform at low over-all fuel-air ratios (fig. IX-2), the differences between the over-all fuel-air ratio and that of the leanest cylinder (fig. IX-9) decrease with decreasing mixture strength.

IMPROVEMENT OF MIXTURE DISTRIBUTION BY MECHANICAL CHANGES

One approach to the problem of elimination of nonuniform distribution is through the use of improved induction devices to permit introduction of more nearly vaporized fuel to the intake manifold. An investigation (reference 4) conducted by the NACA during World War II was concerned with the development of an injection-type impeller that would improve the uniformity of fuel-air mixture and thus promote more uniform distribution to the engine cylinders.

Injection impeller.—The variation in fuel-air ratio among the engine cylinders is influenced by centrifugal and gravitational separation of fuel droplets from the air as well as by coarse, nonuniform injection of fuel into the air stream. Consequently, an improvement in distribution can be achieved by injecting the fuel at a point where the fuel droplets are least likely to separate from the combustion air and at the same time by eliminating the coarse droplets present in the charge-air stream.

The impeller developed in reference 4 was designed to avoid the causes of nonuniform distribution by injecting fuel near the impeller outlet, where elbow and carburetor disturbances are at a minimum and where high velocity and turbulent conditions might be utilized to reduce the effect

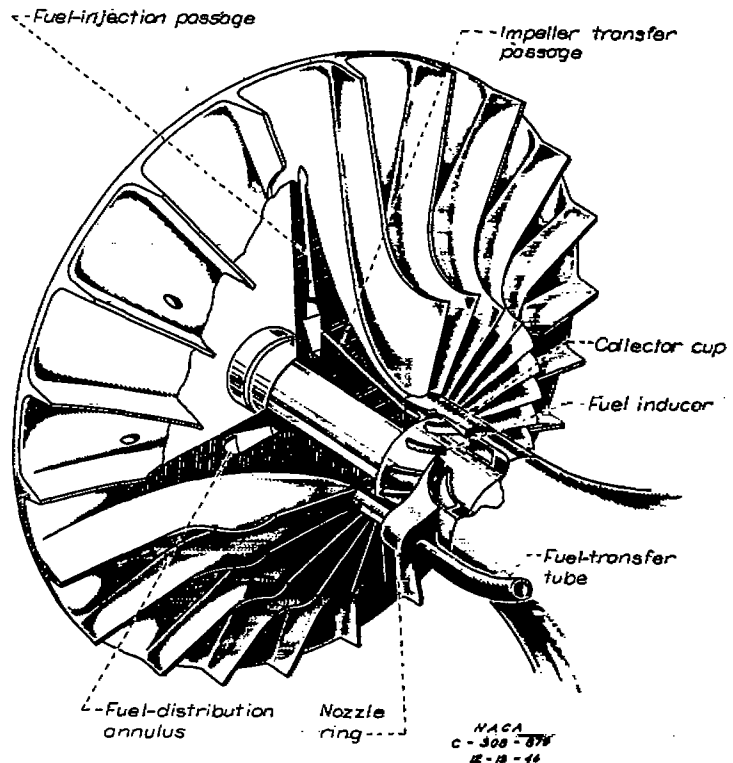


FIGURE IX-10.—Injection impeller. (Fig. 2 of reference 5.)

of gravitational forces and to provide better mixing and fuel evaporation. The impeller (fig. IX-10) is a centrifugal impeller modified to act as a fuel distributor as well as a supercharger. The fuel passages discharge from a centrally located supply chamber into the air passages at a point sufficiently near the impeller tip to avoid fuel impingement on the stationary shroud. Fuel is discharged with a centrifugal force that exceeds the gravitational forces; consequently, a uniform peripheral fuel discharge from the impeller is attained.

Metered fuel passes from the carburetor to a stationary nozzle ring, instead of feeding to the conventional carburetor spray bar, and is delivered from the ring into a collector cup that rotates with the impeller. Between the nozzle ring and the collector cup is an air gap which eliminates surging in the system. The fuel flows by centrifugal action through the collector cup and the impeller transfer passages to the fuel-distribution annulus. From the annulus the fuel is thrown through the radial holes into the air stream.

A comparison of the mixture distribution resulting from

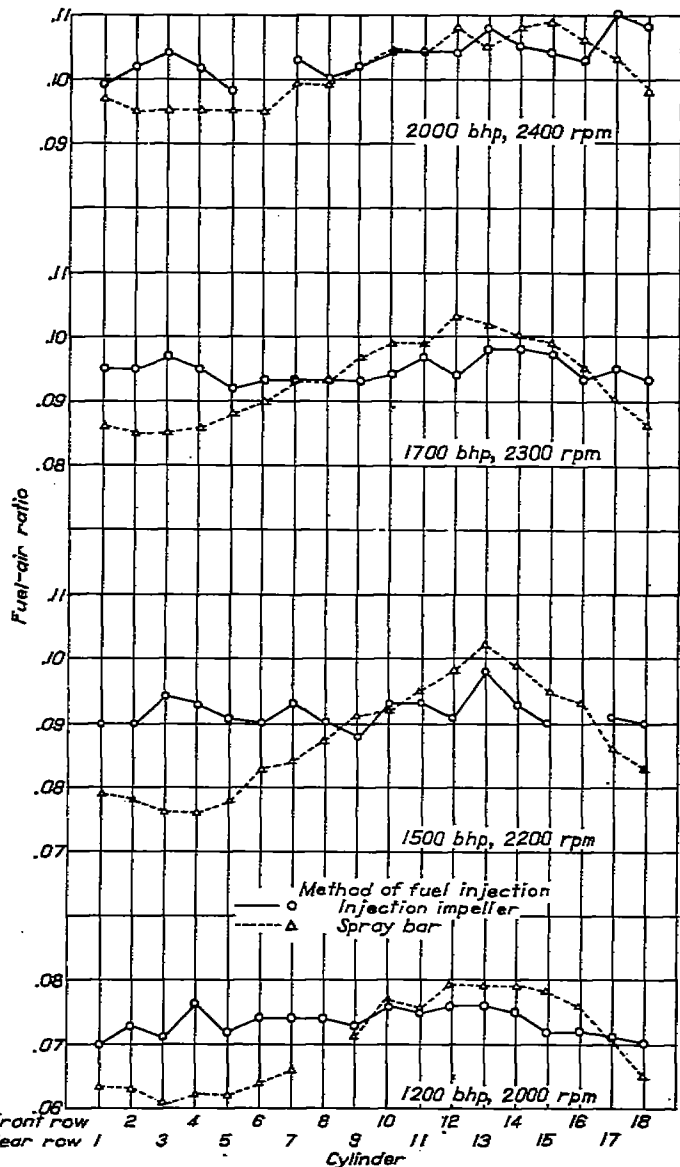


FIGURE IX-11.—Effect of injection impeller on mixture distribution of engine at various engine powers and speeds. (Fig. 6 of reference 4.)

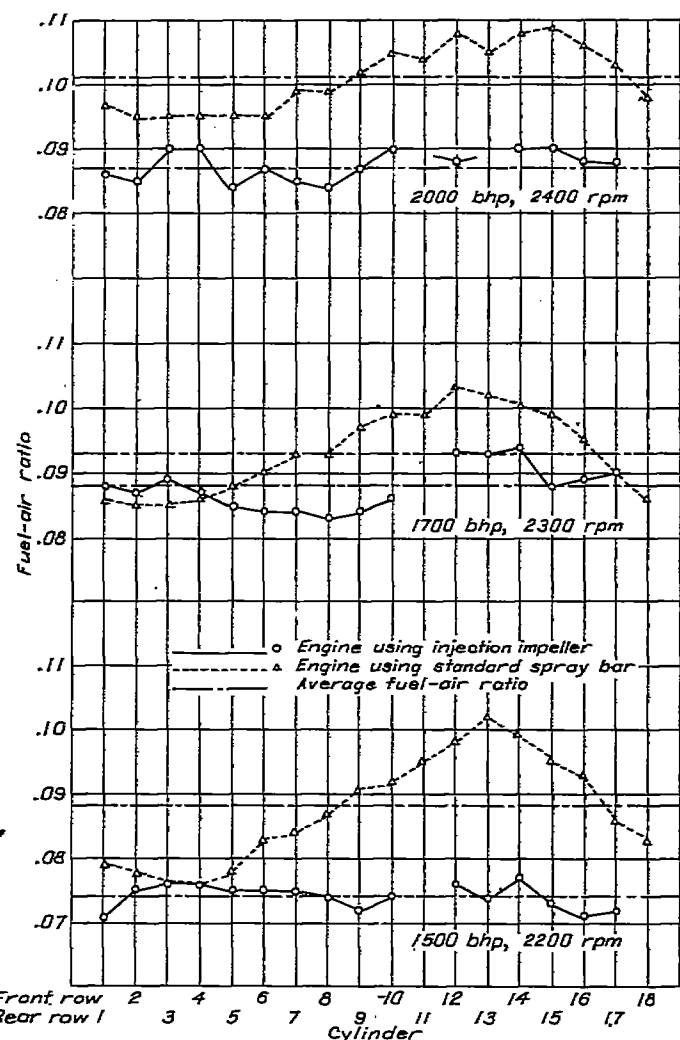


FIGURE IX-12.—Effect of injection impeller on mixture distribution of engine at reduced fuel flows. (Fig. 7 of reference 4.)

a standard carburetor spray bar with that from the injection impeller is presented in figure IX-11. A summary of the data from this figure is given in table IX-1.

At 1200, 1500, and 1700 brake horsepower (table IX-1), the mixture spread was considerably less with the injection impeller than with the standard carburetor spray bar; however, at 2000 brake horsepower the improvement was less noticeable. The poorer showing at 2000 horsepower is attributed in reference 4 to the fact that the impeller does not operate as satisfactorily at the higher fuel flows, whereas

TABLE IX-1.—EFFECT OF INJECTION IMPELLER ON MIXTURE DISTRIBUTION *

Brake horsepower	Fuel-air ratio							
	1200		1500		1700		2000	
Method of fuel injection	Standard spray bar	Injection impeller						
Maximum	0.079	0.076	0.102	0.098	0.103	0.098	0.109	0.110
Minimum	0.061	0.070	0.076	0.068	0.085	0.082	0.095	0.098
Spread	0.018	0.006	0.026	0.010	0.018	0.006	0.014	0.012

* Reproduced from reference 4.

the spray bar apparently provides better mixture distribution at the higher flows.

A comparison of the mixture distribution at reduced fuel flows for the injection impeller with the mixture distribution at higher fuel flows for the standard spray bar is shown in figure IX-12. A summary of the data from this figure is given in table IX-2.

For 1500 and 2000 brake horsepower (table IX-2), the variations in mixture distribution with the impeller at reduced fuel flows are much smaller than the variations at higher fuel flows (table IX-1). At 1700 brake horsepower the variations are greater. On the basis of these data it was suggested (reference 4) that the ability of the injection impeller to overcome the effects of gravitational and centrifugal fuel separation is inhibited at high powers and fuel flows

by some design factor, the effects of which are eliminated at reduced values of fuel flow.

EFFECTS OF THREE FUEL-INJECTION METHODS ON MIXTURE DISTRIBUTION WITH LOW-VOLATILITY FUEL

In order to compare the effects of three methods of fuel injection on engine performance, an investigation (reference 5) was conducted utilizing low-volatility fuel (so-called safety fuel). Low-volatility fuel has long been considered as a substitute fuel for conventional aviation gasoline to reduce the fire hazard in aircraft. Conventional gasoline, because of its high vapor pressure (Reid vapor pressure, 7 lb/sq in.), is much more easily vaporized in an induction system than is low-volatility fuel (Reid vapor pressure, 0.1 lb/sq in.); consequently, safety fuel offers a more rigid test of injection methods. Physical properties for gasoline and low-volatility fuel (reference 5) are compared in the following table:

TABLE IX-2.—EFFECT OF INJECTION IMPELLER ON MIXTURE DISTRIBUTION AT REDUCED FUEL FLOWS

Brake horsepower	Fuel-air ratio					
	1500		1700		2000	
Method of fuel injection	Standard spray bar	Injection impeller	Standard spray bar	Injection impeller	Standard spray bar	Injection impeller
Maximum	0.102	0.077	0.103	0.094	0.109	0.090
Minimum	0.076	0.071	0.085	0.083	0.095	0.084
Spread	0.026	0.006	0.018	0.011	0.014	0.006

• Reproduced from reference 4.

Property	Gasoline	Low-volatility fuel
Grade	100/130	100/139
Tetraethyl lead content, ml/gal	4.55	4.63
Flash point, close cup, °F	Below -30	122
Distillation range, °F		
Initial boiling point	108	320
10-percent evaporated	141	334
30-percent evaporated	205	316
60-percent evaporated	235	302
Final boiling point	332	354
Freezing point, °F	Below -76	Below -76
Reid vapor pressure, lb/sq in.	7	0.1
Residue, copper dish, mg/100 ml	2.0	2.0
Accelerated gum content, mg/100 ml	2.3	2.0
Accelerated gum precipitate, mg/100 ml	0.2	0.6
Sulfur content, percent	0.012	0.0001
Heating value, Btu/lb	18740	18630
Hydrogen-carbon ratio	0.165	0.165
Specific gravity at 60° F	0.719	0.782

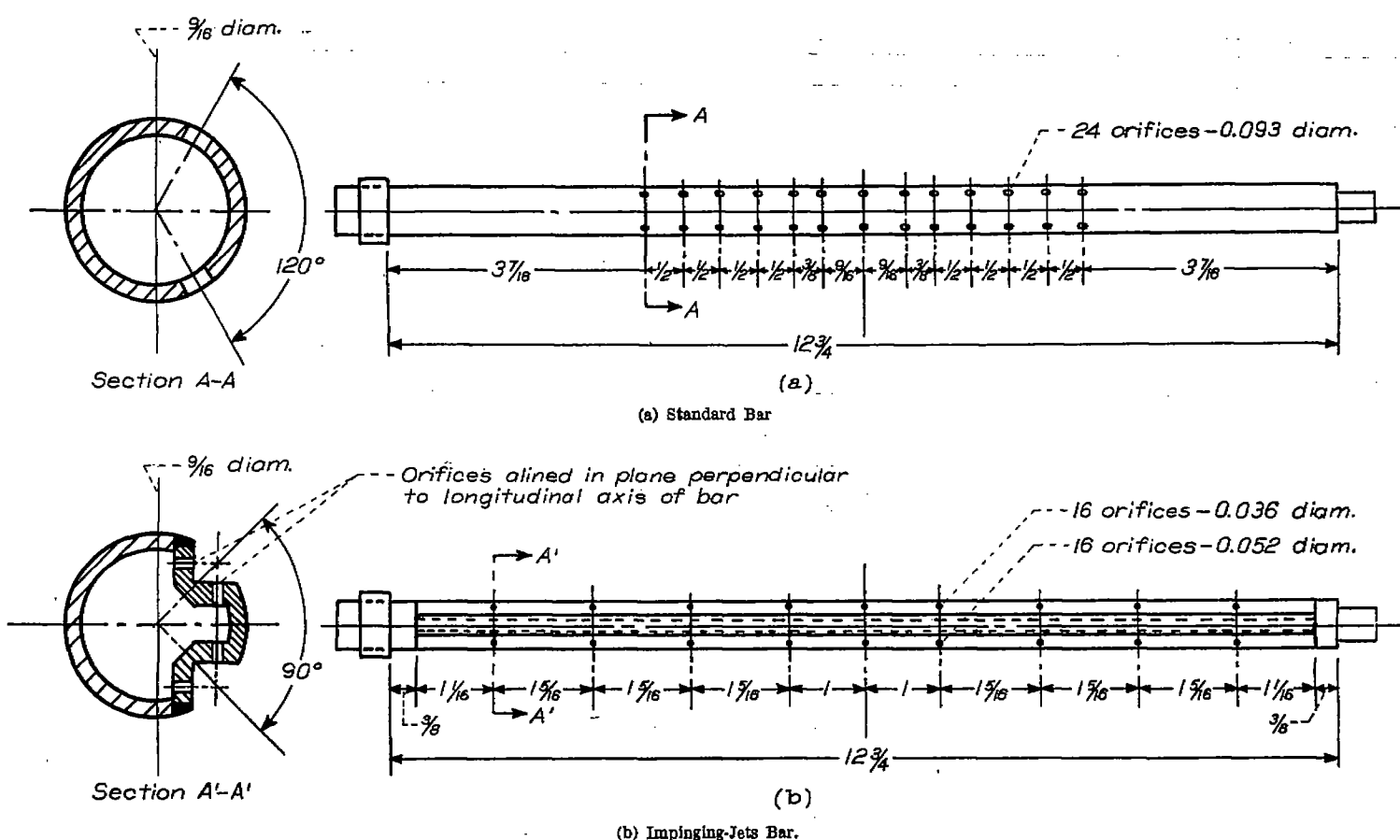
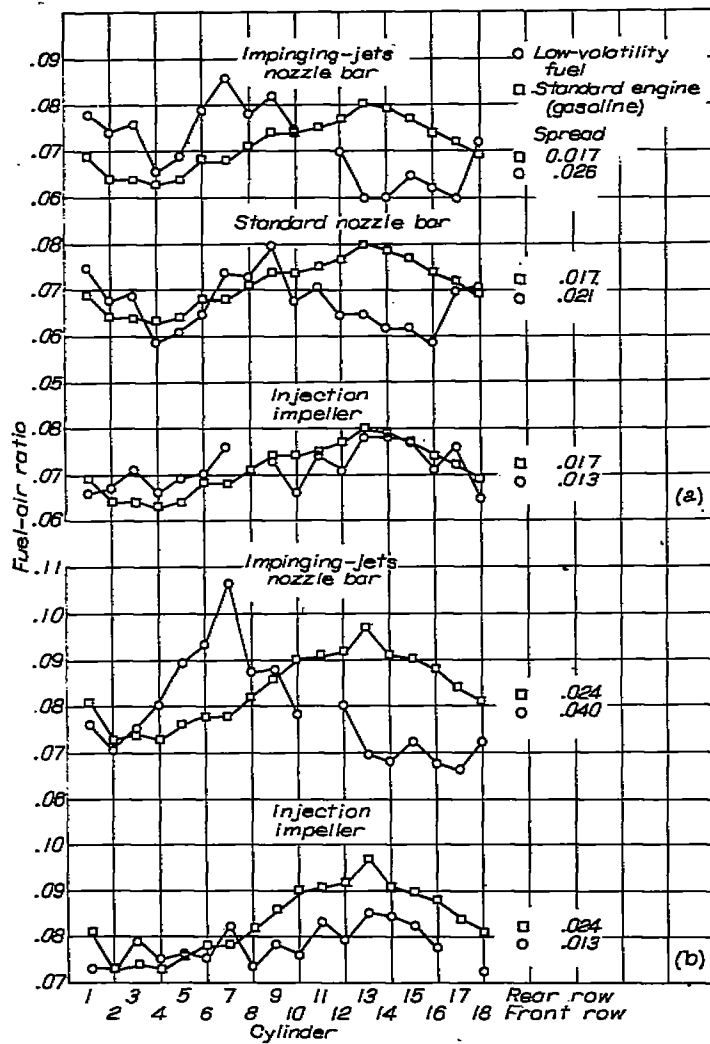


FIGURE IX-13.—Comparison of standard nozzle bar with impinging-jets nozzle bar. (All dimensions given in inches.) (Fig. 3 of reference 5.)

Previous investigations (references 6 and 7) have shown that low-volatility fuel can be utilized successfully in reciprocating engines by direct injection into the cylinders. However, the complexities of a direct injection system can be avoided by better atomization of fuel and injection into the manifold. Aside from the injection impeller discussed in the preceding paragraphs, the NACA has investigated the impinging-jets nozzle bar as a means of achieving better fuel atomization. With the injection impeller, finely dispersed fuel enters the combustion-air stream near the impeller exit, whereas the impinging-jets nozzle bar introduces the finely atomized fuel into the air stream immediately after the carburetor. A standard nozzle bar and the impinging-jets bar are compared in figure IX-13. In the standard bar are located 24 orifices as compared to 32 for the impinging-jets bar. The orifices in the standard bar are larger and the fuel is discharged in less than half the length of the bar. These factors result in poorer atomization and only partial coverage of the combustion-air duct. The orifices in the impinging-jets bar are at right angles to each other and the sprays impinge to form finely atomized fuel.



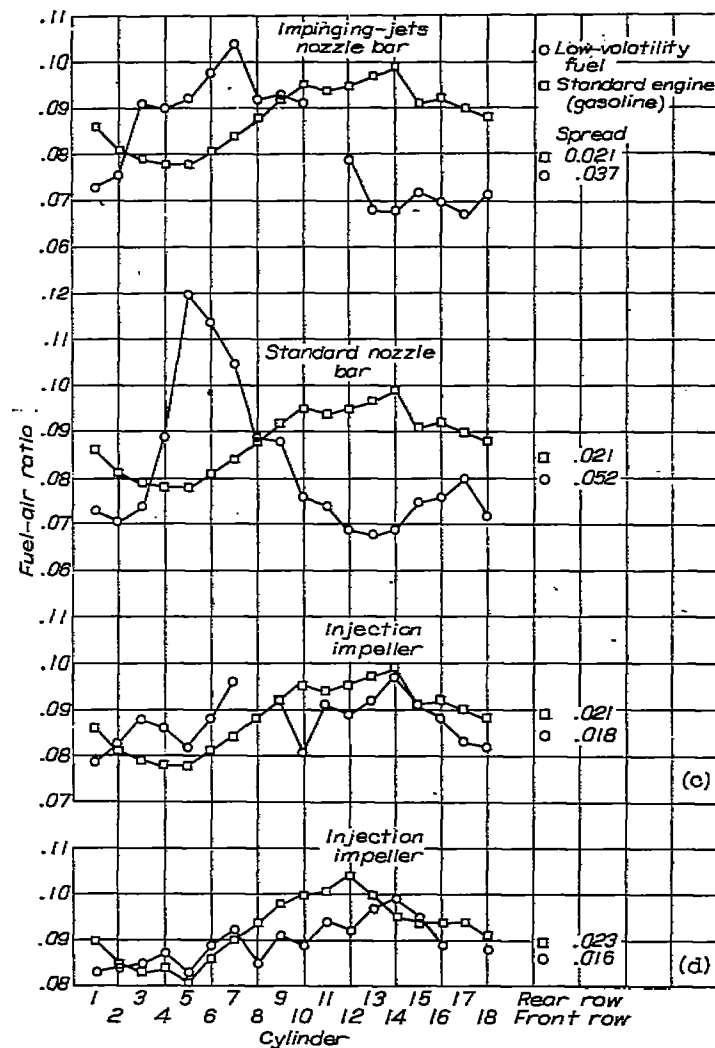
(a) Engine speed, 2000 rpm; engine power, 1200 brake horsepower; approximate average fuel-air ratio, 0.070.
 (b) Engine speed, 2100 rpm; engine power, 1400 brake horsepower; approximate average fuel-air ratio, 0.082.

FIGURE IX-14.—Comparison of mixture distribution obtained with various methods of fuel injection. Combustion-air temperature, 100° F. (Fig. 6 of reference 5.)

In order to evaluate the three methods of injecting low-volatility fuel, a standard mixture-distribution pattern was selected. This pattern was produced at various powers by injection of gasoline through the standard nozzle bar. Comparisons of mixture-distribution patterns for the three methods of injecting low-volatility fuel with the pattern for the standard gasoline test are shown in figure IX-14. The spreads in fuel-air ratio obtained in the standard engine were 0.017, 0.024, 0.021, and 0.023 at 1200, 1400, 1600, and 1800 brake horsepower, respectively.

At 1200 brake horsepower (fig. IX-14(a)) the injection impeller gave a distribution pattern similar to that of the standard engine; the over-all spread in fuel-air ratio was slightly less than that of the standard engine. The other methods gave patterns somewhat different from those of the standard engine in that the over-all spreads in fuel-air ratio were greater.

At 1400 brake horsepower (fig. IX-14(b)) the injection impeller again gave better distribution with low-volatility fuel than the standard engine did with gasoline; however, the impinging-jets bar was worse than the standard engine.



(c) Engine speed, 2200 rpm; engine power, 1600 brake horsepower; approximate average fuel-air ratio, 0.087.
 (d) Engine speed, 2300 rpm; engine power, 1800 brake horsepower; approximate average fuel-air ratio, 0.091.

FIGURE IX-14.—Concluded. Comparison of mixture distribution obtained with various methods of fuel injection. Combustion-air temperature, 100° F. (Fig. 6 of reference 5.)

Similar results were obtained at brake horsepowers of 1600 and 1800 (figs. IX-14(c) and IX-14(d)). Complete data were not obtained at 1800 brake horsepower inasmuch as this power was unattainable with either the standard nozzle bar or the impinging-jets bar.

It can be concluded from the foregoing data that the mixture-distribution patterns produced by the injection impeller with low-volatility fuel are better than those found with a standard nozzle bar and gasoline as a fuel.

EFFECTS OF FUEL VOLATILITY ON ENGINE PERFORMANCE

The effect of fuel volatility on engine performance was investigated by White and Engelman (reference 8). Four fuels were tested over a range of inlet-air temperatures between 46° F and 72° F. In general the results of this study were inconclusive; however, the following summary is offered.

The fuel having the lowest 90-percent point (A. S. T. M. Distillation Procedure D86-40) gave the best power and fuel economy. Differences in performance among the other fuels were relatively slight and could not be attributed to differences in volatility. The 90-percent points of the four fuels were 255°, 270°, 295°, and 306° F. The most volatile fuels were found to give more uniform mixture distribution.

FUEL VAPOR LOSS FROM AIRCRAFT FUEL TANKS

The development of high-altitude, long-range aircraft has resulted in considerable concern over the loss of fuel vapor through fuel tank vents during flight. The loss of fuel represents an increase in the fuel consumed during flight and thus causes a reduction in cruising range and load-carrying capacity.

The variables affecting fuel vapor loss were evaluated in a series of simulated-flight tests (reference 9). A small fuel tank on a bench-test installation (fig. IX-15) was employed to facilitate instrumentation and handling of the equipment during the tests. A similar apparatus was installed in a twin-engine airplane in order to correlate simulated-flight data with actual-flight data. (See fig. IX-16.) Details of the apparatus may be found in reference 9.

Effect of rate of climb on fuel vapor loss.—The fuel in the tank (fig. IX-15) was subjected to simulated flights at rates of climb of 1000, 2000, and 4000 feet per minute to an altitude of 40,000 feet; the results are shown in figure IX-17. These data are replotted in figure IX-18 with fuel vapor loss as a function of altitude. At any given altitude the loss increased only slightly with increased rate of climb for the rates tested; however, the losses due to foaming at the higher rates of climb when the fuel tank is filled close to capacity were not investigated.

Effect of altitude on fuel vapor loss.—The variation of fuel vapor loss with altitude in figure IX-18 is linear above some critical altitude (the theoretical altitude at which fuel vapor loss begins). For this linear portion of the curve the following formula was derived (reference 9):

$$L = \frac{Z - Z_c}{1.9}$$

where

L fuel vapor loss, percent

Z altitude, in 1000 feet

Z_c critical altitude, in 1000 feet (intersection of linear portion of loss-against-altitude curve with base line, fig. IX-18)

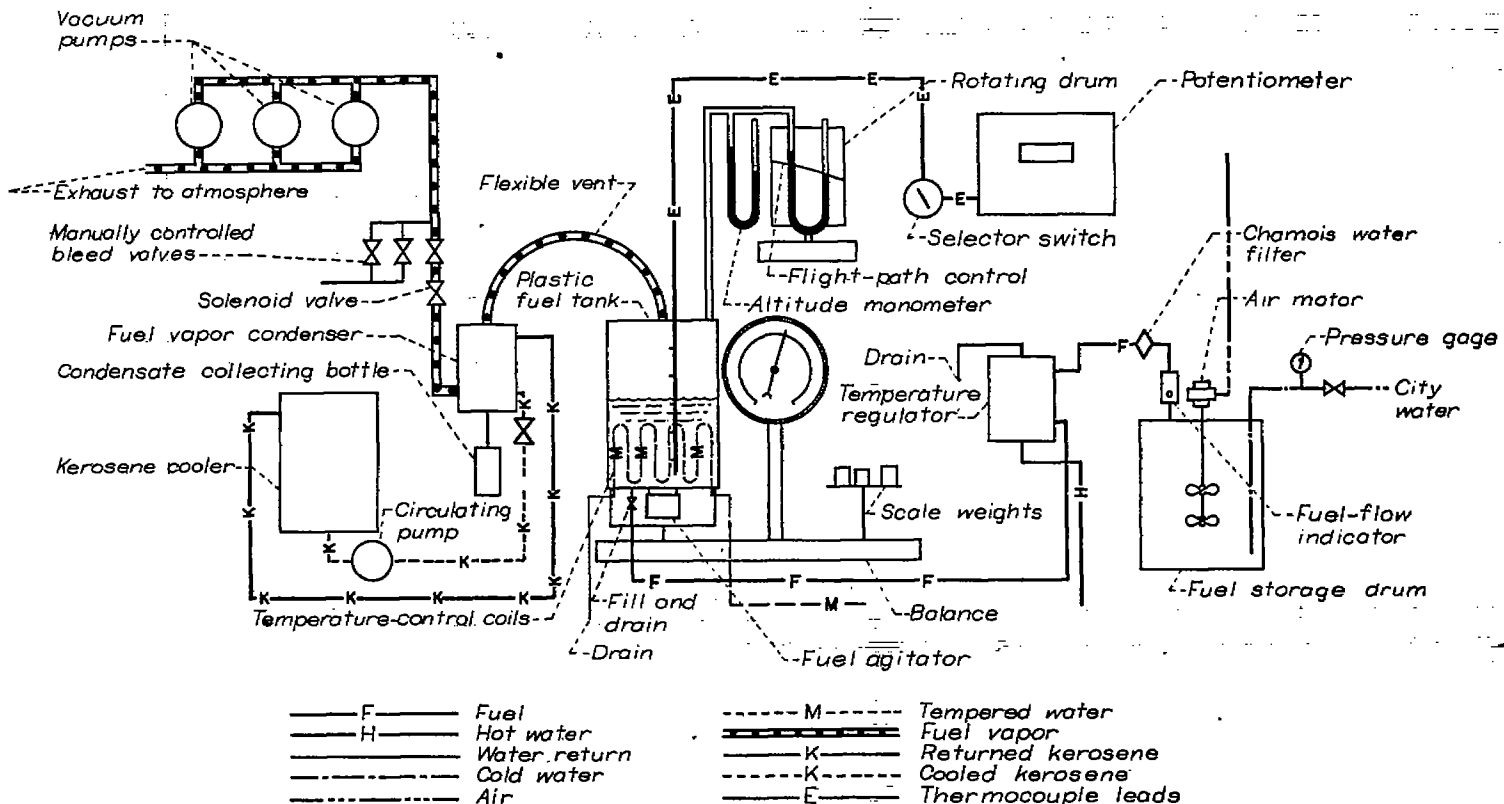


FIGURE IX-15.—Bench-test installation for determination of fuel vapor loss under simulated flight conditions. (Fig. 1 of reference 9.)

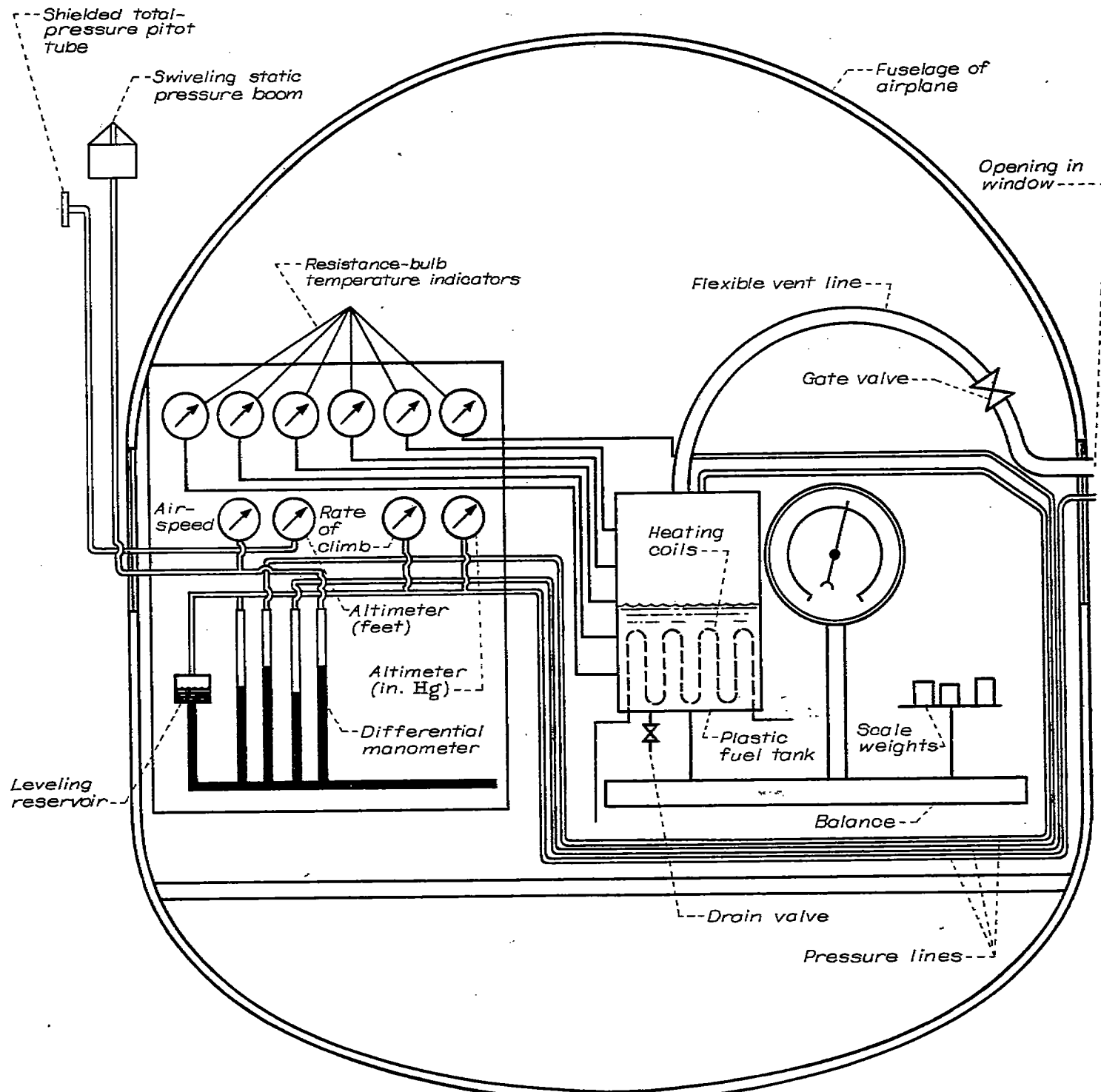


FIGURE IX-16. Flight-test installation for determination of fuel vapor loss. (Fig. 2 of reference 9.)

Effects of initial fuel temperature on fuel vapor loss.—The effect of initial fuel temperature on fuel vapor loss is shown in figure IX-19. These results were obtained from simulated flight tests in which the condition of climb to 30,000 feet was investigated for each of the initial fuel temperatures shown on the figure. These data have been replotted in figure IX-20 to illustrate the variation of fuel vapor loss at the end of climb with initial fuel temperature. Above a fuel temperature of about 70° F the loss varies linearly with fuel temperature. It was suggested in reference 9 that the fuel vapor loss during climb to an altitude of

30,000 feet at initial fuel temperatures above 70° F could possibly be predicted from the following equation:

$$L = K(T - T_c)$$

where

L fuel vapor loss, percent

T initial fuel temperature, °F

T_c temperature above which loss varies linearly with temperature (intersection of linear portion of curve in fig. IX-20 with abscissa), °F.

K constant (0.18 percent per °F, from fig. IX-20)

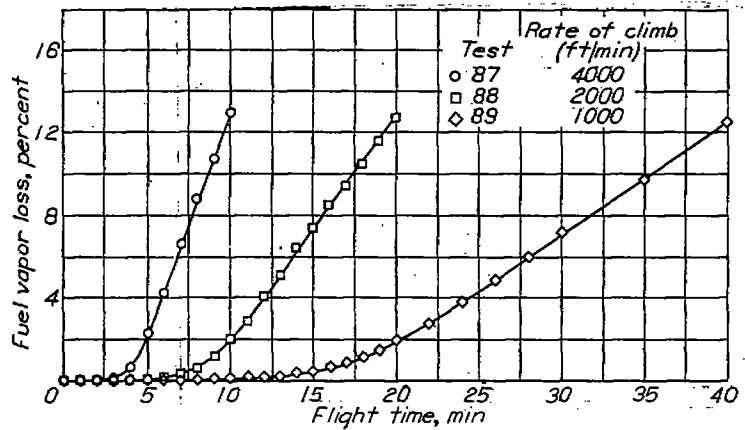


FIGURE IX-17.—Fuel vapor loss during simulated flights to 40,000 feet at various rates of climb. (Fig. 7 of reference 9.)

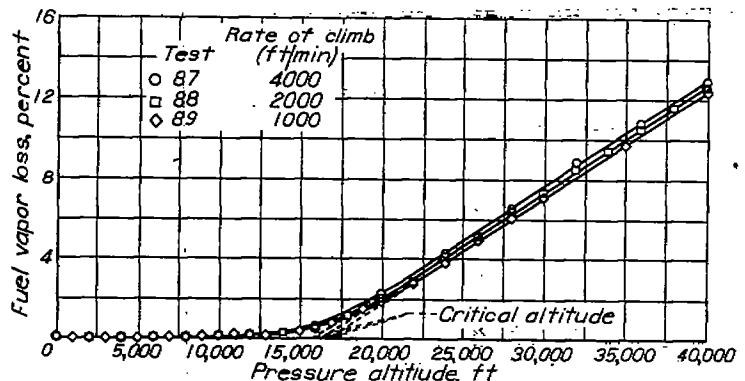


FIGURE IX-18.—Variation of fuel vapor loss with altitude during simulated flights at various rates of climb. (Fig. 8 of reference 9.)

Effect of fuel weathering on fuel vapor loss.—Several successive standard simulated flights were made on the same tank of fuel in order to determine the effect of weathering on vapor loss. (See fig. IX-21.) In this particular test the total volume loss of fuel resulting from the three simulated flights was about 20 percent. The effects of such losses on fuel properties are discussed later in this chapter.

Effects of fuel agitation on fuel vapor loss.—An attempt was made in reference 9 to determine the effects of agitation on vapor loss. The effects of low-amplitude vibrations were investigated by vibrating the tank vertically during a simulated flight. The tank was vibrated at frequencies of 168 and 120 cycles per second at amplitudes of 0.0009 and 0.0018 inch, respectively. An air-operated vibrator attached to the tank was used for this purpose. This type of vibration had no significant effect on fuel vapor loss.

The effect of turbulence on vapor loss was investigated (reference 9) by use of a three-bladed propeller installed in the tank. This mechanism simulated the turbulence arising from use of submerged fuel booster pumps. Two series of tests were made: one in which the fuel was thrust downward, and another in which the fuel was thrust upward. The results are shown in figure IX-22. For the range of speeds investigated the fuel vapor loss increased with speed irrespective of the direction of thrust.

A third method of agitation was investigated in which the fuel tank was oscillated to simulate sloshing of the fuel during flight. The tank was rocked through an angle of 5° at rates

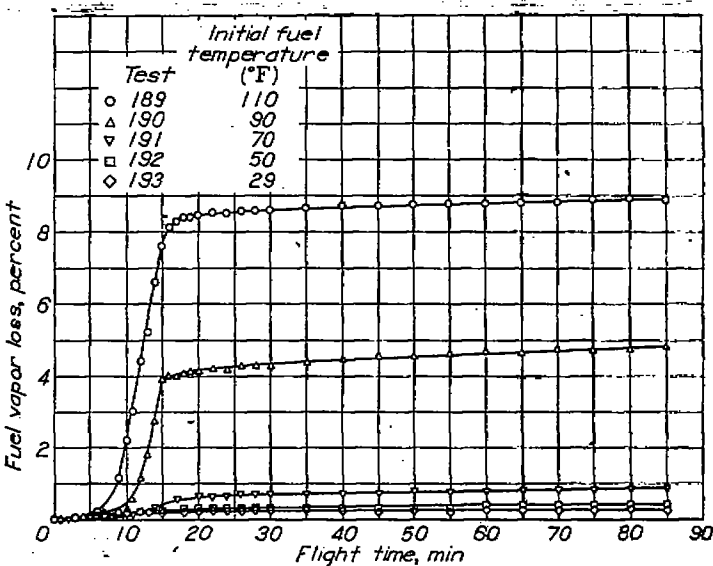


FIGURE IX-19.—Variation of fuel vapor loss with initial fuel temperature, during simulated flight. (Fig. 11 of reference 9.)

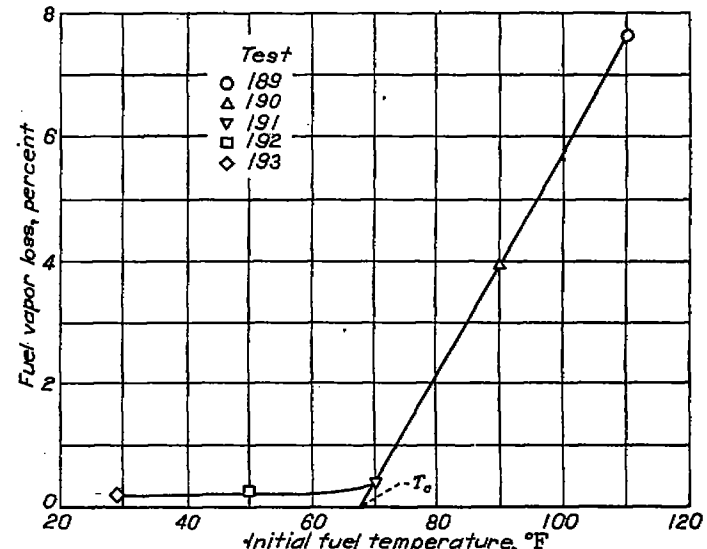


FIGURE IX-20.—Variation of fuel vapor loss at end of climb period with initial fuel temperature during simulated flight. (Fig. 12 of reference 9.)

of 40 and 60 cycles per minute. Fuel vapor loss was increased (fig. IX-23) by this method of agitation.

Flight correlation.—A comparison was made between the flight and bench-test apparatuses used for determination of fuel vapor loss. (See reference 9.) The flight paths followed in these tests are shown in figure IX-24. In both cases the initial fuel temperature was 108° F. The fuel vapor loss resulting from each of the two methods is shown in figure IX-25. The difference in vapor loss measured by the two methods was about 0.06 percent.

EFFECT OF FUEL VAPOR LOSS ON INSPECTION PROPERTIES OF AVIATION FUELS

The effects of fuel vapor loss on the properties of two typical service fuels (AN-F-28 (28-R) and AN-F-33 (33-R)) were investigated in reference 10. These fuels were weathered in a simulated-altitude apparatus shown diagrammatically in figure IX-26. This apparatus represents an improvement over the apparatus described in the preceding section of this chapter. (See fig. IX-15.)

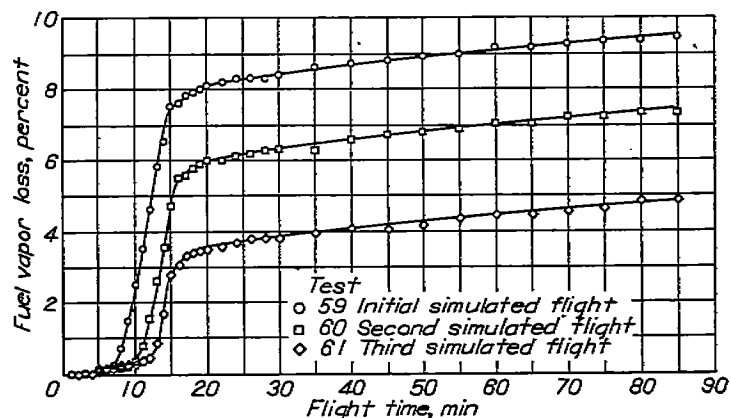


FIGURE IX-21.—Fuel vapor loss during successive standard simulated flights with given fuel sample. (Fig. 13 of reference 9.)

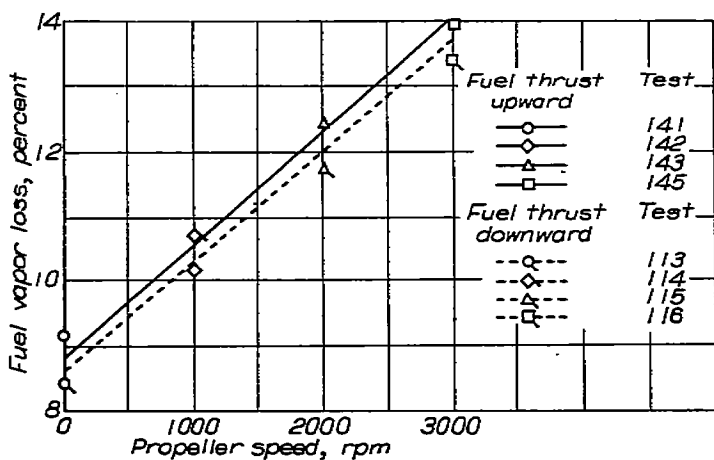


FIGURE IX-22.—Fuel vapor loss at end of standard simulated flight with induced fuel turbulence produced by rotating propeller with blade angle at 30°. (Fig. 17 of reference 9.)

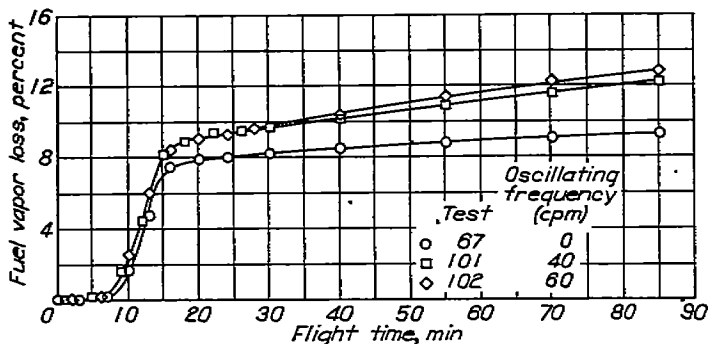


FIGURE IX-23.—Fuel vapor loss during standard simulated flight with fuel tank oscillated through angle of 5°. (Fig. 18 of reference 9.)

The fuels were weathered during a simulated flight consisting of climb at a rate of 1000 feet per minute to an altitude of 30,000 feet. The altitude of 30,000 feet was maintained for approximately 10 minutes after the end of the climb. Because fuel vapor loss is dependent on the temperature (fig. IX-19) of the fuel in an airplane tank at the time of take-off, two initial fuel temperatures (90° and 130° F) were used in the weathering tests of each fuel.

The data obtained from the weathering tests indicated that with 28-R about 3.6 percent (by weight) of the fuel was lost during a simulated flight in which the initial fuel temper-

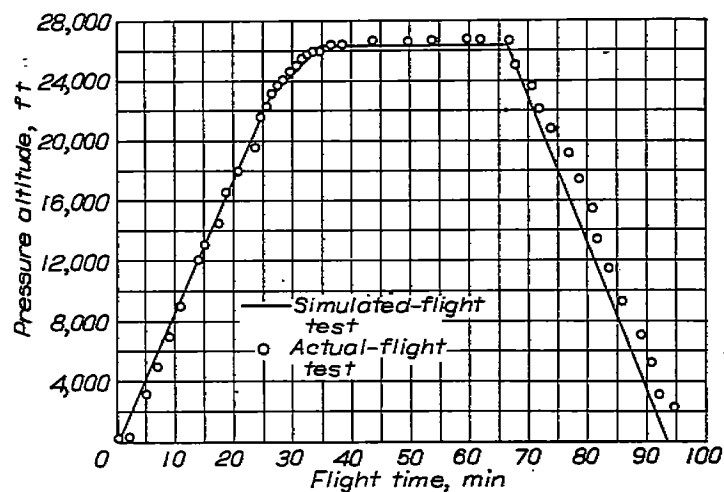


FIGURE IX-24.—Flight paths followed for both simulated and actual flight tests. (Fig. 19 of reference 9.)

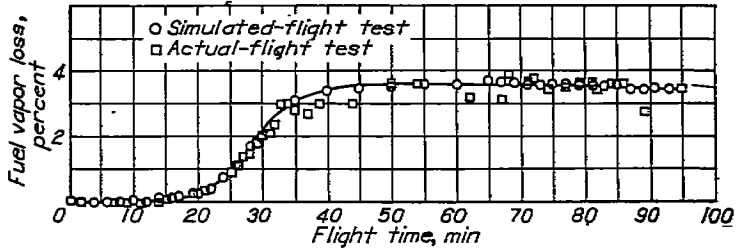


FIGURE IX-25.—Fuel vapor loss during simulated and actual flights. (Fig. 20 of reference 9.) Initial fuel temperature, 108° F.

ature was 90° F. For an initial temperature of 130° F the loss was about 12.8 percent. With 33-R the losses were about 3.5 and 14.3 percent at temperatures of 90° and 130° F, respectively.

Inspection data for both weathered and unweathered fuel samples are shown in table IX-3. The data in this table show that, as a result of the weathering loss, the distillation temperatures were increased and the Reid vapor pressures decreased. The greatest increase in distillation temperature occurred in the low temperature range. Specific gravities, aromatic concentrations, and tetraethyl lead concentrations were increased.

If the data for the weathered samples are compared with the specification limits, it is seen that the samples of 28-R and 33-R fuels, weathered from an initial temperature of 90° F, meet the requirements with the exception of lead concentrations. The 50-percent-evaporated temperature for 33-R is about 3° higher than permitted, but this difference is within the precision of the A. S. T. M. distillation procedure.

For an initial fuel temperature of 130° F the weathered sample of 28-R still meets the requirements with the exception of tetraethyl lead concentration, whereas 33-R is unacceptable because of the high 50-percent-evaporated temperature as well as the high tetraethyl lead concentration. Both weathered samples have a Reid vapor pressure of 4.6 pounds per square inch, which is a lower value than that of most aviation fuels. Under current aviation-fuel specifications, a low Reid vapor pressure is permissible as long as the low-end distillation temperatures are within the specified limits.

TABLE IX-3.—INSPECTION DATA FOR WEATHERED AND UNWEATHERED SAMPLES OF 28-R AND 33-R FUELS*

	28-R			33-R				
	AN-F-28 specifications	Unweathered	Weathered		AN-F-33 specifications	Unweathered	Weathered	
			b 90° F	b 130° F			b 90° F	b 130° F
Tetraethyl lead, ml/gal.....	4.6 (max.)	4.61	4.81	5.49	4.6 (max.)	4.53	4.72	5.29
Specific gravity 60°/60° F.....	0.725	0.729	0.739	0.706	0.710	0.718
Reid vapor pressure, lb/sq in.....	7.0 (max.)	6.6	6.0	4.6	7.0 (max.)	6.6	5.9	4.6
Aromatics, percent by volume.....	15.1	15.3	17.7	7.8	7.7	9.3
A. S. T. M. distillation								
Percentage evaporated		Temperature, ° F						
0.....	109	108	117	167 (max.)	103	104	116	
10.....	137	142	160	167 (min.)	134	140	163	
40.....	194	200	213	167 (min.)	196	204	220	
50.....	221 (max.)	213	217	221 (max.)	219	224	232	
90.....	284 (max.)	274	276	275 (max.)	272	274	279	
End point.....	356 (max.)	322	326	356 (max.)	344	349	357	
Sum of 10- and 50-percent points.....	307 (min.)	360	369	307 (min.)	353	364	365	
Residue, percent.....	1.5 (max.)	0.6	0.4	1.5 (max.)	0.9	0.9	0.8	
Loss, percent.....	1.5 (max.)	1.4	1.4	0.8	1.5 (max.)	1.1	1.1	0.7

* Table I of reference 10.

b Temperature of fuel at start of simulated flight.

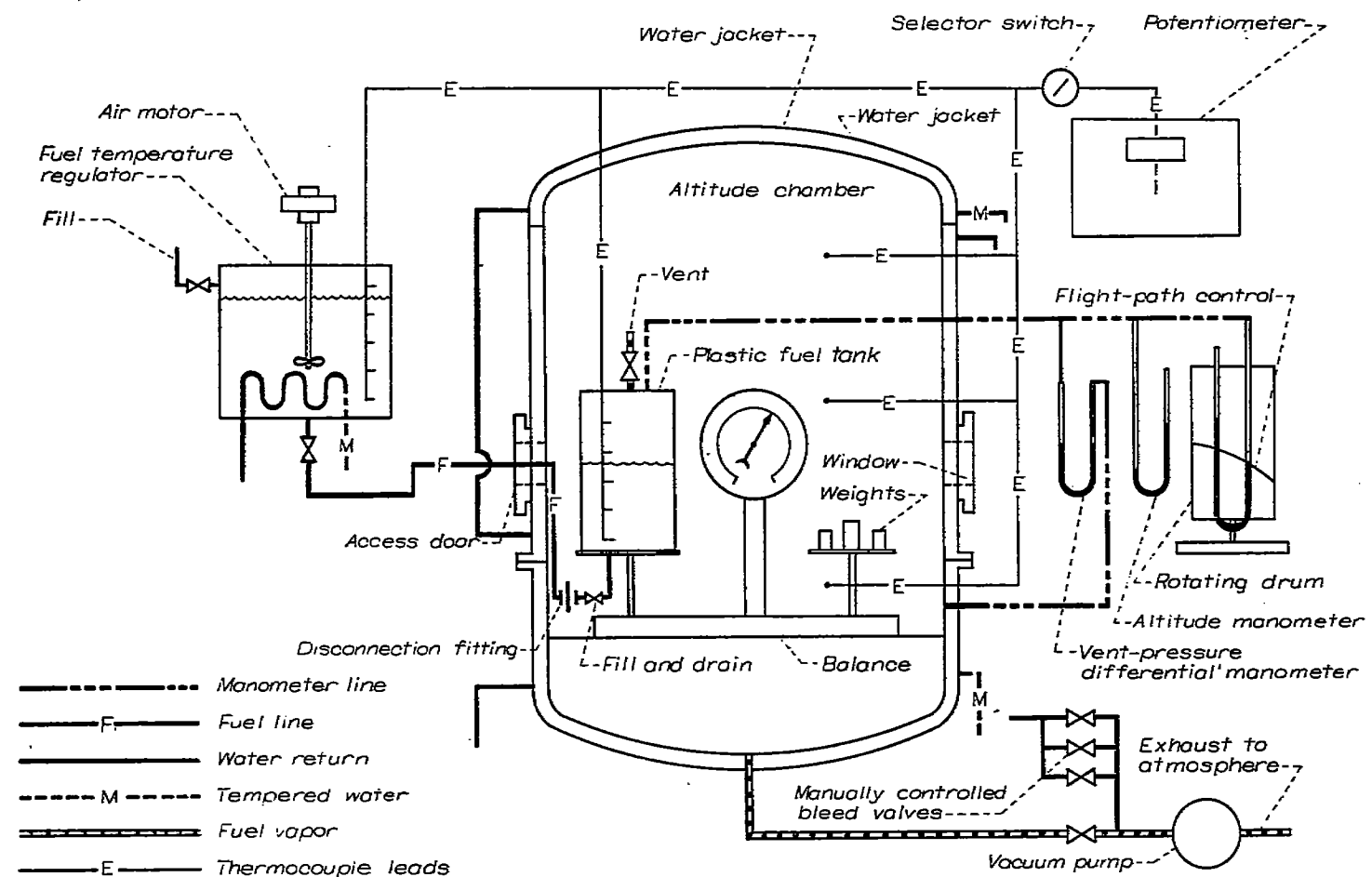


FIGURE IX-28.—Simulated-altitude bench-test installation for determination of fuel vapor loss. (Fig. 1 of reference 10.)

In an earlier investigation (reference 11) an equation was derived to permit estimation of fuel vapor loss by change in specific gravity:

$$L = K(A - A_0)$$

where

L percentage fuel loss

A final specific gravity of fuel at 20° C (68° F)

A_0 initial specific gravity of fuel at 20° C (68° F)

K constant, characteristic of each fuel

The values of the constant K were evaluated (reference 11) for the six fuels used in this study and were plotted against the initial specific gravity (A_0) in figure IX-27.

EFFECT OF FUEL VAPOR LOSS ON KNOCK-LIMITED PERFORMANCE

The A. S. T. M. Aviation (lean) and A. S. T. M. Supercharge (rich) antiknock ratings for 28-R and 33-R are shown in the following table (reference 10). Two rows of ratings are given for each fuel. The first row is milliliters of tetraethyl lead per gallon in S reference fuel and the second row is performance number. The A. S. T. M. Aviation ratings determined for unweathered 28-R and 33-R are higher than the nominal ratings for these fuels.

Fuel	Condition	A. S. T. M. Aviation rating	A. S. T. M. Supercharge rating
28-R	Nominal rating.....	0	1.28
28-R	Unweathered.....	100	1.30
28-R	Weathered (*90° F).....	103	1.31
28-R	Weathered (*130° F).....	108	1.31
33-R	Nominal rating.....	104	1.30
33-R	Unweathered.....	107	1.32
33-R	Weathered (*90° F).....	103	1.33
33-R	Weathered (*130° F).....	115	1.45

*Temperature of fuel at start of simulated flight.

The data indicate that the loss of fuel vapor resulting from weathering has little or no effect on the ratings of the two fuels. If the changes in ratings can be assumed to be significant, the A. S. T. M. Aviation and A. S. T. M. Supercharge performance numbers of both fuels increase slightly. These comparisons should be valid inasmuch as the data were obtained on the same operating day.

REFERENCES

1. Marble, Frank E., Butze, Helmut F., and Hickel, Robert O.: Study of the Mixture Distribution of a Double-Row Radial Aircraft Engine. NACA ARR E5I05, 1945.
2. Gerrish, Harold C., and Meem, J. Lawrence, Jr.: The Measurement of Fuel-Air Ratio by Analysis of the Oxidized Exhaust Gas. NACA Rep. 757, 1943.
3. Cook, Harvey A., and Olson, Walter T.: Small-Orifice Tubes for Minimizing Dilution in Exhaust-Gas Samples. NACA ARR, Feb. 1943.
4. Marble, Frank E., Ritter, William K., and Miller, Mahlon A.: Effect of the NACA Injection Impeller on the Mixture Distribution of a Double-Row Radial Aircraft Engine. NACA Rep. 821, 1945. (Formerly TN 1069.)
5. Michel, Donald J., Hickel, Robert O., and Voit, Charles H.: Performance of a Double-Row Radial Aircraft Engine with Three Methods of Safety-Fuel Injection. NACA TN 1413, 1947.
6. Schey, Oscar W., and Young, Alfred W.: Performance of a Fuel-Injection Spark-Ignition Engine Using a Hydrogenated Safety Fuel. NACA Rep. 471, 1933.
7. Schey, Oscar W.: Performance of Aircraft Spark-Ignition Engines With Fuel Injection. SAE Jour., vol. 46, no. 4, April 1940, pp. 166-176.
8. White, H. Jack, and Engelman, Helmuth M.: Effect of Fuel Volatility on Performance of a Wright R-2600-8 Engine as Influenced by Mixture Distribution. NACA ARR E4I05, 1944.
9. Stone, Charles S., Baker, Sol, and Black, Dugald O.: Flight Variables Affecting Fuel-Vapor Loss from a Fuel Tank. NACA MR E4L28, 1944.
10. Barnett, Henry C., and Marsh, Edred T.: Effects of Fuel-Vapor Loss on Knock-Limited Performance and Inspection Properties of Aviation Fuels. NACA RB E6C01, 1946.
11. Stone, Charles S., and Kramer, Walter E.: Fuel-Vaporization Loss as Determined by the Change in the Specific Gravity of the Fuel in an Aircraft Fuel Tank. NACA RB E5E19, 1945.

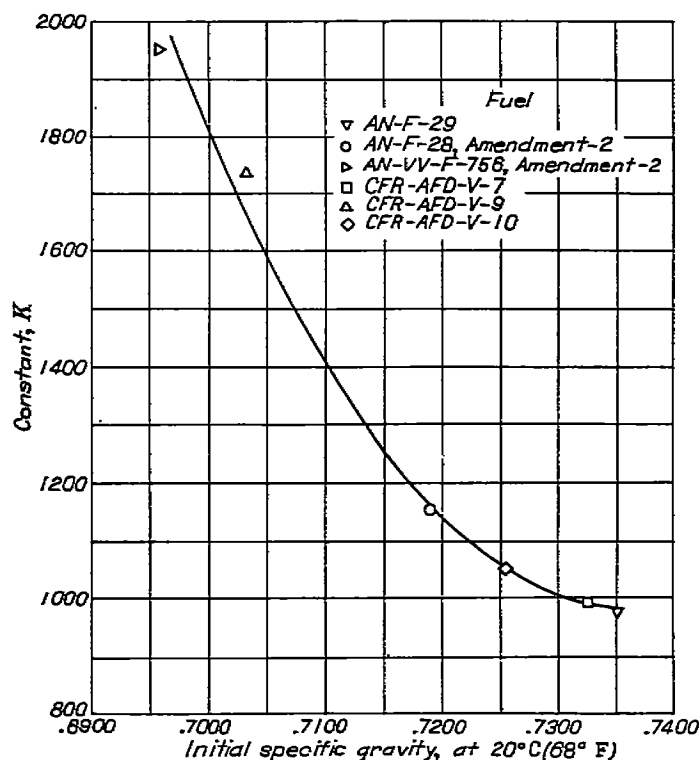


FIGURE IX-27.—Variation of constant K with initial specific gravity of fuel. (Fig. 6 of reference 11.)

CHAPTER X

INTERNAL COOLING

Over a period of years, improvements in fuel performance have made it necessary to improve engine-cooling facilities in order to take full advantage of power potentialities of a given fuel. Cooling studies (reference 1) indicate that more and more heat must be disposed of through the engine walls as the specific power output of the engine is increased. If adequate cooling is assumed to be solely dependent on heat transfer through the cylinder walls, the search for better engine cooling is a continuing process accompanying the ever-increasing antiknock quality of conventional fuels. Although these comments pertain primarily to air-cooled engines, the same might be said of liquid-cooled engines in regard to radiator size and cooling drag.

Complete dependency on heat transfer through cylinder walls for adequate cooling can, however, be avoided by a method commonly called *internal cooling*. Internal cooling may be defined as the injection of an auxiliary liquid into the fuel-air charge at some point before the engine intake port. A desirable liquid for internal cooling should have a high latent heat of vaporization, since the more heat extracted from the charge fuel-air mixture, the greater the cooling attained. The reduction in temperature of the mixture achieved by the use of an internal coolant will result in lower cylinder temperatures and will extend the knock-free performance range. In addition to the advantage of increased permissible power, two other goals in the use of internal coolants are savings in fuel and savings in total liquid consumption.

Each of these objectives may be sought in itself by disregarding changes in the other two or it may be sought in combination with one or both of the others in an effort to balance advantages against disadvantages. The most outstanding advantage of internal cooling is, however, the increase in knock-limited or cooling-limited power that it makes possible.

Where gasoline shortages exist because of out-of-the-way destinations of transport airplanes or because of air routes requiring transportation by air of the gasoline used, the possibility of savings in gasoline is particularly pertinent. Such savings may result from the use of internal cooling rather than fuel enrichment to suppress knock at high

power output. In this case water would be the most efficient internal coolant if freezing temperatures were not encountered in the internal-coolant system. Temperatures below freezing would necessitate either the addition of a freezing-point depressant or the use of a lagged or heated water system. Special cases and requirements must obviously determine which of these methods is most advantageous.

The material that appears in the succeeding portions of this chapter considers only the case of internal cooling wherein the coolant is injected at some point in the intake-air system of the engine. Water injection was treated briefly in chapter I, however, where it was found that knock could be suppressed in an engine by injection of water directly into the combustion end zone. This method was suggested as a means of economizing on the quantity of coolant that might be required to reduce knock.

EFFECT OF INTERNAL COOLANTS ON ENGINE PERFORMANCE

Several investigations (references 2 to 4) have been conducted by the NACA in which the effectiveness of internal cooling with respect to knock-limited and temperature-limited performance has been illustrated. In one of these investigations (reference 4) a V-type 12-cylinder liquid-cooled aircraft engine was used as the test engine.

Water was continuously injected through 12 spray bars inserted into the intake manifolds through holes drilled in the top of the manifolds about 1 inch back from the faces of the manifold mounting flanges, as shown in figure X-1. The spray bars (fig. X-2) were of $\frac{1}{2}$ -inch-diameter, stainless steel tubing about $2\frac{1}{2}$ inches long with six holes, each 0.016 inch in diameter, arranged in two rows of three holes each, to spray water directly into each intake port. Water was applied to the spray bars by individual lines from a tank, which was kept under pressure with compressed air.

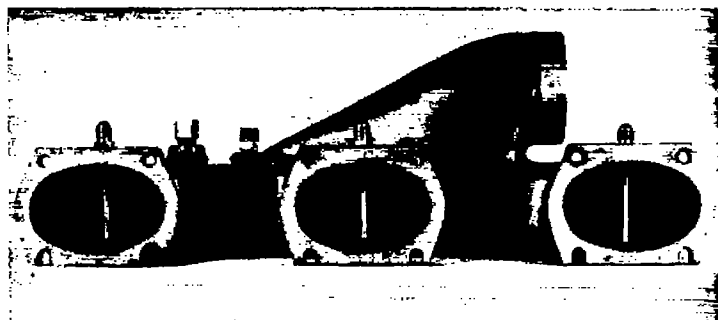


FIGURE X-1.—Intake manifold with water spray bars in position. (Fig. 1 of reference 4.)

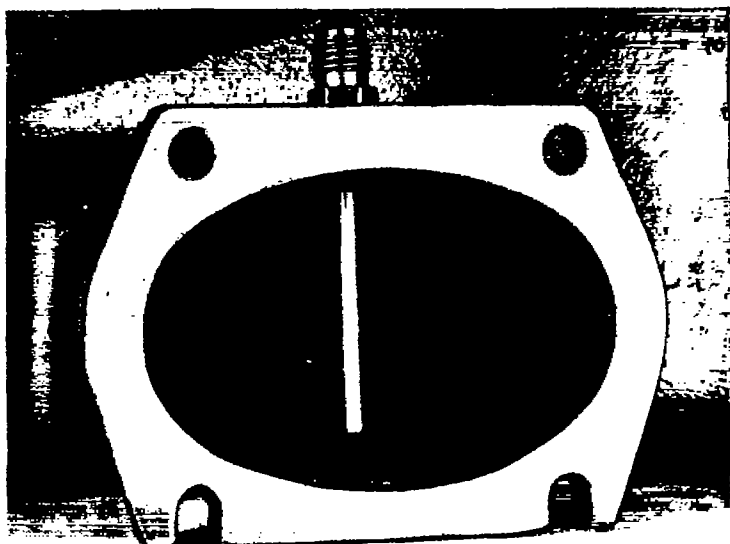
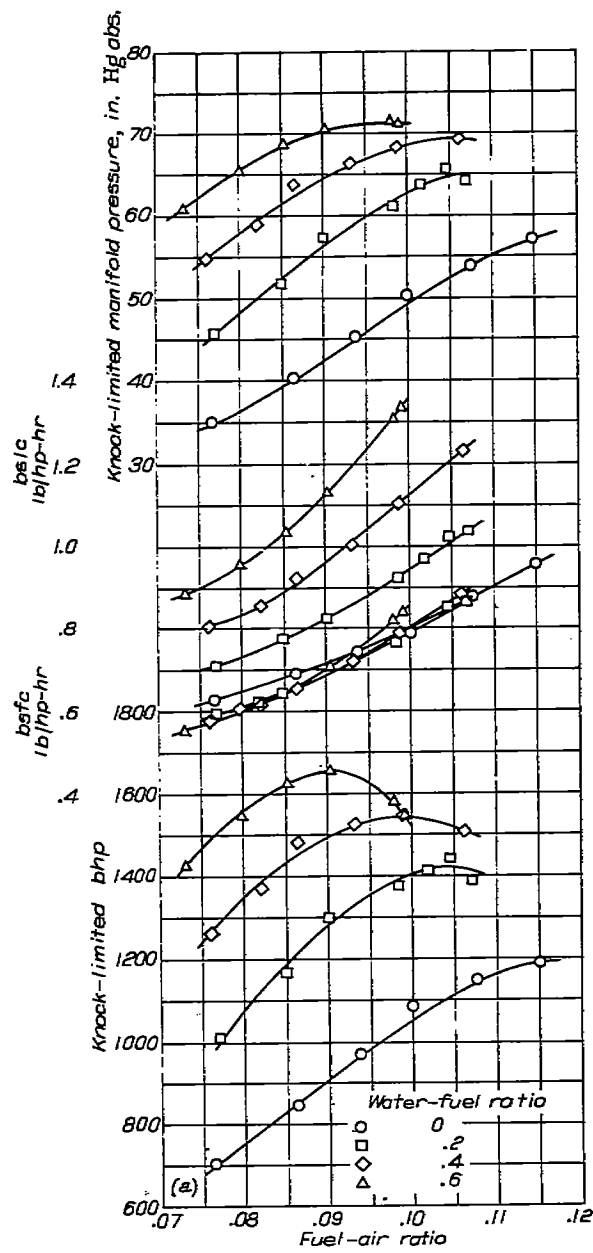


FIGURE X-2.—Closeup of water spray bar inserted in intake manifold. (Fig. 2 of reference 4.)

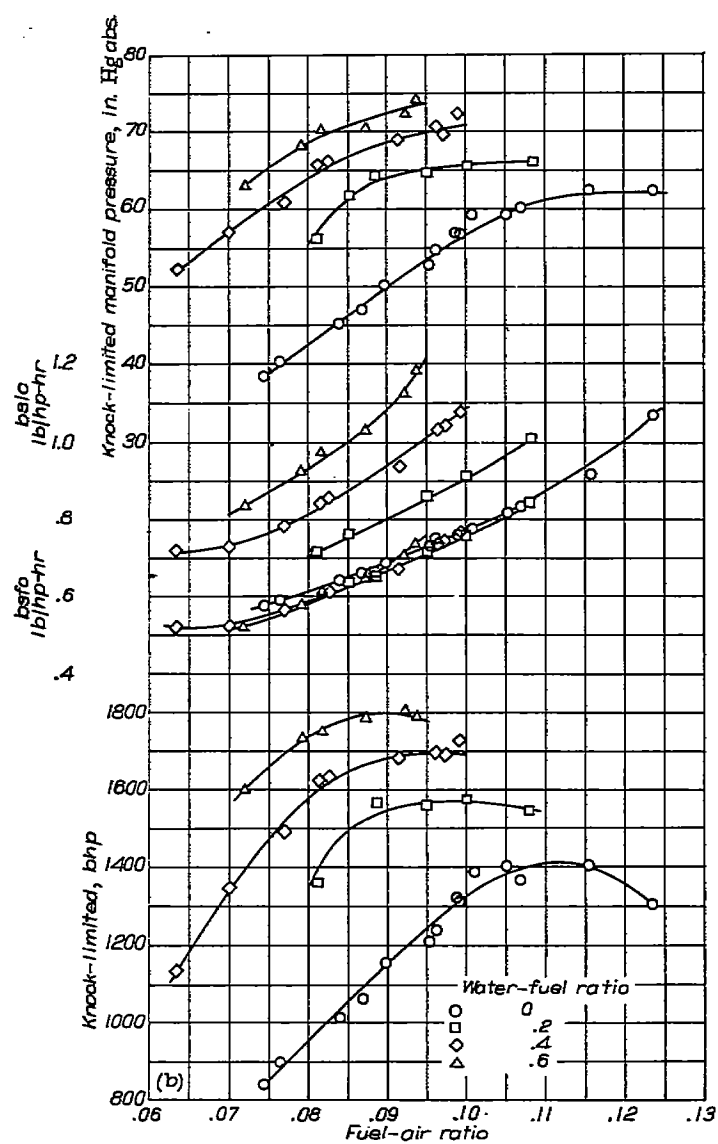
With this injection system, knock-limited performance data were obtained at carburetor-air temperatures of 158°, 101°, and 50° F (fig. X-3). In figure X-3 (a) the peaks of the knock-limited brake horsepower curves occur at successively leaner mixtures as the water-fuel ratio is increased. At a water-fuel ratio of 0.6, a rapid decrease in knock-limited power was found as the fuel-air ratio was increased beyond about 0.092. Similar results were found at the other carburetor-air temperatures; however, at a carburetor-air temperature of 50° F (fig. X-3 (c)) the sharp decline in knock-limited brake horsepower at a water-fuel ratio of 0.6 occurred at fuel-air ratios greater than 0.08.

At the three carburetor-air temperatures investigated, the brake specific fuel consumption was lower with water injection than without at fuel-air ratios leaner than 0.092. This



(a) Carburetor-air temperature, 158° F. (Fig. 4 of reference 4.)

FIGURE X-3.—Knock-limited performance with water injection. V-type 12-cylinder liquid-cooled engine; fuel, AN-F-28, Amendment-2; engine speed, 3000 rpm.



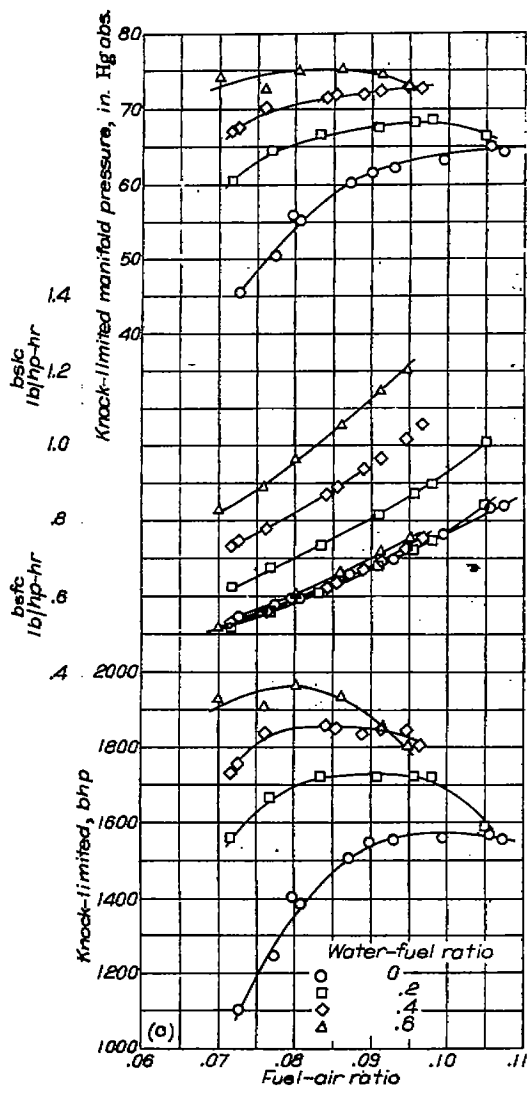
(b) Carburetor-air temperature, 101° F. (Fig. 5 of reference 4.)

FIGURE X-3.—Continued. Knock-limited performance with water injection. V-type 12-cylinder liquid-cooled engine; fuel, AN-F-28, Amendment-2; engine speed, 3000 rpm.

reduction is caused partly by increased mechanical efficiency of the engine at the high power outputs attainable with water injection.

Cross plots of the data in figure X-3 are shown in figure X-4 for two fuel-air ratios. With the exception of the data at 0.095 fuel-air ratio and 50° F carburetor-air temperature, increases of water-fuel ratio resulted in increases of knock-limited brake horsepower. For the excepted data, water-fuel ratios greater than 0.45 resulted in a decrease of knock-limited power.

The effect of internal cooling on cylinder-head temperatures was also observed in reference 4. The average cylinder-head temperatures for the engine are shown in figure X-5 as a function of water-fuel ratio and knock-limited power. It is apparent in this figure that as the water-fuel ratio increases, the power increases continuously; however, the cylinder-head temperatures pass through a maximum. The water-fuel ratio at which this maximum occurs increases as the carburetor-air temperature increases.



(c) Carburetor-air temperature, 50° F. (Fig. 6 of reference 4.)

FIGURE X-3.—Concluded. Knock-limited performance with water injection. V-type 12-cylinder liquid-cooled engine; fuel, AN-F-28, Amendment-2; engine speed, 3000 rpm.

Effect of internal cooling on fuel consumption.—Under high-power cruise operation, over-all fuel enrichment may be necessary in order to prevent an increase in cylinder temperatures beyond the specified maximum. This practice obviously results in higher fuel consumption than would ordinarily be desired in the interest of range considerations. However, the same end result can be achieved by adding additional fuel only to the hottest cylinders.

This fact is substantiated by results obtained in an unpublished NACA investigation conducted in an air-cooled engine. The results indicated that lower brake specific fuel consumptions could be obtained at high cruising power, with no increase in maximum rear-spark-plug-gasket temperatures, by injecting additional fuel to the hottest cylinders and operating the engine in automatic-lean mixture setting instead of the automatic-rich mixture setting usually recommended. The fuel savings varied between 6 and 10 percent for two engines tested in flight and one engine tested in an altitude wind tunnel. It was found, however, that little or no fuel saving

is realized when additional fuel is supplied to the hot cylinders unless the temperature spread among the cylinders before enrichment is very large.

Another investigation conducted in an air-cooled engine (reference 5) showed that further gains in fuel economy could be achieved by using water instead of fuel to cool the hottest cylinders. In this particular study, it was found that the use of water instead of excess fuel to maintain engine temperature limits at powers normally requiring a fuel-air ratio of about 0.09 resulted in a decrease of approximately

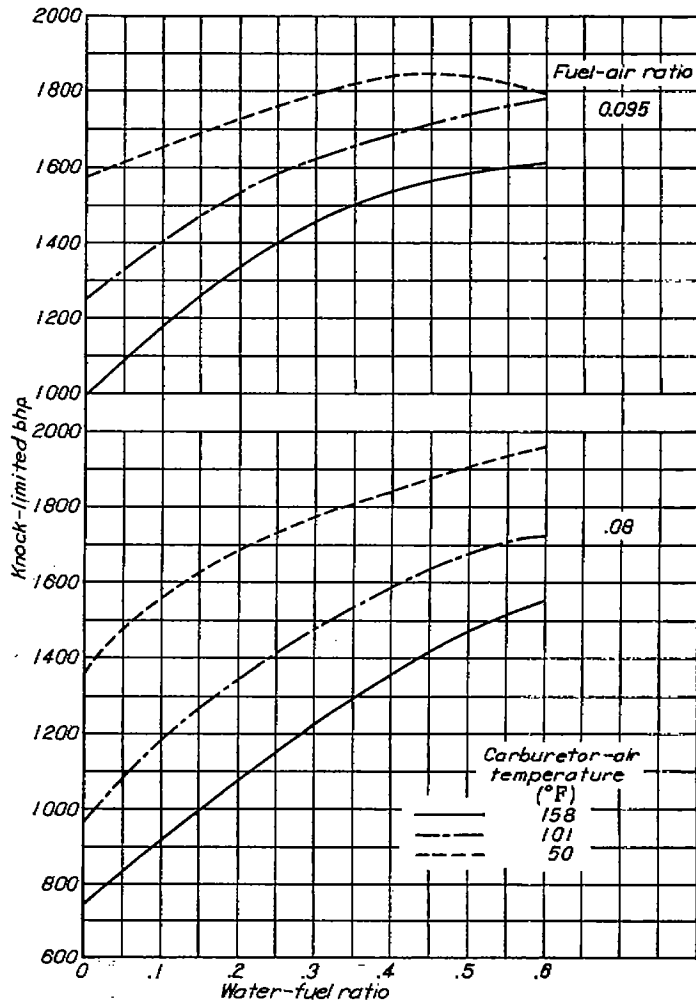


FIGURE X-4.—Variation of knock-limited brake horsepower with water-fuel ratio for three carburetor-air temperatures and two fuel-air ratios. V-type 12-cylinder liquid-cooled engine; fuel, AN-F-28, Amendment-2; engine speed, 3000 rpm. Cross plot from figure X-3. (Fig. 14 of reference 4.)

26 percent in brake specific fuel consumption with an increase of about 3 percent in brake specific liquid consumption.

It is obvious from the foregoing discussion that water injection in aircraft engines permits temperature-limited cruising powers to be reached at reduced engine speeds and increased brake mean effective pressures with fuel-air mixtures very near that for maximum economy. Furthermore, significant improvements in fuel consumption can be attained without appreciable increases in over-all liquid consumption.

These findings have been further substantiated by a study reported in reference 6 in which it was found that for typical air-cooled aircraft engines operating under cruising conditions in which overheating is ordinarily prevented by enriching the fuel-air mixture to the entire engine, the fuel consumption may be reduced 7 to 37 percent by adding water or fuel to only the overheated cylinders.

Effect of internal cooling on spark-advance requirements.—Internal cooling can also be utilized to take advantage of gains that may be achieved by retarding the spark timing of an engine. This fact was demonstrated in an investigation (reference 7) conducted in a liquid-cooled single-cylinder test engine. Two positions were used for the injection of

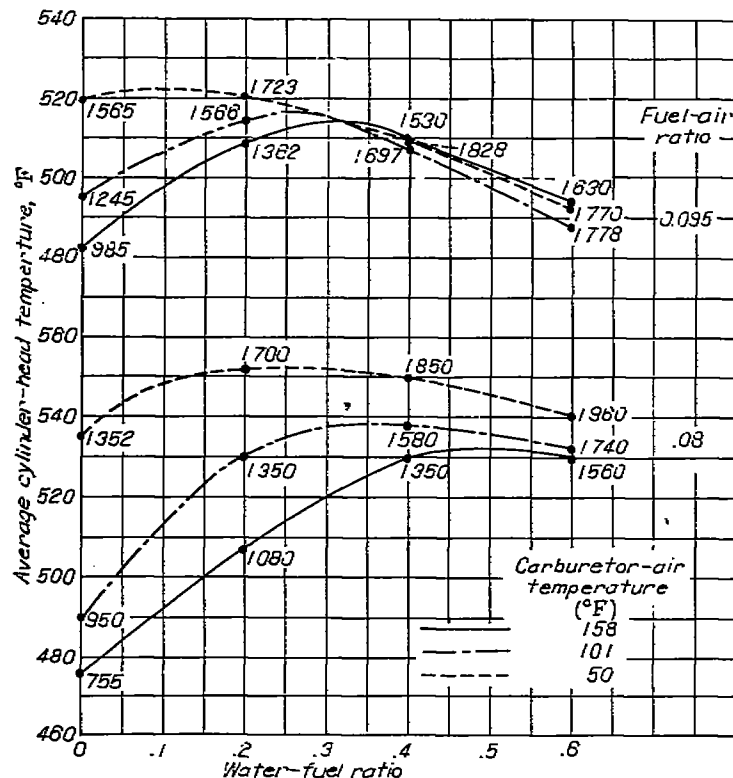


FIGURE X-5.—Variation of average cylinder-head temperature with water-fuel ratio at knock-limited power for three carburetor-air temperatures. V-type 12-cylinder liquid-cooled engine; fuel, AN-F-28, Amendment-2; engine speed, 3000 rpm. (Fig. 13 of reference 4.) Numbers on curves are values of knock-limited brake horsepower.

internal coolant: position A before the vaporization tank and position B at the intake elbow. In both positions the coolant was discharged downstream. The positions of injection are illustrated in figure X-6.

The effect of internal-coolant-fuel ratio on spark advance for peak power is shown in figure X-7. For both types of injection, the spark advance required for peak power was greater when the coolant was injected before the vaporization tank than at the injection elbow; however, the difference was small when a 50:50 mixture of water and ethyl alcohol was used as the coolant. This result indicates that the water, when injected before the vaporization tank and allowed to mix thoroughly with the fuel-air mixture, slowed the flame speed more than when injected at the intake elbow.

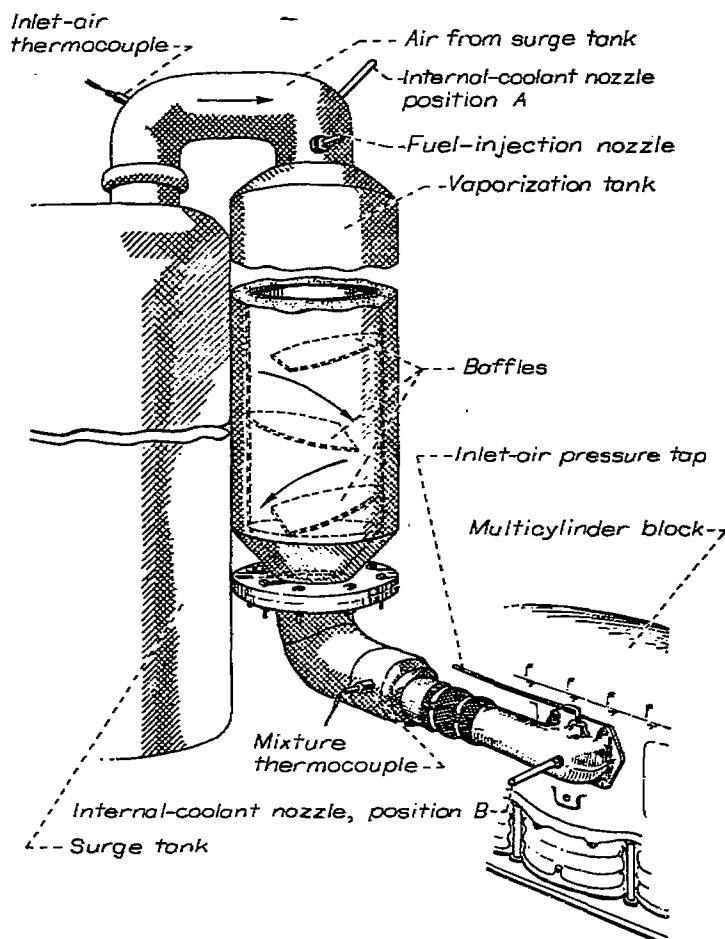


FIGURE X-6.—Induction system used with multicylinder-block adaptation to CUE crankcase showing two positions of internal-coolant nozzle. (Fig. 2 of reference 7).

The flame speed was slowed to about the same degree regardless of injection position for the 50:50 mixture of water and ethyl alcohol.

At the same internal-coolant-fuel ratios (fig. X-7) and for the same coolant injector location, the water-ethyl-alcohol mixture retarded burning less than the injection of pure water. This difference can be attributed to the fact that the alcohol is a fuel and as such is contributing to the combustion process.

In figure X-8 is illustrated the effect of internal-coolant-fuel ratio on the mixture temperatures corresponding to the data of figure X-7. The data for figure X-8 represent the case in which the coolants were injected ahead of the vaporization tank. The mixture temperature decreased until the fuel-air mixture became saturated and for further additions of coolant beyond this point the mixture temperature remained constant. In a similar manner, the power at peak-power spark advance increased because of the increased charge weight inducted into the cylinder until the internal-coolant-fuel ratio for saturation was reached, at which point the power leveled off. (See fig. X-9.) Beyond the point of complete saturation the additional cooling of the mixture must occur after the intake valves close, which makes it impossible to increase engine power through an effect on air flow. Further additions of coolant caused a

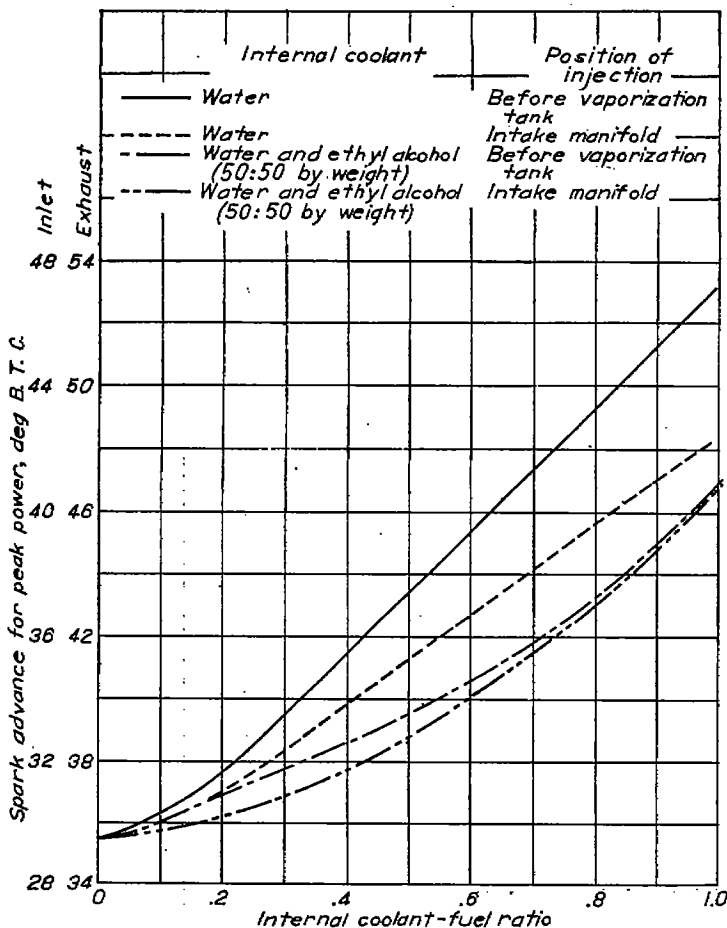


FIGURE X-7.—Effect of internal coolant-fuel ratio on spark advance for peak power for two internal coolants and two positions of injection. Single-cylinder adaptation of multicylinder engine to CUE crankcase; compression ratio, 6.65; engine speed, 3000 rpm; fuel-air ratio 0.03; inlet-oil temperature, 185° F; outlet-coolant temperature, 250° F; inlet-air temperature, 250° F; inlet-air pressure, 30 inches of mercury absolute. (Fig. 11 of reference 7.)

decrease in the power obtainable at peak-power spark advance because some heat of vaporization was extracted from the air during the compression stroke; decreased cycle efficiency resulted. The power increase at peak-power spark advance was small when coolant was injected at the intake elbow (fig. X-9) because so little time was available for charge cooling before the intake valves closed.

The percentage loss in power at various values of spark advance over that obtained by using peak-power spark advance is shown in figure X-10 for each internal-coolant-fuel ratio investigated. The data in this figure indicate that operation with normal spark timing at a given coolant-fuel ratio and position of injection results in a power loss approximately twice as high for water as for the mixture of water and ethyl alcohol.

USE OF INTERNAL COOLING FOR INCREASED TAKE-OFF POWER

In 1944 an analysis was made by the NACA to evaluate the use of internal cooling as a means of increasing take-off power. This study (reference 8) was made for four airplanes to determine the effects of a 25-percent increase in take-off power on the take-off load of the airplane. The operating

characteristics of the airplanes considered are presented in the following table:

Airplane	Normal take-off horse-power	Normal fuel capacity		Gross weight of airplane (lb)
		(gal)	(lb)	
Heavy bomber.....	4800	1433	8598	41,000
Pursuit.....	2000	210	1200	11,870
Torpedo bomber.....	1700	301	1806	15,304
Shipboard fighter.....	2000	344	2064	12,677

For these airplanes the estimated increase in take-off load for a 25-percent increase in take-off power is as follows:

Airplane	Load increase (percent)	Load increase (lb)	Usable load increase (lb)	Usable load (gal of gasoline)	Percentage increase (gal of gasoline)
Heavy bomber.....	11.5	4710	3681	427	30
Pursuit.....	12.0	1430	1097	120	65
Torpedo bomber.....	10.5	1610	1300	153	51
Shipboard fighter.....	10.5	1320	1037	122	36

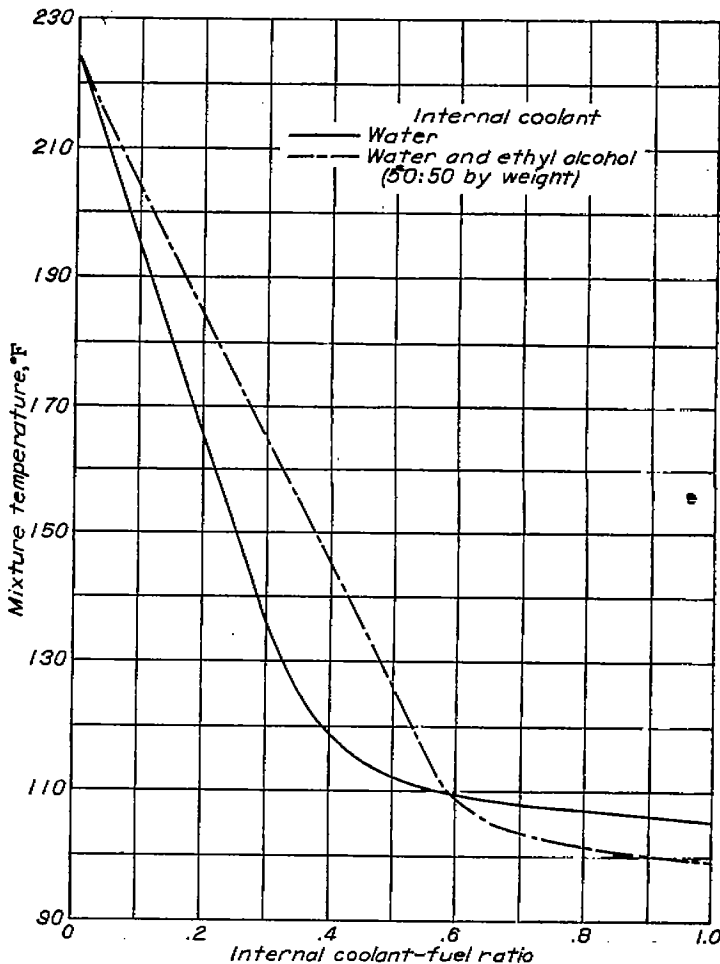


FIGURE X-8.—Effect of internal coolant-fuel ratio on mixture temperature for two internal coolants injected before the vaporization tank. Single-cylinder adaptation of multicylinder engine to CUE crankcase; compression ratio, 6.65; engine speed, 3000 rpm; fuel-air ratio, 0.03; inlet-oil temperature, 185° F; outlet-coolant temperature, 250° F; inlet-air temperature, 250° F; inlet-air pressure, 30 inches of mercury absolute. (Fig. 12 of reference 7.)

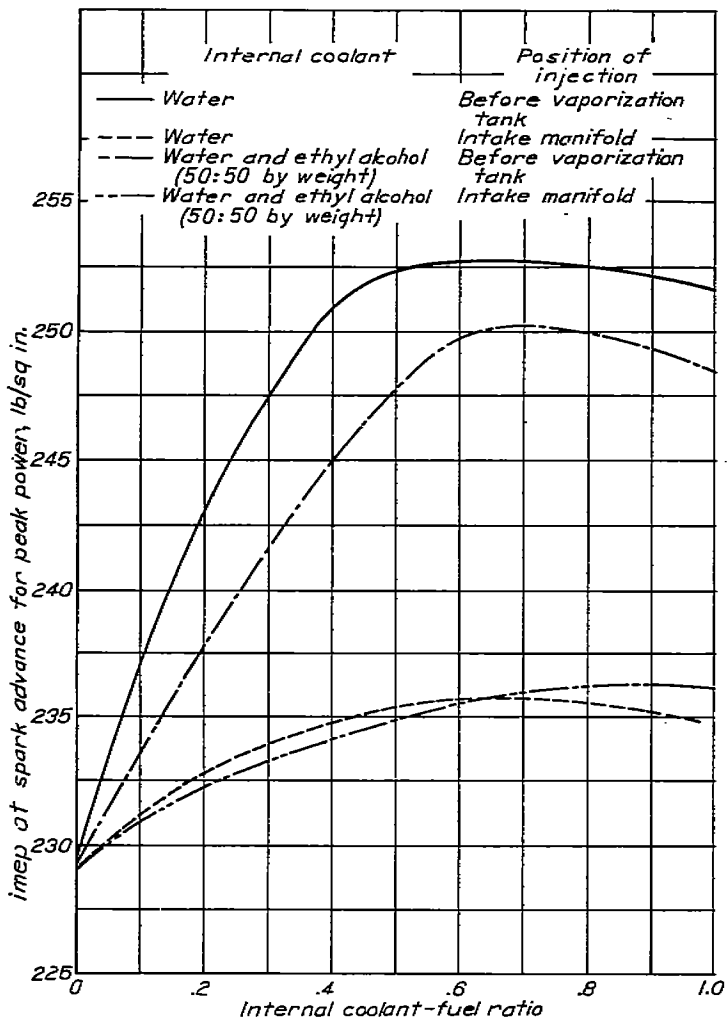


FIGURE X-9.—Effect of internal coolant-fuel ratio on engine power at spark advance for peak power for two internal coolants and two positions of injection. Single-cylinder adaptation of multicylinder engine to CUE crankcase; compression ratio, 6.65; engine speed, 3000 rpm; fuel-air ratio, 0.08; inlet-air temperature, 185° F; outlet-coolant temperature, 250° F; inlet-air temperature, 250° F; inlet-air pressure, 50 inches of mercury absolute. (Fig. 13 of reference 7.)

The data presented in the foregoing table indicate that marked increases in the usable load, or in this usable load translated into gallons of gasoline, may be achieved through use of internal cooling for 25-percent increased take-off power. These numerical estimates are necessarily dependent upon the assumed values for many factors. For example, these particular calculations include the following assumptions:

- (1) that 0.78 pound of coolant per pound of fuel is required to produce a 25-percent increase in take-off power. This quantity of coolant is about 45 percent higher than is indicated by experimental data in order to provide a factor of safety in the calculations.
- (2) that sufficient coolant is provided for 5-minute operation
- (3) that the increase in propeller weight for the additional power output is about 100 pounds
- (4) that the coolant system exclusive of the tank weight is about 75 pounds.

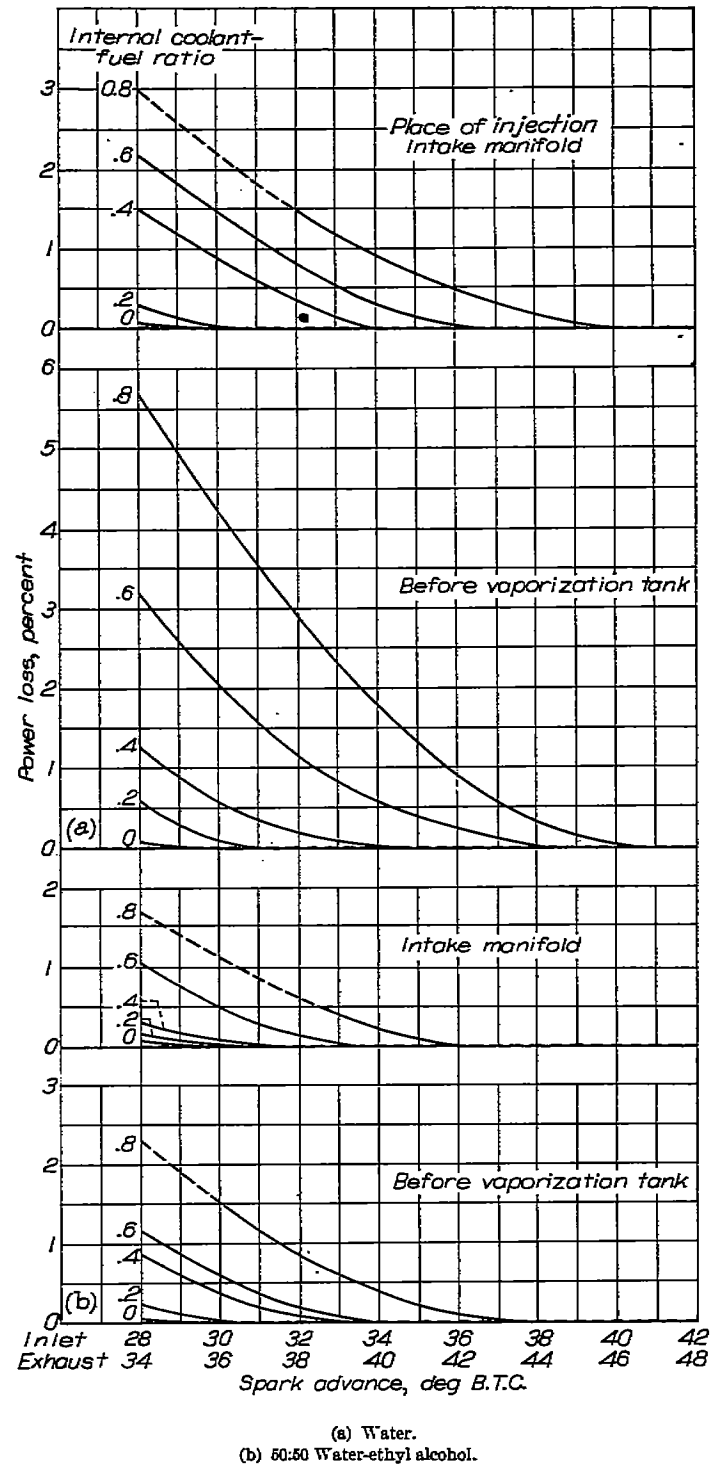


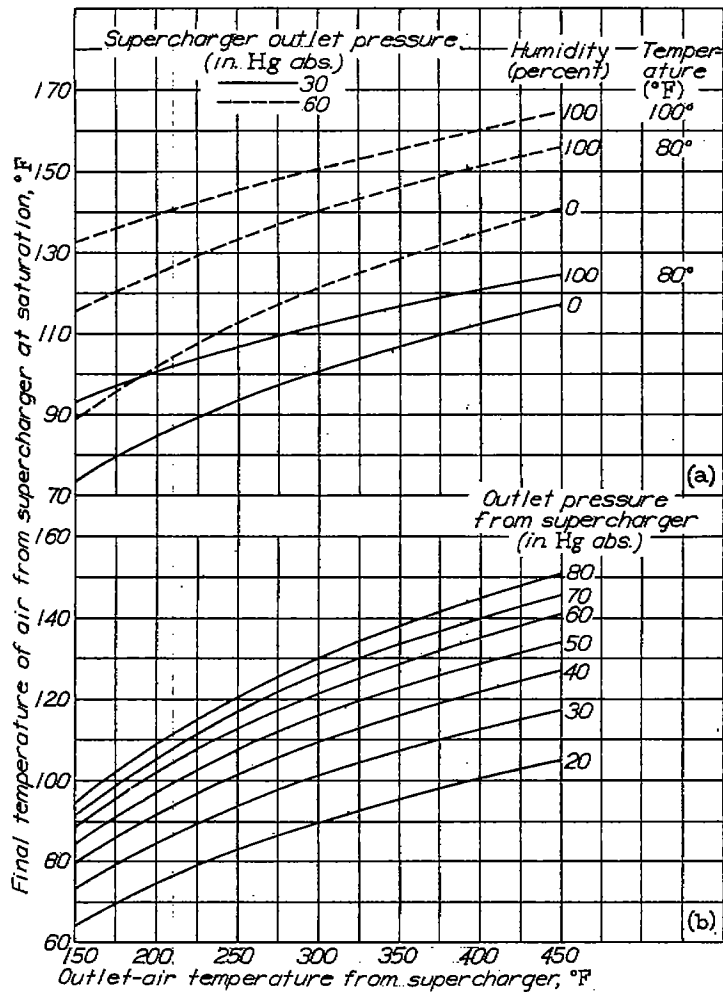
FIGURE X-10.—Loss in power incurred by operating without peak-power spark advance for several internal coolant-fuel ratios and for two positions of injection. Single-cylinder adaptation of multicylinder engine to CUE crankcase; compression ratio, 6.65; engine speed, 3000 rpm; fuel-air ratio, 0.08; inlet-air temperature, 185° F; outlet-coolant temperature, 250° F; inlet-air temperature, 250° F; inlet-air pressure, 50 inches of mercury absolute. (Fig. 14 of reference 8.)

Other details of the estimates may be found in reference 8.

In addition to the gains in usable load, certain gains may be realized in rate of climb and take-off run. The increase of 25 percent in take-off power indicated an increase in rate

of climb from 3100 to 4100 feet per minute up to an altitude of 12,000 feet for the pursuit-type airplane and 1600 to 2200 feet per minute for the torpedo bomber. The estimated take-off distances for the four airplanes are as follows:

Airplane	Normal take-off distance (ft)	Take-off distance 25-percent increase in take-off power (ft)
Heavy bomber.....	1700	1300
Pursuit.....	1300	1000
Torpedo bomber.....	300	200
Shipboard fighter.....	350	250



(a) Air at different humidities into supercharger.
(b) Dry air into supercharger.

FIGURE X-11.—Relation between outlet-air temperature from supercharger and final temperature of air when sufficient cooling water is induced for saturation of air. Water induced as a liquid at 60° F. (Fig. 7 of reference 9.)

PRACTICAL ASPECTS OF INTAKE-AIR COOLING BY WATER INJECTION

Inasmuch as the application of internal cooling to aircraft would necessarily require the installation of additional equipment, consideration has been given to means by which internal cooling might be applied without significant increase in aircraft weight. Calculations have been made (reference 9) to determine the extent to which the engine intake air is cooled by water injection. The results of these calculations,

presented in figure X-11, indicate that the degree of cooling achieved by water injection is sufficient to permit the elimination of normal intercooling and after-cooling in the supercharger. Consequently, the weight of equipment necessary for internal cooling might be offset by the elimination of the supercharger intercooler or aftercooler.

Further calculations reported in reference 9 indicate that the water to be used as internal coolant can be obtained by recovery from the exhaust gas. Sufficient water can be recovered from 50 percent of the exhaust gas to provide an inducted water-fuel ratio of 0.5.

EVALUATION OF VARIOUS LIQUIDS AS INTERNAL COOLANTS

As part of the problem of applying internal cooling to aircraft, extensive investigations have been conducted to evaluate the performance of various liquids as internal coolants. One such investigation, reported in reference 10, compares the performance of (1) water, (2) methyl alcohol and water, (3) ammonia, methyl alcohol, and water, (4) monomethylamine and water, (5) dimethylamine and water, and (6) trimethylamine and water. These studies were made on a high-speed supercharged CFR engine which is described in detail in reference 10. The internal coolant was continuously injected at room temperature into the injection elbow just above the fuel injection nozzle and parallel to the air flow.

The results of the investigation summarized in table X-1 indicate that when water is used as an internal coolant the greatest improvement in knock-limited performance of AN-F-28 fuel is achieved at lean fuel-air ratios. The mixture of methyl alcohol and water is a slightly better coolant than water at lean mixtures but considerably better at rich mixtures. As pointed out earlier in this chapter, the methyl alcohol is a fuel and as such contributes to the combustion process as well as the cooling. Of the coolants listed in table X-1, mixtures of water with monomethylamine or dimethylamine showed the greatest improvements in the knock-limited performance of AN-F-28; the increases in

TABLE X-1.—IMPROVEMENT IN KNOCK-LIMITED ENGINE PERFORMANCE OF AN-F-28 FUEL ACHIEVED BY INTERNAL COOLING

[OFR engine; compression ratio, 7.0; engine speed, 2500 rpm; Inlet-air temperature, 250° F; inlet-coolant temperature, 250° F; spark advance, 30° B. T. C.]

Internal coolant (0.5 lb/lb fuel)	Relative power ratio imep (fuel + internal coolant) — imep (fuel alone)			
	Fuel-air ratio			
	0.05	0.06	0.08	0.09
None.....	1.00	1.00	1.00	1.00
Water.....	1.14	1.52	1.41	1.28
Methylalcohol and water (70:30 by volume)	1.51	1.59	1.80	1.75
Monomethylamine and water (32:68 by weight)	1.98	1.81	1.86	1.83
Dimethylamine and water (26:74 by weight)	1.83	1.78	1.98	—

* Afterfiring encountered.

knock-limited indicated mean effective pressure ranged between 78 and 98 percent for different fuel-air ratios. The use of trimethylamine-water solution as an internal coolant lowered the knock-limited performance of AN-F-28.

The addition of anhydrous ammonia to the solution of methyl alcohol and water before injection (reference 10) reduced the knock-inhibiting effects of the solution of methyl alcohol and water and promoted afterfiring. Afterfiring also occurred when monomethylamine-water solution was used as an internal coolant (table X-1).

The effect of inlet-air temperature on the knock-limited performance of the internal coolants discussed previously is also reported in reference 10. A summary of these data (table X-2) shows that the addition of water reduced the temperature sensitivity of AN-F-28 fuel. The other coolants appeared to increase the sensitivity at lean fuel-air ratios but decreased the sensitivity at rich fuel-air ratios.

Perhaps the most impressive example of the advantages found for the internal coolants evaluated in reference 10 is the knock-limited performance of monomethylamine-water mixture at an inlet-air temperature of 150° F. This particular internal coolant, when added to AN-F-28 fuel, allowed a knock-limited power of 1.96 horsepower per cubic inch of cylinder displacement (imep of 620 lb/sq in.) at a fuel-air ratio of 0.049. The corresponding indicated specific fuel and liquid consumptions were 0.37 and 0.55 pound per horsepower-hour, respectively.

The investigations reported in reference 10 were conducted in an engine installation in which the range of operation was limited to a fuel flow of 30 pounds per hour and an inlet-air pressure of 150 inches of mercury absolute. Because of the continued interest in monomethylamine and dimethylamine as internal coolants, the installation was later revised to extend the range of operation to a fuel flow of 80 pounds per hour and an inlet-air pressure of 225 inches of mercury absolute. Following these revisions the tests with monomethylamine and dimethylamine were resumed; however, two engine cylinders were cracked when the knock-limited performance with the internal coolants reached a level of 700

TABLE X-2.—EFFECT OF INLET-AIR TEMPERATURE ON KNOCK-LIMITED ENGINE PERFORMANCE OF AN-F-28 FUEL USED IN CONJUNCTION WITH INTERNAL COOLANTS

[CFR engine; compression ratio, 7.0; engine speed, 2500 rpm; inlet-coolant temperature, 250° F; spark advance, 30° B. T. C.]

Internal coolant (0.5 lb/lb fuel)	Imep at inlet-air temperature of 150° F			
	Imep at inlet-air temperature of 250° F			
	Fuel-air ratio			
	0.05	0.06	0.08	0.09
None.....	1.24	1.46	1.32	1.20
Water.....	---	1.23	1.11	1.08
Methyl alcohol and water (70:30 by volume).....	1.46	1.57	1.23	1.13
Monomethylamine and water (32:68 by weight).....	1.48	-----	-----	-----
Dimethylamine and water (27:73 by weight).....	1.42	1.51	-----	-----

* Afterfiring encountered at inlet-air temperature of 150° F.

TABLE X-3.—KNOCK-LIMITED RELATIVE POWERS RESULTING FROM THE USE OF INTERNAL COOLANTS WITH AN-F-28 (AMENDMENT 2) FUEL

[CFR engine; compression ratio, 7.0; engine speed, 2500 rpm; inlet-air temperature, 250° F; coolant temperature, 250° F; spark advance, 30° B. T. C.]

Internal coolant	Weight of coolant per pound of fuel (lb)	Imep (fuel+internal coolant) / Imep (fuel alone)					
		Fuel-air ratio *					
		0.05	0.06	0.07	0.08	0.09	0.10
None.....	-----	1.00	1.00	1.00	1.00	1.00	1.00
Water.....	0.25 .50	1.25 1.48	1.21 1.48	1.21 1.37	1.16 1.24	1.08 1.13	1.08 1.13
Monomethylamine and water (32:68 by weight).....	0.25 .50	1.78 2.22	1.46 2.16	1.66 2.18	1.75 2.17	1.70 2.14	1.60 2.18
Dimethylamine and water (27:73 by weight).....	0.25 .50 .75	1.72 1.89	1.42 1.97	1.51 2.60	1.59 2.83	1.57 3.32	1.55 ---

* Any contribution of the amines to the energy of combustion was entirely neglected in computing fuel flows.

pounds per square inch. In order to resume the investigation, a specially designed CFR cylinder was obtained to permit studies at the exceptionally high powers attained with monomethylamine and dimethylamine. The investigation was again resumed and virtually completed before the next engine failure occurred.

In the extended study of the two internal coolants (reference 11) tests were conducted over a wider range of fuel-air ratio and at higher ratios of coolant to fuel. The results are summarized in table X-3. It is seen in this table that the amines are considerably better than water as internal coolants. Of the two amines examined, monomethylamine is superior to dimethylamine at coolant-fuel ratios of 0.25; however, at a coolant-fuel ratio of 0.50, monomethylamine is better than dimethylamine at lean fuel-air ratios but slightly poorer at rich fuel-air ratios. It is of interest to note that the injection of 0.75 pound of dimethylamine-water solution per pound of fuel permitted the attainment of a knock-limited indicated mean effective pressure of 967 pounds per square inch, corresponding to 3.05 indicated horsepower per cubic-inch displacement, at a fuel-air ratio of 0.092. Failure of a cylinder stud terminated the tests at this point; however, after an overhaul the tests were again resumed and the cylinder wall failed at an indicated mean effective pressure of 895 pounds per square inch during a test with dimethylamine-water solution at a coolant-fuel ratio of 0.75.

During the investigation reported in reference 11 a run was made to determine the influence of exhaust back pressure on the knock-limited performance when dimethylamine-water solution was used as an internal coolant. The results indicated that increases in exhaust back pressure had little or no effect on the performance at fuel-air ratios leaner than 0.095. At richer fuel-air ratios serious decreases in power output were encountered and engine operation was quite rough.

An examination of the data in reference 11 indicated that for certain power levels in the rich-mixture range the following combinations of internal coolants resulted in the lowest indicated specific liquid consumptions:

Imep range (lb/sq in.)	Corresponding minimum Islo range (lb/hp-hr)	Internal coolant	Internal coolant-fuel ratio
Below 220	0.44 to 0.58	None	
220 to 370	0.53 to 0.63	Monomethylamine solution	0.25
370 to 440	0.68 to 0.71	Dimethylamine solution	.50
440 to 960	0.71 to 1.10	Dimethylamine solution	.75

The success of aliphatic amines as internal coolants, reported in references 10 and 11, led to further studies with other amines reported in reference 12. The additional amines evaluated were ethylenediamine, diethylamine, triethylamine, and butylamine. The results of the investigation (reference 12) are summarized in table X-4.

It is apparent in table X-4 that of all the amines tested monomethylamine and dimethylamine still offer the greatest possibilities as internal coolants, although ethylenediamine does permit higher knock-free power at lean fuel-air ratios.

In the investigation (reference 12) an effort was made to reach the highest possible knock-limited indicated mean effective pressure with dimethylamine. At a fuel-air ratio of 0.093 and a coolant-fuel ratio of 0.75, a knock-limited indicated mean effective pressure of 1024 pounds per square inch was attained. No engine failure occurred but this test was limited by the available intake-air supply.

TABLE X-4.—RELATIVE KNOCK-LIMITED POWERS RESULTING FROM USE OF INTERNAL-COOLANT ADDITIVES IN WATER AT COOLANT-FUEL RATIO OF 0.50

[CFR engine; fuel AN-F-28, Amendment-2; compression ratio, 7.0; engine speed, 2500 rpm; inlet-air temperature, 250° F; spark advance, 30° B. T. C.; jacket temperature, 250° F]

Internal-coolant additive	Additive in coolant solution (percent by weight)	Imep (fuel+water+additive) Imep (fuel+water alone)					
		Fuel-air ratio *					
		0.05	0.06	0.07	0.08	0.09	0.10
None	0	1.00	1.00	1.00	1.00	1.00	1.00
Monomethylamine	32	1.64	1.32	1.32	1.42	1.91	2.42
Dimethylamine	26	1.64	1.41	1.46	1.82	2.08	2.58
Ethylenediamine	25	1.81	1.61	1.38	1.44	1.45	1.42
Diethylamine	25	1.09	0.86	0.77	0.92	0.96	1.07
Triethylamine	25	—	0.92	0.71	0.80	0.84	0.83
Butylamine	25	1.02	0.82	0.90	0.98	0.93	0.96

* The amines were not considered as fuels and their heats of combustion were neglected in computing the fuel-air ratios.

In a later investigation (reference 13) the following compounds were evaluated as internal coolants; however, none were found to be as effective as monomethylamine, dimethylamine, and ethylenediamine:

Alkyl amines:

Isopropylamine

Isobutylamine

tert-Butylamine

Monoamylamine

Alkanolamines:

Ethanolamine

Diethanolamine

2-Amino-2-methyl-1-propanol

Amides:

Formamide

Amides—Continued

N-Ethylformamide

N-Ethylacetamide

N-Ethylpropionamide

N-N-Dimethylformamide

N,N-Diethylacetamide

Heterocyclic compounds:

2,2-Dimethylethylenimine

Morpholine

Pyridine

2-Methylpyridine

3-Methylpyridine

4-Methylpyridine

2,6-Dimethylpyridine

2-Vinylpyridine

LEWIS FLIGHT PROPULSION LABORATORY,
NATIONAL ADVISORY COMMITTEE FOR AERONAUTICS,
CLEVELAND, OHIO, May 15, 1951.

REFERENCES

1. Pinkel, Benjamin, and Ellerbrock, Herman H., Jr.: Correlation of Cooling Data from an Air-Cooled Cylinder and Several Multi-cylinder Engines. NACA Rep. 683, 1940.
2. Rothrock, Addison M., Krsek, Alois, Jr., and Jones, Anthony W.: The Induction of Water to the Inlet Air as a Means of Internal Cooling in Aircraft-Engine Cylinders. NACA Rep. 756, 1943. (Formerly NACA ARR, Aug. 1942.)
3. Wear, Jerrold D., Held, Louis F., and Slough, James W.: Some Effects of Internal Coolants on Knock Limited and Temperature-Limited Power as Determined in a Single-Cylinder Aircraft Test Engine. NACA ARR E4H31, 1944.
4. Harries, Myron L., Nelson, R. Lee, and Bergeson, Howard E.: Effect of Water Injection on the Knock-Limited Performance of an Allison V-1710-99 Engine. NACA MR, Army Air Forces, Sept. 9, 1944.
5. Engelman, Helmuth W., and White, H. Jack: Use of Water Injection to Decrease Gasoline Consumption in an Aircraft Engine Cruising at High Power. NACA RB E4H12, 1944.
6. Biermann, Arnold E., Miller, George R., and Henneberry, Hugh M.: Economy of Internally Cooling Only the Overheated Cylinders of Aircraft Engines. NACA MR E5G14, Army Air Forces, July 14, 1945.
7. Pfender, John F., Dudugian, Carl, and Lietzke, A. F.: Effect of Engine-Operating Variables and Internal Coolants on Spark-Advance Requirements of an Allison V-1710 Cylinder. NACA MR E5E18, Army Air Forces, May 18, 1945.
8. Rothrock, Addison M.: Use of Internal Coolant as a Means of Permitting Increase in Engine Take-Off Power. NACA RB 4A25, 1944.
9. Rothrock, Addison M.: Calculations of Intake-Air Cooling Resulting from Water Injection and of Water Recovery from Exhaust Gas. NACA RB E4H26, 1944.
10. Bellman, Donald R., and Evvard, John C.: Knock-Limited Performance of Several Internal Coolants. NACA Rep. 812, 1945. (Formerly NACA ACR 4B08.)
11. Bellman, Donald R., Moeckel, W. E., and Evvard, John C.: Knock-Limited Power Outputs from a CFR Engine Using Internal Coolants. I—Monomethylamine and Dimethylamine. NACA ARR E4L21, 1944.
12. Bellman, Donald R., Moeckel, W. E., and Evvard, John C.: Knock-Limited Power Outputs from a CFR Engine Using Internal Coolants. II—Six Aliphatic Amines. NACA ACR E5H31, 1945.
13. Imming, Harry S., and Bellman, Donald R.: Knock-Limited Power Outputs from a CFR Engine Using Internal Coolants. III—Four Alkyl Amines, Three Alkanolamines, Six Amides, and Eight Heterocyclic Compounds. NACA RM E6L05a, 1947.

APPENDIX A

ADDITIONAL DATA ON PERFORMANCE OF VARIOUS FUELS

TABLE A-1.—A. S. T. M. AVIATION AND A. S. T. M. SUPERCHARGE PERFORMANCE NUMBERS OF LEADED AND UNLEADED BLENDS WITH ISOCTANE AND WITH MIXED BASE FUEL CONSISTING OF 87.5 PERCENT (BY VOLUME) ISOCTANE AND 12.5 PERCENT *n*-HEPTANE *

(a) Paraffins and olefins.

Paraffins and olefins	Formula	Performance number											
		A. S. T. M. Aviation method					A. S. T. M. Supercharge method (F/A=0.11)						
		Unleaded		4 ml TEL/gal			4 ml TEL/gal		4 ml TEL/gal				
		Volume percent paraffin or olefin in blend with isooctane					Volume percent paraffin or olefin in blend with mixed base fuel b						
		10	20	10	20		10	25	50	10	25	50	
Paraffins													
2-Methylbutane	C ₅ H ₁₂	128	115	121	130	
2,2-Dimethylbutane	C ₆ H ₁₄	129	117	122	129	
2,3-Dimethylbutane	C ₆ H ₁₄	129	117	130	147	
2,2,3-Trimethylbutane	C ₇ H ₁₆	101	104	151	151	124	135	142	127	146	144	200	
2,3-Dimethylpentane	C ₆ H ₁₄	130	128	141	174	
2,2,3-Trimethylpentane	C ₇ H ₁₆	124	127	133	166	
2,3,4-Trimethylpentane	C ₇ H ₁₆	122	118	132	147	
2,2,3,3-Tetramethylpentane	C ₈ H ₂₀	84	128	107	127	156	>230	
2,2,3,4-Tetramethylpentane	C ₈ H ₂₀	96	96	145	133	120	118	111	125	141	175	
2,2,4-Tetramethylpentane	C ₈ H ₂₀	93	93	137	131	117	118	110	106	125	143	110	
2,3,3,4-Tetramethylpentane	C ₈ H ₂₀	86	140	115	115	127	143	192	
2,4-Dimethyl-3-ethylpentane	C ₈ H ₁₈	
Olefins													
2,3-Dimethyl-2-pentene	C ₇ H ₁₄	78	108	100	117	
2,3,4-Trimethyl-2-pentene	C ₈ H ₁₆	80	77	127	118	113	101	77	112	104	146	77	
2,4,4-Trimethyl-1-pentene	C ₈ H ₁₆	105	131	146	159	
2,4,4-Trimethyl-2-pentene	C ₈ H ₁₆	96	92	183	120	114	108	115	119	103	93	
3,4,4-Trimethyl-2-pentene	C ₈ H ₁₆	106	88	118	108	108	

(b) Aromatics.

Aromatic	Formula	Performance number											
		A. S. T. M. Aviation method					A. S. T. M. Supercharge method (F/A=0.11)						
		Unleaded		4 ml TEL/gal			4 ml TEL/gal		4 ml TEL/gal				
		Volume percent aromatic in blend with isooctane					Volume percent aromatic in blend with mixed base fuel b						
		10	20	10	20		10	25	50	10	25	50	
Benzene													
Benzene	C ₆ H ₆	96	92	121	116	97±6	125	140	175		
Methylbenzene	C ₇ H ₈	94	139	121	117	113	128	152	>290		
Ethylbenzene	C ₈ H ₁₀	97	95	188	120	119	108	180	155	>280		
1,2-Dimethylbenzene	C ₈ H ₁₀	93	88	136	118	113	105	84	104	101	112		
1,3-Dimethylbenzene	C ₈ H ₁₀	100	98	160	125	125	123	122	131	156	297		
1,4-Dimethylbenzene	C ₈ H ₁₀	98	99	148	138	125	122	130	164	>300		
n-Propylbenzene	C ₉ H ₁₂	96	93	146	126	122	118	127	152	205		
Isopropylbenzene	C ₉ H ₁₂	98	124	122	122	133	168	284		
1-Methyl-2-ethylbenzene	C ₉ H ₁₂	86	142	107	124		
1-Methyl-3-ethylbenzene	C ₉ H ₁₂	95	142	124	168		
1-Methyl-4-ethylbenzene	C ₉ H ₁₂	96	88	122	120	134	160	214		
1,2,3-Trimethylbenzene	C ₁₀ H ₁₄	93	85	115	113	105	97	107	113	147		
1,2,4-Trimethylbenzene	C ₁₀ H ₁₄	91	87	141	121	113	101	97	107	113	168		
1,3,5-Trimethylbenzene	C ₁₀ H ₁₄	160	128	127	127	127	137	168	>800		
n-Butylbenzene	C ₁₀ H ₁₄	96	89	118	118	111	123	135	166		
Isobutylbenzene	C ₁₀ H ₁₄	97	93	138	120	119	116	125	144	174		
sec-Butylbenzene	C ₁₀ H ₁₄	96	93	146	151	123	122	112	125	147	177		
tert-Butylbenzene	C ₁₀ H ₁₄	98	99	151	142	125	127	126	135	162	287		
1-Methyl-4-isopropylbenzene	C ₁₁ H ₁₄	98	95	126	123	113	130	153	223		
1,2-Diethylbenzene	C ₁₁ H ₁₄	94	126	107	124		
1,3-Diethylbenzene	C ₁₁ H ₁₄	96	92	146	128	136	165	226		
1,4-Diethylbenzene	C ₁₁ H ₁₄	94	136	119	163		
1,3-Dimethyl-3-ethylbenzene	C ₁₁ H ₁₄	95	140	124	171		
1-Methyl-3-tert-butylbenzene	C ₁₂ H ₁₆	93	141	125	169		
1-Methyl-4-tert-butylbenzene	C ₁₂ H ₁₆	97	142	124	176		
1-Methyl-3,5-diethylbenzene	C ₁₂ H ₁₆	95	140	126	171		
1,3,5-Triethylbenzene	C ₁₃ H ₁₈	93	140	122	170		

* Performance numbers greater than 161 were determined as follows:

Performance number = 161 + (imcp of blend - imcp of isooctane) / 6 ml TEL/gal

† A. S. T. M. Aviation and A. S. T. M. Supercharge performance numbers of mixed base fuel, 120 and 112, respectively.

‡ A. S. T. M. Supercharge data for compound determined at an industrial laboratory; A. S. T. M. Aviation data determined at NACA Lewis laboratory.

TABLE A-1.—A. S. T. M. AVIATION AND A. S. T. M. SUPERCHARGE PERFORMANCE NUMBERS OF LEADED AND UNLEADED BLENDS WITH ISOCTANE AND WITH MIXED BASE FUEL CONSISTING OF 87.5 PERCENT (BY VOLUME) ISOCTANE AND 12.5 PERCENT *n*-HEPTANE—Concluded

(c) Ethers.

Ether	Formula	Performance number											
		A. S. T. M. Aviation method								A. S. T. M. Supercharge method ($F/A = 0.11$)			
		Unleaded		4 ml TEL/gal		4 ml TEL/gal							
		Volume percent aromatics in blend with isoctane				Volume percent ether in blend with mixed base fuel ^b							
		10	20	10	20	10	25	50	10	25	50		
Methyl <i>tert</i> -butyl ether	$C_5H_{12}O$	100	102	149	153	134	143	150	137	175	250		
Ethyl <i>tert</i> -butyl ether	$C_6H_{14}O$	100	104	157	161	140	144	150	132	160	185		
Isopropyl <i>tert</i> -butyl ether	$C_7H_{16}O$	103	104	160	161	137	149	160	126	160	183		
Methyl phenyl ether (anisole)	$C_7H_{12}O$	93	90	141	121	118	107	94	126	142	137		
Ethyl phenyl ether (phenetole)	$C_8H_{14}O$	99	97	140	120	120	111	100	128	146	137		
Methyl <i>p</i> -tolyl ether (<i>p</i> -methylanisole)	$C_9H_{14}O$	99	99	144	133	120	112	100	133	145	136		
<i>m</i> -Methylanisole	$C_8H_{12}O$	—	—	—	—	110	—	—	—	147	—		
<i>o</i> -Methylanisole	$C_7H_{10}O$	—	—	—	—	82	—	—	—	94	—		
<i>p</i> - <i>tert</i> -Butylanisole	$C_9H_{14}O$	—	—	—	—	110	—	—	—	147	—		
<i>n</i> -Propyl phenyl ether	$C_9H_{16}O$	—	—	—	—	110	—	—	—	149	—		
Isopropyl phenyl ether	$C_{10}H_{18}O$	—	—	—	—	110	—	—	—	150	—		
<i>tert</i> -Butyl phenyl ether	$C_{10}H_{14}O$	—	—	—	—	107	—	—	—	137	—		
Methyl benzyl ether	$C_9H_{12}O$	—	—	—	—	104	—	—	—	111	—		
Isopropyl benzyl ether	$C_{10}H_{14}O$	—	—	—	—	119	—	—	—	140	—		
Phenyl methallyl ether	$C_9H_{10}O$	—	—	—	—	48	—	—	—	94	—		
Methyl methallyl ether	$C_8H_{10}O$	—	—	—	—	93	—	—	—	92	—		
Isopropyl methallyl ether	$C_9H_{12}O$	—	—	—	—	106	—	—	—	102	—		
<i>tert</i> -Butyl methallyl ether	$C_9H_{14}O$	—	—	—	—	106	—	—	—	109	—		
Dimethallyl ether	$C_8H_{12}O$	—	—	—	—	77	—	—	—	90	—		
Methyl cyclopropyl ether	C_4H_8O	—	—	—	—	78	—	—	—	94	—		
Methyl cyclopentyl ether	$C_6H_{12}O$	—	—	—	—	80	—	—	—	83	—		
Methyl cyclohexyl ether	$C_7H_{14}O$	—	—	—	—	68	—	—	—	79	—		
Propylene oxide	C_3H_6O	—	—	—	—	100	—	—	—	131	—		

* Performance numbers greater than 161 were determined as follows:

$$\text{Performance number} = 161 \frac{\text{Imep of blend}}{\text{Imep of Isoctane} + 6 \text{ ml TEL/gal}}$$

^b A. S. T. M. Aviation and A. S. T. M. Supercharge performance numbers of mixed base fuel, 120 and 112, respectively.

^c Approximate value.

TABLE A-2.—A. S. T. M. SUPERCHARGE KNOCK-LIMITED INDICATED MEAN EFFECTIVE PRESSURE RATIOS OF BLENDS WITH MIXED BASE FUEL CONSISTING OF 87.5 PERCENT (BY VOLUME) ISOCTANE AND 12.5 PERCENT *n*-HEPTANE + 4 ML TEL PER GALLON

[Standard conditions]

(a) Paraffins and olefins.

Paraffins and olefins	Formula	Imep ratio ^a											
		Volume percent added paraffin or olefin in blend with mixed base fuel											
		10				25				50			
		0.065	0.07	0.085	0.10	0.11	0.065	0.07	0.085	0.10	0.11	0.065	0.07
Paraffins													
2,2,3-Trimethylbutane	C_7H_{16}	1.02	1.05	1.08	1.09	1.11	1.12	1.21	1.26	1.29	1.30	1.49	1.51
2,3-Dimethylpentane	—	—	—	—	—	—	.96	.98	1.00	1.00	—	1.66	1.73
2,2,3,3-Tetramethylpentane	C_9H_{20}	0.90	0.93	1.04	1.08	1.10	0.83	0.83	1.08	1.31	1.39	—	—
2,2,3,4-Tetramethylpentane	—	.95	.94	1.03	1.09	1.11	.85	.88	1.05	1.19	1.24	0.80	0.75
2,3,3,4-Tetramethylpentane	—	—	—	—	—	—	.87	.84	1.06	1.23	1.28	.75	.70
2,4-Dimethyl-3-ethylpentane	—	—	—	—	—	—	1.05	1.05	1.07	1.09	1.10	—	—
Olefins													
2,3-Dimethyl-2-pentene	C_6H_{14}	—	—	—	—	—	0.75	0.79	0.88	0.95	1.02	—	—
2,3,4-Trimethyl-2-pentene	C_6H_{16}	0.84	0.82	0.92	1.00	1.00	0.69	0.67	0.72	0.86	0.93	0.69	0.60
3,4,4-Trimethyl-2-pentene	—	.87	.87	1.00	1.02	1.03	.75	.73	.79	.91	.97	.66	.59

* Imep ratio = $\frac{\text{knock-limited imep of blend with 4 ml TEL/gal}}{\text{knock-limited imep of mixed base fuel with 4 ml TEL/gal}}$

TABLE A-2.—A. S. T. M. SUPERCHARGE KNOCK-LIMITED INDICATED MEAN EFFECTIVE PRESSURE RATIOS OF BLENDS WITH MIXED BASE FUEL CONSISTING OF 87.5 PERCENT (BY VOLUME) ISOOCTANE AND 12.5 PERCENT *n*-HEPTANE + 4 ML TEL PER GALLON—Concluded

[Standard conditions]

(b) Aromatics.

Aromatic	Formula	Imep ratio *														
		Volume percent aromatic in blend with mixed base fuel														
		10					25					50				
		0.065	0.07	0.085	0.10	0.11	0.065	0.07	0.085	0.10	0.11	0.065	0.07	0.085	0.10	0.11
Benzene	C ₆ H ₆	1.08	1.01	1.04	1.05	1.07	1.08	1.10	1.12	1.15	1.19	0.74	0.73	1.23	1.39	1.51
Methylbenzene	C ₇ H ₈	1.01	1.05	1.08	1.10	1.13	1.00	1.04	1.18	1.29	1.37	0.84	0.90	1.27	2.43	----
Ethylbenzene	C ₈ H ₁₀	1.06	1.07	1.11	1.12	1.14	1.02	1.08	1.21	1.29	1.37	0.99	1.07	1.44	1.71	1.77
1,2-Dimethylbenzene		.95	.94	.95	.92	.91	.76	.80	.89	.91	.93	.73	.87	.95	1.00	1.00
1,3-Dimethylbenzene		.93	1.02	1.12	1.15	1.16	.82	.98	1.33	1.45	1.51	.80	.92	1.72	2.36	2.70
1,4-Dimethylbenzene		1.04	1.07	1.10	1.10	1.11	1.01	1.06	1.28	1.39	1.50	.94	1.03	1.37	2.53	----
<i>n</i> -Propylbenzene	C ₉ H ₁₂	0.94	0.99	1.08	1.10	1.11	0.94	1.08	1.24	1.30	1.38	0.73	0.78	1.18	1.37	1.86
Isopropylbenzene		1.14	1.13	1.12	1.11	1.12	1.05	1.07	1.14	1.23	1.30	.93	1.02	1.41	1.92	2.58
1-Methyl-2-ethylbenzene		----	----	----	----	----	.86	.91	1.08	1.08	1.08	----	----	----	----	----
1-Methyl-4-ethylbenzene		1.01	1.04	1.11	1.15	1.15	1.11	1.14	1.28	1.40	1.47	1.08	1.13	1.46	2.28	2.58
1,2,3-Trimethylbenzene		----	----	----	----	----	.96	1.01	1.21	1.34	1.43	.93	.98	1.27	1.51	1.98
1,2,4-Trimethylbenzene		.92	.95	.98	.98	.97	.82	.85	.90	.93	.94	1.02	1.08	1.04	1.21	1.34
1,3,5-Trimethylbenzene		1.09	1.10	1.12	1.16	1.18	.94	.95	1.26	1.39	1.49	1.02	1.04	1.61	2.56	----
<i>n</i> -Butylbenzene	C ₁₀ H ₁₄	0.95	1.00	1.04	1.07	1.08	0.87	0.96	1.12	1.16	1.18	0.77	0.91	1.28	1.84	1.42
Isobutylbenzene		.95	1.04	1.09	1.09	1.11	.97	1.20	1.25	1.30	1.30	.90	1.02	1.26	1.44	1.59
sec-Butylbenzene		1.01	.99	1.03	1.07	1.09	1.03	1.01	1.14	1.25	1.31	.98	.97	1.17	1.43	1.63
tert-Butylbenzene		1.06	1.06	1.10	1.14	1.16	1.12	1.17	1.31	1.42	1.47	1.08	1.13	1.46	2.28	2.58
1-Methyl-4-isopropylbenzene		1.01	1.06	1.12	1.15	1.15	.91	1.03	1.23	1.34	1.48	.77	.87	1.35	1.84	2.03
1,2-Diethylbenzene		1.04	1.09	1.18	1.18	1.19	.98	1.07	1.28	1.42	1.51	.82	.86	1.23	1.81	2.09
1,3-Diethylbenzene		----	----	----	----	----	1.10	1.13	1.22	1.34	1.45	----	----	----	----	----
1,3-Dimethyl-5-ethylbenzene		----	----	----	----	----	1.07	1.11	1.28	1.41	1.49	----	----	----	----	----
1-Methyl-3-tert-butylbenzene	C ₁₁ H ₁₆	----	----	----	----	----	1.10	1.15	1.28	1.40	1.49	----	----	----	----	----
1-Methyl-4-tert-butylbenzene		----	----	----	----	----	1.11	1.14	1.28	1.43	1.53	----	----	----	----	----
1-Methyl-3,5-diethylbenzene		----	----	----	----	----	1.10	1.15	1.27	1.39	1.50	----	----	----	----	----
1,3,5-Triethylbenzene	C ₁₂ H ₁₈	----	----	----	----	----	1.07	1.11	1.25	1.40	1.51	----	----	----	----	----

(c) Ethers.

Ether	Formula	Imep ratio *														
		Volume percent ether in blend with mixed base fuel														
		10					25					50				
		0.065	0.07	0.085	0.10	0.11	0.065	0.07	0.085	0.10	0.11	0.065	0.07	0.085	0.10	0.11
Methyl <i>tert</i> -butyl ether	C ₅ H ₁₂ O	1.07	1.01	1.11	1.18	1.21	1.34	1.13	1.39	1.52	1.59	2.22	1.44	1.85	2.08	2.34
Ethyl <i>tert</i> -butyl ether	C ₆ H ₁₂ O	1.18	1.12	1.14	1.16	1.17	1.27	1.15	1.26	1.34	1.37	1.97	1.25	1.48	1.56	1.70
Isopropyl <i>tert</i> -butyl ether	C ₇ H ₁₂ O	1.13	1.07	1.09	1.10	1.11	1.34	1.26	1.24	1.29	1.33	2.5 ^b	1.45	1.45	1.53	1.66
Methyl phenyl ether (anisole)	C ₇ H ₈ O	.94	.93	1.03	1.07	1.10	.87	.72	.98	1.13	1.25	.89	.83	.55	.92	1.21
Ethyl phenyl ether (phenetole)	C ₈ H ₁₀ O	.97	.94	1.05	1.11	1.12	.99	.81	1.05	1.21	1.30	.95	.85	.64	.96	1.21
Methyl <i>p</i> -tolyl ether (<i>p</i> -methylanisole)	C ₈ H ₁₀ O	.99	.90	1.05	1.13	1.16	.91	.74	.98	1.15	1.29	.94	.85	.56	.98	1.19
<i>m</i> -Methylanisole	C ₇ H ₁₀ O	----	----	----	----	----	.97	.90	1.07	1.21	1.31	----	----	----	----	----
<i>o</i> -Methylanisole	C ₇ H ₁₀ O	----	----	----	----	----	.80	.52	.67	.75	.85	----	----	----	----	----
<i>p</i> -tert-Butylanisole	C ₉ H ₁₂ O	----	----	----	----	----	.95	.91	.94	1.10	1.32	----	----	----	----	----
<i>n</i> -Propyl phenyl ether	C ₈ H ₁₂ O	----	----	----	----	----	1.08	1.00	1.17	1.27	1.35	----	----	----	----	----
<i>tert</i> -Butyl phenyl ether	C ₉ H ₁₂ O	----	----	----	----	----	.98	.90	1.05	1.28	1.35	----	----	----	----	----
Methyl benzyl ether	C ₈ H ₁₀ O	----	----	----	----	----	.88	.81	.92	1.08	1.21	----	----	----	----	----
Isopropyl benzyl ether	C ₉ H ₁₂ O	----	----	----	----	----	.95	.96	1.10	1.20	1.24	----	----	----	----	----
Phenyl methylallyl ether	C ₁₀ H ₁₂ O	----	----	----	----	----	.83	.59	.95	.96	.99	----	----	----	----	----
Methyl methallyl ether	C ₉ H ₁₀ O	----	----	----	----	----	.48	.44	.38	.45	.54	----	----	----	----	----
Isopropyl methallyl ether	C ₁₀ H ₁₄ O	----	----	----	----	----	.77	.71	.85	.81	.83	----	----	----	----	----
Methyl cyclopropyl ether	C ₅ H ₈ O	----	----	----	----	----	.64	.66	.79	.81	.83	----	----	----	----	----
Methyl cyclohexyl ether	C ₇ H ₁₂ O	----	----	----	----	----	.61	.57	.72	.82	.85	----	----	----	----	----
Propylene oxide	C ₃ H ₆ O	----	----	----	----	----	.87	.61	.69	.75	.75	----	----	----	----	----

* Imep ratio = knock-limited imep of blend with 4 ml TEL/gal

** Imep ratio = knock-limited imep of mixed base fuel with 4 ml TEL/gal

* Approximate value.

TABLE A-3.—17.6 ENGINE KNOCK-LIMITED INDICATED MEAN EFFECTIVE PRESSURE RATIOS OF UNLEADED BLENDS WITH ISOCTANE

[Compression ratio, 7.0; engine speed, 1800 rpm; coolant temperature, 212° F; spark advance, 30° B. T. C.]

(a) Paraffins and olefins.

Paraffins and olefins	Formula	Imep ratio *															
		Inlet-air temperature, 250° F								Inlet-air temperature, 100° F							
		Volume percent added paraffin or olefin in blend with isoctane															
		10				25				50							
		Fuel-air ratio															
		0.065	0.07	0.085	0.10	0.11	0.065	0.07	0.085	0.10	0.11	0.065	0.07	0.085	0.10	0.11	0.11
Paraffins																	
2,2,3,3-Trimethylbutane	C ₇ H ₁₆	1.02	1.02	1.03	1.09	1.10	1.08	1.07	1.09	1.17	1.20	1.16	1.15	1.21	1.20	1.20	1.20
2,3-Dimethylpentane		----	----	----	----	----	1.96	1.94	1.94	1.94	1.94	1.93	1.93	1.93	1.94	1.93	1.93
2,2,3,4-Tetramethylpentane	C ₉ H ₂₀	0.90	0.98	1.01	1.11	1.13	1.12	1.14	1.20	1.32	1.31	1.23	1.22	1.27	1.27	1.27	1.27
2,2,3,4-Tetramethylpentane		.97	.98	1.03	1.06	1.13	.95	.91	1.00	1.15	1.23	1.09	1.10	1.15	1.21	1.21	1.22
2,4-Dimethyl-3-ethylpentane		----	----	----	----	----	.99	1.00	1.00	1.01	1.00	1.03	1.17	1.27	1.27	1.27	1.27
Olefins																	
2,3-Dimethyl-2-pentene	C ₇ H ₁₄	----	----	----	----	----	0.99	0.99	1.01	1.09	1.15	1.14	1.12	1.17	1.23	1.27	1.27
2,3,4-Trimethyl-2-pentene	C ₈ H ₁₆	0.90	0.90	0.89	0.91	0.96	0.79	0.79	0.78	0.82	0.89	0.95	0.95	0.96	0.96	0.99	1.02
3,4,4-Trimethyl-2-pentene		.98	.98	.99	1.00	1.05	.93	.94	.94	.98	1.06	1.05	1.04	1.08	1.16	1.20	1.20

(b) Aromatics.

Aromatic	Formula	Imep ratio *															
		Inlet-air temperature, 250° F								Inlet-air temperature, 100° F							
		Volume percent aromatic in blend with isoctane															
		10				25				50							
		0.065	0.07	0.085	0.10	0.11	0.065	0.07	0.085	0.10	0.11	0.065	0.07	0.085	0.10	0.11	0.11
Benzene	C ₆ H ₆	1.00	1.01	1.02	1.03	1.04	1.00	1.01	1.02	1.10	1.17	1.08	1.08	1.12	1.12	1.15	1.15
Methylbenzene	C ₇ H ₈	1.04	1.02	1.05	1.08	1.11	1.04	1.02	1.11	1.21	1.26	1.05	1.07	1.18	1.21	1.24	1.24
Ethylbenzene	C ₈ H ₁₀	1.02	1.02	1.04	1.11	1.16	1.02	1.00	1.07	1.21	1.31	1.19	1.21	1.28	1.35	1.36	1.36
1,2-Dimethylbenzene		.95	.95	.93	.97	1.00	.90	.89	.87	.93	.99	.97	.98	1.00	1.02	1.03	1.03
1,3-Dimethylbenzene		.97	.98	1.03	1.07	1.08	.93	.94	1.08	1.14	1.18	1.14	1.15	1.22	1.36	1.40	1.40
1,4-Dimethylbenzene		1.01	1.01	1.10	1.12	1.14	1.04	1.04	1.16	1.28	1.38	1.16	1.20	1.29	1.34	1.34	1.40
n-Propylbenzene	C ₉ H ₁₂	0.99	0.99	1.00	1.09	1.10	1.16	0.99	0.99	1.02	1.15	1.23	1.14	1.14	1.30	1.32	1.32
Isopropylbenzene		1.01	1.00	1.09	1.14	1.18	1.05	.98	1.07	1.20	1.29	1.18	1.20	1.32	1.32	1.34	1.34
1-Methyl-2-ethylbenzene		----	----	----	----	----	1.03	1.01	1.03	1.07	1.10	1.03	1.04	1.09	1.08	1.10	1.10
1-Methyl-4-ethylbenzene		1.00	1.00	1.05	1.08	1.09	1.00	1.00	1.11	1.11	1.21	1.29	1.28	1.31	1.39	1.41	1.43
1,2,3-Trimethylbenzene		.91	.93	.95	.99	1.01	.87	.87	.93	1.00	1.18	1.11	1.14	1.18	1.11	1.17	1.21
1,2,4-Trimethylbenzene		.96	.98	1.03	1.18	1.21	.91	.95	1.08	1.27	1.42	1.16	1.16	1.31	1.43	1.51	1.51
n-Butylbenzene	C ₉ H ₁₄	0.95	0.98	0.97	0.99	1.02	0.93	0.96	0.96	1.04	1.04	1.04	1.05	1.08	1.10	1.09	1.09
Isobutylbenzene		.98	.98	1.00	1.02	1.07	.97	.94	.96	1.03	1.11	1.11	1.15	1.19	1.20	1.20	1.20
sec-Butylbenzene		.98	1.00	1.06	1.08	1.10	.98	.99	1.08	1.16	1.28	1.14	1.12	1.19	1.23	1.23	1.23
tert-Butylbenzene		.98	1.00	1.05	1.12	1.19	.98	.95	.95	1.08	1.15	1.27	1.24	1.32	1.41	1.43	1.43
1-Methyl-4-isopropylbenzene		.98	.99	1.04	1.07	1.12	.94	.95	1.02	1.10	1.14	1.11	1.14	1.21	1.33	1.37	1.37
1,2-Diethylbenzene		1.01	1.01	1.05	1.12	1.19	1.06	1.01	1.03	1.08	1.11	1.04	1.06	1.11	1.12	1.12	1.12
1,3-Diethylbenzene		----	----	----	----	----	1.11	1.12	1.23	1.34	1.41	1.32	1.33	1.41	1.44	1.46	1.49
1,4-Diethylbenzene		----	----	----	----	----	1.10	1.07	1.17	1.24	1.24	1.24	1.26	1.31	1.35	1.35	1.32
1,3-Dimethyl-2-ethylbenzene		----	----	----	----	----	1.10	1.07	1.17	1.24	1.24	1.24	1.26	1.31	1.35	1.35	1.32
1-Methyl-3-tert-butylbenzene	C ₁₁ H ₁₄	----	----	----	----	----	1.16	1.16	1.26	1.36	1.37	1.30	1.33	1.37	1.39	1.38	1.38
1-Methyl-4-tert-butylbenzene		----	----	----	----	----	1.12	1.14	1.22	1.31	1.37	1.31	1.32	1.37	1.40	1.38	1.38
1-Methyl-3,5-diethylbenzene		----	----	----	----	----	1.10	1.11	1.23	1.36	1.44	1.30	1.36	1.48	1.51	1.51	1.51
1,3,5-Triethylbenzene	C ₁₂ H ₁₈	----	----	----	----	----	1.09	1.09	1.19	1.31	1.42	1.35	1.37	1.46	1.50	1.48	1.48

* Imep ratio = knock-limited imep of blend
 knock-limited imep of isoctane

TABLE A-3.—17.6 ENGINE KNOCK-LIMITED INDICATED MEAN EFFECTIVE PRESSURE RATIOS OF UNLEADED BLENDS WITH ISOCTANE—Concluded

[Compression ratio, 7.0; engine speed, 1800 rpm; coolant temperature, 212° F; spark advance, 30° B. T. C.]
(c) Ethers.

Ether	Formula	Imep ratio *													
		Inlet-air temperature, 250° F							Inlet-air temperature, 100° F						
		Volume percent ether in blend with isoctane													
		10				20				20					
		Fuel-air ratio													
		0.065	0.07	0.085	0.10	0.11	0.065	0.07	0.085	0.10	0.11	0.065	0.07	0.085	0.10
Methyl <i>tert</i> -butyl ether	C ₇ H ₁₆ O	1.06	1.07	1.10	1.10	1.10	1.15	1.14	1.20	1.34	1.38	1.26	1.28	1.35	1.37
Ethyl <i>tert</i> -butyl ether	C ₈ H ₁₆ O	1.14	1.16	1.19	1.20	1.21	1.24	1.25	1.28	1.37	1.45	1.33	1.32	1.31	1.35
Isopropyl <i>tert</i> -butyl ether	C ₉ H ₁₈ O	1.11	1.11	1.12	1.15	1.14	1.19	1.19	1.21	1.27	1.30	1.29	1.29	1.27	1.27
Methyl phenyl ether (anisole)	C ₇ H ₈ O	1.08	1.05	1.07	1.10	1.15	1.12	1.10	1.09	1.20	1.32	1.28	1.27	1.26	1.31
Ethyl phenyl ether (p-phenetole)	C ₈ H ₁₀ O	1.12	1.11	1.11	1.16	1.18	1.27	1.24	1.17	1.31	1.40	1.40	1.37	1.33	1.41
Methyl <i>p</i> -tolyl ether (p-methylanisole)	C ₉ H ₁₂ O	1.12	1.09	1.12	1.18	1.21	1.20	1.14	1.17	1.28	1.38	1.29	1.29	1.34	1.42

* Imep ratio = $\frac{\text{knock-limited imep of blend}}{\text{knock-limited imep of isoctane}}$

TABLE A-4.—17.6 ENGINE KNOCK-LIMITED INDICATED MEAN EFFECTIVE PRESSURE RATIOS OF BLENDS WITH ISOCTANE+4 ML TEL PER GALLON

[Compression ratio, 7.0; engine speed, 1800 rpm; coolant temperature, 212° F; spark advance, 30° B. T. C.]

(a) Paraffins and olefins.

Paraffins and olefins	Formula	Imep ratio *														
		Inlet-air temperature, 250° F							Inlet-air temperature, 100° F							
		Volume percent added paraffin or olefin in blend with isoctane														
		10				20				20						
		Fuel-air ratio														
		0.065	0.07	0.085	0.10	0.11	0.065	0.07	0.085	0.10	0.11	0.065	0.07	0.085	0.10	0.11
Paraffins																
2,2,3-Trimethylbutane	C ₇ H ₁₆	1.05	1.06	1.09	1.10	1.10	1.13 .96	1.16 .97	1.22 .98	1.28 .96	1.24 .96	1.20 .96	1.18 .97	1.22 .97	1.20 .96	1.19 .95
2,3-Dimethylpentane	---	----	----	----	----	----	----	----	----	----	----	----	----	----	----	
2,2,3,8-Tetramethylpentane	C ₈ H ₂₂	1.02	1.03	1.04	1.09	1.11	1.19	1.18	1.31	1.34	1.32	1.28	1.25	1.28	1.29	1.29
2,2,3,4-Tetramethylpentane	1.03	1.05	1.09	1.14	1.17	1.04	1.06	1.10	1.19	1.28	1.28	1.17	1.18	1.21	1.21	1.19
2,3,3,4-Tetramethylpentane	---	----	----	----	----	1.17	1.10	1.10	1.15	1.24	1.27	1.17	1.18	1.20	1.20	1.19
2,4-Dimethyl-3-ethylpentane	---	----	----	----	----	1.01	1.01	1.02	1.01	.99	1.00	1.01	1.01	1.01	1.01	1.00
Olefins																
2,3-Dimethyl-2-pentene	C ₇ H ₁₄	----	----	----	----	----	0.95	0.95	1.00	1.13	1.16	1.14	1.14	1.19	1.24	1.23
2,3,4-Trimethyl-2-pentene	C ₈ H ₁₆	0.91 .96	0.91 .96	0.59 .97	0.94 1.01	0.97 1.05	0.81 .98	0.81 .92	0.78 .92	0.85 .99	0.92 1.07	0.99 1.10	1.00 1.10	1.00 1.10	1.05 1.15	1.09 1.18
3,4,4-Trimethyl-2-pentene	---	----	----	----	----	----	----	----	----	----	----	----	----	----	----	

* Imep ratio = $\frac{\text{knock-limited imep of blend with 4 ml TEL/gal}}{\text{knock-limited imep of isoctane with 4 ml TEL/gal}}$

TABLE A-4.—17.6 ENGINE KNOCK-LIMITED INDICATED MEAN EFFECTIVE PRESSURE RATIOS OF BLENDS WITH ISOCTANE+4 ML TEL PER GALLON—Continued

[Compression ratio, 7.0; engine speed, 1800 rpm; coolant temperature, 212° F; spark advance, 30° B. T. C.]

(b) Aromatics.

Aromatic	Formula	Imep ratio *														
		Inlet-air temperature, 250° F							Inlet-air temperature, 100° F							
		Volume percent aromatic in blend with isoctane														
		10					20					20				
		Fuel-air ratio														
Benzene.....	C ₆ H ₆	1.00	1.02	1.06	1.08	1.09	0.99	1.04	1.10	1.14	1.17	1.11	1.11	1.17	1.21	1.23
Methylbenzene.....	C ₇ H ₈	1.01	1.03	1.04	1.05	1.10	1.05	1.07	1.11	1.19	1.26	1.13	1.17	1.23	1.29	1.31
Ethylbenzene.....	C ₈ H ₁₀	1.07	1.07	1.08	1.10	1.13	1.14	1.17	1.22	1.31	1.36	1.29	1.33	1.36	1.37	1.38
1,2-Dimethylbenzene.....		.89	.91	.88	.87	.86	.77	.82	.84	.83	.82	.81	.82	.84	.86	.87
1,3-Dimethylbenzene.....		1.07	1.09	1.13	1.19	1.23	1.12	1.16	1.29	1.41	1.46	1.28	1.29	1.44	1.48	1.51
1,4-Dimethylbenzene.....		1.04	1.08	1.12	1.14	1.16	1.06	1.13	1.23	1.34	1.41	1.23	1.28	1.42	1.47	1.48
n-Propylbenzene.....	C ₉ H ₁₂	1.05	1.05	1.09	1.14	1.16	1.11	1.13	1.21	1.29	1.38	1.34	1.38	1.42	1.38	1.31
Isopropylbenzene.....		1.04	1.10	1.12	1.16	1.20	1.09	1.12	1.19	1.21	1.38	1.33	1.35	1.36	1.41	1.41
1-Methyl-2-ethylbenzene.....		—	—	—	—	—	—	—	—	—	1.00	1.03	1.01	1.00	1.01	1.00
1-Methyl-3-ethylbenzene.....		—	—	—	—	—	—	—	—	—	1.26	1.32	1.46	1.45	1.42	1.47
1-Methyl-4-ethylbenzene.....		—	—	—	—	—	—	—	—	—	1.11	1.12	1.21	1.33	1.35	1.41
1,2,3-Trimethylbenzene.....		—	—	—	—	—	—	—	—	—	1.38	1.37	1.40	1.41	1.38	1.41
1,2,4-Trimethylbenzene.....		—	—	—	—	—	—	—	—	—	1.91	1.94	1.95	1.96	1.93	1.95
1,3,5-Trimethylbenzene.....		—	—	—	—	—	—	—	—	—	1.00	1.08	1.12	1.16	1.09	1.08
n-Butylbenzene.....	C ₉ H ₁₄	1.01	1.03	1.04	1.08	1.06	1.02	1.04	1.07	1.10	1.11	1.10	1.11	1.12	1.14	1.14
Isobutylbenzene.....		1.09	1.08	1.09	1.14	1.15	1.14	1.15	1.18	1.20	1.29	1.20	1.22	1.23	1.26	1.24
sec-Butylbenzene.....		1.09	1.08	1.08	1.14	1.17	1.16	1.18	1.20	1.29	1.36	1.26	1.28	1.30	1.31	1.31
tert-Butylbenzene.....		1.12	1.12	1.12	1.16	1.18	1.16	1.18	1.20	1.30	1.31	1.37	1.36	1.39	1.41	1.42
1-Methyl-4-isopropylbenzene.....		1.08	1.08	1.08	1.13	1.17	1.16	1.18	1.22	1.32	1.45	1.30	1.32	1.42	1.43	1.43
1,2-Diethylbenzene.....		—	—	—	—	—	—	—	—	—	1.00	1.03	1.07	1.11	1.10	1.08
1,3-Diethylbenzene.....		—	—	—	—	—	—	—	—	—	1.17	1.25	1.32	1.48	1.53	1.53
1,4-Diethylbenzene.....		—	—	—	—	—	—	—	—	—	1.27	1.32	1.42	1.45	1.53	1.47
1,3-Dimethyl-5-ethylbenzene.....		—	—	—	—	—	—	—	—	—	1.17	1.24	1.35	1.38	1.39	1.43
1-Methyl-3-tert-butylbenzene.....	C ₁₁ H ₁₆	—	—	—	—	—	—	—	—	—	1.22	1.24	1.32	1.42	1.36	1.45
1-Methyl-4-tert-butylbenzene.....		—	—	—	—	—	—	—	—	—	1.23	1.26	1.32	1.45	1.44	1.45
1-Methyl-3,5-diethylbenzene.....		—	—	—	—	—	—	—	—	—	1.22	1.25	1.36	1.44	1.47	1.54
1,3,5-Triethylbenzene.....	C ₁₃ H ₁₈	—	—	—	—	—	—	—	—	—	1.20	1.24	1.36	1.49	1.51	1.53

* Imep ratio = $\frac{\text{knock-limited imep of blend with 4 ml TEL/gal}}{\text{knock-limited imep of isoctane with 4 ml TEL/gal}}$

TABLE A-4.—17.6 ENGINE KNOCK-LIMITED INDICATED MEAN EFFECTIVE PRESSURE RATIOS OF BLENDS WITH ISOCTANE+4 ML TEL PER GALLON—Concluded

[Compression ratio, 7.0; engine speed, 1800 rpm; coolant temperature, 212° F; spark advance, 30° B. T. C.]

(c) Ethers.

Ether	Formula	Imep ratio *														
		Inlet-air temperature, 250° F							Inlet-air temperature, 100° F							
		Volume percent ether in blend with isoctane														
		10					20					20				
		0.065	0.07	0.085	0.10	0.11	0.065	0.07	0.085	0.10	0.11	0.065	0.07	0.085	0.10	0.11
Methyl <i>tert</i> -butyl ether.....	C ₅ H ₁₂ O	1.14	1.15	1.19	1.21	1.22	1.26	1.26	1.32	1.42	1.43	1.41	1.43	1.45	1.47	1.48
Ethyl <i>tert</i> -butyl ether.....	C ₆ H ₁₄ O	1.15	1.13	1.12	1.15	1.15	1.41	1.39	1.37	1.37	1.36	1.41	1.42	1.40	1.47	1.33
Isopropyl <i>tert</i> -butyl ether.....	C ₇ H ₁₆ O	1.18	1.11	1.13	1.15	1.15	1.32	1.27	1.24	1.27	1.27	1.33	1.35	1.31	1.27	1.24
Methyl phenyl ether (anisole).....	C ₈ H ₁₀ O	1.07	1.07	1.07	1.13	1.16	1.10	1.14	1.11	1.26	1.27	1.34	1.33	1.39	1.40	1.40
Ethyl phenyl ether (phenetole).....	C ₉ H ₁₀ O	1.11	1.09	1.15	1.18	1.18	1.28	1.25	1.29	1.39	1.45	1.44	1.43	1.43	1.44	1.45
Methyl <i>p</i> -tolyl ether (<i>p</i> -methylanisole).....	C ₉ H ₁₂ O	1.12	1.12	1.16	1.26	1.28	1.16	1.17	1.25	1.36	1.43	1.43	1.41	1.40	1.45	1.43

* Imep ratio = $\frac{\text{knock-limited imep of blend with 4 ml TEL/gal}}{\text{knock-limited imep of isoctane with 4 ml TEL/gal}}$

TABLE A-5.—KNOCK-LIMITED INDICATED MEAN EFFECTIVE PRESSURE RATIOS OF BLENDS WITH MIXED BASE FUEL CONSISTING OF 87.5 PERCENT (BY VOLUME) ISOCTANE AND 12.5 PERCENT *n*-HEPTANE + 4 ML TEL PER GALLON

[For 17.6 engine: compression ratio, 7.0; engine speed, 1800 rpm; coolant temperature, 212° F; spark advance, 30° B. T. C. For full-scale single-cylinder at simulated take-off: compression ratio, 7.3; engine speed, 2500 rpm; inlet-air temperature, 250° F; spark advance, 30° B. T. C.; cooling-air flow such that rear-spark-plug-bushing temperature equals 365° F at 140 bhp and 0.10 fuel-air ratio. For full-scale single-cylinder engine at simulated cruise: same conditions as for take-off except for engine speed, 2000 rpm; inlet-air temperature, 210° F.]

Paraffins and olefins	Formula	Imep ratio *																			
		17.8 engine									Full-scale single-cylinder engine										
		Inlet-air temperature, 250° F					Inlet-air temperature, 100° F				Simulated take-off conditions					Simulated cruise conditions					
		Fuel-air ratio																			
		0.065	0.07	0.085	0.10	0.11	0.065	0.07	0.085	0.10	0.11	0.065	0.07	0.085	0.10	0.11	0.065	0.07	0.085	0.10	0.11
Paraffins																					
2-Methylbutane	C ₅ H ₁₂	---	---	---	---	---	---	---	---	---	1.07	1.05	1.14	1.10	1.09	1.10	1.12	1.14	1.11	1.07	
2,2-Dimethylbutane	C ₆ H ₁₄	---	---	---	---	---	---	---	---	---	1.18	1.10	1.08	1.07	1.05	1.10	1.13	1.10	1.07	1.07	
2,3-Dimethylbutane		---	---	---	---	---	---	---	---	---	1.27	1.26	1.19	1.12	1.10	1.27	1.26	1.19	1.13	1.08	
2,2,3-Trimethylbutane	C ₇ H ₁₆	1.24	1.24	1.82	1.80	1.23	1.28	1.29	1.81	1.81	1.28	1.39	1.31	1.34	1.28	1.27	1.35	1.31	1.26	1.30	1.25
2,3-Dimethylpentane		1.03	1.03	1.06	1.04	1.02	---	---	---	---	---	---	---	---	---	---	---	---	---	---	---
2,2,3-Trimethylpentane	C ₈ H ₁₆	---	---	---	---	---	---	---	---	---	1.26	1.22	1.27	1.25	1.23	1.27	1.26	1.26	1.28	1.24	1.24
2,3,3-Trimethylpentane		---	---	---	---	---	---	---	---	---	1.26	1.21	1.22	1.21	1.20	1.19	1.20	1.18	1.22	1.21	1.21
2,3,4-Trimethylpentane		---	---	---	---	---	---	---	---	---	1.15	1.06	1.16	1.17	1.15	1.17	1.16	1.17	1.18	1.14	1.14
2,2,3,3-Tetramethylpentane	C ₉ H ₂₀	1.26	1.26	1.35	1.39	1.27	1.20	1.21	1.24	1.24	1.24	---	---	---	---	---	1.22	1.20	1.26	1.29	1.22
2,2,3,4-Tetramethylpentane		1.12	1.10	1.16	1.23	1.26	1.20	1.21	1.24	1.24	1.24	1.14	1.06	0.99	0.99	1.02	1.05	1.08	0.98	1.00	1.00
2,2,4,4-Tetramethylpentane		---	---	---	---	---	---	---	---	---	---	---	---	---	---	---	1.21	1.16	1.21	1.27	1.28
2,3,3,4-Tetramethylpentane		1.13	1.11	1.19	1.29	1.30	1.22	1.22	1.27	1.80	1.28	---	---	---	---	---	1.21	1.16	1.21	1.27	1.28
2,4-Dimethyl-3-ethylpentane		1.04	1.06	1.08	1.08	1.07	---	---	---	---	---	---	---	---	---	---	---	---	---	---	
Olefins																					
2,3-Dimethyl-2-pentene	C ₆ H ₁₄	1.03	1.07	1.12	1.16	1.20	1.12	1.11	1.11	1.14	1.16	---	---	---	---	---	0.95	0.96	1.05	1.00	1.04
2,3,4-Trimethyl-2-pentene	C ₇ H ₁₆	.94	.94	.94	.99	1.05	1.12	1.11	1.11	1.14	1.16	---	---	---	---	---	0.95	0.96	1.05	1.00	1.04
2,4,4-Trimethyl-1-pentene		---	---	---	---	---	---	---	---	---	1.04	1.01	1.14	1.32	1.37	1.26	1.23	1.31	1.35	1.33	
2,4,4-Trimethyl-2-pentene		---	---	---	---	---	---	---	---	---	1.06	1.01	1.08	1.12	1.21	1.25	1.20	1.17	1.12	1.15	
3,4,4-Trimethyl-2-pentene		.99	1.01	1.04	1.10	1.13	1.26	1.22	1.20	1.28	1.25	---	---	---	---	---	1.18	1.12	1.17	1.13	1.12

(b) Aromatics

* Imep ratio = $\frac{\text{knock-limited imep of blend with 4 ml TEL/gal}}{\text{knock-limited imep of mixed base fuel with 4 ml TEL/gal}}$

TABLE A-5.—KNOCK-LIMITED INDICATED MEAN EFFECTIVE PRESSURE RATIOS OF BLENDS WITH MIXED BASE FUEL CONSISTING OF 87.5 PERCENT (BY VOLUME) ISOCTANE AND 12.5 PERCENT *n*-HEPTANE+4 ML TEL PER GALLON—Concluded

(c) Ethers.

[Compression ratio, 7.0; engine speed, 1800 rpm; coolant temperature, 212° F; spark advance, 30° B. T. C.]

Ether	Formula	Volume percent ether in blend	17.6 Engine imep ratio*									
			Inlet-air temperature (°F)									
			100					250				
			0.065	0.07	0.085	0.10	0.11	0.065	0.07	0.085	0.10	0.11
Methyl <i>tert</i> -butyl ether	C ₆ H ₁₂ O	10	1.18	1.17	1.17	1.18	1.16	1.14	1.14	1.15	1.15	1.13
Ethyl <i>tert</i> -butyl ether	C ₇ H ₁₄ O		1.11	1.11	1.10	1.09	1.06	1.11	1.12	1.13	1.13	1.13
Isopropyl <i>tert</i> -butyl ether	C ₈ H ₁₆ O		1.11	1.11	1.11	1.10	1.11	1.13	1.13	1.10	1.10	1.11
Methyl phenyl ether (anisole)	C ₇ H ₁₀ O		1.18	1.20	1.17	1.18	1.18	1.11	1.11	1.12	1.15	1.16
Ethyl phenyl ether (phenetole)	C ₈ H ₁₀ O		1.17	1.16	1.16	1.17	1.17	1.15	1.14	1.11	1.12	1.15
Methyl <i>p</i> -tolyl ether (<i>p</i> -methylanisole)	C ₉ H ₁₂ O		1.18	1.15	1.18	1.19	1.20	1.15	1.15	1.19	1.19	1.20
Methyl <i>tert</i> -butyl ether	C ₆ H ₁₂ O	25	1.51	1.50	1.50	1.53	1.51	1.45	1.43	1.49	1.52	1.51
Ethyl <i>tert</i> -butyl ether	C ₇ H ₁₄ O		1.44	1.43	1.41	1.36	1.32	1.47	1.45	1.38	1.39	1.39
Isopropyl <i>tert</i> -butyl ether	C ₈ H ₁₆ O		1.36	1.27	1.28	1.25	1.23	1.33	1.33	1.31	1.31	1.31
Methyl phenyl ether (anisole)	C ₇ H ₁₀ O		1.46	1.48	1.48	1.50	1.54	1.31	1.29	1.27	1.36	1.41
Ethyl phenyl ether (phenetole)	C ₈ H ₁₀ O		1.57	1.65	1.64	1.65	1.68	1.39	1.34	1.30	1.37	1.43
Methyl <i>p</i> -tolyl ether (<i>p</i> -methylanisole)	C ₉ H ₁₂ O		1.55	1.60	1.62	1.69	1.65	1.38	1.33	1.37	1.44	1.62
Methyl <i>tert</i> -butyl ether	C ₆ H ₁₂ O	50	2.28	2.31	2.56	2.59	2.40	2.07	1.84	2.28	2.46	2.44
Ethyl <i>tert</i> -butyl ether	C ₇ H ₁₄ O		2.27	2.35	2.28	2.14	2.02	1.99	1.88	1.76	1.90	2.01
Isopropyl <i>tert</i> -butyl ether	C ₈ H ₁₆ O		2.14	2.18	2.10	2.00	1.98	2.00	1.98	1.98	1.90	1.95
Methyl phenyl ether (anisole)	C ₇ H ₁₀ O		—	—	—	2.63	2.72	1.71	1.50	1.41	1.74	2.07
Ethyl phenyl ether (phenetole)	C ₈ H ₁₀ O		—	2.80	2.61	2.68	2.72	1.77	1.64	1.62	1.99	2.22
Methyl <i>p</i> -tolyl ether (<i>p</i> -methylanisole)	C ₉ H ₁₂ O		—	2.71	2.42	2.74	2.96	1.43	1.28	1.24	1.40	1.68

* Imep ratio = $\frac{\text{knock-limited imep of blend with 4 ml TEL/gal}}{\text{knock-limited imep of mixed base fuel with 4 ml TEL/gal}}$

TABLE A-6.—17.6 ENGINE TEMPERATURE SENSITIVITY OF BLENDS RELATIVE TO ISOCTANE AND MIXED BASE FUEL CONSISTING OF 87.5 PERCENT (BY VOLUME) ISOCTANE AND 12.5 PERCENT *n*-HEPTANE+4 ML TEL PER GALLON

[Compression ratio, 7.0; engine speed, 1800 rpm; coolant temperature, 212° F; spark advance, 30° B. T. C.]

(a) Paraffins and olefins.

Paraffins and olefins	Formula	Relative temperature sensitivity*													
		20 volume percent added paraffin or olefin in blend with isooctane							25 volume percent added paraffin or olefin in blend with mixed base fuel						
		Unleaded					4 ml TEL/gal								
		0.065	0.07	0.085	0.10	0.11	0.065	0.07	0.085	0.10	0.11	0.065	0.07	0.085	0.10
Paraffins															
2, 2, 3-Trimethylbutane	C ₇ H ₁₆	1.06	1.05	1.10	1.06	1.00	1.05	1.00	1.00	1.00	0.95	1.05	1.05	1.00	1.00
2, 4-Dimethylpentane		1.00	.95	1.00	1.00	1.00	1.00	1.00	1.00	1.00	—	—	—	—	—
2, 2, 3, 3-Tetramethylpentane	C ₉ H ₂₂	1.10	1.05	1.06	0.96	0.95	1.05	1.05	1.00	0.95	0.95	—	—	—	—
2, 2, 3, 4-Tetramethylpentane		1.20	1.20	1.15	1.05	1.00	1.10	1.10	1.10	1.00	.95	1.05	1.10	1.05	1.00
2, 3, 3, 4-Tetramethylpentane		1.25	1.25	1.15	1.10	1.00	1.05	1.06	1.05	.95	.95	1.10	1.10	1.05	1.00
2, 4-Dimethyl-3-ethylpentane		1.05	1.00	1.00	1.00	.95	1.00	1.00	1.00	1.00	—	—	—	—	—
Olefins															
2, 3-Dimethyl-2-pentene	C ₆ H ₁₄	1.15	1.15	1.15	1.15	1.10	1.20	1.20	1.20	1.10	1.05	—	—	—	—
2, 3, 4-Trimethyl-2-pentene	C ₇ H ₁₆	1.20	1.20	1.26	1.20	1.15	1.20	1.25	1.30	1.26	1.20	1.20	1.20	1.20	1.10
3, 4-Trimethyl-2-pentene		1.15	1.10	1.15	1.20	1.15	1.20	1.20	1.20	1.15	1.10	1.25	1.20	1.15	1.10

* Relative temperature sensitivity = $\frac{\text{imep ratio of blend (inlet-air temperature, 100° F)}}{\text{imep ratio of blend (inlet-air temperature, 250° F)}}$

TABLE A-6.—17.6 ENGINE TEMPERATURE SENSITIVITY OF BLENDS RELATIVE TO ISOCTANE AND MIXED BASE FUEL CONSISTING OF 87.5 PERCENT (BY VOLUME) ISOCTANE AND 12.5 PERCENT *n*-HEPTANE+4 ML TEL PER GALLON—Continued

[Compression ratio, 7.0; engine speed, 1800 rpm; coolant temperature, 212° F; spark advance, 30° B. T. C.]

(b) Aromatics.

Aromatic	Formula	Relative temperature sensitivity *																		
		20 volume percent aromatic in blend with isooctane										25 volume percent aromatic in blend with mixed base fuel								
		Unleaded					4 ml TEL/gal													
Fuel-air ratio																				
		0.065	0.07	0.085	0.10	0.11	0.065	0.07	0.085	0.10	0.11	0.065	0.07	0.085	0.10	0.11				
Benzene	C_6H_6	1.10	1.05	1.05	1.00	1.00	1.10	1.05	1.05	1.05	1.05	1.15	1.10	1.05	1.05	1.00				
Methylbenzene	C_7H_8	1.00	1.05	1.05	1.00	1.00	1.10	1.10	1.10	1.10	1.10	---	---	---	---	---				
Ethylbenzene	C_8H_{10}	1.15	1.20	1.20	1.10	1.05	1.15	1.15	1.10	1.05	1.00	1.05	1.10	1.05	1.00	1.00				
1, 2-Dimethylbenzene	C_9H_{12}	1.10	1.10	1.15	1.10	1.05	1.05	1.00	1.00	1.05	1.05	1.10	1.05	1.00	1.00	1.00				
1, 3-Dimethylbenzene	C_9H_{12}	1.25	1.20	1.15	1.20	1.20	1.15	1.10	1.10	1.05	1.05	1.10	1.15	1.05	1.00	1.00				
1, 4-Dimethylbenzene	C_9H_{12}	1.10	1.15	1.10	1.05	1.00	1.15	1.15	1.10	1.05	1.05	---	---	---	---	---				
<i>n</i> -Propylbenzene	$C_{10}H_{14}$	1.15	1.15	1.15	1.15	1.05	1.20	1.20	1.15	1.05	1.00	1.10	1.10	1.05	1.05	1.05				
Isopropylbenzene	$C_{10}H_{14}$	1.10	1.20	1.20	1.10	1.05	1.20	1.20	1.15	1.05	1.00	---	---	---	---	---				
1-Methyl-2-ethylbenzene	$C_{10}H_{14}$	1.00	1.05	1.05	1.00	1.00	1.05	1.00	1.00	1.00	1.00	1.00	1.00	1.00	1.00	1.00				
1-Methyl-3-ethylbenzene	$C_{10}H_{14}$	1.15	1.20	1.15	1.10	1.05	1.15	1.10	1.10	1.00	1.00	1.00	1.00	1.00	1.00	1.00				
1-Methyl-4-ethylbenzene	$C_{10}H_{14}$	1.00	1.05	1.00	1.05	1.05	1.20	1.20	1.20	1.05	1.00	1.25	1.20	1.25	1.15	1.05				
1, 2, 2-Trimethylbenzene	$C_{10}H_{14}$	1.05	1.05	1.05	1.05	1.05	1.05	1.00	1.00	1.05	1.05	1.05	1.05	1.05	1.05	1.05				
1, 2, 4-Trimethylbenzene	$C_{10}H_{14}$	1.10	1.10	1.10	1.05	1.05	1.00	1.00	1.00	1.00	1.00	1.10	1.10	1.05	1.00	1.00				
1, 2, 5-Trimethylbenzene	$C_{10}H_{14}$	1.25	1.20	1.20	1.15	1.05	1.25	1.20	1.20	1.10	1.05	---	---	---	---	---				
<i>n</i> -Butylbenzene	$C_{10}H_{14}$	1.10	1.10	1.10	1.10	1.05	1.10	1.05	1.05	1.05	1.05	1.10	1.10	1.05	1.00	1.00				
Isobutylbenzene	$C_{10}H_{14}$	1.15	1.20	1.20	1.15	1.10	1.05	1.05	1.05	1.00	1.00	1.15	1.10	1.05	1.00	1.00				
sec-Butylbenzene	$C_{10}H_{14}$	1.15	1.15	1.10	1.05	1.00	1.10	1.15	1.10	1.00	1.00	1.05	1.05	1.05	1.00	1.00				
tert-Butylbenzene	$C_{10}H_{14}$	1.30	1.30	1.20	1.25	1.15	1.05	1.05	1.05	1.05	1.05	1.20	1.25	1.15	1.10	1.05				
1-Methyl-4-isopropylbenzene	$C_{10}H_{14}$	1.20	1.20	1.20	1.20	1.15	1.15	1.15	1.15	1.15	1.00	1.00	1.15	1.15	1.10	1.05				
1, 2-Diethylbenzene	$C_{10}H_{14}$	1.00	1.05	1.10	1.00	1.00	1.10	1.05	1.05	1.05	1.05	1.00	1.00	1.00	1.00	1.00				
1, 3-Diethylbenzene	$C_{10}H_{14}$	1.20	1.25	1.25	1.20	1.10	1.25	1.20	1.15	1.05	1.05	1.20	1.15	1.10	1.10	1.05				
1, 4-Diethylbenzene	$C_{10}H_{14}$	1.20	1.15	1.15	1.10	1.05	1.10	1.15	1.15	1.05	1.05	1.05	1.05	1.05	1.05	1.05				
1, 3-Dimethyl-5-ethylbenzene	$C_{10}H_{14}$	1.15	1.15	1.15	1.10	1.05	1.20	1.20	1.15	1.15	1.05	1.05	1.05	1.05	1.05	1.05				
1-Methyl-3-tert-butylbenzene	$C_{11}H_{16}$	1.10	1.15	1.10	1.00	1.00	1.10	1.15	1.10	1.05	1.05	1.10	1.10	1.05	1.00	1.00				
1-Methyl-4-tert-butylbenzene	$C_{11}H_{16}$	1.15	1.15	1.10	1.05	1.00	1.10	1.10	1.05	1.05	1.05	1.15	1.10	1.05	1.00	1.00				
1-Methyl-3, 5-diethylbenzene	$C_{11}H_{16}$	1.20	1.20	1.20	1.10	1.05	1.20	1.25	1.10	1.10	1.10	1.05	1.05	1.05	1.05	1.05				
1, 3, 5-Triethylbenzene	$C_{12}H_{18}$	1.25	1.25	1.25	1.15	1.05	1.25	1.25	1.10	1.00	1.00	1.00	1.00	1.00	1.00	1.00				

* Relative temperature sensitivity = $\frac{\text{imep ratio of blend (inlet-air temperature, 100° F)}}{\text{imep ratio of blend (inlet-air temperature, 250° F)}}$.TABLE A-6.—17.6 ENGINE TEMPERATURE SENSITIVITY OF BLENDS RELATIVE TO ISOCTANE AND MIXED BASE FUEL CONSISTING OF 87.5 PERCENT (BY VOLUME) ISOCTANE AND 12.5 PERCENT *n*-HEPTANE+4 ML TEL PER GALLON—Concluded

[Compression ratio, 7.0; engine speed, 1800 rpm; coolant temperature, 212° F; spark advance, 30° B. T. C.]

(c) Ethers.

Ether	Formula	Relative temperature sensitivity *														
		Ether in blend with mixed base fuel, percent by volume														
		20					10					25				
Fuel-air ratio																
		0.065	0.07	0.085	0.10	0.11	0.065	0.07	0.085	0.10	0.11	0.065	0.07	0.085	0.10	0.11
Methyl <i>tert</i> -butylether	$C_4H_{10}O$	1.10	1.10	1.15	1.05	1.00	1.10	1.15	1.10	1.05	1.00	1.05	1.05	1.00	1.00	1.00
Ethyl <i>tert</i> -butylether	$C_5H_{12}O$	1.05	1.05	1.00	1.00	.95	1.00	1.00	1.00	1.00	.95	.95	.95	1.00	1.00	1.00
Isopropyl <i>tert</i> -butylether	$C_7H_{14}O$	1.10	1.10	1.05	1.00	.95	1.00	1.05	1.05	1.00	.95	.95	.95	1.00	1.00	1.00
Methyl phenylether (anisole)	$C_7H_{10}O$	1.15	1.15	1.15	1.10	1.00	1.15	1.15	1.20	1.10	1.05	1.10	1.05	1.10	1.15	1.20
Ethyl phenyl ether (phenetole)	$C_8H_{10}O$	1.10	1.10	1.15	1.10	1.00	1.15	1.15	1.10	1.05	1.05	1.00	1.15	1.15	1.10	1.10
Methyl <i>p</i> -tolyl ether (<i>p</i> -methoxyanisole)	$C_8H_{10}O$	1.05	1.15	1.15	1.10	1.05	1.25	1.20	1.10	1.05	1.00	1.00	1.00	1.10	1.10	1.00

* Relative temperature sensitivity = $\frac{\text{imep ratio of blend (inlet-air temperature, 100° F)}}{\text{imep ratio of blend (inlet-air temperature, 250° F)}}$.

TABLE A-7.—17.6 ENGINE LEAD SUSCEPTIBILITY OF BLENDS RELATIVE TO ISOCTANE

[Compression ratio, 7.0; engine speed, 1800 rpm; coolant temperature, 212° F; spark advance, 30° B. T. C.]

(a) Paraffins and olefins.

Paraffins and olefins	Formula	Relative lead susceptibility *														
		Inlet-air temperature, 250° F								Inlet-air temperature, 100° F						
		Volume percent paraffin or olefin in blend with isoctane														
		10					20					20				
		Fuel-air ratio														
		0.065	0.07	0.085	0.10	0.11	0.065	0.07	0.085	0.10	0.11	0.065	0.07	0.085	0.10	0.11
Paraffins																
2, 2, 3-Trimethylbutane.....	C ₇ H ₁₆	1.05	1.05	1.05	1.00	1.00	1.05	1.10	1.10	1.05	1.05	1.05	1.05	1.05	1.00	1.00
2, 2-Dimethylpentane.....		----	----	----	----	----	1.00	1.00	1.05	1.05	1.00	1.05	1.05	1.05	1.05	1.00
2, 2, 3, 3-Tetramethylpentane.....	C ₉ H ₂₀	1.05	1.05	1.05	1.00	1.00	1.05	1.05	1.10	1.00	1.00	1.00	1.00	1.00	1.00	1.00
2, 2, 3, 4-Tetramethylpentane.....		1.10	1.05	1.05	1.10	1.05	1.15	1.15	1.10	1.05	1.00	1.05	1.05	1.05	1.00	1.00
2, 2, 3, 4-Tetramethylpentane.....		----	----	----	----	----	1.05	1.00	1.05	1.05	1.00	1.00	1.00	1.00	.95	1.00
2, 4-Dimethyl-3-ethylpentane.....		----	----	----	----	----	1.05	1.00	1.00	1.00	1.00	1.00	1.00	1.00	.95	1.05
Olefins																
2, 3-Dimethyl-2-pentene.....	C ₇ H ₁₄	----	----	----	----	----	0.95	0.95	1.00	1.05	1.00	1.00	1.00	1.00	1.00	0.95
2, 3, 4-Trimethyl-2-pentene.....	C ₈ H ₁₆	1.00	1.00	1.00	1.05	1.00	1.05	1.05	1.00	1.05	1.05	1.05	1.05	1.05	1.05	1.05
3, 4, 4-Trimethyl-2-pentene.....		1.00	1.00	1.00	1.00	1.00	1.00	1.00	1.00	1.00	1.00	1.00	1.00	1.00	1.00	1.00

* Relative lead susceptibility = $\frac{\text{Imep ratio of blend with 4 ml TEL/gal}}{\text{Imep ratio of blend with 0 ml TEL/gal}}$

TABLE A-7.—17.6 ENGINE LEAD SUSCEPTIBILITY OF BLENDS RELATIVE TO ISOCTANE—Continued

[Compression ratio, 7.0; engine speed, 1800 rpm; coolant temperature, 212° F; spark advance, 30° B. T. C.]

(b) Aromatics.

Aromatic	Formula	Relative lead susceptibility *														
		Inlet-air temperature, 250° F								Inlet-air temperature, 100° F						
		Volume percent aromatic in blend with isoctane														
		10					20					20				
		0.065	0.07	0.085	0.10	0.11	0.065	0.07	0.085	0.10	0.11	0.065	0.07	0.085	0.10	0.11
Benzene.....	C ₆ H ₆	1.00	1.00	1.05	1.05	1.05	1.00	1.05	1.10	1.05	1.00	1.05	1.05	1.10	1.10	1.05
Methylbenzene.....	C ₇ H ₈	0.95	1.00	1.00	0.95	1.00	1.00	1.05	1.00	1.00	1.00	1.10	1.10	1.05	1.05	1.05
Ethylbenzene.....	C ₈ H ₁₀	1.05	1.05	1.05	1.00	0.95	1.10	1.15	1.15	1.10	1.05	1.10	1.10	1.05	1.00	1.00
1, 2-Dimethylbenzene.....		.95	.95	.95	.90	.85	.85	.90	.95	.90	.85	.85	.85	.85	.85	.85
1, 3-Dimethylbenzene.....		1.10	1.10	1.10	1.10	1.15	1.20	1.25	1.20	1.25	1.10	1.10	1.20	1.10	1.10	1.10
1, 4-Dimethylbenzene.....		1.05	1.05	1.00	1.00	1.00	1.00	1.10	1.05	1.05	1.00	1.05	1.05	1.10	1.10	1.05
n-Propylbenzene.....	C ₉ H ₁₂	1.05	1.05	1.10	1.05	1.00	1.10	1.15	1.20	1.10	1.10	1.20	1.20	1.20	1.05	1.00
Isopropylbenzene.....		1.05	1.10	1.05	1.00	1.05	1.15	1.10	1.10	1.15	1.05	1.15	1.15	1.15	1.05	1.05
1-Methyl-2-ethylbenzene.....		----	----	----	----	----	.95	1.00	1.00	.95	.90	.95	.95	.90	.90	.90
1-Methyl-3-ethylbenzene.....		1.05	1.05	1.10	1.10	1.10	1.15	1.20	1.15	1.15	1.10	1.10	1.10	1.10	1.05	1.05
1-Methyl-4-ethylbenzene.....		1.05	1.05	1.10	1.10	1.10	1.10	1.10	1.10	1.10	1.20	1.35	1.30	1.30	1.15	1.15
1, 2, 3-Trimethylbenzene.....		1.00	1.00	1.00	.95	.95	1.00	.90	.90	.90	.90	.85	.85	.85	.85	.85
1, 2, 4-Trimethylbenzene.....		1.05	1.05	1.10	1.00	.95	1.00	1.00	1.05	1.00	.90	.90	.90	.90	.90	.85
1, 3, 5-Trimethylbenzene.....		1.05	1.05	1.10	1.00	.95	1.10	1.15	1.15	1.10	1.05	1.10	1.10	1.10	1.05	1.05
n-Butylbenzene.....	C ₁₀ H ₁₄	1.05	1.05	1.05	1.05	1.05	1.10	1.10	1.10	1.10	1.05	1.05	1.05	1.05	1.05	1.05
Isobutylbenzene.....		1.10	1.10	1.10	1.10	1.05	1.20	1.20	1.20	1.20	1.15	1.15	1.15	1.15	1.05	1.05
sec-Butylbenzene.....		1.10	1.10	1.05	1.05	1.05	1.20	1.15	1.10	1.10	1.10	1.10	1.10	1.10	1.05	1.05
tert-Butylbenzene.....		1.15	1.10	1.05	1.05	1.00	1.40	1.35	1.20	1.20	1.10	1.10	1.10	1.10	1.05	1.00
1-Methyl-4-isopropylbenzene.....		1.10	1.10	1.10	1.10	1.05	1.20	1.20	1.20	1.20	1.15	1.15	1.15	1.15	1.05	1.05
1, 2-Diethylbenzene.....		1.05	1.10	1.10	1.10	1.05	1.05	1.00	1.05	1.00	1.00	1.05	1.05	1.05	1.05	.95
1, 3-Diethylbenzene.....		1.05	1.10	1.10	1.10	1.05	1.10	1.15	1.15	1.10	1.05	1.05	1.05	1.05	1.05	1.05
1, 4-Diethylbenzene.....		----	----	----	----	----	1.05	1.15	1.15	1.10	1.05	1.05	1.05	1.05	1.05	1.05
1, 3-Dimethyl-5-ethylbenzene.....		----	----	----	----	----	1.05	1.15	1.15	1.10	1.05	1.05	1.05	1.05	1.05	1.05
1-Methyl-3-tert-butylbenzene.....	C ₁₁ H ₁₆	----	----	----	----	----	1.05	1.05	1.05	1.05	1.05	1.05	1.05	1.05	1.05	1.05
1-Methyl-4-tert-butylbenzene.....		----	----	----	----	----	1.10	1.10	1.05	1.05	1.05	1.05	1.05	1.05	1.05	1.05
1-Methyl-3, 5-diethylbenzene.....		----	----	----	----	----	1.10	1.15	1.10	1.05	1.05	1.15	1.15	1.15	1.10	1.05
1, 3, 5-Triethylbenzene.....	C ₁₂ H ₁₈	----	----	----	----	----	1.10	1.15	1.15	1.15	1.15	1.05	1.10	1.15	1.05	1.05

* Relative lead susceptibility = $\frac{\text{Imep ratio of blend with 4 ml TEL/gal}}{\text{Imep ratio of blend with 0 ml TEL/gal}}$

TABLE A-7.—17.6 ENGINE LEAD SUSCEPTIBILITY OF BLENDS RELATIVE TO ISOCTANE—Concluded

[Compression ratio, 7.0; engine speed, 1800 rpm; coolant temperature, 212° F; spark advance, 30° B. T. C.]

(c) Ethers.

Ether	Formula	Relative lead susceptibility *														
		Inlet-air temperature, 250° F							Inlet-air temperature, 100° F							
		Volume percent ether in blend with isoctane														
		10					20					20				
		Fuel-air ratio														
		0.065	0.07	0.085	0.10	0.11	0.065	0.07	0.085	0.10	0.11	0.065	0.07	0.085	0.10	0.11
Methyl <i>tert</i> -butyl ether	C ₄ H ₉ O	1.10	1.05	1.10	1.05	1.05	1.10	1.10	1.05	1.05	1.15	1.10	1.10	1.05	1.10	1.10
Ethyl <i>tert</i> -butyl ether	C ₅ H ₁₁ O	1.00	1.00	.95	.95	1.15	1.10	1.05	1.00	.95	1.05	1.05	1.05	1.00	.95	.95
Isopropyl <i>tert</i> -butyl ether	C ₇ H ₁₅ O	1.00	1.00	1.00	1.00	1.00	1.10	1.05	1.00	1.00	1.05	1.05	1.05	1.05	1.00	1.00
Methyl phenyl ether (anisole)	C ₇ H ₁₁ O	1.00	1.00	1.00	1.00	1.00	1.05	1.05	1.00	1.00	1.05	1.05	1.05	1.05	1.05	1.05
Ethyl phenyl ether (phenetole)	C ₈ H ₁₃ O	1.00	1.00	1.05	1.00	1.00	1.00	1.00	1.00	1.10	1.05	1.05	1.05	1.10	1.00	1.00
Methyl <i>p</i> -tolyl ether (<i>p</i> -methylanisole)	C ₈ H ₁₁ O	1.00	1.05	1.05	1.05	1.05	.95	1.05	1.05	1.05	1.05	1.10	1.10	1.05	1.00	1.05

* Relative lead susceptibility = $\frac{\text{imep ratio of blend with 4 ml TEL/gal}}{\text{imep ratio of blend with 0 ml TEL/gal}}$ TABLE A-8.—FULL-SCALE SINGLE-CYLINDER ENGINE KNOCK-LIMITED INDICATED MEAN EFFECTIVE PRESSURE RATIOS OF ETHER BLENDS WITH MIXED BASE FUEL CONSISTING OF 87.5 PERCENT (BY VOLUME) ISOCTANE AND 12.5 PERCENT *n*-HEPTANE + 4 ML TEL PER GALLON

[Full-scale cruise conditions; compression ratio, 7.3; engine speed, 1800 rpm; inlet-air temperature, 210° F; spark advance, 30° B. T. C.; cooling-air flow such that rear-spark-plug-bushing temperature equals 365° F at 140 bmeep and 0.10 fuel-air ratio]

Ether	Formula	Imep ratio *				
		10 volume percent ether in blend with mixed base fuel				
		Fuel-air ratio				
		0.065	0.07	0.085	0.10	0.11
Methyl <i>tert</i> -butyl ether	C ₄ H ₉ O	1.27	1.21	1.24	1.25	1.19
Ethyl <i>tert</i> -butyl ether	C ₅ H ₁₁ O	1.19	1.16	1.19	1.16	1.11
Isopropyl <i>tert</i> -butyl ether	C ₇ H ₁₅ O	1.17	1.16	1.15	1.15	1.14
Methyl phenyl ether (anisole)	C ₇ H ₁₁ O	1.11	1.08	1.08	1.11	1.11
Ethyl phenyl ether (phenetole)	C ₈ H ₁₃ O	1.13	1.11	1.11	1.15	1.12
Methyl <i>p</i> -tolyl ether (<i>p</i> -methylanisole)	C ₈ H ₁₁ O	1.20	1.16	1.15	1.17	1.19

* Imep ratio = $\frac{\text{knock-limited imep of blend with 4 ml TEL/gal}}{\text{knock-limited imep of mixed base fuel with 4 ml TEL/gal}}$

TABLE A-9.—INSPECTION DATA FOR PURE FUEL STOCKS AND FUEL BLENDS

The following abbreviations are used throughout the table: VBS for virgin base stock; alkylate for aviation alkylate; one-pass stock for one-pass catalytic stock; and MTB ether for methyl *tert*-butyl ether. [

Fuel	Fuel composition		A. S. T. M. distillation data										Specific gravity at 60° F	Copper dish gum (mg/100 ml)	Reid vapor pressure (lb/sq in.)	Aromatics* (percent by volume)	Freezing point (°F)	Hydrogen-carbon ratio	Net heat of combustion (Btu/lb)	Refractive index n _D at 60° F	Bromine number (cst)	Olefins* (percent by weight)	
	Components		TEL concentration (ml/gal)	Initial boiling point (°F)	10% point (°F)	40% point (°F)	50% point (°F)	90% point (°F)	Final boiling point (°F)	Sum of 10 and 50% points (°F)	Residue (percent)	Loss (percent)											
A-202	VBS	0	114	145	172	180	229	298	325	0.4	1.1	0.713	None	5.9	7.3	Below -76	0.175	19,000	1.3988	2.8	1.7		
A-118	50% alkylate+50% VBS	4.04	112	160	188	200	254	336	350	0.7	1.1	0.707	—	5.9	4.7	None	Below -76	0.189	18,100	1.3957	—		
A-203	Alkylate	0	113	160	215	226	272	364	386	.5	1.0	0.688	—	2	4.7	—	—	—	—	1.3928	0.2	0.1	
A-132	30% one-pass stock+70% VBS	4.08	112	140	170	182	251	319	322	0.5	1.3	0.723	—	6.0	—	—	—	—	—	1.4043	—	—	
A-116	50% one-pass stock+50% VBS	4.08	103	134	170	184	269	321	318	.5	1.0	0.727	—	7.1	—	—	—	—	—	1.4080	—	—	
A-119	80% one-pass stock+20% VBS	4.08	116	130	171	190	285	326	320	.4	1.4	0.735	—	7.4	—	—	—	—	—	1.4141	—	—	
A-122	30% one-pass stock+70% alkylate	3.96	110	147	202	218	272	345	365	0.6	1.2	0.718	—	6.8	—	—	—	—	—	1.4005	—	—	
A-117	50% one-pass stock+50% alkylate	4.00	105	140	194	213	280	341	353	.5	1.0	0.721	—	6.5	—	—	—	—	—	1.4051	—	—	
A-121	80% one-pass stock+20% alkylate	4.04	108	131	181	204	288	334	335	.7	1.3	0.782	—	7.2	—	—	—	—	—	1.4123	—	—	
A-204	One-pass stock	0	108	128	170	193	287	362	321	.5	1.0	0.739	—	7.9	24.8	Below -76	0.155	18,700	1.4177	30.4	17.6		
A-136	20% triptane+80% VBS	4.10	124	150	172	178	218	299	328	0.7	0.8	0.712	—	6.0	—	Below -76	—	—	1.3969	—	—		
A-137	40% triptane+60% VBS	4.06	128	156	172	177	205	287	333	.6	0.6	0.707	—	5.3	—	Below -76	—	—	1.3963	—	—		
A-138	60% triptane+40% VBS	4.08	142	162	174	176	194	274	338	.7	0.5	0.704	—	4.5	—	Below -76	—	—	1.3938	—	—		
A-272	20% triptane+80% alkylate	(d)	122	163	202	210	259	346	374	0.9	0.6	0.701	—	4.4	—	Below -76	—	—	—	—	—	—	
A-273	40% triptane+60% alkylate	(d)	130	167	192	198	251	336	366	.7	.8	0.701	—	4.1	—	Below -76	—	—	—	—	—	—	
A-274	60% triptane+40% alkylate	(d)	144	169	183	188	230	326	357	.8	.7	0.700	—	4.0	—	Below -76	—	—	—	—	—	—	
A-275	80% triptane+20% alkylate	(d)	158	172	178	180	202	296	352	.8	.2	0.699	—	3.6	—	Below -76	—	—	—	—	—	—	
A-276	20% triptane+80% one-pass stock	(d)	107	186	172	186	281	321	322	0.4	1.4	0.734	—	6.7	—	Below -76	—	—	—	—	—	—	
A-277	40% triptane+60% one-pass stock	(d)	120	147	174	183	275	320	330	.9	.9	0.725	—	5.9	—	Below -76	—	—	—	—	—	—	
A-278	60% triptane+40% one-pass stock	(d)	128	156	174	179	234	316	335	.4	.6	0.716	—	5.1	—	Below -76	—	—	—	—	—	—	
A-279	80% triptane+20% one-pass stock	(d)	141	166	177	179	196	304	345	.5	.5	0.710	—	4.2	—	Below -76	—	—	—	—	—	—	
A-206	Triptane	0	172	174	174	174	175	180	348	.4	.8	0.694	1	3.0	—	-18	0.191	19,200	1.3898	—	—		
A-397	20% diisopropyl+80% VBS	(d)	120	143	160	168	224	287	311	0.9	0.8	0.705	—	6.6	—	—	—	—	—	—	—	—	—
A-398	40% diisopropyl+60% VBS	(d)	123	138	151	156	214	285	284	.7	1.5	0.696	—	6.8	—	—	—	—	—	—	—	—	—
A-399	60% diisopropyl+40% VBS	(d)	128	138	146	148	197	258	288	.9	1.1	0.686	—	6.8	—	—	—	—	—	—	—	—	—
A-400	80% diisopropyl+20% VBS	(d)	130	136	140	142	165	254	278	.7	1.0	0.677	—	7.0	—	—	—	—	—	—	—	—	—
A-405	20% diisopropyl+80% alkylate	(d)	120	151	187	202	263	344	353	1.1	0.7	0.695	—	5.5	—	—	—	—	—	—	—	—	—
A-406	40% diisopropyl+60% alkylate	(d)	120	140	165	162	222	320	302	1.2	.8	0.687	—	6.3	—	—	—	—	—	—	—	—	—
A-407	60% diisopropyl+40% alkylate	(d)	127	140	160	158	246	322	296	1.1	.6	0.681	—	6.4	—	—	—	—	—	—	—	—	—
A-408	80% diisopropyl+20% alkylate	(d)	130	136	141	143	208	295	279	1.0	.6	0.675	—	6.8	—	—	—	—	—	—	—	—	—
A-401	20% diisopropyl+80% one-pass stock	(d)	112	132	157	172	287	322	304	0.5	1.5	0.728	—	6.9	—	—	—	—	—	—	—	—	—
A-402	40% diisopropyl+60% one-pass stock	(d)	117	133	160	157	277	321	290	.8	.9	0.718	—	7.1	—	—	—	—	—	—	—	—	—
A-403	60% diisopropyl+40% one-pass stock	(d)	121	133	143	147	257	315	280	.4	1.2	0.698	—	7.2	—	—	—	—	—	—	—	—	—
A-404	80% diisopropyl+20% one-pass stock	(d)	127	134	138	140	169	305	274	.7	.7	0.683	—	7.3	—	—	—	—	—	—	—	—	—
A-433	Diisopropyl	0	132	134	135	135	185	138	269	None	1.2	0.666	None	7.4	—	Below -76	0.196	19,100	—	—	—	—	—
A-411	20% neohexane+80% VBS	(d)	118	138	157	165	227	289	303	0.0	0.9	0.705	—	7.0	—	—	—	—	—	—	—	—	—
A-412	40% neohexane+60% VBS	(d)	118	133	145	151	219	286	284	.8	.9	0.694	—	7.5	—	—	—	—	—	—	—	—	—
A-413	60% neohexane+40% VBS	(d)	118	127	138	138	201	266	265	.6	1.3	0.683	—	8.1	—	—	—	—	—	—	—	—	—
A-414	80% neohexane+20% VBS	(d)	118	128	128	128	161	241	251	.9	1.1	0.672	—	9.1	—	—	—	—	—	—	—	—	—
A-415	20% neohexane+80% alkylate	(d)	116	146	183	203	265	345	349	1.1	0.8	0.693	—	5.9	—	—	—	—	—	—	—	—	—
A-416	40% neohexane+60% alkylate	(d)	117	134	167	169	257	332	303	1.2	.8	0.686	—	6.0	—	—	—	—	—	—	—	—	—
A-417	60% neohexane+40% alkylate	(d)	116	125	136	142	247	322	287	1.1	1.1	0.677	—	7.9	—	—	—	—	—	—	—	—	—
A-418	80% neohexane+20% alkylate	(d)	116	122	127	129	220	290	261	.9	1.4	0.670	—	8.8	—	—	—	—	—	—	—	—	—
A-420	20% neohexane+80% one-pass stock	(d)	107	127	151	167	288	323	294	0.6	1.3	0.728	—	7.9	—	—	—	—	—	—	—	—	—
A-421	40% neohexane+60% one-pass stock	(d)	110	125	140	148	275	318	273	.5	1.4	0.712	—	8.3	—	—	—	—	—	—	—	—	—
A-422	60% neohexane+40% one-pass stock	(d)	112	121	130	134	259	313	255	.5	1.2	0.698	—	8.5	—	—	—	—	—	—	—	—	—
A-423	80% neohexane+20% one-pass stock	(d)	116	120	125	126	181	302	246	.6	1.6	0.678	1	9.1	—	—	—	—	—	—	—	—	—
A-500	Neohexane	0	119	120	120	120	211	223	240	None	1.2	0.658	1	9.7	—	—	—	—	—	—	—	—	—
A-123	20% isopentane+80% VBS	4.06	102	122	148	160	224	297	282	0.7	1.3	0.702	—	9.3	—	—	—	—	—	—	—	—	—
A-124	40% isopentane+60% VBS	4.06	96	108	124	134	216	291	242	.7	2.8	0.679	—	11.8	—	—	—	—	—	—	—	—	—
A-134	60% isopentane+40% VBS	4.16	90	98	106	110	200	266	208	.8	2.4	0.664	—	14.4	—	—	—	—	—	—	—	—	—
A-375	20% isopentane+80% alkylate	(d)	104	127	175	208	262	344	336	0.9	2.0	0.687	—	8.4	—	—	—	—	—	—	—	—	—
A-376	40% isopentane+60% alkylate	(d)	97	110	134	154	256	335	264	.7	1.4	0.673	—	11.6	—	—	—	—	—	—	—	—	—
A-388	20% isopentane+80% one-pass stock	(d)	102	118	146	167	288	323	285	0.4	2.4	0.720	—	9.9	—	—	—						

TABLE A-9.—INSPECTION DATA FOR PURE FUEL STOCKS AND FUEL BLENDS—Continued

Fuel composition			A. S. T. M. distillation data										Properties			Refined oil index $\eta_{40,40}$ at 60°F			Bromine number (g/E)			Olefins ^b (percent by weight)			
Fuel	Components		TEL concentration (ml/gal)	Initial boiling point ($^{\circ}\text{F}$)					40% point ($^{\circ}\text{F}$)					Residue (percent)	Loss (percent)	Specific gravity at 60°F	Copper dish gum (mg/100 ml)	Reid vapor pressure (lb/in. 2)	Aromatics ^a (percent by volume)	Freezing point ($^{\circ}\text{F}$)	Hydrogen-carbon ratio	Net heat of combustion (Btu/lb)	Refined oil index $\eta_{40,40}$ at 60°F	Bromine number (g/E)	Olefins ^b (percent by weight)
	Initial boiling point ($^{\circ}\text{F}$)	10% point ($^{\circ}\text{F}$)		Initial boiling point ($^{\circ}\text{F}$)	10% point ($^{\circ}\text{F}$)	40% point ($^{\circ}\text{F}$)	40% point ($^{\circ}\text{F}$)	Initial boiling point ($^{\circ}\text{F}$)	Sum of 10 and 40% points ($^{\circ}\text{F}$)	Initial boiling point ($^{\circ}\text{F}$)	Sum of 10 and 40% points ($^{\circ}\text{F}$)	Initial boiling point ($^{\circ}\text{F}$)													
A-371	20% hot-acid octane+80% one-pass stock	(4)	114	142	189	208	282	322	350	0.4	1.4	0.737	—	—	—	—	—	—	—	—	—	—	—	—	—
A-372	40% hot-acid octane+60% one-pass stock	(4)	124	155	206	218	289	321	373	0.6	1.4	0.732	—	—	—	—	—	—	—	—	—	—	—	—	—
A-373	60% hot-acid octane+40% one-pass stock	(4)	115	165	215	222	250	310	387	0.8	1.1	0.727	—	—	—	—	—	—	—	—	—	—	—	—	—
A-374	80% hot-acid octane+20% one-pass stock	(4)	129	195	222	224	240	294	419	0.7	1.5	0.722	—	—	—	—	—	—	—	—	—	—	—	—	—
A-205	Hot-acid octane	0	174	216	224	224	230	257	440	0.6	0.9	0.715	6	3.6	None	Below -76	0.188	19,200	1,4009	2.6	1.7	—	—	—	
A-148	20% mixed xylenes+80% VBS	±.07	116	152	191	203	272	266	355	0.4	0.6	0.716	—	5.3	26.4	Below -76	—	—	—	—	—	—	—	—	1,4180
A-444	40% mixed xylenes+60% VBS	(4)	122	167	215	232	277	288	399	0.3	0.5	0.715	—	4.2	—	—	—	—	—	—	—	—	—	—	—
A-445	60% mixed xylenes+40% VBS	(4)	128	186	252	264	277	287	460	0.3	0.4	0.805	—	3.0	—	—	—	—	—	—	—	—	—	—	—
A-446	80% mixed xylenes+20% VBS	(4)	140	220	266	270	278	286	490	0.4	0.6	0.824	2	2.2	—	—	—	—	—	—	—	—	—	—	—
A-149	20% mixed xylenes+80% alkylate	3.96	121	176	234	242	276	342	418	0.8	0.7	0.731	1	3.9	20.5	Below -76	—	—	—	—	—	—	—	—	1,4132
A-262	40% mixed xylenes+60% alkylate	(4)	124	191	249	255	281	320	445	0.5	1.3	0.788	—	3.0	—	—	—	—	—	—	—	—	—	—	—
A-263	60% mixed xylenes+40% alkylate	(4)	130	217	262	265	296	306	493	0.5	0.5	0.799	—	2.2	—	—	—	—	—	—	—	—	—	—	—
A-264	80% mixed xylenes+20% alkylate	(4)	136	238	268	271	279	295	509	0.8	0.8	0.821	—	1.9	—	—	—	—	—	—	—	—	—	—	—
A-150	20% mixed xylenes+80% one-pass stock	4.10	106	146	200	230	285	315	376	0.3	0.9	0.767	—	6.5	42.3	Below -76	—	—	—	—	—	—	—	—	1,4333
A-266	40% mixed xylenes+80% one-pass stock	(4)	115	159	244	262	284	311	421	0.8	0.8	0.793	—	5.2	—	—	—	—	—	—	—	—	—	—	—
A-267	60% mixed xylenes+40% one-pass stock	(4)	115	164	251	264	282	303	418	1.1	1.1	0.800	—	4.4	—	—	—	—	—	—	—	—	—	—	—
A-268	80% mixed xylenes+20% one-pass stock	(4)	126	222	273	275	280	294	497	0.2	0.8	0.888	2	2.4	—	—	—	—	—	—	—	—	—	—	—
A-269	Mixed xylenes	0	273	275	276	276	277	278	551	0.2	None	0.867	2	5.5	—	Below -40	0.106	17,600	1,4039	—	—	—	—	—	
A-163	20% cumene+80% VBS	4.12	118	152	188	202	294	321	354	0.5	0.7	0.737	—	5.3	25.8	Below -76	—	—	—	—	—	—	—	—	1,4169
A-244	40% cumene+60% VBS	(4)	123	161	218	238	300	330	399	0.4	0.9	0.775	—	4.4	43.0	Below -76	—	—	—	—	—	—	—	—	1,4333
A-245	60% cumene+40% VBS	(4)	128	180	265	284	302	335	464	0.6	0.6	0.804	—	3.2	62.0	Below -76	—	—	—	—	—	—	—	—	1,4338
A-247	80% cumene+20% VBS	(4)	130	228	296	298	304	342	558	0.5	0.5	0.832	—	2.0	—	Below -76	—	—	—	—	—	—	—	—	1,4338
A-164	20% cumene+80% alkylate	3.99	116	170	234	244	300	342	414	0.7	0.5	0.732	8	4.0	19.7	Below -76	—	—	—	—	—	—	—	1,4122	
A-249	40% cumene+60% alkylate	(4)	118	187	287	307	302	455	545	0.4	0.8	0.767	—	3.2	39.0	Below -76	—	—	—	—	—	—	—	1,4320	
A-250	60% cumene+40% alkylate	(4)	124	206	271	280	304	333	498	0.5	0.5	0.787	—	2.6	—	Below -76	—	—	—	—	—	—	—	—	
A-251	80% cumene+20% alkylate	(4)	140	262	293	296	304	342	558	0.5	0.5	0.831	—	1.4	—	Below -76	—	—	—	—	—	—	—	—	
A-165	20% cumene+80% one-pass stock	3.91	108	136	203	234	298	323	370	0.6	0.4	0.709	—	6.4	40.0	Below -76	—	—	—	—	—	—	—	1,4325	
A-253	40% cumene+60% one-pass stock	(4)	110	144	240	268	301	330	412	1.0	1.0	0.787	—	5.3	—	Below -76	—	—	—	—	—	—	—	—	
A-254	60% cumene+40% one-pass stock	(4)	120	174	256	280	303	336	468	0.4	1.1	0.815	—	3.8	—	Below -76	—	—	—	—	—	—	—	—	
A-255	80% cumene+20% one-pass stock	(4)	125	216	292	295	303	340	511	1.0	1.0	0.836	—	2.4	—	Below -76	—	—	—	—	—	—	—	—	
A-258	Cumene	0	298	298	300	305	349	558	—	0.5	0.5	0.833	—	3	—	• Below -76	0.113	17,800	1,4033	—	—	—	—	—	
A-170	20% benzene+80% VBS	4.11	118	148	167	174	218	298	322	0.5	0.5	0.748	—	6.0	26.0	—	—	—	—	—	—	—	—	1,4175	
A-342	40% benzene+60% VBS	(4)	126	168	218	213	286	327	456	0.5	1.0	0.772	—	5.6	—	—	—	—	—	—	—	—	—	—	
A-343	60% benzene+40% VBS	(4)	144	164	171	174	188	286	338	0.4	1.1	0.823	—	4.6	—	—	—	—	—	—	—	—	—	—	
A-344	80% benzene+20% VBS	(4)	148	188	172	174	179	238	342	0.4	0.6	0.844	—	4.2	—	—	—	—	—	—	—	—	—	—	
A-168	20% benzene+80% alkylate	3.92	120	158	190	200	258	345	356	0.7	0.3	0.734	4	4.8	19.5	—	—	—	—	—	—	—	—	1,4124	
A-349	40% benzene+60% alkylate	(4)	128	162	188	185	245	333	348	0.8	1.2	0.770	—	4.4	—	—	—	—	—	—	—	—	—	—	
A-350	60% benzene+40% alkylate	(4)	148	166	177	179	210	324	345	0.8	0.9	0.808	—	4.4	—	—	—	—	—	—	—	—	—	—	
A-351	80% benzene+20% alkylate	(4)	154	170	176	176	185	233	346	0.8	0.6	0.841	—	3.7	—	—	—	—	—	—	—	—	—	—	
A-169	20% benzene+80% one-pass stock	4.08	107	134	170	182	273	321	316	0.3	0.9	0.768	—	7.0	40.0	—	—	—	—	—	—	—	—	1,4333	
A-363	40% benzene+60% one-pass stock	(4)	117	147	171	179	273	328	326	0.5	1.0	0.822	—	6.0	—	—	—	—	—	—	—	—	—	—	
A-364	60% benzene+40% one-pass stock	(4)	122	163	173	177	211	314	330	0.4	1.1	0.841	—	5.2	—	—	—	—	—	—	—	—	—	—	
A-365	80% benzene+20% one-pass stock	(4)	143	174	175	179	211	316	339	0.4	0.8	0.850	—	4.4	—	—	—	—	—	—	—	—	—	—	
A-210	Benzene	0	170	173	173	173	174	175	346	0.2	0.8	0.833	—	3.5	—	—	—	45	0.084	17,400	1,4033	—	—	—	
A-145	20% toluene+80% VBS	4.10	122	167	186	194	230	294	351	0.6	0.9	0.746	—	5.3	26.2	Below -76	—	—	—	—	—	—	—	1,4178	
A-322	40% toluene+60% VBS	(4)	125	163	193	201	231	282	364	0.4	0.6	0.760	—	5.1</td											

TABLE A-10.—PERFORMANCE RATINGS OBTAINED IN A. S. T. M. AVIATION AND A. S. T. M. SUPERCHARGE ENGINES

Three rows of values are given for each fuel: The first row is l_{mep} , lb/sq in.; the second row for A. S. T. M. Aviation ratings is octane number or tetraethyl lead in S reference fuel, ml/gal; the second row for A. S. T. M. Supercharge ratings is S reference fuel in M reference fuel, percent, or tetraethyl lead in S reference fuel, ml/gal; the third row is performance number. The following abbreviations are used throughout the table: VBS for virgin base stock; alkylate for aviation alkylate; one-pass stock for one-pass catalytic stock; MTBE ether for methyl *tert*-butyl ether.

Fuel	Fuel composition ^a (by volume)	A. S. T. M. Aviation ratings ^b	A. S. T. M. Supercharge ratings ^b					
			Fuel-air ratio					
			0.065	0.070	0.085	0.095	0.100	0.110
A-355	VBS	90.7 75	73 96.6 91	83 99.8 99	122 0.08 103	137 99.8 99	141 99.0 97	143 97.8 94
A-118	50% alkylate+50% VBS	98.8 96	86 0.10 104	99 0.19 107	143 0.34 111	159 0.83 111	162 0.29 110	165 0.24 109
A-356	Alkylate	0.84 110	104 0.65 117	129 0.93 124	178 1.67 134	190 1.71 185	195 2.5 187	201 2.14 140
A-182	30% one-pass stock+70% VBS	90.6 75	72 93.8 84	71 90.0 78	116 100 100	130 98.0 94	136 97.5 94	145 97.7 94
A-116	50% one-pass stock+50% VBS	90.9 76	64 88.6 75	76 93.1 84	116 100 100	137 0.01 101	145 0.01 101	156 0.06 103
A-119	80% one-pass stock+20% VBS	92.7 79	67 90.6 78	76 93.1 84	114 99.2 97	142 0.09 104	154 0.16 106	165 0.24 109
A-122	30% one-pass stock+70% alkylate	0.15 106	82 100	103 0.26	152 0.45	172 0.58	178 0.75	182 0.83
A-117	50% one-pass stock+50% alkylate	100 100	76 96.3 91	91 0.06 103	143 0.34 111	167 0.44 114	178 0.68 117	188 1.17 129
A-121	80% one-pass stock+20% alkylate	96.3 88	72 93.8 84	79 95 96	123 0.09 104	149 0.19 107	160 0.26 110	177 0.48 115
A-410	One-pass stock	93.4 81	73 96.6 91	83 99.8 99	125 0.12 105	151 0.16 106	164 0.28 110	179 0.49 115
A-136	20% triptane+80% VBS	94.2 83	74 96.0 88	90 0.05 102	134 0.23 108	155 0.27 110	162 0.27 110	167 0.28 110
A-187	40% triptane+60% VBS	0.18 107	100 0.43 114	119 0.55 117	164 0.96 125	191 1.75 136	201 2.07 139	205 2.07 139
A-188	60% triptane+40% VBS	0.67 120	117 1.20 129	142 1.58 134	224 5.54 160	260 1.75 175	264 1.75 175	269 1.75 175
A-272	20% triptane+80% alkylate	1.08 127	90 106	128 1.09	186 2.13	218 3.17	225 3.79	287 4.87
A-273	40% triptane+60% alkylate	2.43 142	98 0.38 118	126 0.88 123	225 5.69 160	262 1.77 177	274 2.07 182	283 2.07 184
A-274	60% triptane+40% alkylate	2.70 145	111 0.90 124	159 2.76 145	275 1.09	316 2.18	326 2.16	334 2.18
A-275	80% triptane+20% alkylate	3.06 147	139 2.89 144	190 5.90 161	314 — —	— — —	— — —	— — —

^a Each fuel contains approximately 4 ml TEL/gal.

^b Based on fixed reference-fuel framework (ch. VIII, reference 13).

TABLE A-10.—PERFORMANCE RATINGS OBTAINED IN A. S. T. M. AVIATION AND A. S. T. M. SUPERCHARGE ENGINES—Continued

Fuel	Fuel composition ^a (by volume)	A. S. T. M. Aviation ratings ^b	A. S. T. M. Supercharge ratings ^b					
			Fuel-air ratio					
			0.065	0.070	0.085	0.095	0.100	0.110
A-276	20% triptane+80% one-pass stock ^c	98.8 96	96 90.0 77	72 90.7 78	117 0.01 101	140 0.14 105	160 0.26 110	166 1.17 133
A-277	40% triptane+60% one-pass stock ^c	0.08 103	81 99.4 99	89 0.05 101	129 0.29 111	176 0.88 124	195 1.77 136	231 3.80 152
A-278	60% triptane+40% one-pass stock ^c	0.48 115	100 1.48 114	109 0.38 113	171 1.38 131	218 3.52 150	244 1.62 140	291
A-279	80% triptane+20% one-pass stock ^c	1.80 136	128 1.63 134	147 1.82 137	290 — —	301 — —	391 — —	—
A-271	Triptane ^c	3.30 149	204 191	262 — —	4393 — —	— — —	— — —	— — —
A-397	20% diisopropyl+80% VBS	06.6 90	77 96.9 91	91 0.08 103	132 0.20 108	149 0.19 107	184 0.16 106	155 0.04 101
A-398	40% diisopropyl+60% VBS	0.09 103	81 99.4 98	96 0.16 106	143 0.34 112	167 0.44 114	176 0.50 116	180 0.67 120
A-399	60% diisopropyl+40% VBS	0.33 111	98 0.33 111	108 0.34 112	103 1.58 124	187 1.58 134	197 1.86 137	207 2.21 141
A-400	80% diisopropyl+20% VBS	1.17 128	111 1.10 127	141 1.56 134	202 3.23 149	226 4.14 153	236 5.07 158	280 — 163
A-405	20% diisopropyl+80% alkylate	0.90 124	125 1.78 136	146 2.58 136	192 2.97 144	210 3.21 146	217 3.24 148	222 3.24 146
A-408	40% diisopropyl+60% alkylate	1.45 132	138 2.47 143	158 2.67 144	206 3.49 160	227 4.29 154	234 4.80 156	240 5.00 157
A-407	60% diisopropyl+40% alkylate	1.40 132	132 1.91 138	154 2.29 141	212 3.87 152	210 3.87 162	262 — 167	263 171
A-408	80% diisopropyl+20% alkylate	2.10 139	136 2.24 141	162 3.05 147	226 5.85 161	261 — 176	275 — 182	292 190
A-401	20% diisopropyl+80% one-pass stock	0.81 88	79 98.1 95	89 0.05 102	132 0.20 108	132 0.39 113	163 0.67 120	177 1.60 134
A-402	40% diisopropyl+60% one-pass stock	0.08 102	84 0.05 102	99 0.20 108	150 0.43 114	177 0.95 125	189 1.48 133	209 2.34 142
A-403	60% diisopropyl+40% one-pass stock	0.24 108	96 0.33 111	114 0.44 114	165 1.02 126	196 2.00 138	210 2.72 145	235 4.29 154
A-404	80% diisopropyl+20% one-pass stock	0.68 120	120 1.34 131	143 1.65 135	197 2.90 146	229 4.57 165	245 — 162	272 — 177
A-393	Dilisopropyl ^c	2.41 142	147 3.53 150	173 4.11 153	246 — 175	289 — 195	304 — —	324 — —

^a Each fuel contains approximately 4 ml TEL/gal.

^b Based on fixed reference-fuel framework (ch. VIII, reference 13).

^c Knock-limited performance of the engine with one-pass catalytic stock was low on day fuels were investigated.

^d Estimated value.

^e Values for knock-limited l_{mep} were averaged from three curves.

TABLE A-10.—PERFORMANCE RATINGS OBTAINED IN
A. S. T. M. AVIATION AND A. S. T. M. SUPERCHARGE
ENGINES—Continued

Fuel	Fuel composition ^a (by volume)	A. S. T. M. Aviation ratings ^b	A. S. T. M. Supercharge ratings ^b						
			Fuel-air ratio						
		A. S. T. M. Aviation ratings	0.065	0.070	0.085	0.095	0.100	0.110	
A-411	20% neohexane+80% VBS	91.5 84	74 95.0 88	86 100 100	124 0.10 104	142 0.09 103	147 0.05 102	150 0.02 99.2 98	
A-412	40% neohexane+60% VBS	0.05 102	81 99.4 98	97 0.17 106	138 0.28 110	158 0.31 111	164 0.32 111	167 0.28 110	
A-413	60% neohexane+40% VBS	0.36 112	93 0.26 110	108 0.34 112	189 0.67 120	178 1.03 126	183 1.17 128	187 1.25 130	
A-414	80% neohexane+20% VBS	2.00 138	108 0.75 121	130 1.06 127	182 1.95 138	203 2.48 143	208 2.57 143	210 2.41 142	
A-415	20% neohexane+80% alkylate	1.10 127	112 0.95 125	130 1.06 127	172 1.41 132	193 1.85 137	199 1.95 138	202 1.91 138	
A-416	40% neohexane+60% alkylate	1.50 133	118 1.25 130	137 1.38 131	186 2.19 140	203 2.48 143	207 2.50 143	209 2.35 142	
A-417	60% neohexane+40% alkylate	2.57 143	124 1.53 133	148 1.78 136	195 2.78 145	212 3.10 147	215 3.07 147	216 2.83 145	
A-418	80% neohexane+20% alkylate	3.38 149	137 2.25 142	158 2.67 144	208 3.61 151	224 3.93 152	227 3.93 152	228 3.52 150	
A-420	20% neohexane+80% one-pass stock	96.6 90	79 98.1 95	95 0.14 95	146 0.38 113	171 0.50 116	180 0.92 124	190 1.38 131	
A-421	40% neohexane+60% one-pass stock	0.10 104	86 0.10 104	107 0.23 111	165 1.02 126	190 1.70 135	197 1.86 137	203 1.96 138	
A-422	60% neohexane+40% one-pass stock	0.33 111	106 0.75 121	138 1.43 132	192 2.58 143	210 2.97 146	215 3.07 147	217 2.90 146	
A-423	80% neohexane+20% one-pass stock	1.66 135	132 1.91 133	182 3.08 147	214 4.00 153	230 4.72 156	233 4.67 156	234 4.14 153	
A-394	Neohexane ^c	6.00 161	159 4.76 156	157 5.58 160	230 --- 163	240 5.87 162	242 5.43 161	243 5.43 160	
A-123	20% isopentane+80% VBS	91.4 83	72 98.5 84	87 0.02 101	127 0.14 106	141 0.07 103	146 0.03 101	149 0.09 99	
A-124	40% isopentane+60% VBS	99.1 97	80 98.8 96	99 0.20 108	139 0.21 110	151 0.18 108	155 0.12 107	159 0.12 105	
A-124	60% isopentane+40% VBS	0.23 108	87 0.12 105	112 0.41 114	153 0.48 114	168 0.45 114	172 0.45 114	174 0.42 113	
A-375	20% isopentane+80% alkylate	0.92 124	121 1.39 131	144 1.69 135	186 2.19 143	201 2.34 143	204 2.29 142	204 2.00 138	
A-376	40% isopentane+60% alkylate	0.99 125	121 1.39 131	144 1.69 135	181 2.42 143	203 2.48 143	205 2.36 142	204 2.00 138	
A-388	20% isopentane+80% one-pass stock	95.5 87	78 97.5 94	87 0.02 101	132 0.20 108	160 0.34 111	173 0.47 115	168 1.29 116	168 1.29 113
A-389	40% isopentane+60% one-pass stock	100 100	85 0.07 103	97 0.17 107	140 0.20 111	168 0.46 115	180 0.92 124	192 1.47 133	

^a Each fuel contains approximately 4 ml TEL/gal.^b Based on fixed reference-fuel framework (ch. VII, reference 12).^c Values for knock-limited imep were averaged from two curves.TABLE A-10.—PERFORMANCE RATINGS OBTAINED IN
A. S. T. M. AVIATION AND A. S. T. M. SUPERCHARGE
ENGINES—Continued

Fuel	Fuel composition ^a (by volume)	A. S. T. M. Aviation ratings ^b	A. S. T. M. Supercharge ratings ^b						
			Fuel-air ratio						
		A. S. T. M. Aviation ratings	0.065	0.070	0.085	0.095	0.100	0.110	
A-139	20% hot-acid octane+80% VBS	94.3 83	70 92.5 83	83 98.0 94	128 0.15 106	147 0.16 106	151 0.11 105	154 0.02 101	
A-140	40% hot-acid octane+60% VBS	100 100	74 95.0 94	89 0.03 101	143 0.34 111	168 0.46 114	173 0.58 115	179 0.58 117	
A-141	60% hot-acid octane+40% VBS	0.18 107	84 0.05 111	106 0.31 111	165 1.02 126	191 1.75 136	198 2.21 140	207 2.21 145	
A-387	20% hot-acid octane+80% alkylate	0.82 123	121 1.39 131	142 1.60 134	188 2.32 141	205 2.62 144	210 2.72 145	215 2.76 145	
A-388	40% hot-acid octane+60% alkylate	0.72 121	125 1.58 134	148 1.87 147	200 3.10 147	219 3.59 150	226 3.86 152	235 4.29 154	
A-389	60% hot-acid octane+40% alkylate	0.88 124	129 1.77 136	154 2.29 141	216 4.81 154	240 5.14 162	248 5.60 164	257 5.76 168	
A-370	80% hot-acid octane+20% alkylate	0.72 121	129 1.77 136	154 2.29 141	238 3.00 169	269 3.59 182	276 3.86 183	280 4.12 182	
A-371	20% hot-acid octane+80% one-pass stock	95.1 86	80 98.8 95	90 0.08 102	138 0.28 110	170 0.49 115	185 1.30 130	206 2.14 140	
A-372	40% hot-acid octane+60% one-pass stock	100 100	88 0.14 105	97 0.17 107	154 0.48 115	192 1.80 136	208 2.57 143	229 3.73 151	
A-373	60% hot-acid octane+40% one-pass stock	0.18 107	90 0.19 107	101 0.23 108	184 0.46 125	203 2.42 143	220 3.43 149	245 5.71 160	
A-374	80% hot-acid octane+20% one-pass stock	0.45 115	99 0.41 114	115 0.46 115	224 2.26 141	240 3.93 162	268 5.60 160	288 6.60 175	
A-380	Hot-acid octane ^c	1.08 127	131 1.86 137	230 2.76 145	250 3.78 178	259 4.78 195	304 5.78 195	317 6.78 195	
A-257	20% mixed xylenes+80% VBS	92.6 79	68 91.3 86	78 94.7 86	114 99.2 97	132 98.7 96	138 98.1 94	148 98.6 96	
A-258	40% mixed xylenes+60% VBS	93.5 86	69 91.9 86	78 94.7 86	117 0.03 101	147 0.16 106	160 0.26 110	182 0.58 123	
A-259	60% mixed xylenes+40% VBS	95.2 86	74 95.0 87	85 99.3 99	146 0.38 113	194 1.90 137	216 3.14 148	233 3.59 165	
A-260	80% mixed xylenes+20% VBS	0.04 101	64 0.05 102	95 0.14 105	214 4.00 153	240 4.60 153	259 5.14 153	277 5.78 153	
A-261	20% mixed xylenes+80% alkylate	0.52 116	88 0.14 106	101 0.23 108	153 0.65 119	194 1.90 137	208 2.57 143	227 3.59 150	
A-262	40% mixed xylenes+60% alkylate	0.27 110	82 100 105	95 0.14 105	153 0.46 115	206 2.69 144	225 3.67 167	237 4.57 177	
A-263	60% mixed xylenes+40% alkylate	0.14 105	85 103	96 0.19 107	181 1.89 137	274 1.89 183	274 2.86 183	274 3.86 183	
A-264	80% mixed xylenes+20% alkylate	0.27 110	87 0.12 105	103 0.27 110	260 0.27 185	336 --- ---	370 --- ---	370 --- ---	

^a Each fuel contains approximately 4 ml TEL/gal.^b Based on fixed reference-fuel framework (ch. VIII, reference 12).^c Values for knock-limited imep were averaged from two curves.

TABLE A-10.—PERFORMANCE RATINGS OBTAINED IN A. S. T. M. AVIATION AND A. S. T. M. SUPERCHARGE ENGINES—Continued

Fuel	Fuel composition ^a (by volume)	A. S. T. M. Aviation rat- ings	A. S. T. M. Supercharge ratings ^b						
			Fuel-air ratio						
			0.065	0.070	0.085	0.095	0.100	0.110	
A-265	20% mixed xylenes+80% one-pass stock ^c	94.7 84	71 93.1 83	74 92.0 81	111 97.9 94	138 0.03 101	151 0.11 116	178 0.50 116	
A-266	40% mixed xylenes+60% one-pass stock ^c	97.5 92	80 98.8 95	86 100 100	133 0.21 108	172 0.58 118	198 1.81 136	246 5.88 161	
A-267	60% mixed xylenes+40% one-pass stock ^c	98.8 96	95 0.31 111	100 0.22 108	184 2.06 139	251 1.89 169	232 1.87 187	339 — —	
A-268	80% mixed xylenes+20% one-pass stock ^c	0.16 106	102 0.48 115	106 0.31 111	351 — —	— — —	— — —	— — —	
A-269	Mixed xylenes ^{c,d}	0.92 124	105 0.60 118	122 0.69 120	— — —	— — —	— — —	— — —	
A-245	20% cumene+80% VBS	92.4 78	67 90.6 78	72 90.7 78	98 92.5 82	123 95.7 88	134 96.9 91	154 0.02 101	
A-244	40% cumene+60% VBS	92.7 79	67 90.6 78	70 89.3 76	95 91.8 80	117 93.7 84	130 95.8 88	160 0.14 108	
A-246	60% cumene+40% VBS	94.2 83	67 90.6 78	72 90.7 78	94 90.8 85	118 94.0 86	132 96.3 91	174 0.42 114	
A-247	80% cumene+20% VBS	96.0 88	77 96.9 91	76 93.3 84	90 89.2 76	120 94.7 86	151 0.11 105	— — —	
A-248	20% cumene+80% alkylate	0.32 111	98 0.38 113	102 0.25 109	143 0.34 111	172 0.58 117	187 1.39 131	215 2.78 145	
A-249	40% cumene+60% alkylate	0.11 105	71 93.1 84	76 93.3 84	113 98.8 95	148 0.17 106	171 0.44 114	233 4.00 163	
A-250	60% cumene+40% alkylate	0.03 101	77 96.9 91	76 93.3 84	94 90.8 78	124 96.0 90	149 0.08 103	277 — 180	
A-251	80% cumene+20% alkylate	97.7 93	74 95.0 87	73 91.3 80	86 87.5 73	114 92.7 82	160 0.28 110	— — —	
A-252	20% cumene+80% one-pass stock	93.0 80	70 92.5 82	69 88.6 75	91 89.6 76	120 94.3 85	137 97.8 93	175 0.44 114	
A-253	40% cumene+60% one-pass stock	98.6 82	70 92.5 82	67 87.4 74	75 82.9 67	95 86.3 72	112 90.0 77	168 0.30 111	
A-254	60% cumene+40% one-pass stock	93.0 80	66 90.0 78	62 84.0 68	65 78.8 62	81 81.3 65	94 84.4 69	153 100 100	
A-255	80% cumene+30% one-pass stock	93.0 85	66 90.0 78	68 84.8 69	70 80.8 64	98 87.3 74	141 99.1 98	— — —	
A-240	Cumene ^e	95.0 85	77 96.9 91	75 92.7 88	87 87.9 74	122 96.3 88	— — —	— — —	

^a Each fuel contains approximately 4 ml TEL/gal.^b Based on fixed reference-fuel framework (ch. VIII, reference 13).^c Knock-limited performance of engine with one-pass catalytic stock was low on day fuels

were investigated.

^d Values for knock-limited imep were averaged from three curves.

TABLE A-10.—PERFORMANCE RATINGS OBTAINED IN A. S. T. M. AVIATION AND A. S. T. M. SUPERCHARGE ENGINES—Continued

Fuel	Fuel composition ^a (by volume)	A. S. T. M. Aviation rat- ings	A. S. T. M. Supercharge ratings ^b						
			Fuel-air ratio						
			0.065	0.070	0.085	0.095	0.100	0.110	
A-341	20% benzene+80% VBS	91.4 76	78 97.5 93	88 99.4 97	134 108	155 110	162 110	168 111	
A-342	40% benzene+60% VBS	92.4 78	81 97.4 97	99 102	146 112	178 126	190 134	208 141	
A-343	60% benzene+40% VBS	94.2 83	78 97.5 93	85 99.4 97	244 173	346 —	384 —	— —	
A-344	80% benzene+20% VBS	96.2 88	98 0.38 113	116 0.45 115	— —	— —	— —	— —	
A-358	20% benzene+80% alkylate	0.43 114	117 1.20 129	127 0.92 124	182 1.95 137	212 3.10 147	223 3.57 150	234 4.14 153	
A-359	40% benzene+60% alkylate	0.12 105	102 0.48 115	112 0.41 114	182 1.95 137	230 4.72 166	253 5.33 168	295 192	
A-360	60% benzene+40% alkylate	100 100	102 0.48 115	110 0.38 113	336 —	— —	— —	— —	
A-361	80% benzene+20% alkylate	98.3 94	119 1.30 130	178 4.63 156	— —	— —	— —	— —	
A-362	20% benzene+80% one-pass stock	98.8 82	77 96.9 91	86 100 100	142 0.33 111	172 0.68 118	184 1.26 130	203 1.93 138	
A-363	40% benzene+80% one-pass stock	92.0 78	82 100	79 95.3 88	160 0.73 121	213 2.17 148	238 5.33 159	264 172	
A-364	60% benzene+40% one-pass stock	91.5 77	68 91.3 80	72 90.7 83	191 2.52 143	254 1.72 186	280 —	328 —	
A-365	80% benzene+20% one-pass stock	93.0 80	94 0.29 110	93 0.11 105	— —	— —	— —	— —	
A-340	Benzene ^f	— 87	190 186	— 196	— —	— —	— —	— —	
A-321	20% toluene+80% VBS	92.7 82	85 0.07 103	96 0.15 106	137 0.28 110	166 0.29 110	184 0.32 111	172 0.27 110	
A-322	40% toluene+60% VBS	95.1 85	92 0.24 109	96 0.16 106	175 1.57 134	228 4.43 155	245 1.62 162	266 173	
A-323	60% toluene+40% VBS	97.0 91	88 0.14 105	95 0.14 105	204 3.38 149	303 — —	346 — —	425 —	
A-324	80% toluene+20% VBS	98.8 96	101 0.45 115	113 0.42 114	240 — —	— —	— —	— —	

^a Each fuel contains approximately 4 ml TEL/gal.^b Based on fixed reference-fuel framework (ch. VIII, reference 13).^c Values for knock-limited imep were averaged from two curves.^d

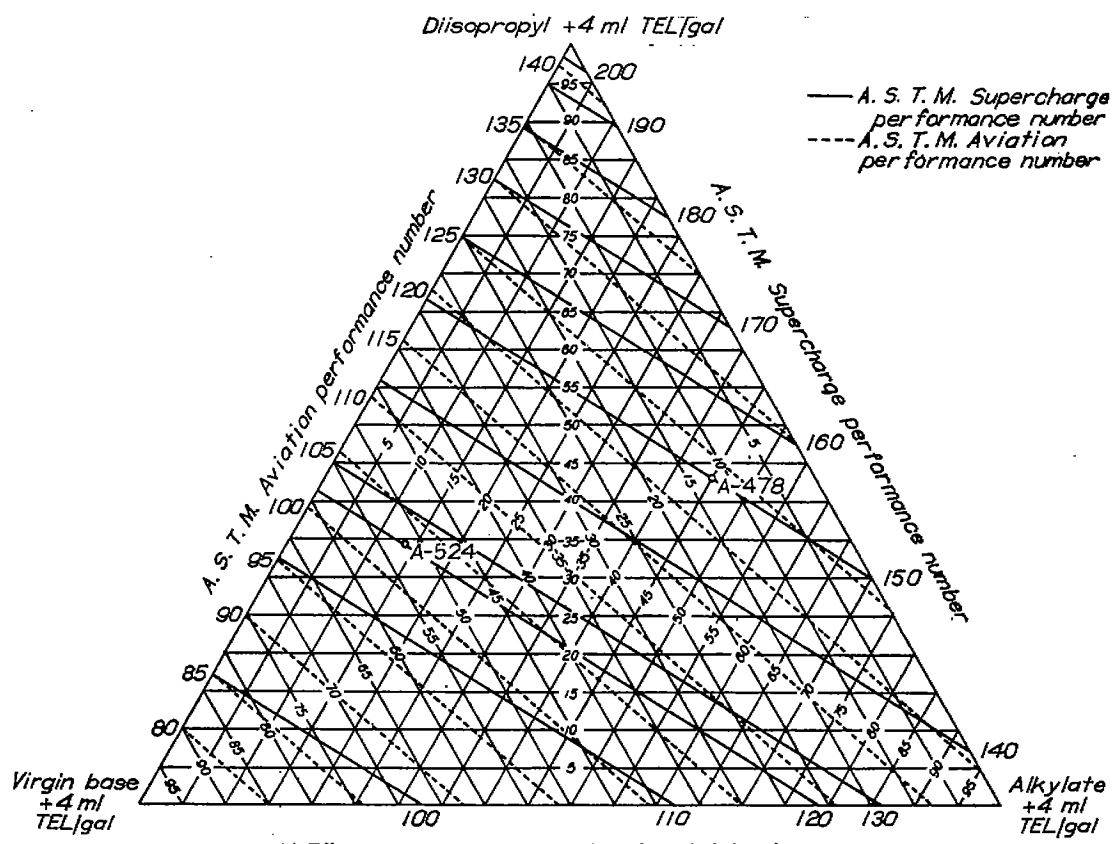
TABLE A-10.—PERFORMANCE RATINGS OBTAINED IN
A. S. T. M. AVIATION AND A. S. T. M. SUPERCHARGE
ENGINES—Concluded

Fuel	Fuel composition ^a (by volume)	M. A. S. T. M. Aviation rating hr ^b	A. S. T. M. Supercharge ratings ^b					
			Fuel-air ratio					
			0.065	0.070	0.085	0.095	0.100	0.110
A-325	20% toluene+80% alkylate	0.48 116	121 1.39 181	139 1.47 132	191 2.52 143	221 3.73 151	232 4.53 155	249 162
A-326	40% toluene+60% alkylate	0.54 116	108 0.75 121	128 0.97 125	223 5.38 159	275 186	308	348
A-327	60% toluene+40% alkylate	0.25 109	100 0.43 114	105 0.30 111	300	—	—	—
A-328	80% toluene+20% alkylate	0.16 106	108 0.75 121	116 0.47 115	—	—	—	—
A-331	20% toluene+80% one-pass stock.	95.1 85	80 98.8 95	90 0.06 103	137 0.26 110	169 0.47 115	184 1.25 130	212 2.55 143
A-332	40% toluene+80% one-pass stock.	95.3 86	85 0.07 103	92 0.09 103	151 0.44 114	202 2.41 142	224 3.72 161	282 171
A-333	60% toluene+40% one-pass stock.	97.4 91	91 0.21 108	95 0.14 105	173 1.73 135	270 182	319	—
A-334	80% toluene+20% one-pass stock.	0.10 104	102 0.48 115	108 0.31 111	—	—	—	—
A-320	Toluene ^c	0.57 118	124 2.00 138	140 1.51 133	—	—	—	—
A-336	20% MTB ether+80% VBS	98.8 96	95 0.31 111	101 0.28 108	144 0.30 111	170 0.49 115	179 0.83 115	187 1.25 130
A-337	40% MTB ether+60% VBS	0.12 105	112 0.95 125	113 0.42 114	185 1.02 126	204 2.55 143	223 3.64 161	253 185
A-338	60% MTB ether+40% VBS	0.92 124	192 3.14 180	163 1.48	228 162	281 190	307	385
A-339	80% MTB ether+20% VBS	2.61 144	—	239	309	379	—	—
A-347	20% MTB ether+80% alkylate.	1.68 135	143 3.06 146	155 2.38 142	230 163	258 174	268 178	281 163
A-348	40% MTB ether+60% alkylate.	2.30 141	166 5.43 159	174 4.21 154	268 188	312 —	338 —	377 —
A-349	60% MTB ether+40% alkylate.	2.50 143	258 —	229 193	327 —	406 —	442 —	—
A-350	80% MTB ether+20% alkylate.	8.0 161	307 —	271 —	374 —	—	—	—
A-351	20% MTB ether+80% one-pass stock.	96.1 88	87 0.12 105	91 0.08 103	144 0.35 112	179 1.10 127	194 1.72 135	218 2.97 146
A-352	40% MTB ether+60% one-pass stock.	0.14 105	118 1.00 126	112 0.41 114	163 0.85 123	204 2.55 143	225 3.79 162	269 175
A-353	60% MTB ether+40% one-pass stock.	0.47 115	185 2.86 173	180 146	230 163	289 195	319 —	376 —
A-354	80% MTB ether+20% one-pass stock.	1.00 126	269 —	237 —	301 —	370 —	—	—
A-355	MTB ether ^c	>6.00 >161	—	330	406	—	—	—

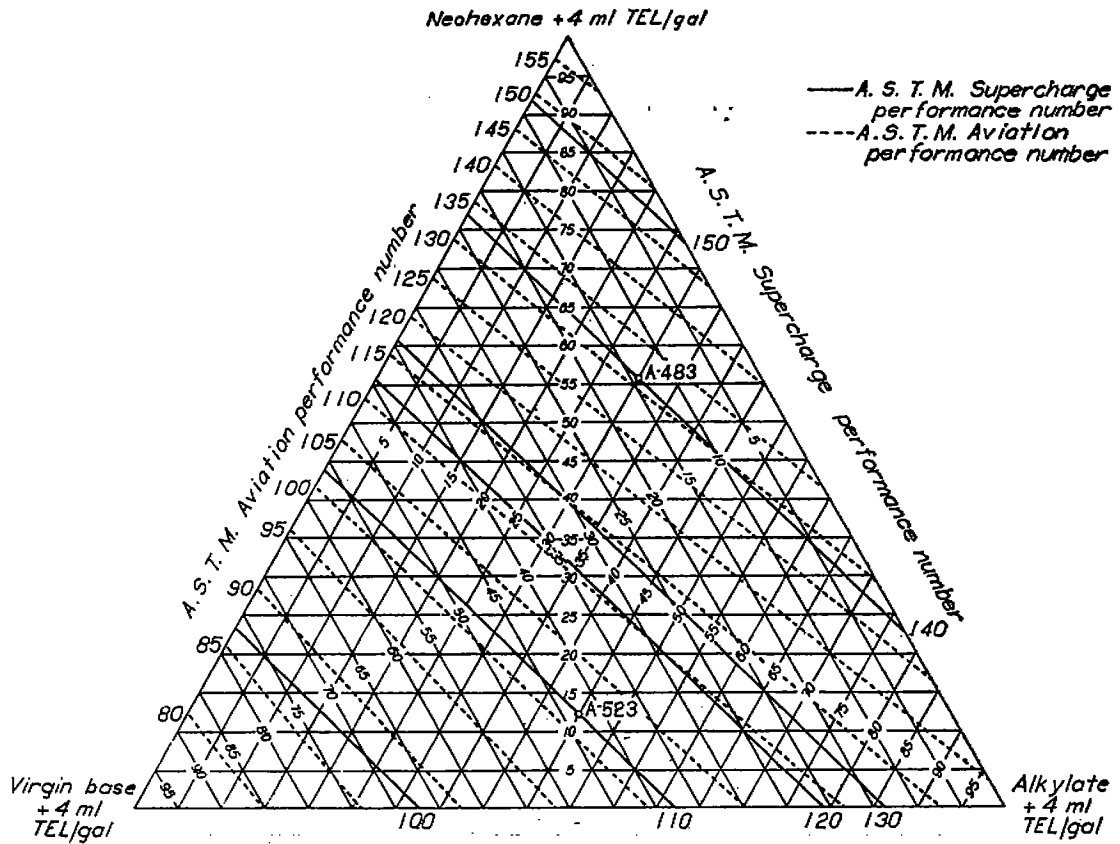
^a Each fuel contains approximately 4 ml TEL/gal.^b Based on fixed reference-fuel framework (ch. VIII, reference 13).^c Values for knock-limited imep were averaged from two curves.

APPENDIX B

ADDITIONAL BLENDING CHARTS FOR TERNARY FUEL BLENDS¹



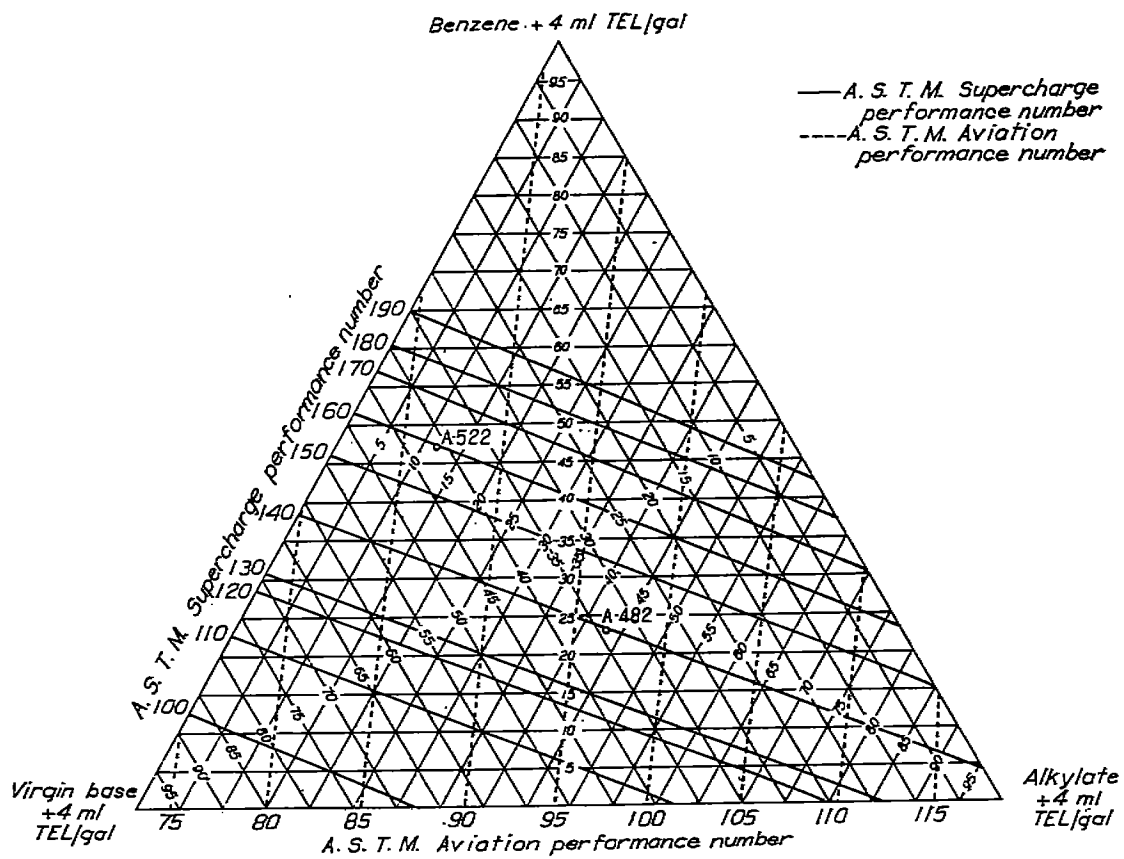
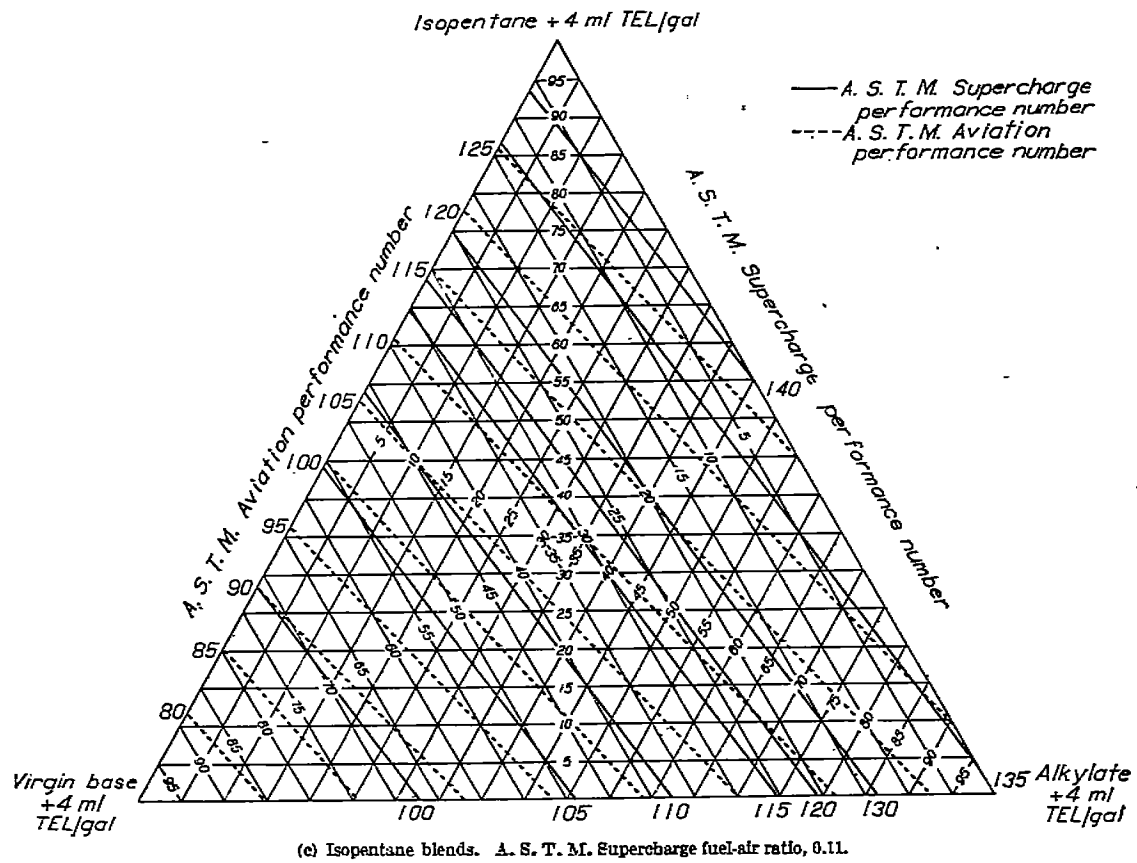
(a) Diisopropyl blends. A. S. T. M. Supercharge fuel-air ratio, 0.11



(b) Neohexane blends. A. S. T. M. Supercharge fuel-air ratio, 0.11.

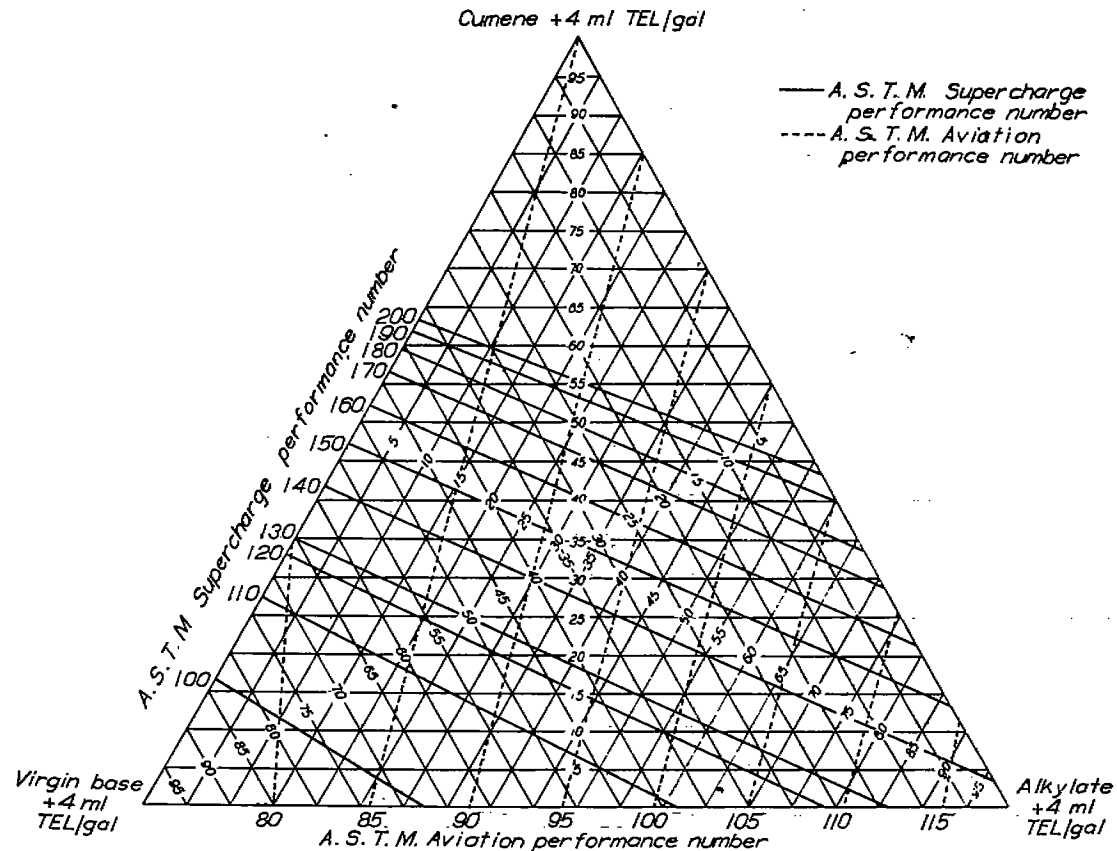
FIGURE B-1.—Blending charts for ternary blends containing high-antiknock blending agents, aviation alkylate, and virgin base stock by A. S. T. M. Aviation and A. S. T. M. Supercharge methods.

¹ The charts of this appendix were reproduced from NACA Report 904 entitled "Estimation of F-8 and F-4 Knock-Limited Performance Ratings for Ternary and Quaternary Blends Containing Triptane or Other High-Antiknock Aviation-Fuel Blending Agents" by Henry C. Barnett.

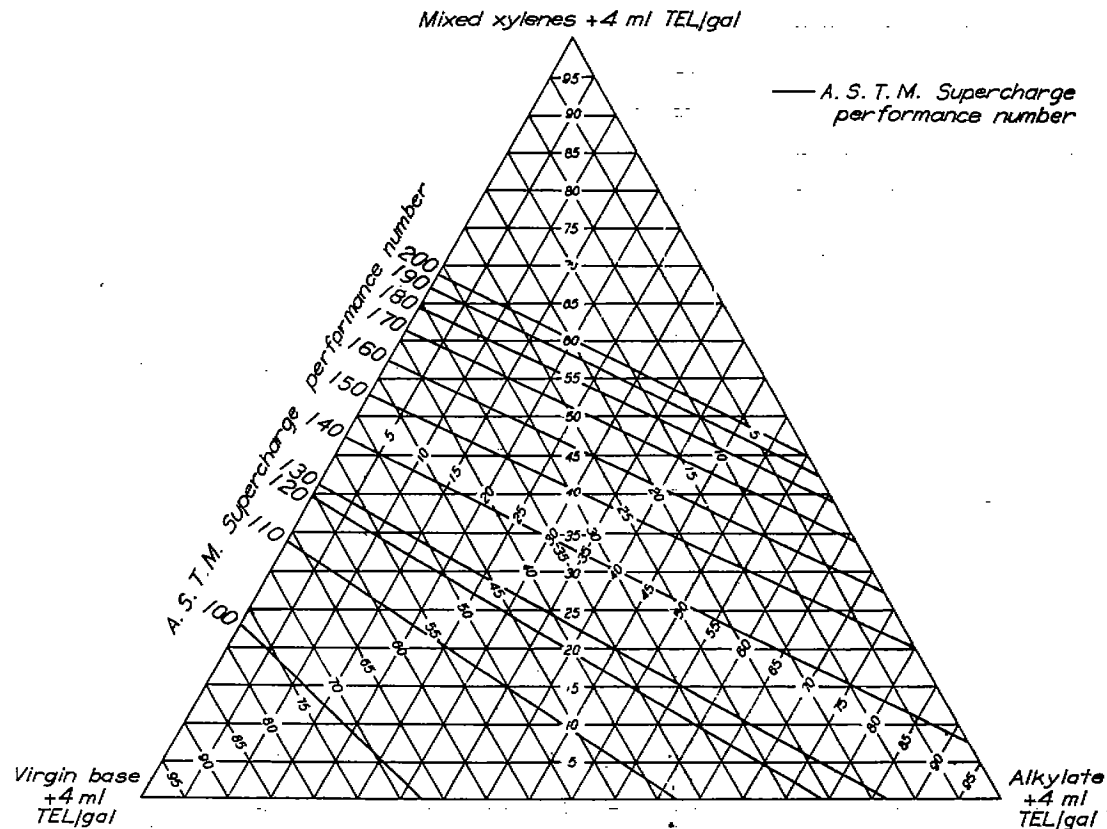


(d) Benzene blends. A. S. T. M. Supercharge fuel-air ratio, 0.11.

FIGURE B-1.—Continued. Blending charts for ternary blends containing high-antiknock blending agents, aviation kerosene, and virgin base stock by A. S. T. M. Aviation and A. S. T. M. Supercharge methods.

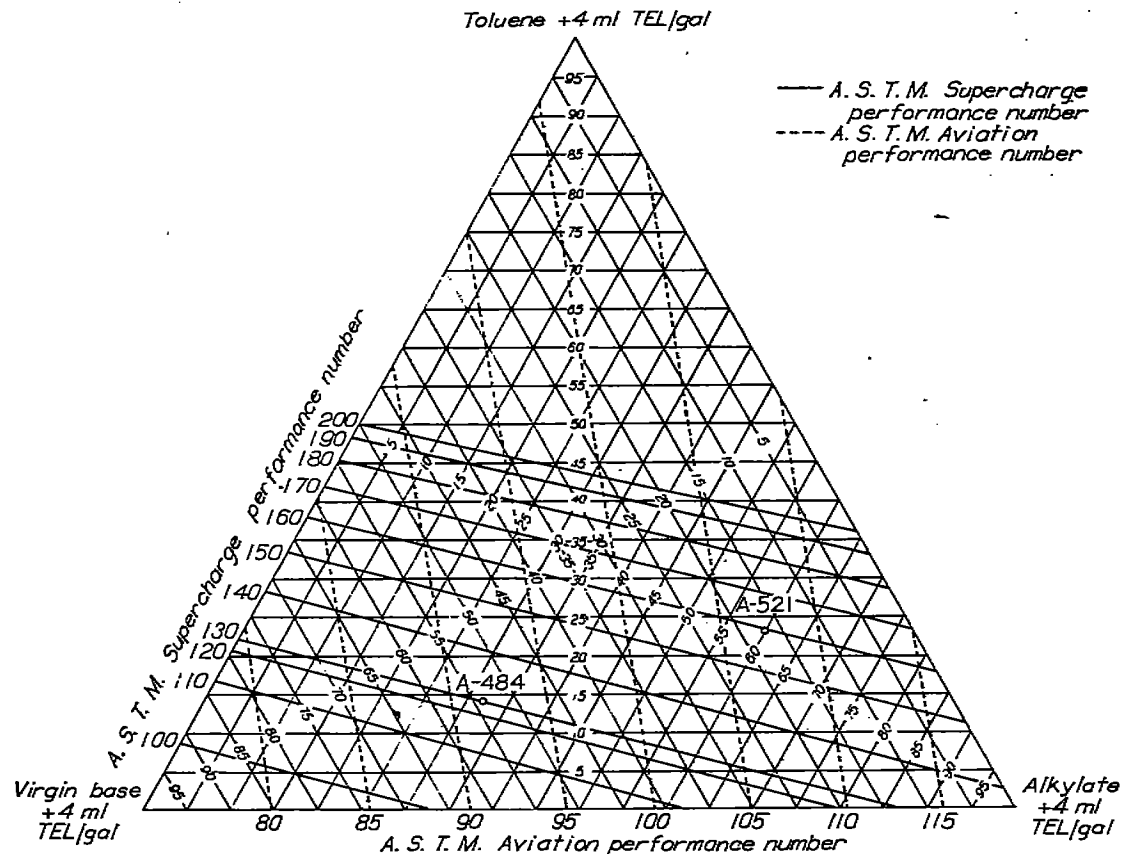


(e) Cumene blends. A. S. T. M. Supercharge ratings at fuel-air ratio for peak power.

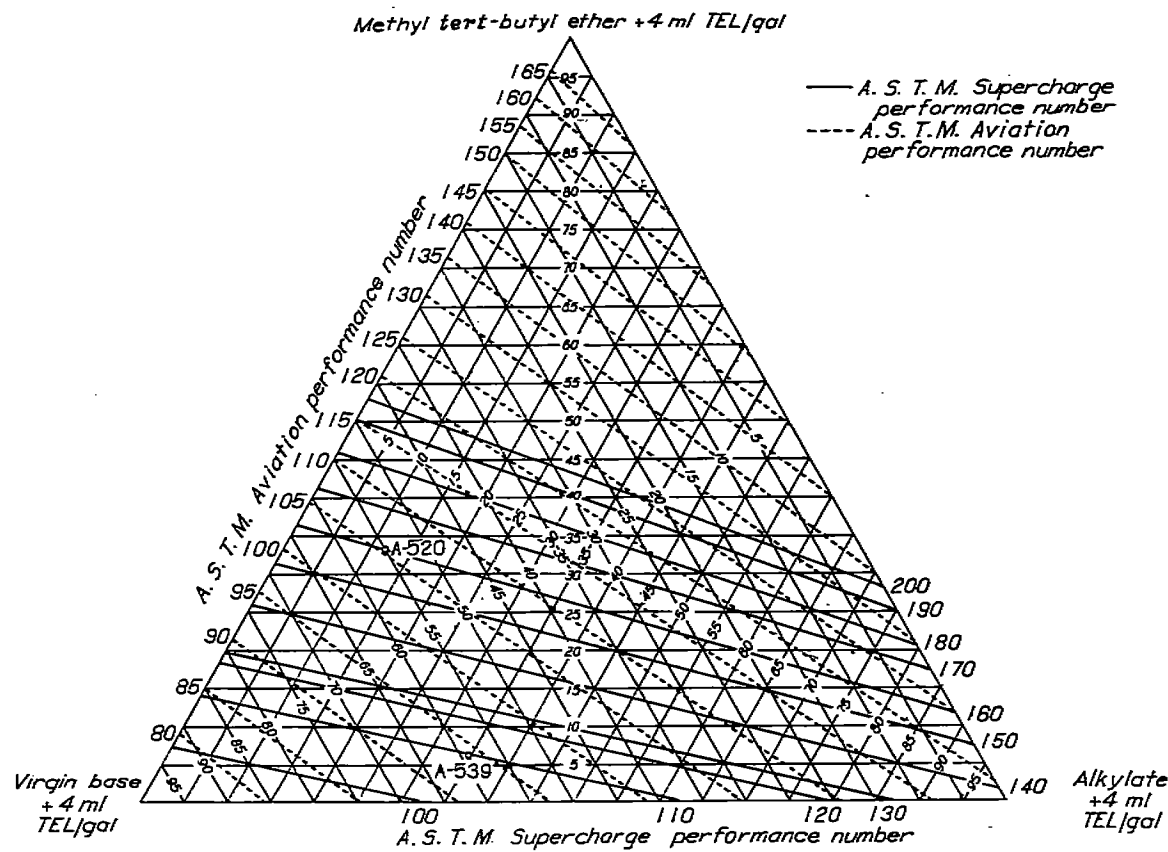


(f) Mixed xylene blends. A. S. T. M. Supercharge fuel-air ratio, 0.11.

FIGURE B-1.—Continued. Blending charts for ternary blends containing high-antiknock blending agents, aviation alkylate, and virgin base stock by A. S. T. M. Aviation and A. S. T. M. Supercharge methods.



(g) Toluene blends. A. S. T. M. Supercharge fuel-air ratio, 0.11.



(h) Methyl *tert*-butyl ether blends. A. S. T. M. Supercharge fuel-air ratio, 0.11.

FIGURE B-1.—Concluded. Blending charts for ternary blends containing high-antiknock blending agents, aviation alkylate, and virgin base stock by A. S. T. M. Aviation and A. S. T. M. Supercharge methods.

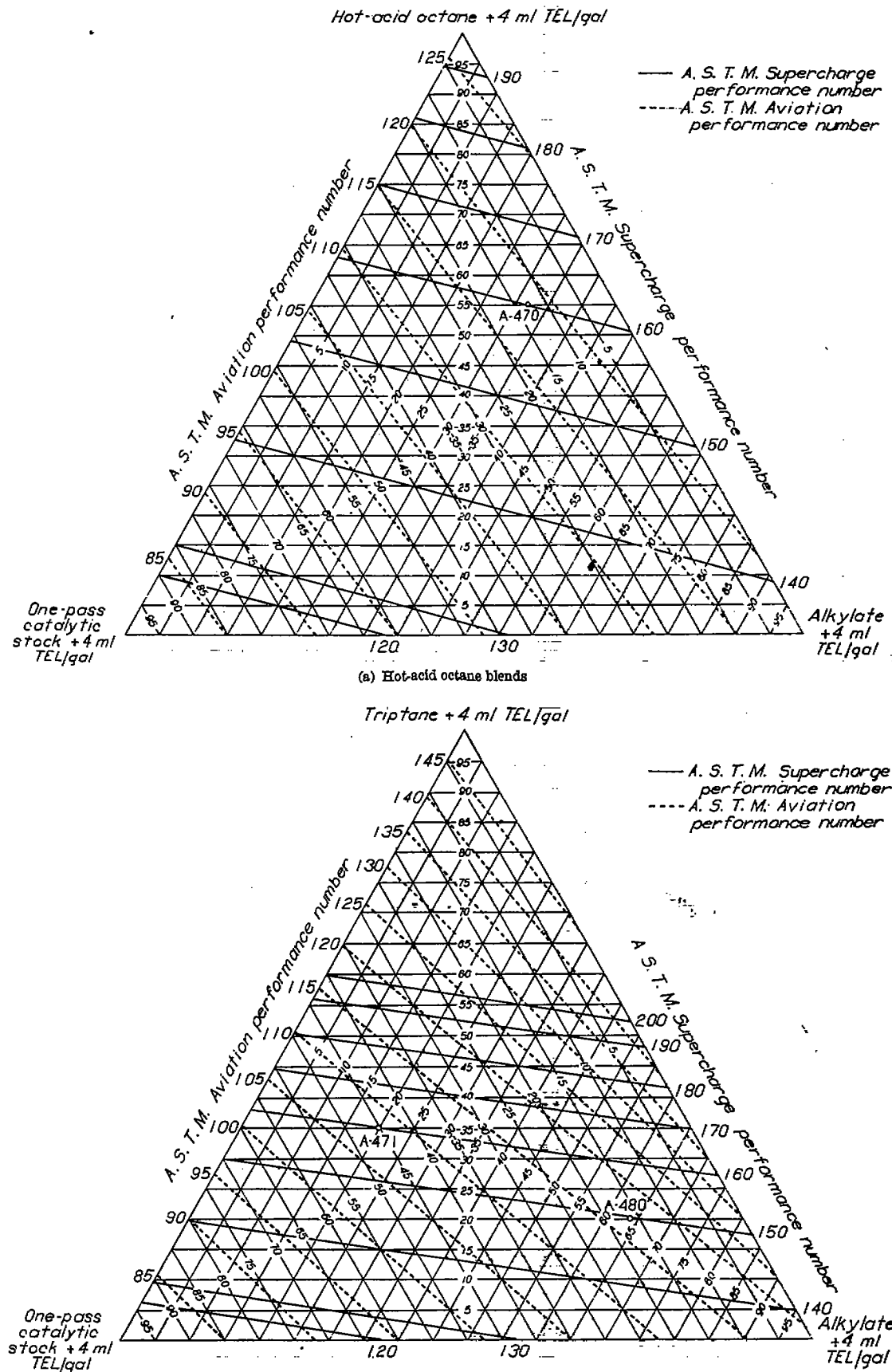


FIGURE B-2.—Blending charts for ternary blends containing high-antiknock blending agents, aviation alkylate, and one-pass catalytic stock by A. S. T. M. Aviation and A. S. T. M. Supercharge methods. A. S. T. M. Supercharge fuel-air ratio, 0.11.

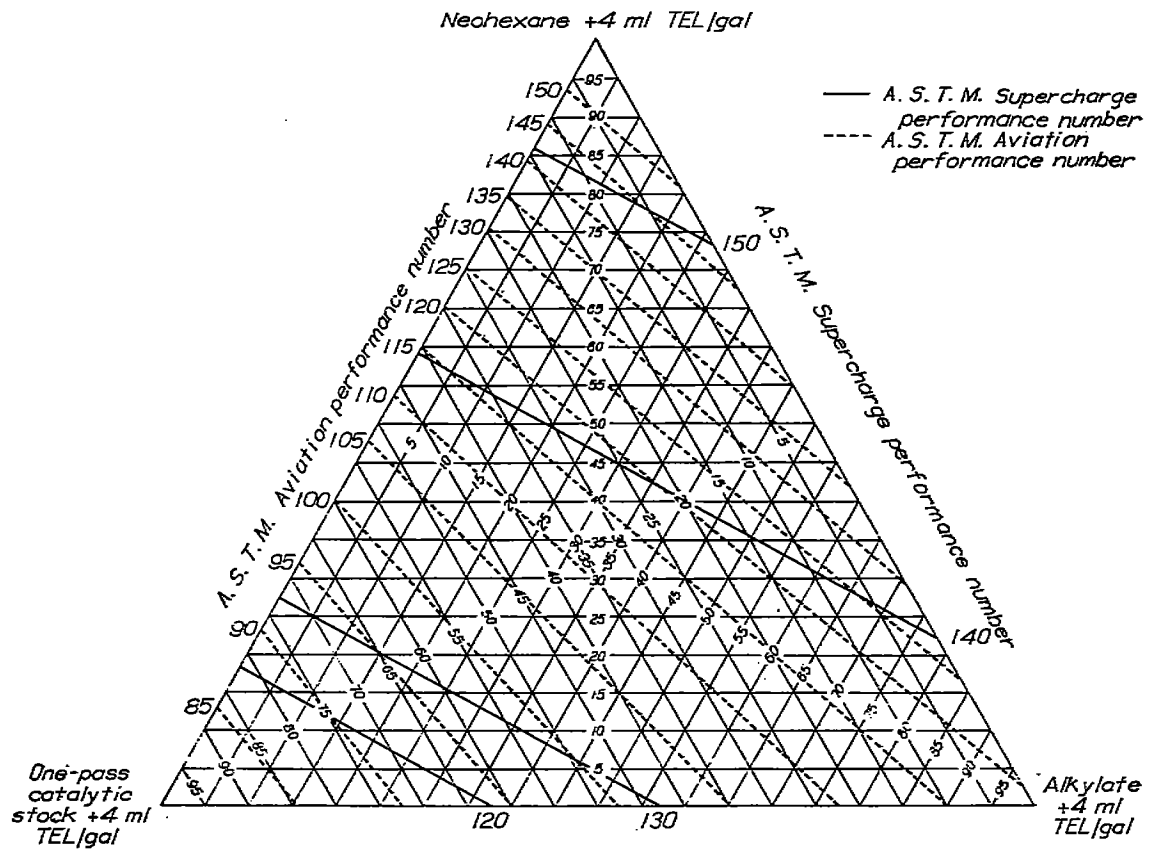
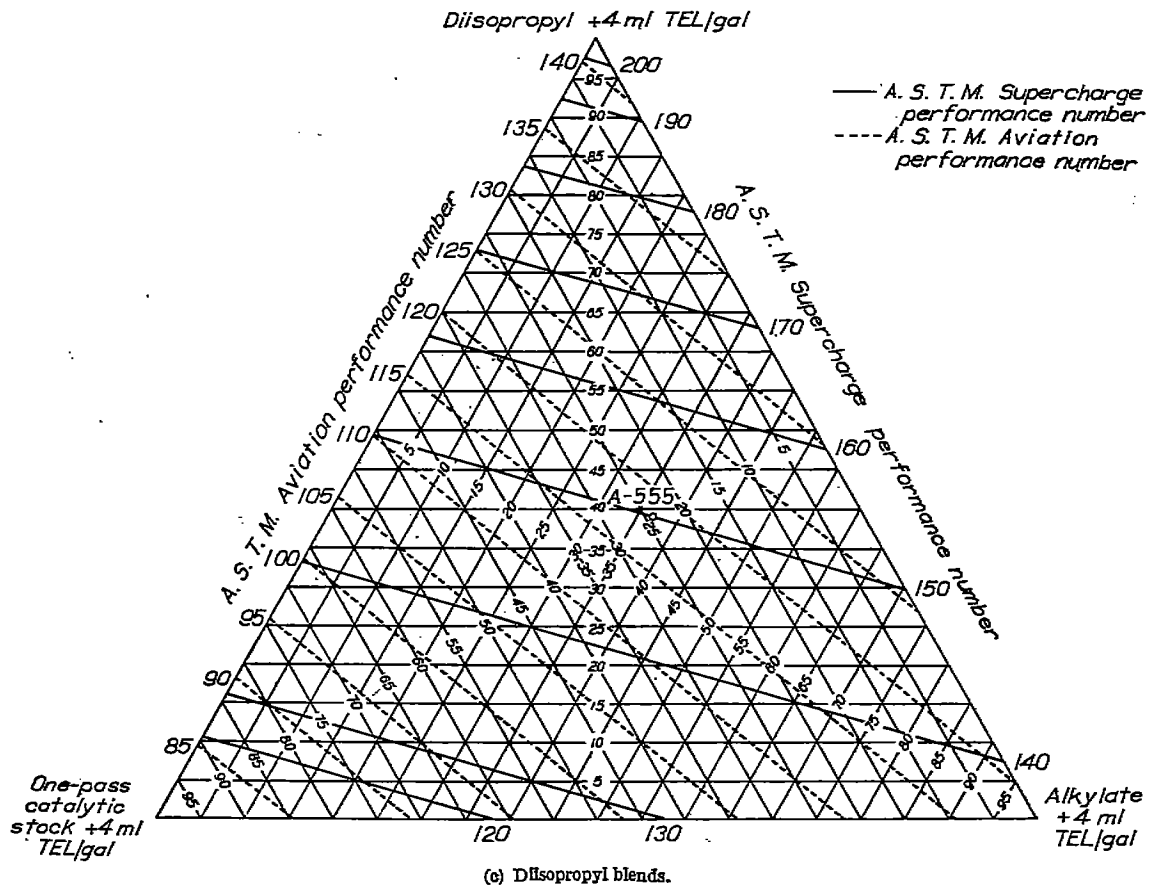
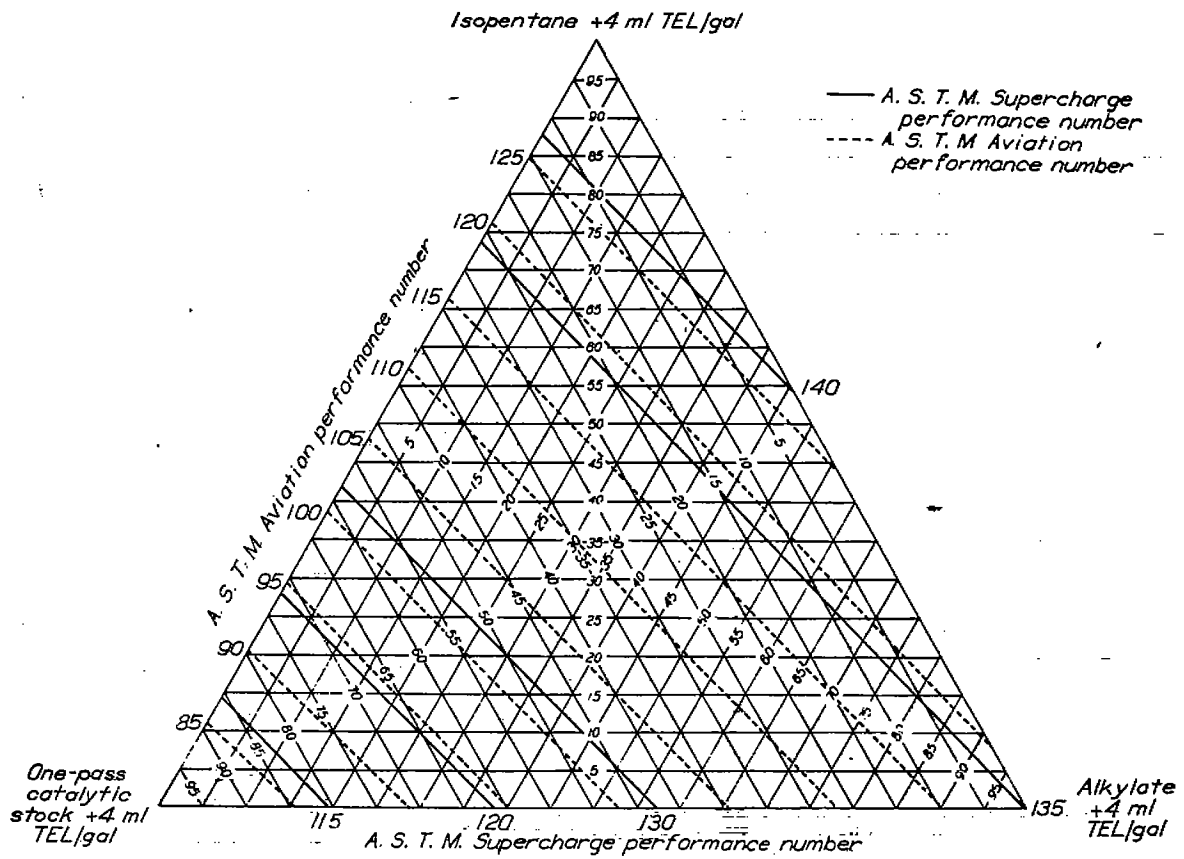
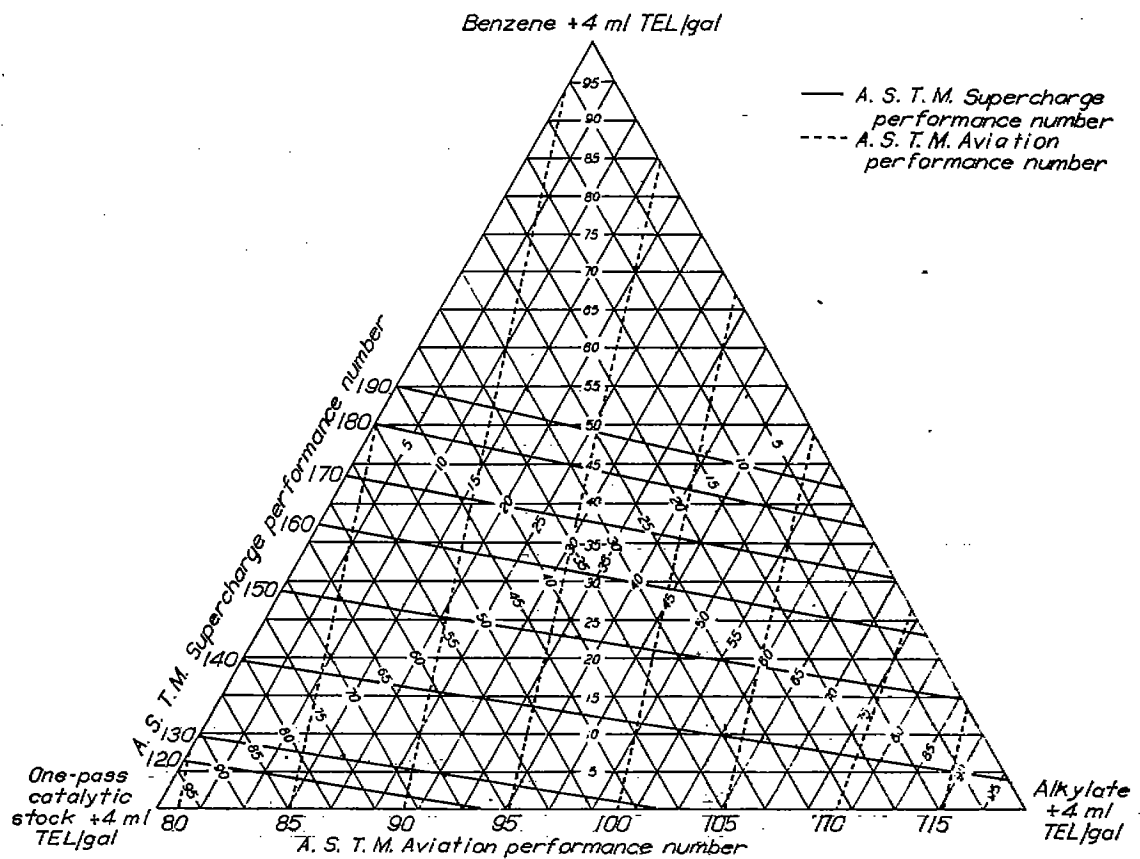


FIGURE B-2.—Continued. Blending charts for ternary blends containing high-antiknock blending agents, aviation alkylate, and one-pass catalytic stock by A. S. T. M. Aviation and A. S. T. M. Supercharge methods. A. S. T. M. Supercharge fuel-air ratio, 0.11.



(e) Isopentane blends.



(f) Benzene blends.

FIGURE B-2.—Continued. Blending charts for ternary blends containing high-antiknock blending agents, aviation alkylate, and one-pass catalytic stock by A. S. T. M. Aviation and A. S. T. M. Supercharge methods. A. S. T. M. Supercharge fuel-air ratio, 0.11.

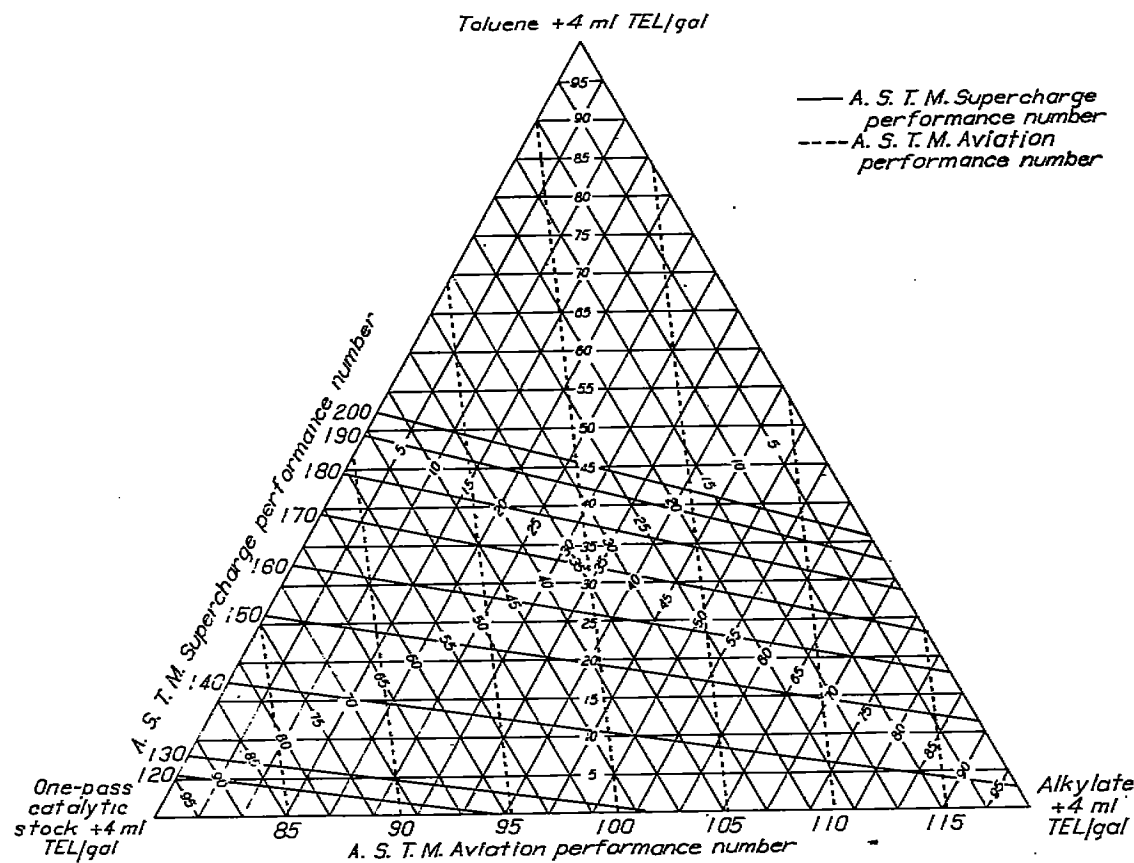
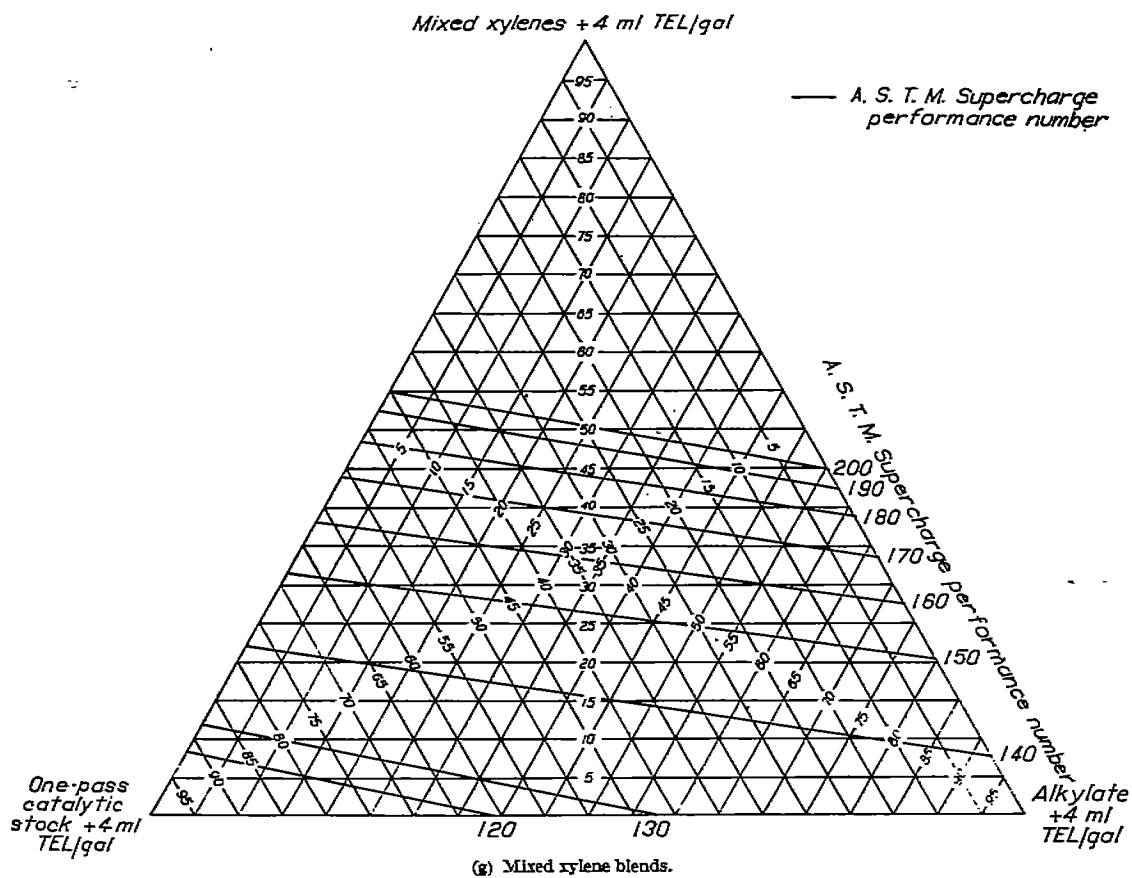


FIGURE B-2.—Continued. Blending charts for ternary blends containing high-antiknock blending agents, aviation alkylate, and one-pass catalytic stock by A. S. T. M. Aviation and A. S. T. M. Supercharge methods. A. S. T. M. Supercharge fuel-air ratio, 0.11.

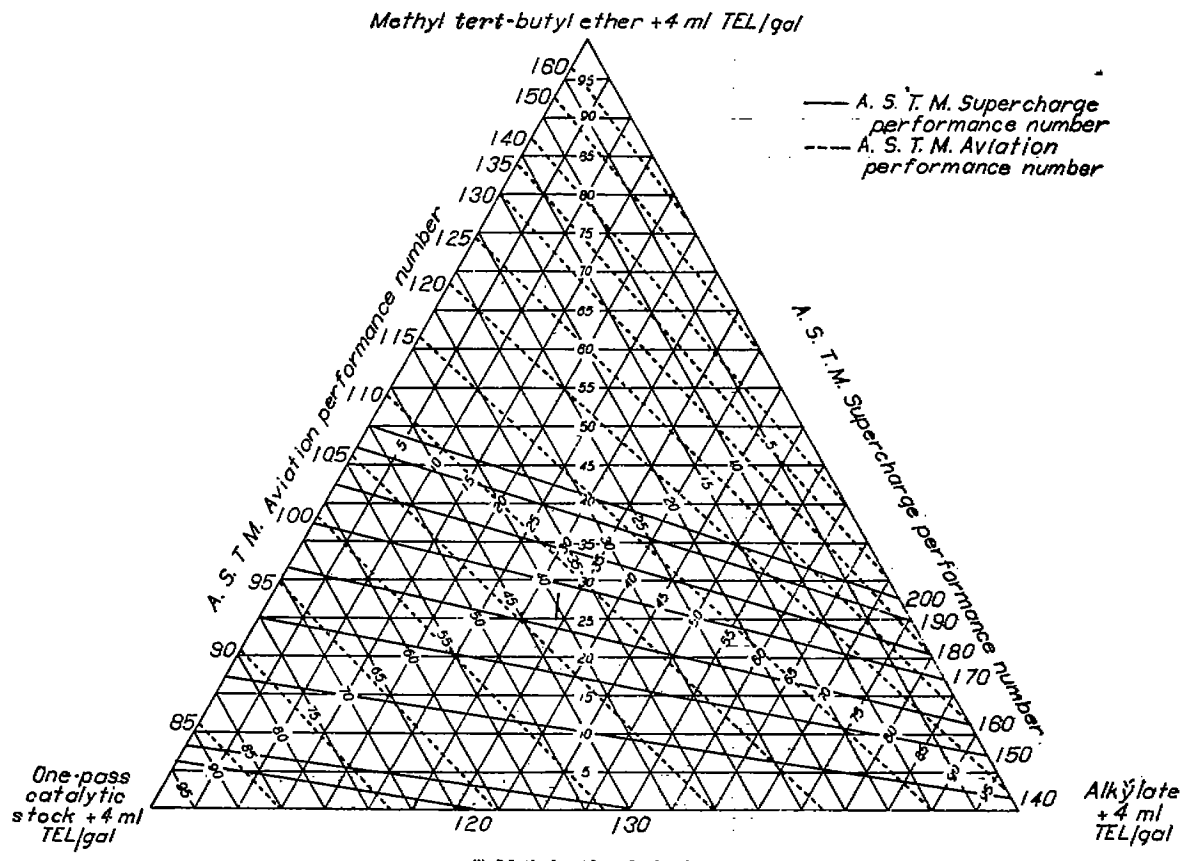


FIGURE B-2.—Concluded. Blending charts for ternary blends containing high-antiknock blending agents, aviation alkylate, and one-pass catalytic stock by A. S. T. M. Aviation and A. S. T. M. Supercharge methods. A. S. T. M. Supercharge fuel-air ratio, 0.11.